INTERNATIONAL COUNCIL FOR RESEARCH AND INNOVATION
IN BUILDING AND CONSTRUCTION

WORKING COMMISSION W18 - TIMBER STRUCTURES

CIB - W18

MEETING THIRTY-FIVE

KYOTO

JAPAN

SEPTEMBER 2002

Lehrstuhl für Ingenieurholzbau und Baukonstruktionen
Universität Karlsruhe
Germany
Compiled by Rainer Görlacher
2002

ISSN 0945-6996

CONTENTS

0 List of Participants
1 Chairman's Introduction
2 Co-operation With Other Organisations
3 Timber Columns
4 Stresses for Solid Timber
5 Timber Joints and Fasteners
6 Load Sharing
7 Laminated Members
8 Structural Stability
9 Fire
10 Statistics and Data Analysis
11 Glued Joints
12 Test Methods
13 Structural Design Codes
14 Any Other Business
15 Venue and Program for Next Meeting
16 Close
17 List of CIB W18 Papers/Kyoto, Japan 2002-10-23
18 Current List of CIB-W18 Papers

CIB-W18 Papers 35-2-1 up to 35-102-2

0 List of Participants

INTERNATIONAL COUNCIL FOR RESEARCH AND INNOVATION IN BUILDING AND CONSTRUCTION
WORKING COMMISSION W18 - TIMBER STRUCTURES

MEETING THIRTY-FIVE
Kyoto, Japan 16-19 September 2002

LIST OF PARTICIPANTS

CANADA

P Quenneville	Royal Military College, Kingston

DENMARK

P Ellegaard	Aalborg University
H J Larsen	Danish Building Research Institute, Hørsholm
S Svensson	Aalborg University

FINLAND

A Kevarinmäki	VTT Technical Research Centre of Finland, Espoo

FRANCE

E Fournely	C.U.S.T. Aubiere Cedex
F Rouger	CTBA, Bordeaux

GERMANY

S Aicher	Otto-Graf-Institute, Stuttgart
H J Blaß	University of Karlsruhe
J Ehlbeck	University of Karlsruhe
R Görlacher	University of Karlsruhe
P Haller	University of Dresden
L Höfflin	Otto-Graf-Institute, Stuttgart
K Rautenstrauch	Bauhaus University, Weimar
K U Schober	Bauhaus University, Weimar

JAPAN

J Jensen	Institute of Wood Technology, Akita Prefectural University
N Kawai	NILIM, Tsukuba
A Kitamosi	Wood Research Institute, Kyoto University
K Komatsu	Wood Research Institute, Kyoto University
S Nakajima	Building Research Institute, Tsukuba
M Noguchi	Wood Research Institute, Kyoto University
T Sasaki	Institute of Wood Technology, Akita Prefectural University
H Sugiyama	University of Tokyo, Tokyo
M Yasumura	Shizuoka University

LATVIA

L Ozola	Latvia University of Agriculture, Jelgava

NORWAY

E Aasheim	Norwegian Institute of Wood Technology, Blindern
I Weider	Norwegian Institute of Wood Technology, Blindern

SLOVENIA

B Dujic	Faculty of Civil and Geodetic Engineering, Ljubljana

SWEDEN

C Bengtsson	Swedish National Testing and Research Institute, Borås
M Hansson	Lund University
B Källsner	Swedish Institute for Wood Technology Research, Stockholm
J König	Swedish Institute for Wood Technology Research, Stockholm
S Thelandersson	Lund University

THE NETHERLANDS

G Gonzalez	Eindhoven University of Technology
A D Leijten	TU Delft

UK

B S Choo	Nottingham University
R F Marsh	Consultant, London

USA

R Gutkowski	Colorado State University
B Yeh	American Plywood Association, Tacoma

1. Chairman's Introduction

2. Co-operation With Other Organisations

3. Timber Columns

4. Stresses for Solid Timber

5. Timber Joints and Fasteners

6. Load Sharing

7. Laminated Members

8. Structural Stability

9. Fire

10. Statistics and Data Analysis

11. Glued Joints

12. Test Methods

13. Structural Design Codes

14. Any Other Business

15. Venue and Program for Next Meeting

16. Close

INTERNATIONAL COUNCIL FOR RESEARCH AND INNOVATION IN BUILDING AND CONSTRUCTION

WORKING COMMISSION W18 - TIMBER STRUCTURES

MEETING THIRTY-FIVE

KYOTO, JAPAN 16 - 19 SEPTEMBER 2002

MINUTES
(B S CHOO)

1. CHAIRMAN'S INTRODUCTION

After welcoming members to the 35th meeting of the Working Commission to Kyoto, H J Blaß, the Chairman informed colleagues that this is the first meeting of the Working Commission to be held in Asia with the exception of one meeting in Israel in 1985. H J Blaß then thanked M Yasumura of Shizuoka University, N Kawai of the Building Research Institute and K Komatsu of Kyoto University for the local arrangements and organisation. M Yasumura then outlined arrangements for social events and for the technical visit to Kyoto University.

2. CO-OPERATION WITH OTHER ORGANISATIONS

(a) RILEM

Members of the Working Commission were not aware of any timber structures related activities at RILEM

(b) CEN

H J Larsen, Chairman of TC 124, announced that product standards for Timber Structures (including structural timber and glulam) are to be published in around 6 months time.

J König, Chairman of the TC 250 reported that the final drafts of EC5 EN 1995-1-1 General Building and EC5 EN 1995-1-2 Fire have been sent to CEN for the formal vote in October and September 2002, respectively. These documents are expected to be available in October 2003 and to be fully implemented (ie with the withdrawal of national standards) in March 2009. He also reported that the second draft of EC5 EN 1995-2 Bridges is expected around November 2002 and the final draft will be prepared by the Project Team in March 2003. After the Examination period (maximum 6 months) the document will be sent to CEN for the formal vote around January 2004. The document is expected to be available in around January 2005 and to be fully implemented (ie with the withdrawal of national standards) around January 2010.

(c) IABSE

Members of the Working Commission were not aware of any timber structures related activities at IABSE.

(d) IUFRO S5.02

It was reported that a new Chairman has been recently elected but members were not aware of his name.

3. TIMBER COLUMNS

Paper 35 - 2 - 1 *Computer Simulations on the Reliability of Timber Columns Regarding Hygrothermal Effects-* ***R Hartnack, K-U Schober, K Rautenstrauch***

Presented by: K U Schober

A number of questions were asked by H J Blaß and H J Larsen about the practical relevance of the research reported in the paper and its implications for service class designations in design situations according to EC5. The author confirmed that the test specimen which were 14x14cm or 16x16 cm cross-section were tested and that it is difficult to model service class 2. This was followed by discussions on the relative values of moisture content in timber members for the various service classes. S Thelandersson then asked for clarification of the work with regard to the creep model used and A Leijten asked about the starting point and the cumulative effect of climate conditions. In addition to clarifying the points raised, K U Schober confirmed that the reported model did not take strength considerations into account.

4. STRESSES FOR SOLID TIMBER

Paper 35 - 6 - 1 *Evaluation of Different Size Effect Models for Tension Perpendicular to Grain Design -* ***S Aicher, G Dill-Langer***

Presented by: S Aicher

H J Larsen and B S Choo asked about the consequences of load shearing and scale effects respectively. S Aicher replied that as the overall effect is conservative the preferred models may be used for design. S Thelandersson asked if the data set used for comparison with the analytical model were tested under a common climate regime. S Aicher replied that of the 20 data set used, 3 were conducted under EN1193 and EN408 recommendations. The remaining 17 data set were those tested by Mistler. J Ehlbeck then confirmed that the Mistler data were obtained from specimens which were at 12% +/- 1 or 2%. Discussion then centred around the question of density effects and the fact that the specimens strengths ranged from C22 to C40.

Paper 35 - 6 - 2 *Tensile Strength of Glulam Perpendicular to Grain - Effects of Moisture Gradients -* ***J Jönsson, S Thelandersson***

Presented by: S Thelandersson

G Gonzalez asked how many replicates were used and if the data was sufficient for statistically valid conclusions. S Thelandersson replied that there were 4 replicates for each of the data points shown and was of the view that it was sufficient to provide a fair impression of the variation in behaviour trend. S Aicher asked if the observed effects could be due to the assumed plane stress or plane strain conditions and R Gutkowski asked if there were shrinkage cracks. S Thelandersson replied that no shrinkage cracks were observed but that there were cracks which were due to the drying process. J Ehlbeck then commented that as k_{mod} for stress perpendicular to grain is generally different from other k_{mod} values, the historical approach has been to use fictitious strength values whilst maintaining a common k_{mod} value in EC5.

6. TIMBER JOINTS AND FASTENERS

Paper 35 - 7 - 1 *New Estimating Method of Bolted Cross-lapped Joints with Timber Side Members* - ***M Noguchi, K Komatsu***

Presented by: M Noguchi

In answer to H J Blaß's question, M Noguchi indicated that the model could not predict ultimate load capacity. A Leijten and H J Blaß then asked about the bolt hole size and the number of test replicates used. Noguchi indicated that the holes were 1 mm oversize and there were 4 replicates per test data point. E Fournely asked about the bending component in the model. This was followed by a brief discussion about the effects of bending in the joint.

Paper 35 - 7 - 2 *Analysis on Multiple Lag Screwed Timber Joints with Timber Side Members* - ***K Komatsu, S Takino, M Nakatani, H Tateishi***

Presented by: K Komatsu

H J Blaß asked if individual load-slip curves were used for the fasteners. K Komatsu indicated that only a generic value was used but that the Monte Carlo approach will be used in future studies. P Ellegaard asked about the apparently more ductile experimental test behaviour than that indicated by the theory. K Komatsu replied that this may be because of errors due to division by zero in the numerical calculations. In reply to questions by H J Larsen and P Quenneville about the experimental design and the approval for use of the type of screw tested, K Komatsu replied that the testing were carried out in response to the requirements of the company producing the screws and it was only after the experimental data have been obtained, that an analytical approach was sought to explain the observed behaviour.

Paper 35 - 7 - 3 *Joints with Inclined Screws* - ***A Kevarinmäki***

Presented by: A Kevarinmäki

P Quenneville and H J Blaß asked about anchorage strength and the contributions of the threaded and head pull through components to the strength of the joint. A Kevarinmäki replied that he was of the view that the addition of the two components of threaded and head pull through strength values is justified but that the resulting value is conservative.

Paper 35 - 7 - 4 *Joints with Inclined Screws* - ***I Bejtka, H J Blaß***

Presented by: H J Blaß

In answer to F Rouger's question H J Blaß indicated that he did not have an explanation for the more conservative values observed for the longer specimens. A Kevarinmäki asked if the effects of the screw head on withdrawal of the screw and about the dowel effect especially for large inclination angles had been considered. H J Blaß replied that the screw head effect was not taken into account as it was not considered to be effective and that the dowel effects were indeed small but would be considered.

Paper 35 - 7 - 5 *Effect of distances, Spacing and Number of Dowels in a Row an the Load Carrying Capacity of Connections with Dowels failing by Splitting* -, ***M Schmid, R Frasson, H J Blaß***

Presented by: H J Blaß

In reply to the questions about the load magnitudes and sequence of loading by P Quenneville, H J Blaß replied that the loading was assumed to be equally distributed even though it was recognised that this does not fully reflect the practical situation and that the model used is justifiable as the results are conservative. E Fournely asked if the frictional effects generated as the dowel moved through the timber on the magnitude the shear force V was taken into account. H J Blaß replied that the frictional effects of the dowel was not considered but he recognised that it would have an effect on the shear load. This was followed by discussion regarding the relevance of the proposed model. It was generally agreed that the model is most relevant to mode 1 failure and that mode 2 failure mode capacity is generally higher than that of mode 1.

Paper 35 - 7 - 6 *Effect of Row Spacing on the Capacity of Bolted Timber Connections Loaded Perpendicular-to-grain* - ***P Quenneville, M Kasim***

Presented by: P Quenneville

H J Larsen and H J Blaß asked about the effect of spacing on the interaction potential of the 2 separate connections – the expressions developed in the presentation seemed to imply that there is interaction even if the connections are very far apart. P Quenneville recognised the limitations of the proposed expressions. This was followed by questions by F Rouger and L Ozola regarding the approach used for calculating cov and the characteristic values presented. P Quenneville replied that the cov values were separately calculated for each data set. This was followed by discussion about the correct approach to calculating cov and it was suggested that a single cov value could be used for the entire test series.

Paper 35 - 7 - 7 *Splitting Strength of Beams Loaded by Connections, Model Comparison* - ***A J M Leijten***

Presented by: A J M Leijten

H J Larsen commented that the proposed expression are almost identical to previously published expression except for the term he/h and so the proposed expression will give identical results when he/h is small and would only have significance when he/h is large and as such the proposed expressions have limited practical significance. This was followed by an interesting in depth discussion by H J Blaß and A Leijten about the fundamental validity of the proposed approach and the significance of the efficiency and behaviour factors used in the proposed expression.

Paper 35 - 7 - 8 *Load-Carrying Capacity of Perpendicular to the Grain Loaded Timber Joints with Multiple Fasteners* - ***O Borth, K U Schober, K Rautenstrauch***

Presented by: K U Schober

In reply to the question by H J Blaß on the practical relevance of the approach presented, K U Schober replied that the equations presented are not for design purposes. A Leijten then asked if failure of the fasteners was considered, K U Schober replied that fastener failure modes were not considered. S Aicher asked if the fictitious crack length of 6mm for 16mm dowel penalises dowels with smaller diameters. Schober agreed that the proposed approach does penalise small diameter dowels.

Paper 35 - 7 - 9 *Determination of fracture parameter for dowel-type joints loaded perpendicular to wooden grain and its application - **M Yasumura***

Presented by: M Yasumura

H J Larsen commented that the test method used is too close to structural application and that it would be better to use independent structural parameters for G and Gc. P Quenneville and S Svensson asked if the rate of loading influenced the test results. M Yasumara replied that he did not think so. K Komatsu and J Ehlbeck respectively asked if the study considered the influences of dowel diameter and moisture content. M Yasumara confirmed that they were not.

Paper 35 - 7 - 10 *Analysis and Design of Modified Attic Trusses with Punched Metal Plate Fasteners - P Ellegaard*

Presented by: P Ellegaard

H J Blaß asked about the relevance of the study to EC5 design approaches and about the load testing arrangement. E Fournely also asked how the loading was applied. After expressing his view on the relevance of his research to EC5, P Ellegaard explained that equal loads at 4 points were applied via a hinged mechanism to the whole frame. G Gonzalez then asked if the suction load on the other side of the frame was considered. P Ellegaard replied that it was not.

Paper 35 - 7 - 11 *Joint Properties of Plybamboo Sheets in Prefabricated Housing - **G E Gonzalez***

Presented by: G E Gonzales

H J Blaß asked about the types of fixing used in the study. G Gonzalez replied that round smooth screws without shanks were used and the holes were predrilled to 80% of the screw diameter. S Svensson asked about the role of the plybamboo sheeting. K Komatsu asked if the timber split due to the nails. After confirming that the plybamboo sheeting were intended to act as normal sheeting G Gonzalez indicated that no splitting due to the nails was observed. B Dujic asked for clarification on the distances between studs and if the tested panel system could be considered to be partially anchored. G Gonzalez agreed that the system is partially anchored and that rotation of the system was not restricted. This was followed by a discussion initiated by B Yeh, S Aicher and S Thelandersson on the issues of storey drift, the transfer of wind loading and general testing arrangement for shear walls.

Paper 35 - 7 - 12 *Fiber-Reinforced Beam-to-Column Connections for Seismic Applications - **B Kasal, A Heiduschke, P Haller***

Presented by: P Haller

H J Blaß asked how the embedding strength of the glass fibre components were calculated. P Haller replied that it could not be measured but that the glass fibre provided ductility and tensile strength to the connection. This led to discussion about the embedding strength of the textile material and B Dujic commented that the glass fibres prevented splitting of the timber by limiting the stress values perpendicular to grain. H Sugiyama then asked if static tests on the connection were also conducted. P Haller indicated that static tests were not carried out. A Leijten asked about the densification of the timber and if secondary effects were considered in analysing the data. P Haller indicated that the softwood was surprisingly amenable to the densification process and that secondary effects were not considered. S

Thelandersson asked about the shrinkage and swelling values of the normal timber and densified wood components of the connection. This was followed by a general discussion about the definition of normal indoor climate and the equilibrium moisture content of the densified veneer wood. B Yeh then asked if P Haller knew of tests on finger joints which have been reinforced in the manner presented and A Leijten asked about the oversize of the dowel holes. P Haller replied that he did not know of similar tests on finger joints and that usual tolerances were used for dowel holes. H J Blaß asked if the type of reinforcement used affected failure loads and the resulting failure modes. P Haller commented that the fibre reinforcement did affect the failure mode and consequently the failure load. He was of the view that the differences in observed failure loads was a function of failure mode rather then direct contribution of the glass fibre's strength.

6. LOAD SHARING

Paper 34 - 8 - 1 *System Effect in Sheathed Parallel Timber Beam Structures part II –* ***M Hansson, T Isaksson***

Presented by: M Hansson

F Rouger and S Thelandersson commented on the weakest link criterion approach to studying system failure. H J Blaß commented on the bending strength used in obtaining the failure criterion and asked if bending - tensile interaction was considered. M Hansson replied that tensile strength values were not taken into account.

7. LAMINATED MEMBERS

Paper 35 - 12 - 1 *Glulam Beams with Round Holes – a Comparison of Different Design Approaches vs. Test Data -* ***S Aicher L Höfflin***

Presented by: L Höfflin

H Larsen provided the background to the approach adopted in EC5 and commented on the implication that EC5 equations would result in non-conservative designs and he then went on to ask if the authors were of the view that the equations in EC5 needed to be altered. S Aicher replied that in his view a scalar modification with an additional term is required.

8. STRUCTURAL STABILITY

Paper 35 - 15 - 1 *On test methods for determining racking strength and stiffness of wood-framed shear walls -* ***B Källsner, U A Girhammar, L Wu***

Presented by: B Källsner

H Sugiyama asked if the authors were familiar with the tests conducted by Tuomi in the 1970s in which proposals for testing perforated shear walls were made. H Sugiyama felt that Tuomi's proposals should be considered even though he did not fully agree with the proposals. B Källsner confirmed that he was aware of the Tuomi tests which assumed an elastic behavior of the various components but despite making arguable assumptions, the Tuomi approach gave good results. He then went on to agree with comments that gypsum boards are difficult to handle.

Paper 35 - 15 - 2 A Plastic Design Model for Partially Anchored Wood-framed Shear Walls with Openings - ***U A Girhammar, L Wu, B Källsner***

Presented by: B Källsner

S Aicher asked about the distribution of loads in the studs and if all the loading eventually located in the end stud. B Källsner confirmed that a lower bound plastic approach was used to model the system tested and that it was one of many possible ways to do so. He also confirmed that the studs used may be considered to be stiff and that the loads were transferred to the end stud. H Larsen asked for a comparative comment on the load testing approach which is frequently used versus the analytical/calculation approach which the Scandinavians seem to prefer. This led to a comment by B Dujic about the need to maintain the vertical loading and the significance of dynamic and monotonic load testing of shear walls. S Thelandersson and H Sugiyama commented on the importance of preventing uplift of the wall end and the differences between testing a floor system and a racked shear wall system.

Paper 35 - 15 - 3 Evaluation and Estimation of the Performance of the Shear Walls in Humid Climate - ***S Nakajima***

Presented by: S Nakajima

S Svensson asked about the moisture content of the components in the tests and S Thelandersson commented on the need for caution when considering appropriate service class allocation and when calculating slip values. S Nakajima clarified the issues raised. B Yeh then commented on the 5-15 % higher strength values described in section 5.2 of the paper and asked for further clarification of the modelling used. S Nakajima clarified that the analysis adopted a process which followed the load-deflection curve of each nail which were then summed to provide an over result.

Paper 35 - 15 - 4 Influence of Vertical Load on Lateral Resistance of Timber Frame Walls - ***B Dujič, R Žarnić***

Presented by: B Dujič

G Gonzalez asked about the embedding strength on both sides of the test system used and S Svensson asked for further details of the vertical loading used in the tests. B Dujič confirmed that failure mode d was observed and the vertical load used represented both dead and live loads which can be expected from a 5 storey building. Comments were then made about the need or otherwise for intermediate studs in a 5 storey building. M Yasumura asked for further details about the model used and its applicability to panels with opening. After further description of the test setup and the model used, B Dujič indicated that the test specimen can be classified as a rigid diaphragm. This was followed by further discussions led by S Thelandersson and H J Blaß about the test rig and the loading system used.

Paper 35 - 15 - 5 Cyclic and Seismic Performances of a Timber-Concrete System - Local and Full Scale Experimental Results - ***E Fournely, P Racher***

Presented by: E Fournely

In answer to a question by G Gonzalez, E Fournely indicated that the slip modulus was measured. H J Blaß asked if bonding between the timber and concrete was prevented during the test. E Fournely replied that plastic sheeting were only provided on the sides of the test specimens and so bonding between the concrete and timber was not prevented.

Paper 35 - 15 - 6 Design of timber-concrete composite structures according to EC5 - 2002 version - ***A Ceccotti, M Fragiacomo, R M Gutkowski***

Presented by: R M Gutkowski

H J Blaß asked if the proposed calculation methods presented were compared against test data. G Gutkowski replied that the presentation refers only to numerically generated data as the testing intended by the authors have yet to be conducted. H J Blaß then commented that the deformations obtained from recent tests conducted at Karlsruhe University were twice the values predicted by EC5 and as such perhaps an approach which is simpler but more accurate than those proposed in the latest version of EC5 or the authors is needed.

Paper 35 - 15 - 7 Design of timber structures in seismic zones according to EC8- 2002 version - ***A Ceccotti, T Toratti, B Dujič***

Presented by: B Dujič

There were no comments or questions for the authors.

Paper 35 - 15 - 8 Design Methods to Prevent Premature Failure of Joints at Shear Wall Corners - ***N Kawai, H Okiura***

Presented by: N Kawai

N Kawai confirmed H J Blaß's observation that although the calculated results are in general larger than test data, this was not so for certain ultimate conditions. B S Choo asked if the assumption that the beams are rigid in the vertical plane is valid and if that could be a reason for large differences observed between calculated and test results. N Kawai agreed that this is possible, especially for the simplified analytical methods but does not explain the differences for the most precise analytical approach. G Gonzalez asked how the yield values were estimated. N Kawai replied that a modified European approach described earlier by B Dujič was used. M Yasumura asked for if the beams used in the tests were of normal proportions or if they could be considered to be rigid. N Kawai confirmed that normal sized glulam beams were used. This was followed by a general discussion relating to the holding down straps and the corner panel size and construction.

9. FIRE

Paper 35 - 16 - 1 Basic and Notional Charring Rates - ***J König***

Presented by: J König

H J Blaß asked why the close comparison of cross-sectional moduli calculated from test data against EC5 values was not reflected in the comparison for beams. J König replied that in the data he presented, he merely wanted to compare the single beam values. J König then commented that EC5 values tend to be conservative for members with narrow cross-sections and is an issue which should be investigated. This was followed by a brief discussion initiated by R Gutkowski around the issues of the needs of the practising designer for simple but generally conservative calculations versus detailed calculations which seek to be accurate and as such may or may not be conservative from a design view point.

10. STATISTICS AND DATA ANALYSIS

Paper 35 - 17 - 1 Probabilistic Modelling of Duration of Load Effects in Timber Structures - ***J Köhler, S Svensson***

Presented by: S Svensson

S Thelandersson asked for clarification regarding the stated intention of the author to model uncertainties versus what was presented which is merely a comparison of the uncertainties between the test data and the model results. This was followed by a detailed discussion about the fundamental assumptions in the 3 models considered and their validity for the cases under consideration. S Svensson cautioned that the test data he presented were derived from specimens with a high moisture content which is not representative of normal building structures and commented on the possible effects on values of k_{mod}.

11. GLUED JOINTS

Paper 35 - 18 - 1 Creep Testing Wood Adhesives for Structural Use - C Bengtsson, B Källander

Presented by: C Bengtsson

S Aicher challenged the authors' recommendation that the 4680 rather than the 3535 test procedures be adopted as the European standard practice for glue testing. The challenge is based on the assertion that the test time to failure obtained ranged from values around 200 to over 10000 hours. Additionally, S Aicher was of the view that the study is not sufficiently detailed or complete to justify the recommendations made. C Bengtsson replied that the authors are not dismissing the 3535 approach completely but the method is only able to differentiate between glues with very different strengths and does not provide data beyond a pass-fail conclusion. C Bengtsson acknowledged that further testing, especially with large or full scale specimens, may well provide data which are able to differentiate and/or confirm the advantages of the two approaches, however until such data is available, C Bengtsson is of the view that the 4680 approach is more sophisticated and should be adopted as the standard European glue testing method.

12. TEST METHODS

Paper 35 - 21 - 1 Full-scale Edgewise Shear Tests for Laminated Veneer Lumber- ***B Yeh, T G Williamson***

Presented by: B Yeh

H J Blaß asked if the author has also tested glulam beams in the same manner as that presented for LVL and if so, how the values compared. B Yeh replied that similar tests were conducted on glulam beams a year ago and that in general the shear strength values for LVL are higher than those for glulam beam. B Yeh felt that the reason for this is the higher volume of glue in the LVL and that the ply in the LVL has been densified.

13. STRUCTURAL DESIGN CODES

Paper 35 - 102 -1 Design Characteristics and Results According to EUROCODE 5 and SNiP Procedures - ***L Ozola, T Keskküla***

Presented by: L Ozola

H J Larsen commented that the classification of building types is not part of the Eurocodes because the activity is the responsibility of the national states in other Standards relating to the design and construction of buildings and structures. He also commented that no EU country has yet formally adopted the Eurocodes for practical design purposes. L Ozola then said that she is an enthusiastic about the Eurocodes because of the scientific content and procedures used in its formulation.

Paper 35 - 102 -2 Model Code for the Reliability-Based Design of Timber Structures - ***H J Larsen***

Presented by: H J Larsen

S Thelandersson suggested the use of a single variable instead of (1 + y) in equation 1 as the use of a single variable will not permit the result being negative. S Thelandersson also commented that the present proposed approach enforces the use of a time-variation approach and advocated the possible inclusion of a simple approach based on modification factors instead of a fully reliability based approach. H J Larsen is in sympathy with the points made and is of the view that a lower limit may be included in the current proposed approach to exclude unreasonable answers. H J Larsen agreed with H J Blaß about the need to include the creep properties of connections on structural systems but that due to the complexity involved, H J Larsen will only be able to deal with the issue in the "next chapter".

14. ANY OTHER BUSINESS

K Komatsu informed delegates about travel arrangements and timetable for visit to the Wood Research Institute and the Disaster Prevention Research Institute.

R Gutkowski informed delegates about the 5 positions which are currently available at the State University of Colorado.

15. VENUE AND PROGRAM FOR NEXT MEETING

R Gutkowski described the venue and travel arrangements to Colorado should members of CIB W18 decide to hold the next meeting in Colorado.

J König read a proposal by Ron Marsh that only every third W18 meeting should be held outside Europe as most participants came from Europe. As a Centre for Timber Engineering has recently been established at Napier University, it would be good to hold the next W18 meeting at Napier even though he has no authority to make the offer of a venue. B S Choo informed delegates that he has been recently appointed Director of the Centre for Timber Engineering and was sure that the Centre will be willing to host the next W18 meeting.

H J Larsen commented that he is content for the next meeting to be held in Colorado and suggested Napier 2004

After a short discussion it was decided to hold the next two meetings in Europe after the Colorado meeting in 2003, possibly in 2004 at Napier University Edinburgh. The date of the Colorado meeting is likely to be the 2nd week of August 2003

16. CLOSE

H J Blass again thanked the Japanese hosts for successfully hosting the meeting and especially Prof. Sugiyama for his support. He also thanked the authors and participants for their contributions and then closed the 35th meeting of CIB-W18 "Timber Structures".

17. List of CIB-W18 Papers,
Kyoto, Japan 2002

List of CIB-W18 Papers, Kyoto, Japan 2002

35 - 2 - 1 Computer Simulations on the Reliability of Timber Columns Regarding Hygrothermal Effects- **R Hartnack, K-U Schober, K Rautenstrauch**

35 - 6 - 1 Evaluation of Different Size Effect Models for Tension Perpendicular to Grain Design - **S Aicher, G Dill-Langer, W Klöck**

35 - 6 - 2 Tensile Strength of Glulam Perpendicular to Grain - Effects of Moisture Gradients - **J Jönsson, S Thelandersson**

35 - 7 - 1 New Estimating Method of Bolted Cross-lapped Joints with Timber Side Members - **M Noguchi, K Komatsu**

35 - 7 - 2 Analysis on Multiple Lag Screwed Timber Joints with Timber Side Members - **K Komatsu, S Takino, M Nakatani, H Tateishi**

35 - 7 - 3 Joints with Inclined Screws - **A Kevarinmäki**

35 - 7 - 4 Joints with Inclined Screws - **I Bejtka, H J Blaß**

35 - 7 - 5 Effect of distances, Spacing and Number of Dowels in a Row an the Load Carrying Capacity of Connections with Dowels failing by Splitting - **M Schmid, R Frasson, H J Blaß**

35 - 7 - 6 Effect of Row Spacing on the Capacity of Bolted Timber Connections Loaded Perpendicular-to-grain - **P Quenneville, M Kasim**

35 - 7 - 7 Splitting Strength of Beams Loaded by Connections, Model Comparison - **A J M Leijten**

35 - 7 - 8 Load-Carrying Capacity of Perpendicular to the Grain Loaded Timber Joints with Multiple Fasteners - **O Borth, K U Schober, K Rautenstrauch**

35 - 7 - 9 Determination of fracture parameter for dowel-type joints loaded perpendicular to wooden grain and its application - **M Yasumura**

35 - 7 - 10 Analysis and Design of Modified Attic Trusses with Punched Metal Plate Fasteners - **P Ellegaard**

35 - 7 - 11 Joint Properties of Plybamboo Sheets in Prefabricated Housing - **G E Gonzalez**

35 - 7 - 12 Fiber-Reinforced Beam-to-Column Connections for Seismic Applications - **B Kasal, A Heiduschke, P Haller**

35 - 8 - 1 System Effects in Sheathed Parallel Timber Beam Structures part II. - **M Hansson, T Isaksson**

35 - 12 - 1 Glulam Beams with Round Holes – a Comparison of Different Design Approaches vs. Test Data - **S Aicher L Höfflin**

35 - 15 - 1 On test methods for determining racking strength and stiffness of wood-framed shear walls - **B Källsner, U A Girhammar, L Wu**

35 - 15 - 2 A Plastic Design Model for Partially Anchored Wood-framed Shear Walls with Openings - **B Källsner, U A Girhammar, L Wu**

35 - 15 - 3 Evaluation and Estimation of the Performance of the Shear Walls in Humid Climate - **S Nakajima**

35 - 15 - 4 Influence of Vertical Load on Lateral Resistance of Timber Frame Walls - **B Dujič, R Žarnić**

35 - 15 - 5 Cyclic and Seismic Performances of a Timber-Concrete System - Local and Full Scale Experimental Results - **E Fournely, P Racher**

35 - 15 - 6 Design of timber-concrete composite structures according to EC5 - 2002 version - **A Ceccotti, M Fragiacomo, R M Gutkowski**

35 - 15 - 7 Design of timber structures in seismic zones according to EC8- 2002 version - **A Ceccotti, T Toratti, B Dujič**

35 - 15 - 8 Design Methods to Prevent Premature Failure of Joints at Shear Wall Corners - **N Kawai, H Okiura**

35 - 16 - 1 Basic and Notional Charring Rates - **J König**

35 - 17 - 1 Probabilistic Modelling of Duration of Load Effects in Timber Structures - **J Köhler, S Svenson**

35 - 18 - 1 Creep Testing Wood Adhesives for Structural Use - **C Bengtsson, B Källander**

35 - 21 - 1 Full-Scale Edgewise Shear Tests for Laminated Veneer Lumber- **B Yeh, T G Williamson**

35 - 102 -1 Design Characteristics and Results According to EUROCODE 5 and SNiP Procedures - **L Ozola, T Keskküla**

35 - 102 -2 Model Code for the Reliability-Based Design of Timber Structures - **H J Larsen**

18. Current List of CIB-W18(A) Papers

CURRENT LIST OF CIB-W18(A) PAPERS

Technical papers presented to CIB-W18(A) are identified by a code CIB-W18(A)/a-b-c, where:

a	denotes the meeting at which the paper was presented. Meetings are classified in chronological order:
1	Princes Risborough, England; March 1973
2	Copenhagen, Denmark; October 1973
3	Delft, Netherlands; June 1974
4	Paris, France; February 1975
5	Karlsruhe, Federal Republic of Germany; October 1975
6	Aalborg, Denmark; June 1976
7	Stockholm, Sweden; February/March 1977
8	Brussels, Belgium; October 1977
9	Perth, Scotland; June 1978
10	Vancouver, Canada; August 1978
11	Vienna, Austria; March 1979
12	Bordeaux, France; October 1979
13	Otaniemi, Finland; June 1980
14	Warsaw, Poland; May 1981
15	Karlsruhe, Federal Republic of Germany; June 1982
16	Lillehammer, Norway; May/June 1983
17	Rapperswil, Switzerland; May 1984
18	Beit Oren, Israel; June 1985
19	Florence, Italy; September 1986
20	Dublin, Ireland; September 1987
21	Parksville, Canada; September 1988
22	Berlin, German Democratic Republic; September 1989
23	Lisbon, Portugal; September 1990
24	Oxford, United Kingdom; September 1991
25	Åhus, Sweden; August 1992
26	Athens, USA; August 1993
27	Sydney, Australia; July 1994
28	Copenhagen, Denmark, April 1995
29	Bordeaux, France, August 1996
30	Vancouver, Canada, August 1997
31	Savonlinna, Finland, August 1998
32	Graz, Austria, August 1999
33	Delft, The Netherlands, August 2000
34	Venice, Italy, August 2001
35	Kyoto, Japan, Septmeber 2002

b denotes the subject:

1	Limit State Design
2	Timber Columns
3	Symbols
4	Plywood
5	Stress Grading
6	Stresses for Solid Timber
7	Timber Joints and Fasteners
8	Load Sharing
9	Duration of Load
10	Timber Beams
11	Environmental Conditions
12	Laminated Members
13	Particle and Fibre Building Boards
14	Trussed Rafters
15	Structural Stability
16	Fire
17	Statistics and Data Analysis
18	Glued Joints
19	Fracture Mechanics
20	Serviceability
21	Test Methods
100	CIB Timber Code
101	Loading Codes
102	Structural Design Codes
103	International Standards Organisation
104	Joint Committee on Structural Safety
105	CIB Programme, Policy and Meetings
106	International Union of Forestry Research Organisations

c is simply a number given to the papers in the order in which they appear:

Example: CIB-W18/4-102-5 refers to paper 5 on subject 102 presented at the fourth meeting of W18.

Listed below, by subjects, are all papers that have to date been presented to W18. When appropriate some papers are listed under more than one subject heading.

LIMIT STATE DESIGN

1-1-1	Limit State Design - H J Larsen
1-1-2	The Use of Partial Safety Factors in the New Norwegian Design Code for Timber Structures - O Brynildsen
1-1-3	Swedish Code Revision Concerning Timber Structures - B Noren
1-1-4	Working Stresses Report to British Standards Institution Committee BLCP/17/2
6-1-1	On the Application of the Uncertainty Theoretical Methods for the Definition of the Fundamental Concepts of Structural Safety - K Skov and O Ditlevsen
11-1-1	Safety Design of Timber Structures - H J Larsen
18-1-1	Notes on the Development of a UK Limit States Design Code for Timber - A R Fewell and C B Pierce
18-1-2	Eurocode 5, Timber Structures - H J Larsen
19-1-1	Duration of Load Effects and Reliability Based Design (Single Member) - R O Foschi and Z C Yao
21-102-1	Research Activities Towards a New GDR Timber Design Code Based on Limit States Design - W Rug and M Badstube
22-1-1	Reliability-Theoretical Investigation into Timber Components Proposal for a Supplement of the Design Concept - M Badstube, W Rug and R Plessow
23-1-1	Some Remarks about the Safety of Timber Structures - J Kuipers
23-1-2	Reliability of Wood Structural Elements: A Probabilistic Method to Eurocode 5 Calibration - F Rouger, N Lheritier, P Racher and M Fogli
31-1-1	A Limit States Design Approach to Timber Framed Walls - C J Mettem, R Bainbridge and J A Gordon
32 -1-1	Determination of Partial Coefficients and Modification Factors- H J Larsen, S Svensson and S Thelandersson
32 -1-2	Design by Testing of Structural Timber Components - V Enjily and L Whale
33-1-1	Aspects on Reliability Calibration of Safety Factors for Timber Structures – S Svensson and S Thelandersson
33-1-2	Sensitivity studies on the reliability of timber structures – A Ranta-Maunus, M Fonselius, J Kurkela and T Toratti

TIMBER COLUMNS

2-2-1	The Design of Solid Timber Columns - H J Larsen
3-2-1	The Design of Built-Up Timber Columns - H J Larsen
4-2-1	Tests with Centrally Loaded Timber Columns - H J Larsen and S S Pedersen
4-2-2	Lateral-Torsional Buckling of Eccentrically Loaded Timber Columns- B Johansson
5-9-1	Strength of a Wood Column in Combined Compression and Bending with Respect to Creep - B Källsner and B Norén
5-100-1	Design of Solid Timber Columns (First Draft) - H J Larsen
6-100-1	Comments on Document 5-100-1, Design of Solid Timber Columns - H J Larsen and E Theilgaard
6-2-1	Lattice Columns - H J Larsen
6-2-2	A Mathematical Basis for Design Aids for Timber Columns - H J Burgess
6-2-3	Comparison of Larsen and Perry Formulas for Solid Timber Columns- H J Burgess

7-2-1	Lateral Bracing of Timber Struts - J A Simon
8-15-1	Laterally Loaded Timber Columns: Tests and Theory - H J Larsen
17-2-1	Model for Timber Strength under Axial Load and Moment - T Poutanen
18-2-1	Column Design Methods for Timber Engineering - A H Buchanan, K C Johns, B Madsen
19-2-1	Creep Buckling Strength of Timber Beams and Columns - R H Leicester
19-12-2	Strength Model for Glulam Columns - H J Blaß
20-2-1	Lateral Buckling Theory for Rectangular Section Deep Beam-Columns- H J Burgess
20-2-2	Design of Timber Columns - H J Blaß
21-2-1	Format for Buckling Strength - R H Leicester
21-2-2	Beam-Column Formulae for Design Codes - R H Leicester
21-15-1	Rectangular Section Deep Beam - Columns with Continuous Lateral Restraint - H J Burgess
21-15-2	Buckling Modes and Permissible Axial Loads for Continuously Braced Columns - H J Burgess
21-15-3	Simple Approaches for Column Bracing Calculations - H J Burgess
21-15-4	Calculations for Discrete Column Restraints - H J Burgess
22-2-1	Buckling and Reliability Checking of Timber Columns - S Huang, P M Yu and J Y Hong
22-2-2	Proposal for the Design of Compressed Timber Members by Adopting the Second-Order Stress Theory - P Kaiser
30-2-1	Beam-Column Formula for Specific Truss Applications - W Lau, F Lam and J D Barrett
31-2-1	Deformation and Stability of Columns of Viscoelastic Material Wood - P Becker and K Rautenstrauch
34-2-1	Long-Term Experiments with Columns: Results and Possible Consequences on Column Design – W Moorkamp, W Schelling, P Becker, K Rautenstrauch
34-2-2	Proposal for Compressive Member Design Based on Long-Term Simulation Studies – P Becker, K Rautenstrauch
35-2-1	Computer Simulations on the Reliability of Timber Columns Regarding Hygrothermal Effects- R Hartnack, K-U Schober, K Rautenstrauch

SYMBOLS

3-3-1	Symbols for Structural Timber Design - J Kuipers and B Norén
4-3-1	Symbols for Timber Structure Design - J Kuipers and B Norén
28-3-1	Symbols for Timber and Wood-Based Materials - J Kuipers and B Noren
1	Symbols for Use in Structural Timber Design

PLYWOOD

2-4-1	The Presentation of Structural Design Data for Plywood - L G Booth
3-4-1	Standard Methods of Testing for the Determination of Mechanical Properties of Plywood - J Kuipers
3-4-2	Bending Strength and Stiffness of Multiple Species Plywood - C K A Stieda

4-4-4	Standard Methods of Testing for the Determination of Mechanical Properties of Plywood - Council of Forest Industries, B.C.
5-4-1	The Determination of Design Stresses for Plywood in the Revision of CP 112 - L G Booth
5-4-2	Veneer Plywood for Construction - Quality Specifications - ISO/TC 139. Plywood, Working Group 6
6-4-1	The Determination of the Mechanical Properties of Plywood Containing Defects - L G Booth
6-4-2	Comparsion of the Size and Type of Specimen and Type of Test on Plywood Bending Strength and Stiffness - C R Wilson and P Eng
6-4-3	Buckling Strength of Plywood: Results of Tests and Recommendations for Calculations - J Kuipers and H Ploos van Amstel
7-4-1	Methods of Test for the Determination of Mechanical Properties of Plywood - L G Booth, J Kuipers, B Norén, C R Wilson
7-4-2	Comments Received on Paper 7-4-1
7-4-3	The Effect of Rate of Testing Speed on the Ultimate Tensile Stress of Plywood - C R Wilson and A V Parasin
7-4-4	Comparison of the Effect of Specimen Size on the Flexural Properties of Plywood Using the Pure Moment Test - C R Wilson and A V Parasin
8-4-1	Sampling Plywood and the Evaluation of Test Results - B Norén
9-4-1	Shear and Torsional Rigidity of Plywood - H J Larsen
9-4-2	The Evaluation of Test Data on the Strength Properties of Plywood - L G Booth
9-4-3	The Sampling of Plywood and the Derivation of Strength Values (Second Draft) - B Norén
9-4-4	On the Use of the CIB/RILEM Plywood Plate Twisting Test: a progress report - L G Booth
10-4-1	Buckling Strength of Plywood - J Dekker, J Kuipers and H Ploos van Amstel
11-4-1	Analysis of Plywood Stressed Skin Panels with Rigid or Semi-Rigid Connections- I Smith
11-4-2	A Comparison of Plywood Modulus of Rigidity Determined by the ASTM and RILEM CIB/3-TT Test Methods - C R Wilson and A V Parasin
11-4-3	Sampling of Plywood for Testing Strength - B Norén
12-4-1	Procedures for Analysis of Plywood Test Data and Determination of Characteristic Values Suitable for Code Presentation - C R Wilson
14-4-1	An Introduction to Performance Standards for Wood-base Panel Products - D H Brown
14-4-2	Proposal for Presenting Data on the Properties of Structural Panels - T Schmidt
16-4-1	Planar Shear Capacity of Plywood in Bending - C K A Stieda
17-4-1	Determination of Panel Shear Strength and Panel Shear Modulus of Beech-Plywood in Structural Sizes - J Ehlbeck and F Colling
17-4-2	Ultimate Strength of Plywood Webs - R H Leicester and L Pham
20-4-1	Considerations of Reliability - Based Design for Structural Composite Products - M R O'Halloran, J A Johnson, E G Elias and T P Cunningham
21-4-1	Modelling for Prediction of Strength of Veneer Having Knots - Y Hirashima
22-4-1	Scientific Research into Plywood and Plywood Building Constructions the Results and Findings of which are Incorporated into Construction Standard Specifications of the USSR - I M Guskov

22-4-2	Evaluation of Characteristic values for Wood-Based Sheet Materials - E G Elias
24-4-1	APA Structural-Use Design Values: An Update to Panel Design Capacities - A L Kuchar, E G Elias, B Yeh and M R O'Halloran

STRESS GRADING

1-5-1	Quality Specifications for Sawn Timber and Precision Timber - Norwegian Standard NS 3080
1-5-2	Specification for Timber Grades for Structural Use - British Standard BS 4978
4-5-1	Draft Proposal for an International Standard for Stress Grading Coniferous Sawn Softwood - ECE Timber Committee
16-5-1	Grading Errors in Practice - B Thunell
16-5-2	On the Effect of Measurement Errors when Grading Structural Timber- L Nordberg and B Thunell
19-5-1	Stress-Grading by ECE Standards of Italian-Grown Douglas-Fir Dimension Lumber from Young Thinnings - L Uzielli
19-5-2	Structural Softwood from Afforestation Regions in Western Norway - R Lackner
21-5-1	Non-Destructive Test by Frequency of Full Size Timber for Grading - T Nakai
22-5-1	Fundamental Vibration Frequency as a Parameter for Grading Sawn Timber - T Nakai, T Tanaka and H Nagao
24-5-1	Influence of Stress Grading System on Length Effect Factors for Lumber Loaded in Compression - A Campos and I Smith
26-5-1	Structural Properties of French Grown Timber According to Various Grading Methods - F Rouger, C De Lafond and A El Quadrani
28-5-1	Grading Methods for Structural Timber - Principles for Approval - S Ohlsson
28-5-2	Relationship of Moduli of Elasticity in Tension and in Bending of Solid Timber - N Burger and P Glos
29-5-1	The Effect of Edge Knots on the Strength of SPF MSR Lumber - T Courchene, F Lam and J D Barrett
29-5-2	Determination of Moment Configuration Factors using Grading Machine Readings - T D G Canisius and T Isaksson
31-5-1	Influence of Varying Growth Characteristics on Stiffness Grading of Structural Timber - S Ormarsson, H Petersson, O Dahlblom and K Persson
31-5-2	A Comparison of In-Grade Test Procedures - R H Leicester, H Breitinger and H Fordham
32-5-1	Actual Possibilities of the Machine Grading of Timber - K Frühwald and A Bernasconi
32-5-2	Detection of Severe Timber Defects by Machine Grading - A Bernasconi, L Boström and B Schacht
34-5-1	Influence of Proof Loading on the Reliability of Members – F Lam, S Abayakoon, S Svensson, C Gyamfi

STRESSES FOR SOLID TIMBER

4-6-1	Derivation of Grade Stresses for Timber in the UK - W T Curry
5-6-1	Standard Methods of Test for Determining some Physical and Mechanical Properties of Timber in Structural Sizes - W T Curry
5-6-2	The Description of Timber Strength Data - J R Tory
5-6-3	Stresses for EC1 and EC2 Stress Grades - J R Tory

6-6-1	Standard Methods of Test for the Determination of some Physical and Mechanical Properties of Timber in Structural Sizes (third draft) - W T Curry
7-6-1	Strength and Long-term Behaviour of Lumber and Glued Laminated Timber under Torsion Loads - K Möhler
9-6-1	Classification of Structural Timber - H J Larsen
9-6-2	Code Rules for Tension Perpendicular to Grain - H J Larsen
9-6-3	Tension at an Angle to the Grain - K Möhler
9-6-4	Consideration of Combined Stresses for Lumber and Glued Laminated Timber - K Möhler
11-6-1	Evaluation of Lumber Properties in the United States - W L Galligan and J H Haskell
11-6-2	Stresses Perpendicular to Grain - K Möhler
11-6-3	Consideration of Combined Stresses for Lumber and Glued Laminated Timber (addition to Paper CIB-W18/9-6-4) - K Möhler
12-6-1	Strength Classifications for Timber Engineering Codes - R H Leicester and W G Keating
12-6-2	Strength Classes for British Standard BS 5268 - J R Tory
13-6-1	Strength Classes for the CIB Code - J R Tory
13-6-2	Consideration of Size Effects and Longitudinal Shear Strength for Uncracked Beams - R O Foschi and J D Barrett
13-6-3	Consideration of Shear Strength on End-Cracked Beams - J D Barrett and R O Foschi
15-6-1	Characteristic Strength Values for the ECE Standard for Timber - J G Sunley
16-6-1	Size Factors for Timber Bending and Tension Stresses - A R Fewell
16-6-2	Strength Classes for International Codes - A R Fewell and J G Sunley
17-6-1	The Determination of Grade Stresses from Characteristic Stresses for BS 5268: Part 2 - A R Fewell
17-6-2	The Determination of Softwood Strength Properties for Grades, Strength Classes and Laminated Timber for BS 5268: Part 2 - A R Fewell
18-6-1	Comment on Papers: 18-6-2 and 18-6-3 - R H Leicester
18-6-2	Configuration Factors for the Bending Strength of Timber - R H Leicester
18-6-3	Notes on Sampling Factors for Characteristic Values - R H Leicester
18-6-4	Size Effects in Timber Explained by a Modified Weakest Link Theory- B Madsen and A H Buchanan
18-6-5	Placement and Selection of Growth Defects in Test Specimens - H Riberholt
18-6-6	Partial Safety-Coefficients for the Load-Carrying Capacity of Timber Structures - B Norén and J-0 Nylander
19-6-1	Effect of Age and/or Load on Timber Strength - J Kuipers
19-6-2	Confidence in Estimates of Characteristic Values - R H Leicester
19-6-3	Fracture Toughness of Wood - Mode I - K Wright and M Fonselius
19-6-4	Fracture Toughness of Pine - Mode II - K Wright
19-6-5	Drying Stresses in Round Timber - A Ranta-Maunus
19-6-6	A Dynamic Method for Determining Elastic Properties of Wood - R Görlacher
20-6-1	A Comparative Investigation of the Engineering Properties of "Whitewoods" Imported to Israel from Various Origins - U Korin

20-6-2	Effects of Yield Class, Tree Section, Forest and Size on Strength of Home Grown Sitka Spruce - V Picardo
20-6-3	Determination of Shear Strength and Strength Perpendicular to Grain - H J Larsen
21-6-1	Draft Australian Standard: Methods for Evaluation of Strength and Stiffness of Graded Timber - R H Leicester
21-6-2	The Determination of Characteristic Strength Values for Stress Grades of Structural Timber. Part 1 - A R Fewell and P Glos
21-6-3	Shear Strength in Bending of Timber - U Korin
22-6-1	Size Effects and Property Relationships for Canadian 2-inch Dimension Lumber - J D Barrett and H Griffin
22-6-2	Moisture Content Adjustements for In-Grade Data - J D Barrett and W Lau
22-6-3	A Discussion of Lumber Property Relationships in Eurocode 5 - D W Green and D E Kretschmann
22-6-4	Effect of Wood Preservatives on the Strength Properties of Wood - F Ronai
23-6-1	Timber in Compression Perpendicular to Grain - U Korin
24-6-1	Discussion of the Failure Criterion for Combined Bending and Compression - T A C M van der Put
24-6-3	Effect of Within Member Variability on Bending Strength of Structural Timber - I Czmoch, S Thelandersson and H J Larsen
24-6-4	Protection of Structural Timber Against Fungal Attack Requirements and Testing- K Jaworska, M Rylko and W Nozynski
24-6-5	Derivation of the Characteristic Bending Strength of Solid Timber According to CEN-Document prEN 384 - A J M Leijten
25-6-1	Moment Configuration Factors for Simple Beams- T D G Canisius
25-6-3	Bearing Capacity of Timber - U Korin
25-6-4	On Design Criteria for Tension Perpendicular to Grain - H Petersson
25-6-5	Size Effects in Visually Graded Softwood Structural Lumber - J D Barrett, F Lam and W Lau
26-6-1	Discussion and Proposal of a General Failure Criterion for Wood - T A C M van der Put
27-6-1	Development of the "Critical Bearing": Design Clause in CSA-086.1 - C Lum and E Karacabeyli
27-6-2	Size Effects in Timber: Novelty Never Ends - F Rouger and T Fewell
27-6-3	Comparison of Full-Size Sugi (Cryptomeria japonica D.Don) Structural Performance in Bending of Round Timber, Two Surfaces Sawn Timber and Square Sawn Timber - T Nakai, H Nagao and T Tanaka
28-6-1	Shear Strength of Canadian Softwood Structural Lumber - F Lam, H Yee and J D Barrett
28-6-2	Shear Strength of Douglas Fir Timbers - B Madsen
28-6-3	On the Influence of the Loading Head Profiles on Determined Bending Strength - L Muszyñsky and R Szukala
28-6-4	Effect of Test Standard, Length and Load Configuration on Bending Strength of Structural Timber- T Isaksson and S Thelandersson
28-6-5	Grading Machine Readings and their Use in the Calculation of Moment Configuration Factors - T Canisius, T Isaksson and S Thelandersson
28-6-6	End Conditions for Tension Testing of Solid Timber Perpendicular to Grain - T Canisius

29-6-1	Effect of Size on Tensile Strength of Timber - N Burger and P Glos
29-6-2	Equivalence of In-Grade Testing Standards - R H Leicester, H O Breitinger and H F Fordham
30-6-1	Strength Relationships in Structural Timber Subjected to Bending and Tension - N Burger and P Glos
30-6-2	Characteristic Design Stresses in Tension for Radiata Pine Grown in Canterbury - A Tsehaye, J C F Walker and A H Buchanan
30-6-3	Timber as a Natural Composite: Explanation of Some Peculiarities in the Mechanical Behaviour - E Gehri
31-6-1	Length and Moment Configuration Factors - T Isaksson
31-6-2	Tensile Strength Perpendicular to Grain According to EN 1193 - H J Blaß and M Schmid
31-6-3	Strength of Small Diameter Round Timber - A Ranta-Maunus, U Saarelainen and H Boren
31-6-4	Compression Strength Perpendicular to Grain of Structural Timber and Glulam - L Damkilde, P Hoffmeyer and T N Pedersen
31-6-5	Bearing Strength of Timber Beams - R H Leicester, H Fordham and H Breitinger
32-6-1	Development of High-Resistance Glued Robinia Products and an Attempt to Assign Such Products to the European System of Strength Classes - G Schickhofer and B Obermayr
32-6-2	Length and Load Configuration Effects in the Code Format - T Isaksson
32-6-3	Length Effect on the Tensile Strength of Truss Chord Members - F Lam
32-6-4	Tensile Strength Perpendicular to Grain of Glued Laminated Timber - H J Blaß and M Schmid
32-6-5	On the Reliability-based Strength Adjustment Factors for Timber Design - T D G Canisius
34-6-1	Material Strength Properties for Canadian Species Used in Japanese Post and Beam Construction - J D Barrett, F Lam, S Nakajima
35-6-1	Evaluation of Different Size Effect Models for Tension Perpendicular to Grain Design - S Aicher, G Dill-Langer
35-6-2	Tensile Strength of Glulam Perpendicular to Grain - Effects of Moisture Gradients - J Jönsson, S Thelandersson

TIMBER JOINTS AND FASTENERS

1-7-1	Mechanical Fasteners and Fastenings in Timber Structures - E G Stern
4-7-1	Proposal for a Basic Test Method for the Evaluation of Structural Timber Joints with Mechanical Fasteners and Connectors - RILEM 3TT Committee
4-7-2	Test Methods for Wood Fasteners - K Möhler
5-7-1	Influence of Loading Procedure on Strength and Slip-Behaviour in Testing Timber Joints - K Möhler
5-7-2	Recommendations for Testing Methods for Joints with Mechanical Fasteners and Connectors in Load-Bearing Timber Structures - RILEM 3 TT Committee
5-7-3	CIB-Recommendations for the Evaluation of Results of Tests on Joints with Mechanical Fasteners and Connectors used in Load-Bearing Timber Structures - J Kuipers
6-7-1	Recommendations for Testing Methods for Joints with Mechanical Fasteners and Connectors in Load-Bearing Timber Structures (seventh draft) - RILEM 3 TT Committee
6-7-2	Proposal for Testing Integral Nail Plates as Timber Joints - K Möhler

6-7-3	Rules for Evaluation of Values of Strength and Deformation from Test Results - Mechanical Timber Joints - M Johansen, J Kuipers, B Norén
6-7-4	Comments to Rules for Testing Timber Joints and Derivation of Characteristic Values for Rigidity and Strength - B Norén
7-7-1	Testing of Integral Nail Plates as Timber Joints - K Möhler
7-7-2	Long Duration Tests on Timber Joints - J Kuipers
7-7-3	Tests with Mechanically Jointed Beams with a Varying Spacing of Fasteners - K Möhler
7-100-1	CIB-Timber Code Chapter 5.3 Mechanical Fasteners;CIB-Timber Standard 06 and 07 - H J Larsen
9-7-1	Design of Truss Plate Joints - F J Keenan
9-7-2	Staples - K Möhler
11-7-1	A Draft Proposal for International Standard: ISO Document ISO/TC 165N 38E
12-7-1	Load-Carrying Capacity and Deformation Characteristics of Nailed Joints - J Ehlbeck
12-7-2	Design of Bolted Joints - H J Larsen
12-7-3	Design of Joints with Nail Plates - B Norén
13-7-1	Polish Standard BN-80/7159-04: Parts 00-01-02-03-04-05. "Structures from Wood and Wood-based Materials. Methods of Test and Strength Criteria for Joints with Mechanical Fasteners"
13-7-2	Investigation of the Effect of Number of Nails in a Joint on its Load Carrying Ability - W Nozynski
13-7-3	International Acceptance of Manufacture, Marking and Control of Finger-jointed Structural Timber - B Norén
13-7-4	Design of Joints with Nail Plates - Calculation of Slip - B Norén
13-7-5	Design of Joints with Nail Plates - The Heel Joint - B Källsner
13-7-6	Nail Deflection Data for Design - H J Burgess
13-7-7	Test on Bolted Joints - P Vermeyden
13-7-8	Comments to paper CIB-W18/12-7-3 "Design of Joints with Nail Plates"- B Norén
13-7-9	Strength of Finger Joints - H J Larsen
13-100-4	CIB Structural Timber Design Code. Proposal for Section 6.1.5 Nail Plates - N I Bovim
14-7-1	Design of Joints with Nail Plates (second edition) - B Norén
14-7-2	Method of Testing Nails in Wood (second draft, August 1980) - B Norén
14-7-3	Load-Slip Relationship of Nailed Joints - J Ehlbeck and H J Larsen
14-7-4	Wood Failure in Joints with Nail Plates - B Norén
14-7-5	The Effect of Support Eccentricity on the Design of W- and WW-Trussed with Nail Plate Connectors - B Källsner
14-7-6	Derivation of the Allowable Load in Case of Nail Plate Joints Perpendicular to Grain - K Möhler
14-7-7	Comments on CIB-W18/14-7-1 - T A C M van der Put
15-7-1	Final Recommendation TT-1A: Testing Methods for Joints with Mechanical Fasteners in Load-Bearing Timber Structures. Annex A Punched Metal Plate Fasteners - Joint Committee RILEM/CIB-3TT

16-7-1	Load Carrying Capacity of Dowels - E Gehri
16-7-2	Bolted Timber Joints: A Literature Survey - N Harding
16-7-3	Bolted Timber Joints: Practical Aspects of Construction and Design; a Survey - N Harding
16-7-4	Bolted Timber Joints: Draft Experimental Work Plan - Building Research Association of New Zealand
17-7-1	Mechanical Properties of Nails and their Influence on Mechanical Properties of Nailed Timber Joints Subjected to Lateral Loads - I Smith, L R J Whale, C Anderson and L Held
17-7-2	Notes on the Effective Number of Dowels and Nails in Timber Joints - G Steck
18-7-1	Model Specification for Driven Fasteners for Assembly of Pallets and Related Structures - E G Stern and W B Wallin
18-7-2	The Influence of the Orientation of Mechanical Joints on their Mechanical Properties - I Smith and L R J Whale
18-7-3	Influence of Number of Rows of Fasteners or Connectors upon the Ultimate Capacity of Axially Loaded Timber Joints - I Smith and G Steck
18-7-4	A Detailed Testing Method for Nailplate Joints - J Kangas
18-7-5	Principles for Design Values of Nailplates in Finland - J Kangas
18-7-6	The Strength of Nailplates - N I Bovim and E Aasheim
19-7-1	Behaviour of Nailed and Bolted Joints under Short-Term Lateral Load - Conclusions from Some Recent Research - L R J Whale, I Smith and B O Hilson
19-7-2	Glued Bolts in Glulam - H Riberholt
19-7-3	Effectiveness of Multiple Fastener Joints According to National Codes and Eurocode 5 (Draft) - G Steck
19-7-4	The Prediction of the Long-Term Load Carrying Capacity of Joints in Wood Structures - Y M Ivanov and Y Y Slavic
19-7-5	Slip in Joints under Long-Term Loading - T Feldborg and M Johansen
19-7-6	The Derivation of Design Clauses for Nailed and Bolted Joints in Eurocode 5 - L R J Whale and I Smith
19-7-7	Design of Joints with Nail Plates - Principles - B Norén
19-7-8	Shear Tests for Nail Plates - B Norén
19-7-9	Advances in Technology of Joints for Laminated Timber - Analyses of the Structural Behaviour - M Piazza and G Turrini
19-15-1	Connections Deformability in Timber Structures: A Theoretical Evaluation of its Influence on Seismic Effects - A Ceccotti and A Vignoli
20-7-1	Design of Nailed and Bolted Joints-Proposals for the Revision of Existing Formulae in Draft Eurocode 5 and the CIB Code - L R J Whale, I Smith and H J Larsen
20-7-2	Slip in Joints under Long Term Loading - T Feldborg and M Johansen
20-7-3	Ultimate Properties of Bolted Joints in Glued-Laminated Timber - M Yasumura, T Murota and H Sakai
20-7-4	Modelling the Load-Deformation Behaviour of Connections with Pin-Type Fasteners under Combined Moment, Thrust and Shear Forces - I Smith
21-7-1	Nails under Long-Term Withdrawal Loading - T Feldborg and M Johansen
21-7-2	Glued Bolts in Glulam-Proposals for CIB Code - H Riberholt
21-7-3	Nail Plate Joint Behaviour under Shear Loading - T Poutanen

21-7-4	Design of Joints with Laterally Loaded Dowels. Proposals for Improving the Design Rules in the CIB Code and the Draft Eurocode 5 - J Ehlbeck and H Werner
21-7-5	Axially Loaded Nails: Proposals for a Supplement to the CIB Code - J Ehlbeck and W Siebert
22-7-1	End Grain Connections with Laterally Loaded Steel Bolts A draft proposal for design rules in the CIB Code - J Ehlbeck and M Gerold
22-7-2	Determination of Perpendicular-to-Grain Tensile Stresses in Joints with Dowel-Type Fasteners - A draft proposal for design rules - J Ehlbeck, R Görlacher and H Werner
22-7-3	Design of Double-Shear Joints with Non-Metallic Dowels A proposal for a supplement of the design concept - J Ehlbeck and O Eberhart
22-7-4	The Effect of Load on Strength of Timber Joints at high Working Load Level - A J M Leijten
22-7-5	Plasticity Requirements for Portal Frame Corners - R Gunnewijk and A J M Leijten
22-7-6	Background Information on Design of Glulam Rivet Connections in CSA/CAN3-086.1-M89 - A proposal for a supplement of the design concept - E Karacabeyli and D P Janssens
22-7-7	Mechanical Properties of Joints in Glued-Laminated Beams under Reversed Cyclic Loading - M Yasumura
22-7-8	Strength of Glued Lap Timber Joints - P Glos and H Horstmann
22-7-9	Toothed Rings Type Bistyp 075 at the Joints of Fir Wood - J Kerste
22-7-10	Calculation of Joints and Fastenings as Compared with the International State - K Zimmer and K Lissner
22-7-11	Joints on Glued-in Steel Bars Present Relatively New and Progressive Solution in Terms of Timber Structure Design - G N Zubarev, F A Boitemirov and V M Golovina
22-7-12	The Development of Design Codes for Timber Structures made of Compositive Bars with Plate Joints based on Cyclindrical Nails - Y V Piskunov
22-7-13	Designing of Glued Wood Structures Joints on Glued-in Bars - S B Turkovsky
23-7-1	Proposal for a Design Code for Nail Plates - E Aasheim and K H Solli
23-7-2	Load Distribution in Nailed Joints - H J Blass
24-7-1	Theoretical and Experimental Tension and Shear Capacity of Nail Plate Connections - B Källsner and J Kangas
24-7-2	Testing Method and Determination of Basic Working Loads for Timber Joints with Mechanical Fasteners - Y Hirashima and F Kamiya
24-7-3	Anchorage Capacity of Nail Plate - J Kangas
25-7-2	Softwood and Hardwood Embedding Strength for Dowel type Fasteners - J Ehlbeck and H Werner
25-7-4	A Guide for Application of Quality Indexes for Driven Fasteners Used in Connections in Wood Structures - E G Stern
25-7-5	35 Years of Experience with Certain Types of Connectors and Connector Plates Used for the Assembly of Wood Structures and their Components- E G Stern
25-7-6	Characteristic Strength of Split-ring and Shear-plate Connections - H J Blass, J Ehlbeck and M Schlager
25-7-7	Characteristic Strength of Tooth-plate Connector Joints - H J Blass, J Ehlbeck and M Schlager

25-7-8	Extending Yield Theory to Screw Connections - T E McLain
25-7-9	Determination of k_{def} for Nailed Joints - J W G van de Kuilen
25-7-10	Characteristic Strength of UK Timber Connectors - A V Page and C J Mettem
25-7-11	Multiple-fastener Dowel-type Joints, a Selected Review of Research and Codes - C J Mettem and A V Page
25-7-12	Load Distributions in Multiple-fastener Bolted Joints in European Whitewood Glulam, with Steel Side Plates - C J Mettem and A V Page
26-7-1	Proposed Test Method for Dynamic Properties of Connections Assembled with Mechanical Fasteners - J D Dolan
26-7-2	Validatory Tests and Proposed Design Formulae for the Load-Carrying Capacity of Toothed-Plate Connectored Joints - C J Mettem, A V Page and G Davis
26-7-3	Definitions of Terms and Multi-Language Terminology Pertaining to Metal Connector Plates - E G Stern
26-7-4	Design of Joints Based on in V-Shape Glued-in Rods - J Kangas
26-7-5	Tests on Timber Concrete Composite Structural Elements (TCCs) - A U Meierhofer
27-7-1	Glulam Arch Bridge and Design of it's Moment-Resisting Joints - K Komatsu and S Usuku
27-7-2	Characteristic Load - Carrying Capacity of Joints with Dowel - type Fasteners in Regard to the System Properties - H Werner
27-7-3	Steel Failure Design in Truss Plate Joints - T Poutanen
28-7-1	Expanded Tube Joint in Locally DP Reinforced Timber - A J M Leijten, P Ragupathy and K S Virdi
28-7-2	A Strength and Stiffness Model for the Expanded Tube Joint - A J M Leijten
28-7-3	Load-carrying Capacity of Steel-to Timber Joints with Annular Ring Shanked Nails. A Comparison with the EC5 Design Method - R Görlacher
28-7-4	Dynamic Effects on Metal-Plate Connected Wood Truss Joints - S Kent, R Gupta and T Miller
28-7-5	Failure of the Timber Bolted Joints Subjected to Lateral Load Perpendicular to Grain - M Yasumura and L Daudeville
28-7-6	Design Procedure for Locally Reinforced Joints with Dowel-type Fasteners - H Werner
28-7-7	Variability and Effects of Moisture Content on the Withdrawal Characteristics for Lumber as Opposed to Clear Wood - J D Dolan and J W Stelmokas
28-7-8	Nail Plate Capacity in Joint Line - A Kevarinmäki and J Kangas
28-7-9	Axial Strength of Glued-In Bolts - Calculation Model Based on Non-Linear Fracture Mechanics - A Preliminary Study - C J Johansson, E Serrano, P J Gustafsson and B Enquist
28-7-10	Cyclic Lateral Dowel Connection Tests for seismic and Wind Evaluation - J D Dolan
29-7-1	A Simple Method for Lateral Load-Carrying Capacity of Dowel-Type Fasteners - J Kangas and J Kurkela
29-7-2	Nail Plate Joint Behaviour at Low Versus High Load Level - T Poutanen
29-7-3	The Moment Resistance of Tee and Butt - Joint Nail Plate Test Specimens - A Comparison with Current Design Methods - A Reffold, L R J Whale and B S Choo

29-7-4	A Critical Review of the Moment Rotation Test Method Proposed in prEN 1075 - M Bettison, B S Choo and L R J Whale
29-7-5	Explanation of the Translation and Rotation Behaviour of Prestressed Moment Timber Joints - A J M Leijten
29-7-6	Design of Joints and Frame Corners using Dowel-Type Fasteners - E Gehri
29-7-7	Quasi-Static Reversed-Cyclic Testing of Nailed Joints - E Karacabeyli and A Ceccotti
29-7-8	Failure of Bolted Joints Loaded Parallel to the Grain: Experiment and Simulation - L Davenne, L Daudeville and M Yasumura
30-7-1	Flexural Behaviour of GLT Beams End-Jointed by Glued-in Hardwood Dowels - K Komatsu, A Koizumi, J Jensen, T Sasaki and Y Iijima
30-7-2	Modelling of the Block Tearing Failure in Nailed Steel-to-Timber Joints - J Kangas, K Aalto and A Kevarinmäki
30-7-3	Cyclic Testing of Joints with Dowels and Slotted-in Steel Plates - E Aasheim
30-7-4	A Steel-to-Timber Dowelled Joint of High Performance in Combination with a High Strength Wood Composite (Parallam) - E Gehri
30-7-5	Multiple Fastener Timber Connections with Dowel Type Fasteners - A Jorissen
30-7-6	Influence of Ductility on Load-Carrying Capacity of Joints with Dowel-Type Fasteners - A Mischler
31-7-1	Mechanical Properties of Dowel Type Joints under Reversed Cyclic Lateral Loading - M Yasumura
31-7-2	Design of Joints with Laterally Loaded Dowels - A Mischler
31-7-3	Flexural Behaviour of Glulam Beams Edge-Jointed by Lagscrews with Steel Splice Plates - K Komatsu
31-7-4	Design on Timber Capacity in Nailed Steel-to-Timber Joints - J Kangas and J Vesa
31-7-5	Timber Contact in Chord Splices of Nail Plate Structures - A Kevarinmäki
31-7-6	The Fastener Yield Strength in Bending - A Jorissen and H J Blaß
31-7-7	A Proposal for Simplification of Johansen`s Formulae, Dealing With the Design of Dowelled-Type Fasteners - F Rouger
31-7-8	Simplified Design of Connections with Dowel-type fasteners - H J Blaß and J Ehlbeck
32-7-1	Behaviour of Wood-Steel-Wood Bolted Glulam Connections - M Mohammad and J H P Quenneville
32-7-2	A new set of experimental tests on beams loaded perpendicular-to-grain by dowel-type joints- M Ballerini
32-7-3	Design and Analysis of Bolted Timber Joints under Lateral Force Perpendicular to Grain - M Yasumura and L Daudeville
32-7-4	Predicting Capacities of Joints with Laterally Loaded Nails - I Smith and P Quenneville
32-7-5	Strength Reduction Rules for Multiple Fastener Joints - A Mischler and E Gehri
32-7-6	The Stiffness of Multiple Bolted Connections - A Jorissen
32-7-7	Concentric Loading Tests on Girder Truss Components - T N Reynolds, A Reffold, V Enjily and L Whale
32-7-8	Dowel Type Connections with Slotted-In Steel Plates - M U Pedersen, C O Clorius, L Damkilde, P Hoffmeyer and L Esklidsen
32-7-9	Creep of Nail Plate Reinforced Bolt Joints - J Vesa and A Kevarinmäki

32-7-10	The Behaviour of Timber Joints with Ring Connectors - E Gehri and A Mischler
32-7-11	Non-Metallic, Adhesiveless Joints for Timber Structures - R D Drake, M P Ansell, C J Mettem and R Bainbridge
32-7-12	Effect of Spacing and Edge Distance on the Axial Strength of Glued-in Rods - H J Blaß and B Laskewitz
32-7-13	Evaluation of Material Combinations for Bonded in Rods to Achieve Improved Timber Connections - C J Mettem, R J Bainbridge, K Harvey, M P Ansell, J G Broughton and A R Hutchinson
33-7-1	Determination of Yield Strength and Ultimate Strength of Dowel-Type Timber Joints – M Yasumura and K Sawata
33-7-2	Lateral Shear Capacity of Nailed Joints – U Korin
33-7-3	Height-Adjustable Connector for Composite Beams – Y V Piskunov and E G Stern
33-7-4	Engineering Ductility Assessment for a Nailed Slotted-In Steel Connection in Glulam– L Stehn and H Johansson
33-7-5	Effective Bending Capacity of Dowel-Type Fasteners - H J Blaß, A Bienhaus and V Krämer
33-7-6	Load-Carrying Capacity of Joints with Dowel-Type Fasteners and Interlayers - H J Blaß and B Laskewitz
33-7-7	Evaluation of Perpendicular to Grain Failure of Beams caused by Concentrated Loads of Joints – A J M Leijten and T A C M van der Put
33-7-8	Test Methods for Glued-In Rods for Timber Structures – C Bengtsson and C J Johansson
33-7-9	Stiffness Analysis of Nail Plates – P Ellegaard
33-7-10	Capacity, Fire Resistance and Gluing Pattern of the Rods in V-Connections – J Kangas
33-7-11	Bonded-In Pultrusions for Moment-Resisting Timber Connections – K Harvey, M P Ansell, C J Mettem, R J Bainbridge and N Alexandre
33-7-12	Fatigue Performance of Bonded-In Rods in Glulam, Using Three Adhesive Types - R J Bainbridge, K Harvey, C J Mettem and M P Ansell
34-7-1	Splitting Strength of Beams Loaded by Connections Perpendicular to Grain, Model Validation – A J M Leijten, A Jorissen
34-7-2	Numerical LEFM analyses for the evaluation of failure loads of beams loaded perpendicular-to-grain by single-dowel connections – M Ballerini, R Bezzi
34-7-3	Dowel joints loaded perpendicular to grain - H J Larsen, P J Gustafsson
34-7-4	Quality Control of Connections based on in V-shape glued-in Steel Rods – J Kangas, A Kevarinmäki
34-7-5	Testing Connector Types for Laminated-Timber-Concrete Composite Elements – M Grosse, S Lehmann, K Rautenstrauch
34-7-6	Behaviour of Axially Loaded Glued-in Rods - Requirements and Resistance, Especially for Spruce Timber Perpendicular to the Grain Direction – A Bernasconi
34-7-7	Embedding characteristics on fibre reinforcement and densified timber joints - P Haller, J Wehsener, T Birk
34-7-8	GIROD – Glued-in Rods for Timber Structures – C Bengtsson, C-J Johansson
34-7-9	Criteria for Damage and Failure of Dowel-Type Joints Subjected to Force Perpendicular to the Grain – M Yasumura
34-7-10	Interaction Between Splitting and Block Shear Failure of Joints – A J M Leijten, A Jorissen, J Kuipers
34-7-11	Limit states design of dowel-fastener joints – Placement of modification factors and partial factors, and calculation of variability in resistance – I Smith, G Foliente

34-7-12	Design and Modelling of Knee Joints - J Nielsen, P Ellegaard
34-7-13	Timber-Steel Shot Fired Nail Connections at Ultimate Limit States - R J Bainbridge, P Larsen, C J Mettem, P Alam, M P Ansell
35-7-1	New Estimating Method of Bolted Cross-lapped Joints with Timber Side Members - M Noguchi, K Komatsu
35-7-2	Analysis on Multiple Lag Screwed Timber Joints with Timber Side Members - K Komatsu, S Takino, M Nakatani, H Tateishi
35-7-3	Joints with Inclined Screws - A Kevarinmäki
35-7-4	Joints with Inclined Screws - I Bejtka, H J Blaß
35-7-5	Effect of distances, Spacing and Number of Dowels in a Row an the Load Carrying Capacity of Connections with Dowels failing by Splitting - M Schmid, R Frasson, H J Blaß
35-7 6	Effect of Row Spacing on the Capacity of Bolted Timber Connections Loaded Perpendicular-to-grain - P Quenneville, M Kasim
35-7-7	Splitting Strength of Beams Loaded by Connections, Model Comparison - A J M Leijten
35-7-8	Load-Carrying Capacity of Perpendicular to the Grain Loaded Timber Joints with Multiple Fasteners - O Borth, K U Schober, K Rautenstrauch
35-7-9	Determination of fracture parameter for dowel-type joints loaded perpendicular to wooden grain and its application - M Yasumura
35-7-10	Analysis and Design of Modified Attic Trusses with Punched Metal Plate Fasteners - P Ellegaard
35-7-11	Joint Properties of Plybamboo Sheets in Prefabricated Housing - G E Gonzalez
35-7-12	Fiber-Reinforced Beam-to-Column Connections for Seismic Applications - B Kasal, A Heiduschke, P Haller

LOAD SHARING

3-8-1	Load Sharing - An Investigation on the State of Research and Development of Design Criteria - E Levin
4-8-1	A Review of Load-Sharing in Theory and Practice - E Levin
4-8-2	Load Sharing - B Norén
19-8-1	Predicting the Natural Frequencies of Light-Weight Wooden Floors - I Smith and Y H Chui
20-8-1	Proposed Code Requirements for Vibrational Serviceability of Timber Floors - Y H Chui and I Smith
21-8-1	An Addendum to Paper 20-8-1 - Proposed Code Requirements for Vibrational Serviceability of Timber Floors - Y H Chui and I Smith
21-8-2	Floor Vibrational Serviceability and the CIB Model Code - S Ohlsson
22-8-1	Reliability Analysis of Viscoelastic Floors - F Rouger, J D Barrett and R O Foschi
24-8-1	On the Possibility of Applying Neutral Vibrational Serviceability Criteria to Joisted Wood Floors - I Smith and Y H Chui
25-8-1	Analysis of Glulam Semi-rigid Portal Frames under Long-term Load - K Komatsu and N Kawamoto
34-8-1	System Effect in Sheathed Parallel Timber Beam Structures – M Hansson, T Isaksson
35-8-1	System Effects in Sheathed Parallel Timber Beam Structures part II. - M Hansson, T Isaksson

DURATION OF LOAD

3-9-1	Definitions of Long Term Loading for the Code of Practice - B Norén
4-9-1	Long Term Loading of Trussed Rafters with Different Connection Systems - T Feldborg and M Johansen
5-9-1	Strength of a Wood Column in Combined Compression and Bending with Respect to Creep - B Källsner and B Norén
6-9-1	Long Term Loading for the Code of Practice (Part 2) - B Norén
6-9-2	Long Term Loading - K Möhler
6-9-3	Deflection of Trussed Rafters under Alternating Loading during a Year - T Feldborg and M Johansen
7-6-1	Strength and Long Term Behaviour of Lumber and Glued-Laminated Timber under Torsion Loads - K Möhler
7-9-1	Code Rules Concerning Strength and Loading Time - H J Larsen and E Theilgaard
17-9-1	On the Long-Term Carrying Capacity of Wood Structures - Y M Ivanov and Y Y Slavic
18-9-1	Prediction of Creep Deformations of Joints - J Kuipers
19-9-1	Another Look at Three Duration of Load Models - R O Foschi and Z C Yao
19-9-2	Duration of Load Effects for Spruce Timber with Special Reference to Moisture Influence - A Status Report - P Hoffmeyer
19-9-3	A Model of Deformation and Damage Processes Based on the Reaction Kinetics of Bond Exchange - T A C M van der Put
19-9-4	Non-Linear Creep Superposition - U Korin
19-9-5	Determination of Creep Data for the Component Parts of Stressed-Skin Panels - R Kliger
19-9-6	Creep an Lifetime of Timber Loaded in Tension and Compression - P Glos
19-1-1	Duration of Load Effects and Reliability Based Design (Single Member) - R O Foschi and Z C Yao
19-6-1	Effect of Age and/or Load on Timber Strength - J Kuipers
19-7-4	The Prediction of the Long-Term Load Carrying Capacity of Joints in Wood Structures - Y M Ivanov and Y Y Slavic
19-7-5	Slip in Joints under Long-Term Loading - T Feldborg and M Johansen
20-7-2	Slip in Joints under Long-Term Loading - T Feldborg and M Johansen
22-9-1	Long-Term Tests with Glued Laminated Timber Girders - M Badstube, W Rug and W Schöne
22-9-2	Strength of One-Layer solid and Lengthways Glued Elements of Wood Structures and its Alteration from Sustained Load - L M Kovaltchuk, I N Boitemirova and G B Uspenskaya
24-9-1	Long Term Bending Creep of Wood - T Toratti
24-9-2	Collection of Creep Data of Timber - A Ranta-Maunus
24-9-3	Deformation Modification Factors for Calculating Built-up Wood-Based Structures - I R Kliger
25-9-2	DVM Analysis of Wood. Lifetime, Residual Strength and Quality - L F Nielsen
26-9-1	Long Term Deformations in Wood Based Panels under Natural Climate Conditions. A Comparative Study - S Thelandersson, J Nordh, T Nordh and S Sandahl

28-9-1	Evaluation of Creep Behavior of Structural Lumber in Natural Environment - R Gupta and R Shen
30-9-1	DOL Effect in Tension Perpendicular to the Grain of Glulam Depending on Service Classes and Volume - S Aicher and G Dill-Langer
30-9-2	Damage Modelling of Glulam in Tension Perpendicular to Grain in Variable Climate - G Dill-Langer and S Aicher
31-9-1	Duration of Load Effect in Tension Perpendicular to Grain in Curved Glulam - A Ranta-Maunus
32-9-1	Bending-Stress-Redistribution Caused by Different Creep in Tension and Compression and Resulting DOL-Effect - P Becker and K Rautenstrauch
32-9-2	The Long Term Performance of Ply-Web Beams - R Grantham and V Enjily

TIMBER BEAMS

4-10-1	The Design of Simple Beams - H J Burgess
4-10-2	Calculation of Timber Beams Subjected to Bending and Normal Force - H J Larsen
5-10-1	The Design of Timber Beams - H J Larsen
9-10-1	The Distribution of Shear Stresses in Timber Beams - F J Keenan
9-10-2	Beams Notched at the Ends - K Möhler
11-10-1	Tapered Timber Beams - H Riberholt
13-6-2	Consideration of Size Effects in Longitudinal Shear Strength for Uncracked Beams - R O Foschi and J D Barrett
13-6-3	Consideration of Shear Strength on End-Cracked Beams - J D Barrett and R O Foschi
18-10-1	Submission to the CIB-W18 Committee on the Design of Ply Web Beams by Consideration of the Type of Stress in the Flanges - J A Baird
18-10-2	Longitudinal Shear Design of Glued Laminated Beams - R O Foschi
19-10-1	Possible Code Approaches to Lateral Buckling in Beams - H J Burgess
19-2-1	Creep Buckling Strength of Timber Beams and Columns - R H Leicester
20-2-1	Lateral Buckling Theory for Rectangular Section Deep Beam-Columns - H J Burgess
20-10-1	Draft Clause for CIB Code for Beams with Initial Imperfections - H J Burgess
20-10-2	Space Joists in Irish Timber - W J Robinson
20-10-3	Composite Structure of Timber Joists and Concrete Slab - T Poutanen
21-10-1	A Study of Strength of Notched Beams - P J Gustafsson
22-10-1	Design of Endnotched Beams - H J Larsen and P J Gustafsson
22-10-2	Dimensions of Wooden Flexural Members under Constant Loads - A Pozgai
22-10-3	Thin-Walled Wood-Based Flanges in Composite Beams - J König
22-10-4	The Calculation of Wooden Bars with flexible Joints in Accordance with the Polish Standart Code and Strict Theoretical Methods - Z Mielczarek
23-10-1	Tension Perpendicular to the Grain at Notches and Joints - T A C M van der Put
23-10-2	Dimensioning of Beams with Cracks, Notches and Holes. An Application of Fracture Mechanics - K Riipola
23-10-3	Size Factors for the Bending and Tension Strength of Structural Timber - J D Barret and A R Fewell

23-12-1	Bending Strength of Glulam Beams, a Design Proposal - J Ehlbeck and F Colling
23-12-3	Glulam Beams, Bending Strength in Relation to the Bending Strength of the Finger Joints - H Riberholt
24-10-1	Shear Strength of Continuous Beams - R H Leicester and F G Young
25-10-1	The Strength of Norwegian Glued Laminated Beams - K Solli, E Aasheim and R H Falk
25-10-2	The Influence of the Elastic Modulus on the Simulated Bending Strength of Hyperstatic Timber Beams - T D G Canisius
27-10-1	Determination of Shear Modulus - R Görlacher and J Kürth
29-10-1	Time Dependent Lateral Buckling of Timber Beams - F Rouger
29-10-2	Determination of Modulus of Elasticity in Bending According to EN 408 - K H Solli
29-10-3	On Determination of Modulus of Elasticity in Bending - L Boström, S Ormarsson and O Dahlblom
29-10-4	Relation of Moduli of Elasticity in Flatwise and Edgewise Bending of Solid Timber - C J Johansson, A Steffen and E W Wormuth
30-10-1	Nondestructive Evaluation of Wood-based Members and Structures with the Help of Modal Analysis - P Kuklik
30-10-2	Measurement of Modulus of Elasticity in Bending - L Boström
30-10-3	A Weak Zone Model for Timber in Bending - B Källsner, K Salmela and O Ditlevsen
30-10-4	Load Carrying Capacity of Timber Beams with Narrow Moment Peaks - T Isaksson and J Freysoldt

ENVIRONMENTAL CONDITIONS

5-11-1	Climate Grading for the Code of Practice - B Norén
6-11-1	Climate Grading (2) - B Norén
9-11-1	Climate Classes for Timber Design - F J Keenan
19-11-1	Experimental Analysis on Ancient Downgraded Timber Structures - B Leggeri and L Paolini
19-6-5	Drying Stresses in Round Timber - A Ranta-Maunus
22-11-1	Corrosion and Adaptation Factors for Chemically Aggressive Media with Timber Structures - K Erler
29-11-1	Load Duration Effect on Structural Beams under Varying Climate Influence of Size and Shape - P Galimard and P Morlier
30-11-1	Probabilistic Design Models for the Durability of Timber Constructions - R H Leicester

LAMINATED MEMBERS

6-12-1	Directives for the Fabrication of Load-Bearing Structures of Glued Timber - A van der Velden and J Kuipers
8-12-1	Testing of Big Glulam Timber Beams - H Kolb and P Frech
8-12-2	Instruction for the Reinforcement of Apertures in Glulam Beams - H Kolb and P Frech
8-12-3	Glulam Standard Part 1: Glued Timber Structures; Requirements for Timber (Second Draft)

9-12-1	Experiments to Provide for Elevated Forces at the Supports of Wooden Beams with Particular Regard to Shearing Stresses and Long-Term Loadings - F Wassipaul and R Lackner
9-12-2	Two Laminated Timber Arch Railway Bridges Built in Perth in 1849 - L G Booth
9-6-4	Consideration of Combined Stresses for Lumber and Glued Laminated Timber - K Möhler
11-6-3	Consideration of Combined Stresses for Lumber and Glued Laminated Timber (addition to Paper CIB-W18/9-6-4) - K Möhler
12-12-1	Glulam Standard Part 2: Glued Timber Structures; Rating (3rd draft)
12-12-2	Glulam Standard Part 3: Glued Timber Structures; Performance (3 rd draft)
13-12-1	Glulam Standard Part 3: Glued Timber Structures; Performance (4th draft)
14-12-1	Proposals for CEI-Bois/CIB-W18 Glulam Standards - H J Larsen
14-12-2	Guidelines for the Manufacturing of Glued Load-Bearing Timber Structures - Stevin Laboratory
14-12-3	Double Tapered Curved Glulam Beams - H Riberholt
14-12-4	Comment on CIB-W18/14-12-3 - E Gehri
18-12-1	Report on European Glulam Control and Production Standard - H Riberholt
18-10-2	Longitudinal Shear Design of Glued Laminated Beams - R O Foschi
19-12-1	Strength of Glued Laminated Timber - J Ehlbeck and F Colling
19-12-2	Strength Model for Glulam Columns - H J Blaß
19-12-3	Influence of Volume and Stress Distribution on the Shear Strength and Tensile Strength Perpendicular to Grain - F Colling
19-12-4	Time-Dependent Behaviour of Glued-Laminated Beams - F Zaupa
21-12-1	Modulus of Rupture of Glulam Beam Composed of Arbitrary Laminae - K Komatsu and N Kawamoto
21-12-2	An Appraisal of the Young's Modulus Values Specified for Glulam in Eurocode 5- L R J Whale, B O Hilson and P D Rodd
21-12-3	The Strength of Glued Laminated Timber (Glulam): Influence of Lamination Qualities and Strength of Finger Joints - J Ehlbeck and F Colling
21-12-4	Comparison of a Shear Strength Design Method in Eurocode 5 and a More Traditional One - H Riberholt
22-12-1	The Dependence of the Bending Strength on the Glued Laminated Timber Girder Depth - M Badstube, W Rug and W Schöne
22-12-2	Acid Deterioration of Glulam Beams in Buildings from the Early Half of the 1960s - Prelimination summary of the research project; Overhead pictures - B A Hedlund
22-12-3	Experimental Investigation of normal Stress Distribution in Glue Laminated Wooden Arches - Z Mielczarek and W Chanaj
22-12-4	Ultimate Strength of Wooden Beams with Tension Reinforcement as a Function of Random Material Properties - R Candowicz and T Dziuba
23-12-1	Bending Strength of Glulam Beams, a Design Proposal - J Ehlbeck and F Colling
23-12-2	Probability Based Design Method for Glued Laminated Timber - M F Stone
23-12-3	Glulam Beams, Bending Strength in Relation to the Bending Strength of the Finger Joints - H Riberholt
23-12-4	Glued Laminated Timber - Strength Classes and Determination of Characteristic Properties - H Riberholt, J Ehlbeck and A Fewell

24-12-1	Contribution to the Determination of the Bending Strength of Glulam Beams - F Colling, J Ehlbeck and R Görlacher
24-12-2	Influence of Perpendicular-to-Grain Stressed Volume on the Load-Carrying Capacity of Curved and Tapered Glulam Beams - J Ehlbeck and J Kürth
25-12-1	Determination of Characteristic Bending Values of Glued Laminated Timber. EN-Approach and Reality - E Gehri
26-12-1	Norwegian Bending Tests with Glued Laminated Beams-Comparative Calculations with the "Karlsruhe Calculation Model" - E Aasheim, K Solli, F Colling, R H Falk, J Ehlbeck and R Görlacher
26-12-2	Simulation Analysis of Norwegian Spruce Glued-Laminated Timber - R Hernandez and R H Falk
26-12-3	Investigation of Laminating Effects in Glued-Laminated Timber - F Colling and R H Falk
26-12-4	Comparing Design Results for Glulam Beams According to Eurocode 5 and to the French Working Stress Design Code (CB71) - F Rouger
27-12-1	State of the Art Report: Glulam Timber Bridge Design in the U.S. - M A Ritter and T G Williamson
27-12-2	Common Design Practice for Timber Bridges in the United Kingdom - C J Mettem, J P Marcroft and G Davis
27-12-3	Influence of Weak Zones on Stress Distribution in Glulam Beams - E Serrano and H J Larsen
28-12-1	Determination of Characteristic Bending Strength of Glued Laminated Timber - E Gehri
28-12-2	Size Factor of Norwegian Glued Laminated Beams - E Aasheim and K H Solli
28-12-3	Design of Glulam Beams with Holes - K Riipola
28-12-4	Compression Resistance of Glued Laminated Timber Short Columns- U Korin
29-12-1	Development of Efficient Glued Laminated Timber - G Schickhofer
30-12-1	Experimental Investigation and Analysis of Reinforced Glulam Beams - K Oiger
31-12-1	Depth Factor for Glued Laminated Timber-Discussion of the Eurocode 5 Approach - B Källsner, O Carling and C J Johansson
32-12-1	The bending stiffness of nail-laminated timber elements in transverse direction- T Wolf and O Schäfer
33-12-1	Internal Stresses in the Cross-Grain Direction of Wood Induced by Climate Variation – J Jönsson and S Svensson
34-12-1	High-Strength I-Joist Compatible Glulam Manufactured with LVL Tension Laminations – B Yeh, T G Williamson
34-12-2	Evaluation of Glulam Shear Strength Using A Full-Size Four-Point Test Method – B Yeh, T G Williamson
34-12-3	Design Model for FRP Reinforced Glulam Beams – M Romani, H J Blaß
34-12-4	Moisture induced stresses in glulam cross sections – J Jönsson
34-12-5	Load Carrying Capacity of Nail-Laminated Timber under Concentrated Loads – V Krämer, H J Blaß
34-12-6	Determination of Shear Strength Values for GLT Using Visual and Machine Graded Spruce Laminations – G Schickhofer
34-12-7	Mechanically Jointed Beams: Possibilities of Analysis and some special Problems – H Kreuzinger

35-12-1	Glulam Beams with Round Holes – a Comparison of Different Design Approaches vs. Test Data - S Aicher L Höfflin

PARTICLE AND FIBRE BUILDING BOARDS

7-13-1	Fibre Building Boards for CIB Timber Code (First Draft)- O Brynildsen
9-13-1	Determination of the Bearing Strength and the Load-Deformation Characteristics of Particleboard - K Möhler, T Budianto and J Ehlbeck
9-13-2	The Structural Use of Tempered Hardboard - W W L Chan
11-13-1	Tests on Laminated Beams from Hardboard under Short- and Longterm Load - W Nozynski
11-13-2	Determination of Deformation of Special Densified Hardboard under Long-term Load and Varying Temperature and Humidity Conditions - W Halfar
11-13-3	Determination of Deformation of Hardboard under Long-term Load in Changing Climate - W Halfar
14-4-1	An Introduction to Performance Standards for Wood-Base Panel Products - D H Brown
14-4-2	Proposal for Presenting Data on the Properties of Structural Panels - T Schmidt
16-13-1	Effect of Test Piece Size on Panel Bending Properties - P W Post
20-4-1	Considerations of Reliability - Based Design for Structural Composite Products - M R O'Halloran, J A Johnson, E G Elias and T P Cunningham
20-13-1	Classification Systems for Structural Wood-Based Sheet Materials - V C Kearley and A R Abbott
21-13-1	Design Values for Nailed Chipboard - Timber Joints - A R Abbott
25-13-1	Bending Strength and Stiffness of Izopanel Plates - Z Mielczarek
28-13-1	Background Information for "Design Rated Oriented Strand Board (OSB)" in CSA Standards - Summary of Short-term Test Results - E Karacabeyli, P Lau, C R Henderson, F V Meakes and W Deacon
28-13-2	Torsional Stiffness of Wood-Hardboard Composed I-Beam - P Olejniczak

TRUSSED RAFTERS

4-9-1	Long-term Loading of Trussed Rafters with Different Connection Systems - T Feldborg and M Johansen
6-9-3	Deflection of Trussed Rafters under Alternating Loading During a Year - T Feldborg and M Johansen
7-2-1	Lateral Bracing of Timber Struts - J A Simon
9-14-1	Timber Trusses - Code Related Problems - T F Williams
9-7-1	Design of Truss Plate Joints - F J Keenan
10-14-1	Design of Roof Bracing - The State of the Art in South Africa - P A V Bryant and J A Simon
11-14-1	Design of Metal Plate Connected Wood Trusses - A R Egerup
12-14-1	A Simple Design Method for Standard Trusses - A R Egerup
13-14-1	Truss Design Method for CIB Timber Code - A R Egerup
13-14-2	Trussed Rafters, Static Models - H Riberholt
13-14-3	Comparison of 3 Truss Models Designed by Different Assumptions for Slip and E-Modulus - K Möhler

14-14-1	Wood Trussed Rafter Design - T Feldborg and M Johansen
14-14-2	Truss-Plate Modelling in the Analysis of Trusses - R O Foschi
14-14-3	Cantilevered Timber Trusses - A R Egerup
14-7-5	The Effect of Support Eccentricity on the Design of W- and WW-Trusses with Nail Plate Connectors - B Källsner
15-14-1	Guidelines for Static Models of Trussed Rafters - H Riberholt
15-14-2	The Influence of Various Factors on the Accuracy of the Structural Analysis of Timber Roof Trusses - F R P Pienaar
15-14-3	Bracing Calculations for Trussed Rafter Roofs - H J Burgess
15-14-4	The Design of Continuous Members in Timber Trussed Rafters with Punched Metal Connector Plates - P O Reece
15-14-5	A Rafter Design Method Matching U.K. Test Results for Trussed Rafters - H J Burgess
16-14-1	Full-Scale Tests on Timber Fink Trusses Made from Irish Grown Sitka Spruce - V Picardo
17-14-1	Data from Full Scale Tests on Prefabricated Trussed Rafters - V Picardo
17-14-2	Simplified Static Analysis and Dimensioning of Trussed Rafters - H Riberholt
17-14-3	Simplified Calculation Method for W-Trusses - B Källsner
18-14-1	Simplified Calculation Method for W-Trusses (Part 2) - B Källsner
18-14-2	Model for Trussed Rafter Design - T Poutanen
19-14-1	Annex on Simplified Design of W-Trusses - H J Larsen
19-14-2	Simplified Static Analysis and Dimensioning of Trussed Rafters - Part 2 - H Riberholt
19-14-3	Joint Eccentricity in Trussed Rafters - T Poutanen
20-14-1	Some Notes about Testing Nail Plates Subjected to Moment Load - T Poutanen
20-14-2	Moment Distribution in Trussed Rafters - T Poutanen
20-14-3	Practical Design Methods for Trussed Rafters - A R Egerup
22-14-1	Guidelines for Design of Timber Trussed Rafters - H Riberholt
23-14-1	Analyses of Timber Trussed Rafters of the W-Type - H Riberholt
23-14-2	Proposal for Eurocode 5 Text on Timber Trussed Rafters - H Riberholt
24-14-1	Capacity of Support Areas Reinforced with Nail Plates in Trussed Rafters - A Kevarinmäki
25-14-1	Moment Anchorage Capacity of Nail Plates in Shear Tests - A Kevarinmaki and J. Kangas
25-14-2	Design Values of Anchorage Strength of Nail Plate Joints by 2-curve Method and Interpolation - J Kangas and A Kevarinmaki
26-14-1	Test of Nail Plates Subjected to Moment - E Aasheim
26-14-2	Moment Anchorage Capacity of Nail Plates - A Kevarinmäki and J Kangas
26-14-3	Rotational Stiffness of Nail Plates in Moment Anchorage - A Kevarinmäki and J Kangas
26-14-4	Solution of Plastic Moment Anchorage Stress in Nail Plates - A Kevarinmäki
26-14-5	Testing of Metal-Plate-Connected Wood-Truss Joints - R Gupta
26-14-6	Simulated Accidental Events on a Trussed Rafter Roofed Building - C J Mettem and J P Marcroft

30-14-1	The Stability Behaviour of Timber Trussed Rafter Roofs - Studies Based on Eurocode 5 and Full Scale Testing - R J Bainbridge, C J Mettern, A Reffold and T Studer
32-14-1	Analysis of Timber Reinforced with Punched Metal Plate Fasteners- J Nielsen
33-14-1	Moment Capacity of Timber Beams Loaded in Four-Point Bending and Reinforced with Punched Metal Plate Fasteners – J Nielsen

STRUCTURAL STABILITY

8-15-1	Laterally Loaded Timber Columns: Tests and Theory - H J Larsen
13-15-1	Timber and Wood-Based Products Structures. Panels for Roof Coverings. Methods of Testing and Strength Assessment Criteria. Polish Standard BN-78/7159-03
16-15-1	Determination of Bracing Structures for Compression Members and Beams - H Brüninghoff
17-15-1	Proposal for Chapter 7.4 Bracing - H Brüninghoff
17-15-2	Seismic Design of Small Wood Framed Houses - K F Hansen
18-15-1	Full-Scale Structures in Glued Laminated Timber, Dynamic Tests: Theoretical and Experimental Studies - A Ceccotti and A Vignoli
18-15-2	Stabilizing Bracings - H Brüninghoff
19-15-1	Connections Deformability in Timber Structures: a Theoretical Evaluation of its Influence on Seismic Effects - A Ceccotti and A Vignoli
19-15-2	The Bracing of Trussed Beams - M H Kessel and J Natterer
19-15-3	Racking Resistance of Wooden Frame Walls with Various Openings - M Yasumura
19-15-4	Some Experiences of Restoration of Timber Structures for Country Buildings - G Cardinale and P Spinelli
19-15-5	Non-Destructive Vibration Tests on Existing Wooden Dwellings - Y Hirashima
20-15-1	Behaviour Factor of Timber Structures in Seismic Zones. - A Ceccotti and A Vignoli
21-15-1	Rectangular Section Deep Beam - Columns with Continuous Lateral Restraint - H J Burgess
21-15-2	Buckling Modes and Permissible Axial Loads for Continuously Braced Columns- H J Burgess
21-15-3	Simple Approaches for Column Bracing Calculations - H J Burgess
21-15-4	Calculations for Discrete Column Restraints - H J Burgess
21-15-5	Behaviour Factor of Timber Structures in Seismic Zones (Part Two) - A Ceccotti and A Vignoli
22-15-1	Suggested Changes in Code Bracing Recommendations for Beams and Columns - H J Burgess
22-15-2	Research and Development of Timber Frame Structures for Agriculture in Poland- S Kus and J Kerste
22-15-3	Ensuring of Three-Dimensional Stiffness of Buildings with Wood Structures - A K Shenghelia
22-15-5	Seismic Behavior of Arched Frames in Timber Construction - M Yasumura
22-15-6	The Robustness of Timber Structures - C J Mettem and J P Marcroft

22-15-7	Influence of Geometrical and Structural Imperfections on the Limit Load of Wood Columns - P Dutko
23-15-1	Calculation of a Wind Girder Loaded also by Discretely Spaced Braces for Roof Members - H J Burgess
23-15-2	Stability Design and Code Rules for Straight Timber Beams - T A C M van der Put
23-15-3	A Brief Description of Formula of Beam-Columns in China Code - S Y Huang
23-15-4	Seismic Behavior of Braced Frames in Timber Construction - M Yasumara
23-15-5	On a Better Evaluation of the Seismic Behavior Factor of Low-Dissipative Timber Structures - A Ceccotti and A Vignoli
23-15-6	Disproportionate Collapse of Timber Structures - C J Mettem and J P Marcroft
23-15-7	Performance of Timber Frame Structures During the Loma Prieta California Earthquake - M R O'Halloran and E G Elias
24-15-2	Discussion About the Description of Timber Beam-Column Formula - S Y Huang
24-15-3	Seismic Behavior of Wood-Framed Shear Walls - M Yasumura
25-15-1	Structural Assessment of Timber Framed Building Systems - U Korin
25-15-3	Mechanical Properties of Wood-framed Shear Walls Subjected to Reversed Cyclic Lateral Loading - M Yasumura
26-15-1	Bracing Requirements to Prevent Lateral Buckling in Trussed Rafters - C J Mettem and P J Moss
26-15-2	Eurocode 8 - Part 1.3 - Chapter 5 - Specific Rules for Timber Buildings in Seismic Regions - K Becker, A Ceccotti, H Charlier, E Katsaragakis, H J Larsen and H Zeitter
26-15-3	Hurricane Andrew - Structural Performance of Buildings in South Florida - M R O'Halloran, E L Keith, J D Rose and T P Cunningham
29-15-1	Lateral Resistance of Wood Based Shear Walls with Oversized Sheathing Panels - F Lam, H G L Prion and M He
29-15-2	Damage of Wooden Buildings Caused by the 1995 Hyogo-Ken Nanbu Earthquake - M Yasumura, N Kawai, N Yamaguchi and S Nakajima
29-15-3	The Racking Resistance of Timber Frame Walls: Design by Test and Calculation - D R Griffiths, C J Mettem, V Enjily, P J Steer
29-15-4	Current Developments in Medium-Rise Timber Frame Buildings in the UK - C J Mettem, G C Pitts, P J Steer, V Enjily
29-15-5	Natural Frequency Prediction for Timber Floors - R J Bainbridge, and C J Mettem
30-15-1	Cyclic Performance of Perforated Wood Shear Walls with Oversize Oriented Strand Board Panels - Ming He, H Magnusson, F Lam, and H G L Prion
30-15-2	A Numerical Analysis of Shear Walls Structural Performances - L Davenne, L Daudeville, N Kawai and M Yasumura
30-15-3	Seismic Force Modification Factors for the Design of Multi-Storey Wood-Frame Platform Construction - E Karacabeyli and A Ceccotti
30-15-4	Evaluation of Wood Framed Shear Walls Subjected to Lateral Load - M Yasumura and N Kawai
31-15-1	Seismic Performance Testing On Wood-Framed Shear Wall - N Kawai
31-15-2	Robustness Principles in the Design of Medium-Rise Timber-Framed Buildings - C J Mettem, M W Milner, R J Bainbridge and V. Enjily
31-15-3	Numerical Simulation of Pseudo-Dynamic Tests Performed to Shear Walls - L Daudeville, L Davenne, N Richard, N Kawai and M Yasumura

31-15-4	Force Modification Factors for Braced Timber Frames - H G L Prion, M Popovski and E Karacabeyli
32-15-1	Three-Dimensional Interaction in Stabilisation of Multi-Storey Timber Frame Buildings - S Andreasson
32-15-2	Application of Capacity Spectrum Method to Timber Houses - N Kawai
32-15-3	Design Methods for Shear Walls with Openings - C Ni, E Karacabeyli and A Ceccotti
32-15-4	Static Cyclic Lateral Loading Tests on Nailed Plywood Shear Walls - K Komatsu, K H Hwang and Y Itou
33-15-1	Lateral Load Capacities of Horizontally Sheathed Unblocked Shear Walls – C Ni, E Karacabeyli and A Ceccotti
33-15-2	Prediction of Earthquake Response of Timber Houses Considering Shear Deformation of Horizontal Frames – N Kawai
33-15-3	Eurocode 5 Rules for Bracing – H J Larsen
34-15-1	A simplified plastic model for design of partially anchored wood-framed shear walls – B Källsner, U A Girhammar, Liping Wu
34-15-2	The Effect of the Moisture Content on the Performance of the Shear Walls – S Nakajima
34-15-3	Evaluation of Damping Capacity of Timber Structures for Seismic Design – M Yasumura
35-15-1	On test methods for determining racking strength and stiffness of wood-framed shear walls - B Källsner, U A Girhammar, L Wu
35-15-2	A Plastic Design Model for Partially Anchored Wood-framed Shear Walls with Openings - U A Girhammar, L Wu, B Källsner
35-15-3	Evaluation and Estimation of the Performance of the Shear Walls in Humid Climate - S Nakajima
35-15-4	Influence of Vertical Load on Lateral Resistance of Timber Frame Walls - B Dujič, R Žarnić
35-15-5	Cyclic and Seismic Performances of a Timber-Concrete System - Local and Full Scale Experimental Results - E Fournely, P Racher
35-15-6	Design of timber-concrete composite structures according to EC5 - 2002 version - A Ceccotti, M Fragiacomo, R M Gutkowski
35-15-7	Design of timber structures in seismic zones according to EC8- 2002 version - A Ceccotti, T Toratti, B Dujič
35-15-8	Design Methods to Prevent Premature Failure of Joints at Shear Wall Corners - N Kawai, H Okiura

FIRE

12-16-1	British Standard BS 5268 the Structural Use of Timber: Part 4 Fire Resistance of Timber Structures
13-100-2	CIB Structural Timber Design Code. Chapter 9. Performance in Fire
19-16-1	Simulation of Fire in Tests of Axially Loaded Wood Wall Studs - J König
24-16-1	Modelling the Effective Cross Section of Timber Frame Members Exposed to Fire - J König
25-16-1	The Effect of Density on Charring and Loss of Bending Strength in Fire - J König
25-16-2	Tests on Glued-Laminated Beams in Bending Exposed to Natural Fires - F Bolonius Olesen and J König
26-16-1	Structural Fire Design According to Eurocode 5, Part 1.2 - J König

31-16-1	Revision of ENV 1995-1-2: Charring and Degradation of Strength and Stiffness - J König
33-16-1	A Design Model for Load-carrying Timber Frame Members in Walls and Floors Exposed to Fire - J König
33-16-2	A Review of Component Additive Methods Used for the Determination of Fire Resistance of Separating Light Timber Frame Construction - J König, T Oksanen and K Towler
33-16-3	Thermal and Mechanical Properties of Timber and Some Other Materials Used in Light Timber Frame Construction - B Källsner and J König
34-16-1	Influence of the Strength Determining Factors on the Fire Resistance Capability of Timber Structural Members – I Totev, D Dakov
34-16-2	Cross section properties of fire exposed rectangular timber members - J König, B Källsner
34-16-3	Pull-Out Tests on Glued-in Rods at High Temperatures – A Mischler, A Frangi
35-16-1	Basic and Notional Charring Rates - J König

STATISTICS AND DATA ANALYSIS

13-17-1	On Testing Whether a Prescribed Exclusion Limit is Attained - W G Warren
16-17-1	Notes on Sampling and Strength Prediction of Stress Graded Structural Timber - P Glos
16-17-2	Sampling to Predict by Testing the Capacity of Joints, Components and Structures - B Norén
16-17-3	Discussion of Sampling and Analysis Procedures - P W Post
17-17-1	Sampling of Wood for Joint Tests on the Basis of Density - I Smith, L R J Whale
17-17-2	Sampling Strategy for Physical and Mechanical Properties of Irish Grown Sitka Spruce - V Picardo
18-17-1	Sampling of Timber in Structural Sizes - P Glos
18-6-3	Notes on Sampling Factors for Characteristic Values - R H Leicester
19-17-1	Load Factors for Proof and Prototype Testing - R H Leicester
19-6-2	Confidence in Estimates of Characteristic Values - R H Leicester
21-6-1	Draft Australian Standard: Methods for Evaluation of Strength and Stiffness of Graded Timber - R H Leicester
21-6-2	The Determination of Characteristic Strength Values for Stress Grades of Structural Timber. Part 1 - A R Fewell and P Glos
22-17-1	Comment on the Strength Classes in Eurocode 5 by an Analysis of a Stochastic Model of Grading - A proposal for a supplement of the design concept - M Kiesel
24-17-1	Use of Small Samples for In-Service Strength Measurement - R H Leicester and F G Young
24-17-2	Equivalence of Characteristic Values - R H Leicester and F G Young
24-17-3	Effect of Sampling Size on Accuracy of Characteristic Values of Machine Grades - Y H Chui, R Turner and I Smith
24-17-4	Harmonisation of LSD Codes - R H Leicester
25-17-2	A Body for Confirming the Declaration of Characteristic Values - J Sunley
25-17-3	Moisture Content Adjustment Procedures for Engineering Standards - D W Green and J W Evans
27-17-1	Statistical Control of Timber Strength - R H Leicester and H O Breitinger

30-17-1	A New Statistical Method for the Establishment of Machine Settings - F Rouger
35-17-1	Probabilistic Modelling of Duration of Load Effects in Timber Structures - J Köhler, S Svenson

GLUED JOINTS

20-18-1	Wood Materials under Combined Mechanical and Hygral Loading - A Martensson and S Thelandersson
20-18-2	Analysis of Generalized Volkersen - Joints in Terms of Linear Fracture Mechanics - P J Gustafsson
20-18-3	The Complete Stress-Slip Curve of Wood-Adhesives in Pure Shear - H Wernersson and P J Gustafsson
22-18-1	Perspective Adhesives and Protective Coatings for Wood Structures - A S Freidin
34-18-1	Performance Based Classification of Adhesives for Structural Timber Applications - R J Bainbridge, C J Mettem, J G Broughton, A R Hutchinson
35-18-1	Creep Testing Wood Adhesives for Structural Use - C Bengtsson, B Källander

FRACTURE MECHANICS

21-10-1	A Study of Strength of Notched Beams - P J Gustafsson
22-10-1	Design of Endnotched Beams - H J Larsen and P J Gustafsson
23-10-1	Tension Perpendicular to the Grain at Notches and Joints - T A C M van der Put
23-10-2	Dimensioning of Beams with Cracks, Notches and Holes. An Application of Fracture Mechanics - K Riipola
23-19-1	Determination of the Fracture Energie of Wood for Tension Perpendicular to the Grain - W Rug, M Badstube and W Schöne
23-19-2	The Fracture Energy of Wood in Tension Perpendicular to the Grain. Results from a Joint Testing Project - H J Larsen and P J Gustafsson
23-19-3	Application of Fracture Mechanics to Timber Structures - A Ranta-Maunus
24-19-1	The Fracture Energy of Wood in Tension Perpendicular to the Grain - H J Larsen and P J Gustafsson
28-19-1	Fracture of Wood in Tension Perpendicular to the Grain: Experiment and Numerical Simulation by Damage Mechanics - L Daudeville, M Yasumura and J D Lanvin
28-19-2	A New Method of Determining Fracture Energy in Forward Shear along the Grain - H D Mansfield-Williams
28-19-3	Fracture Design Analysis of Wooden Beams with Holes and Notches. Finite Element Analysis based on Energy Release Rate Approach - H Petersson
28-19-4	Design of Timber Beams with Holes by Means of Fracture Mechanics - S Aicher, J Schmidt and S Brunold
30-19-1	Failure Analysis of Single-Bolt Joints - L Daudeville, L Davenne and M Yasumura

SERVICEABILITY

27-20-1	Codification of Serviceability Criteria - R H Leicester
27-20-2	On the Experimental Determination of Factor k_{def} and Slip Modulus k_{ser} from Short- and Long-Term Tests on a Timber-Concrete Composite (TCC) Beam - S Capretti and A Ceccotti

27-20-3	Serviceability Limit States: A Proposal for Updating Eurocode 5 with Respect to Eurocode 1 - P Racher and F Rouger
27-20-4	Creep Behavior of Timber under External Conditions - C Le Govic, F Rouger, T Toratti and P Morlier
30-20-1	Design Principles for Timber in Compression Perpendicular to Grain - S Thelandersson and A Mårtensson
30-20-2	Serviceability Performance of Timber Floors - Eurocode 5 and Full Scale Testing - R J Bainbridge and C J Mettem
32-20-1	Floor Vibrations - B Mohr

TEST METHODS

31-21-1	Development of an Optimised Test Configuration to Determine Shear Strength of Glued Laminated Timber - G Schickhofer and B Obermayr
31-21-2	An Impact Strength Test Method for Structural Timber. The Theory and a Preliminary Study - T D G Canisius
35-21-1	Full-Scale Edgewise Shear Tests for Laminated Veneer Lumber- B Yeh, T G Williamson

CIB TIMBER CODE

2-100-1	A Framework for the Production of an International Code of Practice for the Structural Use of Timber - W T Curry
5-100-1	Design of Solid Timber Columns (First Draft) - H J Larsen
5-100-2	A Draft Outline of a Code for Timber Structures - L G Booth
6-100-1	Comments on Document 5-100-1; Design of Solid Timber Columns - H J Larsen and E Theilgaard
6-100-2	CIB Timber Code: CIB Timber Standards - H J Larsen and E Theilgaard
7-100-1	CIB Timber Code Chapter 5.3 Mechanical Fasteners; CIB Timber Standard 06 and 07 - H J Larsen
8-100-1	CIB Timber Code - List of Contents (Second Draft) - H J Larsen
9-100-1	The CIB Timber Code (Second Draft)
11-100-1	CIB Structural Timber Design Code (Third Draft)
11-100-2	Comments Received on the CIB Code a U Saarelainen b Y M Ivanov c R H Leicester d W Nozynski e W R A Meyer f P Beckmann; R Marsh g W R A Meyer h W R A Meyer
11-100-3	CIB Structural Timber Design Code; Chapter 3 - H J Larsen
12-100-1	Comment on the CIB Code - Sous-Commission Glulam
12-100-2	Comment on the CIB Code - R H Leicester
12-100-3	CIB Structural Timber Design Code (Fourth Draft)
13-100-1	Agreed Changes to CIB Structural Timber Design Code
13-100-2	CIB Structural Timber Design Code. Chapter 9: Performance in Fire
13-100-3a	Comments on CIB Structural Timber Design Code

13-100-3b	Comments on CIB Structural Timber Design Code - W R A Meyer
13-100-3c	Comments on CIB Structural Timber Design Code - British Standards Institution
13-100-4	CIB Structural Timber Design Code. Proposal for Section 6.1.5 Nail Plates - N I Bovim
14-103-2	Comments on the CIB Structural Timber Design Code - R H Leicester
15-103-1	Resolutions of TC 165-meeting in Athens 1981-10-12/13
21-100-1	CIB Structural Timber Design Code. Proposed Changes of Sections on Lateral Instability, Columns and Nails - H J Larsen
22-100-1	Proposal for Including an Updated Design Method for Bearing Stresses in CIB W18 - Structural Timber Design Code - B Madsen
22-100-2	Proposal for Including Size Effects in CIB W18A Timber Design Code - B Madsen
22-100-3	CIB Structural Timber Design Code - Proposed Changes of Section on Thin-Flanged Beams - J König
22-100-4	Modification Factor for "Aggressive Media" - a Proposal for a Supplement to the CIB Model Code - K Erler and W Rug
22-100-5	Timber Design Code in Czechoslovakia and Comparison with CIB Model Code - P Dutko and B Kozelouh

LOADING CODES

4-101-1	Loading Regulations - Nordic Committee for Building Regulations
4-101-2	Comments on the Loading Regulations - Nordic Committee for Building Regulations

STRUCTURAL DESIGN CODES

1-102-1	Survey of Status of Building Codes, Specifications etc., in USA - E G Stern
1-102-2	Australian Codes for Use of Timber in Structures - R H Leicester
1-102-3	Contemporary Concepts for Structural Timber Codes - R H Leicester
1-102-4	Revision of CP 112 - First Draft, July 1972 - British Standards Institution
4-102-1	Comparsion of Codes and Safety Requirements for Timber Structures in EEC Countries - Timber Research and Development Association
4-102-2	Nordic Proposals for Safety Code for Structures and Loading Code for Design of Structures - O A Brynildsen
4-102-3	Proposal for Safety Codes for Load-Carrying Structures - Nordic Committee for Building Regulations
4-102-4	Comments to Proposal for Safety Codes for Load-Carrying Structures - Nordic Committee for Building Regulations
4-102-5	Extract from Norwegian Standard NS 3470 "Timber Structures"
4-102-6	Draft for Revision of CP 112 "The Structural Use of Timber" - W T Curry
8-102-1	Polish Standard PN-73/B-03150: Timber Structures; Statistical Calculations and Designing
8-102-2	The Russian Timber Code: Summary of Contents
9-102-1	Svensk Byggnorm 1975 (2nd Edition); Chapter 27: Timber Construction
11-102-1	Eurocodes - H J Larsen
13-102-1	Program of Standardisation Work Involving Timber Structures and Wood-Based Products in Poland

17-102-1	Safety Principles - H J Larsen and H Riberholt
17-102-2	Partial Coefficients Limit States Design Codes for Structural Timberwork - I Smith
18-102-1	Antiseismic Rules for Timber Structures: an Italian Proposal - G Augusti and A Ceccotti
18-1-2	Eurocode 5, Timber Structures - H J Larsen
19-102-1	Eurocode 5 - Requirements to Timber - Drafting Panel Eurocode 5
19-102-2	Eurocode 5 and CIB Structural Timber Design Code - H J Larsen
19-102-3	Comments on the Format of Eurocode 5 - A R Fewell
19-102-4	New Developments of Limit States Design for the New GDR Timber Design Code - W Rug and M Badstube
19-7-3	Effectiveness of Multiple Fastener Joints According to National Codes and Eurocode 5 (Draft) - G Steck
19-7-6	The Derivation of Design Clauses for Nailed and Bolted Joints in Eurocode5 - L R J Whale and I Smith
19-14-1	Annex on Simplified Design of W-Trusses - H J Larsen
20-102-1	Development of a GDR Limit States Design Code for Timber Structures - W Rug and M Badstube
21-102-1	Research Activities Towards a New GDR Timber Design Code Based on Limit States Design - W Rug and M Badstube
22-102-1	New GDR Timber Design Code, State and Development - W Rug, M Badstube and W Kofent
22-102-2	Timber Strength Parameters for the New USSR Design Code and its Comparison with International Code - Y Y Slavik, N D Denesh and E B Ryumina
22-102-3	Norwegian Timber Design Code - Extract from a New Version - E Aasheim and K H Solli
23-7-1	Proposal for a Design Code for Nail Plates - E Aasheim and K H Solli
24-102-2	Timber Footbridges: A Comparison Between Static and Dynamic Design Criteria - A Ceccotti and N de Robertis
25-102-1	Latest Development of Eurocode 5 - H J Larsen
25-102-1A	Annex to Paper CIB-W18/25-102-1. Eurocode 5 - Design of Notched Beams - H J Larsen, H Riberholt and P J Gustafsson
25-102-2	Control of Deflections in Timber Structures with Reference to Eurocode 5 - A Martensson and S Thelandersson
28-102-1	Eurocode 5 - Design of Timber Structures - Part 2: Bridges - D Bajolet, E Gehri, J König, H Kreuzinger, H J Larsen, R Mäkipuro and C Mettem
28-102-2	Racking Strength of Wall Diaphragms - Discussion of the Eurocode 5 Approach - B Källsner
29-102-1	Model Code for the Probabilistic Design of Timber Structures - H J Larsen, T Isaksson and S Thelandersson
30-102-1	Concepts for Drafting International Codes and Standards for Timber Constructions - R H Leicester
33-102-1	International Standards for Bamboo – J J A Janssen
35-102-1	Design Characteristics and Results According to EUROCODE 5 and SNiP Procedures - L Ozola, T Keskküla
35-102-2	Model Code for the Reliability-Based Design of Timber Structures - H J Larsen

INTERNATIONAL STANDARDS ORGANISATION

3-103-1	Method for the Preparation of Standards Concerning the Safety of Structures (ISO/DIS 3250) - International Standards Organisation ISO/TC98
4-103-1	A Proposal for Undertaking the Preparation of an International Standard on Timber Structures - International Standards Organisation
5-103-1	Comments on the Report of the Consultion with Member Bodies Concerning ISO/TC/P129 - Timber Structures - Dansk Ingeniorforening
7-103-1	ISO Technical Committees and Membership of ISO/TC 165
8-103-1	Draft Resolutions of ISO/TC 165
12-103-1	ISO/TC 165 Ottawa, September 1979
13-103-1	Report from ISO/TC 165 - A Sorensen
14-103-1	Comments on ISO/TC 165 N52 "Timber Structures; Solid Timber in Structural Sizes; Determination of Some Physical and Mechanical Properties"
14-103-2	Comments on the CIB Structural Timber Design Code - R H Leicester
21-103-1	Concept of a Complete Set of Standards - R H Leicester

JOINT COMMITTEE ON STRUCTURAL SAFETY

3-104-1	International System on Unified Standard Codes of Practice for Structures - Comité Européen du Béton (CEB)
7-104-1	Volume 1: Common Unified Rules for Different Types of Construction and Material - CEB

CIB PROGRAMME, POLICY AND MEETINGS

1-105-1	A Note on International Organisations Active in the Field of Utilisation of Timber - P Sonnemans
5-105-1	The Work and Objectives of CIB-W18-Timber Structures - J G Sunley
10-105-1	The Work of CIB-W18 Timber Structures - J G Sunley
15-105-1	Terms of Reference for Timber - Framed Housing Sub-Group of CIB-W18
19-105-1	Tropical and Hardwood Timbers Structures - R H Leicester
21-105-1	First Conference of CIB-W18B, Tropical and Hardwood Timber Structures Singapore, 26 - 28 October 1987 - R H Leicester

INTERNATIONAL UNION OF FORESTRY RESEARCH ORGANISATIONS

7-106-1 Time and Moisture Effects - CIB W18/IUFRO 55.02-03 Working Party

CIB-W18/35-2-1

INTERNATIONAL COUNCIL FOR RESEARCH AND INNOVATION
IN BUILDING AND CONSTRUCTION

WORKING COMMISSION W18 - TIMBER STRUCTURES

COMPUTER SIMULATIONS ON THE RELIABILITY OF TIMBER COLUMNS REGARDING HYGROTHERMAL EFFECTS

R Hartnack
K-U Schober
K Rautenstrauch

Bauhaus-University Weimar

GERMANY

Presented by: K U Schober

A number of questions were asked by H J Blaß and H J Larsen about the practical relevance of the research reported in the paper and its implications for service class designations in design situations according to EC5. The author confirmed that the test specimen which were 14x14cm or 16x16 cm cross-section were tested and that it is difficult to model service class 2. This was followed by discussions on the relative values of moisture content in timber members for the various service classes. S Thelandersson then asked for clarification of the work with regard to the creep model used and A Leijten asked about the starting point and the cumulative effect of climate conditions. In addition to clarifying the points raised, K U Schober confirmed that the reported model did not take strength considerations into account.

Computer simulations on the reliability of timber columns regarding hygrothermal effects

Ralf Hartnack, Kay-Uwe Schober, Karl Rautenstrauch
Bauhaus-University Weimar, Chair of Timber and Masonry Engineering, Germany

1 Introduction

The evaluation of the load-bearing capacity of timber columns is based on the interaction of many effects. In particular, hygrothermal long-term effects considerably influence the reliability depending on load and are a decisive criterion for the design of wooden struts.

Nowadays it is almost impossible to evaluate the load-bearing capacity under the influence of hygrothermal long-term effects, because of the long-term nature of such experiments. Furthermore, high costs speak against a purely experimental approach if we consider the dimensions relevant to buildings as well as the large number of specimens as a result of wide-spreading parameters. Computer simulations are a cost reducing and substantially faster alternative for determining long-term effects of the load-bearing capacity behaviour.

For this purpose, a software was developed at the Bauhaus-University Weimar, Chair of Timber and Masonry Engineering, which is based on the theory of finite elements (isoparametric beam elements). It considers both geometrical and physical non-linearity. The influence of the hygrothermal long-term effects were taken into account with the help of a supplementation to a computersimulations program. The adaptation of the underlying rheological model is a result of the simulation of internationally published test series. The results are consistent and verify the model sufficiently.

2 Modelling

The modelling was already explained in detail by BECKER [3] at the last meeting of CIB. The model has been retained basically unchanged. For the respective numerical values see [2]. A substantial change in comparison to BECKER's [2] model, lies in the modelling along the longitudinal axis of the building component. A discretisation along the longitudinal axis replaces the modelling of the so-called length effect.

In the following sections, the components of the model are described briefly.

2.1 Model Components

2.1.1 Creep Law

Different models are used to describe the creep effect properties. HUNT [10] divides these models into two groups, interpolation models and structural models. In this work, the rheological model out of the group of interpolation models is used. The verification was done by adapting data from experiments, as usual with this kind of model.

The creep model used here consists of a Kelvin-chain, with a Hookian spring in series. The four Kelvin-elements (parallel connection of a spring and a dashpot) represent the delayed-elastic deformations (visco-elastic creep), while the spring represents immediate elastic deformations. The deformation caused by the aforementioned four Kelvin-elements depends on the upset load and time, whereas the fifth Kelvin-element is dependent on moisture change in wood and describes the so called mechano-sorptive creep.

This model was also used by BECKER [2]. But these investigations eliminated a non-linear part of creep by using a dashpot. In the opinion of various researchers the visco-elastic creep behaviour of wood can be regarded as linear, when stress lies under a certain threshold. Normally, this proportional limit is set above the service loads (RANTA-MAUNUS [13]). According to HUNT [11], varying climatic conditions do not result in a decrease of the proportional limit but do at the most result in an acceleration of the creep process. Therefore the proportional limit of mechano-sorptive creep is also above the service loads.

2.1.2 Material parameters

The material parameters were also determined with the model used by BECKER [2].

A further alteration of this model exists, however, in the description of the material parameters along the longitudinal axis of the structural member. While the model by BECKER [2] establishes a so-called length-factor, this work will deal with a discretisation along the longitudinal axis.

The material parameters, which are widespread because of the structural composition of wood, are defined by regression equations developed by COLLING [4]. According to these investigations, 15 cm was chosen as the length of one discretisized cell. The normal distributed density and the knot density (KAR) are the significant input parameters. The distribution of the knot density is calculated as done by COLLING [4]. The output parameters are the modulus of elasticity (MOE) and the strength (stress at fracture). The underlying stress-strain relationship by GLOS [6] is derived from these values (Figure 1).

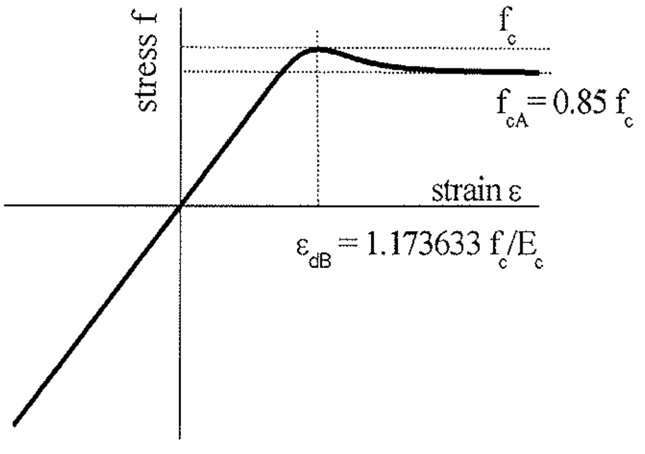

Figure 1: stress-strain-relationship by GLOS [6]

2.1.3 Wood Moisture Content Distribution

Because the material parameters and the mechano-sorptive creep are both dependent on the wood moisture content, its distribution in the cross-section must be known. The wood moisture content of the cross-section is determined by the second Fickian law (equation 1).

$$\frac{\partial u}{\partial t} = \nabla\left(D(u)\cdot\nabla u\right) \tag{1}$$

A two-dimensional solution is used because the dimensions of the cross-section are small in comparison to the length of the building component. Time must be discretisized because it is a non-linear problem which cannot be solved in a closed way. The coefficient of vapour diffusion is constant for one time interval. The transition of moisture from the surrounding climate to the wood surface is considered by a so-called surface emission coefficient.

For more details see BECKER [2].

3 Influence of surrounding Climate

3.1 Assumptions by ENV 1995-1

The impact of moisture is considered in ENV 1995-1 [5] by differentiating various environmental conditions, which are divided into so-called service classes. Together with the class of load duration, the modifying factors k_{mod} and k_{def} are investigated, which influence the verification on the one hand of the load-carrying capacity limit state and on the other hand of the serviceability limit state.

Three service classes corresponding to the climatic influences of the environment are differentiated in ENV 1995-1 [5]. In service classes 1 and 2 a constant temperature of 20°C is assumed. In service class 1, the relative humidity should not exceed 65% for a few weeks in one year [5]. For service class 2, it is required that the relative humidity not top the value of 85 % respectively. All of the climatic scenarios which lead to higher moisture contents than in service class 2, are arranged in service class 3. That implies that the relative humidity must top the value of 85 % for a few weeks per year.

As relative humidity appears to be the decisive influence criterion, it seems justifiable to use a constant temperature as done by ENV 1995-1 [5]. This is reaffirmed by the sorption isotherms for the range of temperatures in the state of accepted usage. According to AVRAMIDIS [1], the equilibrium moisture content can be calculated in dependence of temperature (T) and relative humidity (RH) (equation 2). As a precondition, the surrounding climate must stay in effect long enough for this equilibrium to adjust itself. In reality the duration of varying climate seems to be too short to reach the equilibrium moisture content of wood. Therefore the spectrum of possible wood moisture content is overestimated when calculated with the equation according to AVRAMIDIS [1]. Nevertheless equation (2) is analysed for reference value.

$$u_{wood} = 0.01\cdot\left[\frac{-T\cdot\ln(1-RH)}{0.13\cdot\left(1-\frac{T}{647{,}1}\right)^{-6.46}}\right]^{\frac{1}{110\cdot T^{-0.75}}} \tag{2}$$

If one calculates the equilibrium moisture content of wood via equation (2), a figure of about 12.1 % in service class 1 and 17.7% in service class 2 is obtained.

3.2 Actual Climate Values

The actual measured data of different German climate stations (data set from German weather service DWD), shows that the average daily relative humidity lies between 8 and 21 weeks per year above the threshold. Table 1 shows an overview of different German locations. The values represent the average values over the 20 years of observation between 1981 and 2001.

relative humidity [weeks per year]	Berlin	Hochwacht	Bamberg	Freiburg
≤65 %	14.3	2.7	7.7	18.4
65 % < RH ≤85 %	26.7	28.1	28.6	25.9
> 85 %	11.2	21.4	15.8	7.9

Table 1: frequency of occurrence per year of different relative humidities (service class 3)

That implies that the average daily relative humidity exceeds the value of 85% on average about 14 weeks per year (27 %). According to the definition in ENV 1995-1 [5] the simulation of a wooden building component using real recorded climate data must be assigned to service class 3.

If the real appearance of the averaged wood moisture content under the aforementioned conditions is compared with the values of equation (2), the following distribution in table 2 is obtained:

Averaged wood m.c. [weeks per year]	Berlin	Hochwacht	Bamberg	Freiburg
≤12,1 %	4.2	0.0	0.0	3.9
12,1 % < RH ≤17,7 %	39.6	25.8	35.9	45.5
> 17,7 %	8.4	26.4	16.2	2.7

Table 2: frequency of occurrence per year of different averaged wood moisture contents (service class 3)

Considering the definition according to ENV 1995-1 [5], an obvious affiliation to service class 3 is visible. The moisture content of wood at the beginning of the simulation is based on the value of the equilibrium moisture content on the first day of observation.

The situation in service class 2 is more complex. Commentaries of standards describe such building components as roofed outdoor elements. The influence of the roofing on the climate is not specified in the literature. In order to make comparisions a formulation with measured data will not be undertaken. Only a useful basic approach for describing the relative humidity of such a setting is specified in section 4.

The climate of indoor rooms must be well known for consideration of service class 1. In order to calculate this in dependence to the outdoor climate, an approach by STEIN [15] is chosen:

$$\varphi_i = \frac{\varphi_a \cdot \rho_{sa}}{\rho_{si}} \cdot \frac{T_a}{T_i} + \frac{\dot{m}_{D,add}}{n_L \cdot V_{room} \cdot \rho_{si}} \tag{3}$$

Equation (3) establishes a relationship between the relative humidity outdoors (ϕ_a) and indoors (ϕ_i) under the influence of outdoor temperature (T_a) and indoor temperature (T_i) as well as the appropriate water vapour density at saturation outdoors (ρ_{sa}) and indoors (ρ_{si}). Additionally, a use-conditioned accumulation of water vapour ($m'_{D,add}$) indoors is considered. This additional humidity depends on the rate of air changes (n_L) and on the room volume (V_{room}).

It is assumed that the additional accumulation of water vapour indoors is 150 g/h. The rate of air change is set constantly at 0.8 1/h, the volume of the room to 60 m^3. Furthermore it is assumed that the room temperature is constantly 293 K, whereas there is no cooling of the room for temperatures exceeding this value. Table 3 shows that only a few weeks per year provide humidities above a value of 65 %. For this reason the correlation to service class 1 is obvious.

relative humidity [weeks per year]	Berlin	Hochwacht	Bamberg	Freiburg
≤65 %	49.0	46.4	46.5	47.8
65 % < RH ≤85 %	3.1	5.6	5.5	4.4
> 85 %	0.0	0.1	0.1	0.0

Table 3: frequency of occurrence per year of different relative humidities (service class 1)

Here again the comparison between the timber moisture calculated by equation (2) and the real averaged moisture contents of the wood cross- section can be pointed out:

Averaged wood m.c. [weeks per year]	Berlin	Hochwacht	Bamberg	Freiburg
≤12,1 %	52.2	51.6	51.9	52.2
12,1 % < RH ≤17,7 %	0.0	0.6	0.3	0.0
> 17,7 %	0.0	0.0	0.0	0.0

Table 4: frequency of occurrence per year of different averaged wood moisture contents (service class 1)

The wood moisture at the beginning of the simulation was set to 12 %. Only a few days of the service period show a wood moisture content above the value of 12 %. Therefore the allocation to use service class 1 is justified.

3.3 Influence on Wooden Struts

As previously mentioned the surrounding climate has a decisive influence on the load-bearing capacity of wooden struts. A computer simulation (articulated column Euler case 2, slenderness 100) was done using the real average daily relative humidity over a 20 year period from the four aforementioned locations in Germany. The material and long-term laws described in section 2 are underlying. To compare the results, one simulation was done without paying regard to mechano-sorptive effects.

If the deformations in the middle of the columns for service class 3 are compared, only small differences between the various German locations are evident (figure 2). In addition to the typical curves in the form of saw teeth, the curves lie decisive clearly above the reference curve. This verifies the additional creep deformations caused by the influence of non-constant humidity, which is mentioned in the literature, for example RANTA MAUNUS [12], GRESSEL [7], GROSSMAN [8]. In the interest of clarity, there are only two places (Freiburg and Hochwacht) presented in figure 2. The two other places settle between the represented deformation curves.

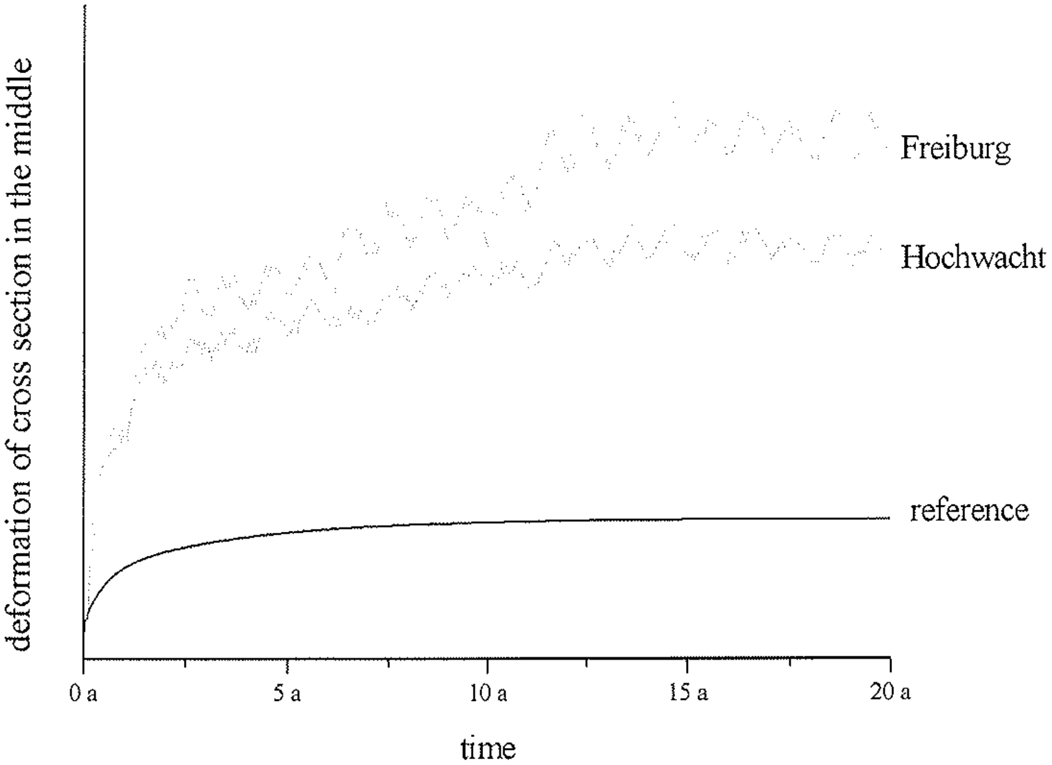

Figure 2: deformation for different locations in the course of time

The deformation curve for Hochwacht lies decisively below the curve for Freiburg. If the average medial wood moisture is compared, a substantially higher value for Hochwacht (17.75 %) than for Freiburg (14.34 %) is evident. The reason for this can be immediately seen, considering the variation of humidity. The fluctuation of the wood moisture is decisively higher in Freiburg, which leads to higher mechano-sorptive creep and therefore to higher deformations.

4 Methods of Approximation

The calculation with exact climate values reaches its limit by determining the load-bearing capacity, which is ascertained by load-increasing until the fracture of a lamella or until the failure of balance. The moisture dependent material parameters are taken from the last time interval during the observation period. The difference in relative humidity between two days can be up to 50 % according to data from the German weather service. Accordingly, the determination of the load-bearing capacity is also dependent on the level of the relative humidity on the last day of observation. There is in fact almost no change in wood moisture content of the core, even though the moisture content of the border is affected considerably. The edge fibres provide the decisive strength for the collapse load at fracture. Moreover it is not the objective to show different conditions for each location in Germany but rather to use the most uniform climate assumptions possible.

This problem definition can be solved by using an approximation for the distribution of climate.

4.1 Method of Approximation for different Service Classes

To harmonise the distribution of moisture content for a chosen period, a sinusoidal modelling is used. Figure 3 shows for one chosen location (Freiburg) in service class 3 the confrontation between the real humidity (gray curve at the top) and the approximated humidity (black curve at the top, equation 4) respectively the real temperature (gray curve at the bottom) and the approximated temperature (black curve at the bottom, equation 5). A possible phase displacement, which arises in dependence of the beginning of observations and on the season, must be considered.

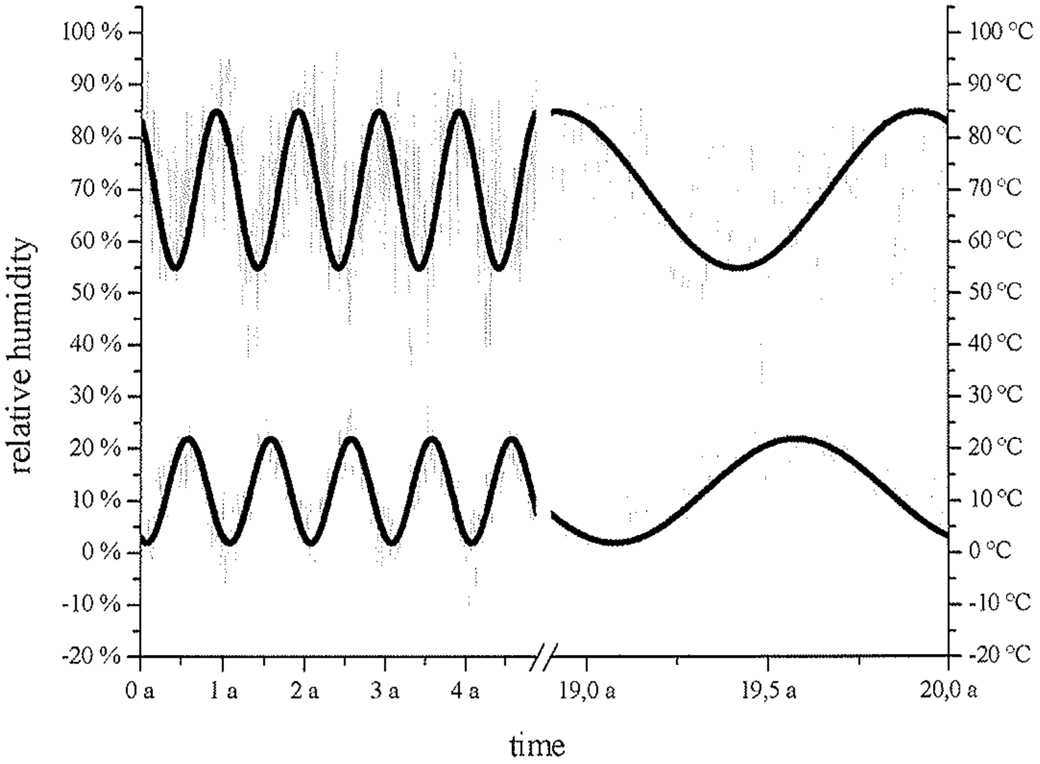

Figure 3: comparison of the approximated and the real climate conditions in service class 3

The following approximated equations are used:

For relative humidity:
$$RH = 70\,\% + 15\,\% \cdot \sin\left(t \cdot \frac{2 \cdot \pi}{365\ d}\right) \tag{4}$$

For temperature:
$$T = 12\,°C + 10\,°C \cdot \sin\left(t \cdot \frac{2 \cdot \pi}{365\ d}\right) \tag{5}$$

In spite of the good conformity of the real values with the approximated values, the comparison between the deformation curves show decisive differences (figure 5). The values calculated on the basis of approximated humidity underestimate regularly the actual values.

The reason for this is that the value of the relative humidity and the resulting wood moisture content is not the only course for mechanosorptive creep. The variations of wood moisture content are reponsible as well. Exactly these changes are minimized by the approximated approach, and the curve is harmonized. Even if the inactivity of the system with regard to the moisture changes is great, the daily changes of moisture content produce a decisive influence.

There are regularly described scenarios in service class 2 which represent outdoor roofed building components. As mentioned above, there are no detailed notations. Only approaches can be taken from the literature:

According to HANHIJÄRVI [9]:
$$RH = 75\,\% + 15\,\% \cdot \sin\left(t \cdot \frac{2 \cdot \pi}{365\ d}\right) \tag{6}$$

According to BECKER [2]:
$$RH = 80\,\% + 6\,\% \cdot \sin\left(t \cdot \frac{2 \cdot \pi}{364\ d}\right) \tag{7}$$

Here it is noticeable that this approach lies above the approaches in service class 3 used in this work. But the fluctuation margin according to BECKER [2] is very slight. That is because there is an additional daily fluctuation considered in his work. On the other hand this fact levels the slight seasonal fluctuation.

In service class 1, only one approximated equation for the relative humidity is indicated.

For relative humidity:
$$RH = 40\,\% + 20\,\% \cdot \sin\left(t \cdot \frac{2 \cdot \pi}{365\ d}\right) \tag{8}$$

For temperature:
$$T = 20\,°C = \text{const.} \tag{9}$$

The temperature is approximated at a constant 20°C. In comparison to service class 3 the higher fluctuation of humidity attracts attention, though on a lower level (figure 4).

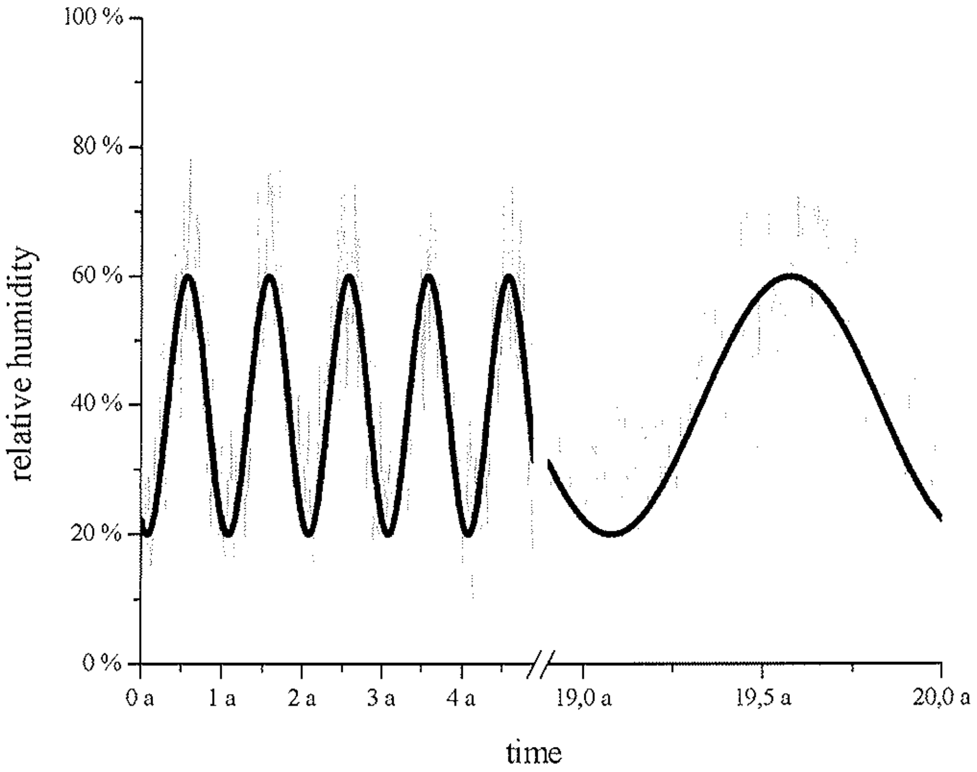

Figure 4: comparison of the approximated and the real climate conditions in service class 1

4.2 Modified Approximation Distributions

The approaches according to BECKER [2] and HANHIJÄRVI [9] already indicate that the equation (4) must be modified. The obtained load-bearing capacity represents a bad comparison criterion. As previously mentioned, there is a type of dependence between the relative humidity on the last day of observation and the reachable load-bearing capacity. Therefore a way must be found to approximate the relative humidity, so that the results, especially the deformation, coincides over the 20-year observation period. Essentially there are four possibilities. First, an increase factor can be added to the approximated curve. This means that both the baseline of the sinusoidal distribution and the amplitude are increased. The increase would be proportional for both influence factors. A second modification could be the exclusive increase of the baseline. Likewise, the third option could be increased amplitude. As the fourth option, a modification of both the baseline and the amplitude is conceivable but with different factors:

Option 1:
$$\mathrm{RH} = \mathrm{f}_1 \cdot \left[70\,\% + 15\,\% \cdot \sin\left(\mathrm{t} \cdot \frac{2 \cdot \pi}{365\,\mathrm{d}}\right)\right] \tag{10}$$

Option 2:
$$\mathrm{RH} = (\mathrm{f}_2 \cdot 70\,\%) + 15\,\% \cdot \sin\left(\mathrm{t} \cdot \frac{2 \cdot \pi}{365\,\mathrm{d}}\right) \tag{11}$$

Option 3:
$$\mathrm{RH} = 70\,\% + (\mathrm{f}_3 \cdot 15\,\%) \cdot \sin\left(\mathrm{t} \cdot \frac{2 \cdot \pi}{365\,\mathrm{d}}\right) \tag{12}$$

Option 4:
$$\mathrm{RH} = \mathrm{f}_{4\mathrm{A}} \cdot 70\,\% + (\mathrm{f}_{4\mathrm{B}} \cdot 15\,\%) \cdot \sin\left(\mathrm{t} \cdot \frac{2 \cdot \pi}{365\,\mathrm{d}}\right) \tag{13}$$

Because of the slight influence of temperature on wood moisture content caused by the relative humidity, the modification of the approximated curve for temperature is neglected.

The options 1 to 3 appear rather inflexible. The increase caused by the factor f_1 shows an increase in the deformation amplitude in addition to the increase of the deformation values. Options 2 and 3 will create similar effects. Above all it has been discovered that in principle the deformation amplitude is too high. This realisation leeds to the conclusion that the baseline of the sinusoidal distribution of humidity must be raised, but at the same time the fluctuation margin must also be reduced. This circumstance can be explained with the inertia of the system. The fast fluctuations caused by the real reproduction of humidity are not represented in the core of the wooden building component, but only in the edge fibers. The approximations show a different behaviour. Here there is an assimilation to the relative humidity more uniformly distributed over the cross-section because the changes are slighter.

Figure 5 shows a comparison between the real distribution, the approximation and the modified approximation for the chosen location (Freiburg). The curve from figure 2 was taken as a reference curve for this place. It is again a matter of service class 3.

It must be emphasised, that during approximation different criterion must be observed. In addition to the good approximation of the actual curve during the entire observation period, the deformation at the last time interval particularly must be approached as closely as possible. This deformation represents the decisive criterion for the determination of the load-bearing capacity.

This results in a modification of the equation (13) as the following approximate formulation for a climate scenario in service class 3:

Option 4 (outdoors)

$$RH = 1.30 \cdot 70\,\% + \left(0.455 \cdot 15\,\%\right) \cdot \sin\left(t \cdot \frac{2 \cdot \pi}{365\,\mathrm{d}}\right) \tag{14}$$

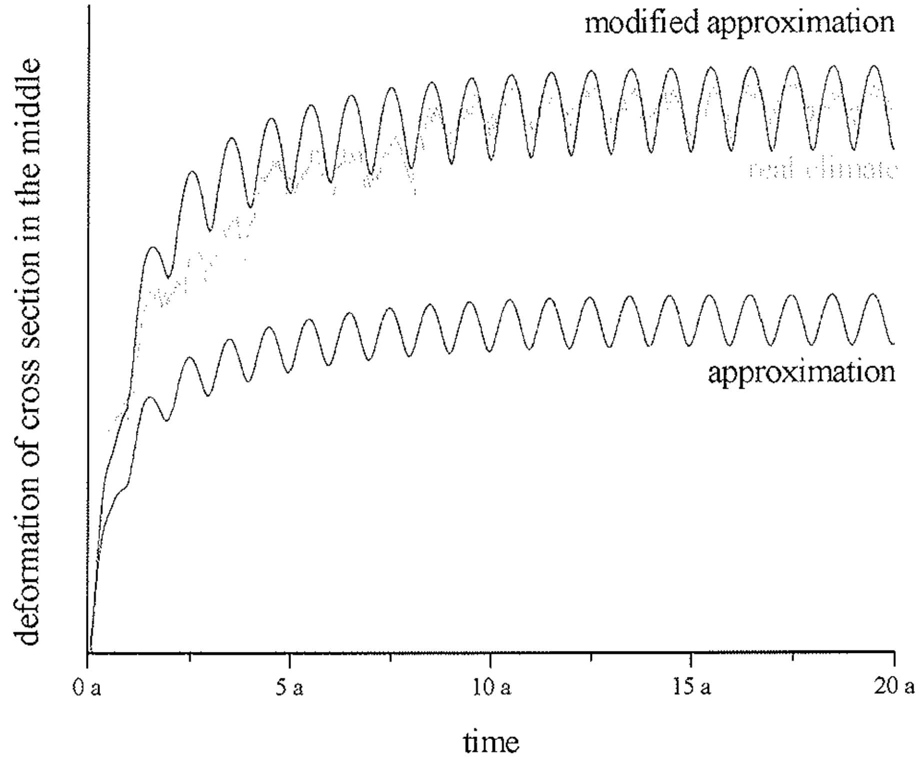

Figure 5: modified approach in service class 3

Figure 6 represents the real deformations and the modified approximated deformations in service class 1. Also the modification of equation (13) shows the best match.

The approximated formulation of the climate scenario for service class 1 is the following:

Option 4 (indoors)
$$RH = 1.4 \cdot 45\,\% + (1.23 \cdot 20\,\%) \cdot \sin\left(t \cdot \frac{2 \cdot \pi}{365\,\mathrm{d}}\right) \tag{15}$$

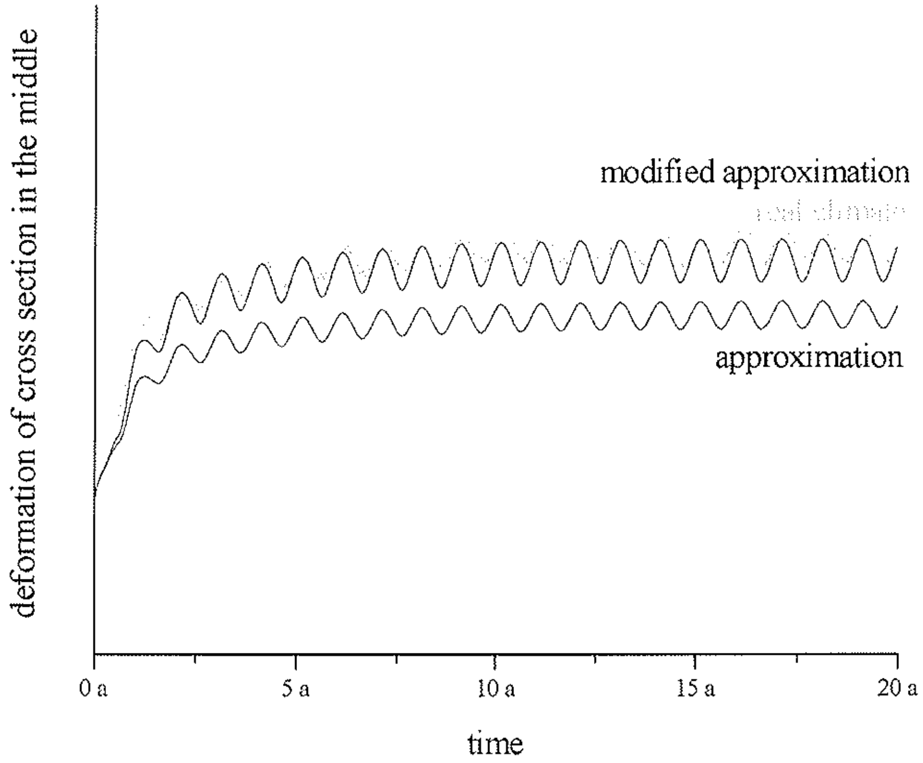

Figure 6: modified approach in service class 1

5 Summary

The wood moisture has a decisive influence on creep deformation of wooden building components and consequently on the load-bearing capacity when stability of the struts is endangered. The investigations point out, that in particular the course of the wood moisture in cross-section has a decisive influence. Meaning that the values of the deformations are more dependent on the moisture fluctuations than on the level of the average wood moisture.

The actual values of the relative humidity and the resulting wood moisture are represented by approximated functions. It is apparent that the direct approximation of the climate does not match the real result very well because the fluctuation margin misses. After modifications, satisfying agreements can be realised, and appropriate climate scenarios can be created for all service classes provided in ENV 1995-1 [5] .

6 Acknowledgements

The results were developed partly in the context of research project RA 887/1, which is sponsored by the Deutsche Forschungsgemeinschaft (DFG).

The climate data was kindly provided by Deutscher Wetterdienst (DWD).

7 References

[1] Avramidis, S., Evaluation of "three-variable" models for the prediction of equilibrium moisture content of wood, Wood Science and Technology 23, S. 251-258, 1989

[2] Becker, P., Modellierung des zeit- und feuchteabhängigen Materialverhaltens zur Untersuchung des Langzeittragverhaltens von Druckstäben aus Holz, Dissertation Universität Weimar, 2002

[3] Becker, P., Rautenstrauch, K., Proposal for compressive member design based on long-term simulation studies, CIB-W18-Proceedings, Paper 34-2-2, Venice, Italy 2001

[4] Colling F., Tragfähigkeit von Biegeträgern aus Brettschichtholz inAbhängigkeit von festigkeitsrelevanten Einflußgrößen, Dissertation Universität Karlsruhe, 1990

[5] ENV 1995-1 (EUROCODE 5) – Timber Structures, Edition 4/94

[6] Glos, P., Zur Bestimmung des Festigkeitsverhaltens von Brettschichtholz bei Druckbeanspruchung aus Werkstoff- und Einwirkungskenngrößen, Dissertation Universität München, 1978

[7] Gressel, P., Kriechverhalten von Holz und Holzwerkstoffen, Bauen mit Holz 4/84, S. 216-223, 1984

[8] Grossman, P.A.U., Requirements for a model that exhibits mechano-sorptive behaviour, Wood Science and Technology Vol 10, S 163-168, 1976

[9] Hanhijärvi, A., Ranta-Maunus, A., A three-dimensional analysis of wooden beams in bending under changing humidity conditions, IUFRO/S5.02 Timber Engineering Meeting New Brunswick, 514 - 525, 1990

[10] Hunt, D.G., Dimensional changes and creep of spruce, and consequent model reqquirements, Wood Science and Technology, Vol. 31, 1997, S. 3-16

[11] Hunt, D.G., Linearity and non-linearity in mechano-sorptive creep of softwood in compression and bending, Wood Science and Technology Vol 23 (1989), S 323-333, 1989

[12] Ranta-Maunus, A., Impact of mechano-sorptive creep to the long-term strength of timber, Holz als Roh- und Werkstoff 48, 67-71, 1990

[13] Ranta-Maunus, A., The viscoelasticity of wood at varying moisture content, Wood Science and Technology, Vol. 9, 189-205, 1975

[14] Rautenstrauch, K., Untersuchungen zur Beurteilung des Kriechverhaltens von Holzbiegeträgern, Dissertation Universität Hannover, 1989

[15] Stein, J., Physik für Bauingenieure – Grundlagen und Anwendungen, Band 2: Wärme und Feuchte, AVH-Verlag Hamburg, 1997

INTERNATIONAL COUNCIL FOR RESEARCH AND INNOVATION
IN BUILDING AND CONSTRUCTION

WORKING COMMISSION W18 - TIMBER STRUCTURES

EVALUATION OF DIFFERENT SIZE EFFECT MODELS FOR TENSION PERPENDICULAR TO GRAIN DESIGN

S Aicher
G Dill-Langer
W Klöck

Otto-Graf-Institute
University of Stuttgart

GERMANY

Presented by: S Aicher

H J Larsen and B S Choo asked about the consequences of load shearing and scale effects respectively. S Aicher replied that as the overall effect is conservative the preferred models may be used for design. S Thelandersson asked if the data set used for comparison with the analytical model were tested under a common climate regime. S Aicher replied that of the 20 data set used, 3 were conducted under EN1193 and EN408 recommendations. The remaining 17 data set were those tested by Mistler. J Ehlbeck then confirmed that the Mistler data were obtained from specimens which were at 12% +/- 1 or 2%. Discussion then centred around the question of density effects and the fact that the specimens strengths ranged from C22 to C40.

Evaluation of different size effect models for tension perpendicular to grain strength of glulam

Aicher, S., Dill-Langer, G. and Klöck, W.
Otto-Graf-Institute, University of Stuttgart, Germany

1 Introduction

Tension perpendicular to grain strength is generally considered to be a volume dependent material property, whereby the volume effect may be modelled by Weibull's weak link theory (Barrett, 1974). Several timber design codes today assume validity of the volume effect and applicability of Weibull modelling for design of tapered, curved and pitched cambered glulam beams. The neglect of stress redistribution in the volume model has evoked a competing approach with almost full stress redistribution in width and length direction of the beam, so reducing the size dependency in an approximation to a pure, however more severe depth effect (Mistler 1982, 1998). The basic empiric argument for the so-called rope and chain model, following termed depth model, is that the volume effect, unquestionably proven on the mean strength level gets considerably weaker at the 5% fractile level.

During redrafting of the German timber design code DIN 1052 the depth model gained appeal. This has to be viewed in relation to the fact that the design of douple tapered, curved and pitched cambered glued laminated timber beams (glulam) based on a volume dependent strength perpendicular to grain results in significantly increased and hence uneconomic cross-sections as compared to todays (deterministic) DIN 1052 design approach without recognition for any size effect at all.

In a pure qualitative sense it can be stated that the application of the weakest-link chain model for prediction of strength in large volumes definitely is a worst case hypothesis. Obviously, possibilities of stress redistribution due to the natural strength and stiffness variability especially in a glulam build-up are neglected in a puristic volume model. It seems to be reasonable that tension strength perpendicular to the grain of large specimens / members follows the law of partial ***parallel systems***, especially in length (parallel to fiber) direction.
The authors have taken up the discussion on preferability of volume vs. pure depth effect hereby including two additional models, a cross-sectional model and a combined 2parameter cross-sectional / length model. The latter models were then first presented in the redrafting process of DIN 1052.

This paper in a first step presents a re-evaluation of some data bases on tension strength perpendicular to grain of glulam made of European spruce. Additional European spruce glulam results and North American test data (i. a. Thut, 1970; Fox, 1974) with other species will be incorporated / evaluated in a second step. A comparison of the evaluations with empiric results from tests with curved and pitched cambered members is given separately.

2 Data bases and evaluation procedure

In an existing evaluation of the here principally regarded data base compiled by (Mistler, 1998) the results of uniaxially loaded specimens and calculated strength values obtained from curved beam tests have been combined in one data set. Further, test series with very small specimen numbers (several series with two specimens) were incorporated in said evaluation based on some special statistical treatment, too. For the purpose of this study, solely results of uniaxially loaded specimens and only test series with 10 or more specimens have been extracted from the cited data base.
Table 1 contains a compilation of the evaluated 20 test series which stem from three sources (Mistler, 1998; Blaß et al., 1998; Aicher et al., 1998). The compilation specifies the dimensions and the number of specimens per series, the median strengths, the coefficients of variation and the 5% fractiles acc. to fitted 2parameter Weibull distributions by means of maximum likelihood method.
The evaluation of the size effect was performed by linear regression fitting (sizes and strengths in logarithmic scale) of the median (50% fractile) and 5% fractile values, assuming four different size relationships / models:

$$f_{t,90} = \text{const.} \cdot \left(\frac{V_0}{V}\right)^{\frac{1}{m_V}} \qquad \text{volume model} \qquad (1a)$$

$$f_{t,90} = \text{const.} \cdot \left(\frac{d_0}{d}\right)^{\frac{1}{m_d}} \qquad \text{depth model} \qquad (1b)$$

$$f_{t,90} = \text{const.} \cdot \left(\frac{Q_0}{Q}\right)^{\frac{1}{m_Q}} \qquad \text{cross-section model} \qquad (1c)$$

$$f_{t,90} = \text{const.} \cdot \left(\frac{Q_0}{Q}\right)^{\frac{1}{m_{Q/L}}} \left(\frac{L_0}{L}\right)^{\frac{1}{m_L}} \qquad \text{cross-section / length model} \qquad (1d)$$

In eqs. (1a-d) the volume is defined by $V = B \cdot d \cdot L$ where B is the specimen (beam) width, d is specimen depth and L is the length parallel to fiber direction. Cross-section Q is defined as $Q = B \cdot d$ in the radial-tangential plane normal to fiber direction. For the respective reference sizes in eqs. (1a-d), however not relevant for the fitting of the exponents, the following values are standardized or proposed, respectively:

$V_0 = 0.01\ m^3$	acc. to EC 5
$d_0 = 0.4\ m$	proposed acc. to test standard EN 408
$Q_0 = 0.04\ m^2$	proposed acc. to test standard EN 408
$Q_0 = 0.04\ m^2$, $L_0 = 0.25\ m$	proposed analogously to $V_0 = 0.01 m^3$

In order to assess the primary important size effect at the lower end of the strength distributions with quantifiable error margins, the statistical uncertainty of the estimated fractile values due to limited number of specimen data per test series was taken into account.
For each 5% (characteristic) and 50% fractile (median) value of all test series the standard deviations of the spread around the expected value were computed assuming a normal distribution of the fractile values. Figure 1 shows exemplarily the cumulative frequencies of the empiric data and the fitted cumulative 2parameter Weibull distribution function; further the calculated probability density functions of the fractile values are given.

Table 1 Compilation of evaluated experimental data sets on tension strength perpendicular to grain $f_{t,90}$ of glulam. All test series were performed with uniaxially loaded prismatic specimens.

No.	Reference	No. of specimens	depth d	width B	length L	cross-section Q	volume V	$f_{t,90}$ median	$f_{t,90}$ C.O.V.	$f_{t,90}$ 5%-frac.
			[mm]	[mm]	[mm]	[dm^2]	[dm^3]	[N/mm^2]	[%]	[N/mm^2]
1	M	36	67	20	20	0.134	0.027	2.44	19.5	1.47
2	M	25	67.1	29	24	0.195	0.047	3.20	15.5	2.15
3	M	93	100	29	24	0.290	0.070	2.09	35.8	0.88
4	M	20	60	31	26.3	0.186	0.049	3.06	20.9	1.88
5	M	18	178	55	20	0.979	0.196	1.72	25.7	0.95
6	M	17	225	55	20.1	1.238	0.249	1.45	33.9	0.64
7	M	156	250	55	19.8	1.375	0.273	1.34	34.0	0.61
8	M	36	133	45	46	0.599	0.275	1.93	23.5	1.15
9	M	10	160	70	41	1.120	0.459	1.57	17.9	1.03
10	M	25	250	60	59.6	1.500	0.894	1.39	19.8	0.93
11	M	12	160	70	70.8	1.120	0.794	1.67	26.1	0.96
12	M	18	294	90	97	2.646	2.567	1.06	31.0	0.52
13	M	87	300	90	97	2.700	2.619	1.10	26.3	0.58
14	M	18	128	139	141	1.779	2.509	1.10	30.4	0.48
15	M	11	1104	200	100	22.080	22.080	0.65	23.0	0.41
16	M	18	1336	139	141	18.570	26.184	0.64	9.2	0.52
17	M	13	28.6	100	250	0.286	0.715	1.55	19.9	0.94
18	B	64	400	100	250	4.000	10.000	0.76	24.9	0.40
19	A	44	400	90	275	3.600	9.900	0.90	10.4	0.71
20	A	43	528	140	405	7.392	29.938	0.68	11.4	0.52

Reference abbreviations:

M:	[Mistler 1998]
B:	[Blaß et al. 1998]
A:	[Aicher et al. 1998]

The spread of the fractile values has been incorporated into the regression procedure by means of Monte-Carlo simulations: For each data set 1000 normally distributed random fractile values were generated and accordingly 1000 regression fits for each investigated size effect model (and for the two fractile levels) were performed, resulting in numerical distributions of the regression values. Thus the uncertainty of the regression values resulting from the varying and limited number of specimens per test series has been taken into account.

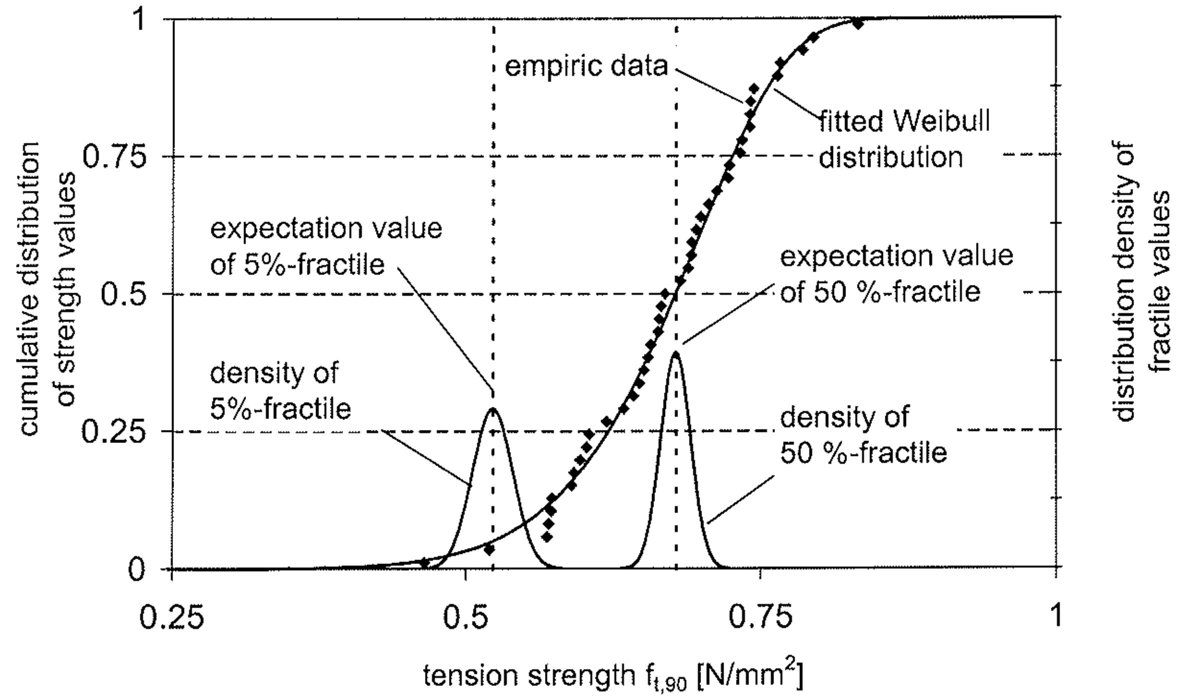

Fig. 1 Exemplary graph for the interrelation of the cumulative distribution of the empiric data set (dots), of the respective fitted Weibull distribution and of the probability densities of the 5% and 50% fractile values distributed around the expected value; data set No. 20: [Aicher et al. 1998]

3 Evaluation results

Figures 2a-c show regression plots through the 5% fractile values and Figures 3a-c give the regression lines through the 50% fractile (median) values for the three considered one-parametric models acc. to eqs. (1a-c). The expected values of the empiric 5% and 50% fractiles, respectively, are given as filled dots and the standard deviations of the respective fractiles are marked by error bars. The thick solid lines indicate the most likely regression line due to the mean value of the regression exponent. The dashed lines in Figs. 2a-c represent the upper and lower bounds, 5% and 95% fractiles of the distribution of the regression exponents resulting from the Monte-Carlo simulation. These bounds, however, solely indicate the influence of the scatter of the fractile value scatter within the respective test series as sketched in Fig.1. As these bounds are very narrow to one another at the median level, they are not depicted in Figs. 3a-c.

The 95% confidence interval for the regression line through the expected values (without recognition of scatter within the test series) is given in Figs. 2a-c and 3a-c by thin solid lines. It is evident that the uncertainty of the mean regression line through the expected values of the fractile values, as arising from the limited number of test series and limited correlation turns out to be much higher than the uncertainty arising from the scatter of the fractile values.

The results of the regression for the two-parametric cross-section / length model are graphed 3-dimensionally in Figs. 4a, b, whereby Fig. 4a shows the results for the 5% fractile level and Fig. 4b gives the results for the strength medians. The two size parameters Q and L span the x-y plane and the z-axis represents the strength values. The regression surface forms a plane in the 3-dimensional space when logarithmic scaling is applied.

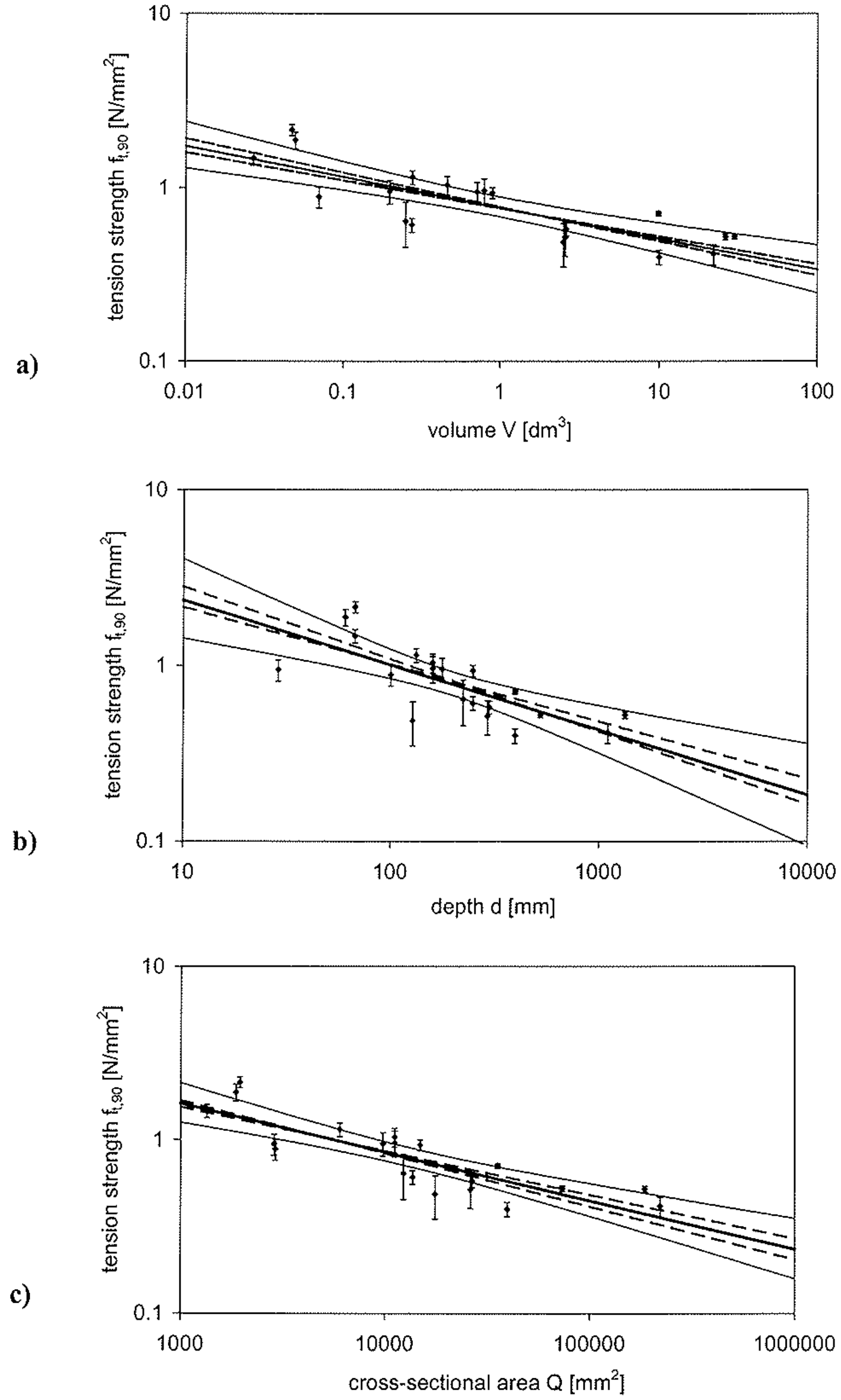

Fig. 2a-c Results of regression analysis for three size effect models applied to the 5% fractile level of tension strength perp. to grain of glulam. Given are the mean regression lines (inner solid thick lines) with 95% confidence intervals (outer solid thin lines) and the 5% and 95% boundaries acc. to scatter of the fractile values (dashed lines)

a) volume model b) depth model c) cross-sectional model

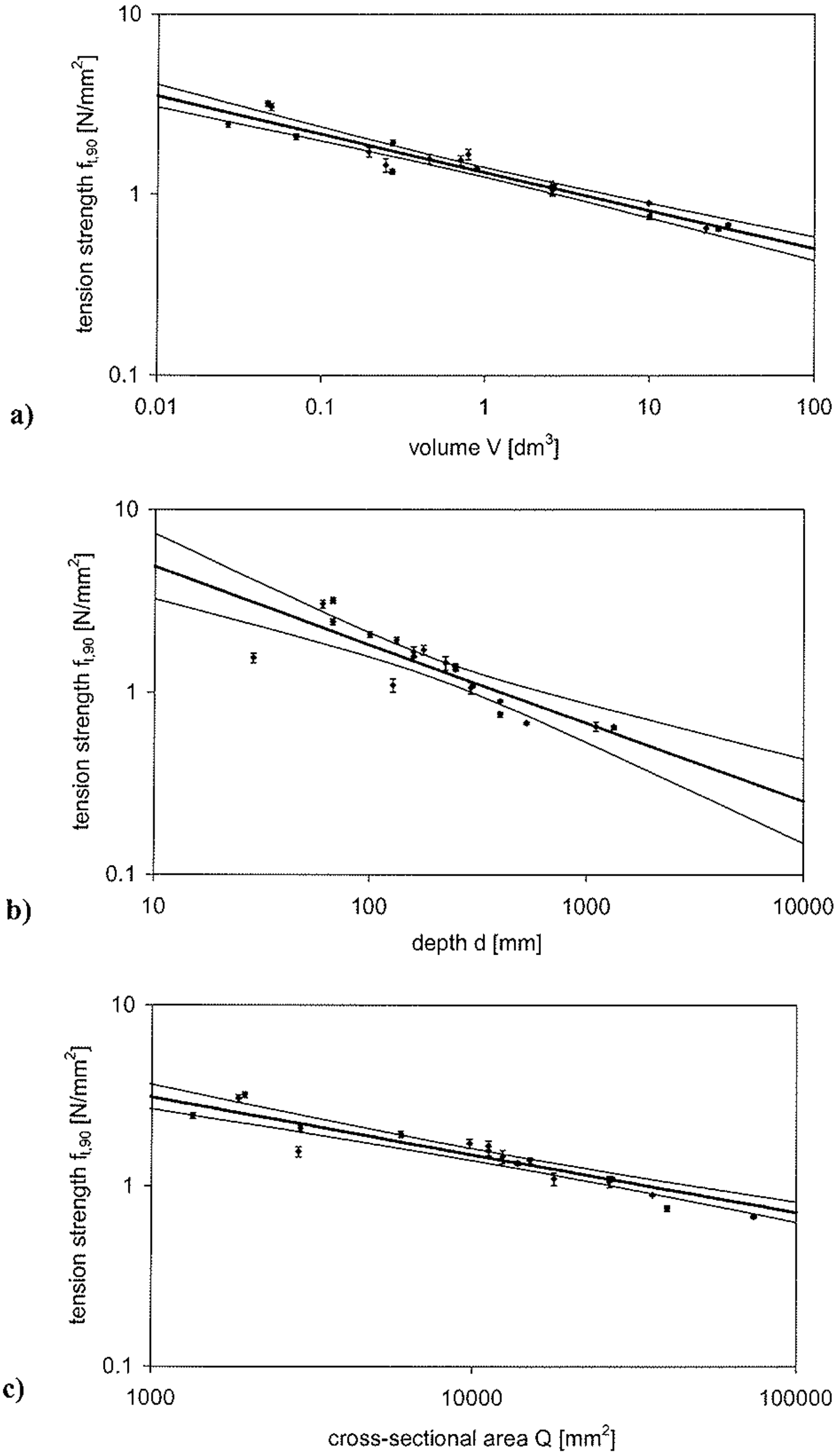

Fig. 3a-c Results of regression analysis for three size effect models applied to the 50% fractile (median) level of tension strength perp. to grain of glulam. The regression line of the mean slope (thick solid line) and the 95% confidence intervalls (solid thin lines) are given.
a) volume model b) depth model c) cross-sectional model

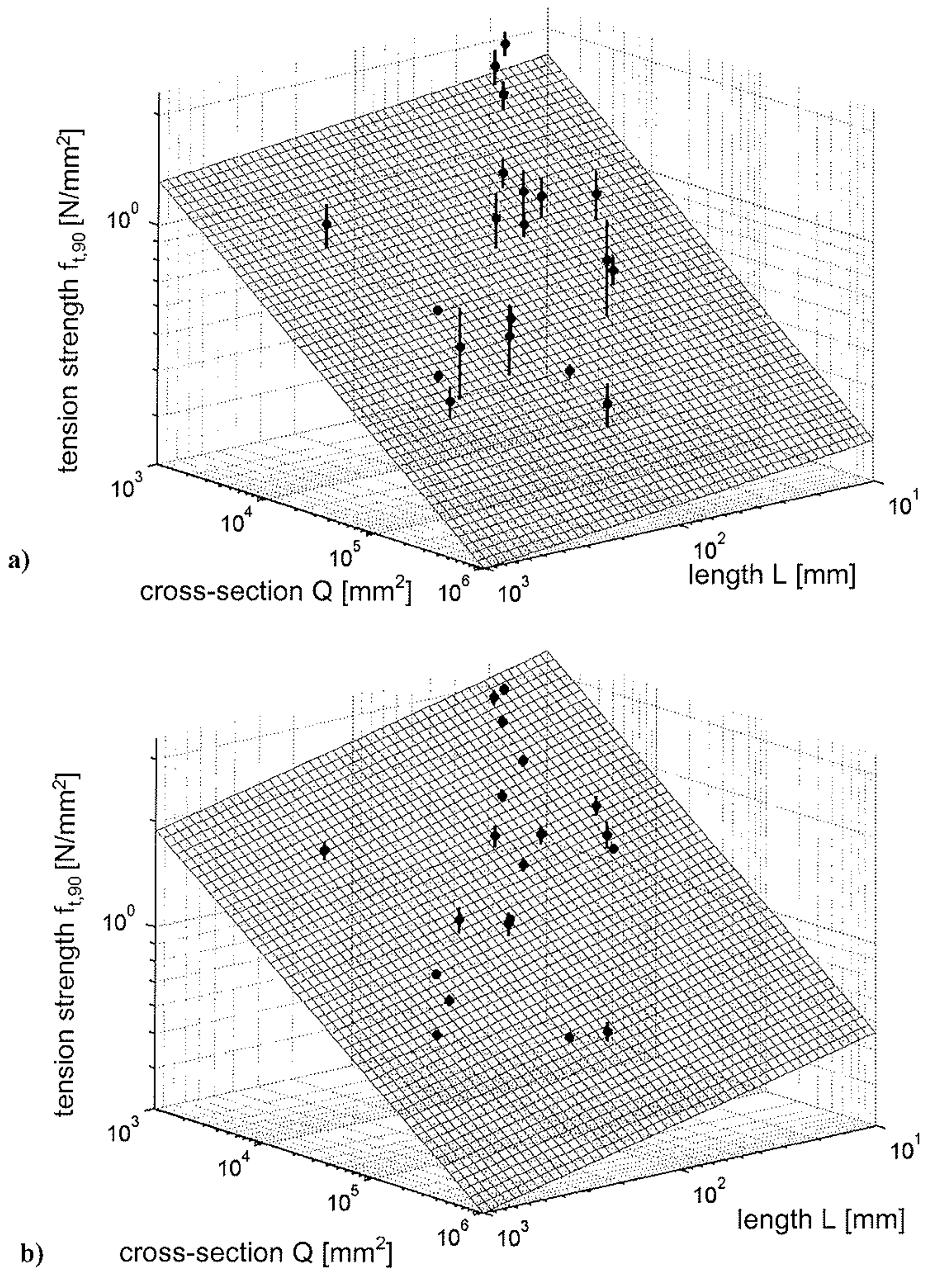

Fig. 4a, b Results of regression analysis for the cross-sectional / length model applied to the 5% and 50% levels of tension strength perp. to grain of glulam. The expected values of the fractiles (medians) are marked as dots and the standard deviations of the fractile values are given as error bars. The meshed plane represents the respective fitted cross-sectional / length model acc. to eq. (1d)

a) 5% fractile strength level b) 50% fractile strength level

Table 2 contains a compilation of the results for the size exponents of the regarded four different size effect models and their coefficients of correlation, both for the 5% (characteristic) and 50% (median) strength level. The mean values and the coefficients of variation due to scatter of the fractile values are given. Additionally, the 95% confidence boundaries of the model exponents regarding mean regression lines are listed.

Table 2 Results of regression analysis for 5% and 50% fractiles of the 20 data sets on tension strength perpendicular to grain of glulam by means of four different size effect models

Size effect model	Size exponent / C.O.C.	5% fractile (= characteristic level)			50% fractile (= median level)		
		mean value [-]	95% confid. interv. of the mean value [-]	C.O.V. (due to scatter of fract. values) [%]	mean value [-]	95% confid. interv. of the mean value [-]	C.O.V. (due to scatter of fract. values) [%]
Volume model Eq. (1a)	$\frac{1}{m_V}$	**0.178**	± 0.0616	6.7	**0.211**	± 0.0292	2.1
	R^2	0.604	-	12.9	0.918	-	1.4
Depth model Eq. (1b)	$\frac{1}{m_d}$	**0.369**	± 0.165	7.0	**0.430**	± 0.131	2.7
	R^2	0.500	-	15.4	0.716	-	3.6
Cross-section model Eq. (1c)	$\frac{1}{m_Q}$	**0.280**	± 0.0888	5.7	**0.319**	± 0.0528	2.2
	R^2	0.641	-	11.4	0.889	-	1.7
Cross-section / Length model Eq. (1d)	$\frac{1}{m_{Q/L}}$	**0.257**	-	10.5	**0.263**	-	4.1
	$\frac{1}{m_L}$	**0.056**	-	85.7	**0.132**	-	11.7
	R^2	0.659	-	11.1	0.938	-	1.1

The performed evaluation forwards the following results:

- **Generally**, as anticipated, the coefficient of correlation is higher and the variation of the model exponent is smaller for the 50% fractile (median) level as compared to the 5% (characteristic) level.

- The **volume model** acc. to eq. (1a) reflects the above statement most expressed with a coefficient of correlation of $R^2 = 0.92$ for the 50% fractile decreasing to $R^2 = 0.60$ for the 5% fractile. The exponent of $1/m_V = 0.21$ for the 50% fractile level conforms very well with the value of $1/m_V = 0.2$ given in Eurocode 5, based on Barrett (1974). In case of the 5% fractile level, the model (size) exponent is somewhat lower ($1/m_V = 0.18$ as compared to 0.21) with a considerably decreased R^2.

- The **depth model** acc. to eq. (1b) yields the worst coefficients of correlation within the evaluated four size effect approaches, both, on the median ($R^2 = 0.72$) and on the characteristic ($R^2 = 0.50$) level. The relatively high values of the model exponents (relatively steep slopes in the diagrams) of $1/m_d = 0.37$ (5%-fractile) and $1/m_d = 0.43$ (median) show that depth seems to be an important parameter for tension strength perpendicular to grain; however, the low correlation quality indicates that the sole recognition of this single dimension does not yield a size effect description with satisfactory prediction quality.

- The **cross-section model** acc. to eq. (1c) yields coefficients of correlation of about the same magnitude as in case of the volume model. For the 50% fractile level the correlation is slightly weaker ($R^2 = 0.89$) and for the 5%-fractile a slightly stronger ($R^2 = 0.64$) relationship than for the volume model is obtained. The model exponent of the cross-sectional approach is markedly higher as compared to the volume model for both fractile levels, being $1/m_Q = 0.28$ and 0.32 for the 5% and 50% level, respectively. Thus, cross-section Q seems to be the most important (single) parameter for the size effect of tension strength perpendicular to grain of commercial grade glulam.

- The **two-parameter model** with combined action of cross-section Q and length L acc. to eq. (1d) turned out to fit the empiric data sets best. Comparing the coefficient of correlation for the median level of the cross-section/length model ($R^2 = 0.94$) to that of the volume model ($R^2 = 0.92$) the difference is still small; however, on the characteristic level an apparently better performance of the 2-parameter model with $R^2 = 0.65$ vs. $R^2 = 0.60$ for the volume model can be stated.
  The most interesting result arises from the ratio of the cross-section exponent $1/m_{Q/L}$ vs. the length exponent $1/m_L$: on the median level a ratio of roughly 2:1 is obtained whereas on the characteristic level the ratio approaches a value of nearly 5:1. The latter result is accompanied by an extremely high coefficient of variation of 85% for the length exponent. Thus the performed evaluation yields a drastic decrease of the length influence vs. the cross-section influence on tension strength perpendicular to grain when proceeding from the 50% to 5% fractile level. This is qualitatively in line with the above given ideas of stress redistribution in length direction.

4 Conclusions

The size effect of tension strength perpendicular to grain of glulam has been assessed by a comparative evaluation of four different model approaches by means of 20 empiric series of uniaxial tension tests with a minimum number of 10 specimens per series. The regression analysis with recognition of scattered input values was carried out, both, on the 5% fractile (characteristic) level and on the 50% fractile (median) level. The results can be summarized as follows:

- The pure depth model shows the worst correlation coefficients of all four evaluated approaches and the largest confidence intervals of the model coefficients both on the median and on the characteristic level.

- The volume model, as anticipated, works well on the median level; however, the correlation coefficients decrease and the confidence intervals increase markedly for the design relevant 5% fractile strength level.
- The cross-section model when compared to the volume model shows roughly a similar performance. On the median level the regression and confidence interval values are slightly worse whereas the model tends to result in better values for the 5% fractile strength level.
- The combined cross-section / length model yields the best results, especially on the 5% fractile level, there with the significantly highest coefficients of correlation. On the characteristic level the exponent of the cross-section $1/m_{Q/L}$ is pronouncedly, by about a factor of 5 higher compared to the length exponent $1/m_L$.

A comparison of the volume model vs. the combined cross-section / length model yields clues for the assumption that tension strength perpendicular to the grain of glulam may be markedly more dependent on cross-sectional dimensions than on length dimensions. Thus the question arises whether the extrapolation from relatively small tension specimens to structural sized beams yields considerably too low resulting strength values when the volume model is applied. This question should be assessed by a (re)-evaluation of existing / new data of curved, tapered and pitched cambered beams. Hereby the problems arising in case of 5% fractile evaluation from the economically bound very small numbers of specimens per test series have to be considered.

5 References

Aicher, S., Dill-Langer, G., Ranta-Maunus, A. (1998): „Duration of load effect in tension perpendicular to grain of glulam in different climates." Holz Roh- Werkstoff 56, 295-305

Barrett, J. D. (1974): „Effect of size on tension perpendicular-to-grain strength of Douglas-Fir". Wood and Fiber Science, 6 (2): 126–143

Blaß, H. J., Ehlbeck, J., Schmid, M. (1998): „Ermittlung der Querzugfestigkeit von Voll- und Brettschichtholz." Research Report, Versuchsanstalt für Stahl, Holz und Steine, University of Karlsruhe

Fox, S. P. (1970): „ Strength and stiffness of laminated Douglas-fir blocks in perpendicular-to-glueline tension". Wood and Fiber Science 6(2): 156-163

Mistler, H.-L. (1982): „Über die Querzugfestigkeit von Fichten-Brettschichtholz in Abhängigkeit von der Bauteilgröße und der Verteilung der Beanspruchung". Ingenieurholzbau in Forschung und Praxis. Edts. J. Ehlbeck and G. Steck, Bruder-Verlag, Karlsruhe, Germany

Mistler, H.-L. (1998): „Design of glulam beams according to EC 5 with regard to perpendicular to grain tensile strength – a comparison with research results." (in German) Holz Roh- Werkstoff 56, 51-59

Thut, W. K. (1970): Stresses in pitched cambered glulam beams. M.S. thesis. Univ. Br. Columbia, Dep. Civ. Eng., Vancouver

CIB-W18/35-6-2

INTERNATIONAL COUNCIL FOR RESEARCH AND INNOVATION
IN BUILDING AND CONSTRUCTION

WORKING COMMISSION W18 - TIMBER STRUCTURES

TENSILE STRENGTH OF GLULAM PERPENDICULAR TO GRAIN - EFFECTS OF MOISTURE GRADIENTS

J Jönsson
S Thelandersson

Div. of Structural Engineering
Lund University

SWEDEN

Presented by: S Thelandersson

G Gonzalez asked how many replicates were used and if the data was sufficient for statistically valid conclusions. S Thelandersson replied that there were 4 replicates for each of the data points shown and was of the view that it was sufficient to provide a fair impression of the variation in behaviour trend. S Aicher asked if the observed effects could be due to the assumed plane stress or plane strain conditions and R Gutkowski asked if there were shrinkage cracks. S Thelandersson replied that no shrinkage cracks were observed but that there were cracks which were due to the drying process. J Ehlbeck then commented that as k_{mod} for stress perpendicular to grain is generally different from other k_{mod} values, the historical approach has been to use fictitious strength values whilst maintaining a common k_{mod} value in EC5.

Tensile strength of glulam perpendicular to grain - effects of moisture gradients

Johan Jönsson, Sven Thelandersson
Div. of Structural Engineering
Lund University, Lund, Sweden

Abstract

Experimental results are presented concerning tension perpendicular to grain in glulam sections where internal stresses induced by climate changes are present. The results reveal that moisture induced internal stresses may affect the tension capacity both in a positive and a negative way compared to reference specimens, free from moisture gradients. The tension capacity is reduced during moistening from RH 40% up to RH 80% whereas it is increased during drying from RH 80% to 40%. The tension capacity during wetting is only 50 % of that observed for drying specimens. This behaviour can be explained by the combination between initial moisture induced stresses and stresses from external loading. The same tendency was observed for specimens exposed to cyclic climate changes, where it was also found that time and numbers of cycles do not affect the tension capacity in any specific direction.

1. Introduction

For timber structures, the majority of failures observed in practice are due to tension perpendicular to grain. Tension perpendicular to grain commonly occurs e.g. in curved elements, in joints in timber structures, and in discontinuities created by wholes and notches in timber members. The values of tensile strength perpendicular to grain used in engineering design are quite low and are assumed to depend on the magnitude of the stressed volume see e.g. Aicher et al (1998). However, the facts that internal moisture induced stresses are more or less always present in timber members are not taken into account. This means that commonly used design procedures are associated with large uncertainty, and the influence of moisture exposure is considered in a very crude and uncertain way. Gustafsson et al (1998) showed that the load bearing capacity of notched beams depends strongly on the time of the year, i.e. on the moisture gradients present in the member.

It was shown in previous papers by Jönsson (2001a) and Jönsson (2001b), that large internal stresses are developed in the cross-grain direction when specimens from glulam beams are exposed to changing climate. The stresses originate from the moisture gradients due to non-uniform shrinkage and swelling perpendicular to grain. Under natural climate exposure outdoors under shelter, the stress level in some part of the specimens exceeded the characteristic value, during several weeks. According to Ranta-Maunus et al (1994), research regarding the capacity of curved beams with moisture gradients showed that *"the conclusions is that the magnitude of the moisture induced stresses is the primary reason for failure, not the number of cycles or duration of load. A combined moisture content and structural analysis indicates that stress distribution is essentially the same during successive moisture cycles"*. This statement is supported by the results in Jönsson (2001a) where measurements of internal stresses were made on specimens exposed to cyclic climate.

Thus, the capacity of timber members subjected to external loads creating tension stresses perpendicular to grain is a result of interaction between moisture induced self-balancing stresses and the stresses induced by the loads. By adding these effects, a stress field is obtained which can be used as a basis to predict failure. The spatial variation of this stress field is however usually quite different from that obtained from the external loading alone and the fact that statistical volume effects are also quite significant means that the failure criterion in this case is far from simple. Ranta-Maunus (1996) introduced a so called Weibull stress, which is a measure of the tension stress intensity in a region considering at the same time the volume under stress. Depending on the spatial stress distribution the perpendicular to grain failure process can be significantly different. Models based on fracture mechanics need to be employed to understand this type of behaviour, Gustafsson et al (1996).
To verify different theoretical methods, experimental results about how the capacity perpendicular to grain is affected by internal stresses are needed. Very few investigations are available for this. The results presented in Jönsson (2001a and b) gives a detailed picture of the distribution and magnitude of the internal stresses induced by moisture exposure. In this paper, static tension tests have been performed on the same type of specimens and with identical moisture exposure. This gives a unique experimental data base for studying the influence of moisture induced stresses on tension capacity, since the initial stress states in all tested specimens are known from the previous investigation. The results from these tests are presented and interpreted in this paper.

2. Material and methods

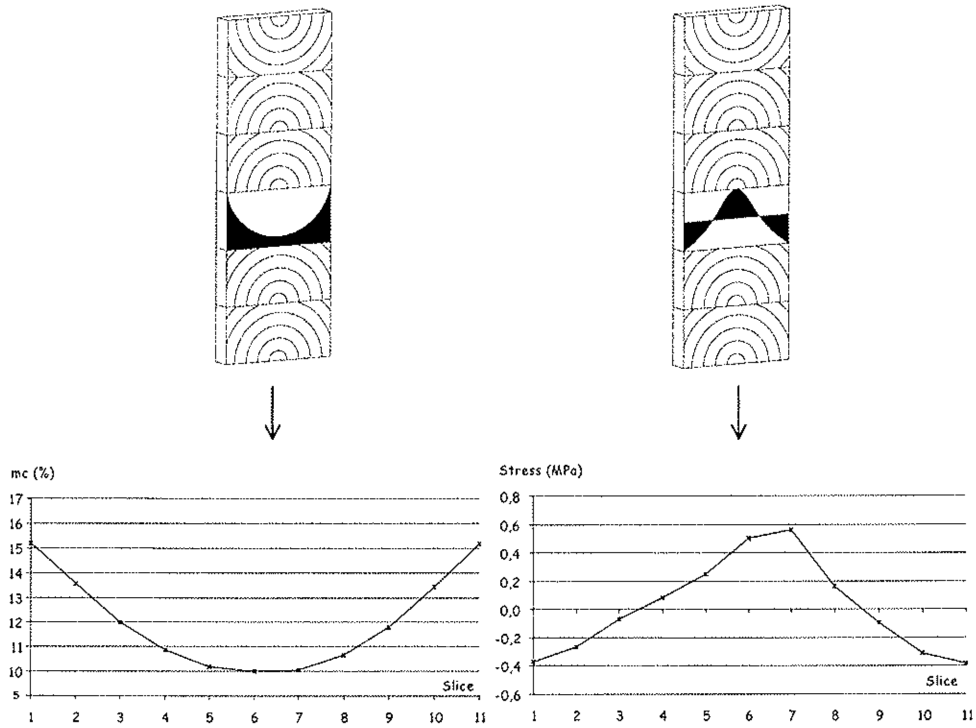

Figure 1. Moisture distribution day 11, after placement in RH 80% for specimen initially conditioned in RH 40% (left) and corresponding internal stresses (right).

The specimens used in the tests are cut from glulam beams (90x270, quality L40) containing 6 lamellae. Their thickness is 16mm so that the size of the specimens becomes 16x90x270mm. The specimens are moisture sealed to ensure a one-dimensional moisture flow, leading to moisture gradients and internal stresses in the cross-grain direction, as shown in figure 1. A thorough description of the material and treatment prior to testing is given in Jönsson and Svensson (2000) and Jönsson and Svensson (2001).
To investigate the influence of internal stresses on the short-term strength perpendicular to grain, the specimens shown in figure 1 were taken direct from the climate chamber and tested in uniaxial tension in a servo hydraulic testing machine. The specimens were clamped in a fixture made for this test, see figure 2. Due to the design of the clamping device, the test length was shorter than the actual length of the specimen. Load was applied by controlling the displacement at the rate of 0.025 mm/sec. The test gives the relation between force and displacement, which is measured over a length of 225 mm.

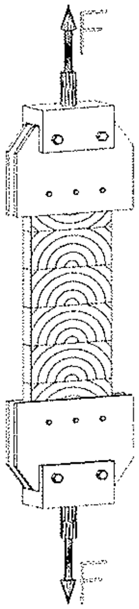

Figure 2.Test arrangement.

3. Test program

The test program is divided in two different types of tests A and B. In both cases, the specimens are affected by internal stresses perpendicular to grain due to climate change. In a test series performed before, the same types of specimens were exposed to the climatic conditions used in the present tests, and the internal stresses were measured. The methodology and results from these tests are presented in Jönsson & Svensson (2000) and Jönsson (2001a,b). This means that the moisture distribution as well as the internal stress distribution has been determined for reference specimens treated in the same way as the specimens used for the present strength tests. For tests of type A, the specimens are exposed to a single climate change. Prior to testing, the specimens were seasoned in RH 40% or 80% and the specimens seasoned in 40% where then placed in 80% and vice versa. For type A tests, a total of 128 specimens were used, divided into 8 groups with 16 specimens in each group, see figure 3. In each group, 8 specimens were kept in the initial constant climate while the rest of them were subjected to drying or wetting, creating internal stresses, see figure 1. All the specimens in one group are taken in a sequence, from the glulam beam. This means that smaller knots are present but no checks or finger joints.

The specimens were taken out from the climatic treatments at different occasions for tension testing.

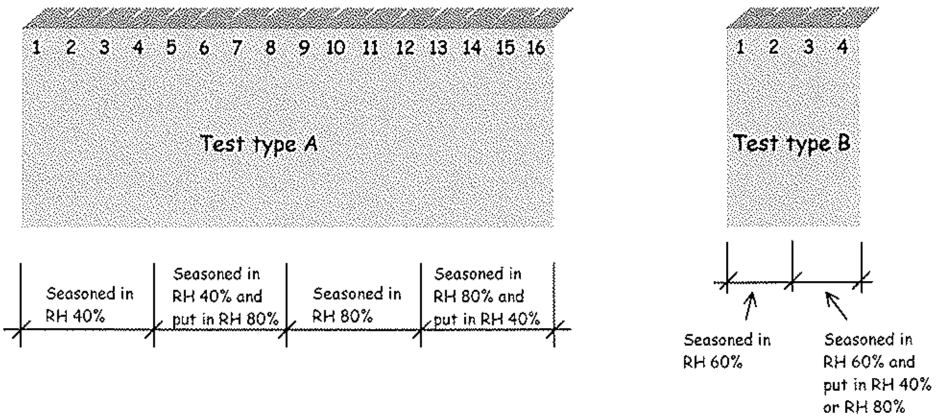
1 2 3 4 5 6 7 8 9 10 11 12 13 14 15 16
Test type A
Seasoned in RH 40%
Seasoned in RH 40% and put in RH 80%
Seasoned in RH 80%
Seasoned in RH 80% and put in RH 40%
1 2 3 4
Test type B
Seasoned in RH 60%
Seasoned in RH 60% and put in RH 40% or RH 80%

Figure 3. Selection of specimens.

In tests type B, the specimens are exposed to cyclic climate and the tension strength perpendicular to grain is again determined at different occasions. The specimens were seasoned in RH 60% and then exposed to drying in RH 40% and wetting in RH 80% during consecutive 7-day periods. For type B, 84 specimens were tested and in this case they were divided into 21 groups with 4 in each group, taken in sequence from the glulam beam, see figure 3. Table 1 summarises the test program.

Table 1 Test program

Test type	Seasoned in relative humidity	Climate exposure	Total number of specimens	Specimens tested each time	Day of testing
A	40%	-	32	4	-
	80%	-	32	4	-
	40%	80%	32	4	1,3,5,7,11,24,36,38
	80%	40%	32	4	1,3,5,7,11,24,36,38
B	60%	-	42	2	-
	60%	Cyclic:40 and 80%	42	2	3.5,10,17,24,31,38, 45,52,59,66,73,80 87,94,101,108,115, 122,129,136,143

4. Results and discussion

4.1 Type A, single climate step, RH 40 to 80% or 80 to 40%

Tests were made on 8 different occasions during the wetting as well as the drying process. The moisture distributions across the width of the glulam cross section on these occasions are shown in figure 4. These results are taken from an earlier test series, with the aim to measure moisture-induced stresses, see Jönsson (2001a,b). Figures 5, 6 and 7 show the tension strengths for reference and gradient specimens versus day of testing, where the data points are average values from 4 specimens. In these figures, the strength is defined as the maximum load F_u at failure divided by the cross section area A.

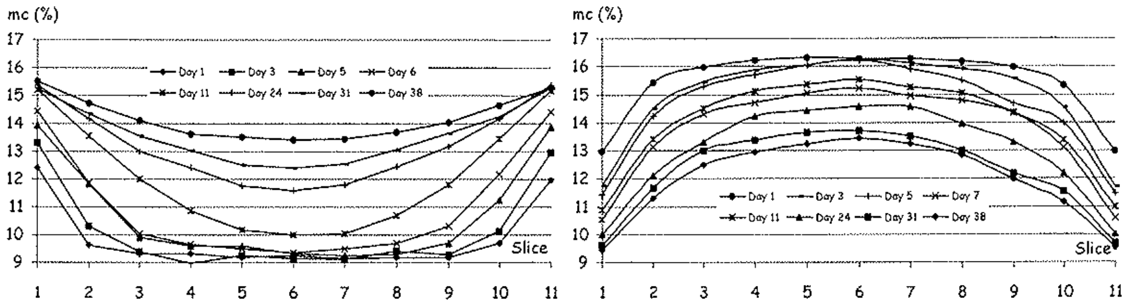

Figure 4. Moisture distribution for wetting and drying specimens between RH 40 and 80%.

Figure 5 shows the strengths from the reference specimens conditioned at RH 40% and 80% up to the time of testing. These reference tests were performed at the same occasions as the gradient specimens exposed to drying or wetting. Reference specimens and gradient specimens tested at the same day are matched with each other as shown in figure 3. Figure 5 shows that the average strength at constant moisture condition is 60 % higher for RH 40 % than for RH 80%. The variation in strength is small between the test occasions. The standard deviations are 0.19 MPa and 0.13 MPa for RH 40% and 80 % respectively, considering all the 32 tests at each moisture level.

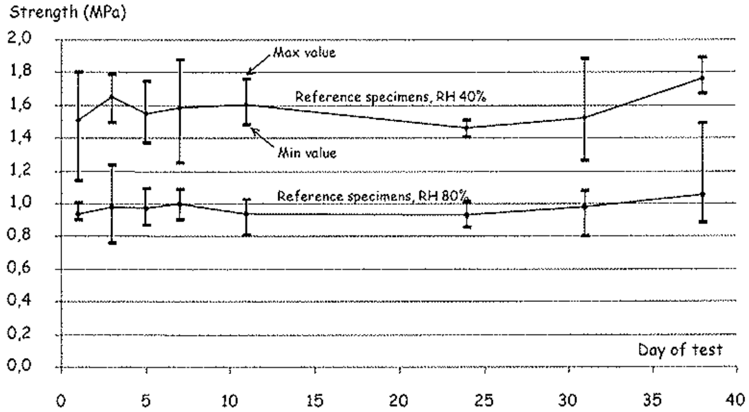

Figure 5. Strength of reference specimens at constant moisture states corresponding to RH 40 and 80 %.

Figure 6 shows that the tension capacity is reduced significantly during the wetting process from RH 40 to RH 80 %. Already after 5 days of moistening, the strength is lower than the reference specimens seasoned in RH 80%. Later in the wetting process the strength is about 30% lower than the strength of the 80% reference specimens and only half of the strength of the 40% reference specimens.

For the opposite case when the specimens are drying, figure 7, an initial increase in strength is observed, and the strength during the continued drying process is only marginally lower than the strength of the 40% reference specimens. The strength development of the gradient specimens is the result of the combined effect of moisture induced stresses and changes in the mechanical properties with moisture content.

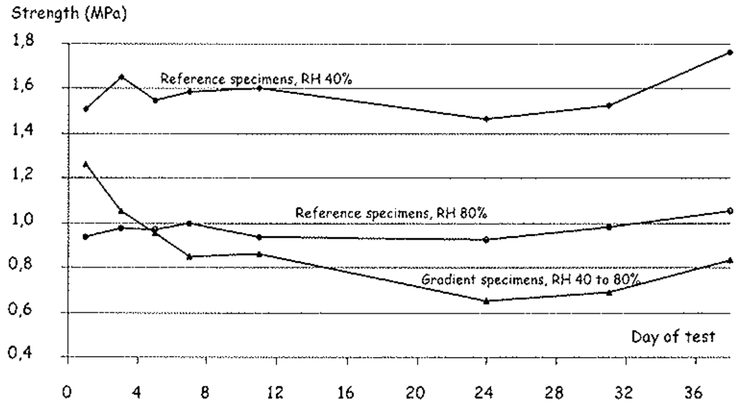

Figure 6. Development of tensile strength perpendicular to grain for gradient specimens in wetting phase compared with reference specimens.

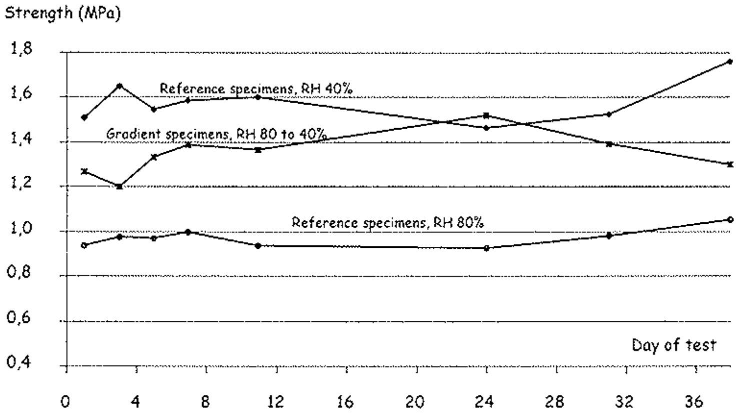

Figure 7. Development of tensile strength perpendicular to grain for gradient specimens in drying phase compared with reference specimens.

For the gradient specimens under wetting, the combination between internal stresses and external force leads to a non-brittle failure. Cracking starts in the middle part with a small crack, which is growing in a stable way until final failure, see figure 8.

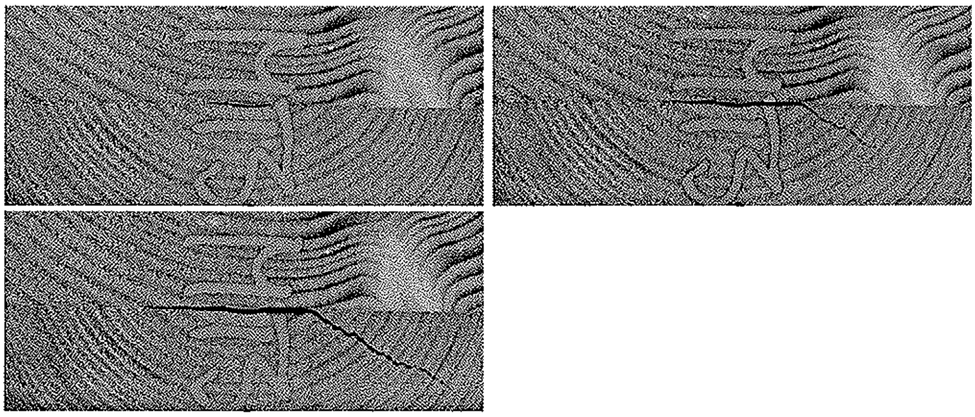

Figure 8. Crack propagation in gradient specimens, RH 40 to 80%, tested at day 5.

For the drying specimens the behaviour is quite different. The cracking seems to start at one of the edges with non-stable crack growth, leading to a brittle failure. This can be seen in figure 9 where stress-deformation curves during the tension tests are plotted. The stress in the gradient specimen, in the wetting phase, increases, even after a crack is formed. This can be seen as a non-linear response in figure 9, whereas for the gradient specimen under drying, the stress–deformation relation is linear up to the point of failure.

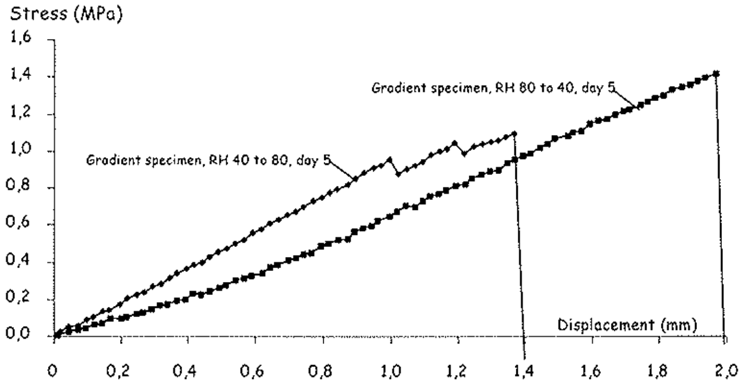

Figure 9. Stress versus deformation for drying and wetting specimens, RH 40 and 80%.

4.2 Type B, cyclic climate change

The specimens in these tests were exposed to cyclic climate, with intervals between drying and wetting phases of 7 days. The specimens where initially seasoned in RH 60%, moisture sealed and then put into a climate chamber were the climate was changing from RH 40 to 80%, see figure 10. Specimens for tension testing, see figure 3, were taken out at the ends of each 7-day period, after a wetting period (W-state) or after a drying period (D-state).

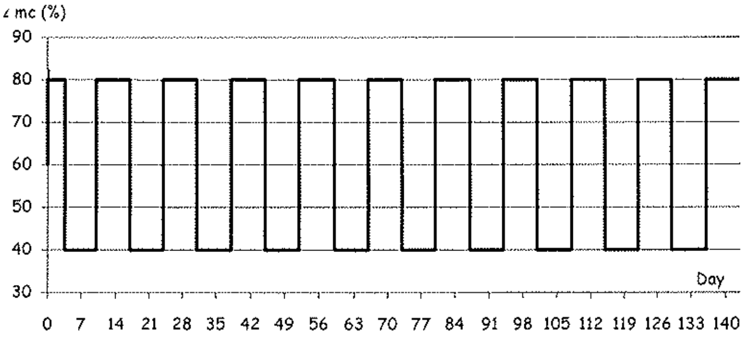

Figure 10. Cyclic climate change.

The same type of exposure was used in a previous investigation of moisture-induced stresses, Jönsson (2001a,b). Typical results after a drying period (D-state) and a wetting period (W-state) are shown in figure 11. It was shown in Jönsson (2001 a,b) that the internal stresses oscillated between these two states during the cyclic tests, with no significant changes from cycle to cycle.

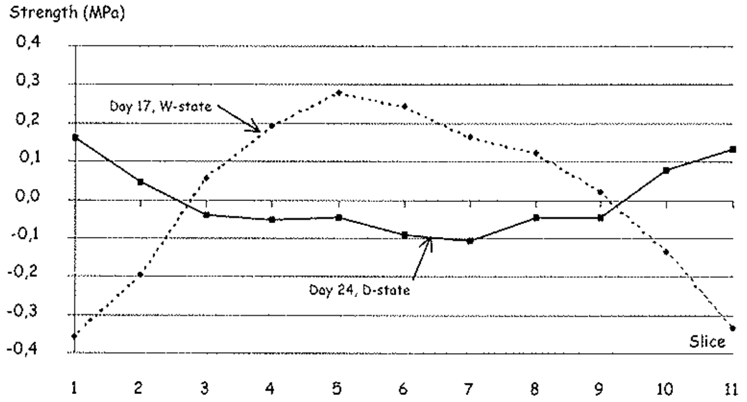

Figure 11. Internal stress state due to cyclic climate change. W=test after a wetting period, D=test after a drying period.

Figure 12 shows the results from the tension tests expressed as failure load F_u divided by area A. Results from two different tests are shown for each day of testing:

1) Average of two matched *reference specimens*, exposed to constant climate (RH 60 %) up to the time of testing.
2) Average of two *gradient specimens* in either W-state or D-state.

The overall variation in strength is from approximately 0.9 to 1.8 MPa. A general pattern is that the strength in W-state is lower, and the strength in D-state is mostly higher than the strength of reference specimens. The differences are displayed in figure 13. There is a considerable variation from cycle to cycle, but there is no tendency showing accumulated effects from repeated cycles. The scatter is probably mostly due to the variation between the different specimens, inevitable since strength cannot be tested more than once for each individual specimen. The overall average values of strengths are shown in table 2. The tension capacity for specimens in W-state is significantly lower than for specimens in D-state. The coefficient of variation (COV) is surprisingly low in view of the fact that a brittle type failure load is observed for specimens taken from different glulam beams. The COV is of the same order of magnitude for gradient specimens and reference specimens.

Table 2. Results from tests type B, failure load per unit area, MPa.

Type	Number of specimens	Mean strength (MPa)	Coefficient of variation (%)
Gradient specimens, W-state	22	1.22	15
Gradient specimens, D-state	20	1.52	17
Reference specimens, RH 60%	42	1.37	17
All together	84	1.37	18

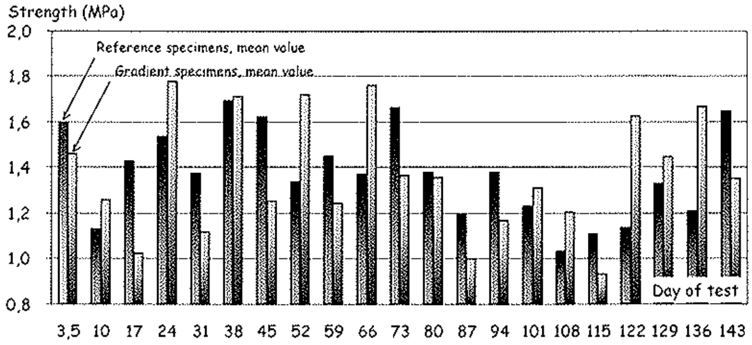

Figure 12. Strengths of gradient and reference specimens.

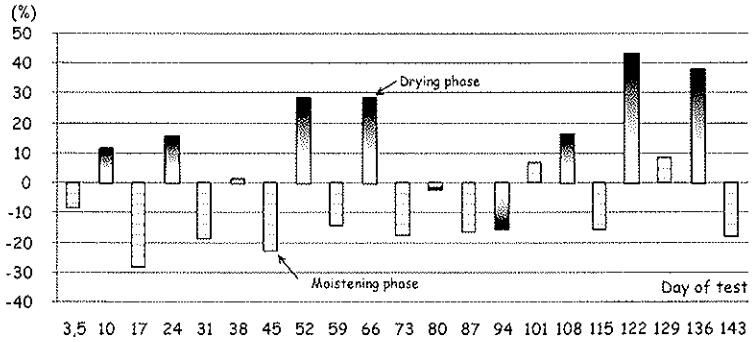

Figure 13. Difference in strength between gradient and reference specimens as a percentage of strength of reference specimens.

5. Analysis of effects of stress distributions in cross section.

For the results shown above, the "strength" is calculated under the assumption that the stress is uniformly distributed over the tested cross section area. This assumption is not valid for two reasons.

1) For specimens with moisture gradients internal self-balancing stresses (eigenstresses) are present before the start of tension testing, see figures 1 and 11.
2) The elastic modulus in the loading direction, varies significantly over the width of the specimen, see Jönsson (2001a,b).

For given moisture content, the elastic modulus is about three times larger in the central part of the specimen than in the outer parts, Jönsson & Svensson (2000). This is due to the orientation of annual rings in the lamellas, with predominant radial directions in the central part.

The actual stress distribution when the specimen fails is a combination of non-uniform initial stress $\sigma_i(x)$ and non-uniform stress $\sigma_e(x)$ imposed by the external loading during the test, where x is a co-ordinate in the width direction of the specimen (perpendicular to the loading direction).

Equilibrium just before failure at load F_u gives

$$F_u = \int_A \sigma_e(x)dA + \int_A \sigma_i(x)dA = \int_A \sigma_e(x)dA \qquad (1)$$

where A is the area of the cross section. The second integral is zero since the initial stress distribution $\sigma_i(x)$ is self-balancing. Assuming elastic behaviour, we have

$$\sigma_e(x) = \varepsilon(x)E(x) = kE(x) \qquad (2)$$

where the strain $\varepsilon(x)$ is assumed to be constant and equal to k over the area A. Equation (1) can now be written as

$$F_u = k\int_A E(x)dA = kA\overline{E} \qquad (3)$$

where $\overline{E} = \frac{1}{A}\int_A E(x)dA$ is the average elastic modulus over the cross section A.
The combined stress $\sigma_c(x)$ is given by

$$\sigma_c(x) = \sigma_e(x) + \sigma_i(x) = \frac{F_u}{A}\frac{E(x)}{\overline{E}} + \sigma_i(x) \qquad (4)$$

where equations (2) and (3) have been utilised.

The initial stress $\sigma_i(x)$ and the variation E(x) is known from a previous investigation, which means that the combined stress distribution $\sigma_c(x)$ at failure can be calculated from equation (4). Figures 14 and 15 show the results from this calculation for one wetting and one drying test respectively (test type A, day 5). The contributions from moisture induced internal stresses and from external loading are also shown together with the mean stress F_u/A. The maximum combined stress for the specimen under wetting, figure 14, is of the order 2 MPa, and occurs in the central part, whereas the stress at the sides is much lower. It is therefore natural that cracking is initiated at the centre in this case, although the local strength is probably higher in this zone with loading in the radial direction.
For the specimens under drying, Figure 15, the maximum combined stress is also found in the centre of the specimen, but the stress is much more uniform in this case. The combined stress is only marginally lower at the sides, where the loading direction is between radial and tangential. Since the tensile strength of wood is very low in this direction, it is not surprising that cracking is first initiated at the sides of the specimen. The fact that the combined stresses are rather uniform implies that the mean stress at failure is higher in this case.

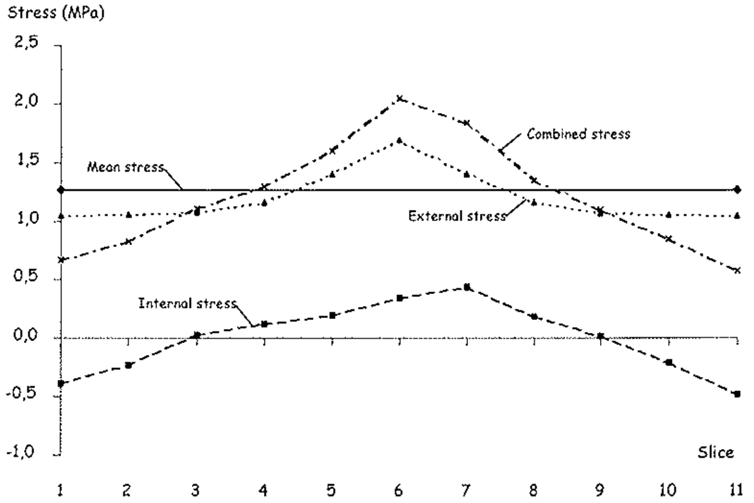

Figure 14. The combination between internal and external stress for specimens under wetting, day 5.

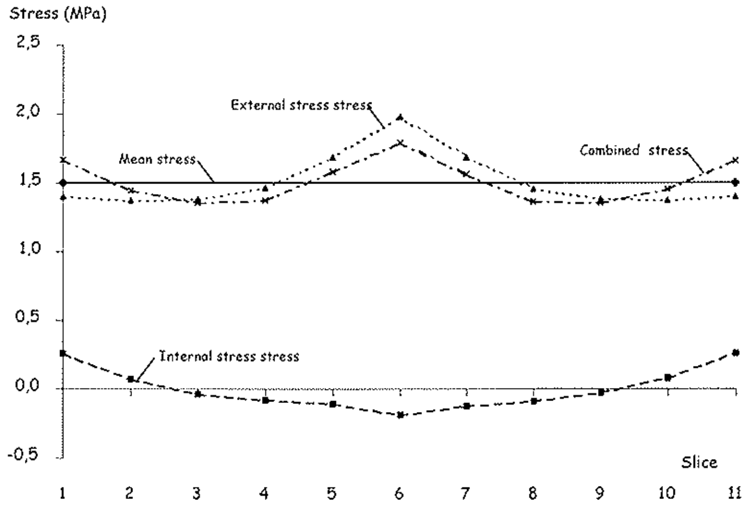

Figure 15. The combination between internal and external stress for specimen under drying, day 5.

Similar calculations have been done for all tests of type A, and the results are plotted in figure 16. The maximum value of the combined stress σ_c is shown together with the average stress for specimens under wetting (dotted curves) and drying (full line curves). For drying specimens, the difference between maximum local stress and mean stress is much lower than for wetting specimens. This explains that the tension capacity is generally very little affected by moisture gradients under drying. The opposite is valid for wetting. For both cases, drying and wetting, the maximum stress is located in the middle of the specimens.

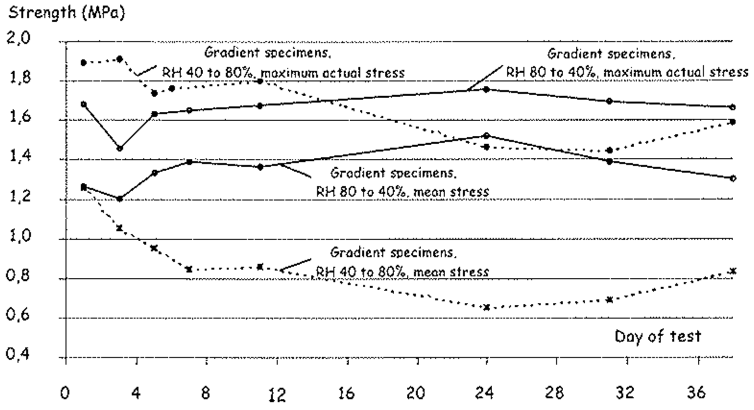

Figure 16. Difference between maximum stress and mean stress

6. Conclusions

The tests presented in this paper were made to investigate the effect of moisture-induced eigenstresses on the tension capacity perpendicular to grain in glulam. The following conclusions can be made

- The tension capacity under constant moisture conditions depends strongly on the moisture content. The strength increases by 60 % from RH 80 % to RH 40 %.
- The influence of moisture-induced stresses on the tension strength depends on whether the specimens are in a drying or in a wetting phase.
- Drying from RH 80 to 40% reduces the tension capacity only marginally.
- Moistening from RH 40% to 80% reduces the tension capacity significantly

- This behaviour was explained by studying the combination between initial moisture induced stresses and stresses from external loading during tension testing.
- In the case of moistening, stresses are added in the inner part leading to a very non-uniform distribution of stress across the width of the specimen.
- In the case of drying, the combined stresses lead to more uniform stress distribution.
- Tests results from cyclic climate changes indicate again that when specimens are in a drying state the tension capacity increases (1.52 MPa), whereas it decreases in the moistening state (1.22 MPa), compared to reference specimens free from moisture gradients (1.37 MPa). Numerical values given here are the mean from all tested specimens
- Time and number of cycles do not seem to affect the tension strength in any specific direction.
- To minimize the moisture gradients in load carrying wooden products during the serviceability state, the surface should be treated with some moisture damping material such as paint, varnish, wax etc.

It is clear that the service class reduction factors in codes need to be re-evaluated in the light of these results and other research findings dealing with interaction between moisture exposure and mechanical performance of wood. The characteristic value of the tensile strength perpendicular to grain for softwood of the type tested here is of the order 0.5 MPa. Eurocode 5, prEN 1995-1 (2001) prescribes a value of k_{mod}=0.9 (short term load) for service class 2, in which the relative humidity may exceed 85 % for a few weeks per year. The moisture exposure used in the tests reported in this paper is less severe than that for service class 2. Still, average tensile strengths as low as 0.6 MPa were observed when the cross section was in a moistening phase. The value of k_{mod} for service class 3 is set to 0.7 in Eurocode 5, which seems to be a too small difference when compared to the value 0.9 for service classes 1 and 2. For instance it was found in the present research that the strength is on average 60 % lower at RH 80% than at RH 40%. It is quite obvious that the climate factors mainly derived for strength properties parallel to grain should not be used for tensile strength perpendicular to grain. An alternative could be to treat moisture exposure as an action, which should be taken into account in relation to failure modes involving tension perpendicular to grain.

Another conclusion from the present research is that any testing of tensile strength of wood perpendicular to grain should be performed under very strict control of moisture conditions in the specimens.

References

Aicher S., Dill Langer G., Ranta-Maunus, A. 1998. Duration of load in tension perpendicular to the grain of glulam in different climates. Holz als Roh- und Werkstoff 56, 295-305.

Gustafsson, P.J., Petersson, H., Stefansson, F. 1996. Fracture analysis of wooden beams with holes and notches. International Wood Engineering Conference, New Orleans, pp 4.281-4.287.

Gustafsson, P.J., Hoffmeyer , P., Valentin, G. 1998. DOL behaviour of end-notched beams. Holz als Roh- und Werkstoff, Vol. 56, No. 5, pp. 307-317.

Jönsson, J., Svensson, S. 2000. Internal stresses in the cross-grain directions of wood induced by climate variations. Proc. of CIB, W18 - Timber Structures. Paper 33-12-1. Meeting 33, Delft, Netherlands.

Jönsson, J., Svensson, S. 2001. A contact free measuring method to determine internal stress states in glulam. Structural Engineering, Lund Institute of Technology. Holzforschung, submitted.

Jönsson, J., 2001a. Moisture induced stresses in glulam cross sections. Proc. of CIB, W18 - Timber Structures. Paper 34-12-4. Meeting 34, Venice, Italy.

Jönsson, J., 2001b. Internal stresses in the cross-grain directions in glulam induced by climate variations. Structural Engineering, Lund Institute of Technology. Holzforschung, submitted.

prEN 1995-1 (2001). Eurocode 5. Design of timber structures, Part 1.1. CEN/TC250/SC5, N316.

Ranta-Maunus, A., Gowda, S. 1994. Curved and cambered glulam beams. Part 2. Long term load tests under cyclically varying humidity. VTT Publications 171, Espoo. 36 p. + app.18 p.

Ranta-Maunus, A. 1996. The influence of changing state of stress caused by mechano-sorptive creep on the duration of load effect. Proceedings International Conference on Wood Mechanics: 187-201, Stuttgart.

CIB-W18/35-7-1

INTERNATIONAL COUNCIL FOR RESEARCH AND INNOVATION
IN BUILDING AND CONSTRUCTION

WORKING COMMISSION W18 - TIMBER STRUCTURES

NEW ESTIMATING METHOD OF BOLTED CROSS-LAPPED JOINTS WITH TIMBER SIDE MEMBERS

M Noguchi
Graduate School of Agriculture, Kyoto University, Uji, Kyoto

K Komatsu
Wood Research Institute, Kyoto University, Uji, Kyoto

JAPAN

Presented by: M Noguchi

In answer to H J Blaß´s question, M Noguchi indicated that the model could not predict ultimate load capacity. A Leijten and H J Blaß then asked about the bolt hole size and the number of test replicates used. Noguchi indicated that the holes were 1 mm oversize and there were 4 replicates per test data point. E Fournely asked about the bending component in the model. This was followed by a brief discussion about the effects of bending in the joint.

New Estimating Method of Bolted Cross-lapped Joints with Timber Side Members

Masahiro Noguchi
(e-mail: noguchan@kuwri.kyoto-u.ac.jp)
Graduate School of Agriculture, Kyoto University, Uji, Kyoto, Japan
and
Kohei Komatsu
Wood Research Institute, Kyoto University, Uji, Kyoto, Japan

1 Introduction

Bolted Cross-lapped Joints (BCLJ) have been used as one of the basic jointing methods in Japan and European countries. There, however, are some problems for BCLJ in design method. For the purpose of expanding industry of large-scale wooden frame structures in Japan, it is necessary to establish the proper estimating methods for predicting actual performance. From this, we exploited a new approach that can estimate the performance of bolted timber joints, not using computer simulation, but in more practical manner.

2 Estimating Methods

2.1 Single Timber to Timber Bolted Joints

2.1.1 Slip modulus (Stiffness)

In Japan, we have been using 'theory of the beam on an elastic foundation' (TBEF) for estimating stiffness of bolted timber joints that had been applied to timber joints first by Kuenzi [1]. Bolt was assumed as a beam, and wood was assumed as an elastic foundation. Deflection of bolted timber joints was governed by following differential equation.

$$\frac{d^4 v(x)}{dx^4} + 4\lambda v(x) = 0$$

General solution is:

$$v(x) = A \sin\lambda x \cos\lambda x + B \sinh\lambda x \cos\lambda x + C \sin\lambda x \cosh\lambda x + D \sinh\lambda x \cosh\lambda x$$

$$\lambda = \sqrt[4]{\frac{k\,d}{4(EI)_s}} \quad \text{.... (1)}$$

where, $(EI)_s$: bending stiffness of bolt, k:

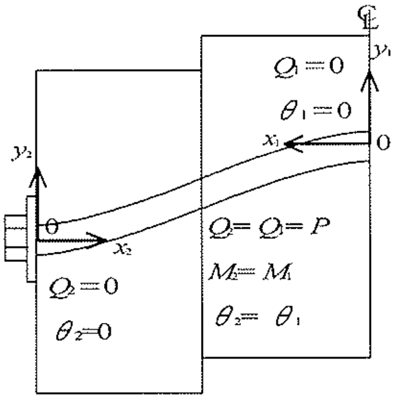

Fig.1 Modeling and boundary condition of Hirai[2] in the case of timber-to-timber bolted joint.

Legend: Qi: shear force at the head of bolt or the interface, M_i: moment at the head of bolt or the interface, θ_i: rotation angle at the head of bolt or the interface, i: 1 is main member, 2 is side member bearing constant of wood, d : diameter of bolt , x: distance from the origin, $v(x)$: bearing displacement of bolt at x point, A,B,C,D: undetermined coefficient

According to "a basic beam theory", rotational angle (θ), moment (M) and shear force (Q) are expressed as;

$$\theta(x) = \frac{\mathrm{d}y}{\mathrm{d}x}, \quad M(x) = (EI)_s \frac{\mathrm{d}y^2}{\mathrm{d}^2x}, \quad Q(x) = (EI)_s \frac{\mathrm{d}y^3}{\mathrm{d}^3x} \quad \text{.... (2)}$$

In the case of bolted timber joints with timber side member, it is necessary to set ordinary differential equation for both main member and side member, simultaneously. Kuenzi model, however, required complicated calculation of 8x8 matrixes to solve differential equations. In consequent, final expression of the equation was very complicated for designers. Therefore, Kuenzi proposed an approximate equation. His approximate equation, nevertheless, was inconsistent except for λl was more than two, slenderness of fastener is large like nails. This result in that Kuenzi's approximate equation was not available in any bolted timber joints.

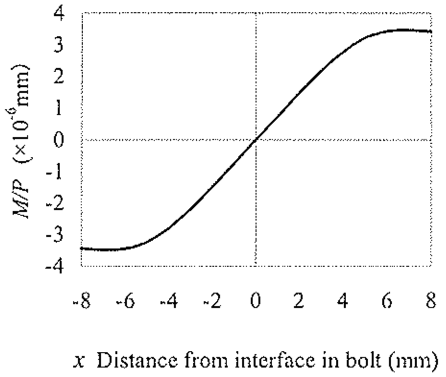

Fig.2 Distribution of moment in bolt.

Legend: x: distance from the interface between main member and side member, P: applied load, M: moment in the bolt

Ohashi [3)] proposed definition of stiffness for both main member and side member in timber dowels joints. In addition, Racher [4)] proposed design method based on Ohashi's proposal in 'Timber Engineering Step1'. If we, however, defined an independent spring to each member in the case where fastener deformation can not be ignored, we will be able to propose more simple equation. By introducing 'independent spring constant' for each member, no more 8x8 matrixes calculation will not be necessary.

In this study, we paid our attention to the moment distribution at the interface between main member and side member. Using Kuenzi's model, moment distributions of bolt were predicted. Fig. 2 shows moment on bolt was equal to zero when the width of main member and side member are same. In order to make main member and side member independent mechanically, we introduced 'Semi-Slip Condition' by setting a new boundary condition at the interface between side member and main member in which moment became almost zero and shear force was equal to the applied load (P). Moreover, we defined fictitious stiffness i.e., Semi-slip modulus, as follows;

$$K_{hi} = \frac{P}{v_i(x_i)} \quad \text{.... (3)}$$

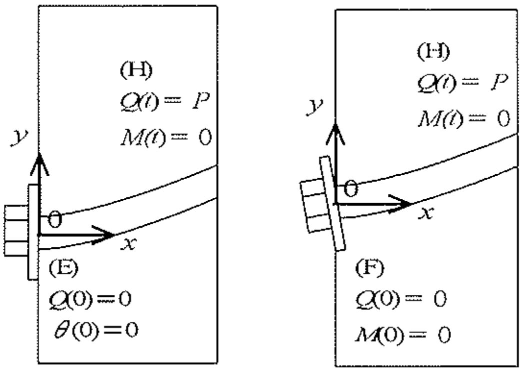

(a) Fixed end condition. (b) Free end condition

Fig.3 Concept and boundary condition of 'Semi-slip condition'.
Legend: (E): boundary condition at the head of bolt (fixed), (F): boundary condition at the head of bolt (free), (H): boundary condition at the interface

In the case of fixed end condition, we defined following hypothesis [2)]:

$$Q\ (0) = 0,\ \theta(0) = 0,\ M\ (l) = 0,\ Q\ (l) = P \qquad \ldots.\ (4)$$

Using eq. (1), (2), (3) and (4), K_h was derived as;

$$K_{hi} = \frac{2\lambda^3 (EI)_s (\sinh \lambda l \cosh \lambda l + \sin \lambda l \cos \lambda l)}{\cosh^2 \lambda l - \sin^2 \lambda l} \qquad \ldots.\ (5)$$

Equation (5) is expressed as;

$$K_{hi} = 2\lambda^3 (EI)_s \Phi(T) \qquad \ldots.\ (6)$$

$$\Phi(T) = \frac{\sinh T \cosh T + \sin T \cos T}{\cosh^2 T - \sin^2 T} \qquad \ldots.\ (7)$$

$$where,\ T = \lambda l$$

Equation (7) was not suitable for designing method, as it contains trigonometry functions and hyperbolic functions. Therefore, eq. (7) was approximated as;

$$T < 2 \qquad \Phi(T) = -0.5111\,T^5 + 3\,T^4 - 5.7631\,T^3 + 3.1093\,T^2 + 1.5127\,T \quad (R^2 = 0.999)$$

$$T \geq 2 \qquad \Phi(T) = 1 \qquad \ldots.\ (8)$$

In the case of free end condition, we defined following hypothesis [2)];

$$M\ (0) = 0,\ Q\ (0) = 0,\ M\ (l) = 0,\ Q\ (l) = P \qquad \ldots.\ (9)$$

From eq. (1), (2), (3) and (9), following equation for K_{hi} was derived as;

$$K_{hi} = \frac{2\lambda^3 (EI)_s (\sin^2 \lambda l - \sinh^2 \lambda l)}{\cos \lambda l \sin \lambda l - \cosh \lambda l \sinh \lambda l} \qquad \ldots.\ (10)$$

Similar to fix end condition, equation (10) is expressed as;

$$K_{hi} = 2\lambda^3 (EI)_s \Psi(T) \qquad \ldots.\ (11)$$

$$\Psi(T) = \frac{\sin^2 T - \sinh^2 T}{\cos T \sin T - \cosh T \sinh T} \qquad \ldots.\ (12)$$

Approximate equation of eq. (12) was obtained as;

$$T < 2.5 \qquad \Psi(T) = 0.0075T^4 - 0.0696\,T^3 + 0.096\,T^2 + 0.4646\,T \quad (R^2 = 0.999)$$

$$T \geq 2.5 \qquad \Psi(T) = 1 \qquad \ldots.\ (13)$$

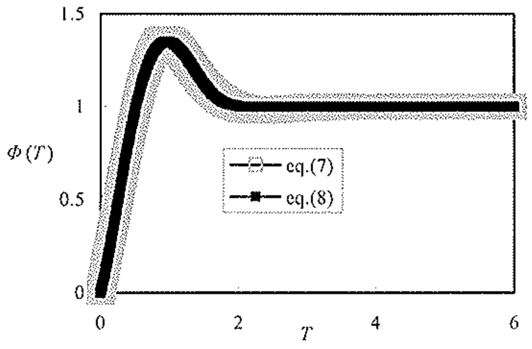

Fig.4 Comparison of eq. (7) and eq. (8)

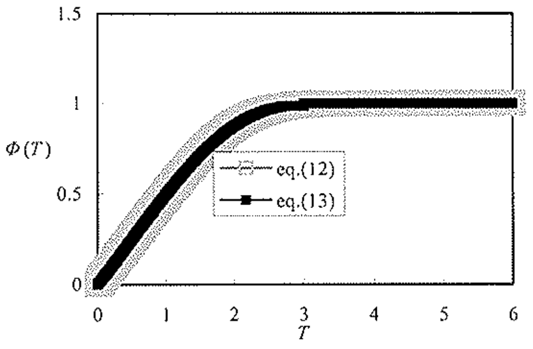

Fig.5 Comparison of eq. (12) and eq. (13)

Semi-slip modulus of arbitrary angle (θ) was assumed to be estimated by Hankinson's formula eq. (14).

$$K_{h0} = \frac{K_{h0}\ K_{h90}}{K_{h0}\sin^2\theta + K_{h90}\cos^2\theta} \quad \dots (14)$$

Slip modulus of bolted timber joint (K_s) can be defined as a modulus of serial spring composed of side member spring (K_{h1}) and main member spring (K_{h2}), as follows;

$$K_s = \frac{K_{h1}\ K_{h2}}{K_{h1} + K_{h2}} \quad \dots. (15)$$

Fig. 6 shows comparison between TBEF and eq. (15). It can be seen from this figure that our proposal can be good in wide range of various parameters.

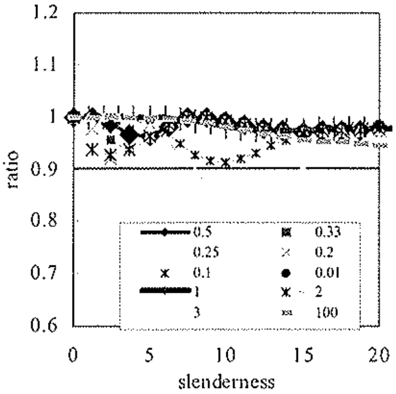

Fig. 6 Comparison between the existence theory (TBEF) and our new proposals on slip modulus, Legend: diameter of bolt: 16mm, angle of force in main member: 0 degrees, angle of force in side member: 90 degrees, ratio: slip modulus by existence theory / slip modulus by our proposal theory, *n*: length of main member divide length of side member.

2.1.1 Yield loads

For estimating yield load of single bolted timber joints, we have been using European yield model theory [5] (EYT) based on rigid-plastic theory. We, nevertheless, thought it is inconsistent to use different theory for estimating stiffness and yield load. Thus, we also tried to use TBEF to estimate stress in wood and bolt for establishing new design method of bolted joints. The yield criteria of bolted joints were thought to be either bearing yield of wood or bending yield of bolt. In this paper, splitting criteria could not be taken into account.

(1) Bearing yield of wood

Yield load on single bolted joint was derived from Kuenzi's hypothesis [1]. Fig. 7 shows semi-slip condition for arbitrary member. Yield load P_{hy} is expressed by Semi-slip modulus K_{hi} and slip of yield point S_y as follows;

$$P_{hw} = K_h\ S_y \quad \dots.(16)$$

While, yield-bearing stress σ_y is expressed by bearing constant k and embedment displacement of yield stress $S_{\sigma y}$.

$$\sigma_{wy} = k\,S_{\sigma y} \quad \dots. (17)$$

So far as semi-slip condition, S_y is equal to $S_{\sigma y}$. Thus from eq. (16), eq. (17) and $S_y = S_{\sigma y}$, P_{hw} was derived as follows;

$$P_{hw} = \frac{K_h\ \sigma_{wy}}{k} \quad \dots. (18)$$

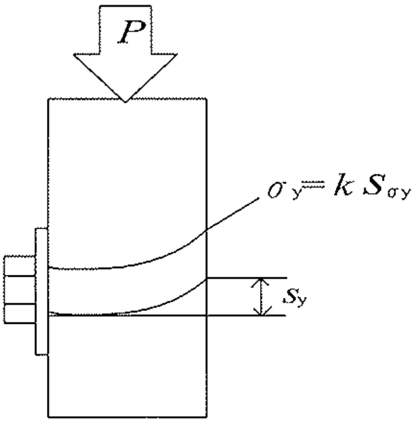

Fig.7 Concept of 'Semi-slip yield load'. Legend: *P*: applied load, S_y: slip yield stress, *k*: bearing constant, S_y: slip at the 'Semi-slip yield load'

(2) Bending yield of bolt

It seemed to be fairly difficult to derive closed-form solution for maximum stress of bolt [1] by TBEF. Therefore, for getting some effective relationships, we used computer simulation for estimating stress on bolt for 15000 combinations.
The combinations were;

Diameter of bolt was from 2 mm to 22 mm per 2 mm. Density of timber (TD) was from 300 kg/m^3 to 700 kg/m^3 per 100 kg/m^3. Slenderness was from 1 to 22 per 1. Angle of load against the grain was 0 degree to 90 degree per 10 degree. The values of several properties were calculated by following regression [6];

$$E_w = 0.0117161\,TD + 3.9029657 \quad \text{(GPa)},$$
$$k_0 = E_w / (0.316 + 0.109d) \quad (\text{N/mm}^3),$$
$$k_{90} = k_0/3.4 \quad (\text{N/mm}^3),$$
$$\sigma_0 = 0.093215\,\text{TD} - 16.074 \quad \text{(MPa)},$$
$$\sigma_{90} = (0.025522\,\text{TD} - 0.527)\,d^{-0.4} \quad \text{(MPa)},$$
$$Es = 204.1 \quad \text{(GPa)},$$
$$\sigma_y = 322.5 \quad \text{(MPa)} \;....(19)$$

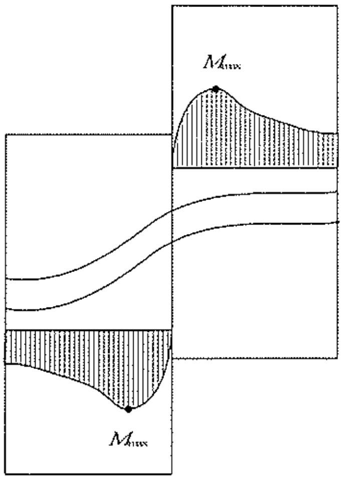

Fig.8 The notion for simulation

Moment on bolt were calculated per 0.01 mm along the shank. The maxum value was defined as maxium moment on bolt. We used following equation for estimating moment of bolt. Fig. 9 showed relationship between M, K_h, k, d, P. From results of simulation, eq. (20) was obtained;

$$\frac{M\,k\,d}{P} = 0.6\,K_h \qquad .... (20)$$

Also, relationship between bending yield stress on bolt (σ_{sy}) and bending moment (M), as following;

$$\sigma_{sy} = \frac{M}{Z}, \qquad Z = \frac{d^3}{6} \qquad .... (21)$$

where, σ_{sy}: yield stress of steel

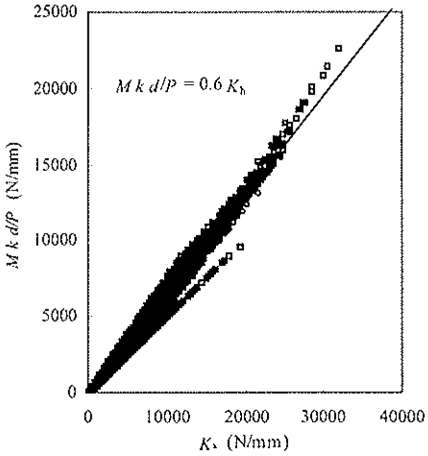

Fig.9 Relationship between maximum moment in bolt and 'Semi-slip' modulus based on simulation.
Legend: M: maximum moment in bolt, P: applied load, k: bearing constant, d: diameter of bolt, K_h: modulus of semi-slip

Using eq. (20) and (21), equation for predicting yield load by loading P_{hb} was obtained;

$$P_{hb} = \frac{k\,\sigma_{sy}\,Z\,d}{0.6\,K_h} \qquad .... (22)$$

Equation. (22) contains all factors except for E_s. E_s, however, were constant value in case of steel. Therefore, eq. (22) was consistent in all case of steel bolt.

Above all, yield load of Semi-slip condition (P_{hy}) was defined as;

$$P_{hy} = \min\,(P_{hw},\ P_{hb}). \qquad .... (23)$$

Semi-slip yield load of any angle against the grain could be predicted as;

$$P_{h\theta} = \frac{P_{h0} \quad P_{h90}}{P_{h0} \sin^2 \theta \; + P_{h90} \cos^2 \theta} \qquad \text{.... (24)}$$

Yield load of bolted joints (P_y) was defined as;

$$P_y = \min \,(P_{hy} \text{ of maim member, } P_{hy} \text{ of side member}) \qquad \text{.... (25)}$$

2.2 Bolted cross-lapped joints

In "Timber Engineering Step 1", BCLJ design method was derived for assuming the member as a rigid body. Ohashi[3)] pointed out that timbers could not be assumed as rigid body in BCLJ, but condition between rigid body and soft body or elasticity. In timber-to-timber bolted joints, super imposition of forces did not work as supposed in conventional theory. Thus, we derived a new analytical model of BCLJ, not assuming rigid body rotational deformation, but assuming that two sets of coupling moment M_1, M_2 resisted by bolts as shear forces P_{1i}, P_{2i} compose twisting moment at joint part.

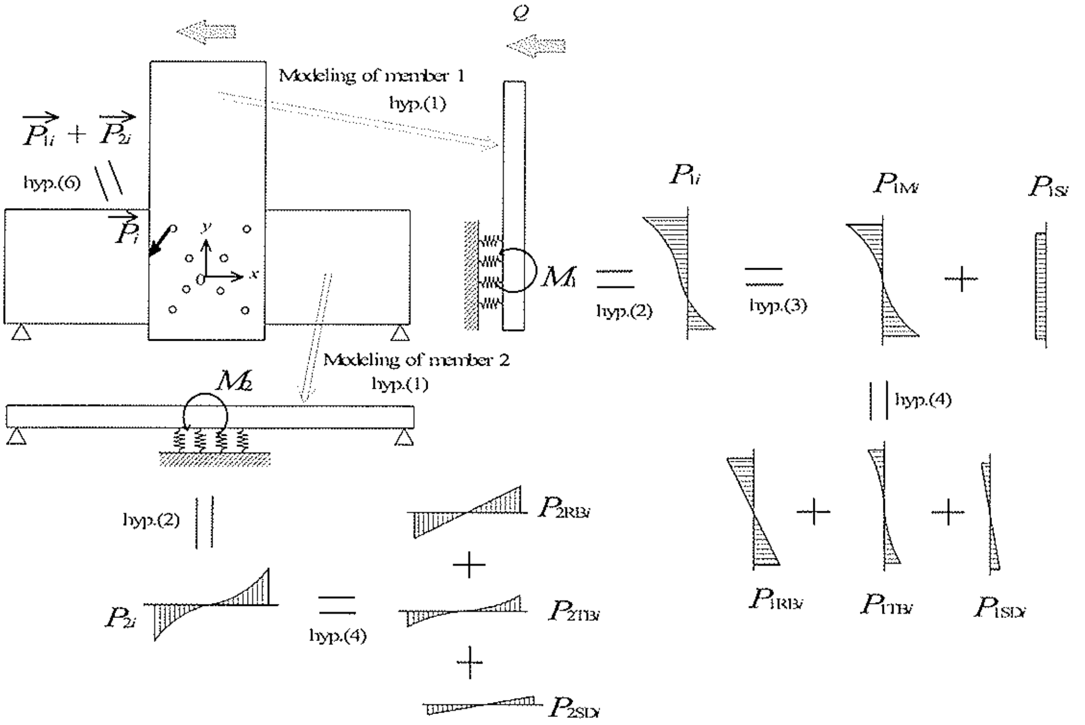
Q
Modeling of member 1
hyp.(1)
$\vec{P_{1i}} + \vec{P_{2i}}$
hyp.(6)
$\vec{P_{1i}}$
y
x
M_1
=
hyp.(2)
P_{1i}
=
hyp.(3)
P_{1Mi}
+
P_{1Si}
hyp.(4)
+
+
P_{1RBi}
P_{1TBi}
P_{1SDi}
Modeling of member 2
hyp.(1)
M_2
hyp.(2)
P_{2i}
=
hyp.(4)
P_{2RBi}
+
P_{2TBi}
+
P_{2SDi}

Fig. 11 Concept for mechanical model of BCLJ.

In order to get equation for estimating rotational stiffness and yield moment, we set following hypothesis;

(1) Each member was subjected to a coupling moment (M_1 and M_2).

(2) Coupling moment M_1, M_2 were resisted by bolts as shear forces P_{1i}, P_{2i}.

(3) Bolt load was decomposed to load by shear force P_{1Si} and bolt load by moment P_{1Mi}.

(4) P_{1i} (P_{2i}) could be decomposed to bolt load by rigid body rotation P_{1RBi}, bolt load by timber bending deformation at panel zone P_{1TBi} and bolt load by timber shear deformation at panel zone P_{1SDi}.

(5)Shear stress distribution of timber at panel zone was constant.

(6) At the rectangular joint part (panel zone), shear force of bolt by coupling moment composed twisting moment.

Keeping these hypothesises in mind; we will derive an equation for estimating yield moment. .

Bolt force $P_{\mathrm{RB}1i}$ due to rigid body rotation is assumed to proportional to the distance x_i from centre of bolt arrangement.

$$P_{1\mathrm{RB}i} = \beta x_i \qquad \beta\text{: undetermined coefficient} \qquad \text{.... (26)}$$

Assuming shear stress distribution of timber at panel zone as constant value, bolt force $P_{1\mathrm{SD}i}$ due to shear deformation of timber is assumed to be also proportional to the distance from centre of bolt arrangement.

$$P_{1\mathrm{SD}i} = \gamma x_i \qquad \gamma\text{: undetermined coefficient} \qquad \text{.... (27)}$$

For simplicity, we use a new parameter as;

$$\alpha = \beta + \gamma \qquad \alpha\text{: undetermined coefficient} \qquad \text{.... (28)}$$

Thinking of timber bending deformation at panel zone, shear stress distribution of timber at panel zone by M_1 could be assumed as constant.

$$Q_{\mathrm{M}} = \frac{M_1}{h} = \frac{d^3\delta}{dx^3} = \text{constant} \qquad \text{where, h: depth of timber 1} \qquad \text{.... (29)}$$

The load distribution of a bolt by timber bending at panel zone by M_1 was expressed bending deformation of timber δ and Semi slip modulus $K_{\mathrm{h}90}$ of bolt perpendicular to the grain. Moreover, the centre of bolt arrangement is thought symmetry - $M(0) = 0$, $\delta(0) = 0$, $\theta(0) = 0$. From these, the load distribution of bolt by bending deformation of timber $P_{1\mathrm{TB}i}$ was obtained as;

$$P_{1\mathrm{TB}i} = \delta \times K_{\mathrm{h}90} = \frac{M_1 K_{\mathrm{h}90}}{6hEI} x_i^3 \qquad \text{.... (30)}$$

Thus, bolt load P_{1i} can be expressed as follows (hyp. 4);

$$P_{1i} = P_{1\mathrm{TB}i} + P_{1\mathrm{RB}i} + P_{1\mathrm{SD}i} \qquad \text{.... (31)}$$

Moment of member 1 is;

$$M_1 = \sum_{i=1}^{n} P_{1i}\, x_i = \alpha \sum_{i=1}^{n} x_i^2 + \frac{\mathrm{K}_{\mathrm{h}90}}{6hEI} \sum_{i=1}^{n} x_i^4 \qquad \text{.... (32)}$$

From above, by eliminating α, we obtained P_{1i}.

$$P_{1\mathrm{M}i} = \frac{M_1\, x_i}{\sum_{i=1}^{n} x_i^2} + \frac{K_{\mathrm{h}90} M_1}{6EIh} \left(x_i^3 - \frac{x_i \sum_{i=1}^{n} x_i^4}{\sum_{i=1}^{n} x_i^2} \right) \qquad \text{.... (33)}$$

Similar to $P_{1\mathrm{M}i}$, $P_{2\mathrm{M}i}$ was obtained as;

$$P_{2Mi} = \frac{M_2\ y_i}{\sum_{i=1}^{n} y_i^2} + \frac{K_{i/90} M_2}{6EIb}\left(y_i^3 + \frac{y_i \sum_{i=1}^{n} y_i^4}{\sum_{i=1}^{n} y_i^2} \right) \quad \text{.... (34)}$$

At jointing part, moment of column must be equilibrium with that of beam. Thus eq. (35) holds good (hyp. 1).

$$M_1 = M_2 = \frac{1}{2} M \quad \text{.... (35)}$$

Here, we assumed that applied shear force Q was distributed to each bolt constantly(hyp. 5).

$$P_{1Si} = \frac{Q}{n} \quad \text{.... (36)}$$

From eq. (31), (32), P_{xi} and P_{yi} are expressed as;

Total bolt load was composed to load by shear force P_{1Si} and bolt load by moment P_{1Mi} (hyp. 3). As shear force of bolt by coupling moment composed twisting moment (hyp. 2),

$$P_{1i} = P_{xi} \qquad P_{2i} = P_{yi} \quad \text{.... (37)}$$

From eq. (33), (34), (35), (36)and (37), P_{xi} and P_{yi} are expressed as;

$$P_{xi} = P_{1i} = \frac{M\,x_i}{2\sum_{i=1}^{n} x_i^2} + \frac{K_{i/90} M}{12EIh}\left(x_i^3 - \frac{x_i \sum_{i=1}^{n} x_i^4}{\sum_{i=1}^{n} x_i^2} \right) + \frac{\varphi}{n} M \quad \text{... (38)}$$

$$P_{yi} = P_{2i} = \frac{M\,y_i}{2\sum_{i=1}^{n} y_i^2} + \frac{K_{i/90} M}{12EIb}\left(y_i^3 + \frac{y_i \sum_{i=1}^{n} y_i^4}{\sum_{i=1}^{n} y_i^2} \right) \quad \text{... (39)}$$

where $\varphi = Q/M$

Now, resultant force P_i are following equation (hyp. 6);

$$P_i = \sqrt{P_{xi}^2 + P_{yi}^2} \quad \text{.... (40)}$$

From above, equation for yield moment of BCLJ (M_y) is obtained as;

$$M_{yi} = \frac{P_{yi}}{\sqrt{\left(\frac{x_i}{2\sum_{i=1}^{n} x_i^2} + \frac{K_{i/90}}{12EIh}\left(x_i^3 - \frac{x_i \sum_{i=1}^{n} x_i^4}{\sum_{i=1}^{n} x_i^2} \right) + \frac{\varphi}{n} \right)^2 + \left(\frac{y_i}{2\sum_{i=1}^{n} y_i^2} + \frac{K_{i/90}}{12EIb}\left(y_i^3 + \frac{y_i \sum_{i=1}^{n} y_i^4}{\sum_{i=1}^{n} y_i^2} \right) \right)^2}} \quad \text{.... (41)}$$

In the case of ignoring timber deformation, eq. (41) can be expanded as;

$$M_{yi} = \frac{P_i}{\sqrt{\dfrac{x_i^2}{4\left(\sum\limits_{i=1}^{n} x_i^2\right)^2} + \dfrac{y_i^2}{4\left(\sum\limits_{i=1}^{n} y_i^2\right)^2}}}$$

$$\textit{where, } M_y = \min\ (M_{yi}) \qquad \text{.... (42)}$$

Next, we will derive the equation of rotational stiffness. Total energy at joint part U_{total} is;

$$U_{\mathrm{total}} = U_{\mathrm{fastner}} + U_{\mathrm{bend}} + U_{\mathrm{shear}} = \sum_{i=1}^{n} \frac{1}{2} P_i S_i + \frac{1}{2}\int_0^{h} \frac{M^2}{EI}\mathrm{d}x + \frac{1}{2}\int \tau\gamma\,\mathrm{d}x \qquad \text{.... (43)}$$

Using Castigliano's first theorem expressed in eq. (44), M-θ relationship is derived as;

$$\theta = \frac{\partial U}{\partial M} \qquad \text{.... (44)}$$

From eq. (40), (43), (44), and 'a basic beam theory', the rotational stiffness of BCLJ (R) was obtained as;

$$R = \frac{1}{\sum\limits_{i=1}^{n}\left(\dfrac{\left(\dfrac{x_i}{2\sum\limits_{i=1}^{n} x_i^2} + \dfrac{K_{H(X)}}{12EIh}\left(x_i^3 - \dfrac{x_i\sum\limits_{i=1}^{n} x_i^4}{\sum\limits_{i=1}^{n} x_i^2}\right)\right)^2 + \left(\dfrac{y_i}{2\sum\limits_{i=1}^{n} y_i^2} + \dfrac{K_{H(X)}}{12EIb}\left(y_i^3 + \dfrac{y_i\sum\limits_{i=1}^{n} y_i^4}{\sum\limits_{i=1}^{n} y_i^2}\right)\right)^2}{K_{Si}}\right) + \dfrac{2}{Gbth} + \dfrac{h^3+b^3}{48EI}} \qquad \text{.... (45)}$$

In the case of ignoring timber deformation, eq. (45) can be simplified as;

$$R = \frac{1}{\dfrac{\sum\limits_{i=1}^{n} \dfrac{x_i^2}{K_{Si}}}{4\left(\sum\limits_{i=1}^{n} x_i^2\right)^2} + \dfrac{\sum\limits_{i=1}^{n} \dfrac{x_i^2}{K_{Si}}}{4\left(\sum\limits_{i=1}^{n} y_i^2\right)^2}} \qquad \text{.... (46)}$$

In the case of cross-grained members, K_{si} could be assumed as constant value K_{s} 4). Thus eq. (46) can be simplified as;

$$R = \frac{K_s}{\dfrac{1}{4\sum\limits_{i=1}^{n} x_i^2} + \dfrac{1}{4\sum\limits_{i=1}^{n} y_i^2}} \qquad \text{.... (47)}$$

Here, in the case of symmetry bolt arrangement on both x-axis and y-axis, eq. (48) is consistent.

$$\sum_{i=1}^{n} x_i^2 = \sum_{i=1}^{n} y_i^2 \qquad \text{.... (48)}$$

Using eq. (47), eq. (48) can be simplified as;

$$R = 2K_S\sum_{i=1}^{n} x_i \qquad \text{.... (49)}$$

While, using eq. (48), conventional theory can be expressed as;

$$R = \sum_{i=1}^{n} K_S r^2 = K_S\sum_{i=1}^{n} r^2 = 2K_S\sum_{i=1}^{n} x_i \qquad \text{.... (50)}$$

Equation. (49) is consistent with eq. (50). From this, in the case of symmetry bolt arrangement on both x-axis and y-axis, rotational stiffness of our proposal theory is the same value with that of conventional theory.

3 Test methods

Two series of experimental study were conducted on the double-sided timber-to-timber joints fastened by a single bolt as well as on BCLJ. Common conditions we set for two series were; Diameter of bolt was 16 mm, Length of bolt was 32 mm, Species of materials was Douglas-fir glulam, JAS grade was E105 – f 300, Mean value of MC was 11 %, Mean value of density was 456 kg/m^3, Thickness of main member was 160 mm, Thickness of side member was 80 mm.

In each double-sided timber-to-timber joints fastened by bolt, the angle of grain for the load varied from 0 degrees to 90 degrees per 30 degrees (Fig.11).

Fig. 12 shows BCLJ specimens prepared in this study. Each BCLJ specimen consists of a column (160 mm × 500 mm × 1500 mm) and a pair of beams (80 mm × 500 mm × 2000 mm). They were joined with bolts and were formed a T-shaped assemblage. We arranged bolts allocation in rectangle or in square by changing the number of bolts from 4 to16.

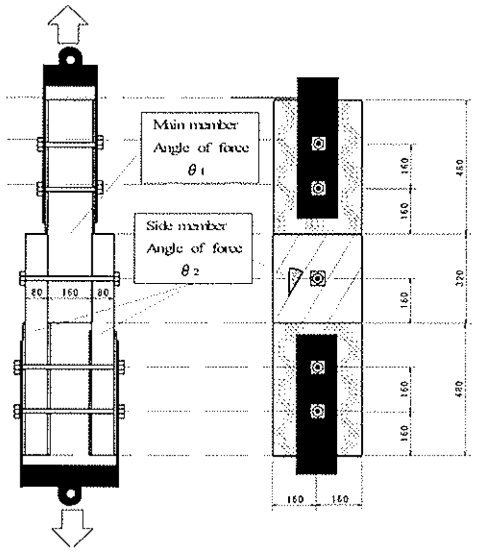
Main member
Angle of force
θ1
Side member
Angle of force
θ2
80
160
80
160
160
160
160
160
480
320
480
160
160

Fig. 11 Specimens for the test of the bolted double shear timber-to-timber joint. (Unit: mm)

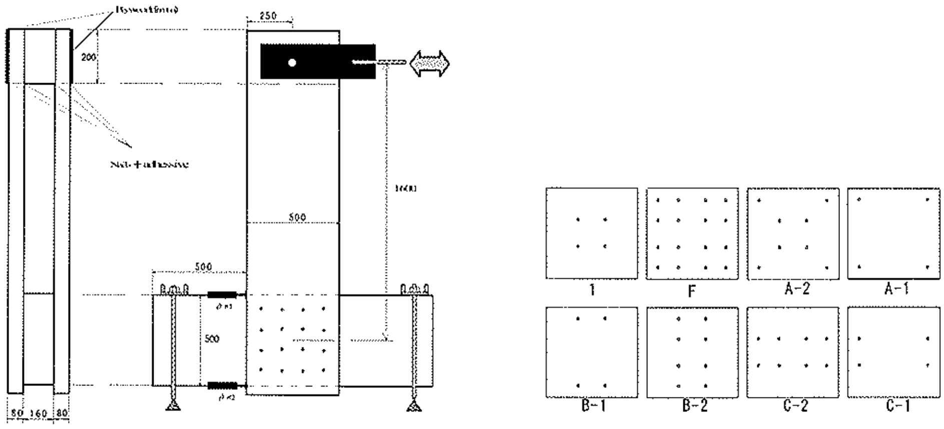
250
200
Nut+adhesive
500
1600
500
500
θ1
θ2
80
160
80
1
F
A-2
A-1
B-1
B-2
C-2
C-1

Fig. 12 Specimen for the test of bolted cross-lapped joints (Unit: mm)

4 Verifying Our Estimating Methods

Material properties for numerical calculating were adopted from the previous study (6), except for bearing properties. Bearing test of bolt was done using finished specimens (Fig. 13, Table 1). Table 2 shows calculating value of rotational stiffness. From this table, effective ratio of rotational stiffness of joints against bending stiffness of timber SR is about half value of the loss of stiffness by timber deformation (100-TR). The reason was thought that both main member and side member deformed 1/SR of R by eq. (47).

Table 1 Result of bearing test

	k (N/mm^3)	σ_y (MPa)
ASTM0	41.7	38.1
ASTM90	22.6	19.4

k: bearing constant, σ_y: bearing yield stress

ASTM0: load parallel to the grain

ASTM90: load perpendicular to the grain

Table 2 Calculating values of rotational stiffness

	SR	TR	(100-TR)/2
T	0.6	98.6	0.7
F	12.2	78.2	10.9
A1	5.5	88.9	5.6
A2	6.1	87.8	6.1
B1	1.1	97.6	1.2
B2	2.0	95.6	2.2
C1	1.1	97.6	1.2
C2	2.0	95.6	2.2

Legend: Unit: % , h : length of panel zone,
TR: eq.(45)/eq.(47), SR: eq.(47)/EIh

From the comparisons between calculations and experimental result (Fig. 14, 15), it was recognized that the stiffness and yield load in double-sided timber-to-timber bolted joints and rotational stiffness and yield moment in bolted cross-lapped joints could be predicted precisely by using our new theory. Thus, the calculation values of BCLJ on Fig.15 were calculated by eq. (41) and (45). While, as to rotational stiffness, estimating values by conventional theory (4) showed much higher than experimental results - about two times - in rectangular bolt-arrangement.

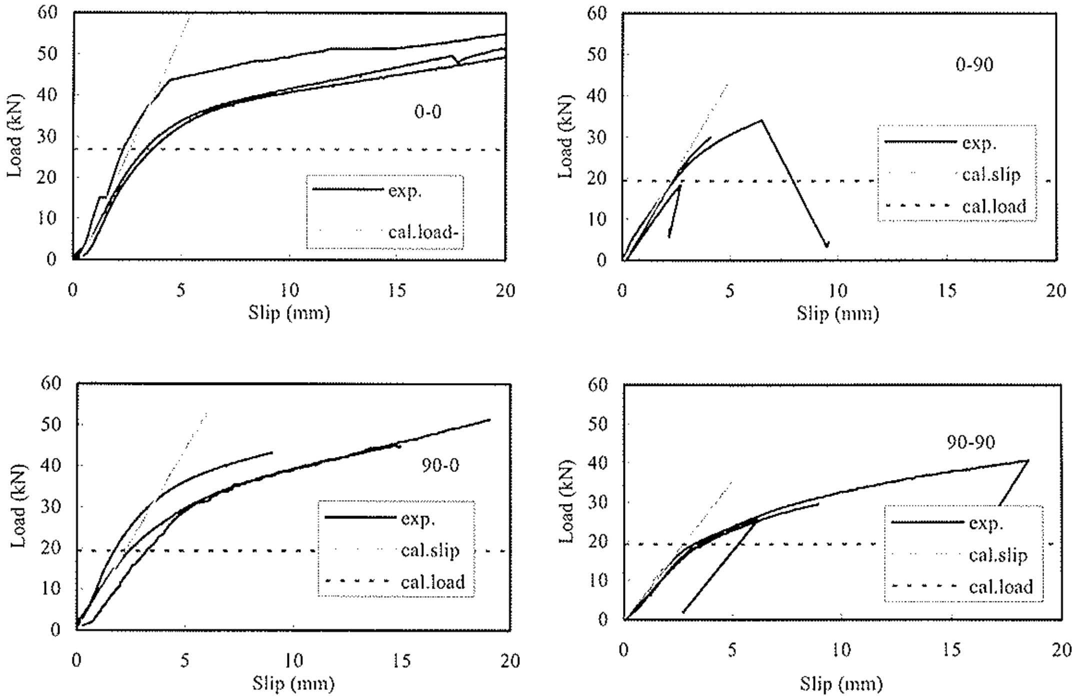

Fig.14 Comparison between experiment and our new proposals on double-shear bolted joints.
exp.: experimental result, cal. slip: slip modulus by our new theory, cal. load: yield load by our new theory

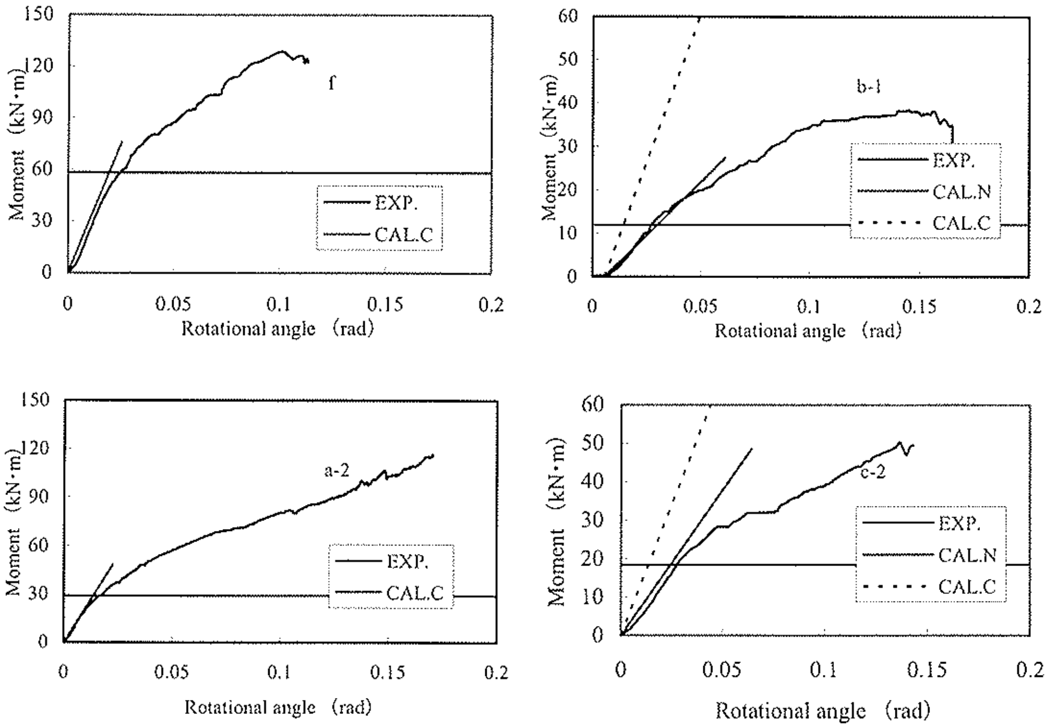

Fig. 15 Comparison between experimental result and estimating value by our proposal in bolted cross-lapped joints. EXP.: experimental result, CAL.C: yield moment by conventional theory, CAL.N: rotational stiffness by our proposal theory

5 Conclusions

(1) Thinking of 'Semi-slip condition', estimating method of Kuenzi could be simplified.

(2) From results of simulation concerning 15000 combinations, we could be derived the closed-form equation to estimate yield load based on TBEF.

(3) It is treacherous to use conventional theory for estimating rotational stiffness, in case of lying bolts out in rectangular. Our proposal theory in this study can predict rotational stiffness and yield moment precisely in both cases of laying bolts out in rectangular and square.

References

(1) Kuenzi, E.W.: Theoretical design of a nail or bolted joint under lateral load, Report D1951, F. P. L. Madison (1955)

(2) T. Hirai, M Sawada: Nominal bearing - stresses of bolted wood - joints at apparent proportional - limits, *mokuzai gakkaishi,* 28, 9, pp. 543-547 (1982).

(3) Y. Ohashi, I. Sakamoto: Study on laminated timber moment resisting joint, Proceedings of the 2nd Pacific Timber Conference, Vol. 2, Auckland, 1989, p. 37-42

(4) P. Racher: Moment resisting connection, Timber Engineering STEP 1, Dusseldorf, 1995, pp. C16/1-C16/11

(5) Larsen L.A.: The yield load of bolted and nailed joints IUFRO-5, Pretoria, 1973, p.646-654

(6) Architectural Institute of Japan (AIJ) edited: Structural Design Note for Timber Structures, Maruzen, Tokyo, 1995. p. 184-221 (in Japanese)

CIB-W18/35-7-2

INTERNATIONAL COUNCIL FOR RESEARCH AND INNOVATION
IN BUILDING AND CONSTRUCTION

WORKING COMMISSION W18 - TIMBER STRUCTURES

ANALYSIS ON MULTIPLE LAG SCREWED TIMBER JOINTS WITH TIMBER SIDE MEMBERS

K Komatsu
S Takino
Wood Research Institute, Kyoto University, Uji, Kyoto

M Nakatani
Graduate School, Kyoto University, Uji, Kyoto

H Tateishi
Tateishi Structural Design Office, Kyoto

JAPAN

Presented by: K Komatsu

H J Blaß asked if individual load-slip curves were used for the fasteners. K Komatsu indicated that only a generic value was used but that the Monte Carlo approach will be used in future studies. P Ellegaard asked about the apparently more ductile experimental test behaviour than that indicated by the theory. K Komatsu replied that this may be because of errors due to division by zero in the numerical calculations. In reply to questions by H J Larsen and P Quenneville about the experimental design and the approval for use of the type of screw tested, K Komatsu replied that the testing were carried out in response to the requirements of the company producing the screws and it was only after the experimental data have been obtained, that an analytical approach was sought to explain the observed behaviour.

Analysis on Multiple Lag Screwed Timber Joints with Timber Side Members

Kohei Komatsu*1 Shinjirou Takino*1 Makoto Nakatani*2 and Hajime Tateishi*3

*1 : Wood Research Institute, Kyoto University, Uji, Kyoto, Japan
*2 : Graduate School, Kyoto University, Uji, Kyoto, Japan
*3 : Tateishi Structural Design Office, Kyoto, Japan

Abstract

Non-linear load-slip relationships of multiple lag screwed timber joints with timber side members were analyzed by making use of the classical Lantos's theory which delt with load distribution in the members of general multiple timber joints under axial force.

Load-slip relationships obtained from single lag screwed joints were fitted by the three parameters exponential function. Then step-wise load incremental calculation method was applied on a series of the finite deferent equations which were obtained by applying Lantos theory to the multiple lag screwed timber joints under axial force.

A series of experimental study was also conducted on the double sided timber to timber joints fastened by single raw lag screws. We prepared basically five different combinations of test specimens composed of single main member and double sided members connected by a several lag screws located along one line.

From the comparisons between calculations and experimental result, it was recognized that the non-linear calculations could predict the non-linear load-slip behavior at least up to the yielding point of each multiple lag screwed joint. So far as using the 'load incremental method', it was difficult to predict precisely on the ultimate stage of each multiple joint specimens.

1. Introduction

Lag screwed timber joint has an big advantage that it can be fastened from a one-sided surface, thus recently it has been getting high reputation in the field of existing wooden post and beam construction in Japan.

In the Japanese timber structures design standards [1994 AIJ], however, an allowable strength for lag screwed timber joint is admitted only for the case where steel side plate is used. Thus, at this moment, a special permission is required if the lag screws are used for timber to timber joints and due to this limitation, design of timber structures using timber to timber lag screwed joints is being faced to a difficult feature. From these backgrounds, we paid our attentions to make the timber to timber lag screwed joints hold a formal recognition as a one of the engineered timber joints.

As the first step of a theoretical approach for understanding non-linear behavior of timber to timber the lag screwed joints, we tried to derive a determinate solutions for the timber to timber multiple lag screwed joints based on the classical Lantos's theory [1969 Lantos], and nonlinear load-slip relationships of them were calculated by applying the step-by-step linear calculation scheme. The validity of theoretical approach was made sure by referring observed results obtained from a series of full size experiments whose details are to be presented in elsewhere [2002 Komatsu].

2. Theoretical Approach

2.1 Original Theory

In 1969, Lantos analyzed a multiple double shear bolted timber joint with timber side members by considering equilibrium condition among axial force in the main member, shear force at the fasteners and axial force in the side member. He derived a kind of finite difference equation for the axial forces, however consequently a closed form solution was obtained by assuming the finite difference equation as an analogous second order differential equation.

In this Lantos's first attempt, it will be the most important part that he defined very skillfully the compatibility condition for the main member and side member by considering both elastic deformation of member as well as elastic slip of fasteners. We would like to use the same compatibility condition for our problem as that set out originally by Lantos.

2.2 Analysis

Figure 1 shows schematically an analytical model of multiple timber to timber lag screwed joint to be analyzed in this study. In this study, from one to five rows of lag screws per single shear plane were considered.

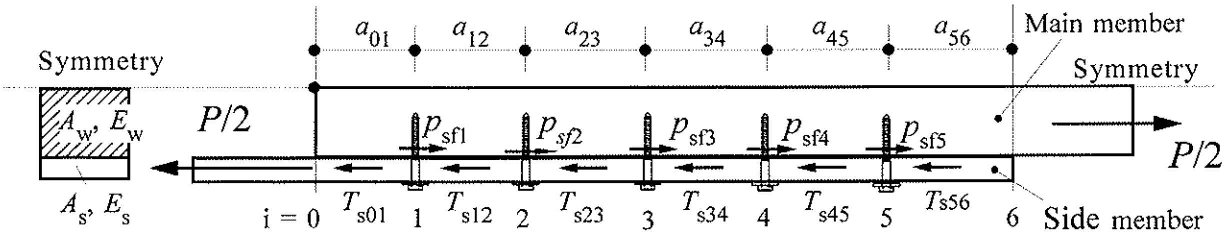

Fig.1 Analytical Model of Multiple Timber to Timber Lag Screwed Joint.

2.2.1 Derivation of Basic Equations for 5 Rows Fasteners

As an example for showing derivation process of basic equations in details, we pay attention to the No.1 and No.2 fasteners shown in Fig.1.

The equilibrium equation of forces around No.1 fastener is;

$$p_{sf1} = T_{s01} - T_{s12} \qquad .....(1)$$

Load-slip relationship for No.1 fastener is;

$$p_{sf1} = K_{s1} \cdot S_1 \qquad ......(2)$$

From eq.(1) and eq.(2) we get;

$$K_{s1} \cdot S_1 = T_{s01} - T_{s12} \qquad .....(3)$$

In the same manner, we also get a same sort of equation for the No.2 fastener;

$$K_{s2} \cdot S_2 = T_{s12} - T_{s23} \qquad .....(4)$$

where,

p_{sfi} : shear force acting at i-th fastener.

$T_{si(i+1)}$: axial force in side member between i-th and (i+1)-th fasteners.

K_{si} : tangent slip modulus of i-th fastener to be defined as $K_{si} = \mathrm{d}p_{si}/\mathrm{d}s_i$
S_i : slip displacement of i-th fastener.

According to the compatibility condition that was first introduced by Lantos [1969 Lantos] as shown in Fig.2, the length a_w* defined at the main member and the length a_S* defined at the side member should be the same.
Namely;

for the main member : $a_w^* = S_1 + (a_{12} + e_{w12})$ .....(5)

for the side member : $a_S^* = S_2 + (a_{12} + e_{S12})$ .....(6)

where,
$a_{i(i+1)}$: initial distance between i-th and (i+1)-th fasteners
$e_{wi(i+1)}$: elongation of main member due to $T_{wi(i+1)}$ between i-th and (i+1)-th fasteners
$e_{Si(i+1)}$: elongation of side member due to $T_{Si(i+1)}$ between i-th and (i+1)-th fasteners

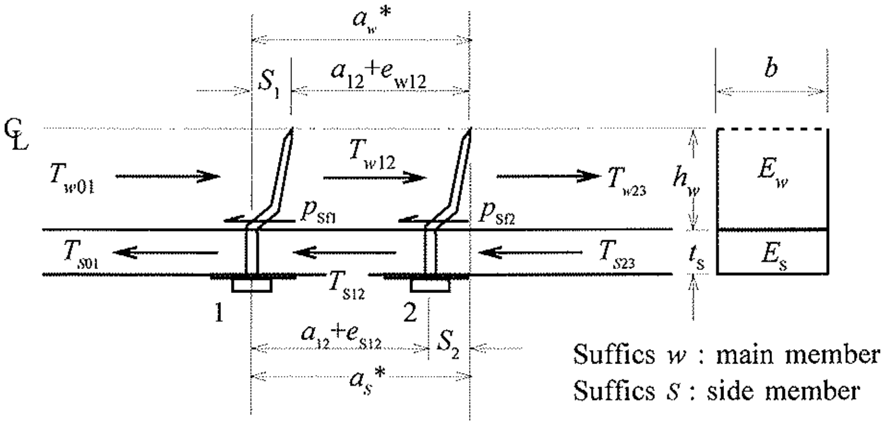

Fig.2 Schematic explanation of the compatibility condition of main member and side member in the case of Lantos's theory

From eqs.(5) and (6), we get;

$$S_1 - S_2 = e_{S12} - e_{w12} \quad .....(7)$$

From Hooke's low, the elongations of each member are expressed as ;

$$e_{w12} = \frac{a_{12}T_{w12}}{E_w A_w} \quad .....(8)$$

$$e_{S12} = \frac{a_{12}T_{S12}}{E_S A_S} \quad .....(9)$$

where,
E_w and E_S : Young's moduli of main member and side member, respectively
A_w and A_S : Cross sectional area of main member and side member, respectively
$T_{wi(i+1)}$: axial force in the main member between i-th and (i+1)-th fasteners.

Substituting eqs.(8), (9) into eq.(7), then considering eqs.(3),(4), we can get a kind of the following finite difference equation;

$$\frac{1}{K_{S1}}T_{S01} - \left(\frac{1}{K_{S1}} + \frac{1}{K_{S2}}\right)T_{S12} + \frac{1}{K_{S2}}T_{S23} = \left(\frac{a_{12}}{E_S A_S}\right)T_{S12} - \left(\frac{a_{12}}{E_w A_w}\right)T_{w12} \qquad \text{.....(10)}$$

The boundary condition at the side member between 0 and 1st fastener is;

$$T_{S01} = \frac{P}{2} \qquad \text{.....(11)}$$

and at arbitrary place, the sum of the axial forces being distributed in both members must be equilibrium with the external force [1969 Lantos];

$$T_{S12} + T_{w12} \equiv \frac{P}{2} \qquad \text{.....(12)}$$

Thus, from eqs.(10), (11) and (12), the following basic finite difference equation relating to No.0, No.1 and No.2 fasteners were obtained ;

$$-\left\{\left(\frac{1}{K_{S1}} + \frac{1}{K_{S2}}\right) + \left(\frac{a_{12}}{E_S A_S} + \frac{a_{12}}{E_w A_w}\right)\right\}T_{S12} + \frac{1}{K_{S2}}T_{S23} = -\left(\frac{a_{12}}{E_w A_w} + \frac{1}{K_{S1}}\right)\frac{P}{2} \qquad \text{.....(13)}$$

In the same manner, a series of following finite difference equations could be derived for the other fastener points.

For No.1, No.2 and No.3 fastener points ;

$$\frac{1}{K_{S2}}T_{S12} - \left\{\left(\frac{1}{K_{S2}} + \frac{1}{K_{S3}}\right) + \left(\frac{a_{23}}{E_S A_S} + \frac{a_{23}}{E_w A_w}\right)\right\}T_{S23} + \frac{1}{K_{S3}}T_{S34} = -\left(\frac{a_{23}}{E_w A_w}\right)\frac{P}{2} \qquad \text{......(14)}$$

For No.2, No.3 and No.4 fastener points ;

$$\frac{1}{K_{S3}}T_{S23} - \left\{\left(\frac{1}{K_{S3}} + \frac{1}{K_{S4}}\right) + \left(\frac{a_{34}}{E_S A_S} + \frac{a_{34}}{E_w A_w}\right)\right\}T_{S34} + \frac{1}{K_{S4}}T_{S45} = -\left(\frac{a_{34}}{E_w A_w}\right)\frac{P}{2} \qquad \text{......(15)}$$

For No.3, No.4 and No.5 fastener points ;

$$\frac{1}{K_{S4}}T_{S34} - \left\{\left(\frac{1}{K_{S4}} + \frac{1}{K_{S5}}\right) + \left(\frac{a_{45}}{E_S A_S} + \frac{a_{45}}{E_w A_w}\right)\right\}T_{S45} = -\left(\frac{a_{45}}{E_w A_w}\right)\frac{P}{2} \qquad \text{......(16)}$$

In eq.(16), another boundary condition of $T_{S56} = 0$ (at free end) was involved in.
Consequently, we obtained a following simultaneous equation for the axial force of side member in the $T_{si(i+1)}$ case of five rows of lag screws;

$$\begin{bmatrix} C_{11} & C_{12} & 0 & 0 \\ C_{21} & C_{22} & C_{23} & 0 \\ 0 & C_{32} & C_{33} & C_{34} \\ 0 & 0 & C_{43} & C_{44} \end{bmatrix} \begin{Bmatrix} T_{S12} \\ T_{S23} \\ T_{S34} \\ T_{S45} \end{Bmatrix} = \begin{Bmatrix} q_1 \\ q_2 \\ q_3 \\ q_4 \end{Bmatrix} \qquad \text{.....(17)}$$

where,

$$C_{ij\ (i=j)} = -\left(\frac{1}{K_{Si}} + \frac{1}{K_{S(j+1)}} + \frac{a_{i(j+1)}}{E_S A_S} + \frac{a_{i(j+1)}}{E_w A_w}\right) \qquad C_{ij\ (i<j)} = \frac{1}{K_{Sj}} \qquad C_{ij\ (i>j)} = \frac{1}{K_{Si}}$$

$$q_1 = \frac{P}{2}\left(\frac{1}{K_{S1}} + \frac{a_{12}}{E_w A_w}\right) \quad q_i = -\frac{P}{2}\left(\frac{a_{i(i+1)}}{E_w A_w}\right) \qquad .....(18)$$

The form of eqs.(17) and (18) can be hold good as they are, even if the number of lag screw decreases or increases. Thus, for the case of another row of lag screws (n = 2, 3 and 4), it was omitted to explain in details.

2.2.2 Load Incremental Calculation Method

In order to obtain the nonlinear load-slip relationship of multiple lag screwed timber to timber joint, simultaneous equation(17) was solved within each load incremental step by substituting tangent slip modulus of each fastener into eq.(18), while moduli of elasticity of side member and main member was assumed to be the same as their initial values.

For expressing the nonlinear load-slip relationship of single lag screwed timber to timber joint, experimental data was fitted to the three parameters exponential equation (19).

$$p_{sfi} = (p_{0i} + K_{ui}S_i)\left\{1 - \exp\left(\frac{-K_{S0i}}{p_{0i}}S_i\right)\right\} \qquad .....(19)$$

where,

p_{0i} : load axis intercept of the second tangential line

K_{ui} : the second tangential modulus

K_{S0i} : the initial or first tangential modulus

p_{Sfi} : shear force on a single lag screwed timber to timber joint

S_i : corresponding slip displacement

In the actual numerical calculation, the differential value of eq.(19) was used for the tangent slip modulus as follows;

$$K_{si} = \frac{dp_{sfi}}{dS_i} = K_{ui}\left\{1 - \exp\left(\frac{-K_{S0i}}{p_{0i}}S_i\right)\right\} + (p_{0i} + K_{ui}S_i)\left(\frac{K_{S0i}}{p_{0i}}\right)\exp\left(\frac{-K_{S0i}}{p_{0i}}S_i\right) \qquad .....(20)$$

For one external force P, different slip displacement S_i were obtained in each fastener's point by solving eqs.(17) then eqs.(3), (4) for example, thus an average value of each slip displacement was defined as the representative slip of the multiple lag screwed joint as follows;

$$S_{\text{rep}} = \frac{\sum_{i=1}^{n}(S_i)}{n} \qquad .....(21)$$

Although we tried to seek any variable incremental load which could avoid ill condition of determinant of eq.(17) at around the final loading level, but at this study no good solution was obtained. Thus, numerical calculation was done by keeping the incremental load as constant as ΔP = 1N until the determinant of eq.(17) become ill condition. Due to this ill condition, it was difficult to calculate the degrading region after maximum load .

3. Experimental Procedures

3.1 Test Specimens

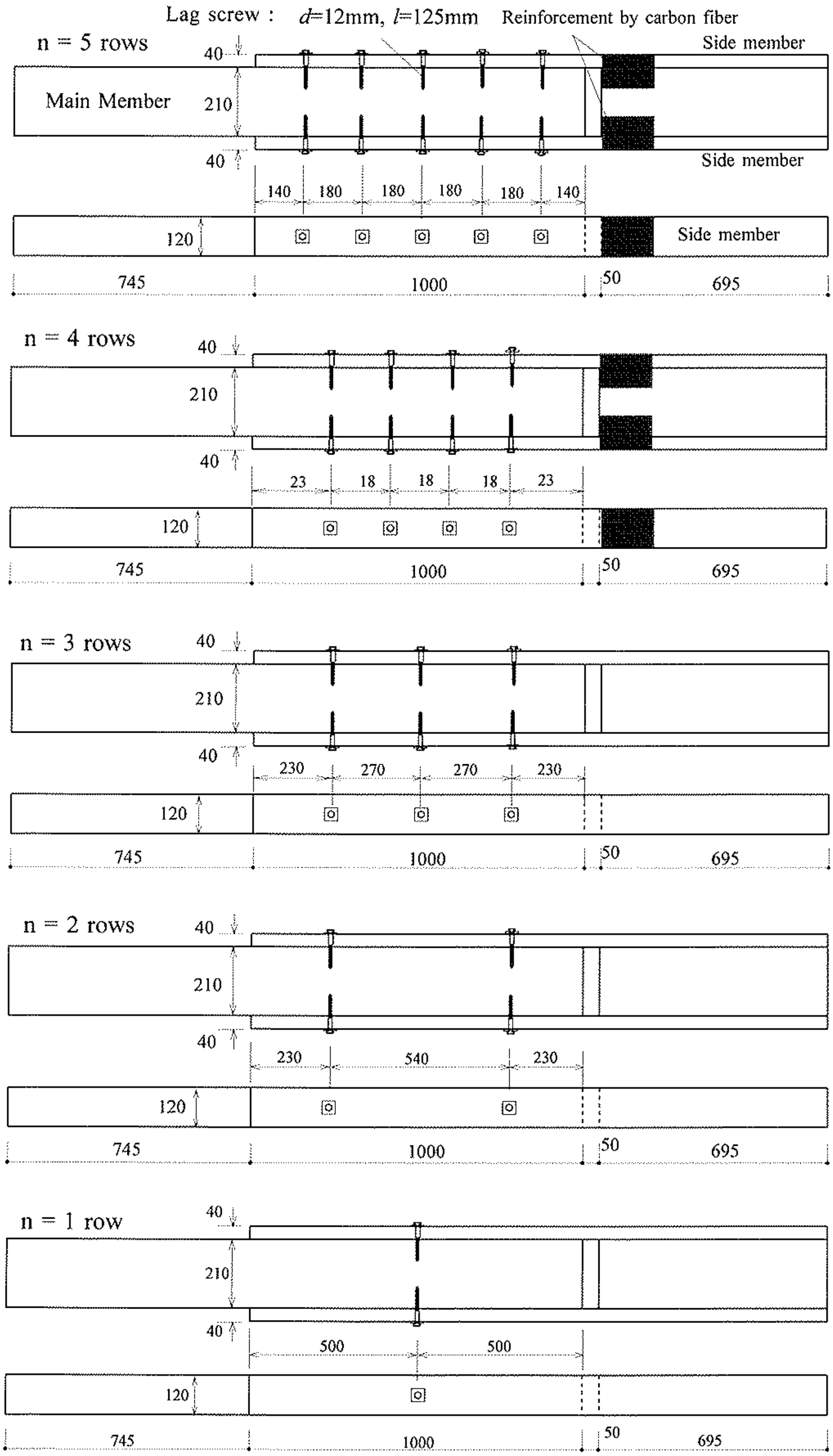
Lag screw : d=12mm, l=125mm
Reinforcement by carbon fiber
n = 5 rows
Side member
Main Member
40
210
40
Side member
140
180
180
180
180
140
120
Side member
745
1000
50
695
n = 4 rows
40
210
40
23
18
18
18
23
120
745
1000
50
695
n = 3 rows
40
210
40
230
270
270
230
120
745
1000
50
695
n = 2 rows
40
210
40
230
540
230
120
745
1000
50
695
n = 1 row
40
210
40
500
500
120
745
1000
50
695

Fig.3 Test Specimens for Multiple Lag Screwed Timber To Timber Joints.

Figure 3 shows test specimens for multiple lag screwed timber to timber joints. Table 1 shows the specification for the test specimens.

Table 1 Configuration and specification of test specimens

Number of lagscrews per shear plane	End distance e_e (mm)	Space between fasteners S (mm)	Main member and cross section (mm)	Side member and cross section (mm)	Lag screw used	Replications
1	500 (41.7d)	—	European red wood glulam 120 x 210 JAS-Grade: E120f330	Western hemlock sawn timber 40 x 120	d=12 mm l=125 mm t =4.5 mm Bearing plate : 40 x 40 mm	3～6
2	230 (19.2d)	540 (41.7d)				
3	230 (19.2d)	270 (22.5d)				
4	230 (19.2d)	180 (15d)				
5	140 (11.7d)	180 (15d)				

3.2 Test Set Up

Photo. 1 shows a servo-actuator type material testing machine (Instron model 8050) whose maximum loading capacity was 1000 kN.

Preliminary, relative slip displacement were measured at various locations, but as the difference of these slip displacement were negligible small, in the main experiments, only one pair of deflection measurement devices were put at the geometrical center of the joint, and the mean of these two displacement was considered as the representative slip S_{rep} of the specimen.

Of three replications in each test series, one specimen was loaded in monotonic tensile load, while the rest of two specimens were loaded in cyclic push-pull loading.

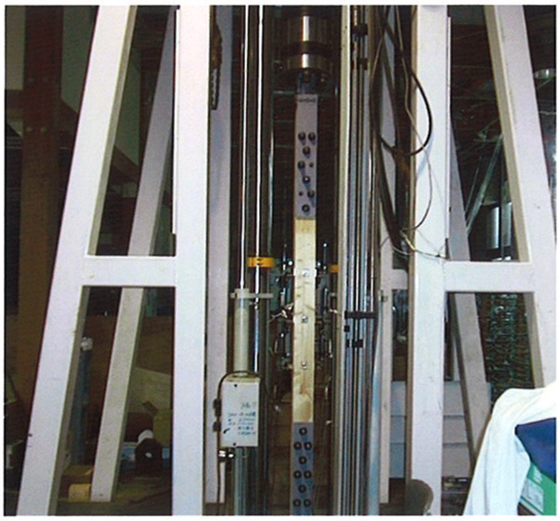

Photo.1 Servo-actuator type testing machine.

4. Results and Discussion

4.1 Best Fit of 3P-exp Function

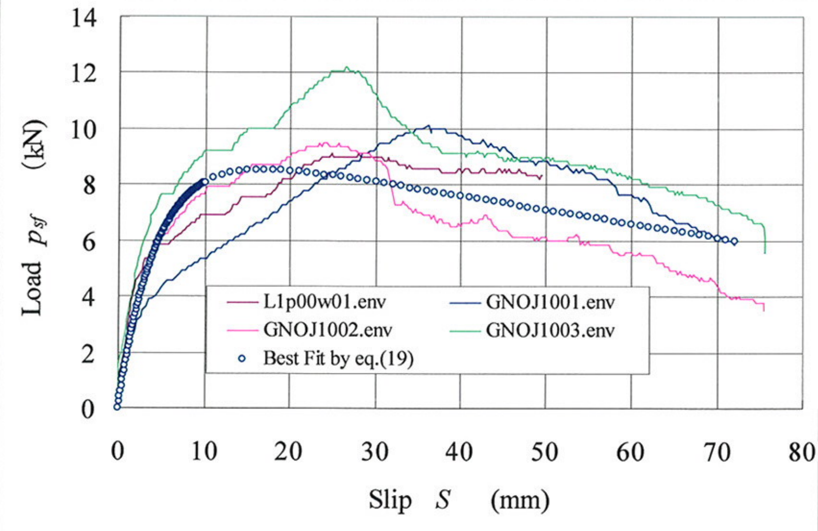

Fig.4 Best fit of experimental data by eq.(19)

Figure 4 shows fitness of 3P-exp function defined by eq.(19) to the experimental load-slip data taken from 1 row lag screwed specimens.

Table 2 shows three parameters obtained by try and error method.

Table 2. 3-parameters

p_o (kN)	K_u (kN/mm)	K_{s0} (kN/mm)
9.6	-0.05	2.1

(refer to eq.(19))

4.2 Comparisons Between Theoretical P-S_{rep} Plots vs Experimental Plots

Figures 5, 6, 7 and 8 show comparisons between theoretical P-S_{rep} plots and those obtained by experiments.

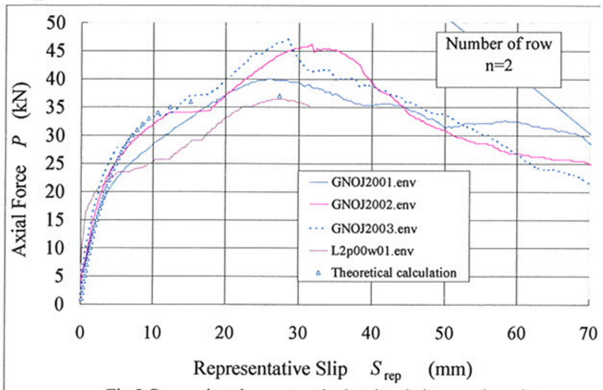

Fig.5 Comparison between calculated and obsereved results

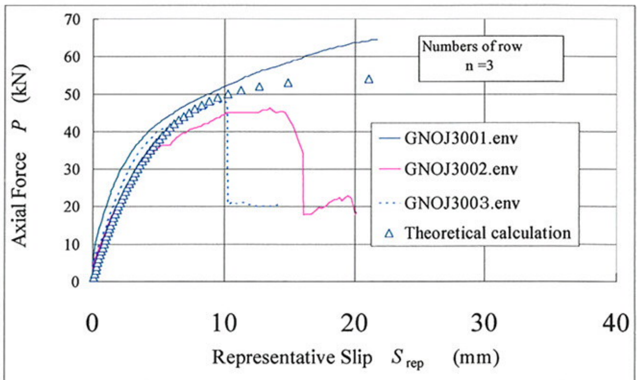

Fig.6 Comparisons beteen Calculated and Observed Results.

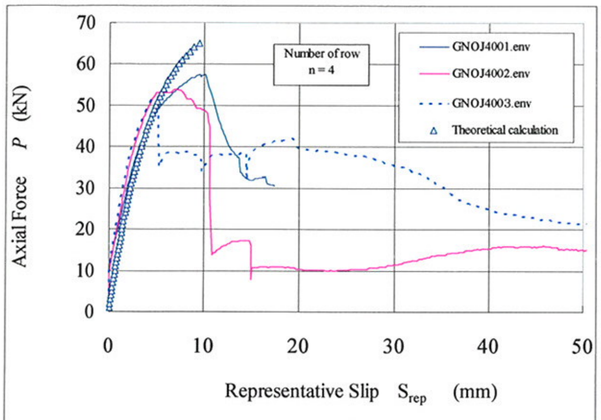

Fig.7 Comparisons between observed and theoretical results.

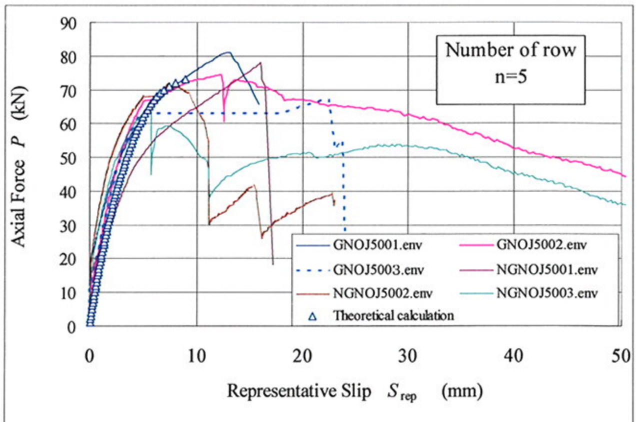

Fig.8 Comparisons between observed and theoretical results.

Up to maximum load, theoretical calculation can predict nonlinear load-slip relationship of multiple lag screwed timber to timber joint fairly well. Once load level exceeds the maximum load, however, it was impossible to predict further nonlinear behavior in which failure phenomena occurs by accompanying with some crack propagation.

4.3 Multiple Effect on the Maximum Strength of the Joints

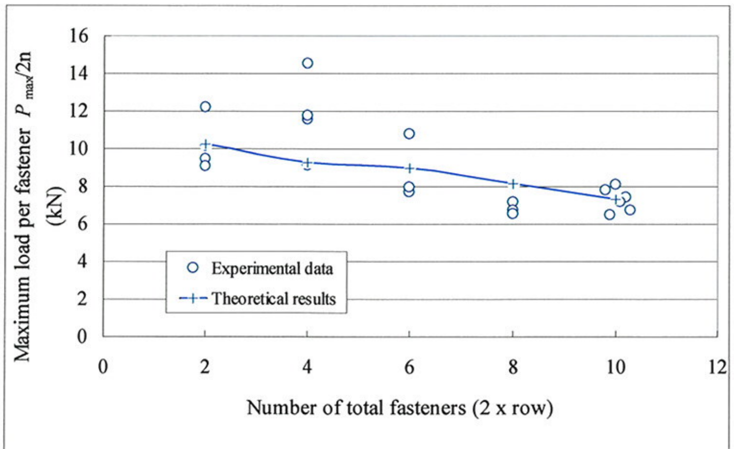

Fig.9 Multiple Effect on the Maxumum Strength per Fastener

Figure 9 shows so-called multiple effect on the maximum strength per fastener. In this fugure, theoretical strength for single fastener joint (n=2) is an average value taken from experiments. It can be seen from this figure that maximum strength per fastener tends to decrease as the number of fastener increases, and also this trend could be predicted theoretically.

5. Conclusions

In this article, we tried to apply the classical Lantos's theory to the nonlinear analysis of the multiple lag screwed timber to timber joints. From the comparisons between calculations and experimental results, it was recognized that the theoretical calculations could predict precisely the nonlinear load-slip behaviors up to the point, which exceeded the yielding point, but before maximum load of each multiple lag screwed joint specimen. So-called multiple effect on the maximum strength per fastener was also recognized by experiment as well as theoretical calculation.

So far as using the 'load incremental method', it was difficult to predict precisely beyond the stage of ultimate load where local cracking or splitting had already occurred.

References

Architectural Institute of Japan (AIJ) edited : Timber Structures Design Standards, Maruzen, Tokyo, 1994. (in Japanese)

G. Lantos : "Load Distribution in a Row of Fasteners Subjected to Lateral Load", Wood Science, **1**(3), 129-136, 1969.

K. Komatsu, S. Takino, M. Nakatani and H. Tateishi: "Lateral Shear Performance of Multiple Lag Screwed Timber Joints with Timber Side Members", Proceeding of the WCTE2002, Shah Alam, Selangor, Malaysia, 2002.

CIB-W18/35-7-3

INTERNATIONAL COUNCIL FOR RESEARCH AND INNOVATION IN BUILDING AND CONSTRUCTION

WORKING COMMISSION W18 - TIMBER STRUCTURES

JOINTS WITH INCLINED SCREWS

A Kevarinmäki

VTT Building and Transport

FINLAND

Presented by: A Kevarinmäki

P Quenneville and H J Blaß asked about anchorage strength and the contributions of the threaded and head pull through components to the strength of the joint. A Kevarinmäki replied that he was of the view that the addition of the two components of threaded and head pull through strength values is justified but that the resulting value is conservative.

Joints with Inclined Screws

Ari Kevarinmäki
VTT Building and Transport, Finland

1 Introduction

The inclined self-tapping screws may be used effectively as fasteners in timber-to-timber connections, because the screws have the particularly high resistance against withdrawal or pushing in (Blass and Bejtka 2001). The test joints of Blass and Bejtka (2001) consisting of screws in tension from 45° to 90° angle between screw axis and the force direction. The maximum value of the load carrying capacity of these tests was reached in direction angle of 60°: about 1,15 times better value than in loading direction of 45° and about 1,5 fold capacity compared to the pure shear joints (90°). However, the clearly best connection stiffness was achieved in loading direction of 45°: about two times higher stiffness than with the angle of 60° and almost 15 times higher than the value for screws loaded perpendicular to the fastener axis. Blass and Bejtka (2001) have presented a modified form of Johansen's yield theory which includes a component where the screw is load in tension and the contact surface between the members is in compression. According to the presented model the maximum load carrying capacity of the tested joints should be reached also with the angle of about 60°, where both the dowel effect of the fasteners and the cosine-component of the axial withdrawal capacity of screws are on the significant high level.

This paper presents the results of a study of screwed joints with inclined screw angle in sawn timber and Kerto-LVL. The aim was to develop design equations for the high stiffness connections using inclined screws with the loading angle of 45°. Two types of single-shear joints were studied: a cross screw joint and a tension screw joint. The cross screw joint is built up of symmetrical screw pairs, in which one screw is under compression and the other under tension. When the joint consisting of only screws in tension, a contact between the wood members is required. The connection stiffness of cross screw joint was believed to be better because small gaps between timber members would have no effect to the initial stiffness of the joint.

2 Withdrawal tests of screws

First the withdrawal capacities and withdrawal stiffnesses of four different types and sizes of screws were tested with different angles between screw axis and the grain direction. An equation for the characteristic withdrawal strength of screw at an angle of the grain has been given in Eurocode 5 (prEN 1995-1-1), but no values for the withdrawal stiffness has not been presented.

Ultimate loading tests were performed on a total of 113 fasteners attached to sawn timber (C24, C40) or Kerto-LVL members in accordance with the EN 1382. Sawn timber material of strength class C24 had been selected in accordance with the method 1 given in EN 28970. The most of test series were loaded with the angle of 45° between the force and grain direction with 5 or 10 parallel test specimens The penetration depth l_p was $8d$ in main test series, when d is the nominal diameter of the screw. The applicability of different types of screws, the behaviour in the compression and the loading angle and the penetration depth were clarified by reference test series. Separate test series were done to determine the withdrawal capacities in standard Kerto-S-LVL and in cross-veneered Kerto-Q-LVL with loading direction 45°. For Kerto-S also edge joint tests with the angle of 45° were done.

The actual test series were made using 6,0 x 90 mm general-purpose screws and 7,5 x 152 mm fully threaded AMO III-screws (see Figure 1.1). In reference test series were used also 4,5x70 mm general-purpose screws and 8,0x140 mm ASSY bore bit screws. No holes were pre-drilled for the fasteners.

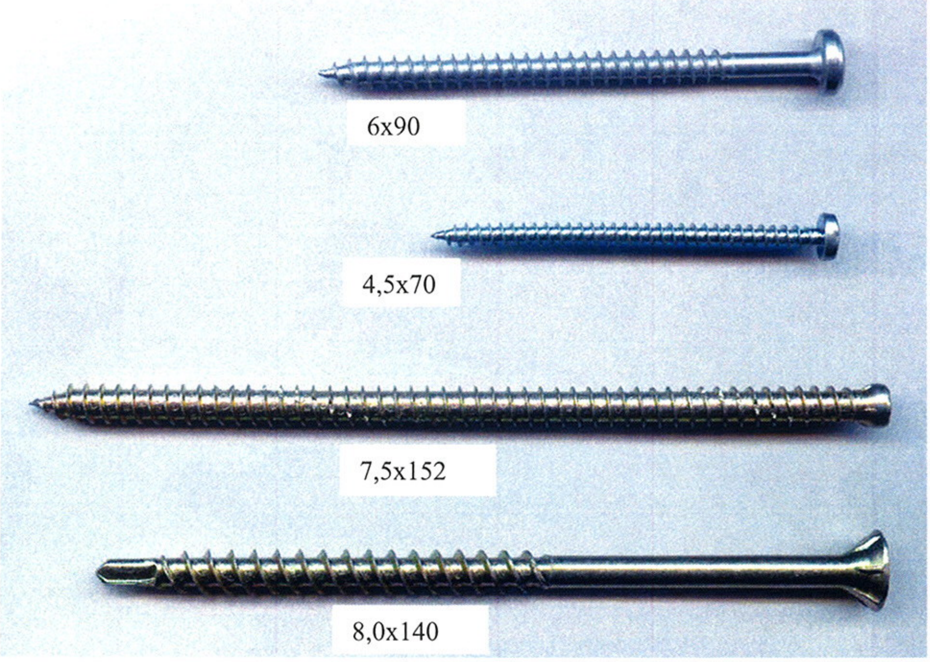

Figure 1.1 *Screws used in withdrawal tests.*

The displacement measurements were made by means of a inductive sensor attached between the timber end and the pulling cylinder. The initial withdrawal stiffness modulus was calculated by the measured slip values for load values $0{,}2F_{\max}$ (δ_{02}) and $0{,}5F_{\max}$ (δ_{05}). The slip values δ_{02} and δ_{05} were chosen as the general edge point of the linear part of load-slip curve. With load values lower than $0{,}2F_{\max}$ there was generally still some effect on the initial displacement due to the looseness of the load attachment.

The failure mode in all of the tests was withdrawal in tension or similar anchorage shear failure in compression tests. No yielding failure of the fastener nor splitting or block shearing of the wood was observed. The test results of direction angle $\alpha = 45°$ are presented in Table 1.1. The used symbols are as follows:

ρ_{65}	is the measured density of wood in moisture content of wood conditioned at RH65,
l_p	is the depth penetration of screw - including the point,
F_{max}	is the mean value of failure load for the test series,
var	is the coefficient of variation of the failure load (= standard deviation/$F_{\max}$),
$f_{ax,45,m}$	is the mean withdrawal strength per the unit area of the effective penetration depth,
K_{ser}	is the withdrawal slip modulus per the unit area of the effective penetration depth and
$F_{ax,45,Rk}$	is the characteristic withdrawal capacity calculated according to Eurocode 5 (prEN 1995-1-1, Final draft version 2002-02-08).

The mean withdrawal strengths have been calculated taken into account the density correction using following formula

$$f_{ax,45,m} = \frac{F_{mean,cor}}{\pi \cdot d \cdot l_{ef}} \tag{1.1}$$

where d is the nominal diameter of the screw (= outer diameter of threaded part),
l_{ef} is the effective penetration depth taken as the penetrationdepth (l_p) minus one screw diameter (d) for 4,5x70, 6x90 and 7,5x152 screws and minus $2d$ for the bore bit screws 8x140 and

$$F_{mean,cor} = F_{max}\left(\frac{\rho_k}{\rho_{65}}\right)^{1,5} \tag{1.2}$$

where ρ_k is the characteristic timber density: 350 kg/m^3 for strength class C24, 420 kg/m^3 for C40 and 480 kg/m^3 for Kerto-LVL.

The slip modulus has been calculated per the unit area of the effective penetration depth:

$$K_{ser} = \frac{k_s}{\pi \cdot d \cdot l_{ef}} \tag{1.3}$$

where
$$k_s = \left(\frac{0{,}5F_{max}}{\frac{5}{3}(\delta_{05} - \delta_{02})}\right) \tag{1.4}$$

where δ_{02} and δ_{05} are the measured mean slip values for the load values $0{,}2F_{max}$ and $0{,}5F_{max}$.

Table 1.1 *Withdrawal test results of series with direction angle $\alpha = 45°$.*

Timber		Screw	l_p	F_{max}	var	$f_{ax,45,m}$	K_{ser}	$F_{ax,45,Rk}$
class	ρ_{65} (kg/m^3)	d x l	(mm)	(N)	(%)	(N/mm^2)	(N/mm^3)	**EC5** (N)
C24	366	6x90	48	4303	8,3	5,08	5,21	3929
C24	356	6x90	70	5275	8,4	4,26	4,06	5504
C24	387	7,5x152	60	6133	7,0	4,26	6,20	5616
C24	389	7,5x152	90	10290	9,6	4,52	5,97	8062
C40	429	6x90	48	5199	5,4	6,36	7,09	5165
C40	429	7,5x152	60	7523	6,8	5,89	7,36	7382
C24	349	4,5x70	36	1792	7,4	4,04	5,23	2480
C24	347	8x140	72	4215	1,3	3,03	1,61	6226
C24 [1)	340	6x90	48	3775	15,4	4,98	3,45	3929
C24 [1)	348	6x90	70	4769	12,3	3,99	4,15	5504
Kerto-S	503	6x90	48	5401	9,3	6,36	7,01	6311
Kerto-Q	543	6x90	48	6474	14,5	6,80	7,76	6311
Kerto-S [2)	499	6x90	48	5021	4,7	5,98	4,92	6311
Kerto-S	498	7,5x152	60	7294	5,0	5,58	6,10	9019
Kerto-Q	539	7,5x152	60	8180	3,5	5,56	4,97	9019
Kerto-S [2)	474	7,5x152	60	7566	6,9	6,23	5,07	9019

[1) Compression test

[2) Edge joint test

The withdrawal tests with sawn timber showed that both the withdrawal capacity and the withdrawal stiffness may be supposed to depend on the timber density in the power of 1,5: $\rho^{1,5}$. The effect of penetration depth may be taken into account by a factor $(l_{p,ref}/l_p)^c$, where $c = 0,2$ for the withdrawal strength and 0,3 for the withdrawal slip modulus.

As mean value the 7,5 mm AMO-screws had 7 % lower withdrawal strength than 6,0 mm general screws, but the slip modulus was as mean value almost the same. The 8 mm bore bit screws had the worst withdrawal strength and slip modulus. The bore bit head of this screw type seems to be too large; it breaks the grain of wood. The general-purpose screws $d = 4,5$ mm and $d = 6,0$ mm had almost equal slip modulus, but the mean withdrawal strength $f_{ax,45,m}$ of 4,5 mm screws was 20 % smaller than the withdrawal strength of 6,0 mm screws. According to Final Draft prEN 1995 the diameter effect should be opposite as in these tests. Probably the thread dimensions of 4,5 mm screws are too small for the effective utilisation of the withdrawal capacity. The withdrawal strength depends in addition of the screw diameter also on the thread type and on the thread dimensions.

The test results of tension and compression test series showed that the withdrawal strength was slightly lower in compression than in tension. The slip modulus was as mean value 15 % lower in compression, but there was a big variation between the test series: with longer penetration depth the slip modulus was higher in compression than in tension.

The withdrawal capacities of Kerto-S, Kerto-Q and edge Kerto-S test series were almost equal. Also the slip modulus was nearly the same with Kerto-S and Kerto-Q. In edge joints of Kerto-S the withdrawal slip modulus was as mean value 23 % lower than with flatwise joint of Kerto-S.

The characteristic withdrawal capacities calculated according to Eurocode 5 (prEN 1995) were exceeded only with the sawn timber test series. EC5 was clearly at the unsafe side (roughly 40 %) both with the 4,5 mm general screws and with the 8,0 mm bore bit screws. The calculation method of Eurocode 5 was at the unsafe side also for Kerto-LVL with all the tested screws (generally about 30 %). The withdrawal strength of different screw types and sizes should be determined separately for different types of timber materials.

3 Joint tests with inclined screws

The shear force capacity and stiffness of altogether 145 inclined screw joint test specimens were tested in Helsinki University of Technology (HUT 2002). The angle between the screw axis and the force direction was 45° and the variables of the tests were as follows: timber material (planed solid timber C24, Kerto-S or Kerto-Q), screw and joint type, member thickness, number of screws, end distances, fastener spacings and moisture changes. There were generally 5 parallel test specimens in each test series. The tests were done as compression tests as shown in Figure 3.1 in accordance with EN 26891. Sawn timber material of strength class C24 had been selected in accordance with EN 28970.

The failure mode of all the test specimens was the withdrawal on the point or head side of the screws. The maximum load was achieved with a small ultimate slip value: it was typically 1..2 mm between timber members. After the maximum load was achieved, the load carrying capacity of the joints were still on the rather high level due to the developed dowel effect. The loading was stopped until the slip value of 15 mm was reached, where the load was generally still about

50 % of the maximum load. Slip-load behaviour of two test series is presented in Figure 3.2 as typical examples. The tension screw joints had generally 25..30% higher load carrying capacity per screw than the cross screw joints due to the friction between timber members occurred only in tension screw joints.

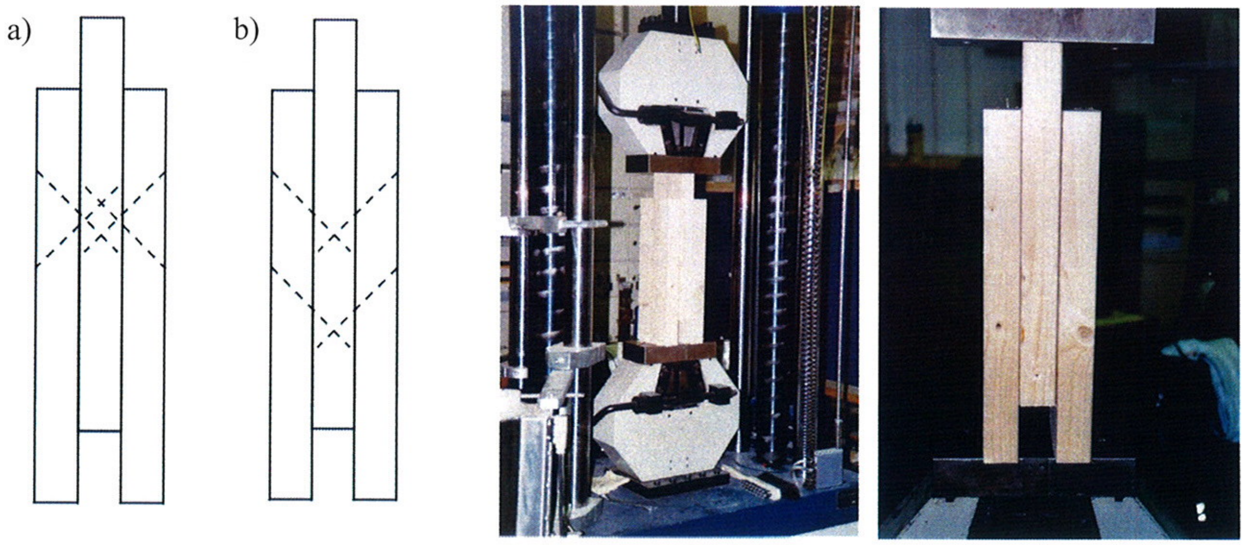

Figure 3.1 *Type of test specimens and compression test set-up. a) a cross screw joint and b) a tension screw joint.*

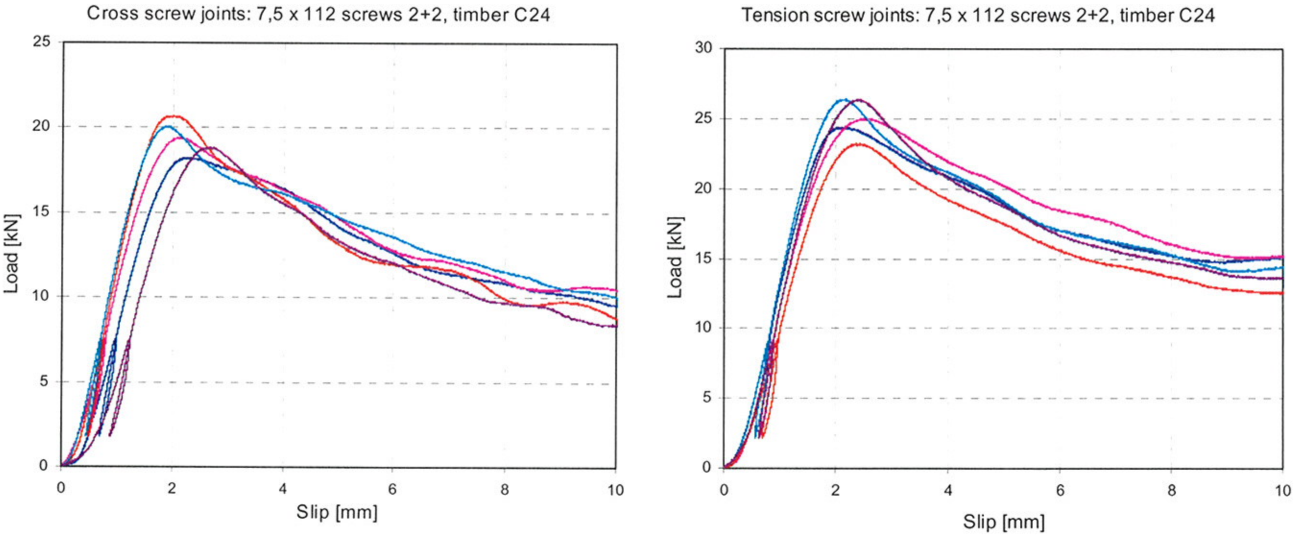

Figure 3.2 *Slip-load behaviour of two test series. Slip has been measured as movement of loading cylinder, which has caused the initial displacement of the curves with load values < 2 kN.*

The summary of the test results are shown in Tables 3.1 – 3.4 together with the calculated comparison values. The comparison values have been calculated according to the design method presented in chapter 4 with the characteristic withdrawal strengths and the mean withdrawal slip modulus determined in the withdrawal tests. The used symbols are as follows:

F_{max} is the mean value of failure loads reduced with the density $= F_{mean}(\rho_k/\rho_{test})^{1,5}$,
var is the coefficient of variation of the failure load (= standard deviation/F_{mean}),

$F_{k,test}$ is the characteristic capacity determined by testing,
F_k is the characteristic capacity calculated as presented in chapter 4,
$k_{s,test}$ is the mean value of slip modulus determined by testing and
nK_s is the slip modulus of joint calculated according to chapter 4.

Table 3.1 *Test results of cross screw joints with solid timber.*

Screws		F_{max}	var	$F_{k,test}$	$F_{k,test}/F_k$	$k_{s,test}$	$k_{s,test}/nK_s$	Note!
d x L	n	kN	%	kN		kN/mm		
6x100	2+2	10,51	5,4 %	7,88	1,09	9,40	1,21	
6x100	2+2	11,11	9,1 %	8,33	1,15	12,91	1,66	fast loading!
6x100	2+2	10,33	7,2 %	7,75	1,07	9,11	1,17	loading cycles, 3 specimens
7,5x112	2+2	17,65	5,0 %	13,24	1,07	12,83	1,02	
7,5x112	2+2	16,64	13,6 %	10,97	0,89	13,59	1,08	loading cycles, 3 specimens
7,5x112	4+4	33,25	5,4 %	24,94	1,01	23,34	0,93	4+4 screws
7,5x112	4+4	30,94	10,0 %	23,21	0,94	23,60	0,94	reduced end distance
7,5x112	4+4	32,09	8,8 %	24,07	0,97	23,22	0,92	reduced screw spacings
7,5x112	8+8	58,97	10,2 %	43,91	0,89	46,50	0,92	8+8 screws
7,5x112	8+8	57,88	3,7 %	43,41	0,88	46,79	0,93	reduced screw spacings
7,5x112	2+2	16,32	8,1 %	12,24	0,99	11,04	0,88	wet timber, RH90
7,5x112	2+2	18,92	9,1 %	14,19	1,15	12,91	1,02	dry timber, RH30
		mean:	8,2 %		0,98		0,96	

Table 3.2 *Test results of cross screw joints with Kerto-LVL.*

Screws		F_{max}	var	$F_{k,test}$	$F_{k,test}/F_k$	$k_{s,test}$	$k_{s,test}/nK_s$	Note!
d x L	n	kN	%	kN		kN/mm		(S = Kerto-S)
7,5x112	2+2	23,01	5,4 %	17,26	1,04	18,36	1,03	Kerto-Q
7,5x112	2+2	23,00	5,1 %	17,25	1,04	14,59	0,90	Kerto-S
7,5x112	2+2	20,37	2,7 %	15,28	1,02	14,36	1,01	Edge joint of Kerto-S
7,5x152	2+2	29,65	2,3 %	22,24	1,08	19,74	1,01	S, long screws
7,5x112	2+2	24,27	10,1 %	18,15	1,09	13,59	0,84	S, loading cycles, 3 specimens
6x100	2+2	15,07	4,0 %	11,30	1,07	9,71	0,96	S, loading cycles, 3 specimens
7,5x112	4+4	46,25	1,6 %	34,69	1,04	39,27	1,10	Kerto-Q, 4+4 screws
7,5x112	4+4	47,16	2,1 %	35,37	1,06	34,85	1,08	Kerto-S, 4+4 screws
7,5x112	4+4	23,23	5,8 %	17,42	1,05	19,03	1,18	S, moisture cycles: RH90-30
		mean:	4,3 %		1,05		1,01	

Table 3.3 *Test results of tension screw joints with solid timber.*

Screws		F_{max}	var	$F_{k,test}$	$F_{k,test}/F_k$	$k_{s,test}$	$k_{s,test}/nK_s$	Note!
d x L	n	kN	%	kN		kN/mm		
6x100	2+2	13,72	9,3 %	10,29	0,94	10,55	1,23	
6x100	2+2	14,7	11,5 %	10,48	0,95	7,91	0,93	small gap between members
7,5x112	2+2	22,41	5,4 %	16,81	1,15	15,73	1,24	
7,5x112	2+2	19,98	15,0 %	12,47	0,85	13,09	1,03	wet timber, RH90
7,5x112	2+2	18,64	10,6 %	13,72	0,94	10,81	0,85	dry timber, RH30
		mean:	10,6 %		0,97		1,01	

Table 3.4 *Test results of tension screw joints with Kerto-LVL.*

Screws		$F_{\max}$	var	$F_{k,test}$	$F_{k,test}/F_k$	$k_{s,test}$	$k_{s,test}/nK_s$	Note!
d x L	n	kN	%	kN		kN/mm		(S = Kerto-S)
7,5x112	2+2	31,47	4,3 %	23,60	1,10	23,79	1,33	Kerto-Q
7,5x112	2+2	31,91	4,5 %	23,93	1,11	17,03	1,05	Kerto-S
7,5x122	2+2	30,64	4,9 %	22,98	1,07	20,46	1,26	S, moisture cycles: RH90-30
		mean:	4,6 %		1,09		1,21	

The calculated capacities and stiffnesses corresponded very well with the test results. The analysis model based on the sum of the cosine-components of the axial withdrawal capacities and stiffness of screws. The friction between timber members has been taken into account in calculation of the capacity of tension screw joints. No dowel effect has been taken into account in calculations. The calculated stiffnesses of tension screw joint were exceeded clearly, when the timber members had been assembled to the contact. However, if there were a gap – purposefully left or developed due to the drying shrinkage of timber members – the calculated stiffnesses were not reached.

4 Proposal for design method of joints with inclined screws

This proposal concerns the use of inclined screws in the single shear joint of Figure 4.1, where the screw inclination angle is $\alpha = 45°$ both in regard to the force direction and the wood grain direction. The withdrawal strength and stiffness of the screws shall be determined by the test procedure described in EN 1382 with an angle of $\alpha = 45°$ between the grain direction and screw axis and using an penetration length of $8d$. This design method is meant to be used in connection with the limit state design described in Eurocode 5. The screws should be fully threaded or partially threaded, where the smooth part diameter is not more then 75 % of the screw nominal diameter (thread outer diameter). No pre-drilling is done.

Cross screw joint capacity

The cross screw joint is built up of symmetrical screw pairs, in which one screw is under compression and the other under tension.

The design shear capacity is

$$R_d = n_p\left(R_{C,d} + R_{T,d}\right)\cos\alpha \tag{4.1}$$

where n_p is the number of screw pairs in the joint and
α is the screw angle = 45° (see Figure 4.1a).

The screw compression capacity is

$$R_{C,d} = \min\begin{cases} f_{a,1,d}\pi d\, s_1 \\ f_{a,2,d}\pi d\, s_2 \\ 0{,}8F_{u,d} \end{cases} \tag{4.2}$$

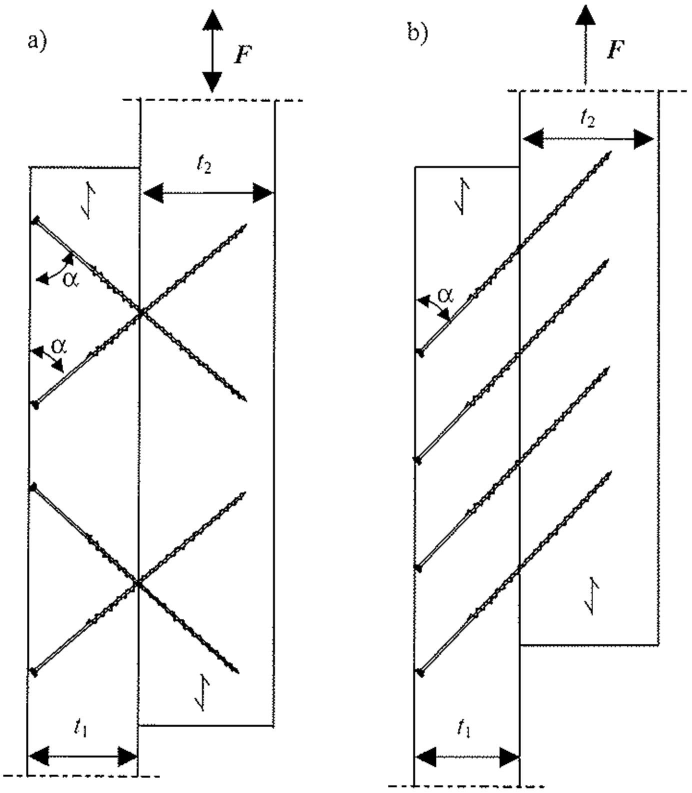

Figure 4.1 *The inclined screw joint a) cross screw joint b) tension screw joint.*

and the screw withdrawal capacity is

$$R_{T,d} = \min \begin{cases} f_{a,1,d} \pi d s_1 + f_{head,d} d_h^2 \\ f_{a,2,d} \pi d (s_2 - d) \\ F_{u,d} \end{cases} \tag{4.3}$$

where		
	d	is the outer diameter of the thread (screw nominal size),
	s_1	is the threaded length of the screw in the member (1) which is towards the screw head,
	s_2	is the threaded length of the screw in the member (2) which is towards the screw tip,
	$F_{u,d}$	is the design value of the screw tension capacity,
	$f_{a,i,d}$	is the design withdrawal strength in member i,
	d_h	is the head diameter of the screw and
	$f_{head,d}$	is the design pull through strength of the screw head determined experimentally according to EN 1383.

The screw withdrawal strength is

$$f_{a,i,d} = \frac{k_{mod}}{\gamma_M} f_{ax,45,k} \left(\frac{8d}{s_i} \right)^{0,2} \tag{4.4}$$

where		
	k_{mod}	is the load duration and moisture influence factor from EC 5 for member i,
	γ_M	the safety factor of timber material for member i (= 1,3),
	s_i	is the length of the threaded part of the screw in member i and

$f_{ax,45,k}$ is the characteristic withdrawal strength of the screw determined in grain direction angle of $\alpha = 45°$ and penetration length of $s_2 = 8d$.

Tension screw joint capacity

A joint consisting of only screws in tension, a contact between the wood members is required. For this reason these joints should not be used in conditions where wood drying could cause a gap of over $0{,}2d$. The gap is determined from the wood shrinkage at a distance of the screw length ($L\sin\alpha$).

The design shear capacity of joints composed of only tension screw is

$$R_d = nR_{T,d}(\cos\alpha + \mu \sin\alpha) \tag{4.5}$$

where
n is the number of screws in the joint,
$R_{T,d}$ is the screw withdrawal capacity, using eq. (4.3),
α is the inclination angle = 45° (see Figure 4.1b) and
μ is the kinetic friction coefficient between the members.

If both member surfaces are planned and uncoated spruce, the kinetic friction coefficient in the grain direction may be taken as $\mu = 0{,}26$ in service classes 1 and 2. If both surfaces are untreated laminated veneer lumber in flatwise (unplanned and uncoated), the kinetic friction coefficient in eq. (4.5) may be taken as $\mu = 0{,}4$.

Joint stiffness

The instantaneous slip of the inclined screw joint is

$$u_{inst} = \frac{F}{nK_s} \tag{4.6}$$

where
F is the external force,
n is the number of screws (for cross screw joints $n = 2n_p$) and
K_s is the slip modulus for an axially loaded screw, eq.(4.7).

In case of tension joints, a term should be added to equation (4.6), which considers the possible drying shrinkage of the members (δ) as a pre-slip: $\delta/\tan\alpha$.

For axially loaded screws the slip modulus is

$$K_s = \frac{1}{\frac{1}{k_1} + \frac{1}{k_2}} \tag{4.7}$$

where $k_1 = K_{1,ser}\pi d s_1$ and $k_2 = K_{2,ser}\pi d(s_2 - d)$ (4.8 and 4.9)

The withdrawal stiffness for the threaded part of the screw is

$$K_{i,ser} = K_{ser}\left(\frac{8d}{s_i}\right)^{0,3} \tag{4.10}$$

where s_i is the length of the threaded part of the screw in member i and
K_{ser} is the mean withdrawal slip modulus per the unit area of the screw determined in grain direction angle of $\alpha = 45°$ and penetration length of $s_2 = 8d$.

Structural detailing

The timber member thickness t has to be at least (does not concern Kerto-Q):

$$t = \max\begin{cases} 7d_s \\ (13d_s - 30)\dfrac{\rho_{k,i}}{400} \end{cases} \tag{4.11}$$

where d_s is for partially threaded screws the diameter of the unthreaded part and for fully threaded screws it is the thread inner diameter in millimetres,
$\rho_{k,i}$ is the characteristic density of the wood member in kg/m^3.

In the same joint, different types or sizes of screws may not be combined. All the screws are placed with the same inclination angle α. The screws are placed centrally to the external force. The wood grain angle should be in the direction of the external force.

The screw penetration length in the member towards the screw tip should be at least $6d$. The screws are screwed deep enough so that the screw head is in full contact with the member surface. The members should be compressed together so that no gaps are present. However, the screwing moment shall be limited under the characteristic torsion capacity of the screw.

The screw spacing and the end and edge distance minimum values are given in Table 4.1, notations described in Figure 4.2. The tensioned and compressed screws of the cross screw pair may be placed, as according to Figure 4.2b, in line ($a_6 = 0$), if the screw pairs penetration point distance is $a_5 \leq 2d$ and the consecutive screw pairs distance is long enough that the screws pointing to different directions do not touch each other. The screws from opposite sides may overlap in the centre member, if $(t_2 - s_2\sin\alpha)$ is higher than $4d_s$.

Table 4.1 *Proposal for minimum screw spacings, end and edge distances for inclined screw joints based on the spacings and distances used in joint tests. For cross joints the distances for tensioned and compressed screws (a_5 and a_6) are given minimum and maximum values. L is the screw length and t_1 is member thickness of the one towards the screw head.*

		Cross screw joint	Tension screw joint
a_1	grain direction	$12d - a_6$	$8d$
$a_{1,p}$	cross joints consecutively	$2L\cos\alpha \geq 14d - a_5$	
a_2	perpendicular to grain direction	$4d$	$4d$
$a_{3,t}$	joint in tension	$12d - a_6$	$8d$
$a_{3,c}$	joint in compression	$10d - a_6$	$6d$
a_4	edge distance	$4d$	$4d$
a_5	cross joints staggered	$0 \dots 3t_1$	
$a_{5,p}$	cross joints consecutively	$0 \dots 2d$	
a_6	cross joints staggered	$2d \dots 4d$	
$a_{6,p}$	cross joints consecutively	0	

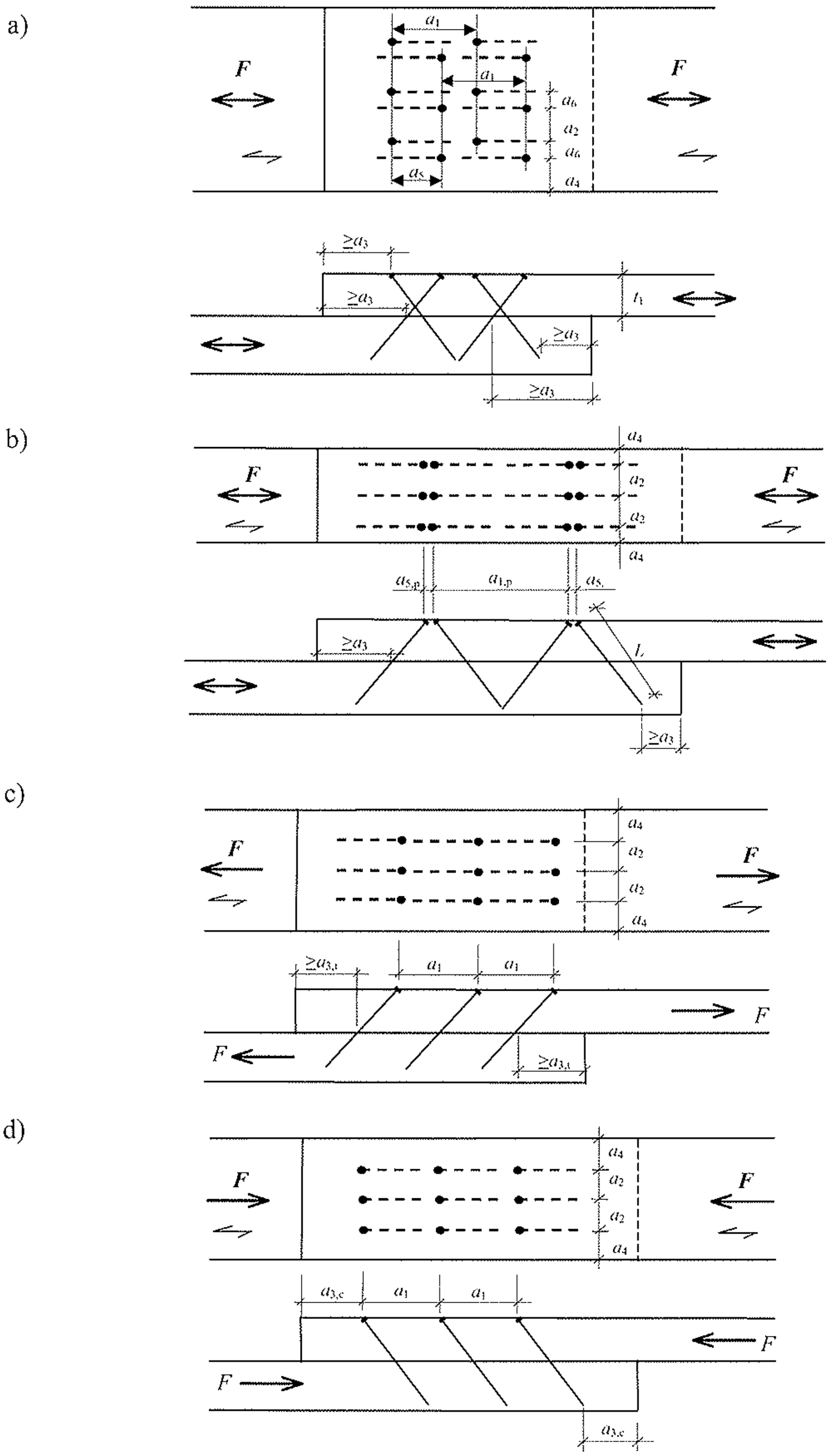
a)
F
F
a_1
a_1
a_6
a_2
a_6
a_4
a_5
$\geq a_3$
$\geq a_3$
t_1
$\geq a_3$
$\geq a_3$
b)
F
F
a_4
a_2
a_2
a_4
$a_{5,p}$
$a_{1,p}$
a_5
L
$\geq a_3$
$\geq a_3$
c)
F
F
a_4
a_2
a_2
a_4
$\geq a_{3,t}$
a_1
a_1
F
F
$\geq a_{3,t}$
d)
F
F
a_4
a_2
a_2
a_4
$a_{3,c}$
a_1
a_1
F
F
$a_{3,c}$

Figure 4.2 *Inclined screw joints: a) staggered cross joint, b) consecutive cross joint, c) tension screw joint under a tension force and d) tension screw joint under a compression force.*

5 Conclusions

The analysis of joint test results showed that the load-carrying capacity and stiffness of the single shear inclined screw joints may be calculated purely by the model of the axial forces of screws, when the angle between screw axis and the joint force direction is 45°. However, the effect of penetration length and timber density to the withdrawal strength and stiffness shall be taken into account, and the effect of screw head and the friction between timber members may be utilised. The ultimate slip of the inclined screw joint with the screw angle of 45° is so small (1..2 mm) that the dowel effect should not be taken into account in the calculation of joint capacity.

The load carrying capacity per a screw was better with the tension screw joint than with the cross screw joint because the friction force is affecting between timber members only with the tension screw joints. However, if there were any gap between timber members, e.g. due to drying of timber, the initial stiffness was clearly better with the cross screw joints.

Utilisation of the withdrawal capacity and stiffness of screws leads to increased load-carrying capacities and stiffnesses. The extremely high stiffness of the inclined screw joints may be utilised for example with mechanically jointed beams and columns. Although the withdrawal failure is brittle, the inclined screw joints have still rather high load-carrying capacity with a long displacement ability after the ultimate load has been exceeded due to the dowel effect of screws. This improves the safety of the structural system.

6 Acknowledgements

Professor Hans Joachim Blass is gratefully acknowledged for directing the Finnish partners for this interesting subject, for the discussions and the advice. Thanks to Simo Koponen and Anu Huovinen from Helsinki University of Technology for the co-operation with the joint tests. This research has been ordered and financed by Finnforest Oyj and Sepa Oy.

7 References

Blass, H.J. & Bejtka, I., 2001, Screws with Continuos Threads in Timber Connection. Proceedings PRO 22: International RILEM Symposium on Joints in Timber Structures. Stuttgart, Germany. pp. 193-201.

HUT, 2002, Research Report No. TRT-PUU-1-02: Screw joints with inclined screw angle in sawn timber and Kerto-LVL. Helsinki University of Technology, Espoo, Finland.

prEN 1995-1-1, 2002, Eurocode 5 – Design of timber structures – Part 1-1: General rules and rules for buildings. Final Draft, Version 2002-02-28.

VTT, 2001, Research Report No. RTE 4420/01: Withdrawal tests of screws at inclined angle to grain in sawn timber and Kerto-LVL. VTT Building and Transport, Espoo, Finland.

CIB-W18/35-7-4

INTERNATIONAL COUNCIL FOR RESEARCH AND INNOVATION
IN BUILDING AND CONSTRUCTION

WORKING COMMISSION W18 - TIMBER STRUCTURES

JOINTS WITH INCLINED SCREWS

I Bejtka
H J Blaß

Universität Karlsruhe (TH)

GERMANY

Presented by: H J Blaß

In answer to F Rouger´s question H J Blaß indicated that he did not have an explanation for the more conservative values observed for the longer specimens. A Kevarinmäki asked if the effects of the screw head on withdrawal of the screw and about the dowel effect especially for large inclination angles had been considered. H J Blaß replied that the screw head effect was not taken into account as it was not considered to be effective and that the dowel effects were indeed small but would be considered.

Joints with Inclined Screws

I. Bejtka, H. J. Blaß - Universität Karlsruhe (TH), Germany

1 Introduction

Screws, bolts and dowels loaded perpendicular to the fastener axis are dowel-type fasteners, whose load-carrying capacity in timber-to-timber connections may be determined based on Johansen's yield theory (Johansen, 1949). The ultimate load of joints with dowel-type fasteners loaded perpendicular to the fastener axis is limited by the embedding strength of the timber members and the bending capacity of the fasteners.

Exploiting the withdrawal capacity of long screws with continuous threads leads to increased load-carrying capacities and hence more economic connections. In order to increase the load-carrying capacity in timber-to-timber connections, the screws are not placed perpendicular to the interface between the members to be connected but arranged under an angle between 75° and 40° between the screw axis and the grain direction. The ultimate load of joints with inclined screws is then limited by the embedding strength of the timber members, the bending capacity and the withdrawal capacity of the fasteners as well as the friction between the timber members. Principally the screw is loaded in tension and the contact surface between the members in compression.

This paper compares the test results of connections with inclined screws and with fasteners loaded perpendicular to their axis. A proposal for design rules for single-shear joints with inclined screws is presented.

2 Timber-to-timber connections with inclined screws

2.1 Theory and design

The load carrying capacity of joints with dowel-type fasteners can be determined by the different equations for the three failure modes based on Johansen's yield theory. The load-carrying capacity for failure mode 1 is limited by the embedding strength of one or two timber members. For failure modes 2 and 3, the load-carrying capacity is limited by the embedding strength of the timber members and the bending capacity of the fastener. In failure mode 2 one plastic hinge and in failure mode 3 two plastic hinges per shear plane and fastener occur.

In order to determine the load-carrying capacity of timber-to-timber connections with inclined screws Johansen's yield theory is extended. For this purpose, the withdrawal capacity of the screws, the angle between the screw axis and the force direction as well as the friction between the timber members are additional parameters influencing the load-carrying capacity. The friction resistance between the timber members is activated as soon as the joint is loaded since the contact surface between the timber members is loaded in compression. A timber-to-timber connection with inclined screws in shown in figure 1.

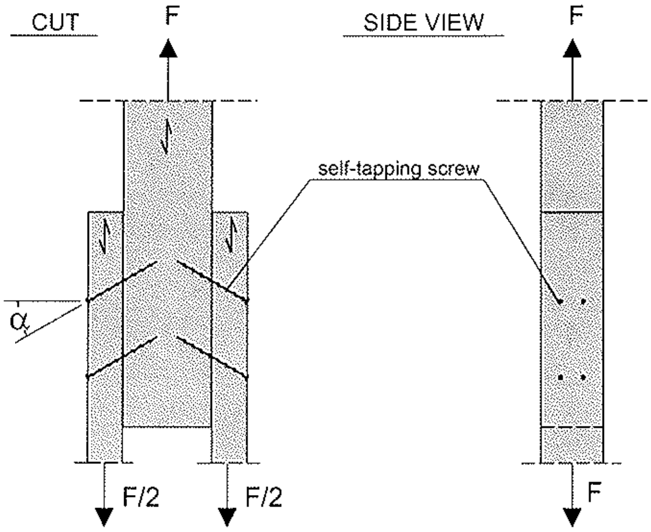

Figure 1: Timber-to-timber connection with inclined screws

One of the basic assumptions in Johansen´s yield theory is an ideal rigid-plastic material behaviour of the timber in embedding and of the fastener in bending. The withdrawal behaviour of screws, however, shows a clear maximum with a subsequent distinct load decrease. For the extension of Johansen's yield theory, the load-displacement behaviour of screws loaded in withdrawal therefore has to be taken into account. Depending on the axial displacement of the screw when reaching the ultimate load of the connection, the screw may or may not have reached its withdrawal capacity. The distribution of the shear stress along the length of the screw consequently has to be taken into account in the model. One possibility is to use a reduced withdrawal parameter taking into account the shear stress distribution along the screw length.

Using a reduced withdrawal parameter also allows to take into account the interaction between embedding and withdrawal strength of fasteners loaded parallel and perpendicular to the fastener axis. Since the distribution of the embedding stresses along the length of the fastener depends on the failure mode, also the modified withdrawal parameter $f_{l,mod}$ depends on the failure mode considered. The derivation of the different modified withdrawal capacity parameters is shown in paragraph 2.2.

In the following the extended design equation for Johansen´s failure mode 3 is derived (see figure 2). Basic assumptions are:

- Ideal rigid-plastic material behaviour for the timber under embedding stresses and of the fastener in bending.
- Averaged modified withdrawal parameters $f_{l,mod,i,j}$ for different failure modes considering the withdrawal behaviour depending on the lateral load. (see paragraph 2.2)

  i timber member (member 1 or 2)

  j Johansen´s failure mode (1a,l - 1a,r - 1b - 2a - 2b or 3)
- The angle or the inclination α is defined as the angle between the screw axis and the direction perpendicular to the grain.

For the notation see figure 2.

The following equations are based on the equilibrium in the undeformed state. If the deformed shape of the fastener is taken into account, the ultimate connection load increases.

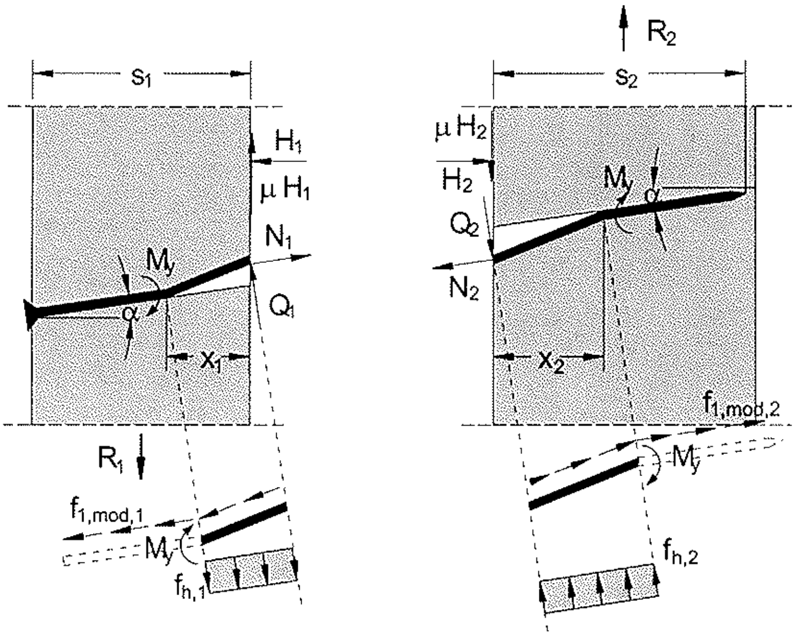

Figure 2: Forces and stresses in a timber-to-timber connection with an inclined screw for Johansen's failure mode 3

The fastener bending moment in the interface between the timber members is:

$$M_1 = M_y - \frac{f_{h,1} \cdot d \cdot x_1^{\;2}}{2 \cdot \cos^2\alpha} \qquad \text{and} \qquad M_2 = -M_y + \frac{f_{h,2} \cdot d \cdot x_2^{\;2}}{2 \cdot \cos^2\alpha}$$

with $M_1 = M_2$ and $f_{h,2} = \beta \cdot f_{h,1}$ follows:

$$x_1^{\;2} + \beta \cdot x_2^{\;2} = \frac{4 \cdot M_y \cdot \cos^2\alpha}{d \cdot f_{h,1}} \tag{1}$$

Forces in the interface between the timber members:

$$R_1 = Q_1 \cdot \cos\alpha + N_1 \cdot \sin\alpha + \mu \cdot H_1 \tag{2a}$$

$$R_2 = Q_2 \cdot \cos\alpha + N_2 \cdot \sin\alpha + \mu \cdot H_2 \tag{2b}$$

$$H_1 = N_1 \cdot \cos\alpha - Q_1 \cdot \sin\alpha \tag{2c}$$

$$H_2 = N_2 \cdot \cos\alpha - Q_2 \cdot \sin\alpha \tag{2d}$$

with:

$$Q_1 = \frac{f_{h,1} \cdot d \cdot x_1}{\cos\alpha} \quad (3a) \qquad\qquad Q_2 = \frac{f_{h,2} \cdot d \cdot x_2}{\cos\alpha} \quad (3b)$$

$$N_1 = \frac{f_{1,mod,1} \cdot d \cdot s_1}{\cos\alpha} \quad (3c) \qquad\qquad N_2 = \frac{f_{1,mod,2} \cdot d \cdot s_2}{\cos\alpha} \quad (3d)$$

Substituting (3a), (3c) and (2c) in (2a) yields equation (4a):

$$R_1 = f_{1,mod,1} \cdot d \cdot s_1 \cdot (\mu + \tan\alpha) + f_{h,1} \cdot d \cdot (1 - \mu \cdot \tan\alpha) \cdot x_1 \tag{4a}$$

Similarly substituting (3b), (3d) and (2d) in (2b) yields equation (4b):

$$R_2 = f_{1,mod,2} \cdot d \cdot s_2 \cdot (\mu + \tan\alpha) + f_{h,2} \cdot d \cdot (1 - \mu \cdot \tan\alpha) \cdot x_2 \tag{4b}$$

Force equilibrium $R_1 = R_2$ results in equation (5):

$$\frac{(\mu + \tan\alpha)\cdot(f_{1,mod,1}\cdot s_1 - f_{1,mod,2}\cdot s_2)}{f_{h,1}\cdot(1-\mu\cdot\tan\alpha)} = \beta\cdot x_2 - x_1 \tag{5}$$

equating (1) and (5) yields equation (6):

$$x_1 = \frac{(\tan\alpha + \mu)\cdot(f_{1,mod,2}\cdot s_2 - f_{1,mod,1}\cdot s_1)}{(1-\mu\cdot\tan\alpha)\cdot f_{h,1}\cdot(1+\beta)} + \sqrt{\frac{2\cdot\beta}{1+\beta}}\cdot\sqrt{\frac{2\cdot M_y\cdot\cos^2\alpha}{f_{h,1}\cdot d} - \frac{(\tan\alpha+\mu)^2\cdot(f_{1,mod,1}\cdot s_1 - f_{1,mod,2}\cdot s_2)^2}{2\cdot {f_{h,1}}^2\cdot(1+\beta)\cdot(1-\mu\cdot\tan\alpha)^2}} \tag{6}$$

In addition to the force equilibrium $R_1 = R_2$, the compressive forces H_1 and H_2 in the contact surface between the timber members are equal: - (2c) = (2d) with (3a,b,c,d):

$$\frac{f_{1,mod,1}\cdot s_1 - f_{1,mod,2}\cdot s_2}{f_{h,1}\cdot\tan\alpha} = -\beta\cdot x_2 + x_1 \tag{7}$$

equating (7) with (5) yields equation (8):

$$-\frac{(f_{1,mod,1}\cdot s_1 - f_{1,mod,2}\cdot s_2)}{\tan\alpha} = \frac{(\mu + \tan\alpha)\cdot(f_{1,mod,1}\cdot s_1 - f_{1,mod,2}\cdot s_2)}{1-\mu\cdot\tan\alpha} \tag{8}$$

Equation (8) has only a solution for $f_{1,mod,1}\cdot s_1 = f_{1,mod,2}\cdot s_2$, since for $f_{1,mod,1}\cdot s_1 \neq f_{1,mod,2}\cdot s_2$ equation (8) results in $-1 = \tan^2\alpha$.

This means that the fastener tensile force in the left side timber member is equal to the tensile force in the right side timber member and the lower of the two fastener withdrawal capacities governs.

for $f_{1,mod,1}\cdot s_1 = f_{1,mod,2}\cdot s_2$ equation (6) may be modified to:

$$x_1 = \sqrt{\frac{2\cdot\beta}{1+\beta}}\cdot\sqrt{\frac{2\cdot M_y\cdot\cos^2\alpha}{f_{h,1}\cdot d}} \tag{9}$$

equation (9) in (4a):

$$R = f_{1,mod}\cdot d\cdot s\cdot(\mu + \tan\alpha) + (1-\mu\cdot\tan\alpha)\cdot\sqrt{\frac{2\cdot\beta}{1+\beta}}\cdot\sqrt{2\cdot M_y\cdot d\cdot f_{h,1}\cdot\cos^2\alpha} \tag{10}$$

The load-carrying capacity in timber-to-timber connections with inclined screws for Johansen´s extended failure mode 3 is then:

$$R_{VM3} = R_{ax,3}\cdot(\mu\cdot\cos\alpha + \sin\alpha) + (1-\mu\cdot\tan\alpha)\cdot\sqrt{\frac{2\cdot\beta}{1+\beta}}\cdot\sqrt{2\cdot M_y\cdot d\cdot f_{h,1}\cdot\cos^2\alpha} \tag{11}$$

with the withdrawal capacity $R_{ax,3}$ for Johansen´s failure mode 3:

$$R_{ax,3} = \min\left\{\begin{matrix} f_{1,mod,1,3}\cdot d\cdot\dfrac{s_1}{\cos\alpha} \\ f_{1,mod,2,3}\cdot d\cdot\dfrac{s_2}{\cos\alpha} \end{matrix}\right\}$$

For timber-to-timber connections with screws arranged perpendicular to the grain ($\alpha \rightarrow 0°$), equation (11) results in equation (12):

$$R_{VM3,0°} = \mu \cdot R_{ax} + \sqrt{\frac{2 \cdot \beta}{1+\beta}} \cdot \sqrt{2 \cdot M_y \cdot d \cdot f_{h,1}} = \mu \cdot R_{ax} + R_{la,VM3} \qquad (12)$$

This equation for the load-carrying capacity in timber-to-timber connections with screws loaded perpendicular to their axis may also be found in the Draft German Timber Design Code E DIN 1052, Mai 2000 using a friction coefficient $\mu = 0{,}25$.

For the other failure modes the following equations are given:

$$R_{VM1a,l} = R_{ax,1al} \cdot \sin\alpha + f_{h,1} \cdot d \cdot s_1 \cdot \cos\alpha$$

$$R_{VM1a,r} = R_{ax,1ar} \cdot \sin\alpha + f_{h,2} \cdot d \cdot s_2 \cdot \cos\alpha$$

$$R_{VM1b} = R_{ax,1b} \cdot (\mu \cdot \cos\alpha + \sin\alpha)$$

$$+ \frac{f_{h,1} \cdot d \cdot s_1}{1+\beta} \cdot (1 - \mu \cdot \tan\alpha) \cdot \left[\sqrt{\beta + 2 \cdot \beta^2 \cdot \left[1 + \frac{s_2}{s_1} + \left(\frac{s_2}{s_1} \right)^2 \right] + \beta^3 \cdot \left(\frac{s_2}{s_1} \right)^2} - \beta \cdot \left(1 + \frac{s_2}{s_1} \right) \right]$$

$$R_{VM2a} = R_{ax,2a} \cdot (\mu \cdot \cos\alpha + \sin\alpha)$$

$$+ (1 - \mu \cdot \tan\alpha) \cdot \frac{f_{h,1} \cdot s_1 \cdot d}{2+\beta} \cdot \left[\sqrt{2 \cdot \beta \cdot (1+\beta) + \frac{4 \cdot \beta \cdot (2+\beta) \cdot M_y \cdot \cos^2\alpha}{f_{h,1} \cdot d \cdot {s_1}^2}} - \beta \right]$$

$$R_{VM2b} = R_{ax,2b} \cdot (\mu \cdot \cos\alpha + \sin\alpha)$$

$$+ (1 - \mu \cdot \tan\alpha) \cdot \frac{f_{h,1} \cdot s_2 \cdot d}{1 + 2 \cdot \beta} \cdot \left[\sqrt{2 \cdot \beta^2 \cdot (1+\beta) + \frac{4 \cdot \beta \cdot (2 \cdot \beta + 1) \cdot M_y \cdot \cos^2\alpha}{f_{h,1} \cdot d \cdot {s_2}^2}} - \beta \right]$$

The load-carrying capacity in timber-to-timber connections with inclined screws is now:

$$R = \min \left\{ \begin{matrix} R_{VM1a,l} \\ R_{VM1a,r} \\ R_{VM1b} \\ R_{VM2a} \\ R_{VM2b} \\ R_{VM3} \end{matrix} \right\} \qquad (13) \qquad\qquad R_{ax,j} = \min \left\{ \begin{matrix} f_{1,mod,1,j} \cdot d \cdot \dfrac{s_1}{\cos\alpha} \\ f_{1,mod,2,j} \cdot d \cdot \dfrac{s_2}{\cos\alpha} \end{matrix} \right\} \qquad (14)$$

with j Johansen's failure mode (failure mode 1a,l; 1a,r; 1b; 2a; 2b or 3)

2.2 Modified withdrawal capacity parameter

Equation (13) may be used to determine the load-carrying capacity of timber-to-timber connections with inclined screws. Johansen's equations for the different failure modes were extended by the withdrawal capacity of the screws, the inclination angle of the screw axis as well as the friction between the timber members.

In order to establish the withdrawal contribution of the screw, the axial displacement Δ of the screw relative to the timber is determined, depending on the relative displacement δ

between the timber members in force direction. Figure 3 shows a timber-to-timber connection with an inclined screw and a total displacement between the timber members in force direction of $\delta_{tot} = \delta_1 + \delta_2$ for Johansen's failure mode 3. It is assumed, that withdrawal failure only occurs in one timber member and the elongation of the screw is neglected. As shown in figure 3 point A is moving to point A*, if the screw is pulled out of the timber member 1. Otherwise point B is moving to point B*.

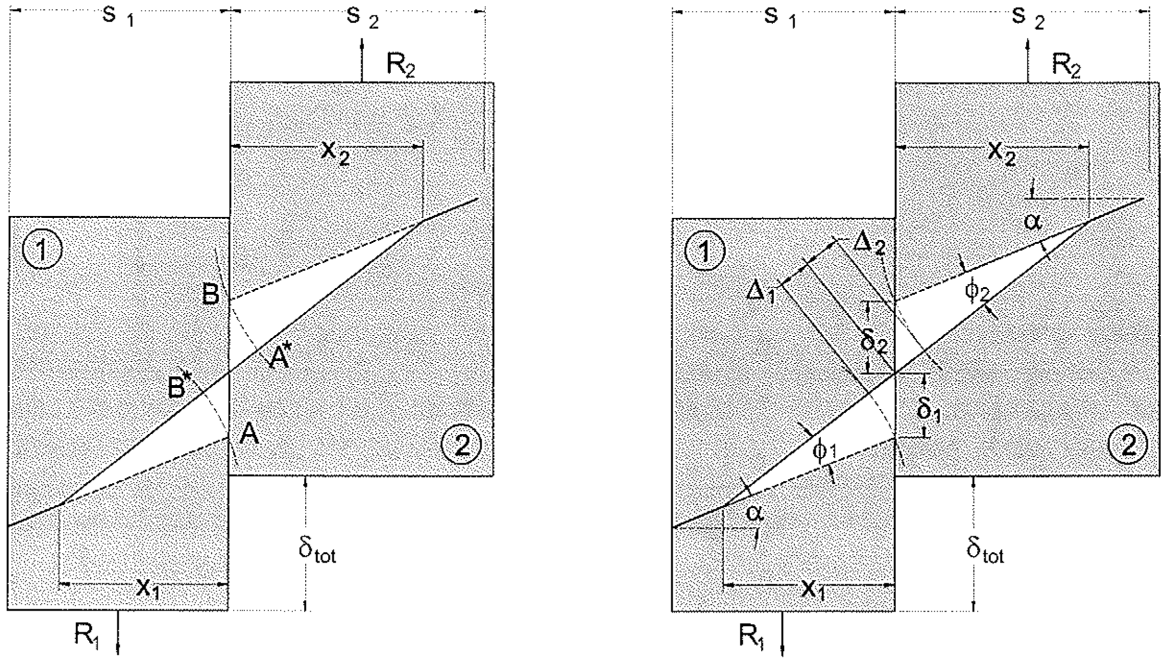

Figure 3: Displacements in a timber-to-timber connection with an inclined screw

For a relative displacement $\Delta_{tot} = \Delta_1 + \Delta_2$ parallel to the screw corresponding to the axial displacement at the ultimate withdrawal load, the ultimate load-carrying capacity of the timber-to-timber connection with inclined screws is reached. At this point the screw is pulled out of either the left or the right timber member.

for all failure modes the following applies (see figure 3):

$$\Delta_i = \frac{x_i}{\cos\alpha} \cdot \left(\left(\sqrt{\left(\frac{\delta_i}{x_i} + \tan\alpha \right)^2 + 1} \right) \cdot \cos\alpha - 1 \right) \qquad i = 1,2 \qquad (15)$$

with

$\phi_1 = \phi_2$ and $\delta_{tot} = \delta_1 + \delta_2$ and $\Delta_{tot} = \Delta_1 + \Delta_2$

follows

$$\Delta_{tot} = \frac{x_1 + x_2}{\cos\alpha} \cdot \left(\left(\sqrt{\left(\frac{\delta_{tot}}{x_1 + x_2} + \tan\alpha \right)^2 + 1} \right) \cdot \cos\alpha - 1 \right) \qquad (16)$$

The relative displacement between the timber members according to ISO 6891 is limited to $\delta_{max} = \delta_{tot} = 15$ mm.

The horizontal distance between the plastic hinge in the fastener and the interface between the timber members for Johansen's failure mode 3 is (see also equation 9):

$$x_{1,VM3} = \sqrt{\frac{2 \cdot \beta}{1+\beta}} \cdot \sqrt{\frac{2 \cdot M_y \cdot \cos^2 \alpha}{f_{h,1} \cdot d}} \qquad \text{and} \qquad x_{2,VM3} = \frac{x_1}{\beta} \tag{17}$$

Average values for material properties of self-tapping screws determined in previous tests:

$$M_y = 500 \frac{N}{mm^2} \cdot \frac{d^3}{6} \qquad \text{and} \qquad f_h = 0{,}050 \cdot (1 - 0{,}01 \cdot d) \cdot \rho$$

Substituting (17) in equation (16) and using as an example the material properties determined in previous tests (ρ = 400 kg/m^3; $\beta = f_{h,2} / f_{h,1} = 1$) results for δ_{tot} = 15 mm in the relative axial displacement Δ_{tot} between the screw and the timber depending on the angle α and the screw diameter d for Johansen's failure mode 3. The displacement Δ_{tot} for Johansen's failure mode 3 is shown in figure 4.

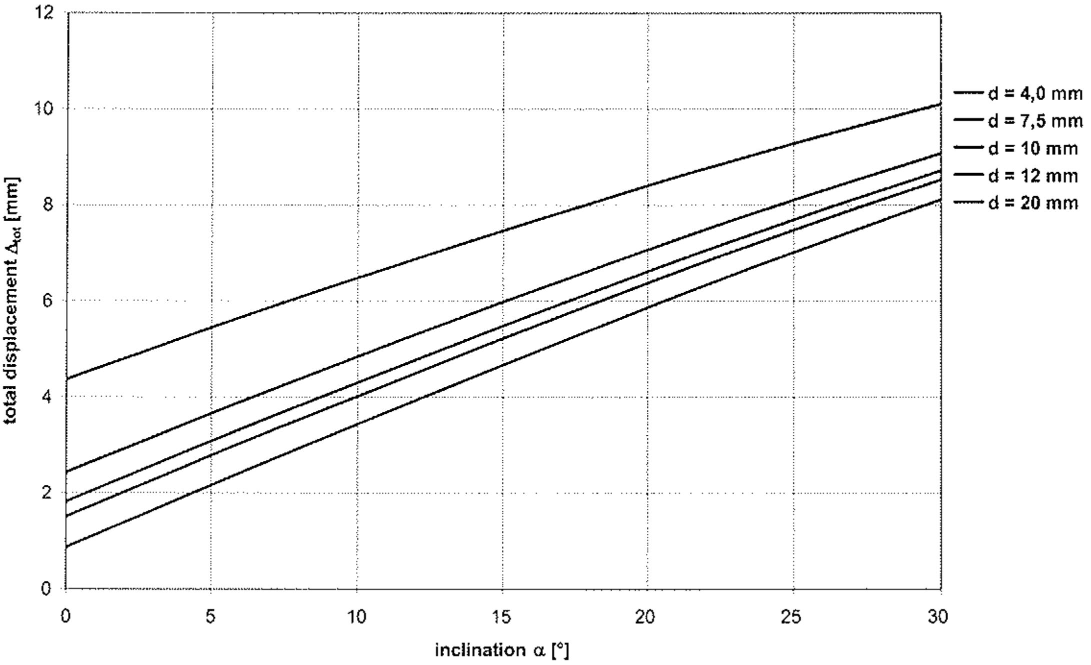

Figure 4: Δ_{tot} for δ_{tot} = 15 mm depending on α for Johansen's failure mode 3

The total displacement Δ_{tot} for the remaining failure modes is determined by using the following expressions in equation (16):

$$x_{1,VM1b} = \frac{s_1}{2 \cdot (1+\beta)} \cdot \left[\sqrt{\beta + 2 \cdot \beta^2 \cdot \left[1 + \frac{s_2}{s_1} + \left(\frac{s_2}{s_1} \right)^2 \right] + \beta^3 \cdot \left(\frac{s_2}{s_1} \right)^2} + 1 - \beta \cdot \frac{s_2}{s_1} \right]$$

$$x_{2,VM1b} = \frac{\beta \cdot s_2 - s_1}{2 \cdot \beta} + \frac{x_1}{\beta}$$

$$x_{1,VM2a} = \frac{s_1}{2 \cdot (2+\beta)} \cdot \left[\sqrt{2 \cdot \beta \cdot (1+\beta) + \frac{4 \cdot \beta \cdot (2+\beta) \cdot M_y \cdot \cos^2 \alpha}{f_{h,1} \cdot d \cdot s_1^2}} + 2 \right]$$

$$x_{2,VM2a} = \frac{2 \cdot x_1 - s_1}{\beta}$$

$$x_{1,VM2b} = \frac{s_2}{1+2\cdot\beta}\cdot\left[\sqrt{2\cdot\beta^2\cdot(1+\beta)+\frac{4\cdot\beta\cdot(2\cdot\beta+1)\cdot M_y\cdot\cos^2\alpha}{f_{h,1}\cdot d\cdot s_2^{\,2}}}-\beta\right]$$

$$x_{2,VM2b} = \frac{1}{2\cdot\beta}\cdot\left[\beta\cdot s_2 + x_1\right]$$

With increasing inclination α the axial displacement Δ in a timber-to-timber connection increases for a fixed value of the connection displacement $\delta_{tot} = 15$ mm. Due to the fact that the withdrawal capacity for screws in a withdrawal test is reached at a displacement of about 1,8 mm (see figure 5), the withdrawal capacity of screws with a diameter up to 8 mm is reached before a connection displacement δ of 15 mm is attained.

Typical withdrawal parameter-displacement curves for screws with a diameter d = 7,5 mm depending on different simultaneous embedding deformations are shown in figure 5. In the tests, the screw was loaded perpendicular to the axis until a prescribed embedding displacement was reached and subsequently pulled out of the timber while maintaining the embedding load. The withdrawal capacity for this diameter was reached at a maximum displacement of about 1,8 mm independent of the lateral displacement.

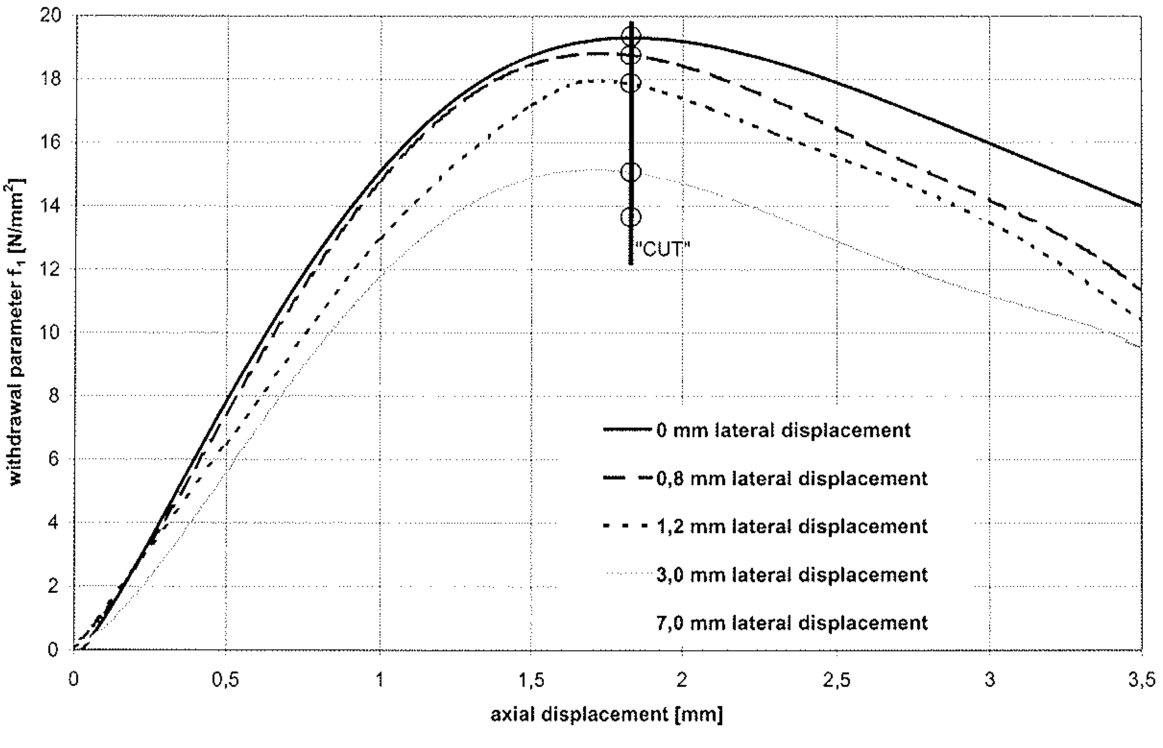

Figure 5: Typical withdrawal curves for screws with a diameter d = 7,5 mm for different lateral embedding displacements

Based on figure 5 the following observations are made:

- The withdrawal capacity is not reduced, as long as no plastic embedding deformation has taken place. This means that the full withdrawal capacity is available in those parts of the screw where the embedding strength is not reached (e.g. outside x_1 and x_2 in figure 3).
- The withdrawal capacity per unit length increases from the interface between the members towards the plastic hinge. The corresponding distribution of the withdrawal

capacity for an axial displacement of 1,8 mm is shown in figure 6, based on the values in figure 5.

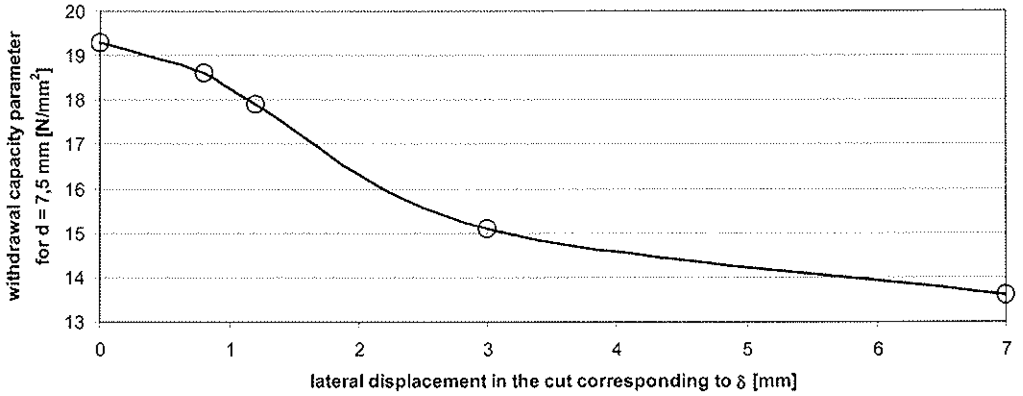

Figure 6: Withdrawal capacity parameter depending on lateral displacement for d = 7,5mm

Based on figure 6, the distribution of the local withdrawal capacity over the total member thickness is shown as a dashed line in figure 7. The solid line represents the modified withdrawal capacity parameter $f_{1,mod,1,3}$ or $f_{1,mod,2,3}$ for Johansen's failure mode 3 as the mean value of the withdrawal capacity over the respective timber member thickness.

Similar withdrawal capacity parameter curves depending on the embedding deformation (see figure 6) and the resulting modified withdrawal capacity parameters (see figure 7) may be derived for the other failure modes based on the procedure described.

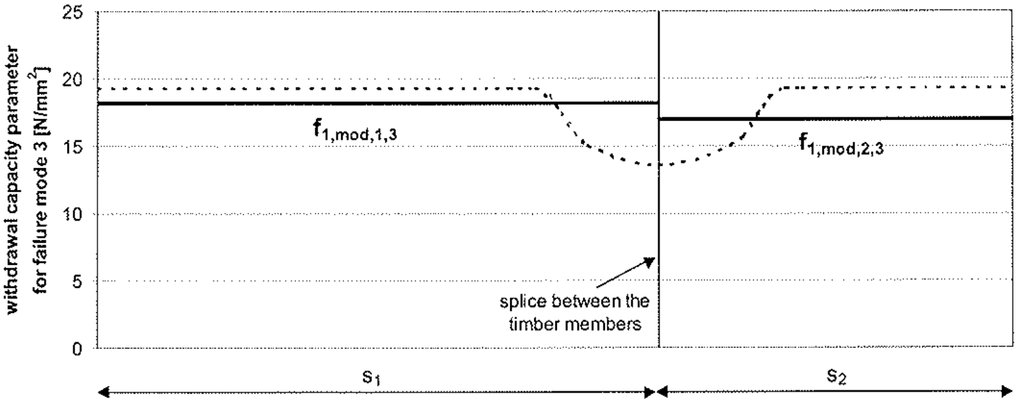

Figure 7: Modified withdrawal capacity parameter $f_{1,mod,1,3}$ or $f_{1,mod,2,3}$ for Johansen's failure mode 3 for a screw diameter d = 7,5 mm in timber member 1 and 2

2.3 Comparison of model prediction and experimental data

Tests were made with specimens containing in each interface between the side and middle timber member either one self-tapping screw with continuous thread for series 1 or four self-tapping screws for series 2, see figure 1. The screw diameter was 7,5 mm and the screw length was 130 mm for series 1 and 180 mm for series 2.

The members were made of glued laminated timber beams with 12 % moisture content. All members within a specimen had similar density. The average density for joint members was 400 kg/m³ for series 1 and 442 kg/m³ for series 2.

Altogether nine sub-series (five sub-series for series 1 and four sub-series for series 2), respectively, were carried out whereby the angle α (0° until 50°) as well as the timber thickness and the penetration depth of the screw was varied.

The values of the load-carrying capacity per fastener and per shear plane reached in the tests is shown in figure 8. In this figure also the calculated load-carrying capacities per fastener and per shear plane based on the extended Johansen theory are shown. Parameters used for the calculated load-carrying capacities were determined in previous tests. Modified withdrawal capacity parameters $f_{1,mod,1,j}$ and $f_{1,mod,2,j}$ were determined as described in paragraph 2.2. In figure 9 the resulting modified withdrawal capacity parameters are shown for all failure modes and all angles α. A uniform value of the embedding strength was used, irrespective of the angle α.

For the timber-to-timber connections with an angle α of about 30°, the load-carrying capacity reached a maximum. This maximum was about 50 % higher than the value for screws arranged and loaded perpendicular to the fastener axis. Due to the decreasing penetration depth of the screws in the middle timber member with increasing angle for series 2, the load-carrying capacity for the timber-to-timber connections with an angle higher than 30° became smaller. The same observation was made in series 1 for an angle of 45° and a minimum penetration depth of about 32 mm. Here, the load-carrying capacity is higher for an inclination of 30° or 50°, where the penetration depth is larger.

An opened specimen with an inclination of 15° between the screw axis and the level direction is shown in figure 10. As expected, the connection failure was caused by reaching the withdrawal and bending capacity of the screw and the timber embedding strength (extended Failure Mode 3).

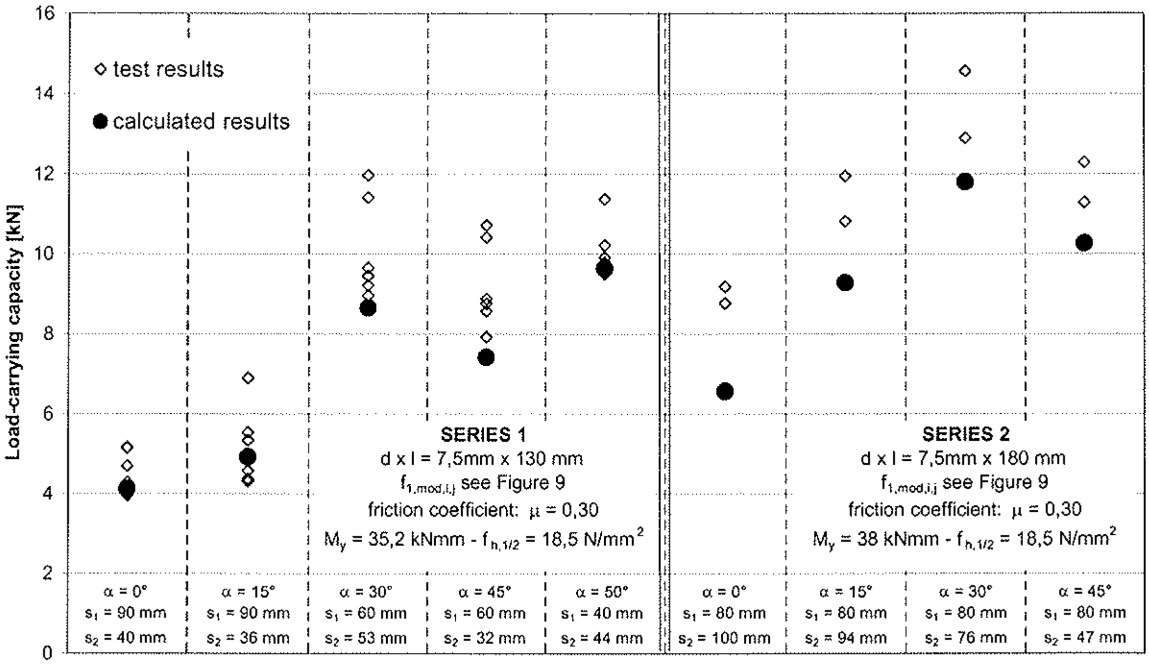

Figure 8: Comparison between test results and calculated load-carrying capacities

SERIES 1													
	failure mode 1a,l		failure mode 1a,r		failure mode 1b		failure mode 2a		failure mode 2b		failure mode 3		
α	$f_{1,mod,1,1al}$ [N/mm²]	$f_{1,mod,2,1al}$ [N/mm²]	$f_{1,mod,1,1ar}$ [N/mm²]	$f_{1,mod,2,1ar}$ [N/mm²]	$f_{1,mod,1,1b}$ [N/mm²]	$f_{1,mod,2,1b}$ [N/mm²]	$f_{1,mod,1,2a}$ [N/mm²]	$f_{1,mod,2,2a}$ [N/mm²]	$f_{1,mod,1,2b}$ [N/mm²]	$f_{1,mod,2,2b}$ [N/mm²]	$f_{1,mod,1,3}$ [N/mm²]	$f_{1,mod,2,3}$ [N/mm²]	**R [kN]**
0	13,6	19,3	19,3	13,6	15,1	15,7	15,1	16,3	18,7	16,6	18,6	17,7	**4,14**
15	14,6	19,3	19,3	14,6	17,4	17,9	17,3	18,0	19,0	17,6	18,9	18,2	**4,93**
30	15,5	19,3	19,3	15,5	18,2	18,3	18,1	18,9	19,0	18,1	18,9	18,9	**8,67**
45	16,5	19,3	19,3	16,5	18,4	18,7	18,3	18,8	19,1	18,4	19,1	18,9	**7,43**
50	17,4	19,3	19,3	17,4	18,6	18,6	18,4	19,1	19,0	18,4	19,0	19,0	**9,65**

SERIES 2													
	failure mode 1a,l		failure mode 1a,r		failure mode 1b		failure mode 2a		failure mode 2b		failure mode 3		
α	$f_{1,mod,1,1al}$ [N/mm²]	$f_{1,mod,2,1al}$ [N/mm²]	$f_{1,mod,1,1ar}$ [N/mm²]	$f_{1,mod,2,1ar}$ [N/mm²]	$f_{1,mod,1,1b}$ [N/mm²]	$f_{1,mod,2,1b}$ [N/mm²]	$f_{1,mod,1,2a}$ [N/mm²]	$f_{1,mod,2,2a}$ [N/mm²]	$f_{1,mod,1,2b}$ [N/mm²]	$f_{1,mod,2,2b}$ [N/mm²]	$f_{1,mod,1,3}$ [N/mm²]	$f_{1,mod,2,3}$ [N/mm²]	**R [kN]**
0	13,6	19,3	19,3	13,6	13,8	13,7	15,5	18,3	17,4	14,5	18,5	18,6	**6,58**
15	14,6	19,3	19,3	14,6	17,7	17,6	17,4	18,8	18,7	17,3	18,8	18,9	**9,29**
30	15,5	19,3	19,3	15,5	18,3	18,3	18,0	19,0	19,0	18,0	19,0	19,0	**11,8**
45	16,5	19,3	19,3	16,5	18,4	18,7	18,3	18,9	19,1	18,4	19,1	19,0	**10,3**

Figure 9: Modified withdrawal capacity parameters for all failure modes and all angles α

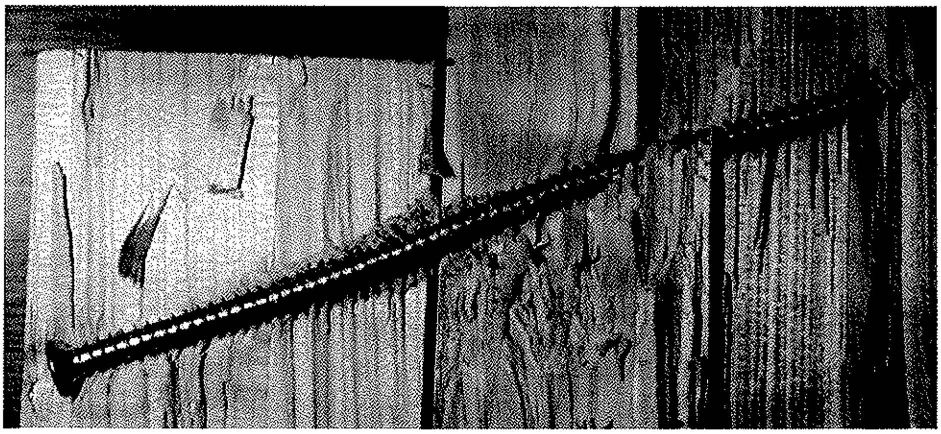

Figure 10: Opened specimen with self-tapping screw - Series 2 - α = 15°

3 Conclusions

Inclined self-tapping screws provide opportunities for rationalisation and cost reduction in timber connections, particularly during design and installation. With the proposed equation (13), it is possible to determine the load-carrying capacity for all timber-to-timber connections with inclined screws taking into account the withdrawal and bending capacity of the screws, the timber embedding strength and the friction stress between the timber members. The withdrawal behaviour of the screws is taken into account in Johansen's extended yield theory using a modified withdrawal capacity parameter.

Evaluating the modified withdrawal parameters for all screw diameters leads to the consequence, that screws with large diameters (d > 8 mm) do not reach their withdrawal capacity in a timber-to-timber connection for angles α close to 0° before a connection displacement of δ_{tot} = 15 mm. Consequently, the modified withdrawal capacity parameters for d > 8 mm and α < 15° are much lower than the withdrawal capacity parameters determined in a withdrawal test. For these timber-to-timber connections the withdrawal action does not significantly increase the load-carrying capacity. However, for inclinations α > 30° the ultimate withdrawal capacity in a timber-to-timber connection is reached for all screw diameters.

For a general use of Johansen's extended yield theory it is necessary to determine both, the modified withdrawal capacity parameters and the embedding strength depending on the angle between the screw axis and the grain direction for the different screw diameters.

To simplify the proposed design, the modified withdrawal capacity parameter $f_{1,mod,i,j}$ for timber member i and failure mode j may be determined as the minimum value $f_{1,mod,i,j} = 0{,}7 \cdot f_{1,i}$ (see figure 9) with the ultimate withdrawal capacity parameter $f_{1,i}$ from an axial withdrawal test for timber member i.

4 References

1. Blass, H.J., Bejtka, I., 'Standardisierung und Typisierung von Anschlüssen und Verbindungen zur Rationalisierung der Planung und Fertigung im Holz-Wohnhausbau - Teil A' Forschungsbericht 2002, Versuchsanstalt für Stahl, Holz und Steine, Universität Karlsruhe (this research project was promoted by "Deutsche Gesellschaft für Holzforschung e.V. mit Mitteln des Bundesministeriums für Verkehr, Bau- und Wohnungswesen (Aktenzeichen: BS 34 - 5 80 01 98 - 18).
2. Blass, H.J., Bejtka, I, 'Screws with continuous threads in timber connections',RILEM, Proceedings PRO 22, Stuttgart, Page 193
3. Blass, H.J., 'Verbindungen mit Nägeln und Schrauben - Bemessung nach E DIN 1052 und neuere Entwicklungen', Ingenieurholzbau - Karlsruher Tage, September, 2000, 56-65
4. Ehlbeck, J., Ehrhardt, W., Screwed joints in 'Timber Engineering STEP 1, Basis of design, material properties, structural components and joints' Centrum Hout, The Netherlands, ISBN 90-5645-001-8
5. Johansen, K.W., 'Theory of timber connections' International Association of Bridge and Structural Engineering, Publication No. 9:249-262, Bern, Switzerland

CIB-W18/35-7-5

INTERNATIONAL COUNCIL FOR RESEARCH AND INNOVATION
IN BUILDING AND CONSTRUCTION

WORKING COMMISSION W18 - TIMBER STRUCTURES

EFFECT OF DISTANCES, SPACING AND NUMBER OF DOWELS IN A ROW ON THE LOAD CARRYING CAPACITY OF CONNECTIONS WITH DOWELS FAILING BY SPLITTING

M Schmid
H J Blaß
University of Karlsruhe

GERMANY

R P M Frasson
Federal University of Espirito Santo

BRAZIL

Presented by: H J Blaß

In reply to the questions about the load magnitudes and sequence of loading by P Quenneville, H J Blaß replied that the loading was assumed to be equally distributed even though it was recognised that this does not fully reflect the practical situation and that the model used is justifiable as the results are conservative. E Fournely asked if the frictional effects generated as the dowel moved through the timber on the magnitude the shear force V was taken into account. H J Blaß replied that the frictional effects of the dowel was not considered but he recognised that it would have an effect on the shear load. This was followed by discussion regarding the relevance of the proposed model. It was generally agreed that the model is most relevant to mode 1 failure and that mode 2 failure mode capacity is generally higher than that of mode 1.

Effect of Distances, Spacing and Number of Dowels in a Row on the Load Carrying Capacity of Connections with Dowels Failing by Splitting

M. Schmid, H.J. Blaß
University of Karlsruhe, Germany
R.P.M. Frasson
Federal University of Espirito Santo, Brazil

1. Introduction

Joints in timber structures often fail in one of the two brittle modes shown in figure 1.

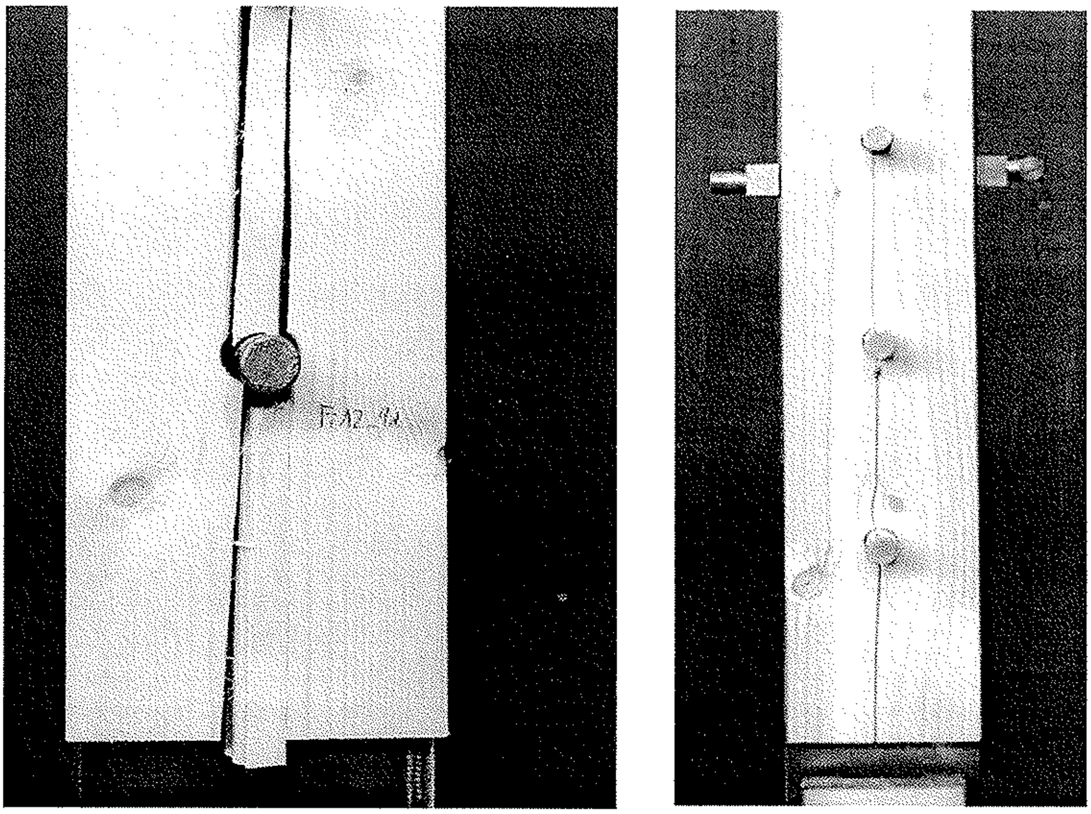

Fig. 1: plug shear failure splitting failure

In order to avoid these brittle failure modes, most timber design codes contain rules based on the experience of craftsmen and results of connection tests in laboratories. These rules mostly consist of prescribed minimum dimensions, such as fastener end and edge distances, fastener spacing, or timber thickness. Regarding these minimum dimensions, no distinction is made between different timber softwood species in many codes. Recent research results e. g. by Jorissen (1998) showed brittle failure modes also in cases where the minimum dimensions were respected. In order to study the influence of the timber species on the splitting tendency, a research project was carried out at Karlsruhe University.

As for economical reasons it is not possible to test all types of fastener using different species and different joint geometry, a mechanical model based on fracture mechanics was developed. In this paper the model for splitting, that was frequently observed in the tests performed both, by Blaß and Schmid (2002) and Masuda (1998), is presented. In terms of fracture mechanics it is a mode I crack extension.

2. Mechanical Model

Stable crack growth in the close neighbourhood of the dowels is often observed (fig. 2), before one of the failure modes shown in figure 1 eventually takes place, leading to an almost complete loss of the joint's strength,.

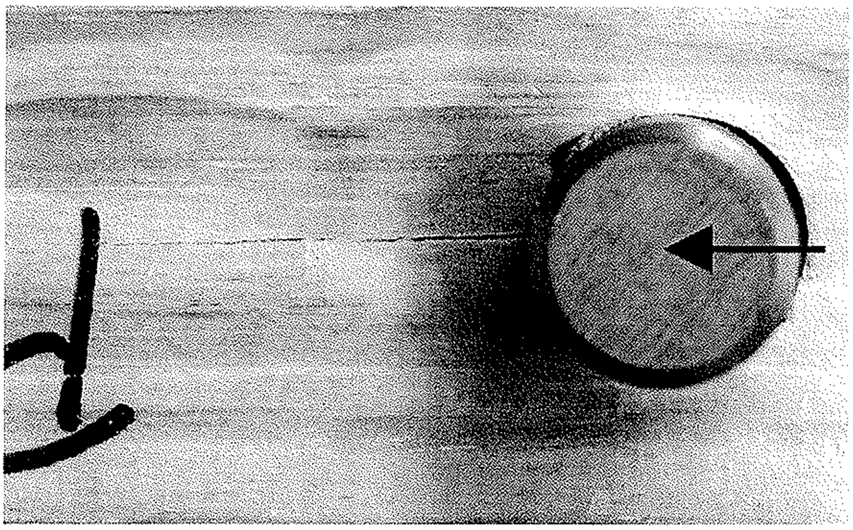

Fig. 2: crack close to the dowel

The joint area including the stable crack propagation is modelled as a beam on elastic foundation (fig. 3). This model seems to be quite crude, the alternative could be a two- or three-dimensional finite element model. But if the large variation of local timber properties is taken into account, as well as the non-linear stress-strain relation in the area close to the fastener and the orthotropic behaviour, it is reasonable to choose this simple model. Jorissen (1998) first used a similar joint area model. Contrary to the model presented here, Jorissen included no crack extension, he instead compared the tensile stresses perpendicular to the grain at the dowel surface with the tensile strength of the material.

Similar to the approach used by Jorissen (1998) the beam is loaded by a transverse force

$$V = F / 7 \qquad (1)$$

and a moment

$$M = F/2 \cdot h/2 = F/2 \cdot a_{4,c}/2 \tag{2}$$

depending on the embedding behaviour and the dowel load F parallel to the grain.

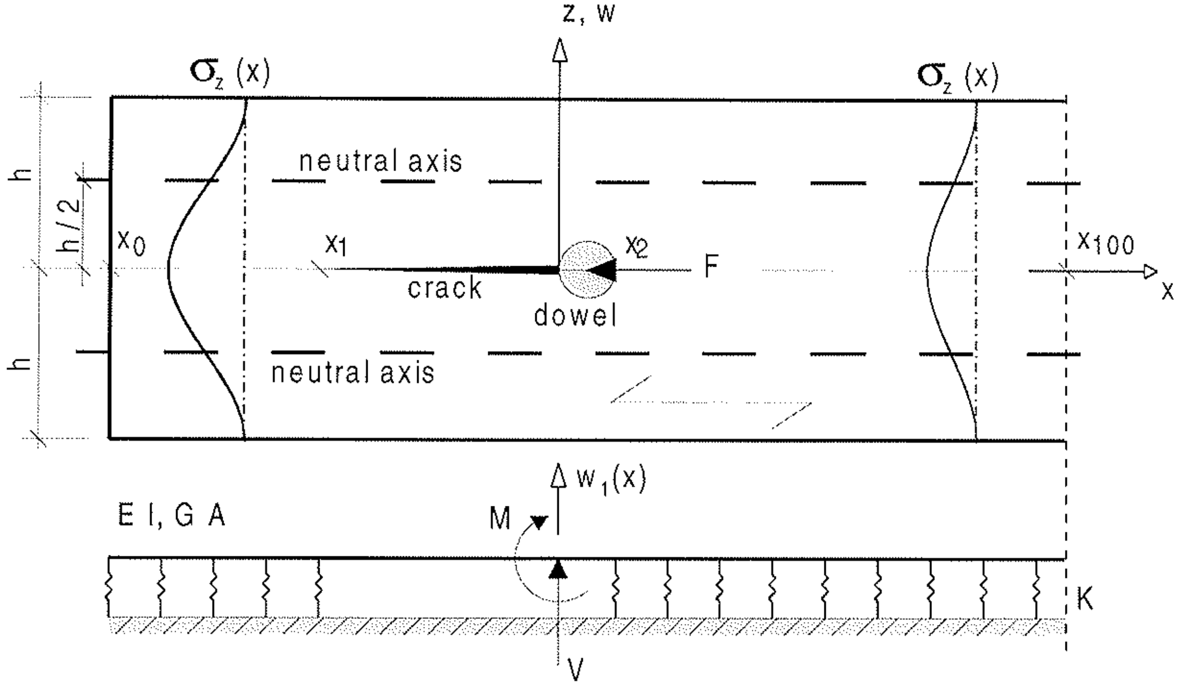

Fig. 3: modelling the cracked joint as a beam on elastic foundation

Assuming a stress distribution perpendicular to the grain $\sigma_z(x,z)$ as shown in figure 3 (Timoshenko and Goodier (1970)), the modulus of foundation K, acting on the neutral axis of the idealised beam, is calculated:

$$\sigma_z(x,z) = \frac{\sigma_z(x,0)}{2} - \left(\frac{3 \cdot (-h/2 + z)}{2 \cdot h} - \frac{2 \cdot (-h/2 + z)^3}{h^3} \right) \cdot \sigma_z(x,0) \qquad (3),$$

$$w(h/2) = \int_{z=0}^{z=h/2} \varepsilon_{90}(z)\, dz = \int_{z=0}^{z=h/2} \frac{\sigma_z(x,z)}{E_{90}}\, dz = \frac{13 \cdot h \cdot \sigma_z(x,0)}{32 \cdot E_{90}} \tag{4}$$

yielding

$$K = \frac{\sigma_z(x,0) \cdot t}{w(h/2)} = \frac{32}{13} \cdot \frac{E_{90} \cdot t}{h} \qquad (5).$$

As the ratio between the depth h of the beam and the length is small, shear deformation is taken into account. Equation (6) follows from equilibrium conditions:

$$\frac{d^4 w_1}{dx^4} - \frac{\kappa \cdot K}{G \cdot A} \cdot \frac{d^2 w_1}{dx^2} + \frac{K \cdot w_1(x)}{E \cdot I} = 0 \tag{6}$$

A displacement shape function satisfying equation (6) is

$$w_1(x) = e^{\alpha \cdot x} \cdot (C_1 \cdot \cos(\beta \cdot x) + C_2 \cdot \sin(\beta \cdot x)) + e^{-\alpha \cdot x} \cdot (C_3 \cdot \cos(\beta \cdot x) + C_4 \cdot \sin(\beta \cdot x)) \tag{7}$$

with

$$\alpha = \sqrt{\lambda^2 + \frac{\kappa \cdot K}{4 \cdot G \cdot A}},\ \beta = \sqrt{\lambda^2 - \frac{\kappa \cdot K}{4 \cdot G \cdot A}},\ \lambda^4 = \frac{K}{4 \cdot E \cdot I} \qquad (8).$$

Fig. 4 shows the distribution of stresses perpendicular to the grain according to a FE-calculation. The following properties were assumed:

$E_{11} = 420\ \mathrm{N/mm^2}$ $E_{22} = 11990\ \mathrm{N/mm^2}$ $G_{12} = 743\ \mathrm{N/mm^2}$ $\nu_{12} = 0{,}027$
coefficient of friction $\mu = 0{,}339$ $d = 16\ \mathrm{mm}$ $a_{3,t} = 7 \cdot d$ $a_{4,c} = 3 \cdot d$
depth $t = d$

The Poisson coefficient ν_{12} and the coefficient of friction μ are not included in the model according to Figure 3.

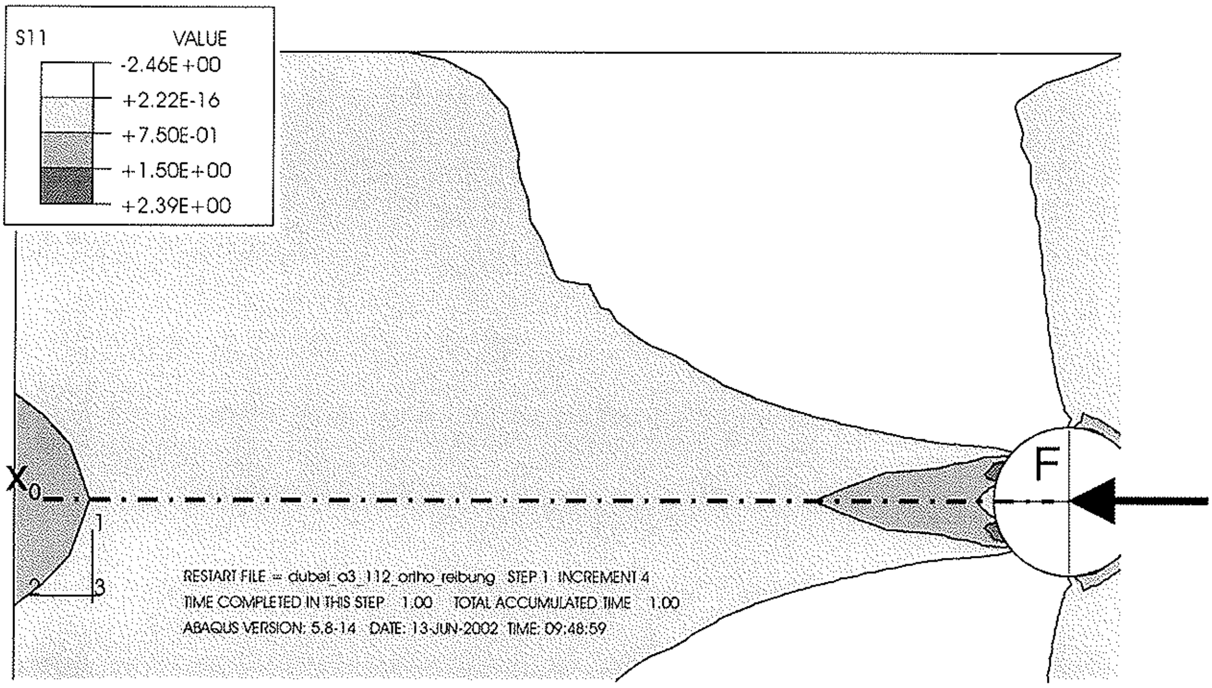

Fig. 4: Stresses perpendicular to the grain according to FE-calculation, coefficient of friction $\mu = 0{,}339$

Fig. 5 shows the stress distribution perpendicular to the grain along the symmetry axis according to both models. Close to the dowel there is a significant difference between the results. Elsewhere the stresses coincide well. As for the FE-calculation linear-elastic behaviour was assumed, which is not true close to the dowel, and the Poisson coefficient ν_{12} is not very well known either, the precision of the FE-calculation has to be considered with care.

Using the model according to fig. 3 crack propagation Δa is modelled by a prolongation of the non embedded part and an equivalent shortening of the embedded beam parts. Consequently the system becomes weaker resulting in deflections and rotations of the points of actions of M_i and V_i.

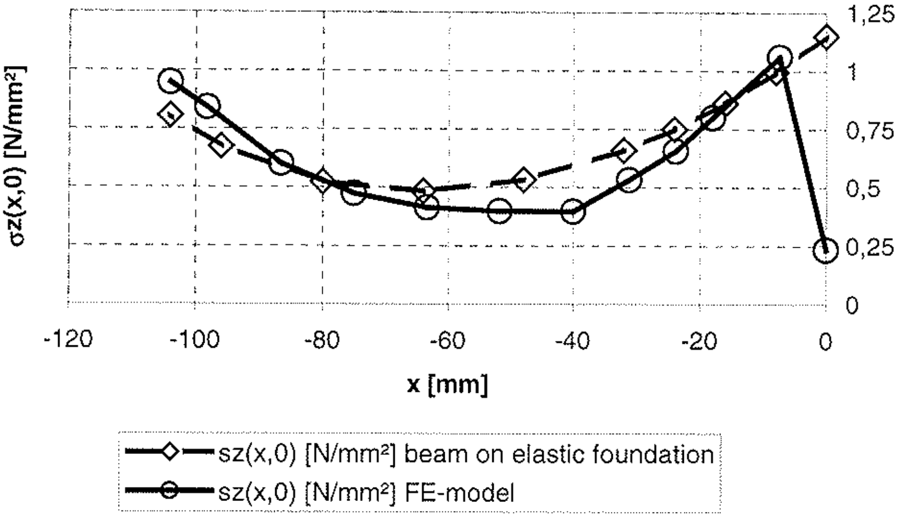

Fig. 5: stresses perpendicular to the grain according to the model and the FE-calculation

The elastic potential is reduced with increasing crack length and the energy release rate is calculated as:

$$G_I = -\frac{\Delta\Pi}{t \cdot \Delta a} = -\frac{\Delta\Pi_V + \Delta\Pi_M}{t \cdot \Delta a} \cdot 2 = \sum_{i=1}^{n} \frac{V_i \cdot \Delta w(x_i)/2 + M_i \cdot \Delta\varphi(x_i)/2}{t \cdot \Delta a} \cdot 2 \qquad (9).$$

The factor 2 in equation (9) results from the symmetry of the joint area, since two beams on elastic foundations form the end of the timber member. For more than one row of fasteners, the model according to figure 3 is only applicable for the outer parts close the member edges, the timber parts between dowel rows are loaded from both sides and basically remain straight. Consequently the energy release rate of mode I for a connection with more than one row is only the half of the value according to equation (9) if crack extension at only one of the outer rows occurs. For this type of joint more often group tear out or shear failure as a mixed mode crack extension (mode I and II) is observed (Quenneville (1998), Mohammad and Quenneville (1999)). A model for calculating the energy release rate G_{II} for this shear failure mode is presented in Blaß and Schmid (2002), but due to a lack of knowledge regarding critical values in mode II and especially for the mixed mode crack extension according to modes I and II a comparison between model and tests remains difficult.

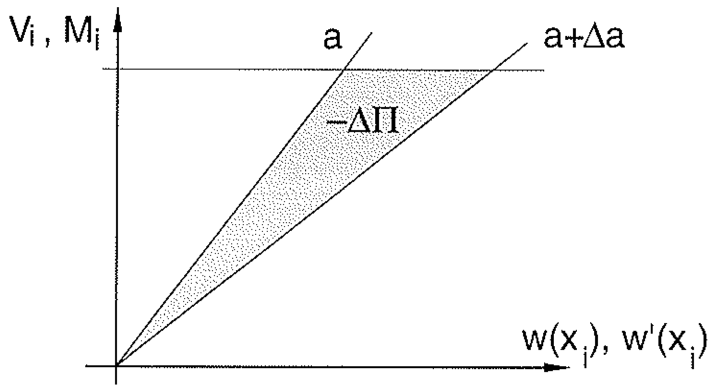

Fig. 6: calculating the energy release rate from the change of the potential ΔΠ

The model shown in figure 3 may easily be extended to a multiple fastener connection. Finally the energy release rate as a criterion for crack propagation can be calculated for different geometry, numbers of fasteners and mechanical properties.

Fig. 7 shows the energy release rates of a model with three dowels and crack extension starting alternatively at the first, the second and the third fastener from the end grain, respectively.

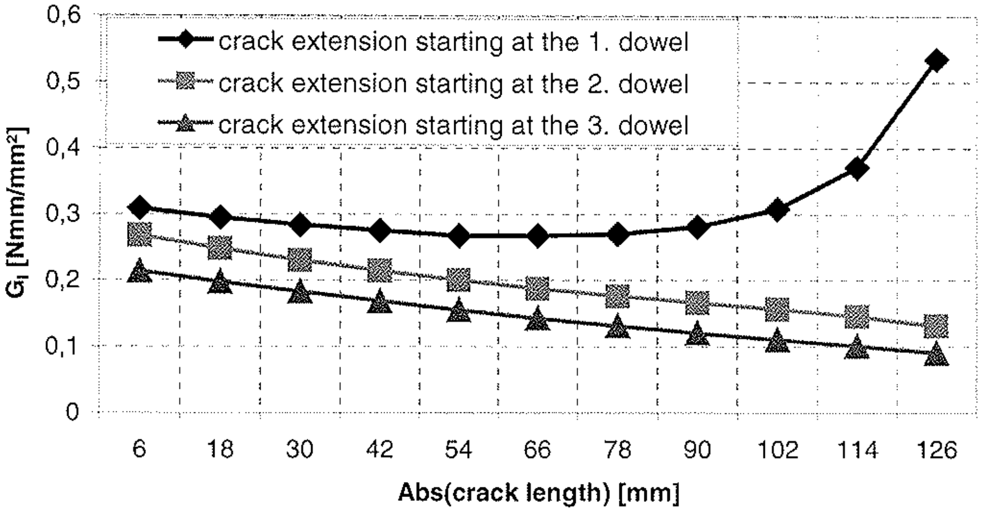

Fig. 7: Energy release rates

Using a critical energy release rate of $G_c = 0{,}214$ Nmm/mm² the corresponding load F_c per fastener per shear plane and a crack extension starting from the first fastener depending on the crack length is calculated for a timber thickness of 1 mm (fig. 8).

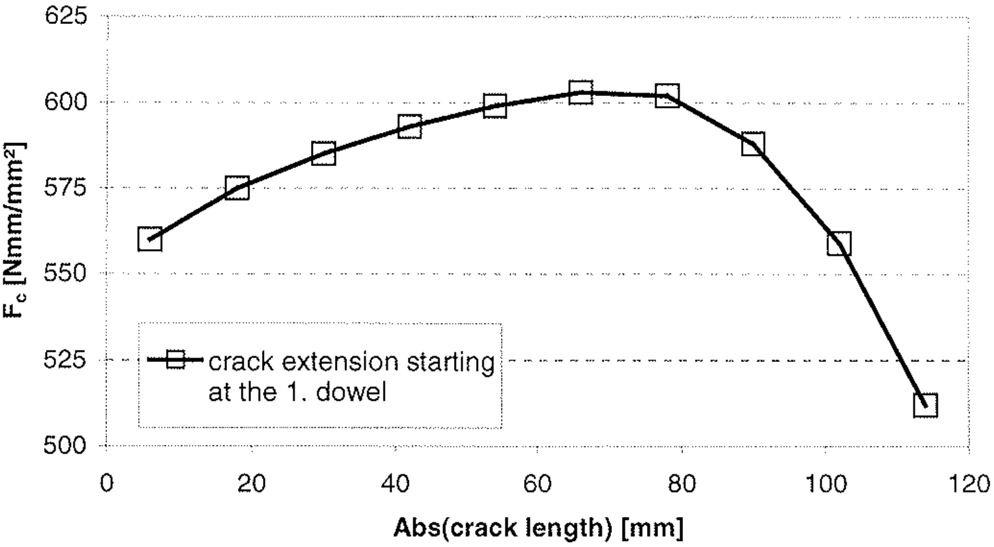

Fig. 8: critical load F_c

The diameter used for the results presented in fig. 7 and 8 was d = 24 mm. Obviously stable crack growth occurs until a crack length of $a \approx 3 \cdot d$ is reached. This was also observed in tests.

3. Results

With models, as e.g. shown for a joint with one fastener in figure 3, calculations of the energy release rate were performed assuming a crack extension starting from the first fastener. An equal load distribution between the fasteners for multiple fastener joints was assumed. For solving the system of equations resulting from the boundary conditions of the model the program mathematica was used. As the boundary conditions lead to quite difficult expressions due to the used shape function (7), the program was only able to solve the system of equations for given values of the studied variables. Contrary to a FE-calculation these solutions are analytical and not numerical.

The influence of the geometry on the energy release rate G_I for a crack extension from $x_I = -d$ until $x_I = -1{,}5 \cdot d$ ($\Delta a = d / 2$) was then studied by fitting a non-linear regression to the numerous results (equation (10)):

$$G_I = 1{,}275 \cdot 10^{-6} \cdot n^{0.155} \cdot d^{0,639} \cdot \rho^{2,00} \cdot \left(\frac{a_1}{d}\right)^{-0,710} \cdot \left(\frac{a_3}{d}\right)^{-0,302} \cdot \left(\frac{a_4}{d}\right)^{-0,074} \quad [\mathrm{N/mm}] \quad (10).$$

For equation (10) only models with more than one fastener in a row were used ($n \geq 2$).

In the studied models mode 1b according to Johansen was assumed. Equation (10) may conservatively also applied for timber members, where the fastener remains straight and is inclined. For timber members, where a plastic hinge occurs in the fastener, equation (10) can easily be extended:

$$G_I = 1{,}275 \cdot 10^{-6} \cdot n^{0.155} \cdot d^{0,639} \cdot \rho^{2,00} \cdot \left(\frac{a_1}{d}\right)^{-0,710} \cdot \left(\frac{a_3}{d}\right)^{-0,302} \cdot \left(\frac{a_4}{d}\right)^{-0,074} \cdot \frac{y^2}{t^2} \quad [\mathrm{N/mm}] \qquad (11),$$

where

$$y = F_{\mathrm{Johansen}} / (f_h \cdot d) = F_{\mathrm{Johansen}} / (0{,}082 \cdot (1 - 0{,}01 \cdot d) \cdot \rho \cdot d) \qquad (12),$$

F_{Johansen} = load-carrying capacity per dowel per shear plane according to Johansen

t	timber thickness,
n	number of fasteners in a row,
d	fastener diameter,
ρ	density,
a_1	distance between fasteners in a row,
a_3	fastener end distance,
a_4	fastener edge distance.

The criterion for crack extension resulting from (11), (12) is

$$G_c \leq G_I = \frac{F^2_{\mathrm{Johansen}} \cdot 1{,}275 \cdot 10^{-6} \cdot n^{0.155} \cdot d^{0,639} \cdot \left(\frac{a_1}{d}\right)^{-0,710} \cdot \left(\frac{a_3}{d}\right)^{-0,302} \cdot \left(\frac{a_4}{d}\right)^{-0,074}}{(0{,}082 \cdot (1 - 0{,}01 \cdot d) \cdot d)^2 \cdot t^2} \quad [\mathrm{N/mm}]\,(13)$$

with the critical energy release rate G_c as a property of resistance.

If equation (13) is not fulfilled the resistance per fastener per shear plane has to be limited according to equation (14):

$$F_{Jo\_red\_1} = \sqrt{\frac{G_c \cdot (0{,}082 \cdot (1-0{,}01 \cdot d) \cdot d)^2 \cdot t^2}{1{,}275 \cdot 10^{-6} \cdot n^{0.155} \cdot d^{0{,}639} \cdot \left(\frac{a_1}{d}\right)^{-0{,}710} \cdot \left(\frac{a_3}{d}\right)^{-0{,}302} \cdot \left(\frac{a_4}{d}\right)^{-0{,}074}}} \; [N] \qquad (14)$$

with $n \geq 2$.

A similar equation was fitted taking also into account models with one fastener ($n \geq 1$), the distance a_1 between the fasteners is then obviously not included:

$$F_{Jo\_red\_2} = \sqrt{\frac{G_c \cdot (0{,}082 \cdot (1-0{,}01 \cdot d) \cdot d)^2 \cdot t^2}{0{,}331 \cdot 10^{-6} \cdot n^{0.248} \cdot d^{0{,}634} \cdot \left(\frac{a_3}{d}\right)^{-0{,}290} \cdot \left(\frac{a_4}{d}\right)^{-0{,}210}}} \; /[N] \qquad (15)$$

with $n \geq 1$.

Equations (14) and (15) are compared to the empirically found result of Jorissen (1998) which was transformed resulting in the load per fastener per shear plane assuming equal load distribution within the fasteners in a row :

$$F_{Jorissen\_1} = 0{,}37 \cdot n^{-0{,}1} \cdot \left(\frac{a_1}{d}\right)^{0{,}30} \cdot (\lambda)^{0{,}20} \cdot F_{Johansen} \qquad (16)$$

with

$$\lambda = \min \begin{cases} t_m/d & t_m: \text{ thickness of the middle member} \\ 2 \cdot t_s/d & t_s: \text{ thickness of the side member} \end{cases} \qquad (17)$$

and $F_{Johansen}$ the load carrying capacity per fastener and shear plane according to Johansen.

As the equation according to Jorissen is based on tests including joints with one fastener, the effect of numbers of fastener n in a row is taken into account using equation (15) and (16). The resulting exponent of n according to equation (15) is:

$$n^{-0{,}248 \cdot 1/2} = n^{-0{,}124} \qquad (18)$$

which is in good agreement to Jorissen's exponent of -0,1.

Using the variables of equation (19) and assuming equal load distribution within the fasteners the diagram in fig. 9 shows the effect of the number of fasteners n per row. The shape of the curves according to (14), (15) and (16) is quite similar. The difference in the values might be caused by the assumption of equal load distribution within the row, an effect which is included in Jorissen's empirically based equation. Furthermore the variation of the embedding strength is included in (16) but not in (14) and (15) using equation (12).

$$\begin{array}{ll} \rho = 450\,\mathrm{kg/m^3} & f_y = 240\,\mathrm{N/mm^2} \\ M_y = \dfrac{f_y \cdot d^3}{6} & t_1 = \dfrac{d}{\sqrt{6}} \cdot \sqrt{\dfrac{f_y}{f_h}} \\ t_2 = 3 \cdot t_1 & d = 24 \\ a_1 = 7 \cdot d & a_3 = 7 \cdot d \\ a_4 = 3 \cdot d & G_c = 0{,}214\,\mathrm{Nmm/mm^2} \\ \beta = \dfrac{f_{h,2}}{f_{h,1}} = 1 & \lambda = \dfrac{2 \cdot t_1}{d} \end{array} \tag{19}$$

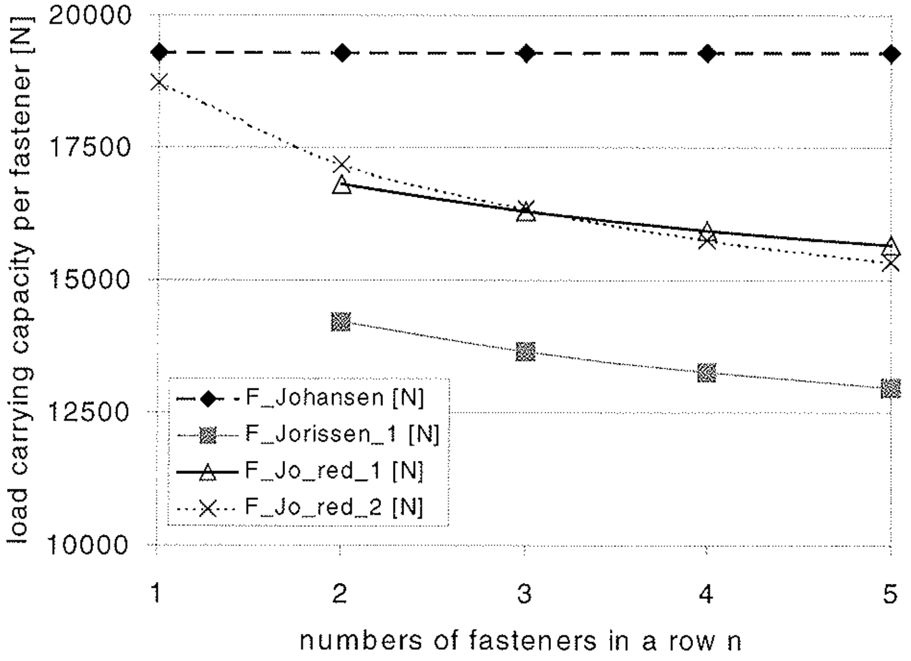

Fig. 9: effect of the number of fasteners per row

Fig. 10 and fig. 11 show the influence of the diameter on the load carrying capacity which is not included in Jorissen's investigations as only 20 from 958 tests had a diameter different from 12 mm.

Values used for fig. 10

$$\begin{array}{llll} \rho = 450\,\mathrm{kg/m^3} & f_y = 240\,\mathrm{N/mm^2} & M_y = \dfrac{f_y \cdot d^3}{6} & t_1 = \dfrac{d}{\sqrt{6}} \cdot \sqrt{\dfrac{f_y}{f_h}} \\ t_2 = 3 \cdot t_1 & n = 3 & a_1 = 7 \cdot d & a_3 = 7 \cdot d \\ a_4 = 3 \cdot d & G_c = 0{,}214\,\mathrm{Nmm/mm^2} & \beta = \dfrac{f_{h,2}}{f_{h,1}} = 1 & \lambda = \dfrac{2 \cdot t_1}{d} \end{array} \tag{20}$$

Values used for fig. 11:

$$\rho = 450\,kg/m^3 \qquad f_y = 240\,N/mm^2 \qquad M_y = \frac{f_y \cdot d^3}{6} \qquad n = 3$$

$$t_1 = \frac{2+\sqrt{2}}{\sqrt{6}} \cdot d \cdot \sqrt{\frac{f_y}{f_h}} \qquad t_2 = t_1 \qquad a_1 = 7 \cdot d \qquad a_3 = 7 \cdot d \tag{21}$$

$$a_4 = 3 \cdot d \qquad G_c = 0{,}214\,Nmm/mm^2 \qquad \beta = 1 \qquad \lambda = \frac{2 \cdot t_1}{d}$$

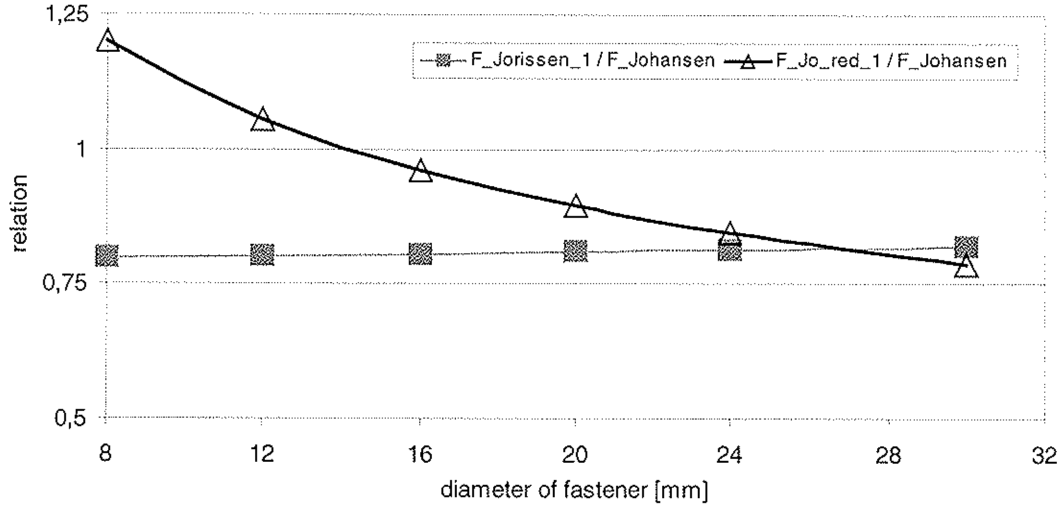

Fig. 10: effect of diameter with a constant slenderness leading to failure mode 1b, properties according to (20)

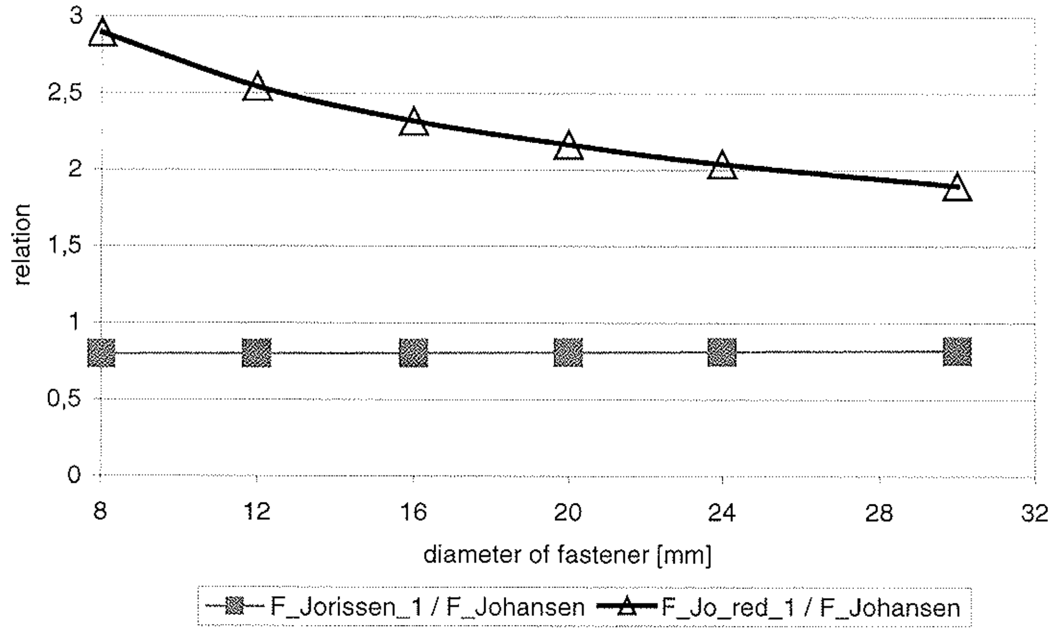

Fig. 11: effect of diameter with a constant slenderness leading to failure mode 3, properties according to (21)

According to fig. 11 splitting would hardly occur if Johansen's failure mode 3 is governing.

Fig. 12 to 14 show the effect of the joint geometry according to equations (14) and (15). The properties were those of (20) except for the variables. The diameter was d = 16 mm.

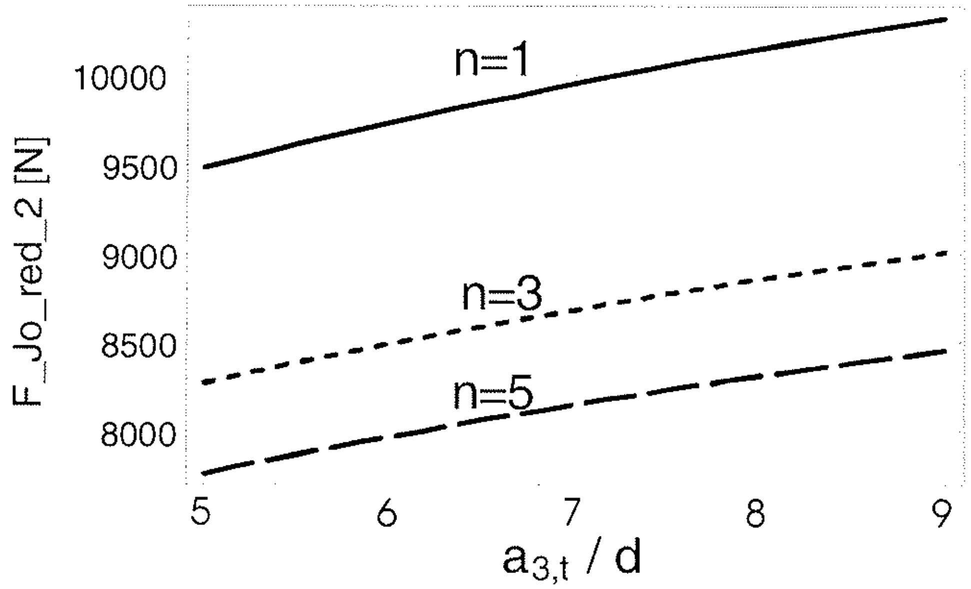

Fig. 12: effect of end distance $a_{3,t}$

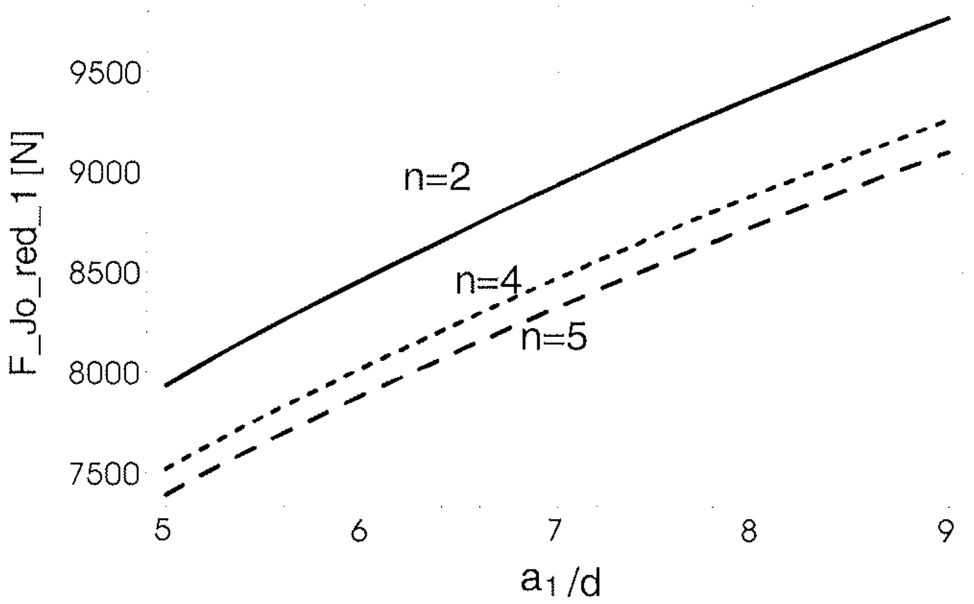

Fig. 13: effect of spacing a_1

The most favourable influence has therefore an increase of the fastener spacing a_1.

Increasing the edge distance increases the load carrying capacity of a single fastener joint (fig. 14). Figures 12 to 14 are based on the fitted equations based on numerous calculations of the energy release rate. If figures 12 to 14 would directly be based on the calculation of energy release rates for the configurations considered, the influence of the parameters would be even more pronounced.

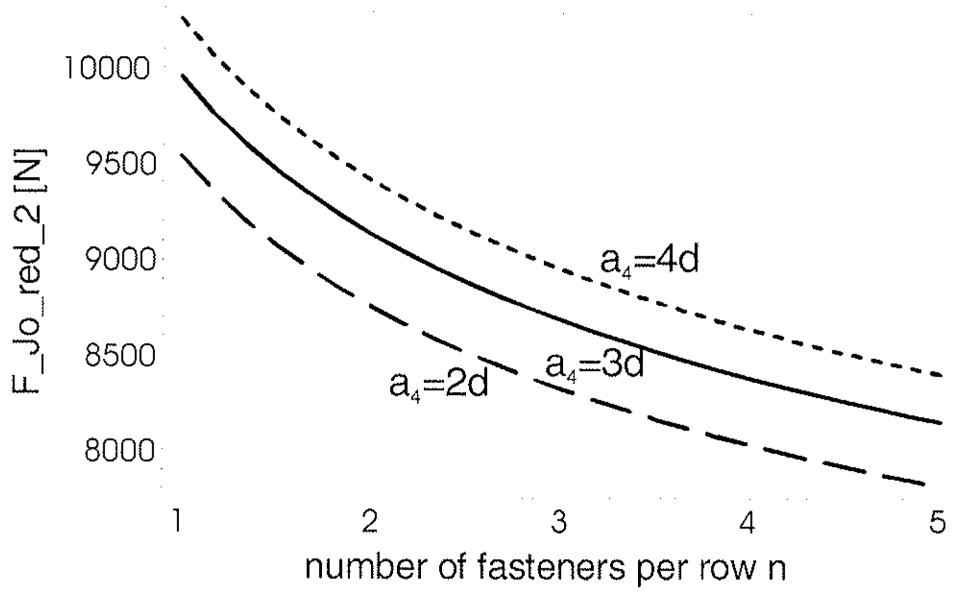

Fig. 14: effect of edge distance $a_{4,c}$

4. Conclusions

The influence of geometry and material properties on the splitting tendency in the connection area of timber members was studied using a fracture mechanics approach. Based on the results of this approach, the model developed by Jorissen (1998) was modified. The predictions of the load-carrying capacity of multiple fastener joints show a good agreement with the test results of Jorissen. The effect of joint geometry was also studied using the model. The major influencing parameter on the splitting tendency of timber in the connection area is the fastener spacing a_1 parallel to the grain, while $a_{3,t}$ and $a_{4,c}$ are of minor influence for joints with more than one fastener. For similar geometry and the same fastener slenderness the absolute diameter has a significant influence as well. Joints, where failure mode 3 according to Johansen's yield theory governs the design should hardly fail by timber splitting.

Further research is necessary for the group tear failure or plug shear failure. These failure modes are a combination of mode I and II crack extension. If mode I dominates, however, the results should be similar those presented here.

Literature

Blaß, H.J.; Schmid, M. (2002). Spaltgefahr von Nadelhölzern. Versuchsanstalt für Stahl, Holz und Steine, Abteilung Ingenieurholzbau, Universität Karlsruhe (TH). In German.

Masuda, M. (1998). Fracture analysis of bolted joints using the finite small area criterion. Fifth World Conference on Timber Engineering. Montreux. Volume I, S. 321-328

Jorissen, A.J.M. (1998). Double Shear Timber Connections with Dowel Type Fasteners. Delft University Press, Delft, 1998.

Timoshenko, S.P. und Goodier, J.N. (1970). Theory of Elasticity. 3. Edition, McGraw-Hill Book Company, Singapore.

Quenneville, P. (1998)Predicting the failure modes and strength of brittle bolted connections. 5th World conference on timber engineering, Montreux, Switzerland.

Mohammad, M.; Quenneville, P. (1999). Behaviour of wood-steel-wood bolted glulam connections. CIB-W18, paper 32-7-1, Graz, Austria.

CIB-W18/35-7-6

INTERNATIONAL COUNCIL FOR RESEARCH AND INNOVATION IN BUILDING AND CONSTRUCTION

WORKING COMMISSION W18 - TIMBER STRUCTURES

EFFECT OF ROW SPACING ON THE CAPACITY OF BOLTED TIMBER CONNECTIONS LOADED PERPENDICULAR-TO-GRAIN

M Kasim
P Quenneville

Royal Military College of Canada

CANADA

Presented by: P Quenneville

H J Larsen and H J Blaß asked about the effect of spacing on the interaction potential of the 2 separate connections – the expressions developed in the presentation seemed to imply that there is interaction even if the connections are very far apart. P Quenneville recognised the limitations of the proposed expressions. This was followed by questions by F Rouger and L Ozola regarding the approach used for calculating cov and the characteristic values presented. P Quenneville replied that the cov values were separately calculated for each data set. This was followed by discussion about the correct approach to calculating cov and it was suggested that a single cov value could be used for the entire test series.

Effect of row spacing on the capacity of bolted timber connections loaded perpendicular-to-grain

M.Kasim and P.Quenneville
Royal Military College of Canada

1 Introduction

When a wood member is loaded perpendicular to the direction of grain by a bolted connection, failure of the joint may result either by yielding of the bolts, crushing of the wood under the bolts or by splitting of the wood member. The first two failures are considered ductile, while splitting or fracture of the wood is brittle and may lead to catastrophic collapse. Most researchers agree that the bolt or line of bolts furthest from the loaded edge initially carries the biggest share of the load, and, therefore, splitting or fracture is more likely to occur at this level. The aim of any connection design is to ensure that brittle failure does not happen prior to yielding of the bolts or the wood, making it necessary to predict the splitting strength of the wood when the joints are subjected to a force perpendicular to grain.

The Canadian design standard for wood structures (CSA O86) [2] lays down minimum requirements for the bolt spacing, edge distance and end distance that define the layout of bolt groups. Tests conducted by many researchers showed that these minimum requirements do not guarantee ductile failure especially in multiple-bolt connections. In bolted connections, the manner in which the load is transferred from the bolts into the wood members affects to a great extent the capacity of the joints. Overlapping of the load paths of adjacent rows of bolts in a joint, for instance, can reduce the effectiveness of the bolts in the group, so that the joint capacity is less than the sum of the capacities of the individual rows.

1.1 Cluster Principle

A load transferred to a wood member perpendicular to grain by a bolt causes compression in the local area under the bolt. The ability of the member to spread the concentrated load and the manner in which the load is spread over the remaining depth can have a significant effect on the capacity of joints. Overlapping of the load path from the bolts in a row with those in adjacent rows within the same joint is not considered in design standards. However, the concept of fastener cluster has been used by many researchers, especially in Europe. Foschi

[4] used the concept of cluster to predict the ultimate capacity of riveted joints. Later, other researchers used and applied the same concept to different types of fasteners. Goerlacher [5] used the concept of cluster in his design proposal for the new EUROCODE 5. He recommended that several groups of fasteners can be considered as one cluster with one load carrying capacity if the distance between the groups is less than 0.5h (h being the depth of the member). On the other hand, they can be considered separate groups if the distance between the groups is more than 2h. The assumed angle of distribution with the grain direction is therefore less than 45° (depending on the unloaded edge distance). A reduction factor is proposed if the distance is between 0.5h and 2h. The 2h limit differs from that used by Ehlbeck, Goerlacher and Werner [3] where only h was assumed. The latter, however, gives a more consistent load distribution with the approach used for interior connections.

Quenneville and Mohammad [6] used the cluster concept to arrive at the splitting capacity of bolted connections. For interior connections, they assumed that a group of bolts in a connection can be assumed as one cluster if the distance between the rows of bolts does not exceed the depth of the member less the unloaded edge distance ($h-e_p$), (Figure 1). The assumed angle of distribution is therefore 63°. On the other hand, if the distance between the rows of bolts exceeds the depth of the member less the unloaded edge distance ($h-e_p$), the resistance of each row is determined and the connection resistance would constitute the sum of the resistance of each of the rows.

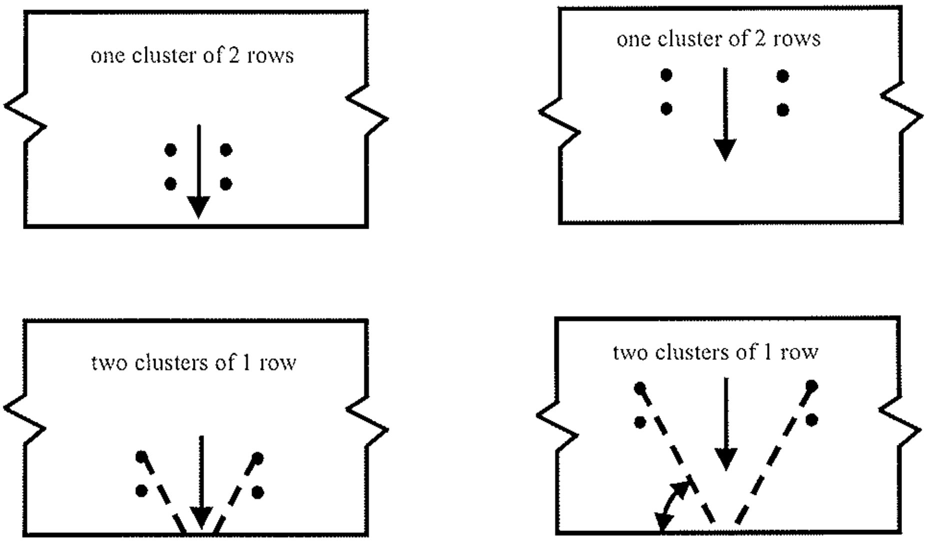

Figure 1 Load distribution in interior joints.

Van der Put and Leijten [8] explained the test results conducted by Ballerini [1] through the use of the spreading of load concept. The tests were confined to a single row with one or two bolts only and therefore do not provide sufficient information on the cluster behavior. They explained the spreading by the equilibrium method of constructing a stress field in the specimen that satisfy the equilibrium and boundary conditions without exceeding the failure criteria. This resulted in a spreading slope of 1 vertical to 1.5 horizontal under each bolt (angle of distribution of 33° with the grain). In other words, the spreading length along the loaded edge of the beam is three times the depth below the bolt (3a).

1.2 Summary

Several researchers have attempted to provide procedures and make recommendations for the estimation of either the tensile strength perpendicular to grain of wood members or the splitting capacity of bolted connections. The approaches, assumptions and theories used for this purpose vary to a great extent. However, the issue of perpendicular to grain loading that can result in brittle failure or splitting of the wood remains neither fully addressed nor well investigated. There is no uniform approach or guidelines in the standards that designers can follow for estimating the splitting capacity of joints.

Research to date does not provide clear ideas as to the optimum joint geometry that can utilize the potential joint capacities while being at the same time sufficiently simple for practical applications. As noted above, the assumed load distribution or the recommended row spacing in the literature are not conclusive. It is necessary to experimentally investigate various joint geometries and locations within the depth of the members to formulate a better idea of the cluster effect and the angle at which the load is transferred within the remaining depth of the member. This study is an attempt to address this gap in the knowledge.

2 Experimental program

The main objective of the experimental program was to determine an upper limit for bolt row spacing beyond which the connection is assumed to behave as two independent clusters as assumed by Quenneville and Mohammad [6], taking into account the effect of the location of the connection with respect to the total depth of the member.

Various row spacings were used in an effort to determine whether the connection is behaving as one cluster or two clusters. The minimum row spacing was determined in accordance with CSA O86 as permitted by linear interpolation for l/d (member thickness/bolt diameter) between 2 and 6. The maximum row spacing was selected on the basis of the maximum angle of load distribution as concluded by different researchers. To examine the influence of the location of the joint within the depth of the member, two different joint locations within the depth of the beam for each row spacing were considered. Configuration 1 joints were fabricated with the minimum loaded edge distance permitted by CSA O86, which is 4d. Configuration 2 joints were fabricated with a larger loaded edge distance of 8.2d. Nine groups consisted of four 19 mm diameter bolts arranged in two rows with 2 bolts in each row. Two groups of one row served as references. The in-row bolt spacing for all the specimens was selected to reflect the minimum requirements of CSA O86, and set at 3d. Using the same in-row bolt spacing for the whole program eliminated the impact of in-row bolt spacing on the results.

2.1 Specimens

All specimens were fabricated using the identical Spruce glulam (80 mm x 304 mm) sections, thus eliminating the impact of the width and depth of the specimens on the load distribution. Connections for all the specimens were fabricated using 19 mm (3/4 inch) diameter bolts, SAE grade 2 which are similar to A307 bolts. The total length of the specimens for each group was determined to be the summation of the bearing lengths, the distances from the support to the closest row of bolts (2 x 1.5 times the depth of the member) and the spacing between row of bolts. This resulted in having different lengths for the groups as shown in Table 1. Figure 2 illustrates the general arrangement of the specimens.

Table 1 Test group configurations.

Group*	e_q mm	e_p mm	s_r mm	s_b mm	N	n_r	Total Length mm
SP-77	77	170	N/A	57	2	1	1100
SP-77-77	77	170	77	57	2	2	1177
SP-77-155	77	170	155	57	2	2	1255
SP-77-225	77	170	225	57	2	2	1325
SP-77-320	77	170	320	57	2	2	1420
SP-157	157	90	N/A	57	2	1	1100

SP-157-77	157	90	77	57	2	2	1177
SP-157-225	157	90	225	57	2	2	1325
SP-157-320	157	90	320	57	2	2	1420
SP-157-418	157	90	418	57	2	2	1518
SP-157-700	157	90	700	57	2	2	1800

*The group name identifies the species (SP), the loaded edge distance (e_q) in mm and then the row spacing (s_r) in mm.

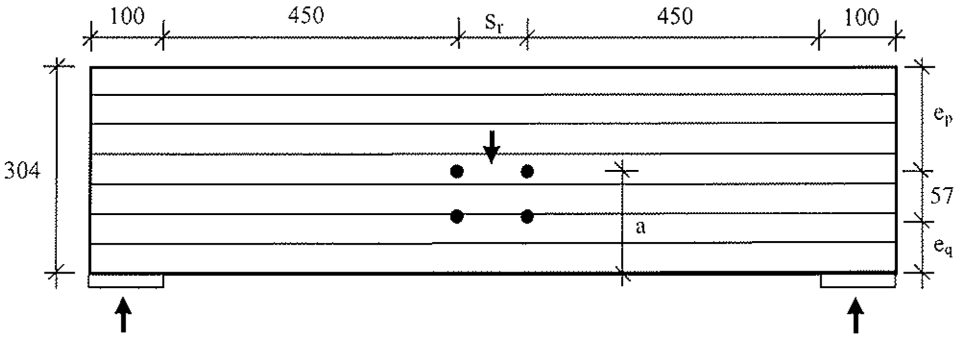

Figure 2 General specimen dimensions.

2.2 Testing procedures

The testing procedure to evaluate the strength of bolted connection joints for all specimens was in accordance with ASTM D 1761-88 (Standard Test Methods for Mechanical Fasteners in Wood/Testing Bolted and Timber Connector Joints) with minor deviations.

Ten replicates of each group were prepared and tested for this experimental program. All specimens had their moisture content measured and recorded using a moisture meter device immediately prior or after testing. The average value of three readings was considered as representative of the actual moisture content of a specimen. The ultimate loads attained during testing for specimens with moisture contents other than the required 12% were adjusted to an equivalent 12% moisture content values using the exponential equation derived by Skaar [7]. The load-deformation curve was monitored on the computer and was updated every 2 seconds, which allowed observation of the load values and deformations due to crack development on the screen. Prior to actual testing, the joint specimen was pre-loaded to approximately 5 kN.

2.3 Displacement Measurements

Linear Voltage Displacement Transducers (LVDTs) were used to measure and record the deformation in the tested specimens. The LVDTs were installed at critical locations such as the supports, the top and bottom of the specimen and at the connection plates, as shown in Figure 3. The LVDTs scheme allowed the calculations of the support bearing, the joint cracking width perpendicular to grain, the joint bearing (bearing of bolts on wood), the total joint slip and the flexural displacements.

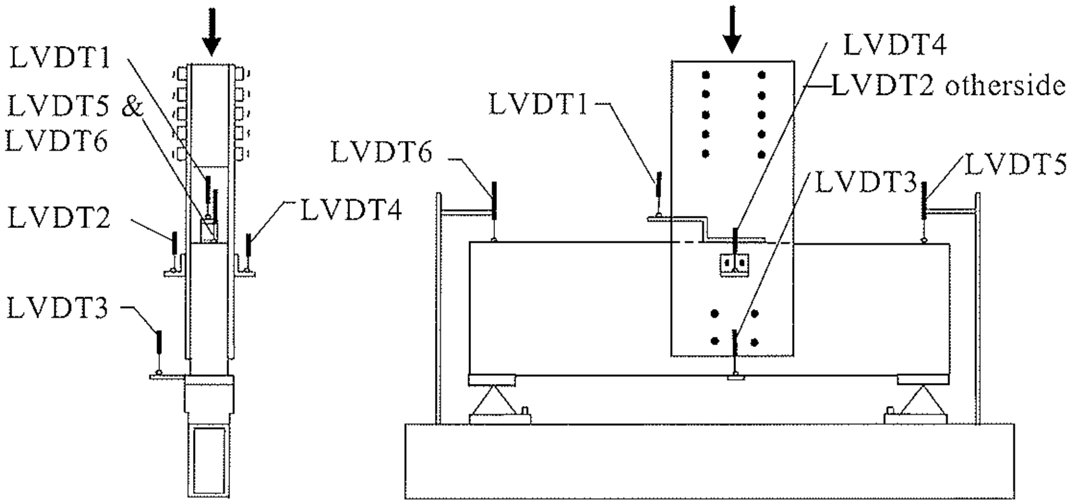

Figure 3 General LVDT set-up.

2.4 Materials

All specimens were fabricated from 80 mm wide Spruce glued-laminated timber with a depth of 304 mm. All glulam was manufactured per CAN\CSA-O122-M89. The two connection plates were mounted on the beams using four19 mm (3/4 inch) diameter bolts, resulting in a bolt slenderness ratio (l/d) of 4.2. The minimum tensile strength of the bolts is 510 MPa which is comparable to the minimum tensile strength of ASTM A307 bolts. The two side plates were 9.5 mm thick, 300W grade steel (F_y = 300 MPa and F_u = 450 MPa).

3 Results

All specimens developed significant cracks shortly prior to failure or at failure. The cracks in all but few specimens passed through the bolt holes furthest from the loaded edge. The presence of the connection plates and the sudden failure of the beams made it difficult to observe the exact locations where the cracks had initiated. Mode II fracture failure is unlikely since the cracks did not propagate all the way to the member ends although the shear force between the joint and the member ends is constant in all beams. The exception with the crack in some specimen reaching one end of the member does not make the case for Mode II fracture failure any stronger. Had the fracture mode of failure been due to shear stresses, an increase in load capacity after the initial splitting would have been unlikely since a shallower lower portion is always weaker in shear than the whole. Since the test was allowed to continue long after the joint failure, it is reasonable to assume that the crack was shorter at joint failure. It can therefore be reasonably argued that the general failure of this group is due to Mode I fracture caused by tensile forces perpendicular to grain.

There were no signs of noticeable bearing/crushing of the wood at all bolt hole locations or through the bearing length of the supports. The bolt holes in the steel plates did not show any sign of bearing failure either. The steel bolts themselves did not bend but remained straight during testing. A typical relationship between the load, normalized cracking (crack difference between subsequent readings divided by the maximum crack difference) and time is illustrated in Figure 4.

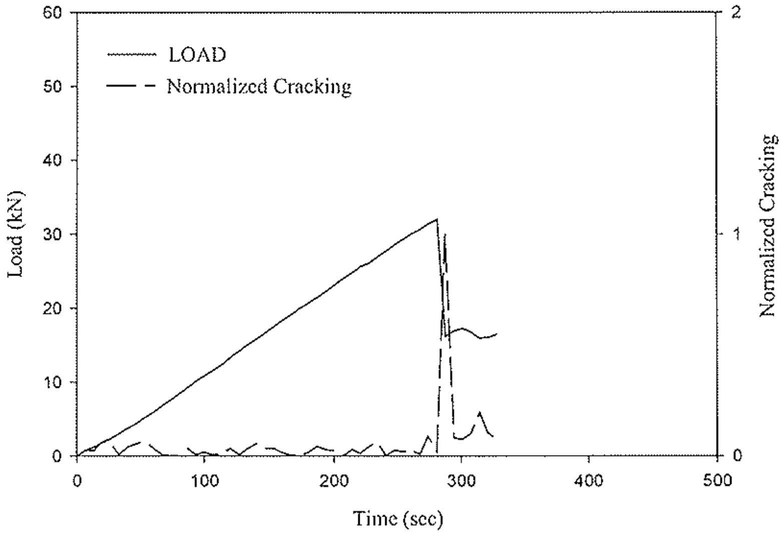

Figure 4 Typical load / cracking curve.

The curves show the normalized cracking pattern reflecting the effect of the crack widths. In most specimens, the maximum normalized cracking (spike) coincides with or is close to the ultimate loads. In some specimens, there is more than one significant spike thus reflecting the behavior of the lower portion of the beam after the joint failure. The value before the first major drop was taken as the ultimate load of the specimen. The ultimate loads were attained within 6-10 minutes. This falls within the acceptable range of ASTM (5 to 20 minutes). The combined effect of joint cracking and joint bearing resulted in a maximum joint slip well below the 15 mm established for bearing failure. Data at failure for each group is listed in Table 2.

Table 2 Group results (10 min duration values).

Group	P_{avg} kN	COV %	P_{5th} kN
SP-77 (one row)	41.1	14.0	27.0
SP-77-77	32.6	19.7	17.5
SP-77-155	41.5	14.8	26.3
SP-77-225	58.7	10.9	39.7
SP-77-320	63.2	13.0	42.0
SP-157 (one row)	68.2	8.3	51.8
SP-157-77	66.6	9.5	48.8
SP-157-225	83.8	11.0	58.8
SP-157-320	83.2	7.1	64.7
SP-157-418	100.4	11.5	69.1
SP-157-700	100.7	9.1	75.6

4 Discussion

The results in Table 2 have been graphed for the two separated loaded edge distances. The one-row connection serves as a reference for the other groups. Simple linear regressions have been plotted for the average and the 5th percentile values (inclined straigth lines). An horizontal line has been drawn from the intersection of the regression line and the "2a" limit (dotted line) for each configuration.

4.1 Connection capacity

It is obvious from Figures 5 and 6 that the resistance of a two-row bolted connection loaded perpendicular-to-grain is not necessarily twice the resistance of a one row bolted connection. Taking the capacity of one-row connections as reference, one can note that the resistance of two-row connections with a row spacing of 3d (minimum by Canadian design standard) is lower or statistically not different. There are thus no advantages to use twice the number of bolts in these cases. As the row spacing is increased, the resistance of the connection increases. This increase in capacity stops or becomes negligible beyond a certain row spacing. Another important point about the connection capacities is that at the row spacing of "2a", the resistance is not twice the capacity of the one-row connection. Beyond that point, the capacity is approximately 75% of twice the capacity of a one-row connection. It is not known experimentally at what row spacing, the resistance of the two row connection equals twice the resistance of a single row connection. This observation should be taken into account in design standards.

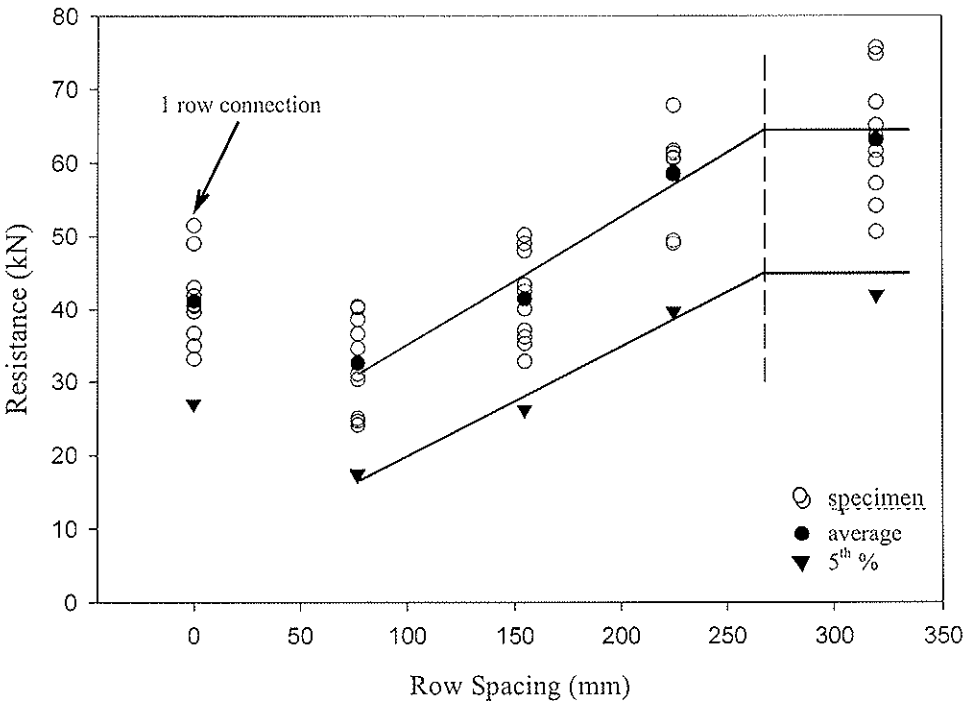

Figure 5 Connection capacity vs. row spacing for 77 mm loaded edge distance.

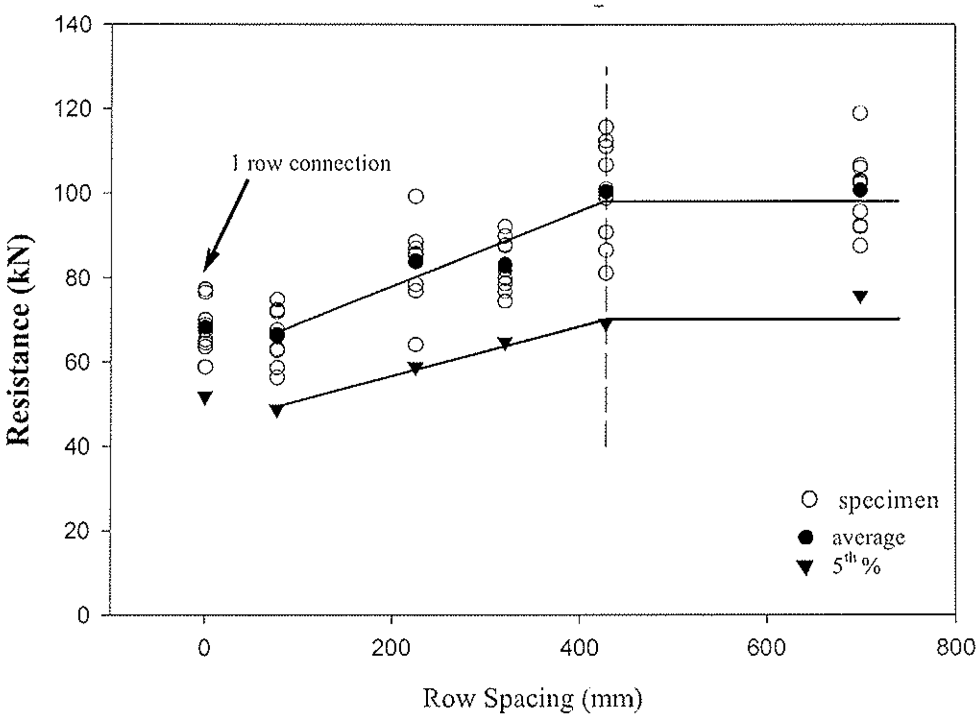

Figure 6 Connection capacity vs. row spacing for 157 mm loaded edge distance.

4.2 Angle of Load Distribution

It is known that a load transmitted from a bolt is distributed in a triangular manner within the depth of the loaded wood member. The spacing between two rows of bolts usually determines the degree of overlapping between them. If the load paths from the adjacent rows overlap, the joint is considered to behave as one cluster. Otherwise, it will act as two independent clusters. It is logical to assume that the joint behaves as one cluster when the distance between the two rows is small and there is a clear overlapping between their triangular load distributions. As the row spacing increases, the common zone (overlap) between the triangular load distribution of each row becomes smaller until this zone vanishes. Once the overlap is eliminated, each row of bolts behaves independently resulting in joint resistance equal to the summation of the capacity of each cluster (row of bolts). Increasing the row spacing further will not necessarily result in an increase of the joint resistance. In other words, the load the joint can resist levels and becomes virtually constant even if the rows are spread further apart.

The overlapping of the stressed areas and the consequent loss of resistance in the common zone is the primary reason why a one cluster joint has a lower resistance than a two cluster joint. However, the resistance of a one cluster joint varies with the degree of overlapping. The more the overlapping, the less the resistance of the joint and eventually the less efficient the design. It is thus critical to determine the joint behavior with respect to the number of clusters in the joint. Once this behavior is identified, the angle of load distribution can be estimated from the joint geometry. Two approaches were employed to analyze the test results from the test groups in each configuration and to study the cluster phenomena. The use of 5th percentile ultimate load values and the average ultimate load values.

The use of the averages and the 5th percentile values in Figures 5 and 6 both reinforces the assumption that the angle of load distribution can be approximated to 45 degrees. One can clearly note that a change in behavior occurs at or near the 268 mm and 428 mm for the in Figures 5 and 6 respectively. These values correspond with the "a" of 134 mm for the first configuration and 214 mm for the second configuration. Thus, one could assume that beyond a row spacing of "2a", the resistance of the connection does not increase significantly and the increase in row spacing to achieve this increase is not practical.

4.3 Design approach

To take into account the effect of the row spacing in the design of two-row connections, a factor is proposed. The factor for the joints used in this experimental program can be estimated from the following equation (for 5th percentile and average values):

$$C_F = 0.75\,[1 + (L_c - 77)/(2a - 77)]/2 \qquad (1)$$

This equation is conservative for the larger loaded edge distances. The value of C_f would be multiplied by the capacity of one row as follows:

$$R_{2\text{-row}} = R_{1\text{-row}} \times C_f \times n_r \qquad (2)$$

5 Conclusions

From testing of spruce glulam specimens by perpendicular to grain loading using two-row bolted joints with various row spacings arranged in two different configurations with respect to the loaded edge distance, the following can be concluded:

a. If "a" is taken as the distance between the furthest line of bolts and the bottom fibers of the member, a two-row joint behaves almost as two separate one row joints if the spacing between the row of bolts is equal to or exceeds "2a". For bolt spacings less than "2a", the joint resistance decreases with the decrease in bolt spacing.

b. Regardless of the location of the joint relative to the member depth, the angle of load distribution from a bolt towards the loaded edge can be estimated at 45°.

c. A cluster factor is proposed. This factor accounts for the increase in joint resistance when the row spacing is larger than the minimum permitted by design standards.

d. The cluster factor for the joints used in this experimental program can be estimated from the following equation (for 5th percentile values):

$$C_F = 0.75\ [1 + (L_c - 77)/(2a - 77)]/2$$

These conclusions are for two-row bolted connections and may not be applicable to three or more row cases.

6 References

[1] Ballerini, M., "A New Set of Experimental Tests on Beams Loaded Perpendicular-to-Grain by Dowel-Type Joints", CIB-W18, Paper 32-7-2, Graz, Austria, 1999.

[2] Canadian Standard Association, O86.1-94, "Engineering Design in Wood (Limit States Design)", Etobicoke, ON., 1994.

[3] Ehlbeck, J., Goerlacher, R., and Werner, H., "Determination of Perpendicular-to-Grain Tensile Stresses in Joints with Dowel-Type Fasteners - A Draft Proposal for Design Rules", CIB-W18 Paper 22-7-2, Berlin, Germany, 1989.

[4] Foschi, R. O., "Stress Analysis and Design of Glulam Rivet Connections for Perpendicular-to-Grain Loading of Wood", Information Report VP-X-117, Department of the Environment, Canadian Forestry Service, 1973.

[5] Goerlacher, R., "Tension Stresses Perpendicular-to-Grain in Joints-A Design Proposal" (Unpublished Notes), 2000.

[6] Quenneville, J.H.P., and Mohammad, M., "Design Method for Bolted Connections Loaded Perpendicular-to-Grain", CJCE, Vol. **28**, 2001.

[7] Skaar, C., "Wood-Water Relations", Springer-Verlag, Berlin, Heidelberg, 1988.

[8] van der Put, T.A.C.M., and Leijten, A.J.M., "Evaluation of Perpendicular to Grain Failure of Beams Caused by Concentrated Loads of Joints", CIB-W18 Paper 33-7-7, Delft, The Netherlands, August 2000.

CIB-W18/35-7-7

INTERNATIONAL COUNCIL FOR RESEARCH AND INNOVATION
IN BUILDING AND CONSTRUCTION

WORKING COMMISSION W18 - TIMBER STRUCTURES

SPLITTING STRENGTH OF BEAMS LOADED BY CONNECTIONS, MODEL COMPARISON

A J M Leijten

Faculty of Civil Engineering
Delft University of Technology

THE NETHERLANDS

Presented by: A J M Leijten

H J Larsen commented that the proposed expression are almost identical to previously published expression except for the term he/h and so the proposed expression will give identical results when he/h is small and would only have significance when he/h is large and as such the proposed expressions have limited practical significance. This was followed by an interesting in depth discussion by H J Blaß and A Leijten about the fundamental validity of the proposed approach and the significance of the efficiency and behaviour factors used in the proposed expression.

Splitting strength of beams loaded by connections, model comparison

A.J.M Leijten, Faculty of Civil Engineering,
Delft University of Technology,
The Netherlands

Abstract

At the previous two CIB/W18 meetings in Delft (2000) and Venice (2001) two fracture mechanical models were proposed for splitting of beams caused by connections. This paper compares models by Van der Put & Leijten [1] and Larsen & Gustafsson [2] both based on fracture theory and an empirical German model. A total number of 767 tests were evaluated. Although the differences between the fracture models are small Model (1), which is the basis for the design by Eurocode 5, shows the best results.

Introduction

Although the problem of perpendicular to grain splitting of beams by connections, see Figure 1, was tried to solve by empirical models, lately models based on fracture mechanics were developed. Empirical models are only valid within the range of parameters tested therefore there is more credit in pursuing general physical oriented models. Empirical models for the problem concerned tend to have many parameters to take all possible influences and effects into account as is shown by the German model evaluated below. The last years two models are published both based on fracture mechanical principles. The first is by Van der Put & Leijten (CIB/W18 paper 33-7-7& 34-7-1) the other by Larsen & Gustafsson (CIB/W18 paper 34-7-3).

The models

The models reviewed are:
Model (1) by v.d.Put/Leijten (Eurocode5)

$$F_u = 2.58\mu b\sqrt{GG_c\frac{h_e}{1-\frac{h_e}{h}}} \qquad (1)$$

Model (2) by Larsen /Gustaffson

$$F_u = 2.82\eta b\sqrt{GG_c h_e} \qquad (2)$$

Model (3) is a simplified Model (1), see equation (18), CIB/W18, paper 33-7-7

$$F_u = 5.16\mu b\sqrt{GG_c}\frac{h_e}{\sqrt{h}} \qquad (3)$$

where:

F_u	is the splitting shear strength of the beam loaded by a connection at mid span in [N]. For connections at the end of a cantilever the splitting strength is $F_u/2$.
b	width in [mm]
μ	behaviour factor, see below
G	shear modulus [N/mm^2]
G_c	fracture energy [N/mm$^{1.5}$]
h	beam depth in [mm]

h_e effective depth, i.e. the distance from the loaded edge to the innermost fastener [mm].

η efficiency factor, see below.

- μ is a behaviour factor that depends on the ratio between the connection and splitting strength and also takes into account the failure mode of the connection in case the connection starts to yield and hardening follows that leads to splitting. It is envisaged in [1] that for the latter case a lower boundary would be found. For over-designed connections (strength ratio >> 1) an upper limit was argued. The limits of the behaviour factor would be are deduced from the available test data evaluated below.
- the variable η, the so-called efficiency factor is taken as a calibration factor in accordance to [2]. Typical values are $0 < \eta < 1.0$

Starting point in the evaluation was $\sqrt{GG_c} = 14$ N/mm$^{1.5}$ for both Model (1), (2)&(3)

For the calibration and evaluation of the models the following procedure was followed:

- Model (1)&(3): for each test series, sometimes consisting of one but usually of more than one test result, the behaviour factor μ value was determined based on the mean splitting strength. Only in cases were the embedment strength of other similar test Series did not signal a different failure mode at splitting, the average μ of all Series was determined and used in the evaluation of the model.
- Model (2): for every test series the efficiency factor η was determined based on the mean splitting strength. In the evaluation the overall mean was taken if more test series were available.

Model (4) is an empirical model used in Germany, which reads:

$$F_{90,k} = k_s k_r \left(6.5 + \frac{18a^2}{h^2}\right).(t_{ef}h)^{0.8}.f_{t,90,k} \qquad (4)$$

where:

$$k_s = \max\begin{cases} 1 \\ 0.7 + \dfrac{1.4\,a_r}{h} \end{cases} \quad and \quad k_r = \frac{n}{\sum_{i=1}^{n}\left(\dfrac{h_1}{h_i}\right)^2}$$

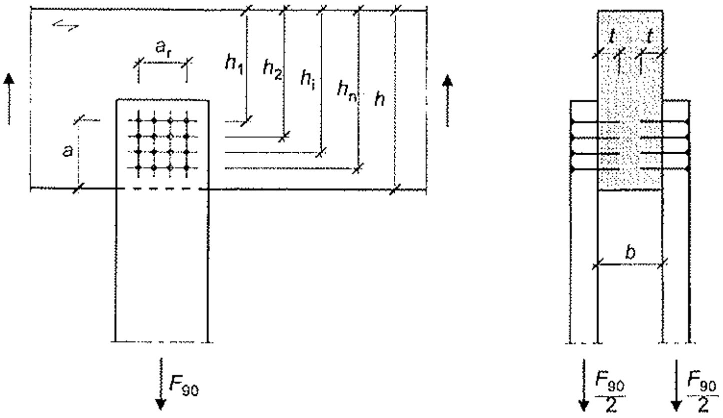

Figure 1: Example of connection with nails.

The parameters of this model are explained in Figure 1. The main field of application is dowel type connections and glued in rods. The model contains only one material parameter, which is the tensile strength perpendicular to grain strength. All other parameters relate to the arrangements of the fasteners and the penetration depth, t_{ef}. For the application of dowels or bolts the effective depth is given as:

$$t_{ef} = \min \begin{cases} \sum t \\ 12d \end{cases}$$

Although the material strength parameter has no physical meaning in the equation originally it had one. In simplifying the equation at later stages this meaning was lost. Now it therefore seems no more than a plug in value and implicitly assumes tension perpendicular to grain as the governing failure mode. Comparing the splitting capacities at the end of a cantilevered beam with one at mid span of a simply supported beam leads to the same result for Model (4) while Model (1) & (3) predict half the capacity. (Later versions of the German DIN1052 standard have corrected this in that half the splitting capacity is assumed as long as the connection is within the beam depth of the cantilever end. However, at the evaluation of the data this correction was unknown and therefore not taken into account. Even if taken into account it assumes tension perpendicular to grain as the governing failure mode while Model (1) to (3) assume shear.) Originally Model (4) was calibrated on the mean values of the available German data sets. The numbers of tests per arrangement of fasteners in the respective data sets was in most cases very limited; mostly 2 to 3.

Below a number of data sets are evaluated versus Models (1), (2) and (3). Linear regression curves that represent the model fit are added. A summary of the results is given at the end.

Evaluation

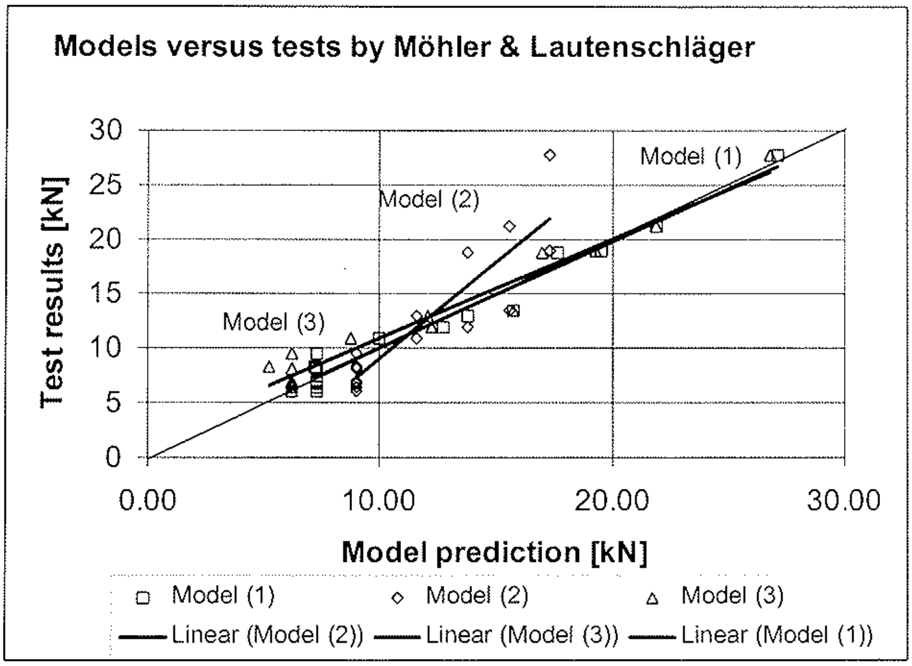

Fig.2: Results of the evaluation, tests reported in CIB-W18/22-7-2

Results of the evaluation of Model (1) & (3)

- series A mean $\mu = 0.86$

- series B mean μ = 1.20
- series C mean μ = 0.84

Justification of different behaviour factor values per Series is the fact that the embedment stresses at splitting failure of these test with nails show significant different values, which suggests nail shapes at time of splitting. Actually, for validation of this approach the load-slip curves are required. However, these curves were not reported.

Model (2)

- overall efficiency factor η = 1.08

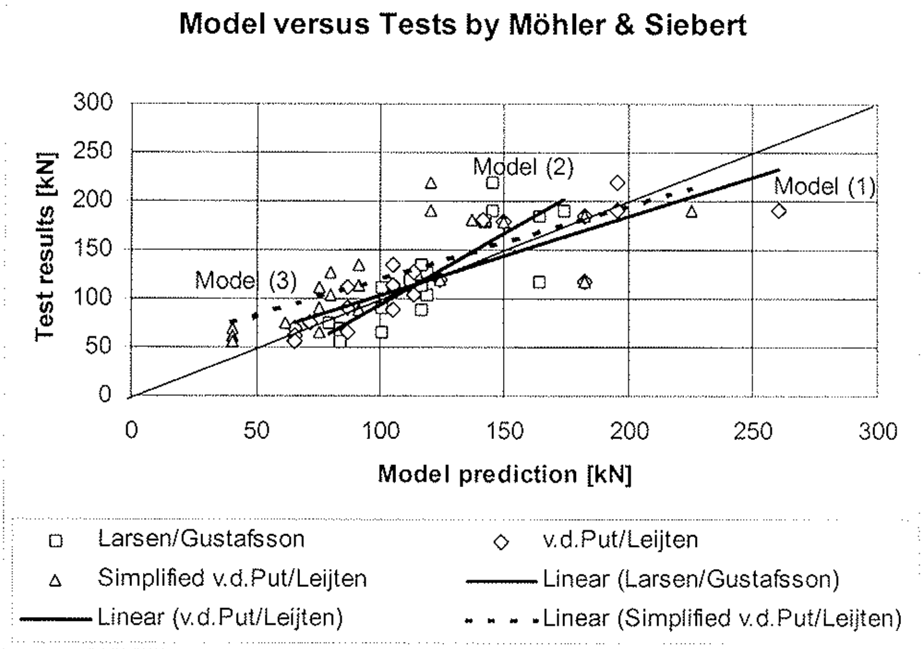

Figure 3: Results of the evaluation: tests reported in CIB-W18/22-7-2

Results of Models (1), (2) and Model (3) are based on the same assumption as in the previous evaluation.

- mean of μ and η are determined as given in the Table below.
- Combinations of test series (V) are arranged according to fastener type (nails and dowels) and timber dimensions

Series	μ	η
V5,V10	0.98	1.17
V2 to V4, V9, V23	1.2	1.48
V11 to 14, V25 to 28	1.27	1.75
V1,V6 to 8, V15 to 18	1.45	1.72

Table 1: Review of model factors for test data of Möhler & Siebert

Evaluation with Model (4) leads to the good fit.

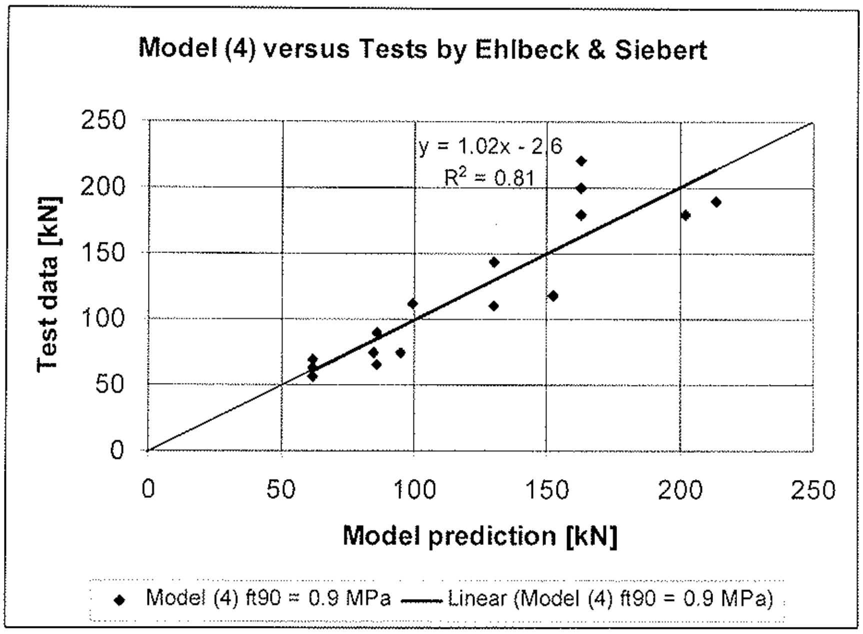

Figure 4: Results of the evaluation: tests reported in CIB-W18/22-7-2

Results of the evaluation of Models (1) & (2) and Model (3)

- mean of μ and η are determined taking all test series together.
  mean $\mu = 0.87$ and $\eta = 1.07$

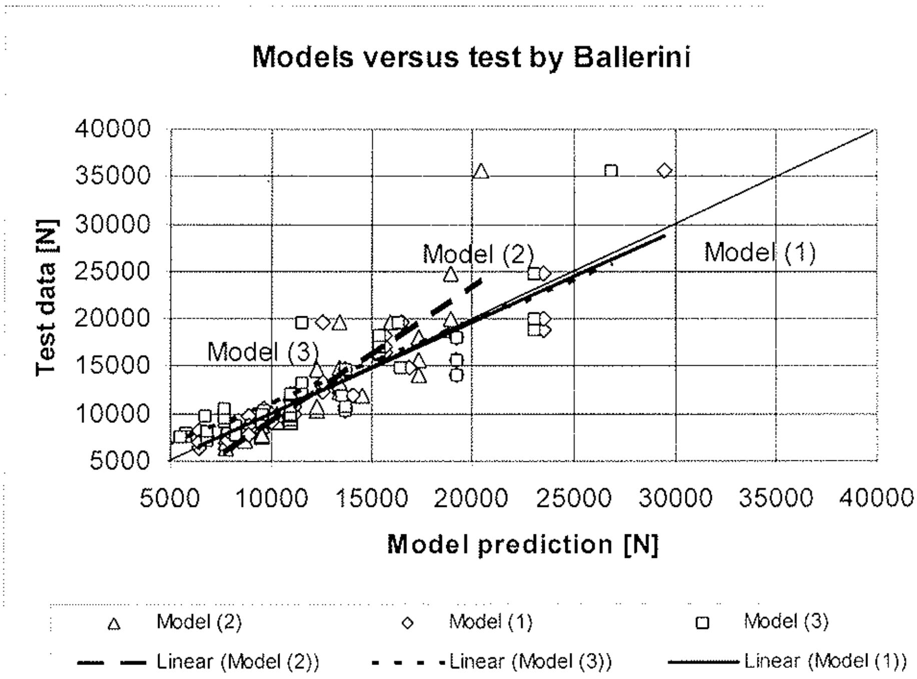

Figure.5: Results of the evaluation: tests reported in CIB-W18/32-7-2

Results of the evaluation of Models (1), (2) and Model (3)

- μ and η are determined for every single test and the overall mean of both parameters is taken in the evaluation.
  Overall mean $\mu = 0.66$ and mean $\eta = 0.78$

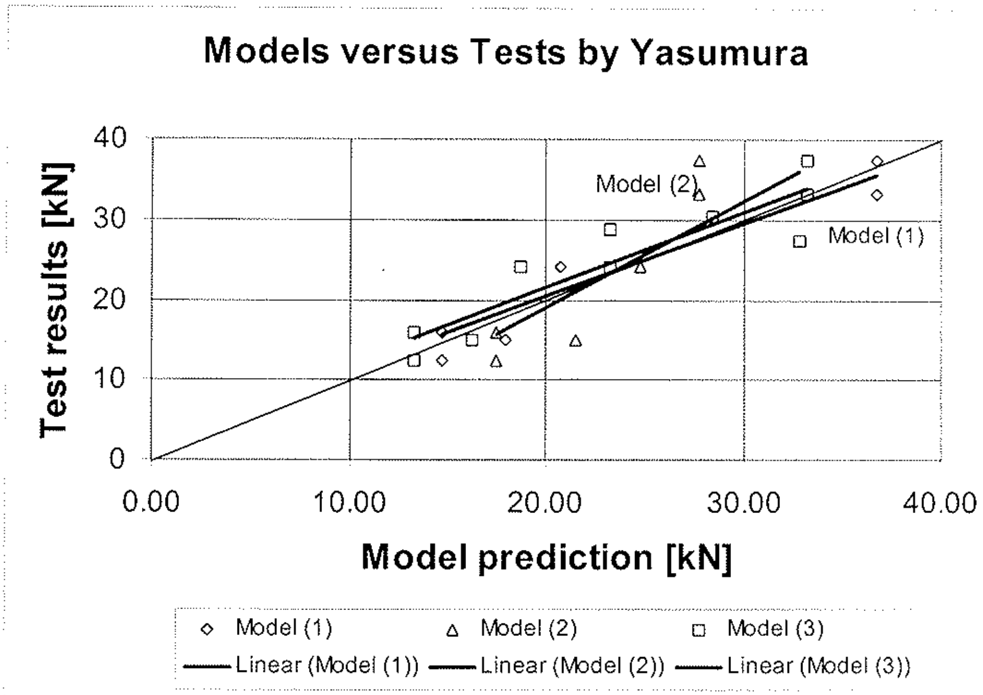

Figure 6: Results of the evaluation: tests rported in CIB-W18/34-7-9

Results of the evaluation of Models (1),(2) & Model (3)

- At first the mean μ and η were determined per test series. In the evaluation the overall mean μ and η of all test series was taken.
  Overall mean μ = 0.67 and η = 0.87

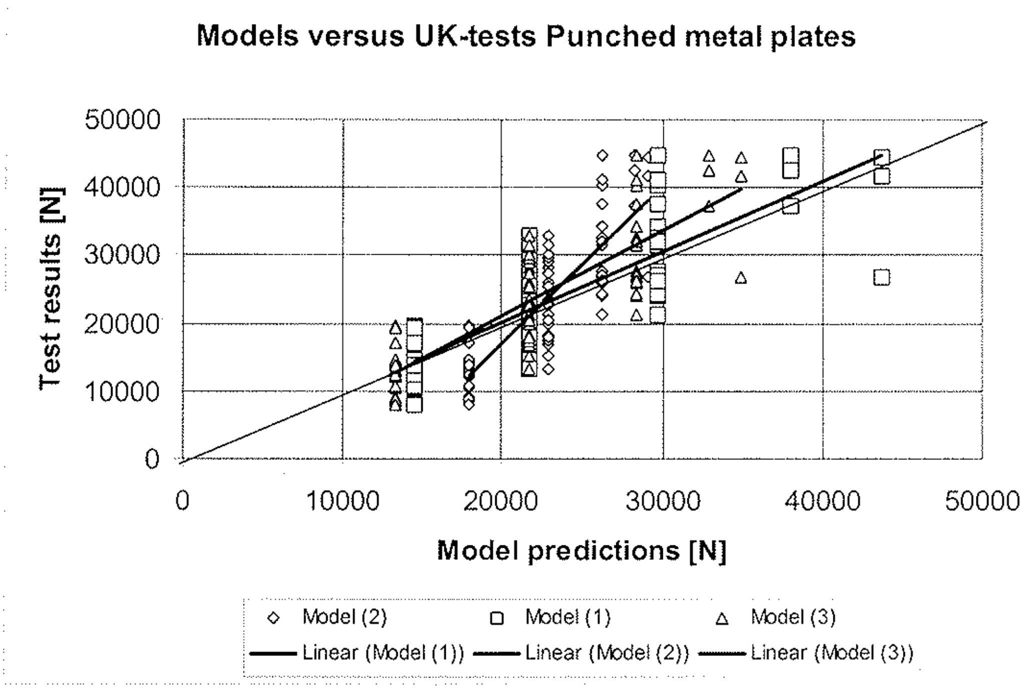

Figure 7: Results of the evaluation: tests reported by Reffolds et al [4]
For calibration purposes of Models (1),(2) & Model (3)

- The overall mean μ and η of all test series was taken.
  Mean μ = 1.44 and η = 1.97

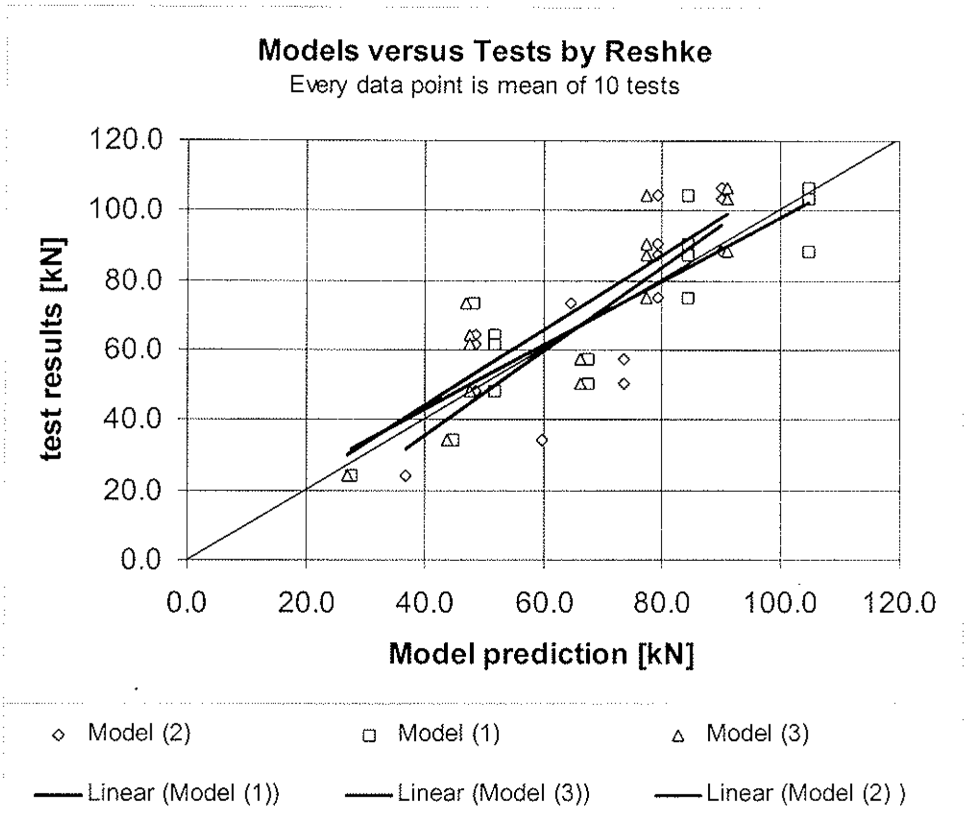

Figure 8: Results of the evaluation: tests reported by Reshke [4]

For calibration purposes of Model (1) to (3):
Tests by Reshke [4] were performed on 15 Series of 10 tests each. They comprise connections with 1, 2, 4, and 6 bolts in a number of arrangements, in total 148 tests.
The data could be divided into two groups; one with connections with 4 to 6 bolts and the other with 1 and 2 bolts because no significant difference was found between the mean behaviour factor of the Series within the two groups. The group means behaviour factors are $\mu = 0.72$ and 0.99, respectively, with an overall mean of 0.86.
In contrast the efficiency factor for the Series with 1, 2, 4 and 6 bolts all had significant different values, 0.86, 1.23, 1.57 and 1.68 respectively with a overall mean of $\eta = 1.34$

For calibration purposes of Model (4):
As this data set has ten tests for every tested arrangement of bolts it allows to make some lower 5% capacity estimate with some more reliability than the other data sets. Therefore, it was assumed that the 5% value = the mean – 2 times the cov (10 tests per Series. The only parameter in Model (4) able to vary and to fit the data is the tensile strength perpendicular to grain. In the graphs below Model (4) predictions of the lower 5% and the mean are presented. The graphs below are made taking 0.9 MPa for the mean tensile strength to fit the mean data and 0.4 MPa to check the fit for the lower 5% data. The latter strength value was taken from the European strength class table (EN308).

The ability of Model (1) to fit the lower 5% data is demonstrated together with Model (4). For this purpose, a behaviour factor of 0.39 is taken which transforms Model (1) into the Eurocde 5 design equation.

Two other Canadian data sets (RMC and NSERC) were evaluated in the same way as the one by Reshke [4], together they comprise a total of 186 tests in Series with ten replicates.

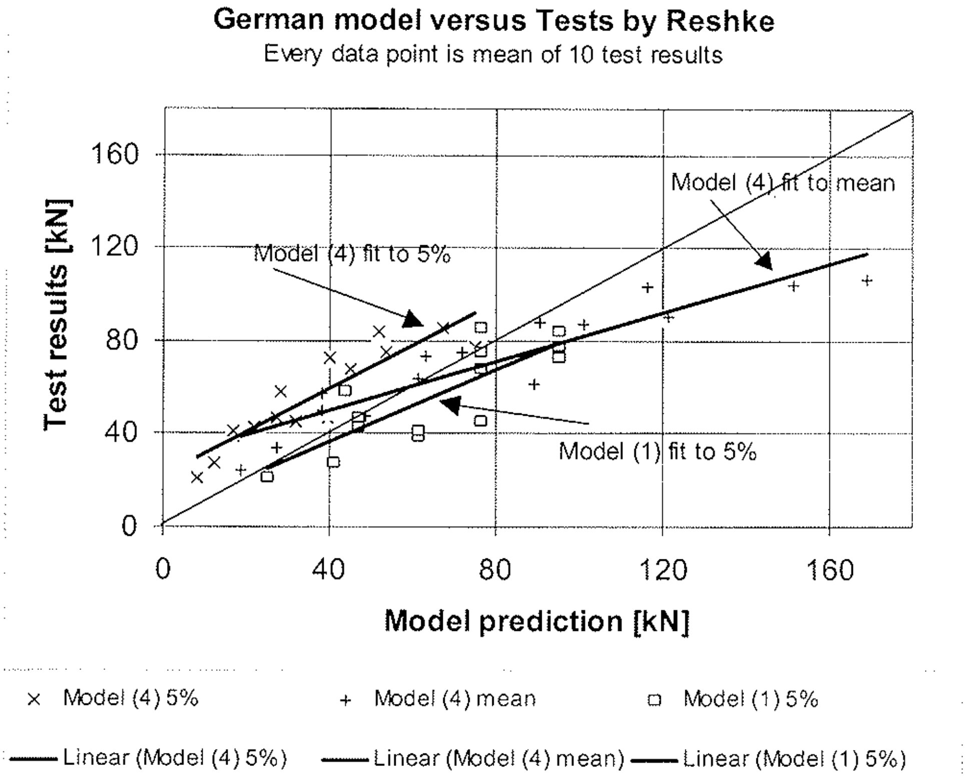

Figure 9: Results of the evaluation: tests reported by Queenville.

Below RMC tests and model prediction of Models (1) to (3) are given based on fit to the mean. (mainly cantilevered beam tests)

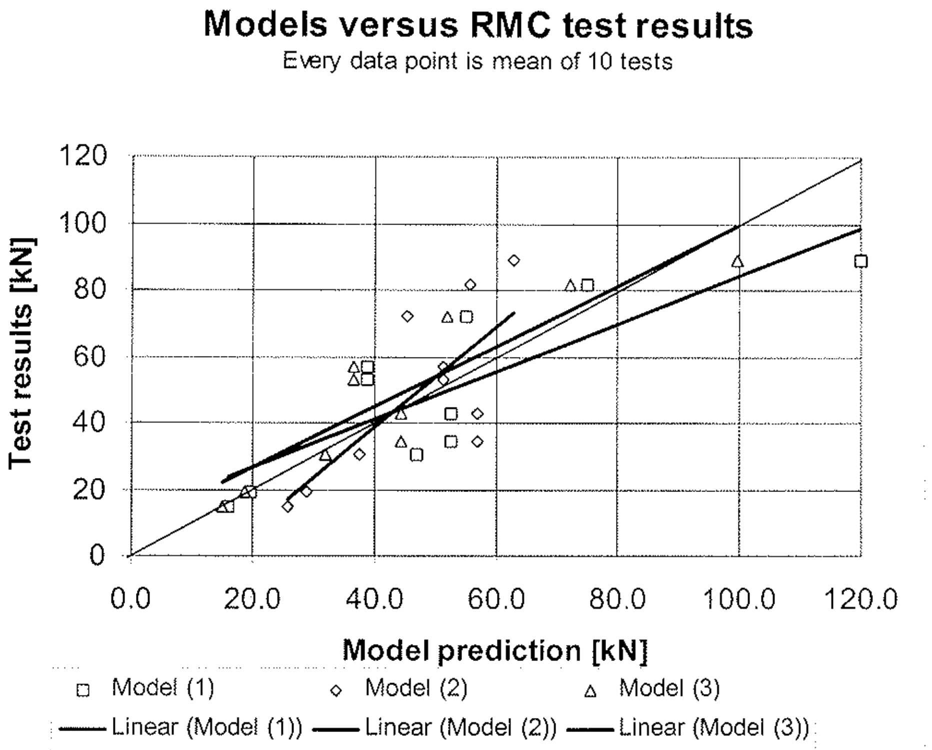

Figure 10: Results of the evaluation Model (1) tp (3): tests reported by Queenville.

As for the tests by Reshke the RMC tests comprise test Series with ten replicates, which enable to some degree a lower 5% estimation..
Models (1) & (4)are used to fit to lower 5% values and in addition Model (4) to fit the mean results This test data consist only of connections at the support.

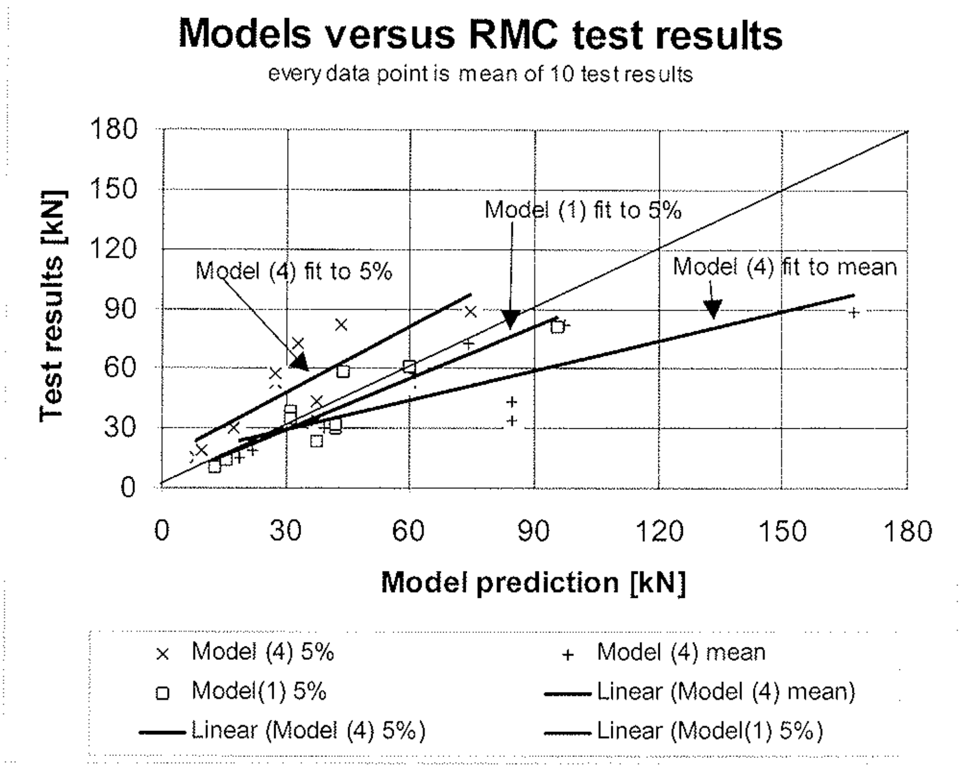

Figure 10: Results of the evaluation: Tests reported by Queenville.

NSERC test with Models (1) to (3)

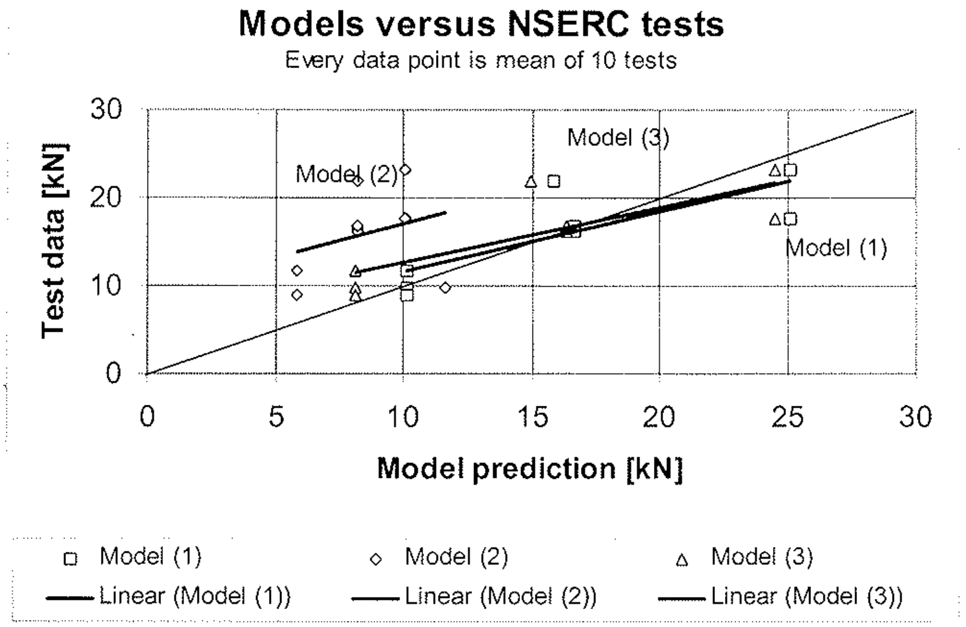

Figure 11: Results of the evaluation: Tests reported by Queenville

NSERC tests: Model (1)&(4) to fit 5% values and Model (4) also for the mean

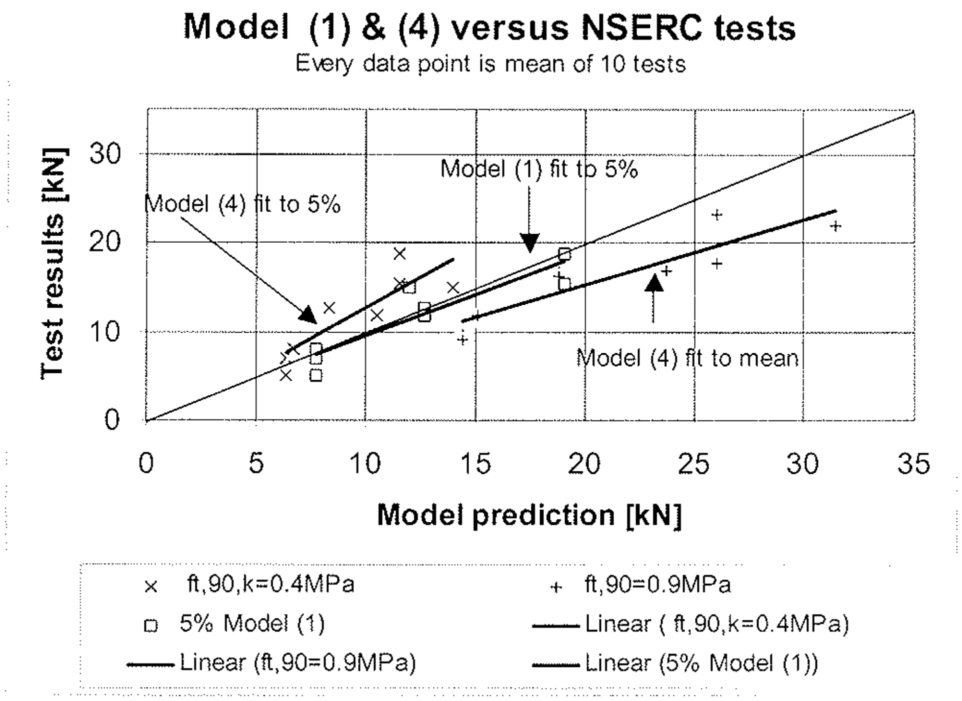

Figure 12: Results of the evaluation: Tests reported by Queenville

Summary of the test results

In Table 2 and 3 a summary is given of results of the evaluation. Table 2 contains the mean of the behaviour and efficiency parameters and Table 3 the goodness of fit parameters of the linear regression.

Table 2: Review of parameters

Tests by	Number of tests	Model (1)&(3) Mean μ	Model (2) Mean η
Validity range			$0 < \eta < 1.0$
Ehlbeck & Lautenschläger	18	0.86	1.08
	13	1.2	
	18	0.84	
Ehlbeck & Siebert	2	0.98	1.17
	5	1.20	1.48
	9	1.27	1.75
	8	1.45	1.72
Ehlbeck & Görlacher	57	0.87	1.07
Ballerini	44	0.66	0.78
Yasumura	30	0.67	0.87
Reffold et. al.	230	0.86	1.34
Reshke	148	0.86	1.34
RMC	96	0.97	0.94
NSERC	90	1.02	0.60

Table 3: Review of r^2-values and parameter A of linear regression fit.

Tests by	Tot. num. of tests	y=Ax+B A^*			(r^2)		
Model number		(1)	(2)	(3)	(1)	(2)	(3)
Ehlbeck & Lautenschläger	18	0.99	1.90	0.93	0.97	0.86	0.97
	13						
	18						
Ehlbeck & Siebert	2	0.78	1.46	0.75	0.72	0.71	0.57
	5						
	9						
	7						
Ehlbeck & Görlacher	57	0.93	1.09	0.92	0.81	0.71	0.79
Ballerini	44	0.96	1.43	0.86	0.83	0.78	0.78
Yasumura	30	0.90	1.33	0.94	0.84	0.62	0.84
Reffold et. al.	230	1.03	2.31	1.24	0.67	0.70	0.70
Reshke	148	0.92	1.21	1.09	0.77	0.66	0.74
RMC	96	0.72	1.52	0.91	0.69	0.55	0.80
NSERC	90	0.68	0.78	0.63	0.63	0.09	0.66
Total / weighted mean	**767**	**0.90**	**1.47**	**0.95**	**0.67**	**0.56**	**0.69**
Model number		(4)					
Tensile strength perp. to grain		$f_{t,90,m}$= 0.9 Mpa			$f_{t,90,k}$= 0.4 Mpa		
		A	B	(r^2)	A	B	(r^2)
Ehlbeck & Siebert	24	1.02	-2.6	0.81	-	-	-
Reshke	148	0.53	28.8	0.86	0.94	+21.9	0.83
RMC	96	0.50	14.2	0.69	1.05	+5.3	0.81
NSERC	90	0.73	0.52	0.82	1.38	-1.15	0.72
	mean	**0.70**	**10.2**	**0.80**	**1.12**	**8.7**	**0.79**

Test results versus model prediction: $A^{*)}$ best value = 1.0

Conclusions:

Based on the results given in Table 2 & 3 it can be concluded:

- The efficiency parameter η of Model (2) is in many cases outside it validity range ($0 < \eta < 1.0$)
- Model (2) is enable to cope with different type of connections and in many cases underestimates high strength results and overestimates low strength results (Table 3, A-values >1)
- Differences between Model (1) and (3) are always small

Based on Table 3 it can be concluded:

- The r^2 - values of Model (1), Model (2) and (3) are about the same.
- The regression parameter A of Model (1) &(3) are closest to 1.00 followed by Model (2).
- As Model (4) is apparently, is unable to cope with the Canadian data sets (Reshke, RMC & NSERC) regarding the mean of the test values and grossly overestimate the capacity. On the lower 5% Model (4) is conservative.
- Model (1) transformed to the Eurocode 5 design equation fits the lower 5% rather well.

Summarising

Evaluation of the models shows that Model (1) and (3) are well able to represent the mean and 5% test values of all data series. The empirical Model (4) fit to the lower 5% test data is conservative while for the mean it grossly overestimates the strength capacity in a number of data sets.

References

[1] Van der Put & Leijten, Proc. of CIB/W18, paper 33-7-7 & 34-7-1

[2] Larsen & Gustafsson, Proc. of CIB/W18, paper 34-7-3.

[3] Reffolds et al, Journal of the Institute of Wood Science, Vol.15. No.1, summer1999

[4]Reshke, R.G., Bolted Timber Connections Loaded Perpendicular-to-Grain, Influence of Joint Configuration Parameters on Strength, M.Eng Thesis, Royal Military College of Canada, Kingston, Ontario, 1999.

CIB-W18/35-7-8

INTERNATIONAL COUNCIL FOR RESEARCH AND INNOVATION
IN BUILDING AND CONSTRUCTION

WORKING COMMISSION W18 - TIMBER STRUCTURES

LOAD-CARRYING CAPACITY OF PERPENDICULAR TO THE GRAIN LOADED TIMBER JOINTS WITH MULTIPLE FASTENERS

O Borth
Fraunhofer-Institut für Werkstoffmechanik, Halle

K-U Schober
K Rautenstrauch

Bauhaus-University Weimar

GERMANY

Presented by: K U Schober

In reply to the question by H J Blaß on the practical relevance of the approach presented, K U Schober replied that the equations presented are not for design purposes. A Leijten then asked if failure of the fasteners was considered, K U Schober replied that fastener failure modes were not considered. S Aicher asked if the fictitious crack length of 6mm for 16mm dowel penalises dowels with smaller diameters. Schober agreed that the proposed approach does penalise small diameter dowels.

Load-carrying capacity of perpendicular to the grain loaded timber joints with multiple fasteners

Olaf Borth
Fraunhofer-Institut für Werkstoffmechanik, Halle, Germany

Kay-Uwe Schober, Karl Rautenstrauch
Bauhaus-University Weimar, Chair of Timber and Masonry Engineering, Germany

1 Abstract

Based on the simple numerical model described in [3] ultimate loads of practice-related joints with multiple fasteners can be estimated easily in the framework of the Linear-Elastic Fracture Mechanic (LEFM). As failure criteria exclusively those of the Linear-Elastic Fracture Mechanics are accepted.

First the numerical model will be checked for a sufficient consideration of properties and parameters of the physical model. For further calculations suitable assumptions and simplifications are made. The assumption of the critical crack length is the main focus of these investigations. They will be verified by acknowledged theoretical approaches and comparisons with experimental results from other scientists.

As a result, ultimate loads of practice-related joints with multiple fasteners can be specified. Using the numerical model described above, the ultimate load of these joints basically depended on the configuration of the fasteners. For beams with a smaller girder depth fracture mechanic concepts can possibly lead to an overestimation of ultimate loads.

2 Introduction

In timber engineering the load-carrying capacity of perpendicular to the grain loaded joints with mechanical fasteners is determined on the one hand by the load-carrying capacity of the fasteners itself and on the other hand by the static strains due to the local load transmission of the fasteners in the structure. The stress condition is stamped by multi-axle stresses and high gradients. Because of the load transmission stresses perpendicular to the grain appear in these areas. Depending on the chosen arrangement of the fasteners tensile stresses may occur. Because of the extremely low tensile strength perpendicular to the grain the load-carrying capacity of these joints is limited and lies below those of the fasteners.

Within the framework of the executed examinations the load-carrying capacity of the fasteners is assumed as sufficient, the failure of the joint shall be exclusively regarded in relation to the load transmission.

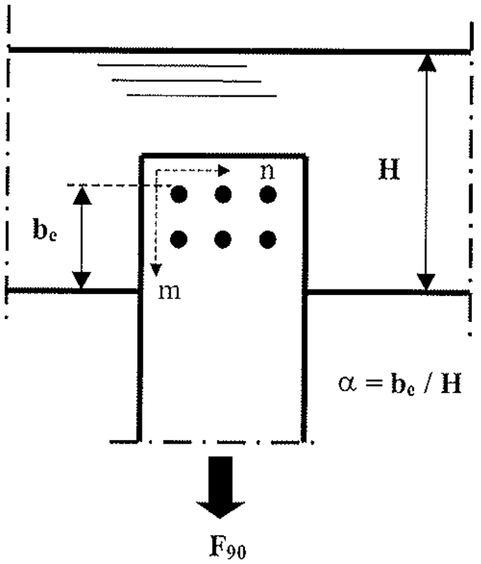

m – number of fasteners per row
n – number of fasteners per column

Fig. 1 Principle sketch of a perpendicular to the grain loaded connection

Existing approaches for the estimation of the load-carrying capacity of perpendicular to the grain loaded connections are based mainly on criteria comparing nominal sizes of tension with the corresponding strength. Within these examinations it is assumed that in the area of multiple fasteners cracks caused on fabrication and humidity change already exist. Possibilities for the assessment of structures with cracks are given by the methods of fracture mechanics.

3 Fundamentals

Nowadays within the framework of fracture mechanics multiple methods are available. Using brittle failure mechanisms the validity of concepts of the Linear-Elastic Fracture Mechanics (LEFM) can be subordinated. In the framework of the LEFM stress intensity factors (SIF K) replace the nominal stresses. The so-called fracture toughness substitutes the strength as the critical material characteristic. Therefore, the following failure criterion arises:

$$K \leq K_c \tag{1}$$

The methods to determine the stress intensity factors are various. Within this considerations the path independent J-integral by RICE is used. The physical parameters used for the calculation of these integrals are determined by the Finite-Element method in acceptance of the theory of elasticity in two-dimensional formulation and orthotropic materials law. The required elasticity constants are based on the experimental examinations of NEUHAUS [1]. Thus the two SIF, K_I (opening mode) and K_{II} (in-plane shear) can be calculated for a mixed failure criterion (mixed mode). The calculation of the J-Integrals was placed according to the following sketch.

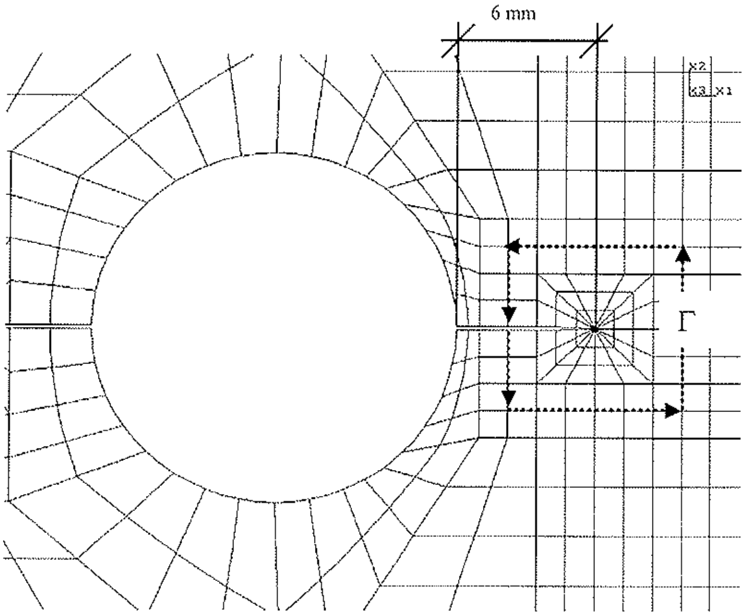

Fig. 2 Integration path around the crack tip on the bolthole

The fracture toughness adopted according to the crack system is

for resistance to tensile stress perpendicular to the grain in the radial-longitudinal-section:	$K_{Ic}^{RL} = 11{,}5\ \mathrm{Nmm}^{-1{,}5}$
in the tangential-longitudinal-section:	$K_{Ic}^{TL} = 9{,}5\ \mathrm{Nmm}^{-1{,}5}$
for shear generally:	$K_{IIc} = 55\ \mathrm{Nmm}^{-1{,}5}$

using the failure criterion formulated by WU [2]:

$$\frac{K_I}{K_{Ic}} + \left(\frac{K_{II}}{K_{IIc}}\right)^2 = 1 \tag{2}$$

Compared to the examinations on single fasteners [3] for practice-related joints the negligibility of the influence of in-plane shear mode was found. The simplification of the fracture criterion by WILLIAMS [4] gives sufficiently exact results:

$$\frac{K_I}{K_{Ic}} = 1 \tag{3}$$

4 Structural model

The analyzed joint is a structure with circular holes and cracks on the loaded edge. The applied structural model also allows the consideration of wood moisture and relevant crack systems (RL, TL). The modeling of the fasteners itself was waived. They were arranged as exterior loads in the numerical model. A cosine-distributed load with regard to the base of the bolthole was a suitable assumption for this problem [3], [5]. The mechanical behavior of cracks in practice-related joints is investigated insufficiently by now. The same assumptions as in the analysis of single fasteners were made, i.e.:

- The crack propagation corresponds with the grain direction.
- The crack tip line starts either in the 90°- or 270°-position of a full circle.
- Crack birth and the crack propagation happen in pairs evenly.
- The SIFs are calculated as functions of the fictitious crack length, because the real crack length is unknown. The authoritative stresses are on cracks, which have the largest distance from the loaded edge of the boltholes.

The examination of possible effects of the crack interaction is described in detail in [3], [5]. All agreements made there are valid.

5 Comparisons with experimental results

In contrast to the consideration of single fasteners a formulation of the ultimate load on basis of stability examinations of the crack growth is not possible for practice-related joints, particularly for joints with multiple fasteners. By the increasingly growing vertical distance between the point of load application and the critical crack on the upper fastener, functions of stress intensity factors without stable crack growth for all fictive crack tip length results. The calculation of the load-carrying capacity, according to the LEFM is only possible if the crack length is known.

For validation, the numerical investigations have to be compared with test results of other research groups. Tests with practice-related joints were made in Karlsruhe in the 70s and 80s of the last century. For the comparison with the numerical results test series with mechanical fasteners [6], [7], [8] were considered. All experiments shown in these test series were modeled numerically and examined to detect the critical crack length. These examinations on multiple fasteners arranged in row pointed out that the relevant stresses can be found in the crack tip turned away of the exterior fasteners ([3]). In the following figure this is crack tip five.

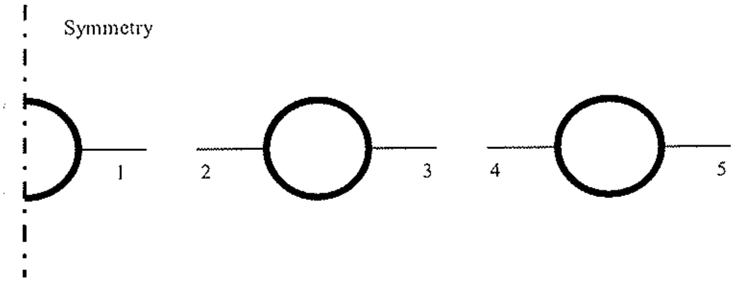

Fig. 3 Crack tips on multicolumn arrangement of fasteners

6 Load application

For joints with multiple mechanical fasteners in load direction the distribution of the total load on the single fasteners is important. Approximately a uniform load distribution was assumed.

$$F_i = \frac{F_{ges}}{n} \tag{4}$$

Normally the load distribution of the single fasteners is not uniform and the quantitative distribution on the fasteners is unknown. This was examined more closely because only few examinations exist [9]. To determine the effects of divergent load directions of (4) on the calculation of the stress intensity factors, the following load application was examined:

$$F_{ges} = \frac{1}{k} \sum_{i=1}^{n} \eta_i \; F_i \tag{5}$$

The investigations done [5] have the following results:

- The assumption of the load distribution has an essentially lower influence on SIF K_I than SIF K_{II}
- The quality of this influence depend on the relative connection depth α, the distance from fastener to fastener, as well as from the crack tip length a and the girder depth H.

As expected the load distribution for the upper fasteners (5) leads to the arise of stresses, because the center of the loads lie nearer to the crack tip. However, the quantity of this effect depends on further conditions. An important parameter is the girder depth H. With an increasing depth the difference in the stresses at the crack tip becomes much lower, e.g., on timber beams with a girder depth of 40 cm and standard fasteners distance a differences of approx. 6% in the SIF K_I appears. Particularly on much higher gluelam beams with joints with more than two rows of fasteners the assumption of a non-uniform load application is redundant. Therefore, a uniform load application in load direction can be a sufficient assumption.

7 Critical crack lengths

The crack tip length is mostly unknown. The critical crack length can be estimated [10] to:

$$a_{crit} = \frac{E_{\perp} G_{Ic}}{4 f_{t,90}^2} \tag{6}$$

This approach uses the characteristic values of timber perpendicular to the grain. The broad variability of the values and the position of the crack area regarding to the natural axes of wood is unknown. Therefore they can range between 2 and 22 mm.

However, such an estimation of the critical crack length is too indifferent for the numerical model. So the crack length was verified on the base of test series examined for practice-related joints [6], [7], [8]. This can be realized with the calculation of the stress intensity factors as a function of the crack length with a certain failure criterion (e.g., [2]).

An associated crack length can be calculated by comparison with the experimentally determined fracture load. The critical crack tip length a_{crit} was determined to approx. 6 mm for the tests made in Karlsruhe [6], [7], [8]. For example, the general procedure is shown in the following figure for the test 2.1 of the series discussed in [8]. Here the critical length was determined to 2 mm.

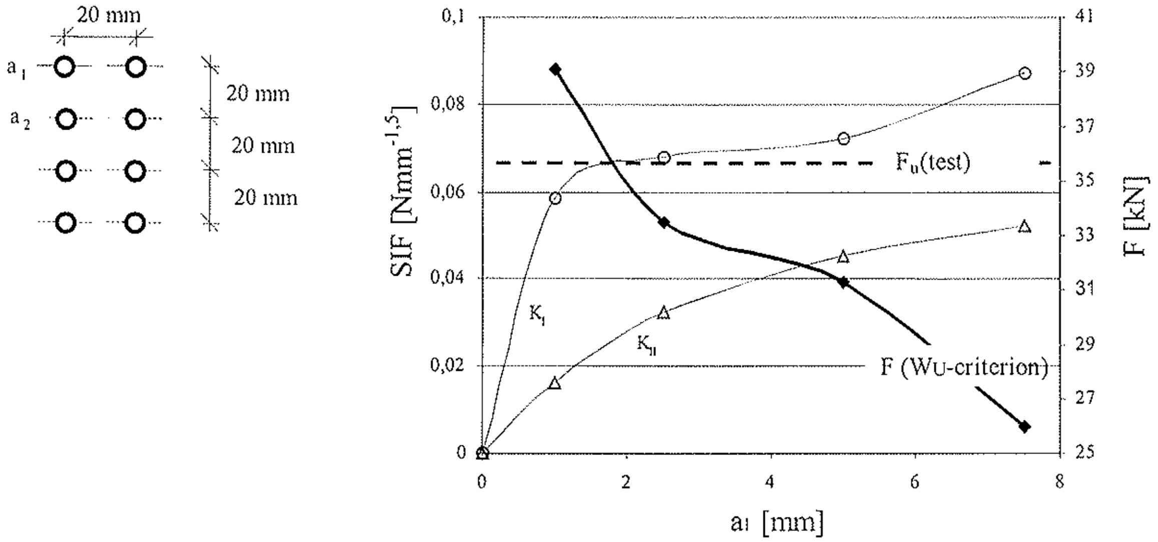

Fig. 4 Stress with corresponding loads of the WU-criterion on the critical crack tip

For the estimation of the ultimate fracture loads of practice-related joints a critical crack tip length of 6 mm is assumed. This is the average value of the critical crack tip length of all test series made in Karlsruhe.

8 Numerical estimation of fracture loads

The following parameters have been used in the numerical model applied here:

- Girder depth $H = 30 \dots 180\ cm$
- Connection depth $\alpha = 0{,}2 \dots 0{,}5$
- Number of rows $m = 1 \dots 4$ (= *number of fasteners per column)*
- Number of columns $n = 1 \dots 5$ (= *number of fasteners per row*

As diameter 16 mm was accepted uniformly. The variation of this parameter has no effects on the estimation of the fracture load. As distances, the recommendations of EC 5 were used. Furthermore the influence of the following boundary conditions was examined:

- Length of the beam (for L >> H)
- Location of the joint regarding to the longitudinal axis
- Additional loads (uniform loads, point loads)

These parameters had only low effects on the calculation of the fracture loads. The influence of the girder depth is also very low by use of the applied numerical model. The number and arrangement of the fasteners itself is very important. In the following figure the fracture loads for different joint configurations are presented.

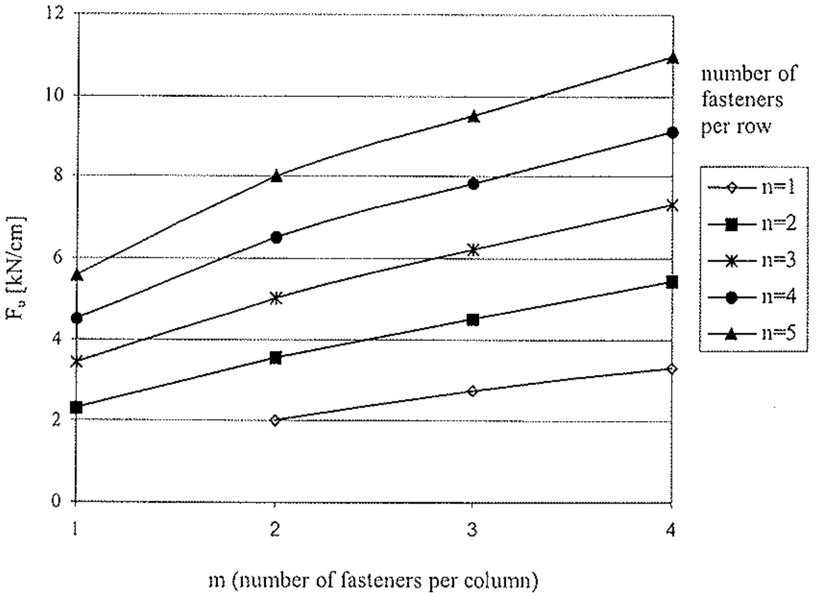

Fig. 5 *Fracture loads as a function of the number of fasteners per row and column for a girder depth of H = 130 cm and a = 0,35 (based on 1 cm of girder thickness)*

F_u [kN/cm]									
	n = 1			**n = 2**			**n = 3**		
m	*α = 0,2*	*α = 0,35*	*α = 0,5*	*α = 0,2*	*α = 0,35*	*α = 0,5*	*α = 0,2*	*α = 0,35*	*α = 0,5*
1				2,24	2,32	2,33	3,28	3,41	3,50
2	1,96	2,03	2,05	3,36	3,54	3,67	4,72	5,03	5,33
3	2,61	2,74	2,79	4,20	4,50	4,75	5,73	6,21	6,74
4	3,16	3,30	3,48	4,87	5,43	5,64	6,35	7,33	7,77
	n = 4			**n = 5**					
	α = 0,2	*α = 0,35*	*α = 0,5*	*α = 0,2*	*α = 0,35*	*α = 0,5*			
1	4,28	4,51	4,66	5,27	5,59	5,81			
2	6,04	6,50	7,00	7,38	8,02	8,73			
3	7,17	7,86	8,68	8,72	9,52	10,71			
4	7,78	9,14	9,85	9,16	10,99	11,94			

m = number of rows (= number of fasteners per column)

n = number of columns (= number of fasteners per row)

Tab. 1 *Fracture loads for practice-related joints (H = 130 cm, based on 1 cm of girder thickness)*

9 Summary

The examinations have shown the possibility to determine the ultimate fracture loads for practice-related joints with mechanical fasteners within the framework of the Linear-Elastic Fracture Mechanics.

An increasing distance between fasteners and loaded edge was represented in the structural model as an increase of the load-carrying capacity. As the most important parameter the arrangement and number of the fasteners itself were determined. Other parameters are circumstantial. By use of fracture-mechanical failure criteria the distribution of the load application has more positive effects on the load-carrying capacity in grain direction than in force direction perpendicular to the grain. Therefore the presented structural model corresponds with experimental results.

Exceptions are perpendicular to the grain loaded joints on structural members with low girder depth (approx. H < 30 cm). Here the low stiffness results in compressing cracks with a lower distance from the loaded edge. The consequence is an overestimation of the load-carrying capacity. The numerical model also supplies an overestimation of the fracture loads of perpendicular to the grain loaded joints arranged above the axis of gravity. For such joint configurations other failure criteria become authoritative.

10 References

[1] Neuhaus: Elastizitätszahlen von Fichtenholz in Abhängigkeit von der Holzfeuchtigkeit. Dissertation, Ruhr-Universität, Bochum, 1981.

[2] Wu: Application of Fracture Mechanics to Anisotropic Plates. In: Journal of Applied Mechanics, 34. Jg. (1967), H. 4, S. 967-974.

[3] Borth, Rautenstrauch: Estimation Of The Load-Carrying Capacity Of Perpendicular-To-Grain Bolted Timber Connections By Fracture Criterion In The Framework Of LEFM. In: Proceedings of the International RILEM Symposium „Joints in Timber Structures“, RILEM Publications S.A.R.L., Stuttgart, 2001, S. 33 - 42.

[4] Williams, Birch: Mixed Mode Fracture in Anisotropic Media. From: ASTM STP 601 Cracks and Fracture, Philadelphia, 1976. S. 125-137.

[5] Borth: Abschätzung der Tragfähigkeit von Queranschlüssen an Trägern aus Voll- und Brettschichtholz im Rahmen der Linear-Elastischen Bruchmechanik. Dissertation, Bauhaus-Universität Weimar, 2002.

[6] Möhler, Lautenschläger: Großflächige Queranschlüsse bei Brettschichtholz. Untersuchungen im Auftrag der EGH in der DGfH, Karlsruhe, 1978.

[7] Möhler, Siebert: Ausbildung von Queranschlüssen bei angehängten Lasten an Brettschichtträger und Vollholzbalken. Untersuchungen im Auftrag der EgH in der DGfH und des Inst. für Bautechnik Berlin, Karlsruhe, 1980.

[8] Ehlbeck, Görlacher: Tragverhalten von Queranschlüssen mittels Stahlblechformteilen, insbesondere Balkenschuhen, im Holzbau. Karlsruhe, 1983. (Forschungsbericht der Versuchsanstalt für Stahl, Holz und Steine).

[9] Mettem, Page: Load Distributions In Multiple-Fastener Bolted Joints In European Whitewood Glulam, With Steel Plates. Aus: Working Commission W 18 - Timber Structures (Ed.): List of CIB-W18 Papers Ahus 1992. Paper 25-7-12.

[10] Gustafsson: Application Of Fracture Mechanics To Timber Structures. Part III Aus: IUFRO S5.02 (Ed.): "Proceedings for the 1990 Conference" Volume I, St. John + Montreal, 1990. S. 210-233.

CIB-W18/35-7-9

**INTERNATIONAL COUNCIL FOR RESEARCH AND INNOVATION
IN BUILDING AND CONSTRUCTION**

WORKING COMMISSION W18 - TIMBER STRUCTURES

DETERMINATION OF FRACTURE PARAMETER FOR DOWEL-TYPE JOINTS LOADED PERPENDICULAR TO WOODEN GRAIN AND ITS APPLICATION

M Yasumura

Department of Forest Resources Science
Shizuoka University

JAPAN

Presented by: M Yasumura

H J Larsen commented that the test method used is too close to structural application and that it would be better to use independent structural parameters for G and Gc. P Quenneville and S Svensson asked if the rate of loading influenced the test results. M Yasumara replied that he did not think so. K Komatsu and J Ehlbeck respectively asked if the study considered the influences of dowel diameter and moisture content. M Yasumara confirmed that they were not.

Determination of fracture parameter for dowel-type joints loaded perpendicular to wooden grain and its application

Motoi YASUMURA
Department of Forest Resources Science, Shizuoka University, Japan

1 Introduction

During the CIB-W18 Meeting in Delft, 2000, a formula to predict the lateral capacity of dowel-type joints loaded perpendicular to the wooden grain was proposed[1]. This formula includes what we call the "fracture parameter" consisting of G and Gc. Instead of applying individual material properties of ***G*** and ***Gc*** which are difficult to determine from the material tests, fracture parameters will be obtained by conducting simple tension test of dowel-type joints consisting of a single or multiple dowel fasteners. This study proposes the test method to determine the fracture parameter for dowel-type joints loaded perpendicular to the wooden grain. Tension tests of dowel-type joints were conducted with different edge and end distances, and the suitable configuration of specimen and dowel disposition are proposed with the aid of FE analysis. The obtained fracture parameters were applied to validate the formula for predicting the failure load of dowel-type joints.

2 Background

A design formula for predicting the lateral capacity of dowel-type joints loaded on the center of beam is expressed as follows[1][2];

$$\frac{F_u}{2b\sqrt{h}} = C_1\sqrt{\frac{\alpha}{1-\alpha}} \quad ; \quad C_1 = \sqrt{\frac{GG_C}{0.6}} \tag{1}$$

where, ***Fu*** is the ultimate load, ***b*** is the thickness of beam, ***h*** is the height of beam, ***he*** is the edge distance and α is the ratio of the edge distance to beam height (***he/h***).
Equation (1) is expressed as (2) by dividing each side of the equation by $\sqrt{\alpha}$.

$$\frac{F_u}{2b\sqrt{h_e}} = C_1\sqrt{\frac{1}{1-\alpha}} \tag{2}$$

Assuming ***h*** is close to infinitive; that is α is close to null in equation (2), the fracture parameter C_I is expressed by the following equation;

$$C_1 = \frac{F_u}{2b\sqrt{h_e}} \tag{3}$$

Thus the fracture parameter C_I may be obtained by conducting a simple tension test of the joints subjected to a force perpendicular to the grain as shown in Fig. 1. For this purpose, appropriate configuration of specimen and bolt geometry such as the width, height, thickness and edge distance should be studied. In this study the joints with different configuration were subjected to forces perpendicular to the grain and an appropriate test method to determine the fracture parameter C_I is proposed.

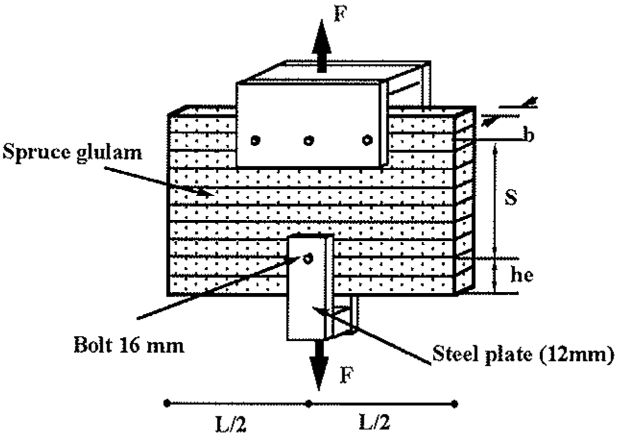

Fig.1 Lateral loading test of dowel-type joints for determining the fracture parameter.

3 Specimen and test method

Specimens consisted of spruce glued laminated wood and 12mm thick steel side plates on both sides of the wooden member, connected with bolts 16mm in diameter (*d*) except for T30-7-2L. The glued laminated wood was made of laminae 30mm thick with an average density 440kg/m^3. For T30-7-2L spruce sawn lumber was applied. The quality of steel used for the side plates and bolts was JIS (Japanese Industrial Standard) SS 400. The pre-drilled holes of wooden members were equal to or slightly larger than the bolt diameters, and the diameters of the bolt holes of steel plates were 1mm larger than the bolt diameter. The thickness of the wooden member was of 32mm(2*d*) and 64mm (4*d*) and the schematic diagrams and outline of specimens are shown in Fig.2 and Table 1. Six specimens of each type were subjected to lateral loads as shown in Fig.1. The quasi-static tension loads were applied to the steel side plates by a hydraulic jack. The nuts were attached to the joints with little tightening.

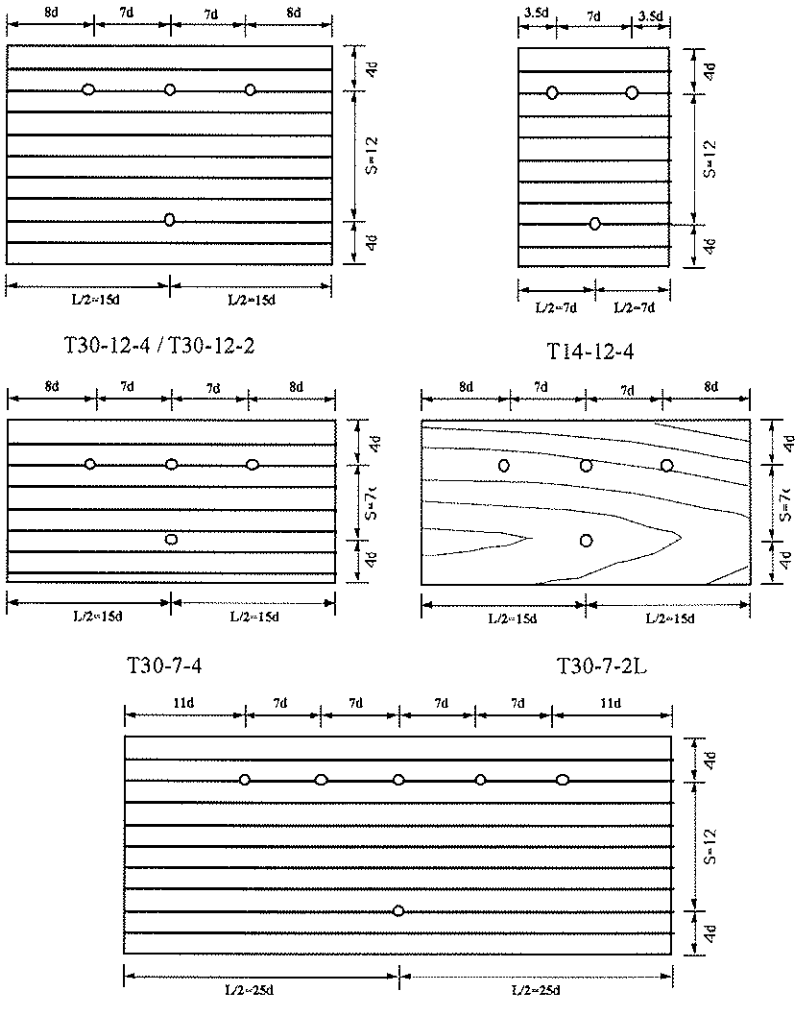
8d
7d
7d
8d
4d
S=12
4d
L/2=15d
L/2=15d
3.5d
7d
3.5d
L/2=7d
L/2=7d
S=7d
11d
L/2=25d
L/2=25d

T30-12-4 / T30-12-2

T14-12-4

T30-7-4

T30-7-2L

T50-12-4

Fig.2 Schematic diagram of specimens

4 Modeling and analysis

The crack propagation under Mode I fracture can be calculated by using the energy release rate (G_I). The energy release rate in Mode I (G_I) can be calculated by the following formula[3];

$$\frac{G_I}{F^2} = \frac{1}{2b}\frac{\partial C}{\partial A} = \frac{1}{2b}\frac{1}{\Delta A}\left(\frac{1}{k_{i+1}} - \frac{1}{k_i}\right) \quad ; \quad \Delta A = A_{i+1} - A_i \qquad (4)$$

where, k_i = Stiffness of structure in state (i) and A=crack length.

Tested joints were modeled with the finite elements. A half of the specimen was modeled considering the symmetry. Young's modulus of spruce was assumed to be 12,000 MPa in the longitudinal direction and 600 MPa in the transverse direction and the shear modulus and Poisson's ratio of 300 MPa and 0.5 were assumed, respectively. The bolt hole boundary was fixed in the radial direction but only in the positive direction and free in the tangential direction[4]. The forced displacements were applied downwards at the supports. The FEM code CASTEM 2000 developed by the French Atomic Energy Commissariat (*CEA*) was used for the analysis.

5 Results and discussion

5.1 Comparison of experimental results with simulation

Table 1 shows the comparison of the ultimate lateral loads between experimental results and simulation by LEFM. For the simulation, Gc of 240N/m was assumed from the following equation with ***Fu/b*** = 176N/mm and ***G*** = 300MPa;

$$G_C = \frac{0.15}{h_e \cdot G}\left(\frac{Fu}{b}\right)^2 \qquad (5)$$

It shows that the simulated ultimate load agreed quite well with the experimental results in the specimens having the thickness of 64mm(4*d*). Experimental results were 12 to 16% smaller than the simulation in the specimens having the thickness of 32mm (2*d*).

Table 1 Comparison of test results with the LEFM simulation.

Specimen	**Width (L)**	**Loading distance (S)**	**Thickness (mm)**	**Ultimate load (Fu/b) (N/mm)**			
				Experim-ent	**C.O.V. (%)**	**LEFM**	**ratio**
T14-12-4	**14d**	**12d**	**4d**	**157**	**20.3**	**158**	**0.99**
T30-12-4	**30d**	**12d**	**4d**	**176**	**6.77**	**171**	**1.03**
T50-12-4	**50d**	**12d**	**4d**	**180**	**0.97**	**177**	**1.02**
T30-7-4	**30d**	**7d**	**4d**	**176**	**7.86**	**172**	**1.02**
T30-12-2	**30d**	**12d**	**2d**	**143**	**16.8**	**171**	**0.84**
T30-7-2L	**30d**	**7d**	**2d**	**152**	**15.3**	**172**	**0.88**

These results indicate that the specimens with small thickness tend to provide smaller strength than the thicker specimen, and appropriate thickness should be chosen for testing this type of specimen.

5.2 Specimen width

Figure 3 shows the relation between the specimen width and the ultimate load in experiments and simulations. Both experimental and simulated ultimate load increased as the specimen width was lager, and approached to the theoretical value when the half width of specimen was 15***d***. This indicates that the width of specimen (***L***) should be at least 30 times as large as the dowel diameter (30***d***).

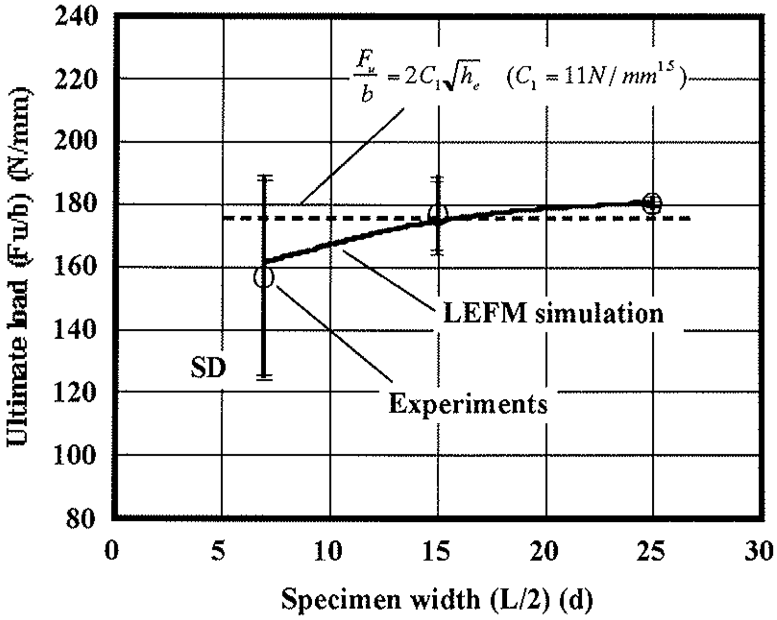

Fig.3 Relation between the specimen width and the ultimate load.

5.3 Specimen height

Figure 4 shows the relation between the distance between the loading point and supports (***S***) and the ultimate load in experiments and simulation. It shows that the ultimate load increased slightly as the distance (***S***) was lager, and showed constant values when the distance (***S***) was equal to or larger than seven times of dowel diameter (7***d***). This indicates that the space between the loading point and the supports (***S***) should be equal to or larger than 7 times as large as the dowel diameter.

5.4 Validation of formula

Figure 5 shows the comparison between the calculated values of $Fu/2b\sqrt{h}$ with C_1

value of 11N/mm$^{1.5}$ obtained from the test results of the specimen T30-12-4 and the experimental and simulated results of bolted joints loaded at the center of beam[5].

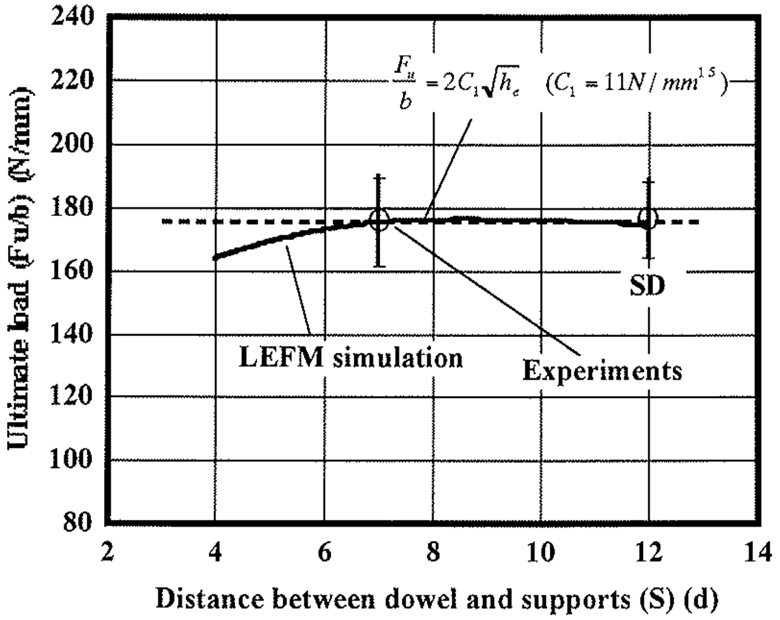

Fig.4 Relation between the distance (*S*) and the ultimate load.

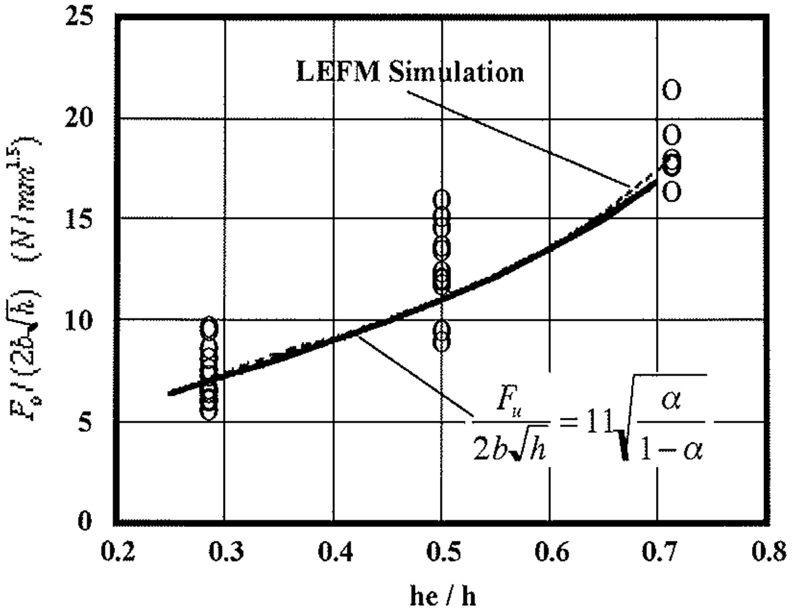

Fig.5 Comparison between the calculated values of $Fu/2b\sqrt{h}$ with C_1 value of 11N/mm$^{1.5}$ obtained from the test results of the specimen T30-12-4 and the experimental and simulated results of bolted joints loaded at the center of beam[5]

The calculated values by the equation (1) with the C_I value obtained from the test proposed in this paper agreed quite well with both experimental results and LEFM simulation. This means the test method proposed in this paper is appropriate to obtain the fracture parameter (C_I).

6 Conclusions

From this study it was shown that the fracture parameter C_I can be obtained by conducting simple tension test of dowel-type joints consisting of a single dowel fastener. Typical specimen configuration is proposed in Fig.6. The failure load predicted by the equation (1) with the C_I value obtained from the test proposed in this paper agreed quite well with both experimental results and LEFM simulation.

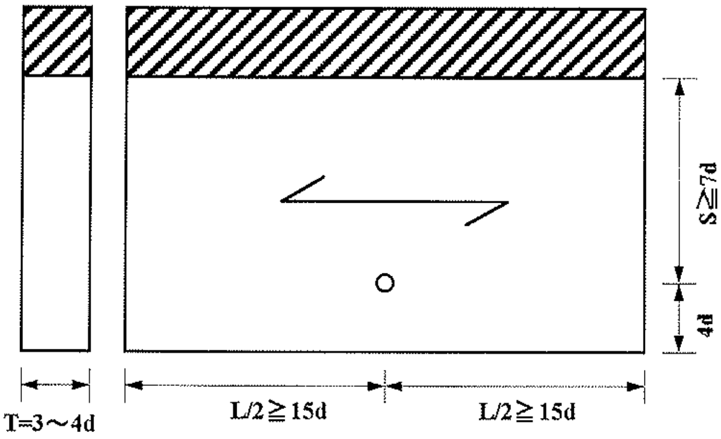

Fig.6 Configuration of proposed specimen

7 Acknowledgments

The author thanks Yuki TATEYAMA, undergraduate student of Shizuoka University, for his assistance in experiments.

8 References

1. Van der Put, T.A.C.M. and Leijten, A.J.M.:2000:"Evaluation of Perpendicular to Grain Failure of Beams caused by Concentrated Loads of Joints", Proceeding of CIB-W18, paper 33-7-7
2. Leijten, A.J.M., Jorissen, A.J.M.:2001:"Splitting Strength of Beam Loaded by Connections perpendicular to grain, Model Validation", Proceeding of CIB-W18, paper 34-7-1

3. Yasumura,M. and Daudeville,L.: 1996: "Fracture Analysis of Bolted Timber Joints under Lateral Force Perpendicular to the Grain", Mokuzai Gakkaishi 42(3), pp225-233
4. Yasumura, M. and Daudeville,L.: 2000: "Fracture of multiply-bolted joints under lateral force perpendicular to wooden grain", J. Wood Sci 46, pp187-192
5. Yasumura, M.:2001:"Criteria for Damage and Failure of Dowel-type Joints subjected to Force perpendicular to the Grain", Proceeding of CIB-W18, paper 34-7-9

CIB-W18/35-7-10

**INTERNATIONAL COUNCIL FOR RESEARCH AND INNOVATION
IN BUILDING AND CONSTRUCTION**

WORKING COMMISSION W18 - TIMBER STRUCTURES

ANALYSIS AND DESIGN OF MODIFIED ATTIC TRUSSES WITH PUNCHED METAL PLATE FASTENERS

P Ellegaard

Department of Building Technology and Structural Engineering
Aalborg University

DENMARK

Presented by: P Ellegaard

H J Blaß asked about the relevance of the study to EC5 design approaches and about the load testing arrangement. E Fournely also asked how the loading was applied. After expressing his view on the relevance of his research to EC5, P Ellegaard explained that equal loads at 4 points were applied via a hinged mechanism to the whole frame. G Gonzalez then asked if the suction load on the other side of the frame was considered. P Ellegaard replied that it was not.

Analysis and Design of Modified Attic Trusses with Punched Metal Plate Fasteners

Peter Ellegaard, Assistant Professor

Department of Building Technology and Structural Engineering,
Aalborg University, Sohngaardsholmsvej 57
DK-9000 Aalborg, Denmark

1 Abstract

Analysis and tests of knee joints as part of a modified attic truss has been made in several projects at Aalborg University during recent years. The modified attic truss is an alternative to the attic truss, see figure 1. The results from these projects have led to a stiff and strong design of this knee joint when punched metal plate fasteners (nail plates) are used as connectors.

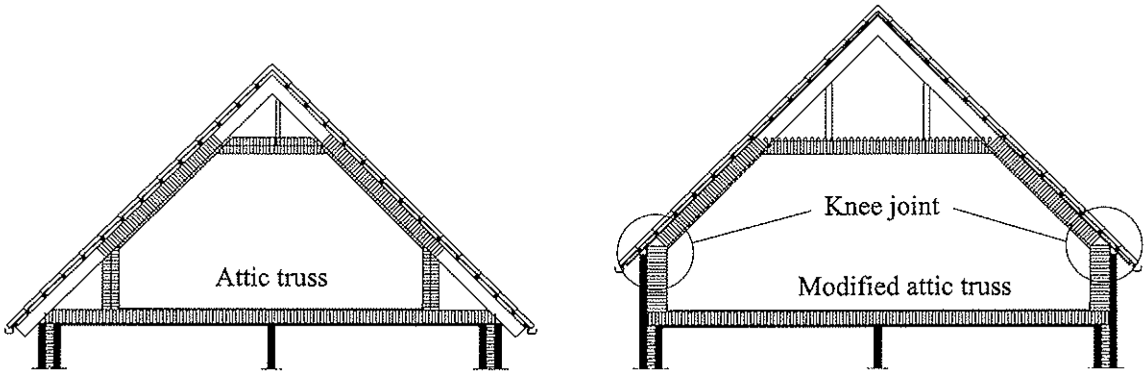

Figure 1. Attic truss versus modified attic truss.

Traditionally the knee joints of the modified attic trusses are designed with plywood sheets that are glued and nailed to the rafter and the leg of the truss. However, this type of joint is expensive and it is preferable that these knee joints can be made with nail plates.

20 full-scale tests with the modified attic truss have been performed within this study. In 10 of these tests the knee joints are produced with nail plates and in rest of the tests the knee joints are produced with plywood sheets to be able to compare the two types of joints. The results from these tests are compared with results from a finite element model (named TRUSSLAB) that includes the non-linear behaviour of the nail plate joints and contact between the timber members. The comparison is performed considering both the stiffness and the strength of the trusses.

For the truss manufactures' commercial use, a simple design method for knee joints with nail plates has been set up (calculation of the ultimate loads). The method is based on sectional forces that are determined from a relatively simple numerical model of the frame truss, where the knee joint is modelled as fully stiff – which is the way truss producers model the modified attic truss today. The test results are compared with results from the method.

In section 6 the *Eurocode 5 (2001)* methods for design of the plate capacities are investigated. Deficiencies when using this method for a knee joint are outlined.

2 Test Description

The dimensions of the modified attic truss are based on a span on 8.5 m, see figure 2. A Danish truss producer has determined the dimensions of the timber beams. Structural timber (Nordic origin) is used and the qualities are shown in the figure.

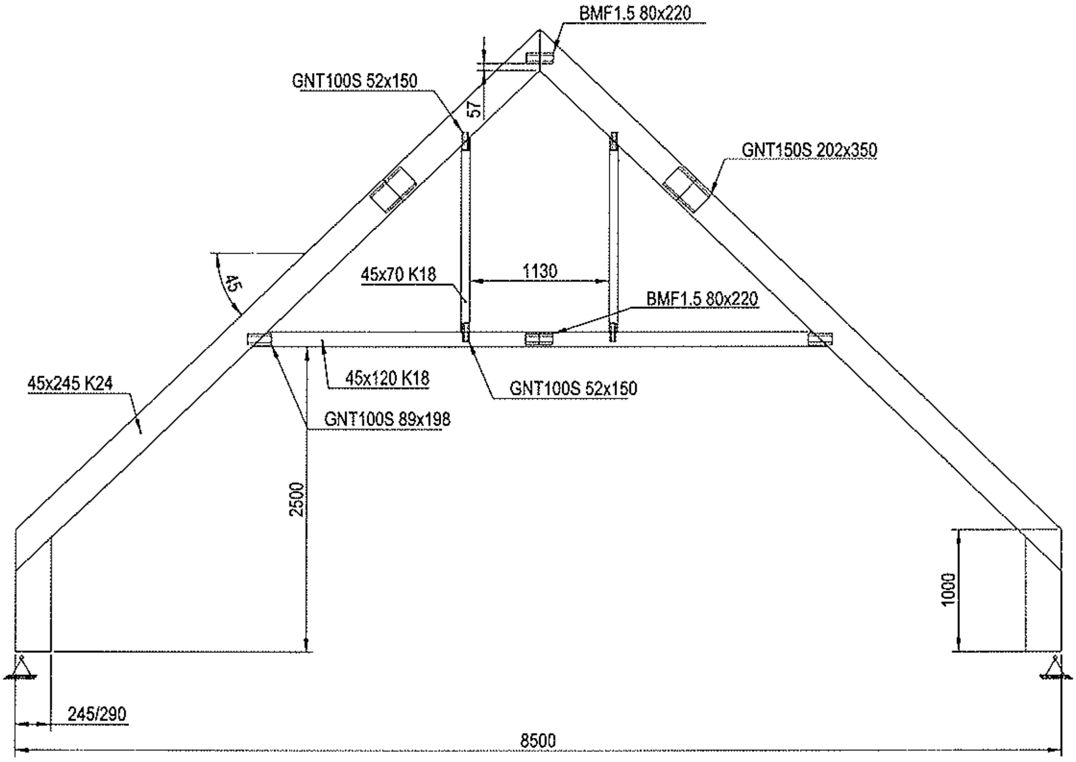

Figure 2. Dimensions (in mm) of the tested modified attic truss. Double lines indicate the main direction of the nail plates.

Prior to production of the trusses, the timber beams have been stored at a relative humidity (RH) of 85% and a temperature of 20°C (according to *DS/EN 408 (1995)*). After production and before testing the trusses were stored at 65% RH and 20°C.

For the beams used as rafters the modulus of elasticity has been measured (the influence of the stiffness of rest of the beams is assumed to be small).

2.1 The Four Different Test Series

Besides the design of the knee joints and the width of the legs all four test series are identical. The dimensions of the leg/knee joints of each test series are given in figure 3.

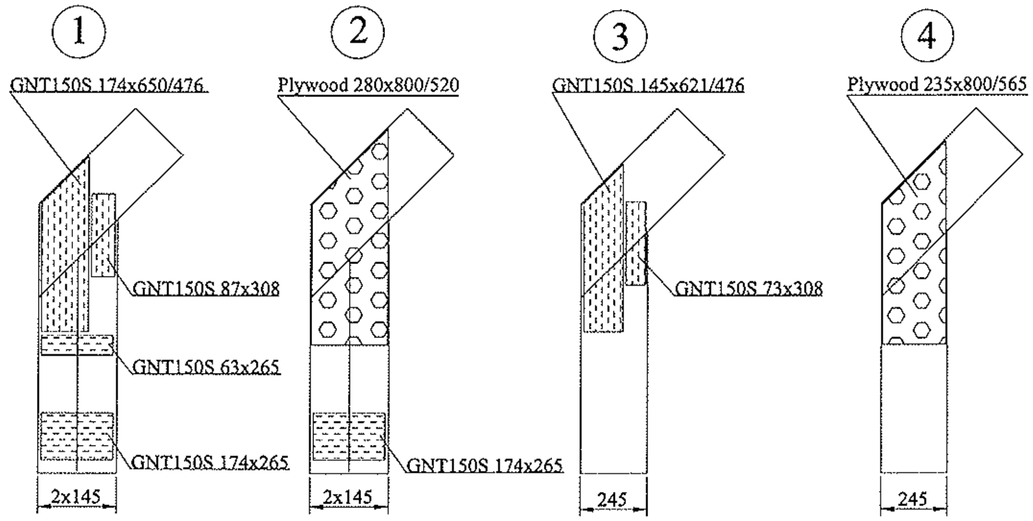
①
②
③
④
GNT150S 174x650/476
Plywood 280x800/520
GNT150S 145x621/476
Plywood 235x800/565
GNT150S 87x308
GNT150S 63x265
GNT150S 174x265
GNT150S 174x265
GNT150S 73x308
2x145
2x145
245
245

Figure 3. Dimensions (in mm) of the four different knee joints. Double lines indicate the main direction of the nail plates.

The nail plate type GNT100S has a thickness of 1.0 mm and a tooth length of 8 mm, whereas the GNT150S have a thickness of 1.5 mm and a tooth length of 14 mm. The nail plates are produced by MiTek. The thickness of the plywood is 22 mm (for each member) and the quality is P30.

Five identical specimens have been tested in each series (only four in series 4). The Danish truss producer has determined the dimensions of the two knee joints with plywood, whereas the dimensions of the knee joints with nail plates are based on tests with sections of knee joints, see *Ellegaard, P. (2002)*. The dimensions of all other joints with nail plates are designed by the truss producer.

2.2 Test Setup and Load Arrangement

The trusses are subjected to the load case shown in figure 4. This load case simulates wind load from the left (according to the Danish code *DS 410 (1998)*) and creates horizontal deformations at the knee joint which often control the dimensions of the truss (since the deformations should be limited not to destroy the adjoining building parts, which is often a brick wall at the outside of the truss). The locations and directions of the 7 displacement transducers are also shown in figure 4.

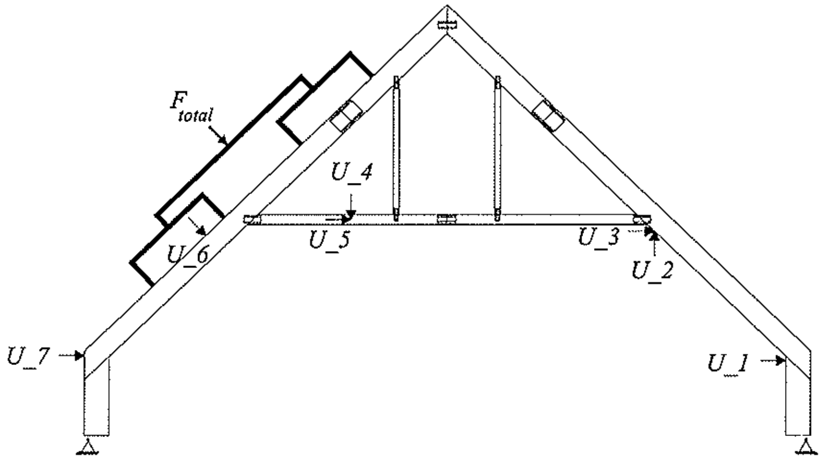
F_total
U_4
U_5
U_6
U_3
U_2
U_7
U_1

Figure 4. Load arrangement and location of displacement transducers. Dimensions in mm.

The supports are modelled as hinges and at 14 locations the truss is supported against distortion motion and buckling out of plane as shown in figure 5.

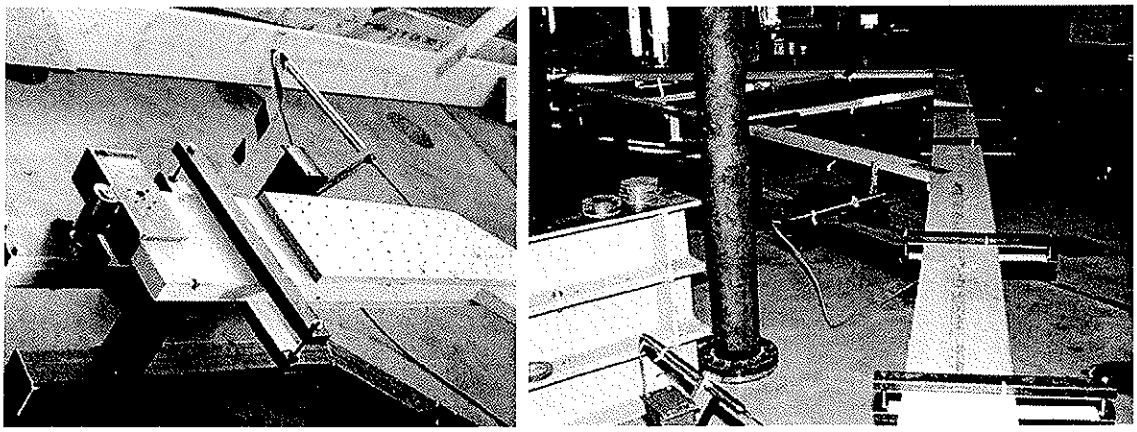

Figure 5. Support of the truss and arrangement to prevent the truss from distortion and buckling out of plane.

3 The Finite Element Model TRUSSLAB

The theory behind TRUSSLAB is in general based on the ideas of joint modelling proposed by R. O. Foschi, see *Foschi, R. O. (1977)* and *Foschi, R. O. (1979)*. J. Nielsen developed some of the elements further, see *Nielsen, J. (1996)*. These improvements also form the basic of the TRUSSLAB model where additional modifications have been implemented. For a detailed description of TRUSSLAB, see *Ellegaard, P. (2002)*.

Both the locations and the dimensions of the nail plates are taken into account in TRUSSLAB and therefore, the sectional forces required for design are directly given in each nail group and plate connection.

The different elements used in the joint modelling are described considering a heel joint of a timber truss, see figure 6.

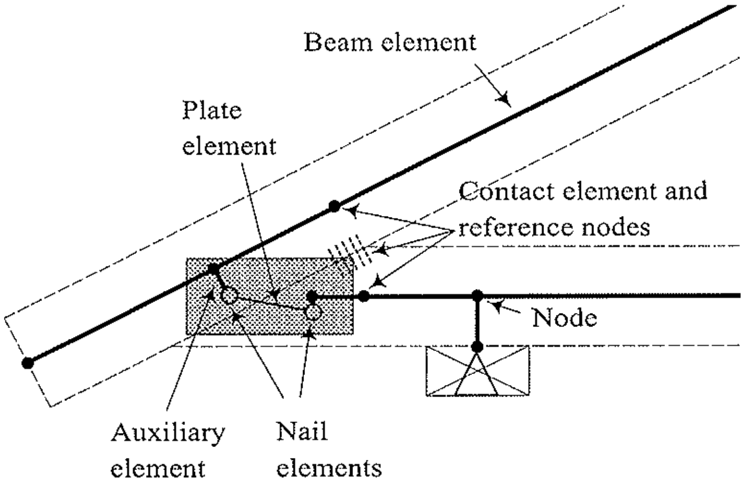

Figure 6. Heel joint used to explain the use of elements in TRUSSLAB.

Beam elements are used to model the timber members. The elements are located in the system line. Beam elements are also used as auxiliary elements. These auxiliary elements are used to transfer forces from nail groups to the system lines.

The stiffness of nail groups is taken into account by special nail elements. The nail elements connect beam elements with plate elements.

The behaviour of the nail plate over the joint line is modelled by a plate element. A plate element connects two nail elements. The nodes of a plate element and the corresponding nail elements are located at the centre of the respective nail groups.

Contact between timber members is modelled by a contact element. If there is an initial gap between the timber members the contact element is not activated until this gap is closed. The contact element refers to two nodes.

The material properties of the nail and plate elements are non-linear and the properties are determined from a number of tests, see *Ellegaard, P. (2002)*. The properties of the contact element are bilinear elastic. TRUSSLAB is a plane frame finite element program with three degrees of freedom for each node: two displacements and one rotation. Second order theory has not yet been implemented.

4 Comparison of Stiffness Test Results Versus TRUSSLAB

In the following results from the tests are compared with results by TRUSSLAB. In figures 7, 8, 9 and 10 the stiffness from the tests are compared with simulations by TRUSSLAB.

The displacement transducer measuring the horizontal displacement at the knee joint to the right is considered (displacement transducer *U_1* in figure 4). The calculations by TRUSSLAB are stopped at a load level of 25 kN (total load, F_{total}). For the test series 2 and 4 the knee joints are assumed to be fully stiff (test series where the knee joints are made up of plywood).

To account for the influence of second order theory, the displacements calculated by TRUSSLAB are multiplied by 1.08, see *Ellegaard, P. (2002)*.

The results from the calculations by TRUSSLAB are indicated by a "+" and the test results by a solid line. It is noted that the test results are only plotted until the load level where TRUSSLAB is assumed to be able to predict the behaviour of the truss. In several test series suddenly arising cracks in the timber make the load-displacement curves show either horizontal or vertical jumps.

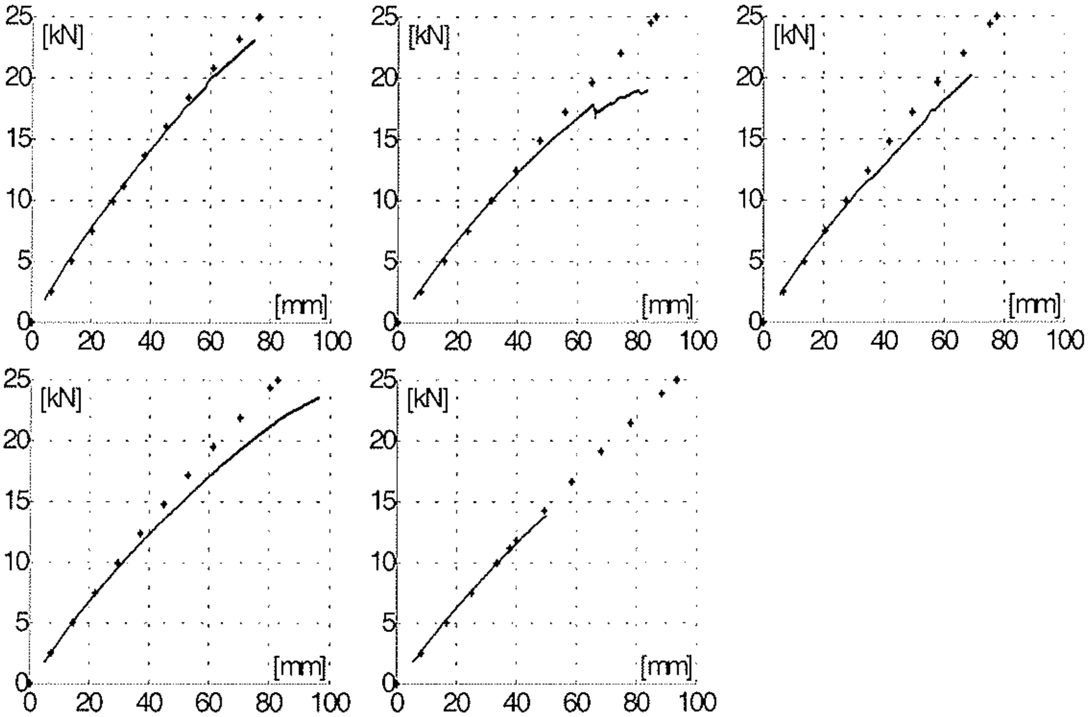

Figure 7. Load-displacement curves for test series 1. The force is shown on the vertical axis and the displacement U_1 on the horizontal axis.

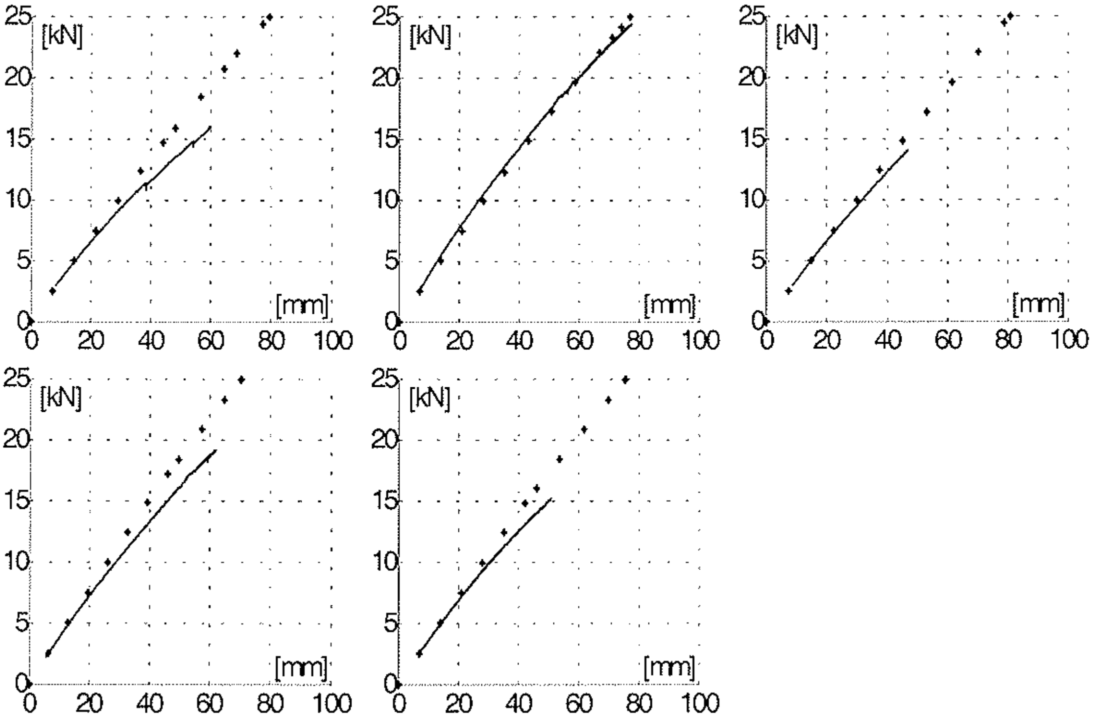

Figure 8. Load-displacement curves for test series 2. The force is shown on the vertical axis and the displacement U_1 on the horizontal axis.

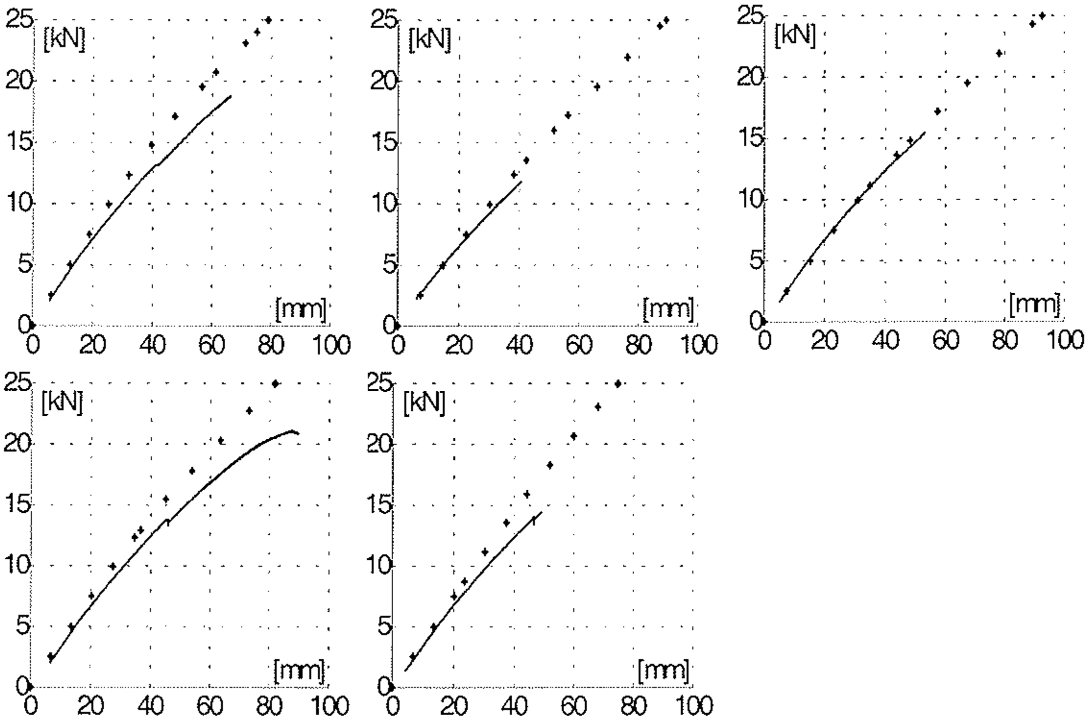

Figure 9. Load-displacement curves for test series 3. The force is shown on the vertical axis and the displacement U_1 on the horizontal axis.

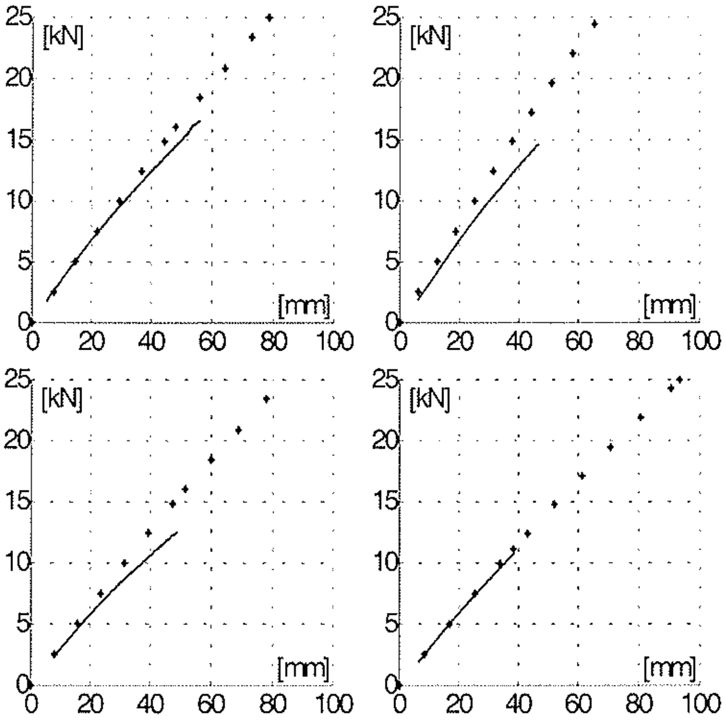

Figure 10. Load-displacement curves for test series 4. The force is shown on the vertical axis and the displacement U_1 on the horizontal axis.

When considering the load-displacement curves it is found that TRUSSLAB for most of the test specimens is able to predict the stiffness of the modified attic truss accurately – especially for load levels up to 10-15 kN. At higher load levels TRUSSLAB overestimates the stiffness of the trusses. In none of the test specimens TRUSSLAB underestimates the stiffness.

These overestimations may be caused by the fact that the properties of the timber beams are modelled as linear elastic (without any plasticity in compression). Moreover, splitting of the timber is not taken into account and the influence of second order effects are estimated to be 8%. In most of the test specimens one or several cracks were observed in the rafter before testing, see figure 11. These cracks are probably caused by the climate conditions before and after production (85% RH/65% RH) and they are propagating during testing.

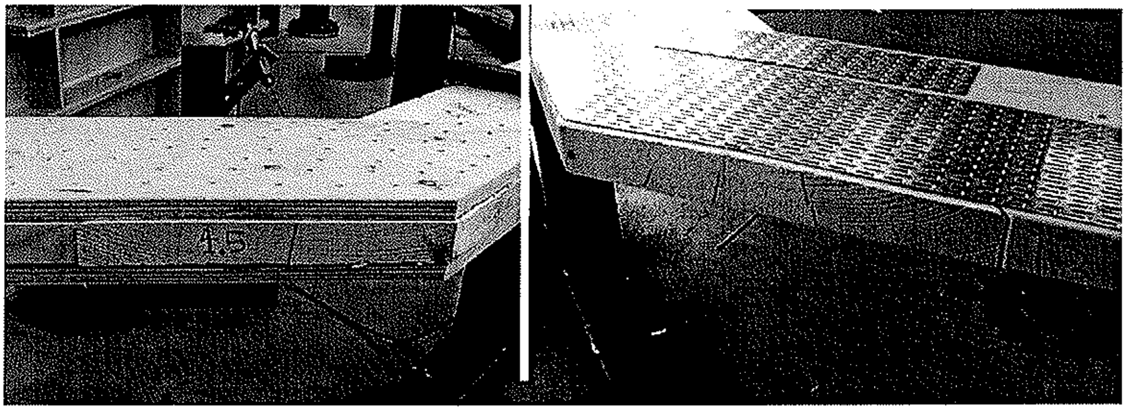

Figure 11. Initial cracks in the rafter before testing.

When comparing results by TRUSSLAB with test results for rest of the displacement transducers similar correspondence as for displacement transducer *U_1* is found.

In table 1 the initial stiffness (defined as the displacement *U_1* at a load level of 10 kN) is listed.

	Displacement at a load level of 10 kN					Average
Test specimen	1	2	3	4	5	1-5
Series 1	27.0	29.2	31.2	31.2	34.0	30.5
Series 2	26.5	29.0	30.5	32.0	32.5	30.1
Series 3	29.5	30.8	31.3	31.3	33.2	31.2
Series 4	--	30.3	31.4	35.6	37.5	33.7

Table 1. Initial stiffness for the modified attic trusses. Units in mm.

From table 1 an increase of 1% is found when comparing the average initial stiffness of series 1 (knee joint with nail plates) with that of series 2 (knee joint with plywood) that both have 290 mm leg widths. When comparing series 3 (knee joint with nail plates) with series 4 (knee joint with plywood) the initial stiffness is 8% larger for the trusses where the knee joints are made with nail plates. As expected the test series 1 and 2, where the trusses are produced with a total leg width of 295 mm, have higher initial stiffness than the series 3 and 4, where the width of the legs are 245 mm.

When considering the stiffness of the modified attic trusses it is found that the trusses can be produced with nail plates as connector in the knee joints.

5 Comparison of Ultimate Loads and Failure Modes From Tests Versus TRUSSLAB

In the following the ultimate loads and the failure modes for the modified attic trusses are analysed. The failure criteria implemented in TRUSSLAB are:

- **Timber beam elements:** Design rules from *Eurocode 5 (2001)*. The timber strength values (mean values) are from the Danish Code *DS413 (1998)*.
- **Nail elements:** Design rules from *Eurocode 5 (2001)*. The anchorage strength values (mean values) are determined from tests, see *Ellegaard, P. (2002)*.
- **Plate elements:** Special failure criteria have been implemented since the design rules in Eurocode 5 may lead to false capacities (see section 7). The plate strength values (mean values) are determined from tests, see *Ellegaard, P. (2002)*.

A comparison of the load level and failure type, where the first "failure" is predicted by TRUSSLAB, and the first "failure" observed during testing is shown in table 2. Normally, the ultimate load capacities of the trusses have not been reached at these load levels, since e.g. contact is established after plate buckling. "T" denotes timber failure, "P.B". denotes plate buckling, "P". denotes plate failure (no distinction of buckling, shear or tension) and -- denotes that the first failure type has not been registered. It is noted that there is some uncertainty in the load levels and failure types observed during testing.

Test series	Tests		TRUSSLAB		Test series	Tests		TRUSSLAB	
	Load level [kN]	Failure type	Load level [kN]	Failure type		Load level [kN]	Failure type	Load level [kN]	Failure type
1.1	15	P.B.	12	P	3.1	12	P.B.	10	P
1.2	10	P.B.	10	P	3.2	13	T	10	P
1.3	11	P.B.	11	P	3.3	18*)	T	10	P
1.4	12	P.B.	10	P	3.4	11	P.B.	10	P
1.5	12	P.B.	10	P	3.5	12	P.B.	10	P
2.1	12	T	12	P					
2.2	25*)	P.B.	10	P	4.2	20**)	--	14	P
2.3	15*)	T	12	P	4.3	16**)	--	12	P
2.4	21*)	T	12	P	4.4	13**)	--	12	P
2.5	11	P.B.	12	P	4.5	11	P.B.	10	P

*Table 2. Predictions by TRUSSLAB of first "failure" load level versus observations during testing. *) The load level at the first observed failure type coincides maximum load level. **) Maximum load level.*

For all test specimens TRUSSLAB predicts plate failure at a load level lower than observed during testing, which is on the safe side. The location of the nail plates where failure is predicted by TRUSSLAB are, however, in several cases different from what is observed during testing.

Post-plate buckling, failure occurs either as timber failure or tension failure in the nail plates. The ultimate load levels for these failure modes are listed in table 3. It should be pointed out that only specimens 3.1 and 3.4 failed in the knee joint. In figure 12 the failed knee joints are shown.

	Ultimate load level [kN]					Average [kN]
Test specimen	1	2	3	4	5	1-5
Series 1	23.8	19.8	22.6	24.1	20.5	22.2
Series 2	17.1	25.3	14.9	21.5	18.9	19.5
Series 3	20.9	16.9	18.4	21.7	16.9	18.9
Series 4	--	20.4	16.5	13.3	13.7	16.0

Table 3. Ultimate load levels - F_{total}.

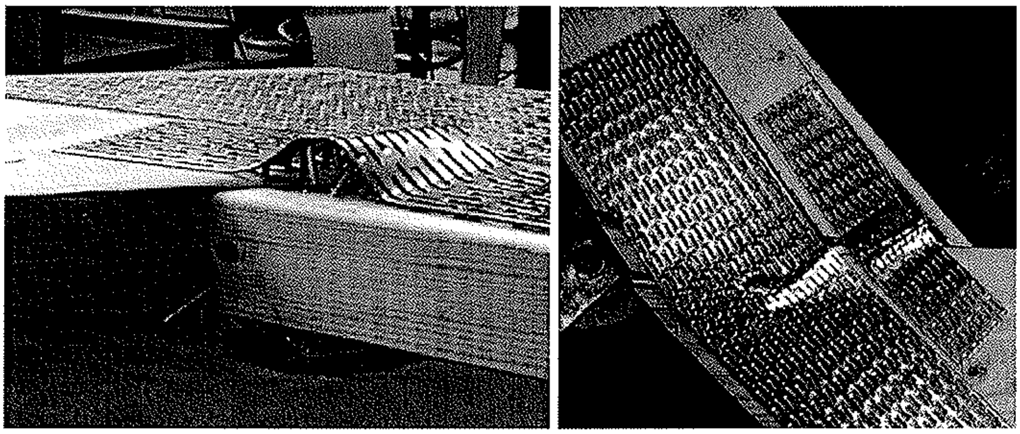

Figure 12. Failure mode for test specimens 3.1 and 3.4.

Considering the strength of the modified attic trusses it can be concluded that the trusses with nail plates in the knee joints (series 1 and 3) have average ultimate loads exceeding the ultimate loads for the trusses where the knee joints are connected with plywood, glue and nails (series 2 and 4). It is difficult to tell whether this is caused by the knee joints with nail plates, since the knee joints only failed in the series 3.1 and 3.4.

As expected the test series 1 and 2 have higher average ultimate loads compared to test series 3 and 4 caused by the total leg width of 245 mm and 295 mm, respectively.

6 Calculation of Ultimate Loads for the Knee Joints With Nail Plates

The design method described in the following has been derived as an application tool for truss manufacturers. The load capacities predicted by the method are compared to the test results. Direct comparison between the method and the tests may, however, only be done for the two trusses that failed in the knee joint (test specimens 3.1 and 3.4). The method was set up considering tests with knee sections of the modified attic truss, where it was found that the method can be used to predict the capacities of the knee joints, see *Ellegaard, P. (2002).*

The failure mode of cross-grain splitting has not been considered in the method.

In the method the leg is considered to be one single beam, even though some of the tested knee joints consist of two beams. This assumption requires that the legs are connected by a sufficient number of nail plates.

Since the method is meant for use by the truss producers the statical model is similar to the one they use at present where the knee joint is assumed fully stiff. The sectional forces at the middle of the joint line are considered, see figure 13.

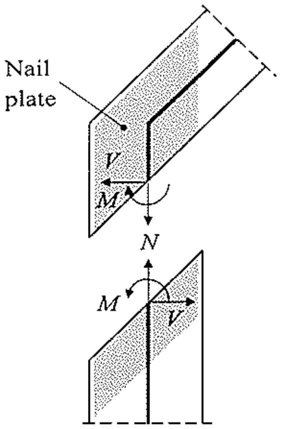

Figure 13. Sectional forces from the finite element model.

The bending moment *M* and the axial force *N* are converted to the forces N_1 and N_2, see figure 14. For the load case analysed and considering the right-hand knee joint the force N_2 is a tension force and N_1 is a compression force. The force N_2 and the shear force V are assumed to be transferred by the nail plates over the outer 1/3 of the width of the leg (measured horizontally) – denoted the *tension zone*. The force N_1 is transferred through the inner 60 mm of the joint line (measured horizontally) – denoted the *compression zone*, see figure 14 (only the forces on the leg are shown).

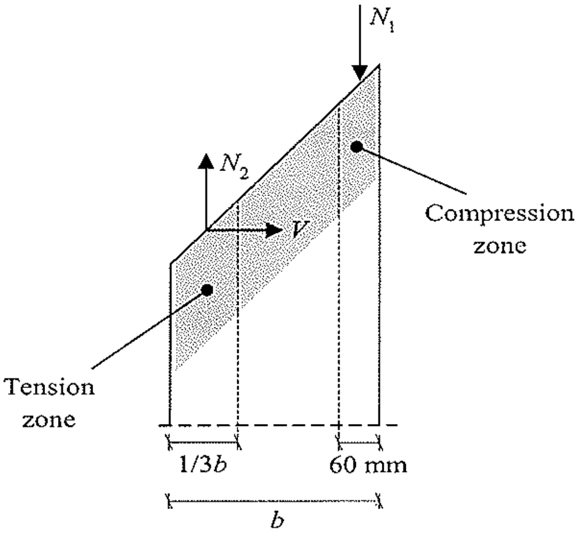

Figure 14. Assumed force distribution in the joint line.

50% of N_1 is transferred as compression in the nail plates and 50% of N_1 is transferred as contact between the timber members.

The contact force between the timber members is converted to a force $F_{c,perp}$ perpendicular to the grain direction of the rafter and a force $F_{c,par}$ parallel to the joint line. This is shown in figure 15. Possible stress distribution in the rafter is not taken into account. The force $F_{c,par}$ is transferred by the remaining parts of the nail plates located between the outer 1/3 of the width of the leg and the inner 60 mm – denoted the *shear zone*.

The nail plates, where 50% of the compression force N_1 is transferred, are assumed to be centrally loaded, even though the nail plates may be located 10 mm from the edge of the inner side of the leg. The anchorage areas for transferring 50% of N_1 are determined as the area of the nail plates located within 60 mm from the inner side of the leg. These areas are shown as cross-hatched areas in figure 15.

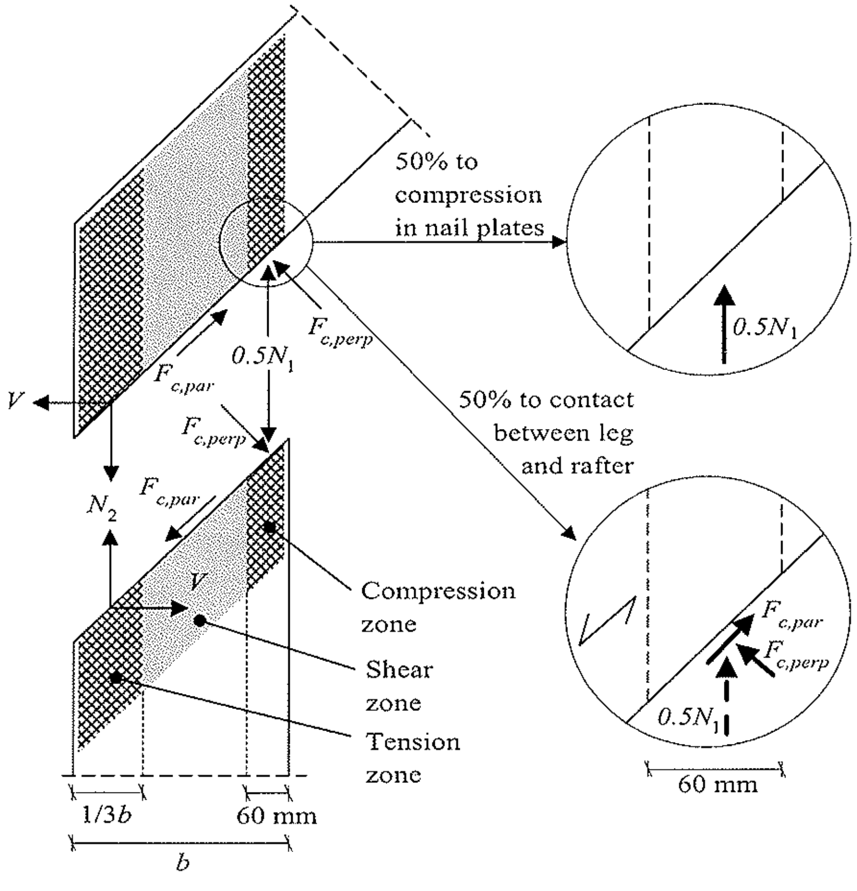
50% to compression in nail plates
$0.5N_1$
$F_{c,perp}$
$F_{c,par}$
V
N_2
50% to contact between leg and rafter
Compression zone
Shear zone
Tension zone
1/3b
60 mm
b
$F_{c,par}$
$F_{c,perp}$
$0.5N_1$
60 mm

Figure 15. The distribution of the contact forces results in an "extra" force along the joint line. At the right-hand side only the forces on the rafter are considered.

Similar to the compression zone, it is assumed that the nail plate areas located in the tension zone (shown as cross-hatched areas) transfer the force N_2 and the shear force V.

The calculations are performed with the design equations for plate and anchorage capacities given in *Eurocode 5 (2001)*, mean strength values used for the timber are as given in *DS 413 (1998)* and mean strength values used for the plate and anchorage capacities were determined by tests, see *Ellegaard, P. (2002).*

The results from the calculations of the two test series 1 and 3, where the knee joints are produced with nail plates, are shown in table 4. The results are shown as a coefficient of utilization compared to the actual ultimate load achieved in the tests. A coefficient below 1.0 means that the calculation method predicts a capacity of the knee joint that is higher than the ultimate load achieved in the tests and vice versa.

Test specimen	Coefficient of utilization	Test specimen	Coefficient of utilization
1.1	0.98	3.1	1.03
1.2	0.81	3.2	0.85
1.3	0.86	3.3	0.82
1.4	0.99	3.4	1.08
1.5	0.64	3.5	0.75

Table 4. Coefficient of utilization from the calculations compared to the actual ultimate load achieved in the tests.

For both series the controlling part of the knee joints is compression perpendicular to the grain direction of the rafter - $F_{c,perp}$.

From the table it is found that the calculation method predicts failure for the test specimens 3.1 and 3.4 at a load level that is up to 8% lower than that observed during testing. These two test specimens were the only ones who failed in the knee joints during testing, which is predicted well by the calculation method. For the rest of the test specimens the calculation method predicts the load-carrying capacity of the knee joints to be up to 36% higher that the ultimate load achieved in the tests. This cannot be verified from the test results, since these specimens did not fail in the knee joints. However, as mentioned above, the calculation method is calibrated against test results with sections of the modified attic truss and the method showed good agreement with the ultimate loads from the tests.

7 Use of EC5 Rules to Estimate the Ultimate Loads of the Knee Joints

If the nail plate covers more than one joint line Eurocode 5 (2001) suggests the following:

"If the plate covers more than two elements then the forces in each straight part of the connection line should be determined so that the equilibrium is fulfilled and that the condition in 3.8 is satisfied in each straight part."

The condition in 3.8 is given by:

$$\left(\frac{F_x}{R_x}\right)^2 + \left(\frac{F_y}{R_y}\right)^2 \leq 1$$

where R_x and R_y are the strength values of the plate capacity in the x and y directions, respectively and F_x and F_y are the corresponding actual forces.

In TRUSSLAB the plate element is composed of beams with nonlinear material properties. If the nail plate covers e.g. two straight parts the forces at the midpoint of each straight part can be determined from the sectional forces at the ends of the small beams. When more than one joints line is considered it seems, however, that the plate design rules in Eurocode 5 lead to wrong load capacities. To explain this two similar joints, as shown in figure 16, are analysed.

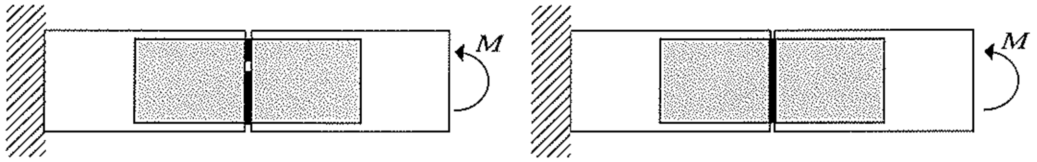
A: Joint where the plate line consists of two joint lines

B: Joint where the plate line consists of one joint line

Figure 16. Two similar joints where the expressions in Eurocode 5 lead to different load capacities.

In joint type A the nail plate is divided into two straight joint lines, whereas in joint type B the nail plate is treated as one straight line. In practice the joints only cover one line, but could easily be converted to a joint with two straight lines if one of the line parts in joint type A is rotated by a small angle. In TRUSSLAB the nail plates are identical for the two cases A and B.

In order to design the nail plate according to Eurocode 5, sectional forces are to be at the middle of each joint line as shown in figure 17. The moment M_1 is smaller than M_2 for two reasons:

1. The lengths of the joint lines are different.
2. The plate becomes plastic in compression at a lower stress level than in tension, see *Ellegaard, P. (2002).*

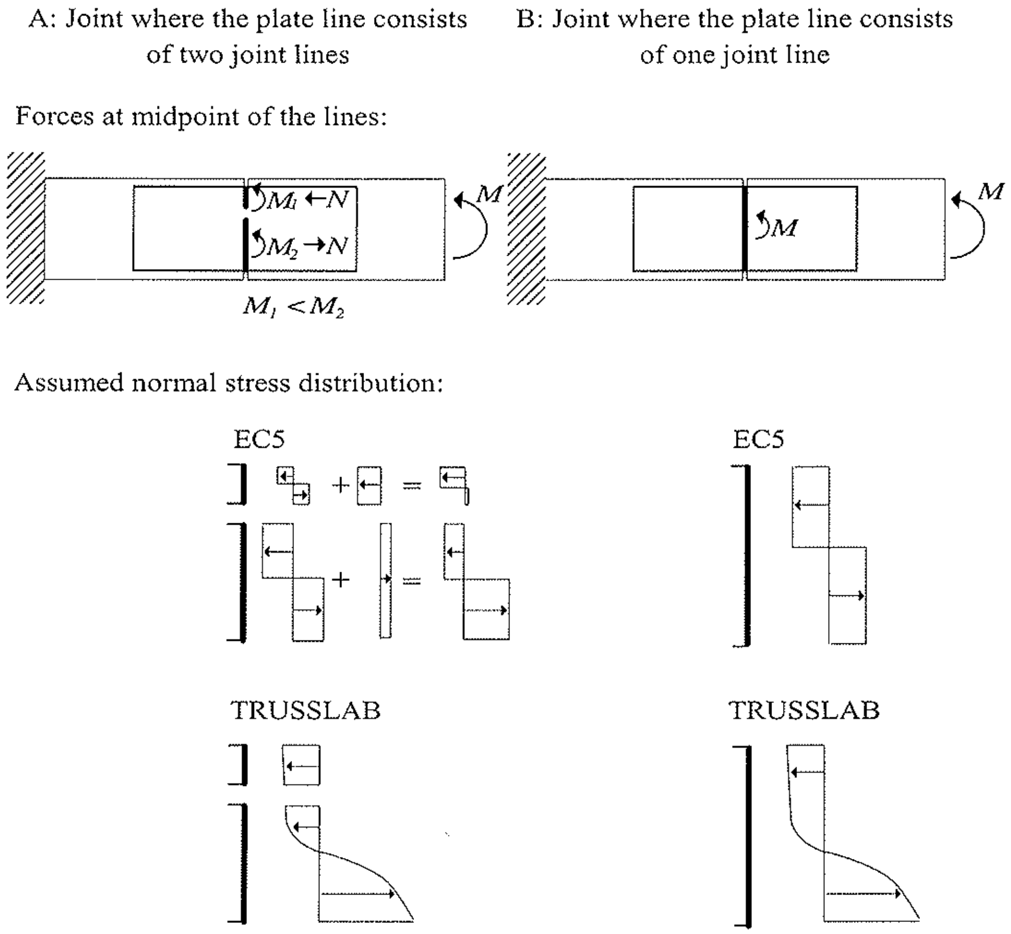
A: Joint where the plate line consists of two joint lines
B: Joint where the plate line consists of one joint line
Forces at midpoint of the lines:
M_1 ←N
M_2 →N
M
$M_1 < M_2$
M
M
Assumed normal stress distribution:
EC5
EC5
TRUSSLAB
TRUSSLAB

Figure 17. Sectional forces and stresses at the middle of each straight part.

From the figures it is seen that the two similar joints are treated differently in Eurocode 5 and a consequence is that the load-carrying capacity of joint type A is approximately 50% less than the load-carrying capacity of joint type B.

The problem described above arises for the knee joint shown in figure 18. This knee joint type was one of the tested segments of the modified attic truss. In the figure two possible failure paths in the nail plates are shown as thick lines. It should be noted that the outer leg goes to the top of the rafter.

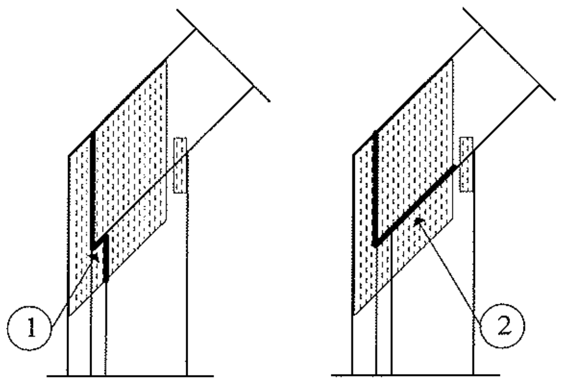

Figure 18. Complex knee joint type where two possible failure modes are shown.

From the calculated sectional forces at each of the midpoints of the straight joint lines 1 and 2, respectively, it is found that plate failure according to Eurocode 5 (2001) arises at an unrealistically low load level for joint line 1 of the plate. For joint line 2 of the plate the failure load level according to Eurocode 5 (2001) is significantly higher. However, since part 2 includes part 1 of the plate it seems unrealistic that part 1 fails and part 2 does not fail at the same load level.

8 Conclusion

Based on the tests and the analysis of the modified attic trusses it can be concluded that the knee joints produced with nail plates have sufficient stiffness and strength compared to the knee joints with plywood, glue and nails.

The TRUSSLAB model is able to predict the behaviour of the modified attic truss quite well, especially at lower load levels. At higher load levels TRUSSLAB overestimates the stiffness.

TRUSSLAB predicts the load level where the first "failure" arises at a load level that is lower than that observed during testing.

The design rules in Eurocode 5 (2001) cannot directly be used for design of the more complex types of knee joints with nail plates.

A calculation method has been set up and this method predicts the lowest load-carrying capacity for the two test specimens where failure was also observed during testing.

9 References

DS 410 (1998), 'Norm for last på konstruktioner' (in Danish) (Code of Practice for Loads for the Design of Structures), Dansk Standard, 4. udgave/1.oplag, 1998.

DS 413 (1998), 'Norm for trækonstruktioner' (in Danish) (Code of Practice for the Structural Use of Timber), Dansk Standard, 5. udgave/1.oplag, 1998.

DS/EN 408 (1995), 'Timber structures – Structural Timber and Glued Laminated Timber – Determination of some Physical and Mechanical Properties', 1995.

Ellegaard, P. (2002), 'Analysis of Timber Joints With Punched Metal Plate Fasteners – With Focus on Knee Joints' Ph.D. Thesis, Department of Building Technology and Structural Engineering, University of Aalborg, Denmark, 2002.

Eurocode 5 (2001) - prEN 1995-1-1. Final draft of 1995-1-1, 'Eurocode 5 – Design of Timber Structures – Part 1-1: General Rules, General Rules and Rules for Buildings'. CEN Brussels, 2001.

Foschi, R. O. (1977), 'Analysis of Wood Diaphragms and Trusses. Part II: Truss-Plate Connections', Can. J. Eng. Vol. 4, 1977.

Foschi, R. O. (1979), 'Truss Plate Modelling in the Analysis of Trusses'. Metal-Plate Wood-Truss Conference 1979, pp 88-97, 1979.

Nielsen, J. (1996), 'Stiffness Analysis of Nail-Plate Joints Subjected to Short-Term Loads', Ph.D.-Thesis, Dept. of Building Technology and Structural Engineering, University of Aalborg, Denmark, 1996.

CIB-W18/35-7-11

INTERNATIONAL COUNCIL FOR RESEARCH AND INNOVATION
IN BUILDING AND CONSTRUCTION

WORKING COMMISSION W18 - TIMBER STRUCTURES

JOINT PROPERTIES OF PLYBAMBOO SHEETS IN PREFABRICATED HOUSING

G González

Eindhoven University of Technology

THE NETHERLANDS

Presented by: G E Gonzales

H J Blaß asked about the types of fixing used in the study. G Gonzalez replied that round smooth screws without shanks were used and the holes were predrilled to 80% of the screw diameter. S Svensson asked about the role of the plybamboo sheeting. K Komatsu asked if the timber split due to the nails. After confirming that the plybamboo sheeting were intended to act as normal sheeting G Gonzalez indicated that no splitting due to the nails was observed. B Dujic asked for clarification on the distances between studs and if the tested panel system could be considered to be partially anchored. G Gonzalez agreed that the system is partially anchored and that rotation of the system was not restricted. This was followed by a discussion initiated by B Yeh, S Aicher and S Thelandersson on the issues of storey drift, the transfer of wind loading and general testing arrangement for shear walls.

Joint properties of plybamboo sheets in prefabricated housing

Guillermo González
Eindhoven University of Technology, The Netherlands

Abstract- This paper deals with the theoretical and experimental structural analysis of several wall-to-wall connections of plybamboo and wood panels that have been proposed by the author and his supervisors in his PhD research. The panels consist of a wooden frame on which one plybamboo sheet is fixed to. These wall-panels could be suitable for social housing in developing countries. Corner, T- and sheet-to-frame connections are three types of joints that have been tested and analyzed. The obtained results show that all connections present ductile behavior adequate for expected wind and seismic loads.

1 Introduction

This paper deals with the experimental analysis of wall-to-wall connections regarding the wall-panel system of plybamboo (kind of plywood or wood-based panel made out of bamboo) and wood that has been proposed by the author and his supervisors [1]. The advantage of using these type of walls is that they could be industrially produced (prefabrication) in developing countries where wood lacks. The construction on-site would be rather simple and makes the system a superb alternative for social housing. The purpose of this research is to obtain the structural response and capacity of several plybamboo-wood wall-panel connections. The paper concentrates on wall-to-wall connections such as corners, T- and sheet-to-frame connection under lateral load. For the experimental tests, scale models were built and tested in order to obtain information about the structural behavior and capacity of such connections. The following section describes the wall-panel system including different types of prefabricated panels, the wall-to-foundation (and roof) connection and an example of a house floor plan with details of the vertical connections. Section 3 is more related to the followed methodology and the experimental setups for each of the tested connection. Section 4 presents the most relevant results with their respective analyses. Several concluding remarks finish the paper in section 5. All unspecified dimensions are in millimeters.

2 The wall-panel system

The following sections describe the wall-panel system that has been proposed by the author and his supervisors in the article 'Selection criteria for a house design method using plybamboo sheets' [1].

2.1 Prefabricated panels

The walls consist of prefabricated panels transported from the factory and mounted on-site. Figure 1 shows three different types of prefabricated walls regarding the building process and the structural design. Panel A consists of a plybamboo sheet between 12 and 18 mm thick joined to a wooden frame. In this case, the size of the frame coincides with the size of the sheet (2450x1225 mm). The studs and the horizontal members are joined in the corners by steel angles. Panel B consists of a smaller wooden frame than panel A. The idea is to cover the top plate and soleplates with the plybamboo sheet as will be explained in the following section. In this way, the top and sole plates would not be exposed to the outside. Besides, structural capacity to resist lateral load is improved. Nevertheless, more work on-site would be needed. The purpose of panel C is to eliminate horizontal members. In this case, the joint between the studs and top and bottom plates must be made on-site as well as the joint between the sheet and the plates. The previous would have an impact on the structural design of the top plate.

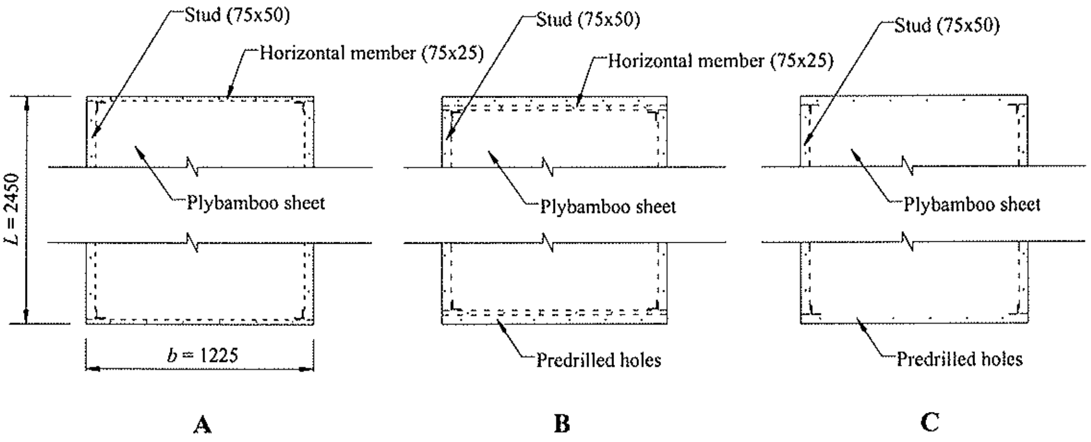

Figure 1. Different types of prefabricated panels.

2.2 Wall-to-foundation connection

Figure 2-a shows a vertical section of a possible wall-to-foundation connection based on the footing system that has been used by the Costa Rican Bamboo Foundation [2]. It consists of a reinforced concrete strip footing (this one might be another type depending on the soil conditions in which the method is being applied). Two concrete hollow blocks (i.e. 12x20x40 cm) are placed above the concrete strip. Steel bars coming from the footing are passed through the hollow part of the blocks. This part is afterwards filled with mortar. These blocks provide a barrier against humidity and termites [2]. The soleplate is fixed to the concrete blocks by means of steel bars coming from the foundation. Passing the steel bars through predrilled holes on the soleplate over 10 cm and hammering them to anchor the soleplate to the blocks achieves this. Figure 2-b shows how each of the different types of panel would be connected to the soleplate. Note that for panel A, screws are needed to join the panel to the soleplate because these fasteners must prevent uplifting whereas for panel B or C nails would be sufficient because the sheet is joined directly to the soleplate.

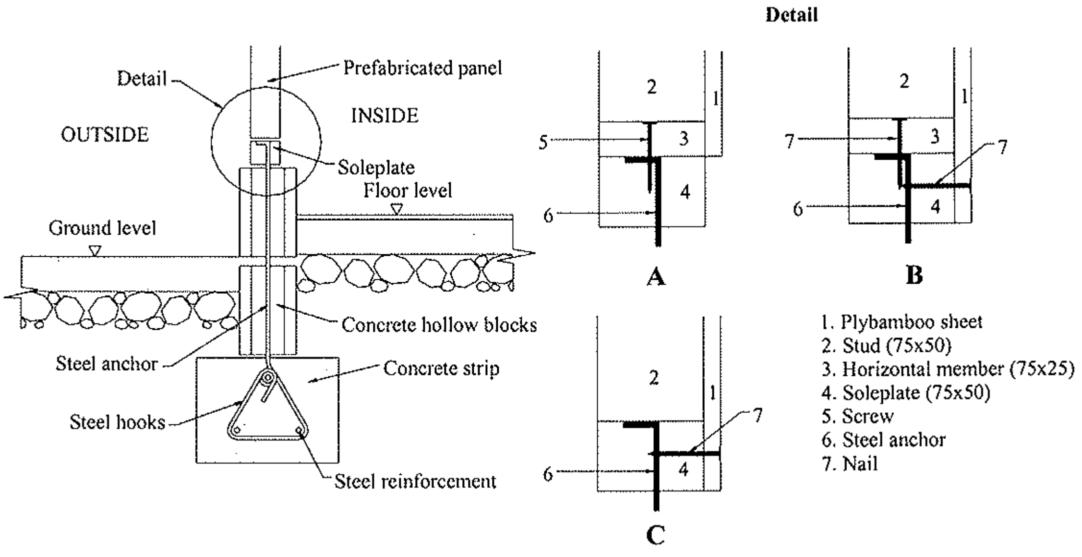
Detail
Detail
Prefabricated panel
OUTSIDE
INSIDE
Soleplate
Floor level
Ground level
Concrete hollow blocks
Steel anchor
Concrete strip
Steel hooks
Steel reinforcement
A
B
C
1
2
3
4
5
6
7
1. Plybamboo sheet
2. Stud (75x50)
3. Horizontal member (75x25)
4. Soleplate (75x50)
5. Screw
6. Steel anchor
7. Nail

(a) Vertical section **(b) Detail for each type of panel.**

Figure 2. Wall-to-foundation connection

2.3 Wall-to-roof connection

The wall to roof connection will depend on the type of roof structure that is going to be utilized. Basically, this structure could be easily joined to the top plate using fasteners or other kind of connectors.

2.4 Floor plan example

Figure 3 shows a plan view of a possible one-story house constructed with the prefabricated panels previously described. It also shows a modular basis of 1225 mm (plybamboo sheet width), the different types of wall-to-wall joints for this plan (Corner 1, Corner 2, T1, T2, T3 and parallel) and the places in which the walls should have a window or door opening. The details of the wall-to-wall connections are shown in Figure 4. Corner 1 (Figure 4-a) would be commonly used and requires an extra stud placed on-site. Corner 2 (Figure 4-b) may also be used in cases where the house has five external corners or for some internal walls. There are three possible T-connections as shown in Figure 3. T1 (Figure 4-d) would be used when a parallel connection (Figure 4-c) meets a perpendicular wall. T2 (Figure 4-e) would be used when two parallel walls on opposite sides from the modular basis line meet a perpendicular wall. Finally, T3 (Figure 4-f) would be used when two perpendicular walls meet.

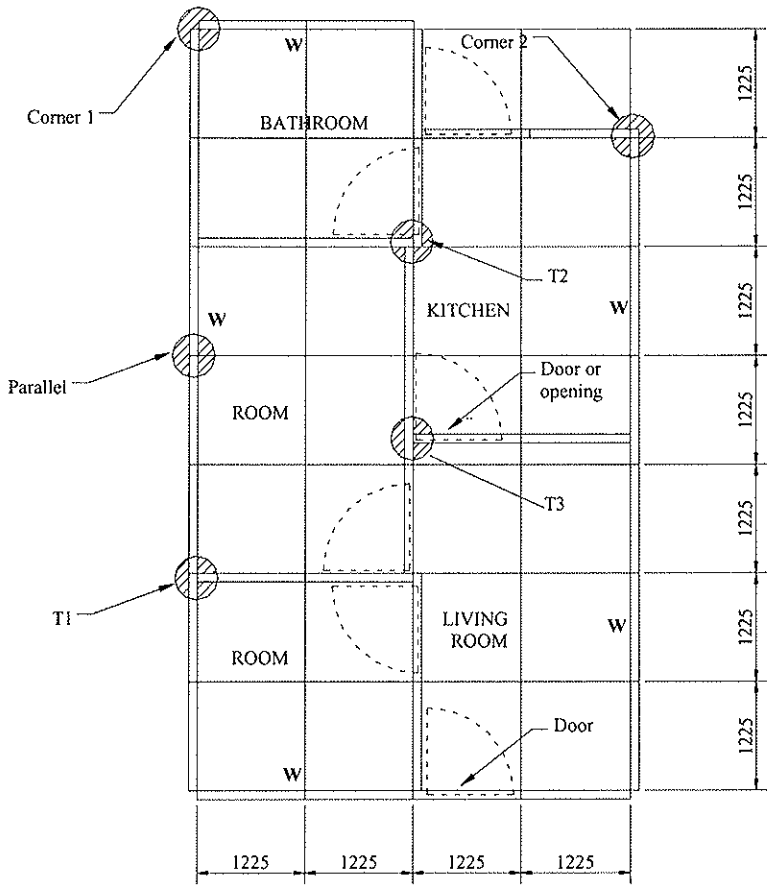
Corner 1
W
BATHROOM
Corner 2
1225
1225
1225
1225
1225
1225
1225
T2
KITCHEN
W
W
Parallel
ROOM
Door or opening
T3
T1
LIVING ROOM
W
ROOM
Door
W
1225
1225
1225
1225

Figure 3. Floor plan example.

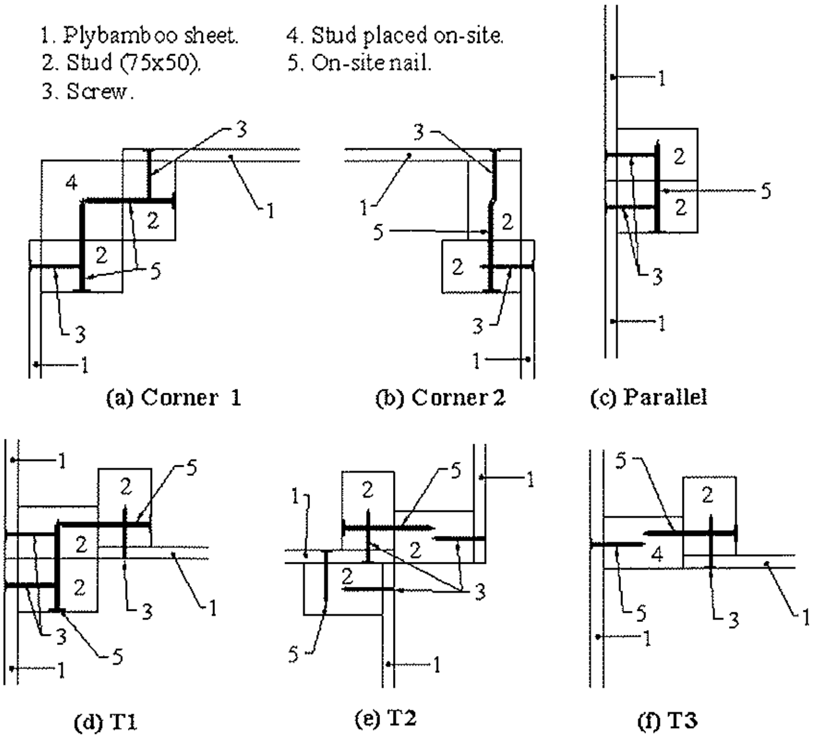
1. Plybamboo sheet.
2. Stud (75x50).
3. Screw.
4. Stud placed on-site.
5. On-site nail.
1
2
3
4
5

(a) Corner 1 (b) Corner 2 (c) Parallel

(d) T1 (e) T2 (f) T3

Figure 4. Details of the wall-to-wall connections according to Figure 3.

3 Methodology and experimental setup

3.1 Methodology

Three issues regarding the wall-panel system are investigated: corner connection, T-connection and sheet-to-frame connection under lateral load. The research concentrates on Corner 1 (Figure 4-a) and T1 (Figure 4-d) because they would be most commonly used. Besides, when the structural response of these two connections is known, the rest could be predicted. On the other hand, Corner 2 (Figure 4-b) seems to be stronger than Corner 1 because of a smaller arm causing bending moments in one direction and a larger nail on the other direction. T2 (Figure 4-e) and T3 (Figure 4-f) seem to be as strong as T1. Instead of the parallel connection (Figure 4-c) the sheet-to-frame connection was selected because when the parallel connection is analyzed as the corner and T-connections it becomes unstable [7].

In order to analyze the previous connections, part of the whole connection is modeled (see Figure 5, 6 and 7) neglecting the effect of the roof and foundation connection with the exception of the sheet-to-frame connection. This approach is conservative because the roof and foundation connections strengthen the global capacity of the connection. The wall width is taken as 625 mm, which is half the sheet width. The length of 450 mm is related to the spacing of the fasteners used to join the sheet to the studs. The spacing used was 150 mm (3 fasteners). The horizontal wind or seismic forces are modeled as a resultant load acting along the length of one of the studs. In the case of the sheet-to-frame connection a 1200x1200 mm wall-panel was used with a lateral load applied to the top plate.

For the theoretical calculations, some physical and mechanical properties obtained by manuals, personal contact or the author were used [3,4,5,6]. Some of these properties are density (ρ), moisture content (%w), bending and compression modulus of elasticity (E_m, E_c), bending strength (f_m) and embedding strength (f_h). The values are shown in Table 1.

Table 1. Several properties of the materials used during the experiments.

Material	ρ [kg/m^3]	%w	E_m [N/mm^2]	E_c [N/mm^2]	f_m [N/mm^2]	f_h [N/mm^2]
BMB	790	4.2	5700	3000	60	92
BSB	720	8-10	6500	-	94	86
W	490	12	11000	-	29	-

BMB [3]: Bamboo mat board (Board made out of woven bamboo mats glued together). BSB [4]: Bamboo strip board (Board made out of bamboo strips glued together). W: Soft wood class K24 [5].

3.2 Experimental setup

3.2.1 Corner connection

In order to fixate the model for the corner connection a steel frame was built. This frame is useful for the structure's supports and the placing of the dial gages and load cell. The frame offers an independent fixed reference system for measurement of displacements. Figure 5 shows the specimen and steel frame. The specimen is composed by two 12(18)x625x450 mm plybamboo sheets, two 75x50x450 mm studs and one 75x75x450 mm stud joined together as shown in Figure 4-a. The sizes of the screws and the nails are 4.9x49 mm and 4.1x88 mm respectively. The support for the horizontal sheet consists of a steel cylinder joined to a steel plate at the extremes and is able to rotate around its longitudinal axis. The sheet is fastened to the cylinder so that when the load is applied it can rotate. The vertical sheet rests on a wood piece with a small channel, which allows the rotation of the sheet. A 10 kN load cell that measures the load transmitted by the connection supports the wood piece. H-steel beams compose the steel frame and its function is to support the steel cylinder and the load cell. The loading system consists of two hydraulic jacks and a load cell previously mentioned. One jack is placed in a compression machine and the other one is placed above the specimen and is held by an upper H-beam. The two jacks are connected by an oil pressure tube that transmits the pressure applied to the jack on the compression machine to the one above the specimen. The advantage of doing so is that the displacement is controlled by the speed system of the compression machine. The load cell under the specimen measures the transmitted load every five seconds at a speed rate of 1 mm/min. The deformation measurement system consists of five digital dial gages placed on different positions of the specimen (see Figure 8-a).

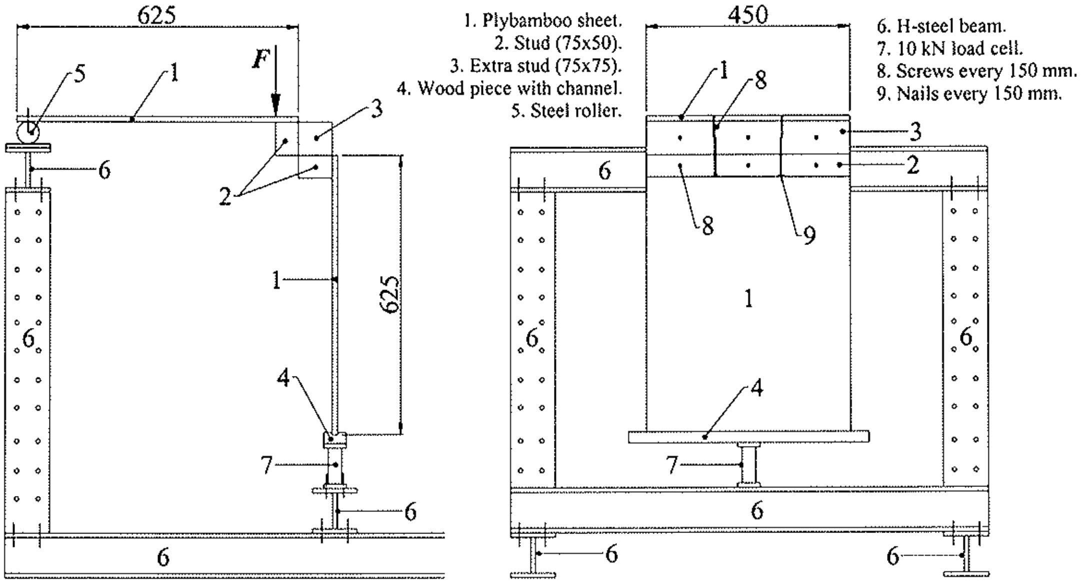

Front view **Side view**

Figure 5. Corner connection test setup.

3.2.2 T-connection

The steel frame used for the corner connection tests was modified in order to fixate the model for the T-connection. The frame offers an independent fixed reference system for measurement of displacements as well. Figure 6 shows the specimen and steel frame. The part numbers are referred to Figure 5. The specimen consists of three 12(18)x625x450 mm plybamboo sheets and three 75x50x450 mm studs joined together as shown in Figure 4-d. The supports for the horizontal and vertical sheets are the same as the ones used for the corner connection. H-steel beams compose the steel frame. As for the corner connection, two hydraulic jacks and a load cell are used to measure loads. The loading system is the same as the one applied for the corner connection. The deflection measurement system consists of three digital dial gages placed on different positions of the specimen (see Figure 8-b).

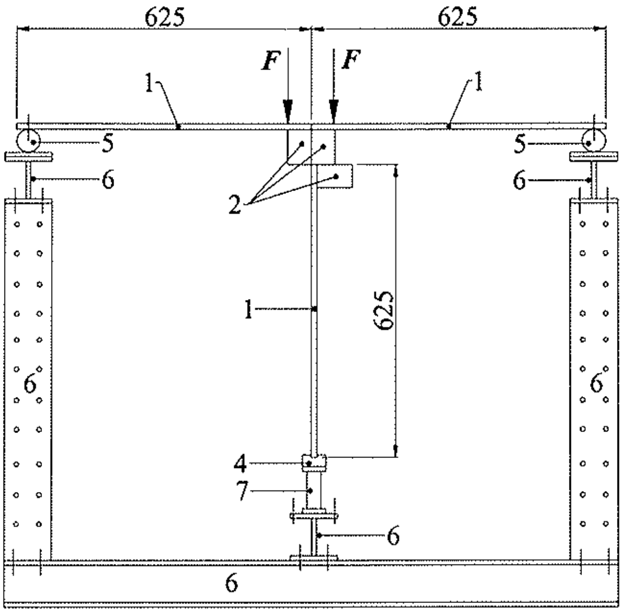

Front view

Figure 6. T-connection test setup.

3.2.3 Sheet-to-frame connection under lateral load

The test specimen consists of a plybamboo sheet joined to a wooden frame as shown in Figure 7. Screws (4.9x49 mm) spaced every 190 mm were used to join the studs to the sheets whereas nails (2.8x55 mm) were used to join the sheet to the top and sole plates. The test specimen was mounted on a steel frame consisting of two H-steel beams joined together forming a corner. The specimen is joined to the horizontal H-beam using two bolts at the extremes of the soleplate. Two steel bars joined to steel plates at each end are placed at the top of the specimen as shown in Figure 7. A hydraulic jack and a load cell are fixed to one of the steel plates and the vertical H-beam. The idea is to produce a concentrated load at the center of the top plate's cross-section. When the jack starts to pull the plate, the steel bars are pulled as well and transmit the load to the plate on the other extreme producing the wanted load. If the jack were pushing instead of pulling it would restrict the rotation of the loading point. A pneumatic pump at an approximate rate of 1 kN/min applied the load. The measurement of deformations system consists of three different displacements: diagonal elongation of the wooden frame, diagonal elongation of the sheet and horizontal displacement of the top plate. For the diagonal deformations, an aluminum tube is fixed to the opposite corners of the wooden frame or sheet and a LVDT that can freely rotate (Figure 8-c).

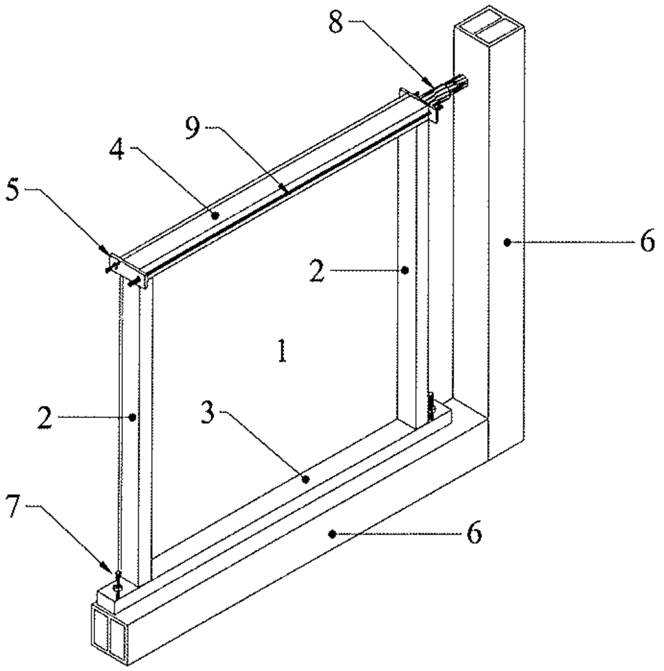

1. Plybamboo sheet (12 or 18 x1200x1200).
2. Studs (75x50x1100).
3. Soleplate (75x50x1400).
4. Top plate (75x50x1200).
5. Steel plate.
6. H-steel beams.
7. Bolts.
8. Hydraulic jack and load cell.
9. Steel bars.

Figure 7. Sheet-to-frame connection under lateral load test setup.

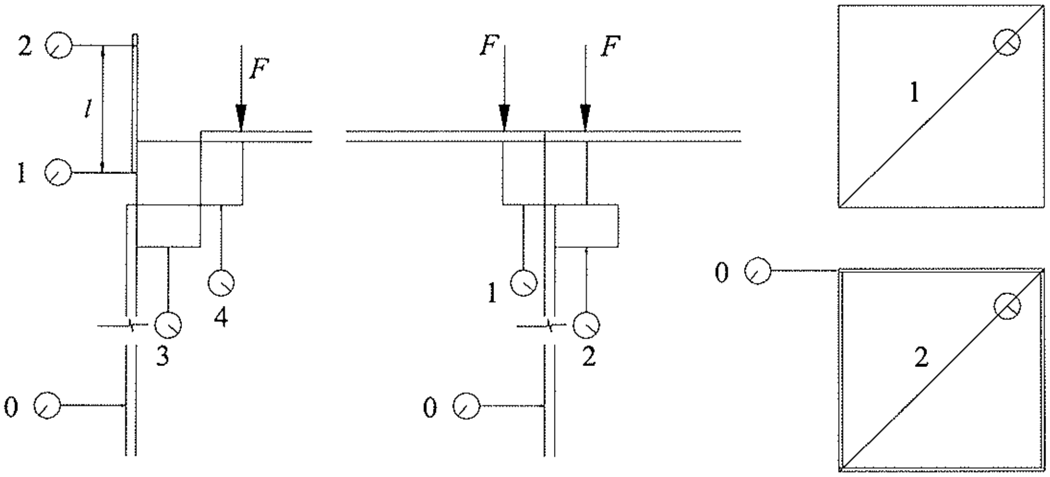

(a) Corner connection deformations

(b) T-connection deformations

(c) Sheet-to-frame connection deformations

Figure 8. Measurement of deformation details.

4 Discussion of results

4.1 Corner connection

Nine experimental tests were carried out in total. The first three (M-n, M-g, M-s) were part of an exploratory phase. M-n is the corner connection shown in Figure 4-a but using nails (2.8x55 mm) instead of screws (4.9x49 mm). The ultimate load for this test was around 0.5

kN (see Figure 9) or 0.17 kN/nail (see Table 2). It seems that the bending moments produced at the connections between the studs and the sheets are causing the withdrawal of the nails that join them. The moment capacity of these regions is so small that with a low load the connection becomes a mechanism where two hinges are formed. From this test, it was concluded that the corner connection becomes weak if only nails are used to join the studs and the sheets. M-g is the same as M-n but using glue between the studs and sheets. As expected, M-g was stronger than M-n (see Figure 9). The ultimate load was 2.4 kN or 0.8 kN/nail, which is almost five times higher than M-n. The reason is that now the moment capacities are higher due to the glue. M-s is the screwed connection shown in Figure 4-a. It behaved similar to M-g in terms of ultimate load and stiffness. The ultimate load was 2.46 kN or 0.82 kN/screw. The capacity of the load cell utilized for the previous three tests was 2 kN. Hence, the Load-Displacement curves were obtained until 2 kN of load. The ultimate load for M-g and M-s was derived from the maximum load registered by the compression machine and the relation between the previous readings of the load cell and compression machine. After the exploratory phase, six more tests were carried out based on the M-s prototype. Three were done using bamboo mat boards (M1, M2, M3) and three using bamboo strip boards (S1, S2, S3). The results can be seen in Figure 9. The ultimate loads for M1, M2 and M3 were 2.6, 3.2 and 3.6 kN or 0.87, 1.07 and 1.20 kN/screw respectively. The behavior of these tests can be summarized in three phases: linear-elastic, loss of stiffness and ductile phase. During the first phase, the screws that have not yet plastically deformed take the bending moments produced in the connection. In the second phase the screws yield and the nails are withdrawn from one of the studs (Figure 9, top photograph). In the last phase, the screws keep deforming plastically and the nails are constantly being withdrawn with no increasing of the load. During the previous process, the vertical sheet is bent due to eccentric loading. The ultimate loads for S1, S2 and S3 were 4.3, 3.95 and 3.80 kN or 1.43, 1.32 and 1.27 kN/screw respectively. The behavior of these three tests is similar to the previous ones but stronger and stiffer due to the thickness of the strip boards (18 mm) that avoids the bending out-of-plane (Figure 9, bottom photograph). Nevertheless, the ductile phase is not present. Theoretical analyses of the corner connection were carried out based on the failure modes observed during the tests, theoretical capacities of the joints [8] and equilibrium equations. The results were close to the experimental values considering the variability that could be expected in these type of structures [7].

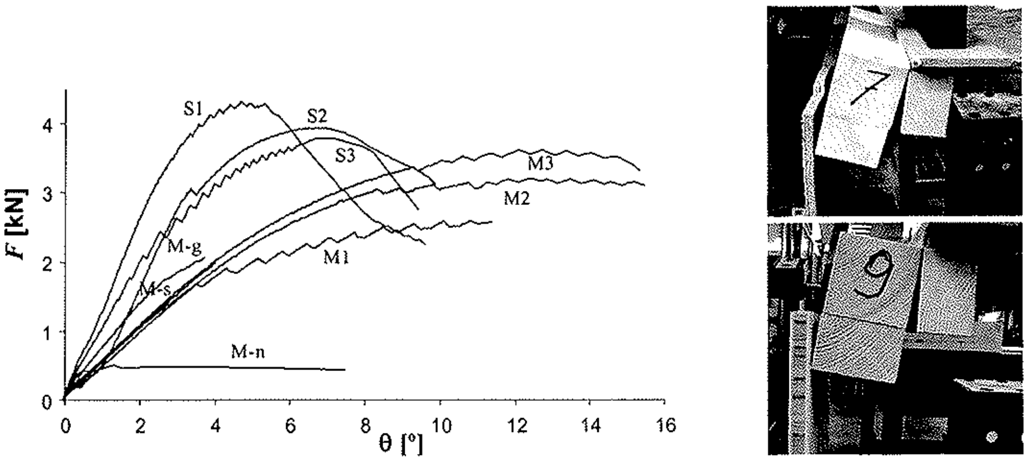

Figure 9. Load-Displacement curves and failure modes for corner connection.

4.2 T-connection

For the T-connection seven tests were performed. Four were made using bamboo mat boards (M1, M2, M3, M4) and three using bamboo strip boards (S1, S2, S3). The results can be seen in Figure 10. The ultimate loads for M1, M2, M3 and M4 were 16.1, 15.3, 12.5 and 13.0 kN or 5.37, 5.10, 4.17 and 4.33 kN/nail respectively. The structural response shown in Figure 10 is basically that one of the vertical sheet under eccentrically axial compressive loading and hence the strength is limited by the load at which buckling of the sheet occurs. Moreover, there are other factors that affect the behavior such as the nailed connection between the studs. At failure, the vertical panel is allowed to rotate at the top due to the withdrawal of the nail joining two of the studs (see Figure 10, top photograph). The ultimate loads for S1, S2 and S3 were 16.0, 14.0 and 20.0 kN or 5.33, 4.67 and 6.67 kN/nail respectively. Since the axial compression strength of the strip boards is much higher, the tests were stopped when displacement number 1 was around 5 mm (see Figure 8-b and Figure 10, bottom photograph).

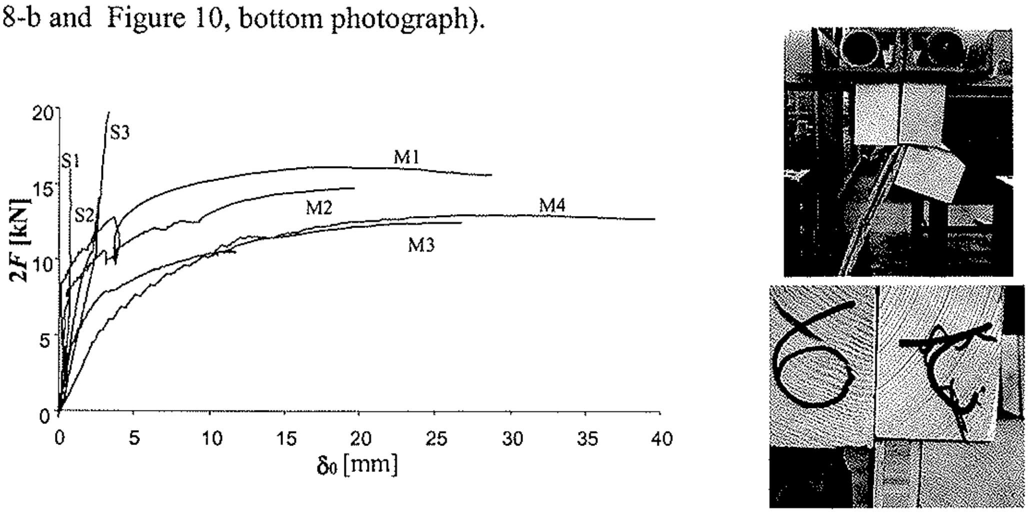

Figure 10. Load-Displacement curves and failure modes for T- connection.

4.3 Sheet-to-frame connection under lateral load

Seven tests were made in total. The first four were done using bamboo mat boards (M1, M2, M3, M4) whereas the other three were done using bamboo strip boards (S1, S2, S3). The results can be seen in Figure 11. The ultimate loads for the mat boards were 5.4, 4.4, 5.4 and 1.8 kN or 0.77, 0.63, 0.77 and 0.26 kN/nail. The latter one was carried out without the angle plates that join the studs to the top and bottom soleplates and hence the lower value (see Figure 11, top photograph). For the strip boards, the ultimate loads were 4.7, 4.1 and 4.6 kN or 0.67, 0.58 and 0.66 kN/nail. Since the embedding strength of the mat boards (92 N/mm^2) is higher than that one of strip boards (86 N/mm^2), the slightly higher value obtained for mat boards is understandable [6]. The structural response shown in the experimental tests is quite typical for wooden-framed walls under lateral load. That is, nonlinear behavior due to the nailed connections between sheet and frame controlling the stiffness [9,10]. It must be added that the failure was due to the withdrawal of the steel angle screws joining the stud and the soleplate (Figure 11, bottom photograph). If this connection had been stronger, the specimen would have probably deformed more gaining ductility like M4 at higher load levels. The theoretical capacity of the sheet-to-frame connection per nail is 0.89 kN for mat boards [7]. An easy way to calculate the lateral capacity of the specimen is multiplying this capacity by the number of nails joining the sheet to the top and sole plates. For the specimen used in the tests, 7 nails were used in this connection and hence the theoretical capacity would be 0.89x7 = 6.2 kN. The strength loss in the experiments is due to the uplifting of the stud as previously explained.

Table 2. Experimental capacities for each test.

	Capacity per fastener in kN						
Connection	M1	M2	M3	S1	S2	S3	M4
Corner	0.87	1.07	1.20	1.43	1.32	1.27	0.17*
T	5.37	5.10	4.17	5.33	4.67	6.67	4.33
Sheet-to-frame	0.77	0.63	0.77	0.67	0.58	0.66	0.26

* Value corresponding to the M-n test.

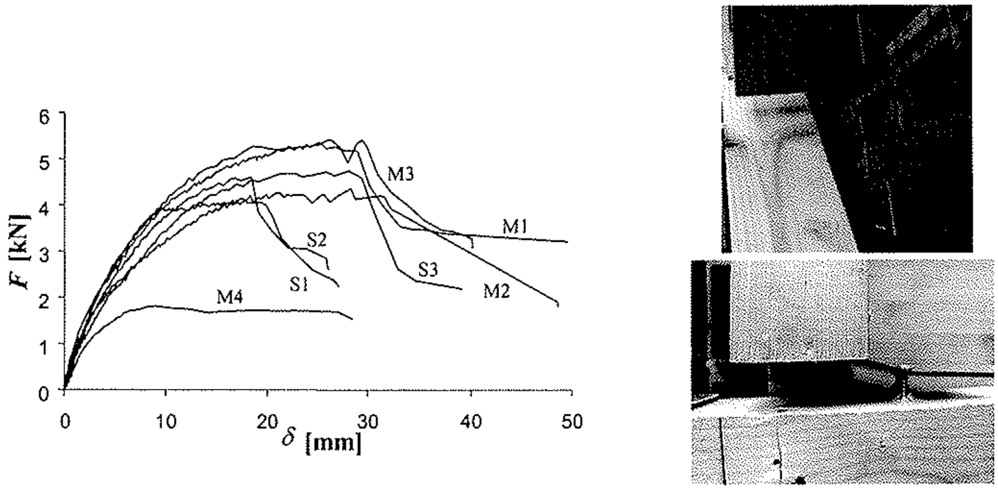

Figure 11. **Load-Displacement curves and failure modes for the sheet-to-frame connection. Top photo: uplifting of stud due to nail deformation. Bottom photo: Uplifting of stud due to withdrawal of the screws.**

5 Conclusions

The capacity of the corner connection shown in Figure 4-a needs certain withdrawal strength, which cannot be provided if nails are used instead of screws. It can be calculated that the required load per fastener in this corner connection is about 0.35 kN for a wind load pressure of 1.9 kN/m^2 and a tributary width of 1.22 m (1.9x1.22x0.15). This load is higher than the experimental value (0.17 kN/nail, Table 2). It would be then necessary to test the full-scale corner connection with roof and foundation to find whether the withdrawal effect occurs. The use of glue (in addition to nails) or screws increases more than five times the capacity of the corner connection according to the experimental results. However, the one with screws is able to deform more than the glued one. Both the glued and screwed corner connections seem to be able to withstand the required load for high wind with a safety factor higher than two. The corner connection with bamboo strip boards is stronger and stiffer but less ductile than that one with bamboo mat boards.

The lowest experimental capacity obtained for the T-connection of Figure 4-d (4.2 kN/nail) is about six times higher than the required capacity for high wind load (0.7 kN/fastener) which makes it the strongest link of the structural chain covered by the experiments. The T-connection using strip boards is stronger than that one using mat boards because of the higher stiffness (due to the thickness) of the first ones.

The sheet-to-frame connection under lateral load showed in all cases ductile behavior (capacity to deform with small increase of load), which is adequate for seismic or wind load. The theoretical capacity (0.89 kN/nail) is higher than the experimental one (0.68 kN/nail in average) due to the connection between the studs and the soleplate, which in the end limits the strength of the connection. The shear capacity of the wall-panel is around 4.8 kN/m (0.68x7) and the capacity of a house against seismic or wind loading will depend on the wall-panel arrangement. Tests on full-scale panels should be carried out in order to corroborate this result. Attention must be paid to the steel angle connections.

To finish the paper, it can be concluded that the obtained results show that all the investigated connections present ductile behavior adequate for seismic and wind loads. Both mat boards or strip boards could be implemented but strip boards are more suitable for furniture or floors and more expensive and hence the mat boards are preferred and will be further investigated. The next step would be to investigate the element behavior (wall-panel) and full-scale connections including roof and foundation connections.

References

1. González, G.E et al (2001). Selection criteria for a house design method using plybamboo sheets. Journal of Bamboo and Rattan. Vol.1, No.1, p59-70. ISSN 1569-1568.
2. FUNBAMBU (1998). Bamboo Housing Technology Transfer Workshop. Costa Rican Bamboo Foundation. Guápiles. Costa Rica.
3. IPIRTI (1999). Manufacture of Bamboo Mat Boards, a manual. Project Bamboo Mat Board. India. 27p.
4. Yao, S. (1999). Bamboo Strip Boards properties. Values provided to the author. Internet page: http://www.china-qingfeng.com.
5. NEN 6760 (1997). Nederlands Normalisatie Instituut (Dutch Institute for Standardization). Houtconstructies (Timber construction) TGB 1990. Technische Grondslagen voor Bouwconstructies (Technical principles for buildings). Basiseisen (Basic demands). Eisen en bepalingsmethoden (Demands and determination methods). 102 p.
6. González, G.E. (2000). Determination of the embedding strength of plybamboo. Eindhoven University of technology. Report CO-01-03. The Netherlands. 42p.
7. González, G.E. (2001). Joint properties of plybamboo sheets in prefabricated housing. Eindhoven University of technology. Report CO-01-19. The Netherlands. 76p.
8. Eurocode 5 (1993). Timber structures. Part 1-1. General rules and rules for buildings. European Committee for Standardization (CEN). English version. 110p.
9. Filiatrault, A., Folz, B. (2002). Performance-based seismic design of wood framed buildings. ASCE Journal of Structural Engineering. January, 2002. Volume 128, number 1, p39-47. ISSN 0733-9445.
10. ASTM E 564-95 (1995). Static load test for shear resistance of framed walls for buildings. USA. 4p.

CIB-W18/35-7-12

INTERNATIONAL COUNCIL FOR RESEARCH AND INNOVATION
IN BUILDING AND CONSTRUCTION

WORKING COMMISSION W18 - TIMBER STRUCTURES

FIBER-REINFORCED BEAM-TO-COLUMN CONNECTIONS FOR SEISMIC APPLICATIONS

B Kasal
North Carolina State University

USA

A Heiduschke
P Haller
Technical University Dresden

GERMANY

Presented by: P Haller

H J Blaß asked how the embedding strength of the glass fibre components were calculated. P Haller replied that it could not be measured but that the glass fibre provided ductility and tensile strength to the connection. This led to discussion about the embedding strength of the textile material and B Dujic commented that the glass fibres prevented splitting of the timber by limiting the stress values perpendicular to grain. H Sugiyama then asked if static tests on the connection were also conducted. P Haller indicated that static tests were not carried out. A Leijten asked about the densification of the timber and if secondary effects were considered in analysing the data. P Haller indicated that the softwood was surprisingly amenable to the densification process and that secondary effects were not considered. S Thelandersson asked about the shrinkage and swelling values of the normal timber and densified wood components of the connection. This was followed by a general discussion about the definition of normal indoor climate and the equilibrium moisture content of the densified veneer wood. B Yeh then asked if P Haller knew of tests on finger joints which have been reinforced in the manner presented and A Leijten asked about the oversize of the dowel holes. P Haller replied that he did not know of similar tests on finger joints and that usual tolerances were used for dowel holes. H J Blaß asked if the type of reinforcement used affected failure loads and the resulting failure modes. P Haller commented that the fibre reinforcement did affect the failure mode and consequently the failure load. He was of the view that the differences in observed failure loads was a function of failure mode rather then direct contribution of the glass fibre's strength.

Fiber-reinforced beam-to-column connections for seismic applications

Bo Kasal
Department of Wood and Paper Science, North Carolina State University, NC, USA;
Senior Fulbright Fellow, Department of Civil Engineering, TU Dresden, Germany.
Andreas Heiduschke, Peer Haller
Department of Civil Engineering, Technical University Dresden, Germany.

1 Introduction

Wood structures perform extremely well when subjected to earthquake loading. Low mass, good dissipative parameters of connections and the capability to undergo large deformations result in wood structures having relatively high safety under dynamic loads. Numerous examples from the US document that light-frame structures are among the safest structures in earthquake regions (over 90% of the US residential homes are built as light-frame wood buildings). Light-frame structures contain low-mass members, a large number of ductile connections in shear walls and are subjected to low dead and live loads. However, heavy timber frames are designed to carry relatively high loads and must rely on few engineered connections. The dissipative capacity of the wood is low due to its low material damping. Therefore, if heavy timber construction is to perform well in an earthquake, the connections must be able to carry the loads while deforming plastically to dissipate enough energy. This may create contradictory design requirements when we require the connection to have high capacity and ductility at the same time. The use of timber frames in Europe is limited to two stories, in exceptional cases up to four stories (Lignatec 2001), and applications in seismic areas are rare. The research work presented herein shows the potential for use of multistory timber frames in seismic areas due to their excellent dissipative properties, high load-carrying capacity and low mass. In addition to the dynamic properties, high fire resistance makes these structures good candidates for commercial and public buildings.

As mentioned above, a key issue in heavy timber frame application is connection performance. Typically, beam-to-column connections are facilitated by steel mechanical fasteners, such as dowels, drift pins or bolts. Steel plates are sometimes used to facilitate the moment transfer. Use of atypical, fastening techniques, such as glued-in rods or large finger joints, is rare. While connections with mechanical fasteners have high ductility, they suffer from low moment carrying capacity relative to the solid members and brittle-type of failure in wood material around dowel-type fasteners due to tension perpendicular to wood fibers. Past research in application of technical textiles in timber connections showed that fiber-reinforced joints have significantly higher capacity when loaded by a monotonic static load (Haller et al. 2001). Research performed at TU Dresden shows as the ultimate capacity and the ductility of the monotonically loaded connection increases (Haller 1997 and Haller et al. 1994). This is due to the prevention of tensile failure in perpendicular-to-fibers direction that results in an increase in apparent dowel-bearing strength. Recent experiments with fiber-reinforced densified wood indicate that dowel-bearing strength can be further improved without joints suffering from brittle failures due to tensile stresses perpendicular to fibers. While most of the research has been carried out on monotonically loaded spliced joints, no data for fiber-reinforced joints are available for beam-to-column connections and cyclic loads. Such experiments are necessary to evaluate the behavior of joints subjected to dynamic or even wind loads.

The goal of the experimental research program was to investigate cyclic performance of fiber reinforced and densified beam-to-column connections to design an effective joint capable of performing under extreme earthquake loads. The ultimate goal was to design, manufacture and tests a full-size, two-story glue-laminated heavy timber frame under dynamic loading.

2 Materials and Methods

Since no prior experiments with fiber reinforced and densified beam-to-column connections were available, the scaled models of connections and frames were manufactured and tested followed by full-scale tests of beam-to-columns connections and frames. The beam-to-column connections were tested under static-cyclic loads while the frames were tested on a shake table using sinusoidal sweep function and arbitrary dynamic load.

Wood of European spruce (Picea excelsa) was used. The undensified material had an average density of 0.44 g/cm^3 and a moisture content of 9 %. Densification was performed in a hydraulic press with a pressure of 7 MPa and a plate temperature of 150 °C. The densification lasted 90 min with resulting average density of 0.87 g/cm^3 (MC of 9 %). Small- and full-scale beam-to-column connections were manufactured and tested using the DIN EN 12512 (1996) cyclic test protocol – see Tables 1a, 1b, and Figure 1.

Table 1a. Test protocol for cyclic tests of the scaled beam-to-column connections.

Yield displacement v_y = 8mm; (constant test speed 5 mm/s); (3 loops/cycle)

Cycle number	1	2	3	**4**	5	6	7	8	9	10	11	12
(value)*v_y	0,25	0,5	0,75	**1**	1,5	2	2,5	3	4	5	6	7
Amplitude (mm)	2	4	6	**8**	12	16	20	24	32	40	48	56
Joint rotation (rad)	0,01	0,02	0,03	**0,04**	0,06	0,08	0,10	0,12	0,16	0,20	0,24	0,28

Table 1b. Test protocol for cyclic tests of the full-size beam-to-column connections.

Yield displacement v_y = 28mm (see Figure 2c); (constant test speed 2 mm/s); (3 loops/cycle)

Cycle number	1	2	3	**4**	5	6	7
(value)* v_y	0,25	0,5	0,75	**1**	1,8	2,6	3,4
Amplitude (mm)	7	14	21	**28**	50	72	94
Joint rotation (rad)	0,01	0,02	0,03	**0,04**	0,07	0,10	0,13

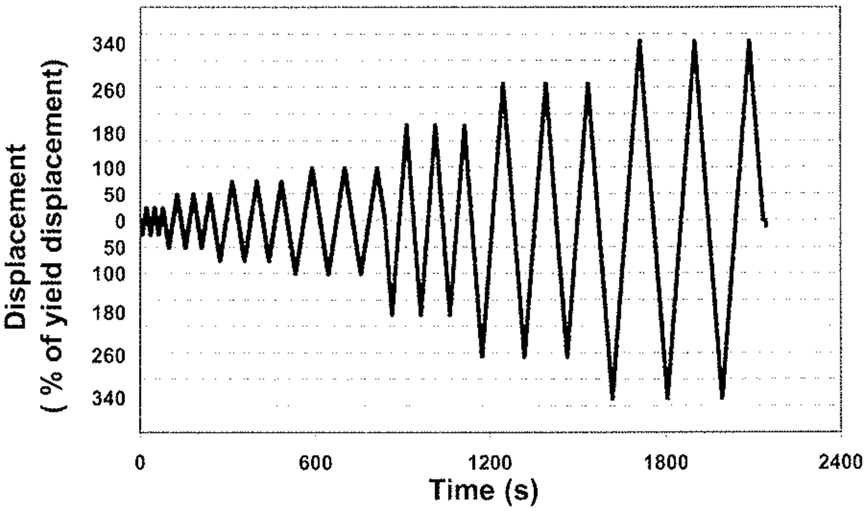

Figure 1. Test protocol used for cyclic tests of full-size beam-to-column connections.

Different loading speeds for scaled and full-size connections were due to the equipment limitations. However, both deformation rates can be considered as quasi-static and will have no significant effect on the behavior of the tested connections. The cycle number 4 (bold font) represents a 100% displacement at maximum load. Data in Tables 1a and 1b indicate that after the yield displacement was reached the increment in amplitude was smaller than the one required by the DIN EN 12512 (1996) standard.

It appears that the standard test protocol for cyclic loading requires testing the joints in displacements that are unrealistic in practical applications. Let's assume that the model frame is 1200 mm high. A rotation of the beam-to-column connection of 0.2 rad (11.5°) will cause a drift of 240 mm; the drift at the joint ultimate capacity will be about 48 mm – 1/25 of the frame height. Clearly, such drifts are well beyond generally accepted safe values and it is unlikely that a frame will reach such magnitudes of drift without catastrophic failure due to the second order effects.

2.1 Scaled model tests

The dimensions of scaled specimens (Figure 2a) were based on the geometry of the full-size test specimens (Figure 3) with a scaling factor of 0.25 (1:4). This scaling was selected to maintain the relative geometry of the joints since the joints were the focus of interest. The pins were made of structural steel with a yield point of 235 MPa.

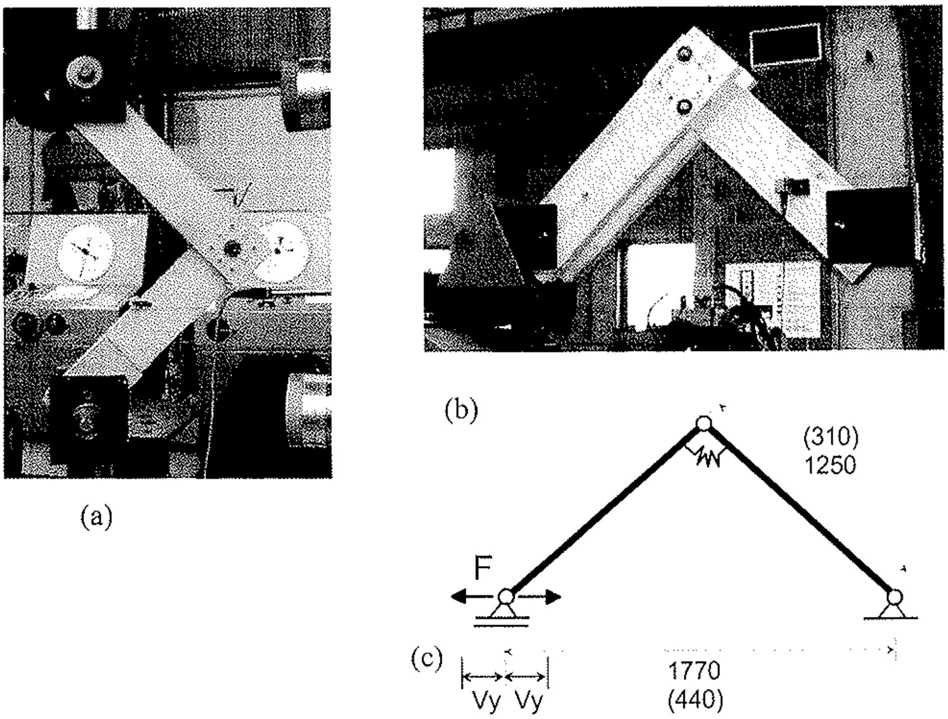

Figure 2. Test specimens of beam-to-column connections tested under cyclic load: (a) scaled specimens (1:4), (b) full-size specimens (c) schematic of the tests (values in parenthesis represent dimensions for scaled specimens).

The parameters of the E-glass fiber-reinforcing non-woven fabric with the weight of 200 g/m^2 are listed in Table 2 ((3)).

Table 2. Parameters of materials used in composites for the reinforcement.

Material	Tensile strength [MPa]	MOE [GPa]	Failure strain [%]	Density [g/ cm ^{3}]
E-Glass	1300-1600	73	2	2,6
Epoxy [(1)]	60-90	3,7	4	1,2
Melamine [(2)]	30	N/A	N/A	1,3
Composite (Glass/EP) (BD-Fabric 200g/m^2) [(3)]	220	12	2	1,6
Composite (Glass/EP) (TD-Fabric 1300g/m^2) [(4)]	550	8,5	3	1,7
Composite (Glass/MH) (TD-Fabric 1300g/m^2) [(4)]	N/A	N/A	N/A	1,7

[(1)] EP = Epoxy resin (Dow chemical: EPON Resin 828; CURING AGENT 9551).
[(2)] MH = Melamine resin (BASF: Kauramin Resin 691; Kauramin Hardener 686).
[(3)] BD = Bi-Directional woven fabric with 0°/90° oriented fiber
[(4)] TD = Tri-Directional stitch bonded fabric with –45°/0°/45° oriented fiber placement

Epoxy resin was used to bond the fabric to wood. The fabric was attached to each surface of the beams and column such that the glass fiber was oriented across the wood fiber.

Three different joint configurations were designed to test various options – see the first column in Table 3. The first connection type was a circle 54 mm in diameter consisting of 12 dowels with a diameter of 3mm. The second joint had total of 8 dowels (4 dowels (d = 5mm) and 4 dowels (d = 3mm)), the third connection had only 4 dowels (d = 5mm). The joints were designed to meet the requirements of DIN 1052 T2 (1988) for edge distance, end distance and spacing.

The experiments were performed using a servo mechanical testing machine with the full-scale load cell capacity of 10 kN. The deformations of the crosshead were used but the error was checked using an independent displacement transducer. Since the translational deformations were large, the error from the crosshead reading was negligible (less than 1 %) and crosshead position was used for displacement measurement. A constant speed of the crosshead of 300 mm/min was used. This means that the frequency of the displacement was decreasing with increasing amplitude. The angular displacement was calculated from the specimen geometry and deflection of the members was neglected.

2.2 Full-scale beam-to-column connection tests

Figure 2b shows the full-size beam-to-column connection. The beams and columns were vertically laminated and each interface between layers was reinforced by glass-fiber non-woven fabric (see Table 2 (4)). The cross sections of the columns were 160x290 mm, with lamination thickness of 2x20mm (Figure 3). To achieve a width of 290 mm, laminations were edge-glued from two pieces 100 mm and 200 mm wide. This configuration was staggered in adjacent layers. The beams had a cross section of 80x290 mm and were laminated in the same manner as columns. The relatively large width of the members was a result of the gravity load design and the need to facilitate sufficient area for the beam-to-column connection. Melamine resin was used to connect wood and the glass fiber in the laminated beams and columns. The contact surface between beams and columns was reinforced using the same fabric and epoxy resin was used to connect fabric and wood.

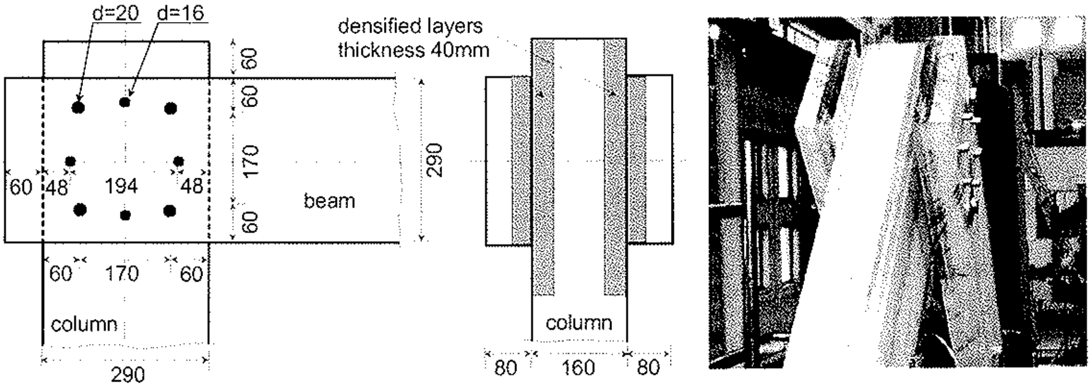

Figure 3. Connection detail and three-dimensional view of a partially densified and reinforced full-size specimen. Only first two laminations (2x20mm) at the interface between the beams and column were densified.

Again, the spacing requirements followed the German standards (DIN 1052) as did the scaled models. The German standard allows closer spacing and end and edge distances than the EUROCODE 5 (1995) and EUROCODE 8 (1998). Tests of groups of fasteners and fiber-reinforced joints indicate that the spacing requirements originally designed for unreinforced wood can be too conservative. This is because the reinforcement prevents or postpones initiations of cracks due to stresses in tension perpendicular to wood fibers. Some of the specimens did not have all layers made of densified wood (Table 4). This configuration was selected to investigate the failure modes of vertically laminated members with uneven dowel bearing capacities. The tests were performed at ENEL (ENEL.Hydro) in Bergamo, Italy, using a servo-hydraulic testing machine with a full load cell capacity of 100 kN. Again, the DIN EN 12512 (1996) test protocol was used to apply cyclic loading (see Table 1b and Figure 1).

3 Results and Discussion

The moment-rotation relationship for the scaled specimens and for full-size specimens is shown in Figure 4 a, b and c.

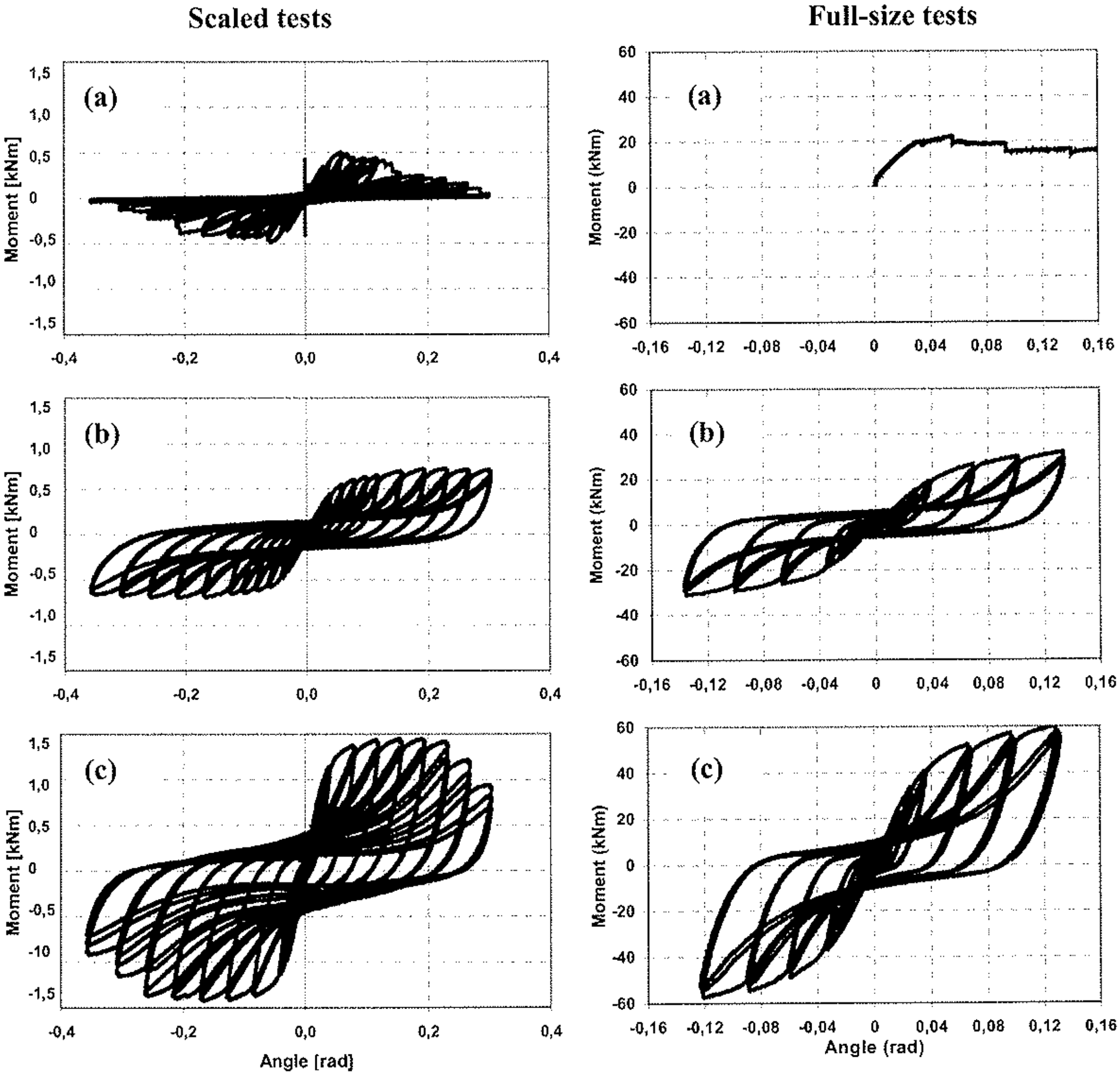

Figure 4. Moment-rotation relationships for (a) unreinforced and undensified joint, (b) reinforced and undensified joint and (c) reinforced and densified joint.

3.1 Scaled models tests

Typical moment-rotation relationship for the three different types of connections is shown in Figure 4. The data indicate that all different configurations behave similarly.
Table 3 lists the average ultimate capacities, rotations and dissipated energy of the joints.

Table 3. Test results of scaled models of beam-to-column connections

Number of dowels and diameter	Material	Ultimate capacity [M_{max}] (kNm)	Joint rotation [φ] at M_{max} (rad)	Number of cycles at M_{max}	Dissipated energy [E_φ] at rotation φ (kNm-rad)	
					$E_{0,04}$	$E_{0,2}$
12 dowels (12x3mm)	Undensified, unreinforced	0,512	0,117	8	0,061	0,69
		0,503	0,144	9	0,031	0,55
		0,526	0,155	9	0,034	0,67
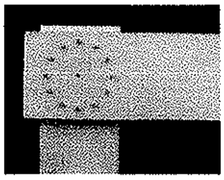		0,521	0,155	9	0,033	0,59
	$\overline{X}$ (1)	**0,516**	**0,143**		**0,040**	**0,625**
	Undensified, reinforced	0,720	0,192	10	0,038	0,80
		0,717	0,192	10	0,042	0,79
		0,722	0,192	10	0,040	0,78
		0,704	0,192	10	0,039	0,77
	$\overline{X}$	**0,715**	**0,192**		**0,040**	**0,785**
	Densified, reinforced	1,161	0,155	9	0,093	2,58
		1,174	0,079	6	0,139	2,95
		1,152	0,155	8	0,102	2,76
	$\overline{X}$	**1,162**	**0,130**		**0,111**	**2,76**
8 dowels (4x5mm; 4x3mm)	Undensified, unreinforced	0,492	0,068	6	0,047	0,58
		0,502	0,055	5	0,046	0,56
		0,501	0,061	5	0,034	0,53
		0,578	0,079	6	0,049	0,65
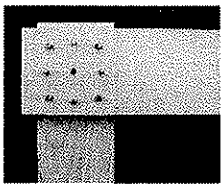	$\overline{X}$	**0,518**	**0,173**		**0,044**	**0,58**
	Undensified, reinforced	0,725	0,154	9	0,051	1,03
		0,830	0,154	9	0,054	1,09
		0,726	0,192	10	0,045	1,00
		0,748	0,192	10	0,047	1,01
	$\overline{X}$	**0,767**	**0,192**		**0,049**	**1,03**
	Densified, reinforced	1,437	0,155	9	0,116	2,89
		1,548	0,154	9	0,113	3,42
		1,447	0,154	9	0,115	2,69
	$\overline{X}$	**1,477**	**0,154**		**0,114**	**3,00**
4 dowels (4x5mm)	Undensified, unreinforced	0,406	0,126	8	0,039	0,63
		0,397	0,098	7	0,026	0,45
		0,383	0079	6	0,033	0,41
		0,435	0,098	7	0,037	0,57
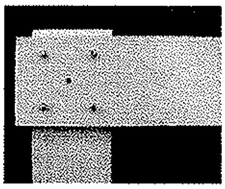	$\overline{X}$	**0,405**	**0,100**		**0,037**	**0,52**
	Undensified, reinforced	0,556	0,192	10	0,052	0,94
		0,537	0,192	10	0,038	0,78
		0,560	0,192	10	0,041	0,85
		0,542	0,192	10	0,042	0,81
	$\overline{X}$	**0,549**	**0,192**		**0,043**	**0,85**
	Densified, reinforced	-	-	-	-	-
		-	-	-	-	-

(1) $\overline{X}$ = average value

The data in Table 3 show that the densified and reinforced joints have a higher capacity than undensified and unreinforced connections. The deformation at the ultimate capacity indicates that fiber reinforced connections will exhibit high ductility while having increased stiffness and strength. The energy dissipation capacity expressed as an area enclosed by a hysteretic loop is compared in Figure 5. Figure 5 shows that the densified and reinforced joints are superior to the other two and will dissipate more energy.

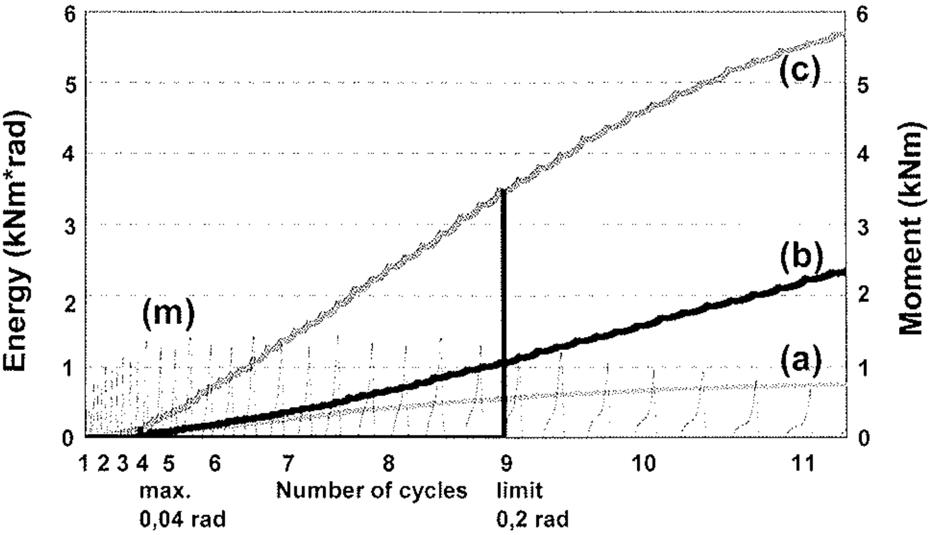

Figure 5. Scaled model (1:4) experiments. Energy dissipation measured as the area enclosed by hysteretic loops: (a) unreinforced and undensified joint, (b) reinforced and undensified joint, (c) reinforced and densified joint and (m) moment (3 loops per cycle)

3.2 Full-size beam-to-column connection tests

Typical moment-rotation relationships for the three different types of connections are shown in Figure 4. Figure 4 indicates that all different configurations behave similarly. Table 4 lists the average ultimate capacities and deformations of the joints, and shows that the densified and reinforced joints have about 3-times higher capacity as compared to undensified and unreinforced connections. The deformation at the ultimate capacity indicates that fiber reinforced connections will exhibit high ductility while having increased stiffness and strength.

Table 4. Test results of full-size beam-to-column connections

Number of dowels and diameter	Materials	Ultimate capacity [M_{max}] (kNm)	Joint rotation [φ] at M_{max} (rad)	Number of cycles at M_{max}	Dissipated energy [E_φ] at rotation φ (kNm-rad)	
					$E_{0,04}$	$E_{0,2}$
8 dowels (4x20mm; 4x16mm)	Undensified, unreinforced	19,7	0,032	monotonic test	monotonic test	monotonic test
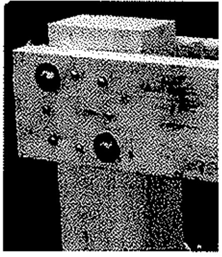	Undensified, reinforced	28,1	0,131	7	2,62	24,9
	Partially densified, reinforced	(43,3)$^{(*)}$ 60,4	(0,052) 0,128	(5) 7	(5,24) 5,16	(-) 47,6
	Fully densified, reinforced	63,5	0,117	7	5,57	54,7

(*) Shear failure at the interface between densified and undensified laminations in the reinforcement layer. The failure was due to the insufficient volume fraction of the matrix.

The average backbone curves are shown in Figure 6.

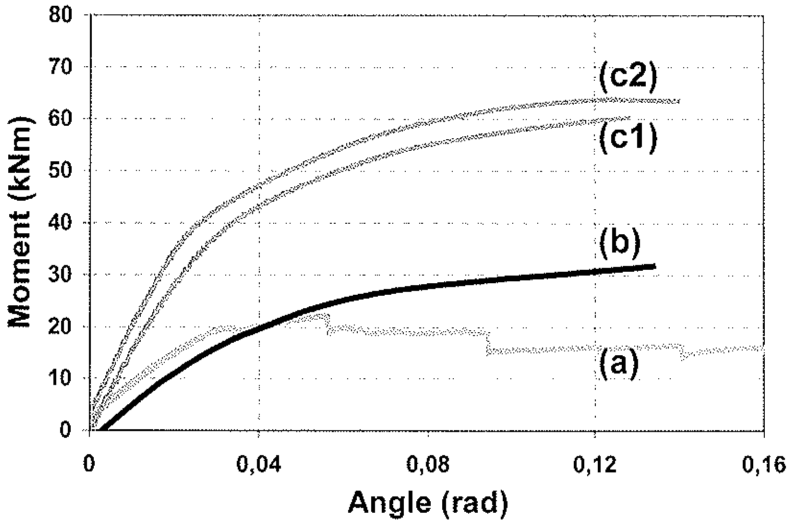

Figure 6. Full-size experiments. Average backbone curves for the four different joint configurations. (a) unreinforced and undensified joint, (b) reinforced and undensified joint, (c1) partially densified and reinforced joint and (c2) fully densified and reinforced joint.

The energy dissipation capacities expressed as an area enclosed by a hysteretic loop are compared in Figure 7 shows that the densified and reinforced joints are superior to the other two and will dissipate more energy. The differences increase with increased rotation of the joint.

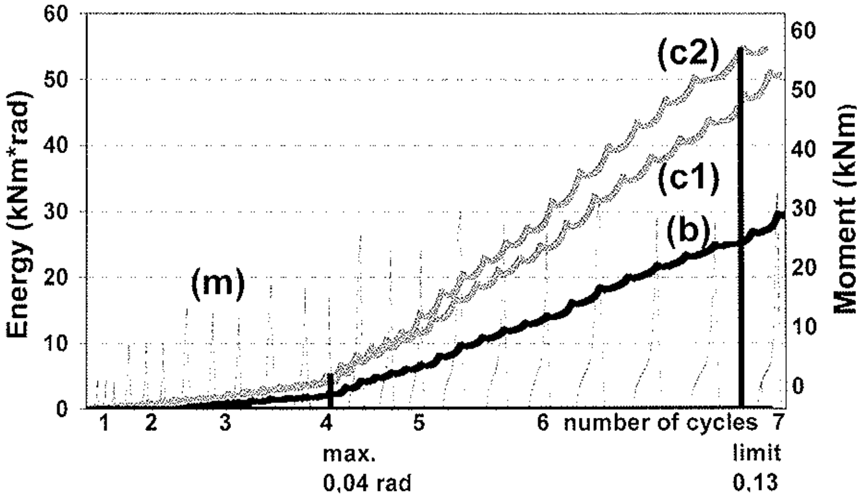

Figure 7. Full-size experiments. Energy dissipation measured as the area enclosed by hysteretic loops. (b) reinforced and undensified joint, (c1) partially densified and reinforced joint, (c2) full densified and reinforced joint and (m) moment (3 loops per cycle).

4 Conclusions

From these experiments it follows that densified material can significantly increase strength and energy dissipation capacity of beam-to-column connections. Using densified wood increases the dowel bearing strength of the material and dowels or pins of larger diameter can be used while still exhibiting plastic hinges. The low strength of wood in tension perpendicular to grain can cause a brittle failure, especially when densified material is used. Application of non-woven reinforcing fabric minimizes the risk of brittle failure and significantly increases ductility of the connections. It appears that the standard test protocols for cyclic tests of connections may not fully consider the range of realistic deformations that a connection can undergo in the structure. The test of reduced scale (1:4) and full-scale connections under cyclic loads indicate that the scaled models are excellent indicators of properties of full-size joints. Similar failure modes, behavior and relative properties of scaled and full-size connections allow one to use the scaled experiments to investigate dynamic behavior of subsystems and systems containing these connections. The experiments on scaled models and full-size two-story heavy timber frames will be reported in subsequent papers.

5 References

DIN 1052 T2 (1988). Timber Structures – Mechanical joints; Beuth Verlag, Berlin, Germany.

DIN EN 12512 (1996). Timber Structures – Test methods – Cyclic testing of joints made with mechanical fasteners; German version prEN 12512 : 1996, Beuth Verlag, Berlin, Germany.

EUROCODE 5 (1995). Design of timber structures, Part 1-1:General rules and rules for buildings; German version ENV 1995-1-1 : 1993, Beuth Verlag, Berlin, Germany.

EUROCODE 8 (1993). Constructions in seismic regions. Under preparation by TC 250 of CEN, Brussels, Belgium.

EUROCODE 8 (1998). Design provisions for earthquake resistance of structures – Part 1-3: General Rules – Specific rules for various materials and elements; German version ENV 1998-1-3 : 1995, Beuth Verlag, Berlin, Germany.

Haller P., Wehsener J., Birk T. (2001). Embedding characteristics on fibre reinforced and densified timber joints; proceedings, CIB-W18-meeting, Venice, Italy, August 2001.

Haller, P. (1997). Technische Textilien im Holzbau und ihre Möglichkeiten in der Verbindungstechnik, Bauen mit Textilien, Berlin: Ernst & Sohn, 1997 Heft 1, S. 11-12.

Haller, P., Chen, C. J., Natterer, J. (1994). Experimental study of fibre reinforced timber joints, Proceedings, Pacific Timber Engineering Conference, Gold Coast, Australia, July 1994, Vol. 2, p. 66-72.

Lignatec (2001). Holz und Brandschutz; Nr. 12/2001, Schück Söhne AG, Rüschlikon, Schweiz.

6 Acknowledment

This research was supported by the Fulbright Foundation, European Commission Human Potential Program and TU Dresden Sonderforschungsbereich SFB 528. The full-scale experimens were performed at ISMES Seismic Research Laboratory, Bergamo, Italy. The help of Paul Stephan Holzleimbau in Gaildorf (Germany) is gratefully acknowledged.

CIB-W18/35-8-1

INTERNATIONAL COUNCIL FOR RESEARCH AND INNOVATION
IN BUILDING AND CONSTRUCTION

WORKING COMMISSION W18 - TIMBER STRUCTURES

SYSTEM EFFECT IN SHEATHED PARALLEL TIMBER BEAM STRUCTURES

PARTII

M Hansson
T Isaksson

Division of Structural Engineering
Lund University

SWEDEN

Presented by: M Hansson

F Rouger and S Thelandersson commented on the weakest link criterion approach to studying system failure. H J Blaß commented on the bending strength used in obtaining the failure criterion and asked if bending - tensile interaction was considered. M Hansson replied that tensile strength values were not taken into account.

System Effect in Sheathed Parallel Timber Beam Structures

Part II

Martin Hansson, Tord Isaksson
Division of Structural Engineering
Lund University, Sweden

1 Abstract

This is a continuation of a paper by Hansson and Isaksson (2001) presented at meeting 34. A study on the system effect in sheathed parallel timber beam elements is presented. In Eurocode 5 a factor of 1.1 is given for such systems. In the present study Monte Carlo simulations are used to generate systems and to evaluate the influence of different parameters on the system behaviour. The variability within and between timber elements is accounted for using a model by Isaksson (1999). The properties of the sheathing are assumed to be deterministic and the property of the joint between beam and sheathing is varied. Reliability theory is used to evaluate the system effect. For a given reliability of a single member the reliability of a system is calculated. The reliability of a system is in general lower than for a single member. The study showed a system effect somewhere between 1.2 and 1.3, i.e. the load carrying capacity of a system is 20 to 30 % higher compared to the capacity of a system when it is evaluated on a single member basis.

2 Introduction

The design of timber structures or systems is usually based on the design of single elements. Two different effects are usually not taken into account:

- the fact that the single elements are interacting in the system, i.e. stronger beams carry more load than weaker ones.
- the lower probability that a weak part of the material coincides with a highly stressed part of the member.

The system is built up by a number of parallel, equally spaced, solid structural timber beams and a sheathing of plywood. The joint between sheathing and beam can be nailed, screwed or glued resulting in different effective bending stiffness and bending strength.

The background and a first outline of the system effect factor for sheathed parallel timber beam structures was presented in Hansson and Isaksson (2001).

3 Modelling of the system

3.1 Bending strength and modulus of elasticity of the beams

The bending strength is modelled using a statistical model of variability within and between members, Isaksson (1999). The strength of a section *i* in beam *j* is given by eq. (1), see also Figure 1.

$$f_{ij} = \exp(\mu + \tau_i + \varepsilon_{ij}) \quad (1)$$

where

μ is the logarithm mean of all weak sections in all beams.

τ_i is the difference between the logarithm mean of weak sections within a beam *i* and μ. The mean equals zero and the standard deviation is σ_i.

ε_{ij} is the difference between weak section *j* in beam *i* and the value $\mu + \tau_i$. The mean equals zero and the standard deviation is σ_j.

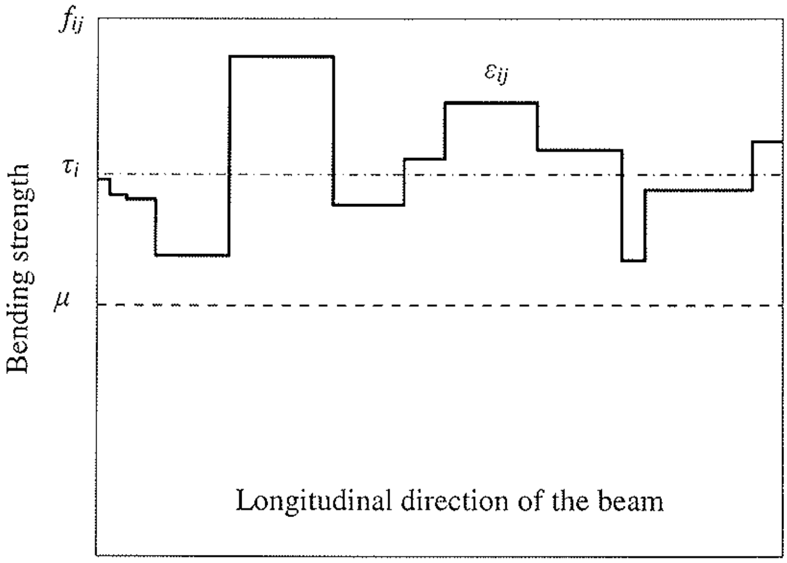

Figure 1: Modelling of longitudinal variation of bending strength, Isaksson (1999).

Using this model results in a coefficient of variation of 25 % for bending strength. 40 % of this variation is due to the variability between members and the rest is due to the variability within members.

The strength is modelled using the following parameters:

μ	log N(3.8924,0) (expected value 50 MPa)
τ_i	log N(0,0.0375)
ε_{ij}	log N(0,0.025)

The modulus of elasticity (*MOE*) is correlated to the bending strength according to eq. (2), Sørensen (2002). The *MOE* is further assumed to be constant within each timber beam. Based on experimental data, see Isaksson (1999), the correlation between bending strength and *MOE* is set to 0.8.

$$MOE_i = \mu_f \left[\ln(300) + 0.13\left(u_{f,i}\rho + u_E\sqrt{1-\rho^2}\right)\right] \quad (2)$$

where

μ_f expected bending strength (50 MPa)

ρ correlation between bending strength and MOE (0.8)

$u_{f,i}$ outcome from a normal distribution N(0,1) used to generate bending strength in member *i*.

u_E outcome from a normal distribution N(0,1) independent of u_f

The length of a weak section is given by a gamma distribution Γ(2.5445, 194.12), i.e. the mean length of a weak section is around 500 mm, Isaksson (1999).

3.2 Composite cross sectional properties

The properties and normal stresses of the T-section are calculated according to Eurocode 5. Figure 2 shows the bending strength for a T-section (solid line) with an applied uniform load (parabola). The dashed line is the bending strength for the solid timber beam without sheathing. The dot-dashed line is the apparent bending strength for this T-section subjected to a uniform load.

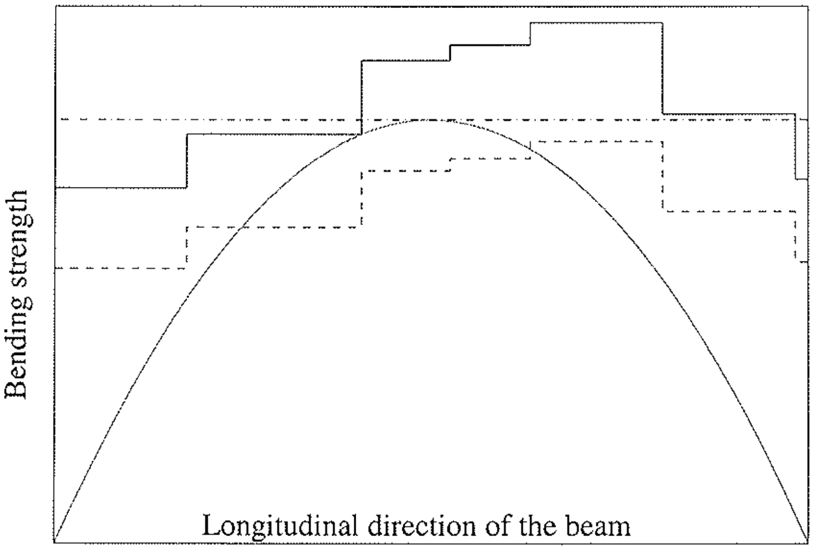

Figure 2: Bending strength for a T-section (solid line) and an applied uniform load (parabola). The dashed line is the bending strength for the timber beam. The horizontal dash-doted line indicates the effective strength for this T-section.

3.3 Beam-Spring model

The load distribution in the transverse direction to the beams is calculated using an analogue beam model, see Figure 3, originally proposed by McCutcheon (1977, 1984) for analysing deflections of a system in the serviceability limit state. Further in McCutcheon the springs were elastic brittle.

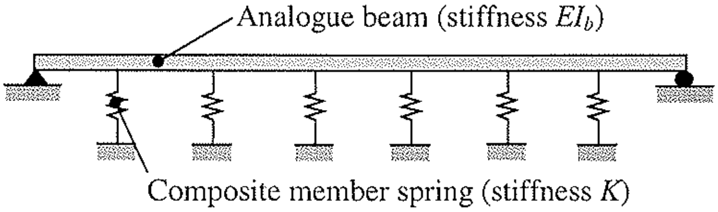
Analogue beam (stiffness EI_b)
Composite member spring (stiffness K)

Figure 3: The beam - spring model.

The present study is focussed on the ultimate limit state. To be able to account for the behaviour of a T-beam after first failure, the spring model is extended to be tri-linear (Liu and Bulleit 1995) see Figure 4. After first failure of the beam, the remaining strength equals ΘR, where R is the original strength and Θ is reduction parameter. The stiffness of the spring after failure is ηK, where K is the stiffness of the unbroken beam and η is a reduction parameter.

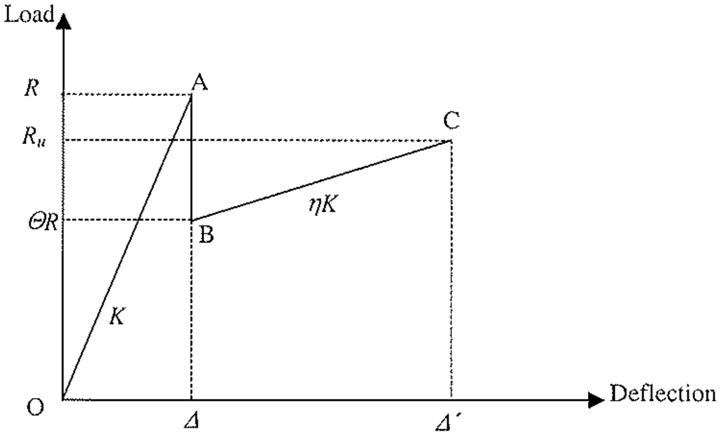

Figure 4: Load-Deformation curve for the composite member spring, Liu and Bulleit (1995).

The cross member stiffness, EI_b to be used in the beam-spring model is taken from Liu and Bulleit (1995):

$$EI_b = I_{cross} E_v \left(1 - \frac{s}{l_v}\right) \tag{3}$$

where the second term in the brackets considers the discontinuities of the sheathing in the cross-member direction.

l_v is the length of sheathing in the cross-member direction (2.4 m).
s is the member spacing of the beams.
I_{cross} is the moment of inertia of the plywood in the cross-member direction. Only veneers in the cross-member direction are taken into account.
E_v is the modulus of elasticity of the plywood in the cross member direction.

4 Simulation and parameter study

4.1 Parameters

Using Monte Carlo simulations the influence of various parameters on the system behaviour is investigated. The parameters of interest are selected based on the results presented in Hansson and Isaksson (2001) and are given in Table 1. The parameters have a reference value and alternative values. Different values of the parameters are combined according to Table 2. The governing property for the strength of the T-section is the bending strength. Other failure modes such as shear failure, buckling of the sheathing or failure in the connectors are not included in this study.

Table 1: Input values to the parameter study.

Parameter	Description	Reference value	Alternative values
c	Centre to centre distance of the timber beams. [m]	0.6	0.4
n	Number of timber beams in each system	15	10
L_j	Beam span [m]	4	5
Layer	Number of veneers in the plywood []	5	7
k	Stiffness of the connection between sheathing and timber beam [N/m], Spacing is constant 0.15 m.	1 (no connection) and $1\cdot10^{75}$	-
t	Thickness of plywood [m]	0.012	0.018
Θ	Remaining bending strength of the beam after first failure (See Figure 4)	0.4	0.2
η	Remaining stiffness of the beam after first failure (See Figure 4)	0.2	0.1

Table 2: The different sets of parameters. The dense shaded values are the alternative values found in Table 1.

Parameter set	c [m]	n []	Lj [m]	*layer* []	k [N/m]	t [m]	Θ []	η []
1	0.60	15	4.00	5	1	0.012	0.40	0.20
2	0.60	15	4.00	5	1.E+75	0.012	0.40	0.20
3	0.60	15	5.00	5	1	0.012	0.40	0.20
4	0.60	15	5.00	5	1.E+75	0.012	0.40	0.20
5	0.60	15	4.00	7	1	0.018	0.40	0.20
6	0.60	15	4.00	7	1.E+75	0.018	0.40	0.20
7	0.60	10	4.00	5	1	0.012	0.40	0.20
8	0.60	10	4.00	5	1.E+75	0.012	0.40	0.20
9	0.40	15	4.00	5	1	0.012	0.40	0.20
10	0.40	15	4.00	5	1.E+75	0.012	0.40	0.20
11	0.60	15	4.00	5	1	0.012	0.20	0.10
12	0.60	15	4.00	5	1.E+75	0.012	0.20	0.10

Compared to the simulations presented in Hansson and Isaksson (2001) the following differences are made:

- New generated sample of data with properties according to section 3.1.
- The properties of the T section are determined according to Eurocode 5.
- Another description of the MOE in the timber beams using a correlation of 0.8 between MOE and bending strength.

4.2 Bending strength variation in single T-sections

Using the model described in section 3 the bending strength for the simulated timber beams can be calculated. The strength of each beam under a uniform load is determined and the results are given in Table 3.

Table 3: Bending strength data for solid timber beams subjected to a uniform load. (Non-parametric).

5th percentile [MPa]	**Mean value** [MPa]	**COV** [%]
31.28	45.23	20.9

The data in Table 3 can be converted to a T-section using data in Table 2. The mean values of the maximum uniform load (kN/m^2) that can be applied on a single T-section are given in Table 4 for the different combinations of parameters according to Table 2.

Table 4: Bending strength for single T-sections. The coefficient of variation is the same as in Table 3.

Parameter set	1	2	3	4	5	6	7	8	9	10	11	12
Uniform load mean [kN/m^2]	5.95	8.07	3.81	5.17	5.97	9.71	5.95	8.07	8.92	12.1	5.95	8.07

4.3 Weakest T-section in a system

Table 5 shows the results from selecting the weakest T-section in each system (10 or 15 beams in each system). This corresponds to weakest link theory without load sharing. From the whole population of timber beams 1000 systems are generated. Since the beam-spring model according to Figure 3 is a continuous beam the reaction in the spring next to the end of the beam is the highest, i.e. this beam is deciding the load carrying capacity. For a beam on several supports, the influence width for the support next to the beam end is 10 % higher than the centre-to-centre distance between beams.

4.4 Failure of a system

Using the beam-spring model, cross-sectional properties and the material data as described earlier the failure load of the systems can be calculated, see Table 5. For each data set in the parameter study 1000 simulations are performed.

Table 5: Simulation results for weakest T-section in the system and for the failure load of the system.

Parameter set	c	n	Lj	layer	k	t	Θ	η	Weakest T-section in system			Failure load		
									5th percentile	mean	COV	5th percentile	mean	COV
	[m]	[]	[m]	[]	[N/m]	[m]	[]	[]	[kN/m²]	[kN/m²]	[%]	[kN/m²]	[kN/m²]	[%]
1	0.60	15	4.00	5	1	0.012	0.40	0.20	3.19	4.05	12.09	4.01	4.84	10.07
2	0.60	15	4.00	5	1.E+75	0.012	0.40	0.20	4.42	5.54	11.36	5.40	6.50	9.63
3	0.60	15	5.00	5	1	0.012	0.40	0.20	2.04	2.56	11.88	2.59	3.08	9.29
4	0.60	15	5.00	5	1.E+75	0.012	0.40	0.20	2.84	3.51	11.11	3.48	4.12	8.87
5	0.60	15	4.00	7	1	0.018	0.40	0.20	3.20	4.06	12.07	4.14	4.92	9.64
6	0.60	15	4.00	7	1.E+75	0.018	0.40	0.20	5.28	6.60	11.33	6.52	7.76	9.49
7	0.60	10	4.00	5	1	0.012	0.40	0.20	3.36	4.25	12.98	4.14	5.02	10.91
8	0.60	10	4.00	5	1.E+75	0.012	0.40	0.20	4.64	5.79	12.19	5.59	6.72	10.28
9	0.40	15	4.00	5	1	0.012	0.40	0.20	4.78	6.07	12.09	6.20	7.37	9.60
10	0.40	15	4.00	5	1.E+75	0.012	0.40	0.20	6.63	8.31	11.36	8.29	9.82	9.34
11	0.60	15	4.00	5	1	0.012	0.20	0.10	3.19	4.05	12.09	3.94	4.74	10.41
12	0.60	15	4.00	5	1.E+75	0.012	0.20	0.10	4.42	5.54	11.36	5.26	6.34	10.09

The system behaviour is depending on the relation between the stiffness of the T-section (spring) and the load-distributing system (the sheathing). Stiff springs compared to a relatively weak load-distributing system results in spring forces similar to the reaction forces found for a continuous beam i.e. with an influence width 10 % higher for the spring next to the end support. This results in a higher frequency of failure in these beams.
The failure load is nearly independent of the properties Θ and η of the broken beam after failure.
The simplest approach to interpret the difference between load carrying capacity of the weakest T-section in each system with the load carrying capacity of the system is to compare the 5th percentile and/or the mean values. The ratio can be found in Table 6.

Table 6: Ration between the weakest T-section in system and the failure load shown in Table 5 for both 5th percentile and mean values.

Parameter set	1	2	3	4	5	6	7	8	9	10	11	12
Ratio for 5th percentile	1.26	1.22	1.27	1.23	1.29	1.23	1.23	1.21	1.30	1.25	1.23	1.19
Ratio for mean values	1.20	1.17	1.20	1.17	1.21	1.18	1.18	1.16	1.21	1.18	1.17	1.14

6 Evaluation of the system effect

6.1 Reliability evaluation

Today's design codes are based on the design of single elements. This results in a lower reliability of the load carrying capacity of a system compared to a single member. Based on the accepted reliability of single elements, the reliability of a system can be determined. This is necessary to be able to determine the system effects. The evaluation is done using the statistical data on the load-carrying capacity presented in previous sections.

The first step is to determine the maximum load which can be applied on a single T-section for a given reliability index. This load is then applied on a weakest link system and the reliability index is calculated for this system. This can be interpreted as the system reliability index implicitly accepted by the. Now the extended model of a system including load redistribution together with the system reliability index is used to determine the load level. The ratio between the load applied on the single T-section and the load on the extended model will be the searched system effect factor. The evaluation is summarised in Figure 5. The code and probabilistic format used in the evaluation is described in the following.

The code format can be written as eq. 4. R is the resistance and S the action.

$$\frac{R_k}{\gamma_m \gamma_n} - \sum \gamma_i S_{ki} \geq 0 \tag{4}$$

γ_m, γ_n and γ_i are partial coefficients related to the material, safety class and action, respectively.

The characteristic resistance R is given by eq. 5.

$$R_k = C_k \kappa f_k a \tag{5}$$

where

C_k	uncertainty in the model
κ	reflects climate and duration of load (not included in this study, set to 1)
f_k	characteristic strength
a	dimension variable

The designing load combination is given by eq. 6.

$$S_d = G_d + Q_d = \gamma_G G_k + \gamma_Q Q_k \tag{6}$$

where

γ_G is the partial coefficient for dead load

γ_Q is the partial coefficient for variable load

G_k is the characteristic permanent load equal to its mean.

Q_k is the characteristic variable load equal to the upper 98:th percentile.

The probabilistic format for the strength can be written as a product of several stochastic variables, eq.7.

$$R = C f a \kappa \tag{7}$$

where

C	uncertainty in the calculation model (μ_C, COV_C)
f	strength (μ_f and COV_f can be found in the simulation results)
a	uncertainty in dimensions (μ_a, COV_a=0.02)
κ	climate and duration of load parameter (κ=1)

The loads are all assumed to be normal distributed and can be written as

$$S = \lambda(G + Q) \tag{8}$$

where

G	permanent load, N(μ_G, COV_G)
Q	variable load, N(μ_Q, COV_Q)
λ	a factor to set the load level

In this investigation COV_G equals 5 % and COV_Q equals 40 %.

The failure function can then be written as

$$R - S = 0 \quad => \quad R - \lambda(G + Q) = 0 \tag{9}$$

A variable, α, is defined to be the ratio between design variable load to the total design load

$$\alpha = \frac{Q_d}{Q_d + G_d} \tag{10}$$

The following relationship between G and Q is assumed

$$\mu_G + \mu_Q = 1 \tag{11}$$

where

μ_G is the mean of the permanent load, G

μ_Q is the mean of the variable load, Q

For a given properties of the resistance (μ_R, COV_R) and actions (μ_G, COV_G, μ_Q, COV_Q), α-value and reliability index, β, the magnification factor, λ, can be found using the failure function found in eq. 9.

Using the target reliability index, $\beta^{single} = 4.8$ and the load capacity, μ_R^{single}, from the design of a single component (see Table 4) the calculated load magnification factor, λ^{single}, will show which load can be applied in a regular design for this safety level.

Codes generally accept that a system will have a lower reliability for the overall safety where the weakest part/component is determining the overall capacity. In an element with many beams this is equivalent to determining the safety of a system only regarding the weakest member within each system. The statistical data for this kind of weakest link system are found in Table 5.

If the resistance properties of the weakest link system is used with the same load i.e. the same magnification factor, λ^{single}, as above, eq. 9 gives the reliability index of the system, β^{system}.

Using the system reliability, β^{system}, together with the resistance properties of system failure (including the beam-spring model) according to Table 5, eq. (9) can be used to calculate a new load magnification factor λ^{system}.

The procedure is summarised in Figure 5.

Finally, to determine the system effect factor the following design equations are used.

The code format for a single member can be written as

$$\frac{f_k a_k C_k}{\gamma_m \gamma_n} = \lambda^{single}\left(G_d + Q_d\right) \tag{12}$$

For a system the allowed reliability and the load capacity will be different,

$$k_{sys}\frac{f_k a_k C_k}{\gamma_m \gamma_n} = \lambda^{system}\left(G_d + Q_d\right) \tag{13}$$

Using the two equations above the system effect factor, k_{sys}, can be written as

$$k_{sys} = \frac{\lambda^{system}}{\lambda^{single}} \tag{14}$$

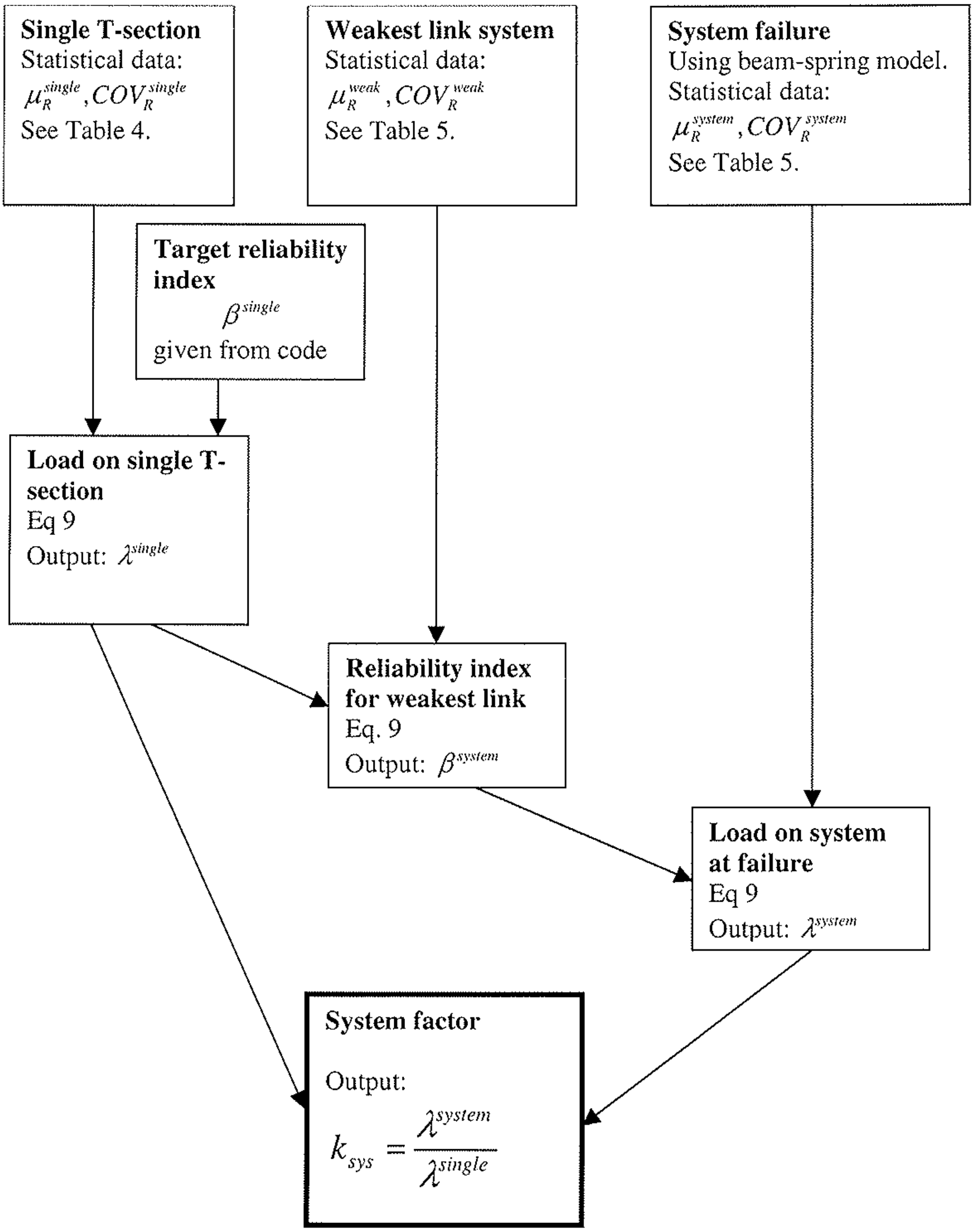
Single T-section
Statistical data:
$\mu_R^{single}, COV_R^{single}$
See Table 4.
Weakest link system
Statistical data:
$\mu_R^{weak}, COV_R^{weak}$
See Table 5.
System failure
Using beam-spring model.
Statistical data:
$\mu_R^{system}, COV_R^{system}$
See Table 5.
Target reliability index
β^{single}
given from code
Load on single T-section
Eq 9
Output: λ^{single}
Reliability index for weakest link
Eq. 9
Output: β^{system}
Load on system at failure
Eq 9
Output: λ^{system}
System factor
Output:
$k_{sys} = \frac{\lambda^{system}}{\lambda^{single}}$

Figure 5: Flow chart of determination of system effect factor, k_{sys}.

Different national codes may have different recommendations about which distributions to select for the stochastic variables, e.g. resistance R, dead load G and variable load Q. The partial coefficient for the designing load combination may differ as well. The following example is using the Swedish code (BKR 99), which means that the load variables in the failure function are assumed to be normal distributed and the strength variables are log normal distributed. The partial coefficients for dead load, γ_G, and for variable load, γ_Q, are set to 1.0 and 1.3 respectively. The numerical results can be seen in Appendix and graphically for parameter set 1 & 2 in Figure 6.

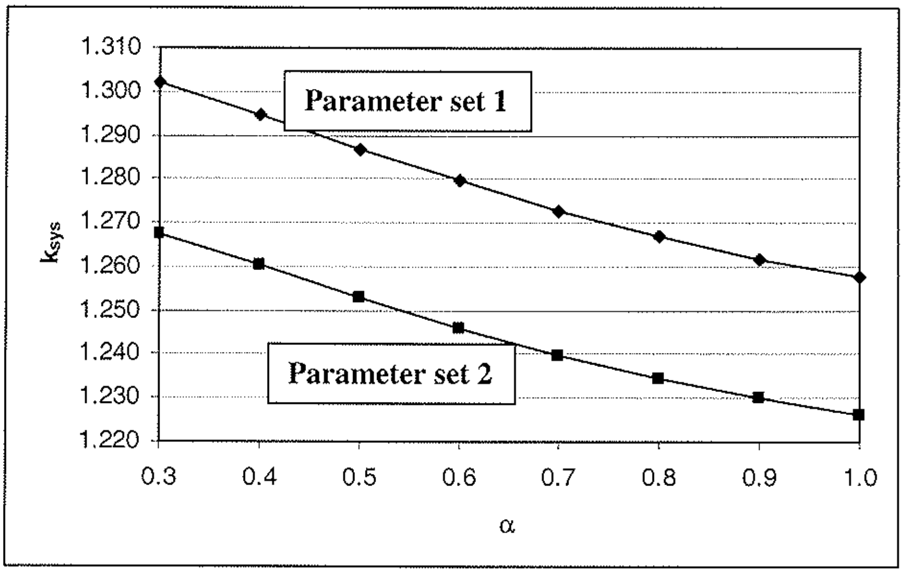

Figure 6: Calculated system effect factor, k_{sys}, as a function to the variable load ratio, α=$Qd/(Qd+Gd)$.

For a typical timber system, α is usually found to be between 0.4 and 1. In Thelandersson et. al. (1999) weighting for different intervals of α is suggested, see Table 7.

Table 7: Weighting of structures according to the ratio between variable and total load, α. Thelandersson et al (1999).

Interval for α	Structures within respective interval [%]
0-0.4	0
0.4-0.6	20
0.6-0.8	60
0.8-1	20

The weighted k_{sys} for the different parameter sets can be found in Table 8.

Table 8: Weighted system effect factors for the different parameter sets.

Parameter set	1	2	3	4	5	6	7	8	9	10	11	12
k_{sys}	1.27	1.24	1.30	1.26	1.31	1.25	1.27	1.24	1.31	1.26	1.23	1.19

7 Conclusions

The codes generally accept that a system will have a lower reliability for the overall safety compared to the reliability of a single member. Using first order reliability method the reliability of a system based on the design of a single T-section can be compared to the reliability of a system using load sharing. Monte Carlo simulations are used to determine the load carrying capacity of single beams and systems. The parameter study shows that the different parameters only have minor influence on the system effect.

A general method based on reliability theory was used to evaluate the system effect factor. To quantify the effect, the statistical distribution of the variables in the failure function and the partial coefficients for the loads must be known. Using the Swedish code (BKR 99) the system effect factor was found to be between 1.19 and 1.31. A simpler way to evaluate the system effect is to determine the ratio between failure load of a system and the weakest T-section in each system. For the 5th percentile and the mean value the system effect is in the interval 1.19-1.30 and 1.14-1.21 respectively. This can be compared to a factor of 1.1 given in Eurocode 5.

8 References

BKR 99, 1998. *Boverkets Konstruktionsregler* (Swedish code, in Swedish). Boverket BFS 1993:58 and BFS 1998:39.

EN408. *Timber structures – Structural timber and glued laminated timber – Determination of some physical and mechanical properties.*

Eurocode 5. *Design of timber structures. – Part 1-1 : General rules and rules for buildings.* European Committee for Standardization, Bruxelles, Belgium.

Foschi, R.O, Folz, B.R. and Yao F.Z., 1989. *Reliability-Based Design of Wood Structures.* Structural Research Series, Report No. 34, Department of Civil Engineering, University of British Columbia, Vancouver, Canada.

Hansson, M. and Isaksson T., 2001. *System Effect in Sheathed Parallel Timber Beam Structures,* CIB-W18 34-8-1 Venice, Italy.

Isaksson, T., 1999. *Modelling the variability of bending strength in structural timber.* Report TVBK-1015, Dept. of Structural Engineering, Lund University Sweden.

Liu, W-F and Bulleit, W. M., 1995. *Overload behaviour of sheathed lumber systems.* ASCE Journal of Structural Engineering, vol 121, No 7.

McCutcheon, W. J., 1977. *Method for predicting the stiffness of wood-joist floor systems with partial composite action.* Research paper FPL 289, Forest Products Lab, U.S Dept. of Agriculture, Forest Service, Madison, Wisconsin.

McCutcheon, W. J., 1984. *Deflections of uniformly loaded floors: a beam-spring analog.* Research paper FPL 449, Forest Products Lab, U.S Dept. of Agriculture, Forest Service, Madison, Wisconsin.

Sørensen Dalsgaard, J., Hoffmeyer, P. (2001). *Statistical analysis of data for timber strength.* Report, Aalborg University, Denmark.

Sørensen Dalsgaard, J., Damkilde L. (2002). *Load bearing capacity of roof trusses.* To be published. Aalborg University, Denmark.

Thelandersson, S., Larsen, H. J., Östlund L., Isaksson, T., Svensson, S., 1999. *Reliability levels for timber and timber products used in construction* (in Swedish). Report TVBK-3039, Dept. of Structural Engineering, Lund University, Sweden.

Appendix:

Results from the calculations of the system factor k_{sys}

Parameter set 1 α	Single beams λ^{single}	Weakest β^{system}	Failure λ^{system}	k_{sys}
1.0	1.214	4.381	1.527	1.258
0.9	1.371	4.420	1.730	1.262
0.8	1.519	4.469	1.925	1.267
0.7	1.657	4.531	2.108	1.273
0.6	1.780	4.605	2.277	1.280
0.5	1.885	4.691	2.426	1.287
0.4	1.970	4.784	2.550	1.295
0.3	2.031	4.871	2.645	1.302

Parameter set 2 α	Single beams λ^{single}	Weakest β^{system}	Failure λ^{system}	k_{sys}
1.0	1.647	4.519	2.019	1.226
0.9	1.859	4.573	2.287	1.230
0.8	2.061	4.639	2.544	1.235
0.7	2.247	4.723	2.786	1.240
0.6	2.414	4.822	3.007	1.246
0.5	2.557	4.936	3.203	1.253
0.4	2.671	5.059	3.366	1.260
0.3	2.755	5.176	3.491	1.267

Parameter set 3 α	Single beams λ^{single}	Weakest β^{system}	Failure λ^{system}	k_{sys}
1.0	0.777	4.345	0.996	1.281
0.9	0.878	4.384	1.129	1.287
0.8	0.973	4.432	1.258	1.293
0.7	1.061	4.494	1.380	1.301
0.6	1.140	4.570	1.493	1.310
0.5	1.207	4.658	1.593	1.320
0.4	1.261	4.752	1.678	1.330
0.3	1.301	4.843	1.743	1.340

Parameter set 4 α	Single beams λ^{single}	Weakest β^{system}	Failure λ^{system}	k_{sys}
1.0	1.055	4.496	1.308	1.240
0.9	1.191	4.551	1.483	1.245
0.8	1.320	4.620	1.652	1.251
0.7	1.439	4.705	1.811	1.258
0.6	1.546	4.808	1.958	1.266
0.5	1.638	4.926	2.089	1.275
0.4	1.711	5.054	2.200	1.286
0.3	1.765	5.178	2.286	1.295

Parameter set 5	**Single beams**	**Weakest**	**Failure**	
α	λ^{single}	β^{system}	λ^{system}	k_{sys}
1.0	1.218	4.378	1.569	1.288
0.9	1.375	4.418	1.778	1.293
0.8	1.524	4.468	1.980	1.299
0.7	1.662	4.529	2.171	1.306
0.6	1.786	4.604	2.347	1.314
0.5	1.891	4.690	2.504	1.324
0.4	1.976	4.783	2.635	1.334
0.3	2.038	4.872	2.737	1.343

Parameter set 6	**Single beams**	**Weakest**	**Failure**	
α	λ^{single}	β^{system}	λ^{system}	k_{sys}
1.0	1.982	4.473	2.439	1.231
0.9	2.237	4.524	2.763	1.235
0.8	2.479	4.589	3.074	1.240
0.7	2.703	4.669	3.367	1.246
0.6	2.904	4.765	3.636	1.252
0.5	3.076	4.876	3.874	1.259
0.4	3.214	4.996	4.073	1.267
0.3	3.315	5.110	4.226	1.275

Parameter set 7	**Single beams**	**Weakest**	**Failure**	
α	λ^{single}	β^{system}	λ^{system}	k_{sys}
1.0	1.214	4.495	1.517	1.250
0.9	1.371	4.532	1.719	1.254
0.8	1.519	4.579	1.913	1.259
0.7	1.657	4.636	2.095	1.265
0.6	1.780	4.704	2.263	1.272
0.5	1.885	4.780	2.410	1.279
0.4	1.970	4.860	2.533	1.286
0.3	2.031	4.936	2.627	1.293

Parameter set 8	**Single beams**	**Weakest**	**Failure**	
α	λ^{single}	β^{system}	λ^{system}	k_{sys}
1.0	1.647	4.625	2.013	1.223
0.9	1.859	4.677	2.281	1.227
0.8	2.061	4.740	2.538	1.232
0.7	2.247	4.817	2.781	1.238
0.6	2.414	4.908	3.003	1.244
0.5	2.557	5.010	3.200	1.252
0.4	2.671	5.119	3.363	1.259
0.3	2.755	5.220	3.489	1.266

Parameter set 9 α	Single beams λ^{single}	Weakest β^{system}	Failure λ^{system}	k_{sys}
1.0	1.820	4.380	2.351	1.292
0.9	2.055	4.418	2.666	1.297
0.8	2.277	4.468	2.969	1.304
0.7	2.484	4.529	3.256	1.311
0.6	2.668	4.603	3.521	1.320
0.5	2.826	4.689	3.756	1.329
0.4	2.953	4.782	3.954	1.339
0.3	3.045	4.870	4.107	1.349

Parameter set 10 α	Single beams λ^{single}	Weakest β^{system}	Failure λ^{system}	k_{sys}
1.0	2.469	4.521	3.071	1.244
0.9	2.787	4.576	3.479	1.248
0.8	3.089	4.643	3.872	1.253
0.7	3.369	4.724	4.245	1.260
0.6	3.619	4.824	4.586	1.267
0.5	3.833	4.939	4.889	1.275
0.4	4.005	5.062	5.143	1.284
0.3	4.131	5.179	5.340	1.293

Parameter set 11 α	Single beams λ^{single}	Weakest β^{system}	Failure λ^{system}	k_{sys}
1.0	1.214	4.381	1.483	1.222
0.9	1.371	4.420	1.679	1.225
0.8	1.519	4.469	1.867	1.229
0.7	1.657	4.531	2.044	1.234
0.6	1.780	4.605	2.205	1.239
0.5	1.885	4.691	2.347	1.245
0.4	1.970	4.784	2.464	1.251
0.3	2.031	4.871	2.554	1.257

Parameter set 12 α	Single beams λ^{single}	Weakest β^{system}	Failure λ^{system}	k_{sys}
1.0	1.647	4.519	1.947	1.183
0.9	1.859	4.573	2.203	1.185
0.8	2.061	4.639	2.449	1.189
0.7	2.247	4.723	2.679	1.192
0.6	2.414	4.822	2.888	1.197
0.5	2.557	4.936	3.071	1.201
0.4	2.671	5.059	3.223	1.206
0.3	2.755	5.176	3.338	1.211

CIB-W18/35-12-1

**INTERNATIONAL COUNCIL FOR RESEARCH AND INNOVATION
IN BUILDING AND CONSTRUCTION**

WORKING COMMISSION W18 - TIMBER STRUCTURES

GLULAM BEAMS WITH ROUND HOLES – A COMPARISON OF DIFFERENT DESIGN APPROACHES VS. TEST DATA

S Aicher
L Höfflin

Otto-Graf-Institute, Stuttgart

GERMANY

Presented by: L Höfflin

H Larsen provided the background to the approach adopted in EC5 and commented on the implication that EC5 equations would result in non-conservative designs and he then went on to ask if the authors were of the view that the equations in EC5 needed to be altered. S Aicher replied that in his view a scalar modification with an additional term is required.

Glulam beams with round holes – a comparison of different design approaches vs. test data

Aicher, S. and Höfflin, L.

Otto-Graf-Institute, Stuttgart, Germany

1 Introduction

The design of glulam beams with holes is treated considerably different in timber design codes. Examples are the latest drafts of Eurocode 5 and of the German timber design code DIN 1052. In the first case a solution based on a linear fracture mechanics approach is stated whereas in the latter case a strength of materials design is given. In both cases the underlying mechanical models represent rather crude idealizations, especially when round holes are regarded.

The paper first shortly reveals the mechanical problem. Second, both mentioned design approaches are discussed and compared quantitatively. Thirdly, both approaches are evaluated vs. results of some recent experiments with different sized beam specimens. Some amendments of the design approaches are proposed.

2 Stress distributions perpendicular to grain

Holes in glulam members in general are subject to combined shear force and moment action. In rare occasions pure moment loading of the member section with the hole may occur. Holes in axially loaded glulam columns are not regarded here.

The hole disturbs the stress flow due to shear force, V, and/or bending moment, M, and the rearrangement of the stresses produces tension stresses perpendicular to grain at distinct locations at the periphery of the hole. The locations and the extension of the tension perpendicular to grain stress fields depend distinctly on the loading situation, i.e. on the M/V ratio. Figures 1a and b give schematic illustrations of the distributions of stresses perpendicular to grain in the hole vicinity for two extreme M/V ratios. Figure 1a shows the case $M/V \to \infty$, i.e. pure moment loading ($V = 0$), and Fig. 1b reveals the situation $M/V \to 0$ being the fictive load case with a "pure" shear force ($M = 0$). A superposition approach for derivation of solutions for the load case $M = 0$ was shown by (Aicher and Höfflin, 2001).

The graphs illustrate that in case of pure moment there are three fields of tension stresses perpendicular to grain of rather small extension as compared to the case of "pure" shear force. In the latter case there are only two tension stress fields. In a general M/V action, exclusively the M and V bound tension stresses perpendicular to grain in the first quadrant are additive.

Figures 1c, d depict for the two regarded extreme section force configurations the distributions of tension stresses perpendicular to grain along the highest stressed sections along beam axis. The magnitude of the stresses and their extension denoted by the distribution lengths, l_M and l_V, respectively, are shown in a qualitative manner. The shear force action produces higher and more extended tension stresses perpendicular to grain.

Figures 2a, b illustrate schematically the tension stress distribution perpendicular to grain along the highest stressed sections for two different realistic M/V ratios. With increasing M/V ratio the tension stress distribution in the first quadrant becomes dominant.

The failures in glulam beams with holes are almost entirely determined by the tension stresses perpendicular to grain. Except hereof are loading situations with very high M/V ratios (almost pure moment action) where the failure of the beam is bound to the interaction of bending tension stresses and stresses perpendicular to grain at the whole periphery.

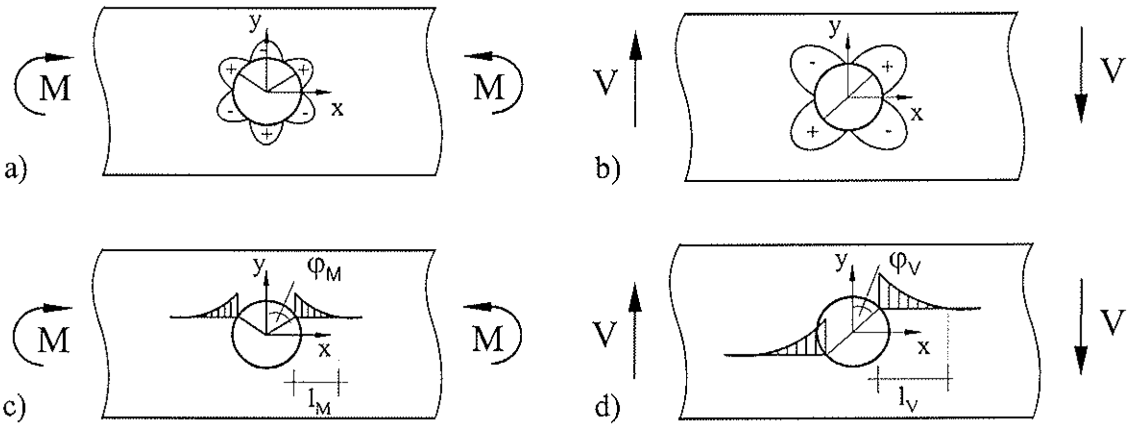

Fig. 1a-d: Schematic illustrations of stress fields and sections with high tension stresses perpendicular to grain at the periphery of round holes in a glulam beam for two extreme section force cases

a) stress field perpendicular to grain for pure moment action (M/V → ∞)

b) stress field perpendicular to grain for „pure“ shear force action (M/V = 0)

c) sections with highest tension stresses perpendicular to grain for pure moment action

d) sections with highest tension stresses perpendicular to grain for „pure“ shear action

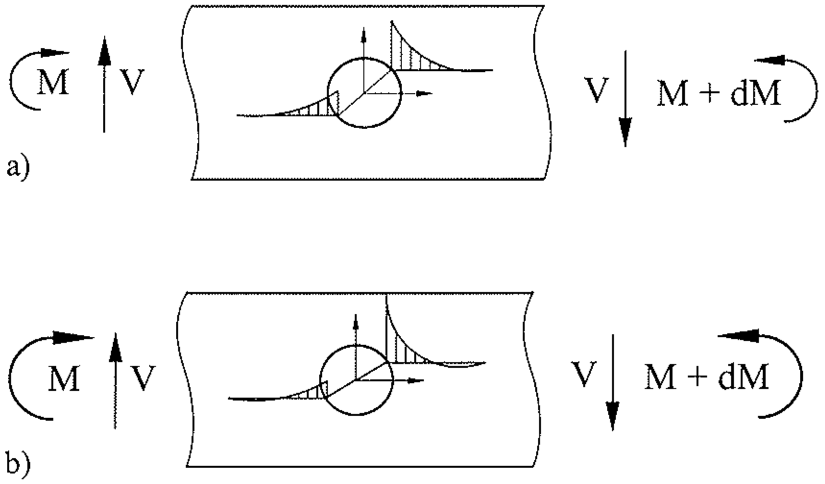

Fig. 2a, b: Schematic illustrations of distribution of tension stresses perpendicular to grain along highest stressed sections at the hole periphery for two different moment/shear force ratios

a) small M/V ratio b) large M/V ratio

3 Design of round holes according to draft DIN 1052

Following the design for round holes as specified in the draft of the revised semi-probabilistic German timber design code [1] is given (the design of rectangular holes is in principle similar). As mentioned above, the design approach represents a classical strength of materials approach. Hereby the design tension force perpendicular to grain at the hole periphery, $F_{t,90,d}$, is compared to the design value of the resistance $R_{t,90,d}$ ($R_{t,90,d}$ not specified explicitly)

$$\frac{F_{t,90,d}}{R_{t,90,d}} = \frac{F_{t,90,d}}{0{,}5\ l_{t,90}\ b\ f_{t,90,d}} \leq 1 \tag{1a}$$

where (in case of round holes)

$$l_{t,90} = 0{,}353\ h_d + 0{,}5\ h \tag{2}$$

is the distribution length of the assumed triangular stress distribution perpendicular to grain, b is beam width and $f_{t,90,d}$ is the design tension strength perpendicular to grain (see also Fig. 3). Rewritten as the ratio of a design stress $\sigma_{t,90,d}$ vs. design strength, eq. (1a) reads

$$\frac{\sigma_{t,90,d}}{f_{t,90,d}} \leq 1 \qquad \text{where} \qquad \sigma_{t,90,d} = \frac{F_{t,90,d}}{0{,}5\ l_{t,90}\ b} \tag{1b, 3}$$

The design value of the tension force is composed of two additive parts bound to the separate actions of the shear force and the bending moment

$$F_{t,90,d} = F_{t,V,d} + F_{t,M,d} \tag{4}$$

where[1] (in case of round holes)

$$F_{t,V,d} = \frac{V_d\ (0{,}7\ h_d)}{4\ h}\left[3 - \frac{(0{,}7\ h_d)^2}{h^2}\right] = V_d\ \eta\ , \tag{5}$$

$$F_{t,M,d} = 0{,}008\frac{M_d}{h_r} \tag{6}$$

and V_d, M_d absolute values of design shear force and moment at the hole edge (= hole center ± d/2); sign of ± d/2 to be chosen such as to give unfavourable results

and

$$h_r = \min\ \{h_{ru} + 0{,}15\ h_d,\ h_{rl} + 0{,}15\ h_d\}^2 \tag{7}$$

---

[1] Subsequent eq. (5) is a corrected equation according to the latest draft revision

[2] DIN notations h_{ro} and h_{ru} were changed to EC 5 notations h_{ru} and h_{rl}

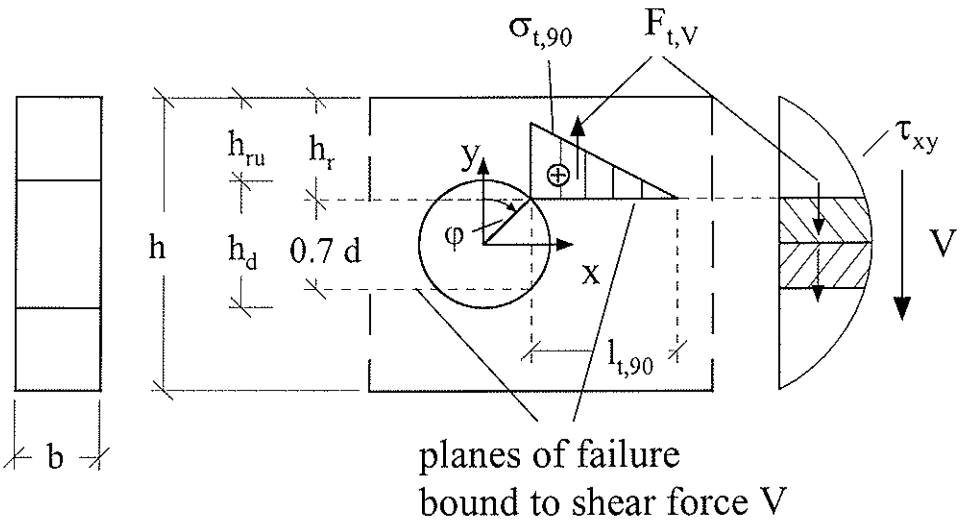

Fig. 3: Geometry notations [1)] of a round hole in glulam beam according to DIN 1052 and schematic illustration of the derivation of the tension force $F_{t,V}$ bound to shear force V [1)] notations h_{ru}, h_{rl} chosen according to EC 5

Further, the maximum/minimum restrictions

$h_d \leq 0,4$ h and $h_{ro(ru)} \geq 0,25$ h

apply.

Some comments to the background and limits of the specified equations seem appropriate (in the following for sake of simplicity the subscript d is omitted, i.e. nominal resp. characteristic values are regarded):

- Tension force $F_{t,V}$ bound to the shear force V, specified in eq. (5), represents the resultant of the shear stresses τ_{xy} which can not be transferred in the hole area (see Fig. 3)

  $$F_{t,V} = b \int_{0}^{0,5\,d\cos\varphi} \tau_{xy}\,dy \tag{8}$$

  The integration boundary y = c = 0,5 d cosφ defines the plane with the highest stresses perpendicular to grain and thus at ultimate load the plane of failure. The offset of c from mid-hole depends i.a. to some extent on the stiffness ratios. In an approximation c is defined by $\varphi = 45°$, thus $y = 0,5\ d/\sqrt{2}$. By integration of the stresses perpendicular to grain (resulting from FE analysis) it can be shown that eqs. (8) and (5) deliver the correct stress resultant (evident from principle of force equilibrium).

- Tension force $F_{t,M}$ bound to the bending moment, specified in eq. (6), is not based analytically but results from a calibration to experimental data in different literature sources (Kolb and Epple, 1985). The performed calibration procedure can be questioned. A finite element based determination of $F_{t,M}$ delivers a considerably different result (Aicher and Höfflin, 2001)

$$F_{t,M} = 0{,}084 \frac{M\, d^2}{h^3} \tag{9}$$

which gives, depending on the ratio d/h, pronouncedly smaller values for $F_{t,M}$.

- From a continuum analysis point of view it can be stated that the distribution length of the assumed triangular stress distribution perpendicular to grain, given by eq. (2), is too long. This is illustrated exemplarily in Figs. 4a, b and Tab. 1. The graphs show the distribution of tension stress perpendicular to grain for two ratios of hole to depth d/h = 0,2 and 0,4 for a beam with depth of 900 mm according to finite element analysis and according to the given DIN design approach. In detail, the comparison of the stress

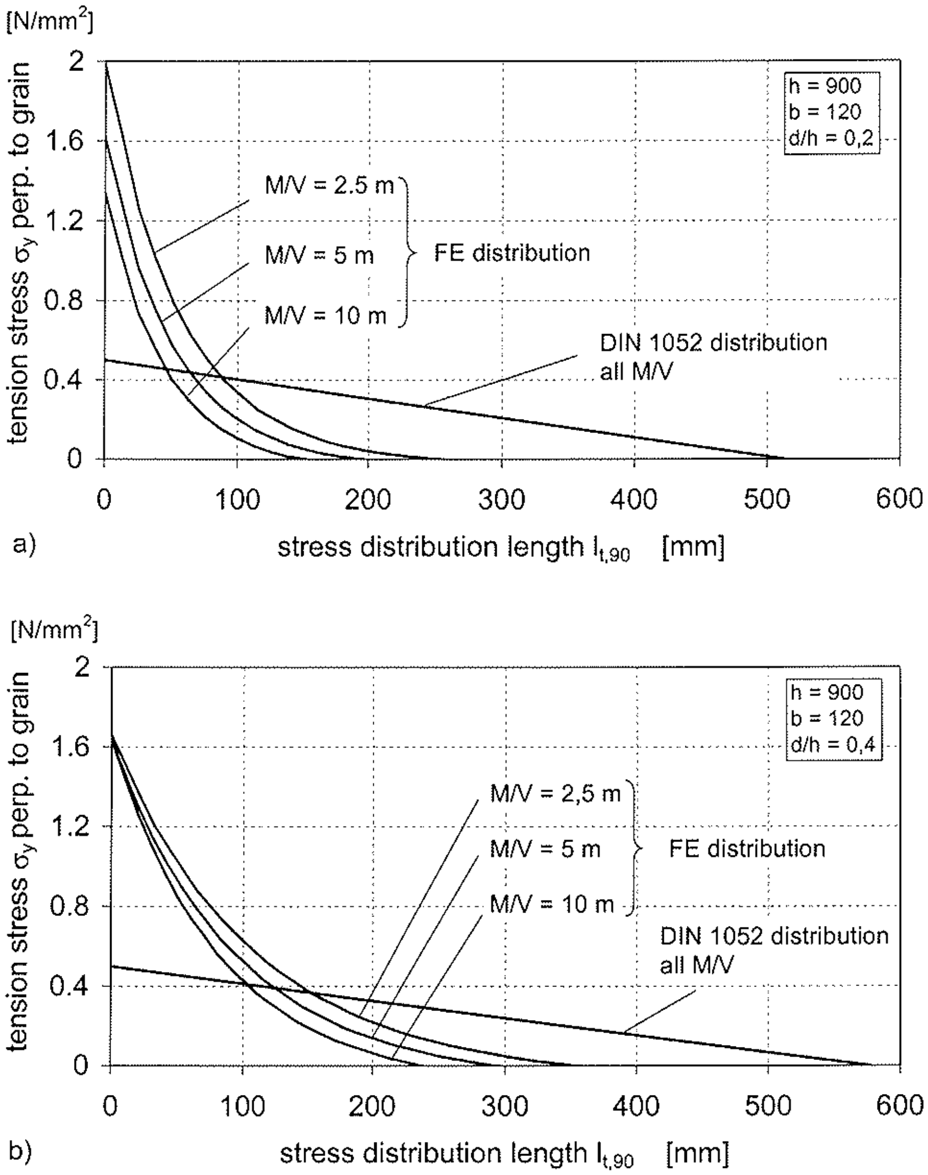

Fig. 4a, b: Tension stress σ_y perpendicular to grain vs. stress distribution length $l_{t,90}$ at highest stressed section at failure state V_k according to DIN 1052 and according to continuum analysis bound to load $V_{k(DIN)}$ for different hole to depth ratios and moment/shear force ratios
a) d/h = 0,2 b) d/h = 0,4

hole to depth ratio	moment shear force ratio	charact. shear force	charact. tension force		distribution length		maximum tension stress	
d/h	M/V	$V_{k(DIN)}$	$F_{t,90,k(DIN)}$	$F_{t,90,k(FE)}$	$l_{t,90(DIN)}$	$l_{t,90(FE)}$	$\sigma_{y,max(DIN)}$	$\sigma_{y,max(FE)}$
-	-	kN	kN	kN	mm	mm	N/mm^2	N/mm^2
0.2	2.5	98.1	15.4	12.6	514	252	0.5	1.98
	5	73.8		9.2		196		1.62
	10	49.4		6.5		151		1.34
0.4	2.5	64.5	17.3	18.6	577	359	0.5	1.66
	5	52.5		16.1		295		1.63
	10	38.1		13.7		237		1.64

Table 1: Comparison of resultant characteristic tension forces perpendicular to grain $F_{t,90,k}$, of stress distribution length $l_{t,90}$ and of maximum tension stress $\sigma_{y,max}$ according to DIN 1052 and FE analysis for different d/h and M/V ratios (beam depth and width: d = 900 mm, b = 120 mm)

distribution is performed for the ultimate (= characteristic) load resp. shear force state V_k defined by the DIN approach through eqs. (1a), (4), (5) and (6) giving

$$V_{k(DIN)} = f_{t,90,k}\ 0{,}5\ l_{t,90}\ b \Big/ \left(\eta + \frac{0{,}008}{h_r} \frac{M_{(k)}}{V_{(k)}} \right) \qquad (10)$$

Shear force $V_{k(DIN)}$ is evaluated for three different realistic $M_{(k)}/V_{(k)}$ ratios of 2,5; 5 and 10 [(kNm/kN) = m]. Tension strength $f_{t,90,k}$ was taken as 0,5 N/mm^2 for assumed glulam strength class GL 32h. The given FE stress distributions are based on $V_{k(DIN)}$ and the respective M/V ratios. It can be seen from the graphs that the nonlinear stress distribution according to continuum analysis shows a distinctly higher stress gradient and a higher stress level closer to the hole periphery and in general considerably smaller stress distribution lengths $l_{t,90}$. Table 1 gives for the different regarded hole to depth and section force ratios the characteristic shear force capacity $V_{k(DIN)}$ and the resultant characteristic tension force perpendicular to grain, $F_{t,90,k(DIN)}$, according to DIN 1052. Further, the resultant tension force $F_{t,90,FE}$ according to integration of stresses σ_y along highest stressed section bound to the characteristic DIN 1052 shear force capacity $V_{k(DIN)}$

$$F_{t,90,FE} = b \int_0^{l_{t,90,FE}} \sigma_y \, dx \qquad (11)$$

is given. Further, the table gives the stress distribution lengths $l_{t,90}$ and the maximum tension stress $\sigma_{y,max}$ at the hole periphery according to DIN 1052 and FE analysis. Considerable differences between DIN 1052 and the FE analysis are revealed for all regarded configurations. Except hereof is a rather good agreement for the characteristic tension forces in case of hole to depth ratio d/h = 0,4.

The maximum stresses according to continuum analysis might be considered to high; however for this judgement the actually stressed volume has to be taken into account.

4 Design of round holes according to draft EC 5

The linear fracture mechanics based strength verification for a shear force V at a hole placed at the centre axis of the beam is conducted as for a notched beam subjected to a shear force of V/2 (see Fig. 5). The effect of the additional moment on the load capacity is not considered. For a round hole, the strength verification is performed as for a notched beam with inclination of 1:1. The design equation formally reads as an approach based on the comparison of design shear stress τ_d vs. design shear strength $f_{v,d}$ reduced by some factor k_V

$$\frac{\tau_d}{k_V\ f_{v,d}} \le 1 \qquad \text{and} \qquad \tau_d = \frac{1{,}5\ V_d}{b\ h_{ef}} \tag{12a, b}$$

Factor k_V is defined by

$$k_V = \min\begin{cases} 1 \\ \dfrac{k_n\left(1+\dfrac{1{,}1\ i^{1{,}5}}{\sqrt{h^*}}\right)}{\sqrt{h^*}\left(\sqrt{\alpha\left(1-\alpha\right)}+0{,}8\dfrac{x}{h^*}\sqrt{\dfrac{1}{\alpha}-\alpha^2}\right)} \end{cases} \tag{13}$$

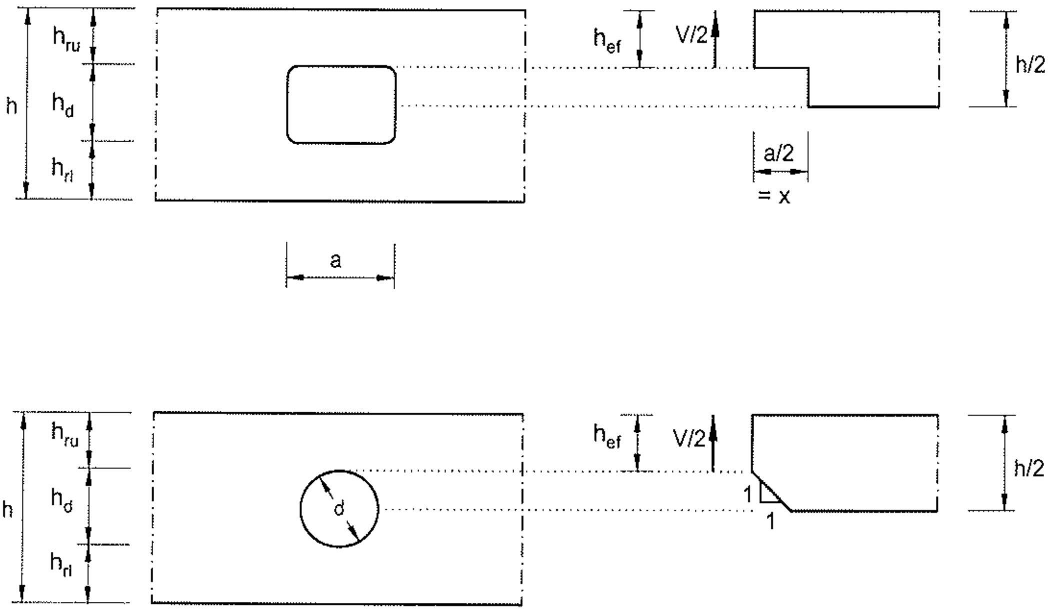

Fig. 5: Dimensions of holes in beams and respective approximations of the notched beam design approximation; leftside: actual geometry; rightside: notched beam approximations (after EC 5)
a) rectangular holes b) round holes

where

i = notch inclination
$h^* = h/2$
x = distance from line of action to the corner
$\alpha = h_{ef}/h^*$
$$k_n = \begin{cases} 5 & \text{for solid timber} \\ 6{,}5 & \text{for glulam} \end{cases}$$

In case of round holes, where $i = 1$ and $x = 0$, factor k_V reduces to

$$k_V = \min \begin{cases} 1 \\ \dfrac{k_n}{\sqrt{\alpha(1-\alpha)}} \dfrac{1+\dfrac{1{,}1}{\sqrt{h^*}}}{\sqrt{h^*}} \end{cases} \tag{14}$$

Further, minimum/maximum restrictions

$$h_d \leq 0.4\ h \text{ and } h_{ru(rl)} \geq 0.25\ h \tag{15}$$

apply.

Some comments to the background and limits of the specific equations seem appropriate:

- The design approach is based on linear elastic fracture mechanics based on total energy release rate for an end-notched beam (Gustafsson, 1988). As fracture mechanism, a Mode I fracture mechanics problem was assumed; hereby the material resistance is highly determined by characteristic fracture energy $G_{f,k}$ in tension perpendicular to grain. The formally shear strength based resistance side in eq. (12a) is simply the result of an equation multiplication by $f_{v,k}/f_{v,k}$.

- The basic analytical solution was calibrated to experimental results for the **end-notched beam case** with a factor of 2/3.

- Characteristic fracture energy $G_{f,k}$ was eliminated from the resistance side by the approximation that expression

  $$k_n = \frac{1}{3}\sqrt{\frac{G_{f,k} E_{0,05}}{f_{v,k}^2}} \tag{16}$$

  is approximately 5 and 6,5 for solid wood and glulam, respectively, throughout all strength classes.

5 Comparison of load capacities according to drafts of EC 5 and DIN 1052

For a comparison of both design approaches these are evaluated for characteristic shear force with and without consideration of a bending moment influence. The evaluation is based on glulam strength class GL 32h with the respective strength values given in EN 1194. For the EC 5 solution, characteristic shear strength and for DIN 1052 characteristic tension strength perpendicular to grain

$f_{v,k} = 3{,}8\ \text{N/mm}^2$ and $f_{t,90,k} = 0{,}5\ \text{N/mm}^2$

are employed. Three different beam depths being

h1 = 450 mm, h2 = 2 h1 = 900 mm and h3 = 3,33 h1 = 1500 mm

are regarded; beam width is constant 120 mm. The comparison comprises round holes with hole to depth ratios of d/h = 0,1 to 0,4 and considerably different moment to shear force ratios (M/V = 0 ... 10).

First, the computational shear force capacity without consideration of a bending moment influence (M/V = 0) is regarded. Figure 6 shows the shear capacity depending on the hole to depth ratio for the 3 different beam depth as resulting from the EC 5 and DIN 1052 (there M = 0 in eq. (4)) approach. A comparison of the results of the different design approaches reveals in general considerable discrepancies. For beam depth ≤ 1300 mm the design equation according to EC 5 in general predicts (considerably) higher characteristic shear force capacities whereby the differences between the two approaches (EC 5/ DIN 1052) become smaller with increasing beam depths up to about equal numbers at h ≈ 1300 mm. This is an immediate consequence of the different recognition of the depth effect in the linear fracture mechanics approach (EC 5) and in the strength of materials approach (DIN 1052), respectively. In the first case, load capacities increase proportional to quasi $\sqrt{h}$ and in the second case proportional to h.

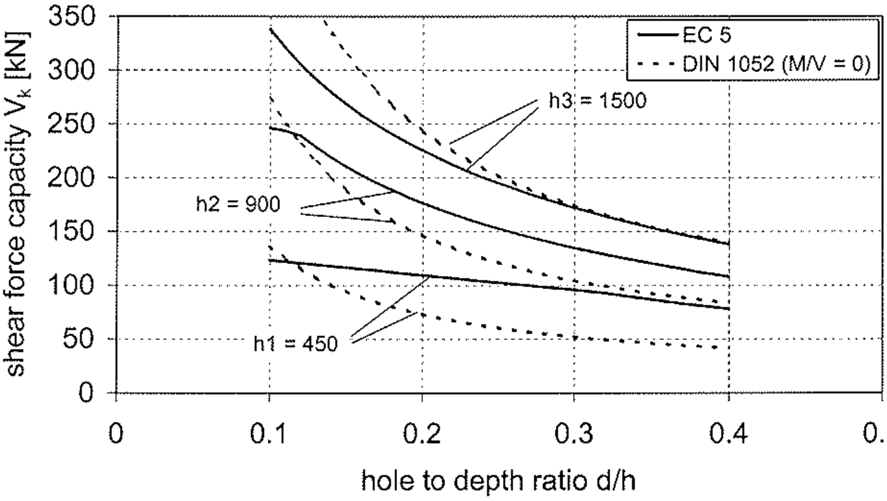

Fig. 6: Characteristic shear force capacity of glulam beams with round holes without consideration of a bending moment influence according to drafts of EC 5 and DIN 1052 depending on the hole to depth ratio and on the beam depth

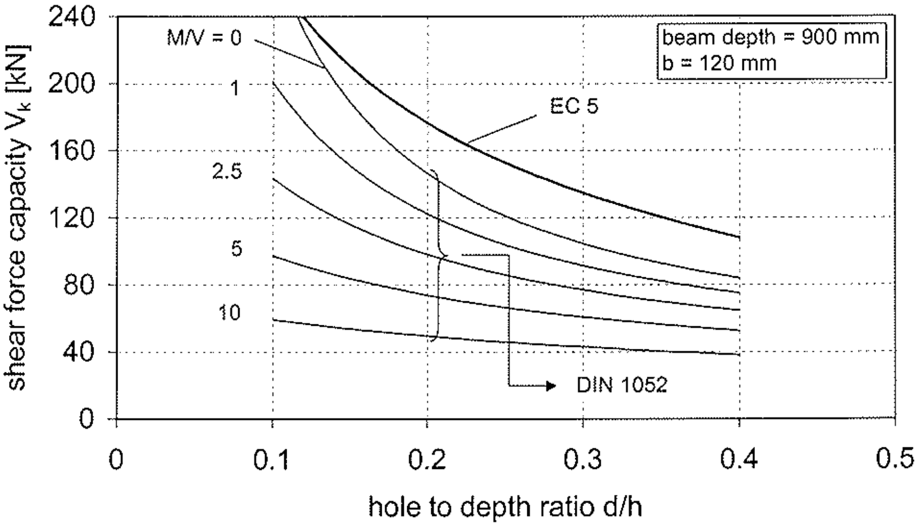

Fig. 7: Characteristic shear force capacity of a glulam beam (depth h2 = 900 mm) with a round hole depending on the hole to depth ratio for different moment shear force ratios M/V according to drafts of EC 5 and DIN 1052

Quantitatively, the differences for the regarded extreme (in practice not possible) section force ratio M/V = 0 are partly considerable. For beam depths of h1 = 450 mm and h2 = 900 mm and medium to larger sized d/h ratios of 0,2 to 0,3 the EC 5 load capacities are 1,5 to 1,7 and 1,2 to 1,3 times higher as compared to the DIN 1052 solution. The quantitative discussion is not be deepened for this artificial section force ratio as the DIN 1052 design approach accounts for the moment contribution on the load capacity, too.

Figure 7 shows the shear force capacity for a beam of constant depth of h2 = 900 mm depending on the hole to depth ratio d/h and on the section force ratio M/V. In detail the parametric dependency of the DIN solution on the section force ratio M/V in the realistic range of M/V = 0 to 10 [m] is given. Ratios M/V of about 2,5 [m] relate to holes very close to the supports, the larger ratios increasingly mirror constructions with holes closer to mid-span. It can be taken from the graph that the additional incorporation of the bending moment influence results in a tremendous reduction of the load (shear force) capacity of the beam according to DIN 1052 as compared to the EC 5 approach. For practically typical M/V ratios in the range of 2,5 to 5, throughout all regarded hole to depth ratios of 0,1 to 0,4, EC 5 predicts , in a rough average, a 2 times higher load capacity as compared to DIN 1052. For M/V = 10 and d/h = 0,1 the difference of EC 5 vs. DIN 1052 is more than 400%.

6 Comparison of test results vs. design approaches

In order to verify/calibrate the presented designs and a new alternative approach for glulam beams with holes first tests in the frame of a research project were performed; the existing data base (i.a. Kolb and Frech, 1977; Pentalla, 1980; Johanesson, 1983) is re-evaluated, too. Following, exclusively the results of two new test series at Otto-Graf-Institute with significantly different beam sizes (h1 = 450 mm and h2 = 900 mm) and hole to depth ratios of d/h = 0,2 and 0,4 are regarded. The tests with single span beams with very small M/V ratios (0,675 m and 1,35 m) were performed with homogeneously built-up glulam beams of strength class GL 32h. In each test series four beams were tested. Table 2 specifies the investigated beam configurations. The test results concerning the mean (± standard deviation), minimum and characteristic shear force capacities obtained in both test series are given in table 3.

test series	beam depth h	dimensions		hole to depth ratio d/h	M/V ratio
		width b	hole diameter d		
-	mm	mm	mm	-	-
h1_0,4	450	120	180	0.4	0.675
h2_0,2	900	120	180	0.2	1.35

Table 2: Investigated configurations of glulam beams with holes

test series	shear force capacity V in [kN]		
	mean ± std.	minimum	5% fractile
h1_0,4	48.55 ± 7.33	38.25	36.90
h2_0,2	96.94 ± 13.17	81.90	74.45

Table 3: Compilation of test results of two test series with different glulam beam sizes and hole to depth ratios

Figures 8a, b show the test results in comparison to the characteristic shear force capacities predicted by both design approaches. It can be seen that in case of test series h1_0,4 the estimated 5% fractile of the test results coincides with the DIN 1052 solution whereas EC 5 gives a highly unconservative overestimation by a factor of about 2. In case of test series h2_0,2 both design approaches forward a considerable overestimation of the experimental 5% fractile; the characteristic load capacities according to DIN 1052 and EC 5 are 1,6 and 2,4 times higher, respectively, compared to the test results.

Disregarding the very small experimental basis for final conclusions the following can be stated:

- The DIN 1052 strength of materials approach seems to give good load capacity predictions for beams with rather small depth (verified for a large hole to depth ratio of d/h = 0,4). For medium/large beam depths a considerable (unconservative) overestimation of the test results was obtained.

- The EC 5 approach is throughout highly on the unconservative side, overestimating the experimental results by a factor of 2 and more.

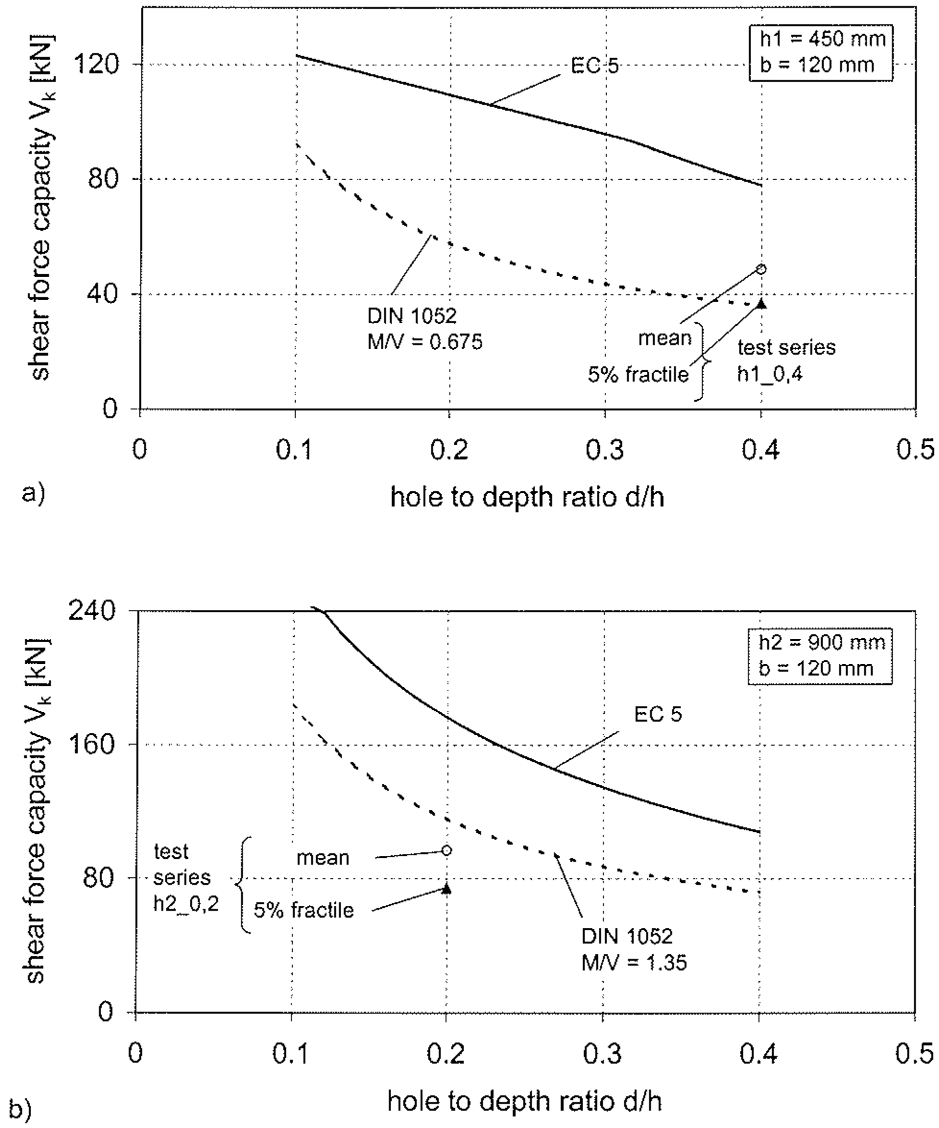

Fig. 8a, b: Comparison of experimental and calculated (EC 5, DIN 1052) mean and characteristic load capacities of different sized glulam beams with round holes of different hole to depth ratios
a) test series h1_0,4 b) test series h2_0,2

7 Proposal for design equation changes

Any scalar changes to the DIN approach improving the agreement with the test results for large beams produce a less good agreement for beams with small dimensions. The approach, method inherent, does not reflect the experimentally obvious size effect of the fracture mechanism correctly, what is inline with former evaluations of the size effect problem (Aicher et al., 1995).

Looking at the reasons for the extreme load capacity overestimation by the EC 5 approach (compare chap. 4) at least two points are important:

- Factor k_n according to eq. (16) depends on (characteristic) fracture energy $G_{f,k}$ in tension perpendicular to grain. For the mean value of G_f the relationship

  $$G_f = 0,65\ \rho \qquad (17)$$

  was found in (Larsen and Gustafsson, 1990; Larsen et al., 1992); For derivation of a characteristic value it was assumed that the ratio of characteristic to mean fracture

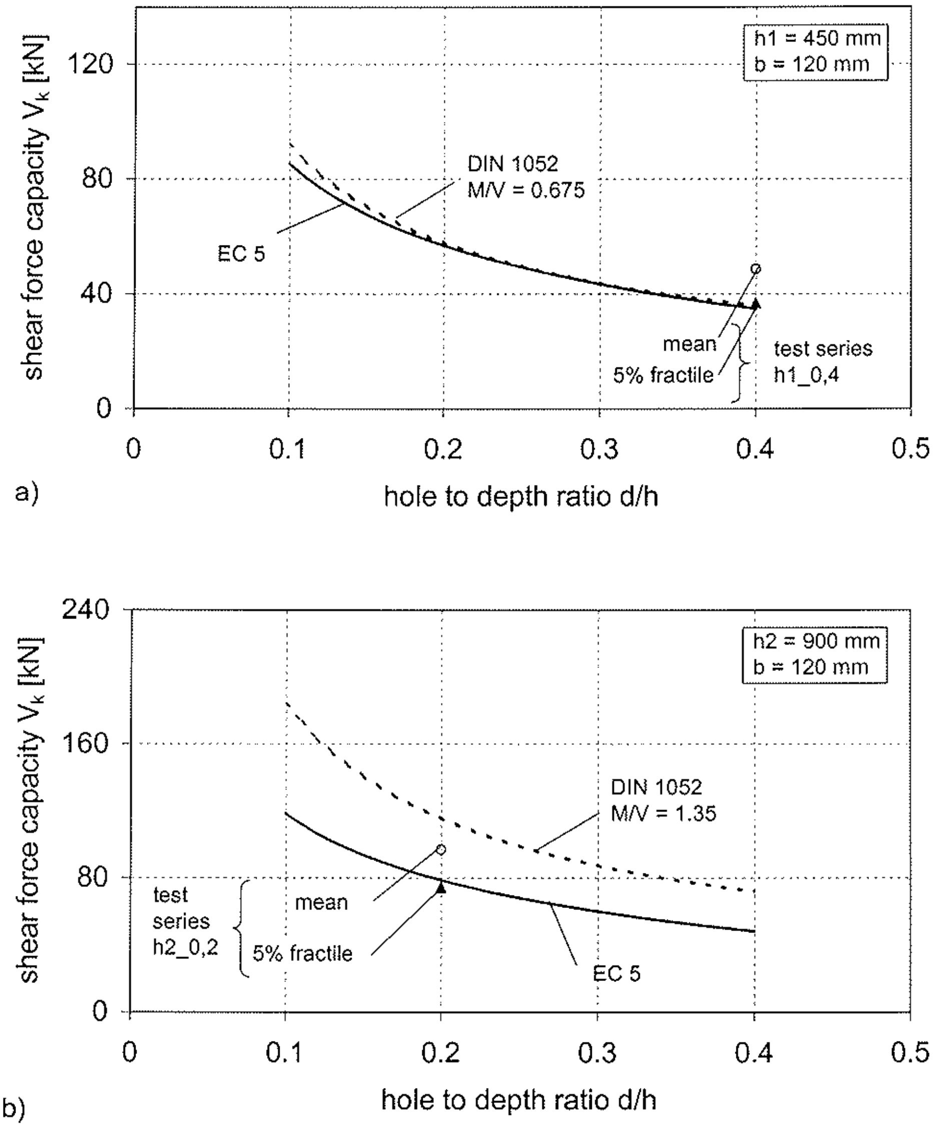

Fig. 9a, b: Comparison of mean and characteristic load capacities for glulam beams with a round hole depending on the hole to depth ratio according to draft of DIN 1052 and a slightly modified EC 5 draft equation (now: k_n = 2.9) vs. some test results
a) test series h1_0,4 b) test series h2_0,2

energy corresponds to the ratio of characteristic to mean density, the latter taken to be 0,83, so:

$$\rho_k/\rho_{mean} = 0.83 = G_{f,k}/G_{f,mean} \qquad (18)$$

The mean value for the fracture energy according to eq. (17) represents a good approximation for European spruce, however eq. (18) may be considered to forward a pronounced overestimation of the 5% fractile of the G_f value. In a different investigation on fracture energy perpendicular to grain of European spruce the mean level relationship $G_f = 0,62\ \rho$ was found (Aicher, 1994). However for the ratio of characteristic vs. mean value $G_{f,k}/G_{f,mean}$ a considerably smaller value of about 0,65 as compared to 0,83 in eq. (18) was obtained.

- There is no widely known theoretical/experimental evidence that the experimental calibration factor of 2/3 applied to the theoretical end-notched beam solution applies similarly to beams with round holes, too.

Assuming for the time being approximate validity of the linear fracture mechanics based EC 5 approach, a scalar modification of eqs. (13) and (14), justified partly by above arguments, should give a better agreement between tests and the design equation.
Figures 9a, b repeat the graphs shown in Figs. 8a, b, now however with a modified factor $k_n = 2,9$ as compared to $k_n = 6,5$ in eq. (13). It can be seen that now a very good agreement between the calculated and experimental characteristic values is obtained for the investigated test configurations defined by very small M/V ratios.
In order to account more differentiated for the influence of the moment to shear force ratio and for the size effect, a Weibull theory based design model is currently developed.

8 References

Aicher, S. (1994): Fracture energy, critical strain energy release rate and fracture toughness of spruce in tension perpendicular to grain. Holz Roh- und Werkstoff 52, pp. 361–370

Aicher, S., Gustafsson, P.J., Haller, P., Petersson, H. (2002): Fracture mechanics models for strength analysis of timber beams with a hole or a notch. RILEM Report. Edt. P.J. Gustafsson, Lund University

Aicher, S., Höfflin, L. (2001): Round holes in glulam members. Part 1: Analysis (in German). Bautechnik 78 (10), pp. 706-715

Aicher, S., Höfflin, L. (2001): A contribution to the analysis of glulam beams with round holes. Otto-Graf-J., Vol. 11, pp. 167 –180, University of Stuttgart

Aicher, S., Schmidt, J., Brunold, S. (1995): Design of timber beams with holes by means of fracture mechanics. CIB Meeting 28, paper CIB-W18/28-19-4, Copenhagen

DIN 1052: Design of timber structures – General rules and rules for buildings. Draft version E DIN 1052 : 2000-05

Eurocode 5: Design of timber structures – Part 1-1; General rules and rules for buildings. Final draft prEN 1995-1-1, CEN/TC 250/SC5 N173

Gustafsson, P.J. (1988): A study of strength of notched beams. Proc. CIB Meeting 21, paper CIB-W18A/21-10-1, Vancouver Island

Johannesson, B. (1983): Design problems for glulam beams with holes. Div. Steel and Timber Structures, Chalmers University of Technology, Göteborg

Kolb, H., Frech, P. (1977): Untersuchungen an durchbrochenen Bindern aus Brettschichtholz. Holz Roh- und Werkstoff 35, pp. 125 – 134.

Kolb, H., Frech, P. (1977): Untersuchungen an durchbrochenen Bindern aus Brettschichtholz. Research Report FMPA, Otto-Graf-Institute, Stuttgart

Larsen, H. J., Gustafsson, P. J. (1990): The fracture energy of wood in tension perpendicular to grain – results from a joint testing project. Proc. CIB Meeting 23, paper CIB-W18A/23-10-12, Lisbon

Larsen, H. J., Riberholt, H., Gustafsson, P. J. (1992): Note on Eurocode 5. Design of notched beams. CEN SC5 paper

Pentalla, V (1980): Reiällinen liimapuupalkki. Julkaisu 33, Div. Structural Eng. Helsinki University of Technology, Otaniemi

CIB-W18/35-15-1

INTERNATIONAL COUNCIL FOR RESEARCH AND INNOVATION
IN BUILDING AND CONSTRUCTION

WORKING COMMISSION W18 - TIMBER STRUCTURES

ON TEST METHODS FOR DETERMINING RACKING STRENGTH AND STIFFNESS OF WOOD-FRAMED SHEAR WALLS

U A Girhammar
L Wu
Civil Engineering, Department of Applied Physics, Umeå University

B Källsner
Växjö University
Trätek - Swedish Institute for Wood Technology Research

SWEDEN

Presented by: B Källsner

H Sugiyama asked if the authors were familiar with the tests conducted by Tuomi in the 1970s in which proposals for testing perforated shear walls were made. H Sugiyama felt that Tuomi's proposals should be considered even though he did not fully agree with the proposals. B Källsner confirmed that he was aware of the Tuomi tests which assumed an elastic behavior of the various components but despite making arguable assumptions, the Tuomi approach gave good results. He then went on to agree with comments that gypsum boards are difficult to handle.

On test methods for determining racking strength and stiffness of wood-framed shear walls

Ulf Arne Girhammar and Liping Wu
Civil Engineering Group, Department of Applied Physics, Umeå University, Sweden
Bo Källsner
Växjö University, Sweden
Trätek - Swedish Institute for Wood Technology Research, Sweden

Abstract

It is proposed that the present standard EN 594 is revised by using, as the main alternative, a test method that evaluates the strength and stiffness of the shear wall in a pure shearing mode. This mode will render boundary and loading conditions corresponding to a fully anchored shear wall. This pure shear mode is introduced in a rational way in the wall by applying a diagonal tensile load at the top corner of the wall. This method will render basic test results that have general applicability as far as the actual sheathing and fastener materials are concerned. Different materials can then easily be compared. The necessary adjustment of the design value for shear walls applied in a specific construction with certain boundary and loading conditions is then proposed to be made either by supplementary testing or by using theoretical reduction factors that depend on these conditions and that can be obtained by analytical models for partially anchored shear walls.

The mechanical properties of the sheathing-to-timber joints have a major influence on the stiffness and strength of shear walls. Therefore, the racking test standard would need to be supplemented by a relevant method for testing of the joint characteristics. The present standard for load bearing nailed joints is not appropriate. A revised test standard is needed that incorporate testing of the parameters of special interest, such as edge distance of the fasteners and loading direction vis-à-vis the edge of the sheet. By such a test standard for joints, design values for shear walls can be evaluated using general calculation models and the results can be compared to full-scale tests.

By realising this proposal we open up for use of advanced methods in design of shear walls.

1 Introduction

1.1 Background

1.1.1 General

For the horizontal stability of multi-storey buildings, diaphragm action in the walls is of vital importance. Shear walls and diaphragms are the main structural elements used to resist the forces of wind and seismic loads. In wooden houses, such wall panels usually comprise of wood-based sheets nailed on a timber framework. Roof and floor diaphragms distribute lateral loads to the shear walls, which in turn transfer the loads to the foundations. These sheathed wood shear walls should be designed and optimised with respect to their overall functions, especially with regard to the joints, different kinds of restraining devices against uplift and various strength enhancing details.

Important factors that have great influence on the load-carrying capacity and the structural performance are:

(a) Fastener characteristics – both for sheathing-to-timber connections and framing joints – including the effect of different load-grain directions and edge distances;

(b) Boundary conditions – both for internal components and external boundaries of the shear wall – fully or partially anchored leading stud and/or bottom rail, characteristics of the inter-component connections to transverse walls and floors, and the flexural and shear stiffness of floors;

(c) Loading conditions – both with respect to the magnitude and distribution (depending on the rigidity of the roof and floor structures) of the dead weight and other permanent loads; and

(d) Sheathing design – fully or partially sheathed segments.

The designations, fully and partially anchored shear walls, refer to walls where the vertical stud on the tension side of the wall is fully or partially anchored to the substrate, respectively. The bottom rail may be anchored or not.

The terms, fully and partially sheathed shear walls, refer to walls where the sheet in each segment covers fully the frame of that segment or where the sheet in at least one segment only partially covers the frame of that segment, respectively. Each sheet is always fastened on framing members along the whole perimeter, usually also along intermediate studs.

Different testing standards diverge when it comes to the type and degree of anchoring of or overturning restraint for the shear wall.

1.1.2 American standards

The former American Society of Testing and Materials (now ASTM International) has worked out the standard procedure, E 72 "Standard Test Method of Constructing Strength Tests of Panels for Building Construction", for determining racking performance of shear walls [1]. This test procedure uses steel hold-down rods to resist over-turning forces. A 'stop' is placed at the end of the wall to prevent lateral slipping. The main purpose of this test was to compare the performance of sheathing types. The test is considered to be a monotonic test since the load is only one directional and each loading stage is applied separately. The procedure stipulates a steel tie-down rod tying the top plate to a rigid base to prevent uplift at one end of the wall where the load is applied [2, 3].

Due to criticism of ASTM E 72 because of the use of the rigid hold-down mechanism, ASTM E564 "Standard Practice for Static Load Test for Shear Resistance of Framed Walls for Buildings" was developed [4]. ASTM E 564 uses tie-down anchorage to attach the end studs to the rigid base and does not include a 'stop' to prevent lateral slipping [2, 3].

For example, Price & Gromala (1980) used ASTM E 72 to compare ultimate strength and stiffness of panels sheathed with different structural sheets [5]. The most common monotonic failure mode was bending of the nail shank and withdrawal from the framing material. Wolfe (1983) used ASTM E 564 to evaluate the racking performance of shear walls [6]. Griffiths (1984) pointed out that the tie-down mechanisms according to ASTM E72 over restrain the panel, which result in unrealistic failure values [7]. Dolan (1989) found that the overturning anchor connection fastening the end studs of the test walls to the foundation greatly enhanced wall performance. The anchor prevented the walls from rotating as a rigid body and averted separation from the bottom plate [8].

1.1.3 European standards

Griffiths (1984) summarized the results of monotonic shear wall tests under different conditions [7]. As mentioned above, he found ASTM E 72 unsuitable for racking tests because it over restrains the panel giving unrealistic failures. Therefore, the Princes Risborough Laboratories in England introduced a different monotonic testing procedure. Rather than restraining the wall panels from uplift using tie-down anchors, the English method incorporates vertical load applied to the panels using jacks. Stiffness and ultimate strength tests of walls were conducted at different vertical load levels. Griffiths pointed out that a zero vertical load level represented a 'lower bound case' accounting for light-weight structures subjected to 'hurricane type uplift conditions'. In this test method the bottom rail of the panel is bolted to the test rig. The lack of hold-downs for the studs will result in a lower racking capacity for the wall panel [2, 3].

Most walls Griffiths tested sustained 90 percent of the maximum load over a reasonably large displacement. He indicated that the modes of failure vary with board types, nail size, vertical loading and frame timber.

This English method is the basis for the European test standard EN 594 "Racking strength and stiffness of timber frame wall panels" [9].

1.1.4 Other standards

Australian testing organizations, for example, do not require any uplift restraints, Reardon (1980) [10]. However, Stewart (1987) concluded from his shear wall tests that anchorage connections have a large influence on capacity and stiffness of shear walls [11].

1.2 Eurocode 5

In Eurocode 5, 2001, two methods are presented in order to determine the racking strength of cantilevered wall diaphragms [12]:

(1) Calculation according to a simplified procedure based on a lower limit value on the plastic capacity (equals approximately the elastic capacity value) of fully anchored shear walls (i.e. fully restrained studs and bottom rail); and

(2) Determining the racking strength by testing of prototype structures (European Standard EN 594 "Timber structures – Test methods – Racking strength and stiffness of timber frame wall panels", December 1995 [9]).

The engineered design method (1) for shear walls assumes that the shear wall segment acts as a cantilevered 'I-beam' (the leading and trailing studs act as flanges and the sheet as web) and the force couple at the ends of the wall equals the tilting moment. The individual segment is fully restrained against these overturning forces. The overturning anchors or tie-down connections, fastening the end studs of shear walls to the foundation, prevent the walls from rotating as a rigid body and restrain the tension studs against uplift from the bottom plate. The load-slip characteristics of the sheathing-to-timber connections are assumed to govern the wall performance in the ultimate limit state.

Testing according to the test standard (2) is an alternative method for determining the racking resistance of wall diaphragms. However, the shear wall according to this standard (which is supposed to imitate the conditions in practice) will only be partially anchored depending on the value of the applied vertical loads on the studs (that work similar to a tie-down device) and the spreading of holding down bolts through the bottom rail to the base of the test rig.

If the stud on the tension side of the wall panel is not directly anchored to the base, this stud will normally be subjected to substantial vertical displacement (at least in a testing situation). Consequently, the structural behaviour will deviate considerably from what is assumed in the calculation procedure (1). This means that the sheathing-to-timber joints located along the bottom rail on the tension side of the test panel will be subjected to vertical tension forces, which strive to draw the sheet apart from the bottom rail in a perpendicular direction. This redistribution of the fastener forces will result in a lower racking capacity for a tested wall panel according to EN 594 than for a diaphragm designed according to the simplified theory with a fully anchored tensile stud. An additional effect is that the tensile forces will act almost perpendicular to the edge of the sheet. The strength of the connection is often considerably lower when the fastener forces act perpendicular to the edge of the sheet than when they act parallel to the edge. This is especially the case when the fasteners are located close to the edges of the sheathing and framing materials.

The end object desire would be to have a test standard for the sheathing-to-timber joints, which are governing the response of the shear wall (the present standard EN 1380 "Timber structures - Test methods – Load bearing nailed joints" [13] should be elaborated on). In evaluating the characteristics of those joints it is important to include the effect of loading-to-grain direction and edge distance in the sheathing and framing materials. Knowing the properties of the joints, it is possible to apply a general calculation model in order to evaluate the shear wall behaviour.

This study is part of an ongoing Nordic project, dealing with the design of wood-based diaphragm structures, especially with respect to shear walls that are incompletely anchored to the substrate.

1.3 Aim and Scope

The main objective of this paper is to discuss appropriate test methods for racking performance of wood-framed shear walls with various loading and boundary conditions. The aim is to provide a basis for a possible improvement of the present test standard in order to obtain consistency between test procedures, calculation methods and actual behaviour of shear walls.

The different American and European test standards are discussed. The influence of full or partial anchoring of the leading or tensile studs and bottom rail is at the focus of the study. A testing program has been conducted for various shear wall configurations in order to evaluate these effects. This program is not presented here in any detail. A plastic design method has been developed to be able to account for these effects.

A revised testing standard is proposed that will provide results for the racking strength and stiffness corresponding to a fully anchored shear wall. The results reflect the maximum racking load-carrying capacity and stiffness of the actual sheathing materials and fasteners. The influence of the actual boundary and loading conditions is proposed to be account for separately by testing or by calculation.

2 Models for simplified design of shear walls

2.1 General

Presently there exist two simplified methods, an elastic and a plastic one, for the design of fully anchored shear walls [14]. The methods are based on linear elastic or rigidly plastic characteristics of the sheathing-to-timber joints, respectively.

A new simplified method for design of incompletely anchored but fully sheathed wall diaphragms has been presented, Källsner et al. (2001) [15], and a corresponding one for partially anchored and partially sheathed shear walls will be presented in a companion paper, Källsner et al. (2002) [16]. The method is based on a plastic lower bound value of the load-carrying capacity of the shear wall.

The horizontal load-carrying capacity, H, can in general terms be written as

$$H = n_{s,eff} \cdot f_p \, b \tag{1}$$

where b = width of a sheet or shear wall unit, $n_{s,eff}$ = effective number of sheet segments or shear wall units of width b, a number that depends on the actual boundary and loading conditions ($n_{s,eff} b$ = effective length of the shear wall that contribute to the horizontal load transfer), and f_p = plastic capacity of the sheathing-to-timber joints per unit length of framing member, i.e.

$$f_p = \frac{F_v}{s} \tag{2}$$

where F_v = fully plastic capacity of a individual sheathing-to-timber joint, and s = fastener spacing along the top rail.

The full or actual number of sheet segments corresponds to the (maximum) horizontal load-carrying capacity of a shear wall *fully* anchored with respect to the leading stud and bottom rail, i.e.

$$H_{full} = n_s \cdot f_p \, b \tag{3}$$

where n_s = number of sheet segments or shear wall units.

2.2 Fully anchored shear walls

The elastic and plastic models are based on the assumptions that the shear wall is fully anchored to the substrate, the frame members are rigid and hinged to each other, the sheet is rigid, the load-displacement relationships of the sheathing-to-timber joints are linear-elastic until failure (f_p) or fully plastic (f_p), respectively, and the displacements are small compared with the width (b) and height (h) of the sheet segment or shear wall unit.

2.3 Partially anchored shear walls

Using the new simplified method for design of incompletely anchored wall diaphragms, the effective number of sheet segments that contribute to the horizontal load-carrying capacity can be derived as a function of the boundary and loading conditions.

For the boundary and loading conditions shown in Figure 1, the effective number of sheet segments versus the relative vertical load acting on the studs is illustrated in Figure 2 (for a shear wall with four sheet segments, n_s = 4). The (maximum) relative value $V/f_p h = 1$ corresponds to a vertical load that causes the full plastic capacity of the sheathing-to-timber joints to occur along the whole length of the stud, which the vertical load is acting on.

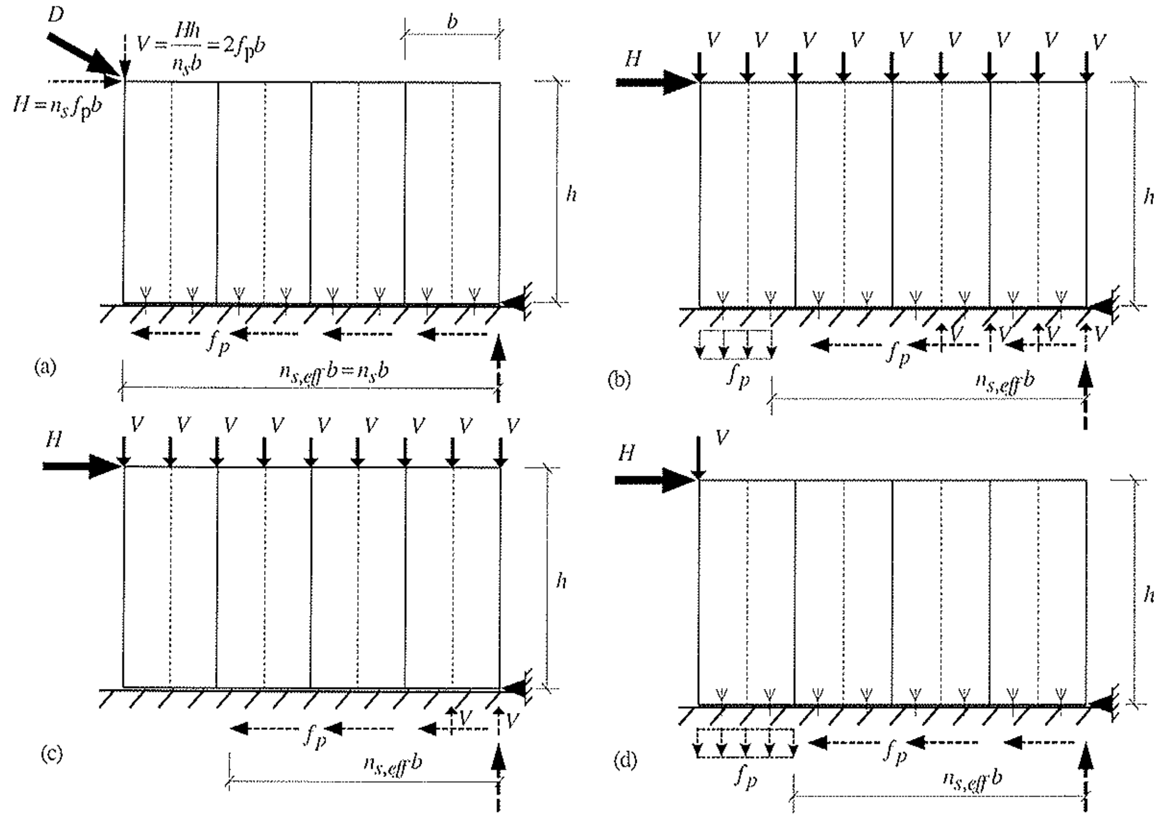

Figure 1. Shear walls on rigid foundation with different boundary and loading conditions: (a) Fully anchored bottom rail – diagonal load that corresponds to a fully anchored leading stud; (b) Fully anchored bottom rail – vertical loads on all studs; (c) Not anchored bottom rail – vertical loads on all studs; and (d) Fully anchored bottom rail – vertical load on leading stud. The dashed arrows are reaction forces relative to the bottom rail.

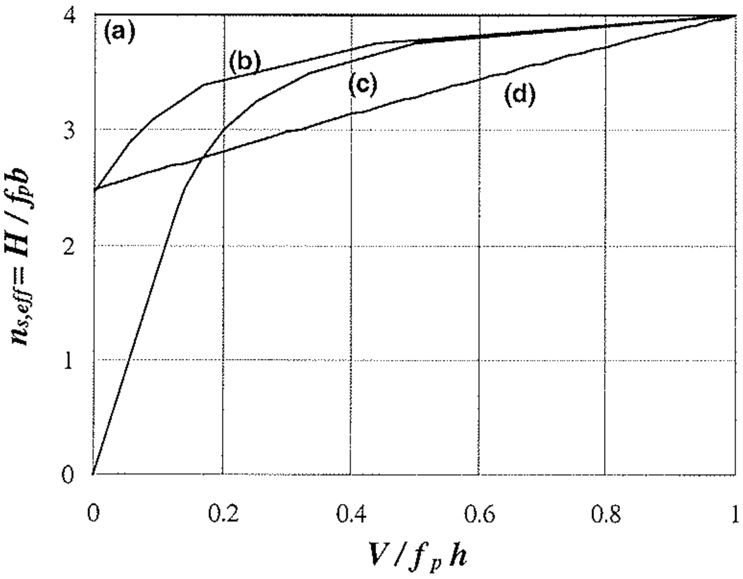

Figure 2. Effective number of sheet segments or shear wall units, $n_{s,eff}$, contributing to the horizontal load-carrying capacity, H, versus the relative vertical load for the different boundary and loading conditions according to Figure 1. The curves are valid for shear walls of 4 sheet segments ($n_s = 4$). Curve (b) is only approximate.

3 Standards for prototype testing of shear walls

3.1 Fully anchored shear walls

3.1.1 American standard ASTM E 72

The American test standard, E 72 "Standard Test Methods of Conducting Strength Tests of Panels for Building Construction" [1], specifies among other things the test method to be used in evaluation of the racking resistance of sheathing materials on a standard wood frame. The test specimen shall be 2.4 by 2.4 m and the framing shall be constructed in a specified way.

The test panel shall be attached to a timber or steel plate that is in turn attached rigidly to the base of the loading frame, Figure 3. Means shall be provided to bolt or otherwise attach the sole plate of the panel firmly to this member. A hold-down shall be provided as shown in Figure 3.

Load shall be applied to the specimen through a timber member firmly bolted to the upper plate of the panel. Lateral guides shall be provided so that the specimen will deflect in a plane.

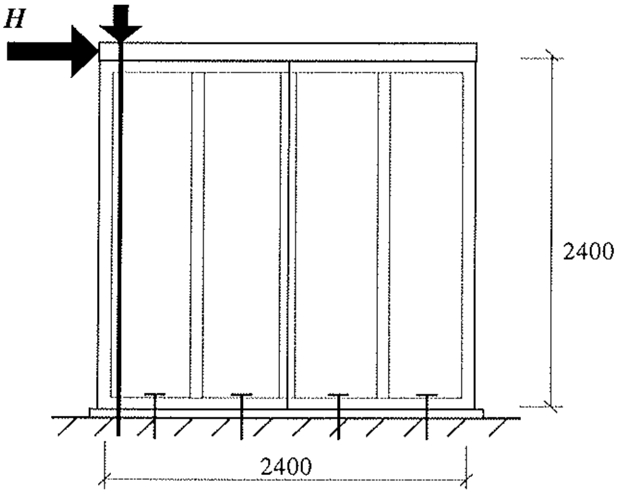

Figure 3. Details of test panels and requirements for test apparatus.

3.2 Partially anchored shear walls

3.2.1 European standard EN 594

The present test standard, EN 594 "Racking strength and stiffness of timber frame wall panels" [9], specifies the test method to be used in determining the racking strength and stiffness of timber frame wall panels. The test method is intended to provide (i) comparative performance values for the materials used in the manufacture of the panels and (ii) datum information for use in structural design. The requirements for test panels and test apparatus are as given in Figure 4.

The test method measures the resistance to racking load of wall panels, which can deform both vertically and horizontally in the plane of the wall panel.

In this test method, the bottom rail of the wall panel is bolted to the test rig and uplift is resisted by the sheathing fixings and also by the vertical loads on the top rail of the wall panel. Normally it is sufficient to test the maximum and minimum conditions of vertical load appropriate to the design of the wall panel. Due to incomplete anchoring and/or, normally, small vertical loads, these conditions render only partially shearing action in the wall panel.

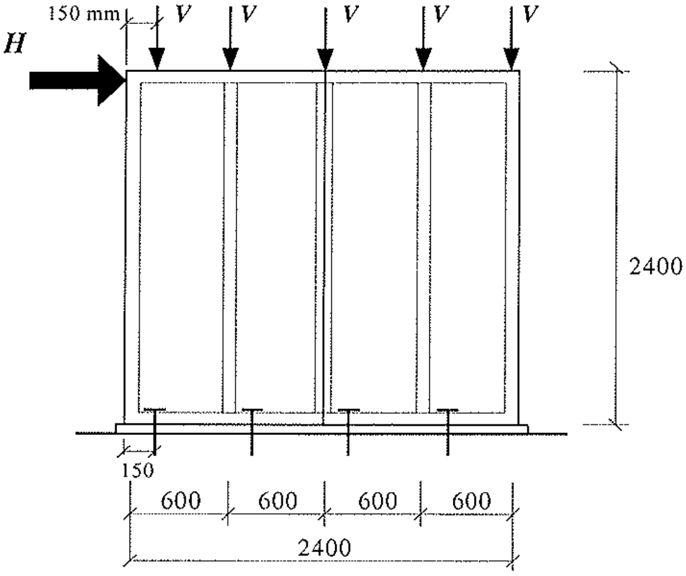

Figure 4. Details of test panels and requirements for test apparatus.

The racking load capacity of the wall panel is defined as the maximum value of the load-slip curve (panel failure) or when the wall panel attains a deformation of 100 mm, whichever first occurs.

The test results can only be used to determine the racking load for the wall panel with the specific design, the anchoring and loading conditions at hand.

3.2.2 American standard ASTM E 564

The American test standard, E 564 "Standard Practice for Static Load Test for Shear Resistance of Framed Walls for Buildings" [4], specifies a basis for evaluation of the shear stiffness and strength of a typical section of a framed shear wall, supported on a rigid foundation. Test wall size will vary with the specific objectives of the test. Tests conducted to assess the structural performance of actual building construction shall have dimensions commensurate with those of the shear walls being simulated.

The apparatus shall be assembled in a similar manner as shown in Figure 4. Provisions shall be made to resist rigid-body rotation in the plane of the wall where this reflects the use of the assembly in actual building constructions. This shall be done by application of relevant gravity or other loadings simultaneously with the racking loads. The bottom of the assembly shall be attached to the test base with anchorage connections simulating those that will be used in service. Load distribution along the top edge of the wall shall simulate floor or roof members that will be used in the actual building construction. The wall test assembly shall be laterally supported along its top.

4 Testing of shear walls with various anchoring and loading conditions

4.1 General

Strength and stiffness of sheathed wood shear walls can be tested in several ways. There are different schools concerning what type of testing is the most expedient one. Two extreme conditions are at hand:

(1) Pure shearing mode of behaviour of the wall panel, which requires that no uplift from the bottom plate is taking place.

   This mode will make possible the use of the full capacity of the shear wall. There are three ways to achieve this condition of pure shear:

   (i) the racking load is applied diagonally;

   (ii) the racking load is applied horizontally together with a load applied vertically on the leading stud and with a magnitude that is greater than or at least equal to what corresponds to the tilting moment (it is implicit that this vertical load must not induce any other type of failure mode); or

   (iii) the racking load is applied horizontally and the leading stud is rigidly tied down to the substrate;

   (These conditions apply strictly only to a wall segment comprised of a sheet attached to a frame only along its perimeter.)

(2) Pure tilting of the wall panel, which imply that it freely separates from the bottom plate and rotates around the lower corner at the trailing stud.

   This mode will render minimum utilization of the load-bearing capacity of the wall panel because of the total lack of anchoring of the wall panel to the substrate (implying that the self-weight of the wall panel is neglected). In case of pure tilting, the racking load is applied horizontally only.

The real behaviour of shear walls in practice be somewhere in between those extreme cases, depending on the anchoring of studs and bottom rail, inter-component connections between and flexibility of the surrounding walls and floors, and vertical loads from storeys or roof above the shear wall.

4.2 Boundary and loading conditions

The main kinds of boundary and loading conditions that represent various designs of shear walls in practise and in laboratory and that correspond to fully anchored leading stud and bottom rail are illustrated in Figure 5a & 5b, and 5c, respectively.

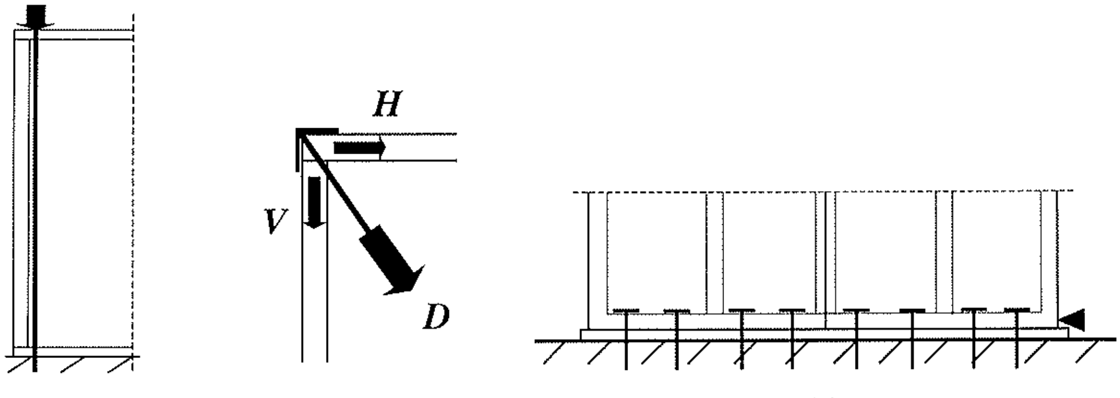

(a) (b) (c)

Figure 5. (a) Boundary condition corresponding to full anchoring of leading or tensile stud; (b) Loading condition - diagonal load or its horizontal and vertical components at leading stud and top rail corresponding to a fully anchored leading stud; and (c) Boundary condition corresponding to bottom rail continuously anchored to the rigid foundation;

The diagonal load case (b) in Figure 5 corresponds to a fully anchored leading stud according to the boundary condition case (a). The vertical component of the diagonal load will hold down the leading stud so it will act as fully anchored.

Thus, applying a diagonal load is a simple and rational way to imitate a fully anchored shear wall. This kind of test method is proposed to form the basis for a standard for prototype testing of shear walls.

4.3 Testing program

4.3.1 Background

Racking tests of shear walls have been conducted in order to evaluate the effect of different kinds of boundary and loading conditions. All wall tests consist of four segments of sheets fastened to a timber frame. The different boundary and loading conditions for the shear wall configurations are the ones shown in Figure 1 and others.

The dimension of framing members is 45 x 120 mm, the sheets consist of 8.0 mm hard fibreboard (Masonite AB, Sweden), and the sheathing-to-timber connectors is composed of annular ringed shank nails of dimension 50 x 2.1 mm (Nordisk Kartro AB).

A view of the set-up for tests where the racking load is applied diagonally in the upper corner of the shear wall, a diagonal tensile load as shown in Figure 6.

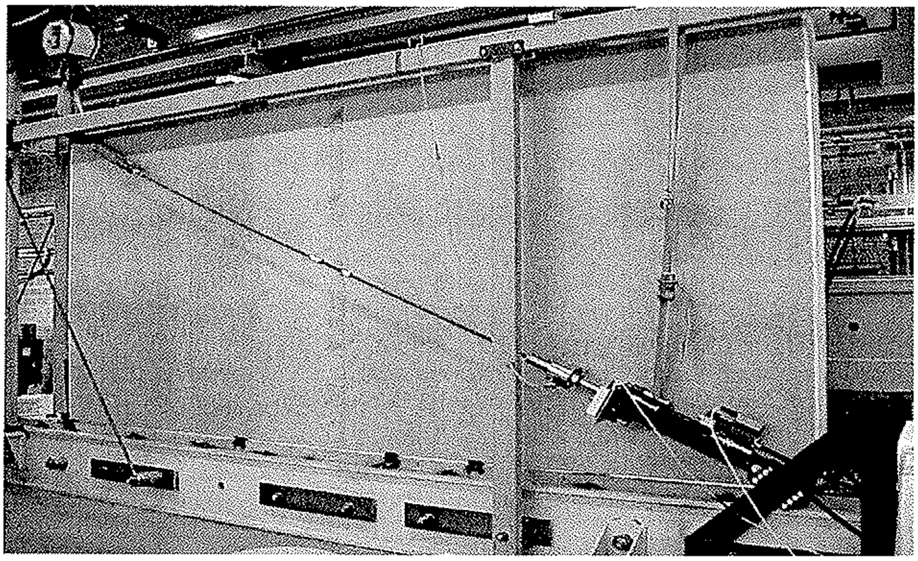

Figure 6. Racking load is applied as a diagonal tensile load.

4.3.2 Test results

For illustration purposes a few comments concerning the test results are given here.

For a *fully anchored shear wall* according to Figure 1a, the failure mode at the bottom of the loaded end is shown in Figure 7a. As is evident from the figure, no uplift of the leading stud occurred. The first failure occurred for a racking load of 51.5 kN at a displacement of 40 mm. Maximum load is 52.3 kN at a displacement of 43 mm. The plastic bending capacity of the sheathing-to-timber joints was reached and the final failure occurred after withdrawal of the nails out of the bottom rail. The first failure occurred when the sheathing-to-timber joint in the corner or next to the corner in the bottom rail failed. The final failure occurred when the sheathing-to-timber joints in a large part of the corner failed.

It was observed during the testing that it is hard to apply the racking load exactly in the corner. From other tests it has also been observed that crushing of wood takes place to a large extent at the point of application of the diagonal load and at the framing joint between the trailing stud and the bottom rail. This is true especially for long shear walls and/or short fastener spacing when very high racking loads are attained.

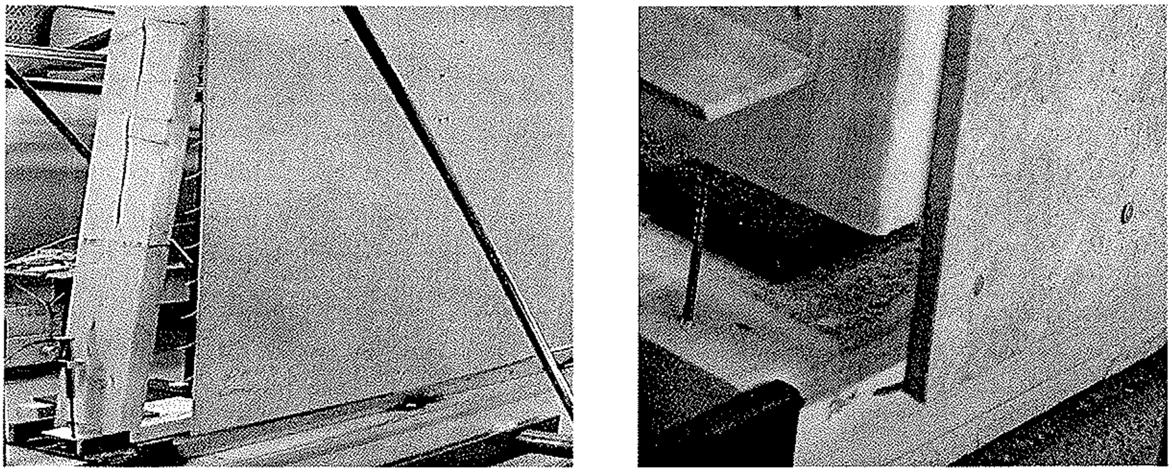

(a) (b)

Figure 7. (a) Failure of the sheathing-to-timber joints for a shear wall with boundary and loading conditions according to Figure 1a; and (b) Uplift of the leading stud and failure of the sheathing-to-timber joints for a shear wall with boundary and loading conditions according to Figure 1b and with $V = 0$.

For a *partially anchored shear wall* according to Figure 1b but with no vertical loads, the failure mode at the bottom of the loaded end is shown in Figure 7b. As is evident from the figure, considerable uplift of the leading stud took place. The first failure occurred for a racking load of 33.1 kN at a displacement of 17 mm. Maximum load is 36.6 kN at a displacement of 22 mm. The plastic bending capacity of the sheathing-to-timber joints was reached and the final failure occurred after withdrawal of the nails out of the bottom rail. The first failure started at the corner. The failure of the sheathing-to-timber joints occurred only in the bottom rail and not along the leading stud.

It is evident that the effect of uplift of the leading stud is considerable with respect to the horizontal load-carrying capacity of the shear wall. The reduction in this case with respect to the boundary and loading conditions at hand compared to the fully anchored case is 36.6/52.3 = 0.700.

This test result can only be used in applications for shear walls with these particular boundary and loading conditions. However, if use is made of the plastic theory for the boundary and loading conditions at hand compared to the fully anchored case, the reduction is given by 2.47/4 = 0.618 according to Figure 2. By applying the general test result for a fully anchored shear wall and this theoretical reduction factor, the horizontal load-carrying capacity for this particular case would differ only 13 % on the safe side compared to the test results for a partially anchored shear wall.

5 Conclusions

The design principles for shear walls given in Eurocode 5 are not satisfactory. There are shortcomings with respect to calculation of both stiffness and strength. It has been demonstrated that the structural behaviour of shear walls is very sensitive to wall geometry, boundary conditions and load configuration. The present European standard EN 594 for testing of shear walls recommends a test set-up that is very sensitive to the magnitude of the applied vertical load. Therefore, the test results obtained by this test standard are not unequivocally and generally applicable.

It is proposed that the present standard EN 594 is revised by using, as the main alternative, a test method that evaluates the strength and stiffness of the shear wall in a pure shearing mode. This mode will render boundary and loading conditions corresponding to a fully anchored shear wall. This pure shear mode is introduced in a rational way in the wall by applying a diagonal tensile load at the top corner of the wall. The vertical component of the diagonal load will hold down the leading stud so it will act as fully anchored. It is recommended that the bottom rail be anchored continuously to the rigid test base.

The proposed test method will render basic test results that have general applicability as far as the actual sheathing and fastener materials are concerned. Different materials can then easily be compared. The necessary adjustment of the design value for shear walls applied in a specific construction with certain boundary and loading conditions is then proposed to be made either by supplementary testing or by using theoretical reduction factors that depend on these conditions and that can be obtained by analytical models for partially anchored shear walls.

The mechanical properties of the sheathing-to-timber joints have a major influence on the stiffness and strength of shear walls. Therefore, the racking test standard would need to be supplemented by a relevant method for testing of the joint characteristics. The present standard for load bearing nailed joints is not appropriate. A new test standard is needed that incorporate testing of the parameters of special interest, such as edge distance of the fasteners and loading direction vis-à-vis the edge of the sheet.

By such a test standard for joints, design values for shear walls can be evaluated using general calculation models and the results can be compared to full-scale tests.

Proposal:

1) A new or revised test standard for determining basic stiffness and strength properties of sheathing-to-timber joints should be developed. Influence of edge distance and force direction should be included in this standard.
2) The main load configuration in test standard EN 594 should be changed to pure shear. This load configuration is more neutral with respect to different boundary conditions and could serve as a reference value for comparison of test results.
3) EN 594 should also include rules for testing of other load configurations that may occur in practice (e.g. the present main alternative).

By realising this proposal we open up for use of advanced methods in design of shear walls.

6 References

[1] ASTM 1998, "Annual Book of ASTM Standards", Designation: E 72 – 98 "Standard Test Methods of Conducting Strength Tests of Panels for Building Construction", American Society of Testing and Materials, Philadelphia, PA, pp. 1-11.

[2] Johnson, A.C., 1997, "Monotonic and Cyclic Performance of Long Shear Walls with Openings", Thesis submitted in partial fulfilment of the Masters of Science Degree at Virginia Polytechnic Institute and State University, Blacksburg, Virginia.

[3] Heine, C., 1997, "The Effect of Overturning Restraint on the Performance of Fully Sheathed and Perforated Timber Framed Shear Walls", Thesis submitted in partial fulfilment of the Masters of Science Degree at Virginia Polytechnic Institute and State University, Blacksburg, Virginia.

[4] ASTM 1995, "Annual Book of ASTM Standards", Designation: E 564 – 95 "Standard Practice for Static Load Test for Shear Resistance of Framed Walls for Buildings", American Society of Testing and Materials, Philadelphia, PA, pp. 83-86.

[5] Price, E.W. and Gromala, D.S., 1980. "Racking Strength of Walls Sheathed With Structural Flakeboards Made From Southern Species," *Forest Products Journal*, Vol. 30, No. 12, pp. 19-23.

[6] Wolfe, R.W., 1983, "Contribution of Gypsum Wallboard to Racking Resistance of Light-Frame Walls", Research Paper FPL 439, United States Department of Agriculture, Forest Products Laboratory.

[7] Griffiths, D.R., 1984. "Determining the Racking Resistance of Timber Framed Walls," *Proceedings of the Pacific Timber Engineering Conference, Auckland, New Zealand,* Vol. I "Timber Construction", Institution of Professional Engineers, Wellington, New Zealand, pp. 504-512.

[8] Dolan, J.D., 1989, "The Dynamic Response of Timber Shear Walls", Thesis submitted in partial fulfilment of the Doctor of Philosophy Degree at the University of British Columbia, Vancouver, British Columbia.

[9] CEN 1995, European standard EN 594 "Timber structures - Test methods - Racking strength and stiffness of timber frame wall panels", European Committee for Standardization, Brussels.

[10] Reardon, G.F., 1980, "Recommendations for the Testing of Roofs and Walls to Resist Wind Forces", Technical Report No. 5, Cyclone Testing Station, James Cook Structural Testing Station, Queensland.

[11] Stewart, W.G., 1987, "The Seismic Design of Plywood Sheathed Shearwalls", Thesis submitted in partial fulfilment of the Doctor of Philosophy Degree at the University of Canterbury, New Zealand.

[12] CEN 2001, European prestandard prEN 1995-1-1 "Eurocode 5 – Design of timber structures – Part 1.1: General rules and rules for buildings", European Committee for Standardization, Final Draft, CEN/TC 250/SC5 N158, September 2001, Brussels.

[13] CEN 1999, European standard EN 1380 "Timber structures - Test methods – Load bearing nailed joints", European Committee for Standardization, Brussels.

[14] Källsner, B. and Lam, F., 1995, "Diaphragms and shear walls", Holzbauwerke nach Eurocode 5 - STEP 3, Arbeitsgemeinschaft Holz e.V., Düsseldorf, pp. 15/1-15/19.

[15] Källsner, B., Girhammar, U.A. and Wu, L., 2001, "A simplified plastic model for design of partially anchored wood-framed shear walls", CIB/W18 Meeting, Venice, Italy, 22-24 August, 2001, 19 pp.

[16] Källsner, B., Girhammar, U.A. and Wu, L., 2002, "A plastic design model for partially anchored wood-framed shear walls with openings", CIB/W18 Meeting, Kyoto, Japan, 16-19 September, 2002, 17 pp.

CIB-W18/35-15-2

INTERNATIONAL COUNCIL FOR RESEARCH AND INNOVATION
IN BUILDING AND CONSTRUCTION

WORKING COMMISSION W18 - TIMBER STRUCTURES

A PLASTIC DESIGN MODEL FOR PARTIALLY ANCHORED WOOD-FRAMED SHEAR WALLS WITH OPENINGS

B Källsner
Växjö University
Trätek - Swedish Institute for Wood Technology Research

U A Girhammar
L Wu
Civil Engineering, Department of Applied Physics, Umeå University

SWEDEN

Presented by: B Källsner

S Aicher asked about the distribution of loads in the studs and if all the loading eventually located in the end stud. B Källsner confirmed that a lower bound plastic approach was used to model the system tested and that it was one of many possible ways to do so. He also confirmed that the studs used may be considered to be stiff and that the loads were transferred to the end stud. H Larsen asked for a comparative comment on the load testing approach which is frequently used versus the analytical/calculation approach which the Scandinavians seem to prefer. This led to a comment by B Dujic about the need to maintain the vertical loading and the significance of dynamic and monotonic load testing of shear walls. S Thelandersson and H Sugiyama commented on the importance of preventing uplift of the wall end and the differences between testing a floor system and a racked shear wall system.

A plastic design model for partially anchored wood-framed shear walls with openings

Bo Källsner
Växjö University, Sweden
Trätek - Swedish Institute for Wood Technology Research, Sweden

Ulf Arne Girhammar and Liping Wu
Department of Applied Physics, Umeå University, Sweden

Abstract

Design of shear walls has been a topic of major discussions during the Eurocode 5 work. The main problem has been that shear walls are fastened to the substrate in different ways in different countries and that this fact must be reflected in the code.

At the CIB-W18 meeting in Venice 2001, a simplified plastic model for design of partially anchored wood-framed shear walls in the ultimate limit state was presented. The method covers static loads and can be applied when mechanical fasteners with plastic characteristics are used.

The main focus of the present paper is to extend this plastic model to design of partially anchored shear walls with openings. The method is applied to a few typical wall configurations with openings.

A few introductory tests of shear walls with openings have been conducted where the bottom rail was completely fixed to the substrate. The test results indicate that the proposed basic theory should be somewhat modified in order to obtain good agreement between measured and calculated load-carrying capacity.

1 Introduction

1.1 Background

Design of shear walls has been a topic of major discussions during the Eurocode 5 work. The European test standard EN 594 has often been criticised for giving very conservative test results. The main problem has been that shear walls are fastened to the substrate in different ways in different countries and that this fact must be reflected in the code.

Different methods suitable for calculation by hand have been presented by Källsner et al (1995). Andreasson (2000) has demonstrated the importance of considering the three-dimensional interaction in stabilisation of multi-storey timber frame buildings.

At the previous CIB-W18 meeting, Källsner et al (2001) presented a plastic lower bound method for design of shear walls in the ultimate limit state. The advantage of this model is that it can be applied on shear walls that are completely as well as incompletely anchored to the substrate.

1.2 Objective

The objective of this paper is to extend the plastic lower bound model for design of partially anchored wood-framed shear walls presented by Källsner et al (2001) to include also the influence of openings in walls.

The purpose of this paper is not to present the final version of the model but rather to give some basic principles that can be discussed.

1.3 Limitations

The simplified model can only be applied on shear walls where the sheet material is fixed by mechanical fasteners to the frame members and where these sheathing-to-timber joints show plastic behaviour.

The model covers only static loads in the ultimate limit state. The model can not be used for determination of deformations in the serviceability limit state.

In some cases there are risks of brittle failure modes in the shear walls. An example of such a failure mode is when cracks occur in the frame members due to small edge distances of the fasteners. The influence of such failure modes is not treated.

In connection with openings in shear walls, high concentrated contact forces between adjacent sheets may give raise to local buckling failures in the sheets. These failure modes are not dealt with in this paper.

2 Basic assumptions

For design of partially anchored shear walls a plastic lower bound method is proposed. This means that a force distribution is chosen that fulfils the conditions of force and moment equilibrium for each timber member and sheet. The basic assumptions are identical to those given by Källsner et al (2001) and are as follows:

- the sheathing-to-timber joints, referring to the vertical studs and the top rail, are assumed to transfer shear forces only parallel to the timber members
- the sheathing-to-timber joints, referring to the bottom rail, are assumed to transfer forces both parallel and perpendicular to the bottom rail
- the framing joints are not assumed to transfer any tensile or shear forces
- compressive forces can be transferred via contact between adjacent sheets.

In order to obtain simple expressions for the racking resistance of the shear walls, the fasteners are assumed to be continuously distributed along the timber members. The load-carrying capacity of the sheathing-to-timber joints is consequently given in force per unit length. In all the examples presented below, it is assumed that the fastener spacing around the perimeter of the sheets is constant.

3 Fully anchored bottom rail – no vertical loads

3.1 Sheets of different depths. Low sheet on the leeward side.

In order to understand the structural behaviour of shear walls with openings, a fundamental wall configuration consisting of two sheets according to Figure 1 will first be studied. The bottom rail is assumed to be fully anchored to the substrate. h and b denote the depth and the width of the full format sheets respectively. The depth of the lower sheet is denoted by h_l and the length of the wall is denoted by l ($=2b$). The leading stud is assumed to be completely free from the bottom rail. The forces acting on the wall in the ultimate limit state are assumed to be distributed according to Figure 1. The forces acting along the lower part of the wall are shown in a section immediately above the bottom rail and represent the sheathing-to-timber joints. It is assumed that the plastic capacity per unit length of these joints f_p has been attained. The factor μ opens for the possibility of using reduced strength properties when the fastener forces act perpendicular to the sheet edges. If nothing else is said, it is assumed that $\mu = 1$ in this paper. Further, it is assumed that the plastic shear capacity of the sheathing-to-timber joints between the two sheets has not been attained. The notation l_{eff} is used to indicate that this length of the wall is fully effective for horizontal load transfer.

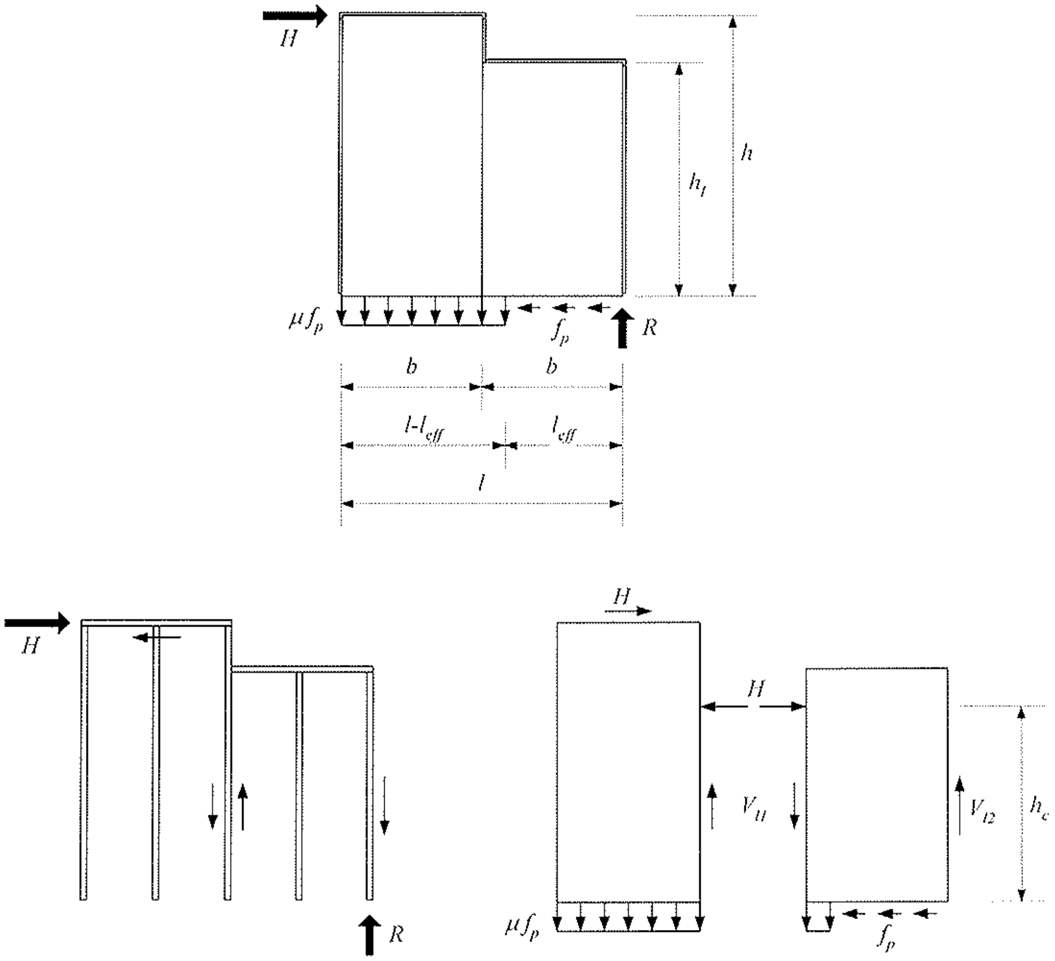

Figure 1: Forces acting on a shear wall in the case of a low sheet on the leeward side ($h_l \geq h_c$).

Moment equilibrium around the lower right corner of the wall diaphragm gives

$$H\,h = \mu f_p (l - l_{eff})\left(\frac{l + l_{eff}}{2}\right) \tag{1}$$

Force equilibrium in horizontal direction gives

$$H = f_p l_{eff} \tag{2}$$

By introducing the notation

$$\alpha = \frac{l}{h} \tag{3}$$

and using equations (1) and (2) the effective wall length can be calculated as

$$l_{eff} = l\left(\sqrt{1 + \left(\frac{1}{\alpha\mu}\right)^2} - \frac{1}{\alpha\mu}\right) \tag{4}$$

Force equilibrium in the vertical direction gives

$$R = \mu f_p (l - l_{eff}) \tag{5}$$

By studying the vertical force equilibrium of the left sheet, the shear force V_{l1} between the two sheets is obtained as

$$V_{l1} = \mu f_p b \tag{6}$$

This force must of course be lower than the plastic capacity $f_p h_l$.

The assumed external force distribution for the shear wall configuration in Figure 1 is identical to the one used by Källsner et al (2001) for a wall configuration consisting of one or several sheets of full format forming a row of sheets. In order to fulfil the moment of equilibrium of the two sheets a contact force must be transferred between them. The position of this contact force defined by the distance h_c can be calculated by studying the moment of equilibrium of the left sheet in Figure 1. A moment equation around the lower right corner gives

$$H(h - h_c) = \mu f_p \frac{b^2}{2} \tag{7}$$

By inserting equation (2) into equation (7), the position of the contact force is obtained as

$$h_c = h - \frac{\mu b^2}{2 l_{eff}} \tag{8}$$

This means that the depth h_l of the right sheet in Figure 1 must be larger than or equal to h_c in order to attain the full plastic capacity f_p of the sheathing-to-timber joints along the bottom rail. For $h/b = 2$ and $\mu = 1$ the distance h_c is calculated from equation (8) to 0,698 h. It is observed that in the case of two sheets of full format connected by a common top rail, the distance h_c represents the position of the resultant horizontal force corresponding to the contact force between the two sheets and the force in the top rail.

In the derivation of the equations above it was demonstrated that the depth h_l of the low sheet had to be at least equal to h_c. Now a wall configuration according to Figure 2 in which the depth h_l is less than h_c will be studied. In this case the full plastic capacity f_p of the sheathing-to-timber joints along the bottom rail of the low sheet can not be attained.

The maximum racking capacity H of this wall configuration will be obtained if the left sheet is assumed only to transfer vertical force components to the bottom rail.

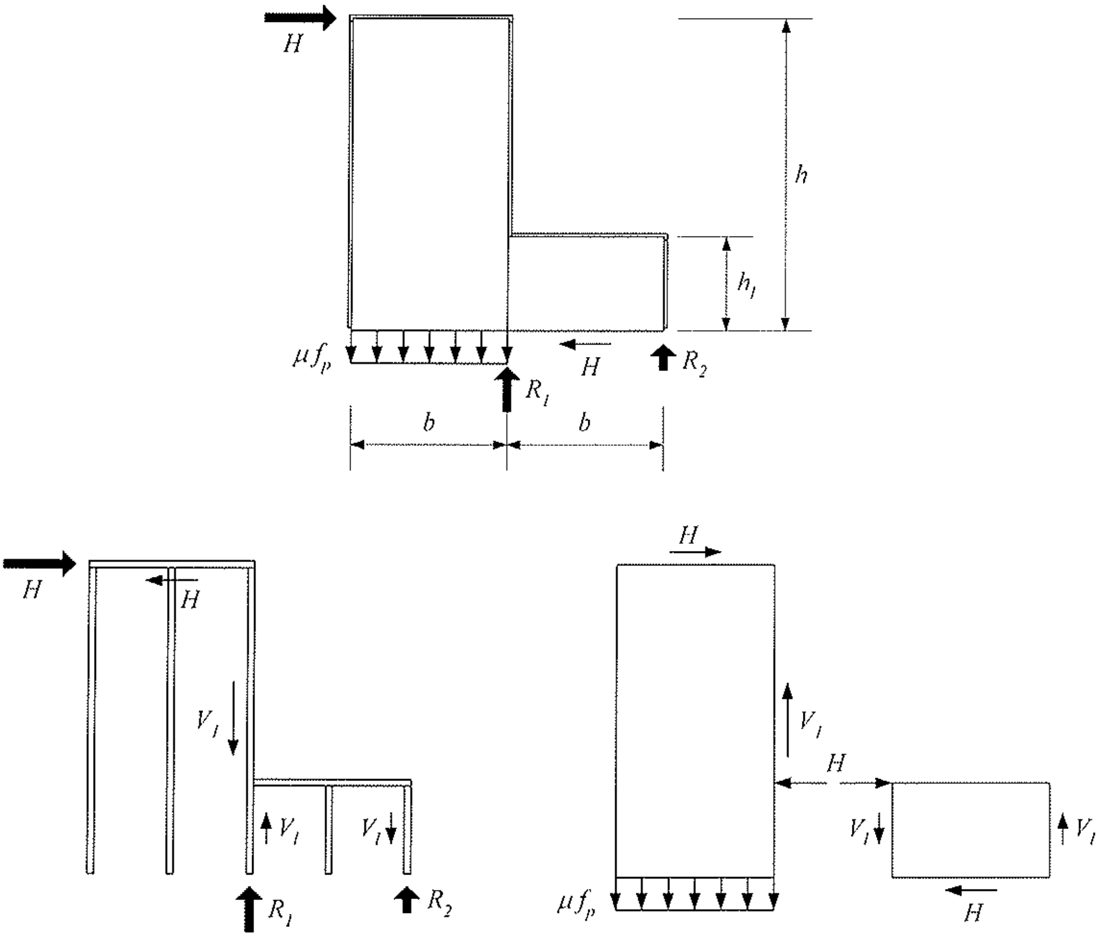

Figure 2: Forces acting on a shear wall in the case of a low sheet on the leeward side ($h_l \le 2/3\ h$).

A moment equation with respect to the left sheet around the lower right corner gives

$$H = \mu f_p \frac{b^2}{2(h - h_l)} \tag{9}$$

Moment equilibrium for the right sheet gives

$$V_l = \frac{h_l}{b} H = \mu f_p \frac{b h_l}{2(h - h_l)} \tag{10}$$

A vertical equilibrium equation for the stud furthest to the right gives

$$R_2 = V_l = \mu f_p \frac{b h_l}{2(h - h_l)} \tag{11}$$

Force equilibrium in vertical direction with respect to the entire shear wall gives

$$R_1 = \mu f_p b - R_2 = \mu f_p b \frac{2h - 3h_l}{2(h - h_l)} \tag{12}$$

From equation (12) it is obvious that the reaction force R_1 will only be positive if the depth of the sheet $h_l < 2/3\ h$. This means that for depths h_l in the range between 2/3 h and h_c there must be a force distribution according to Figure 3.

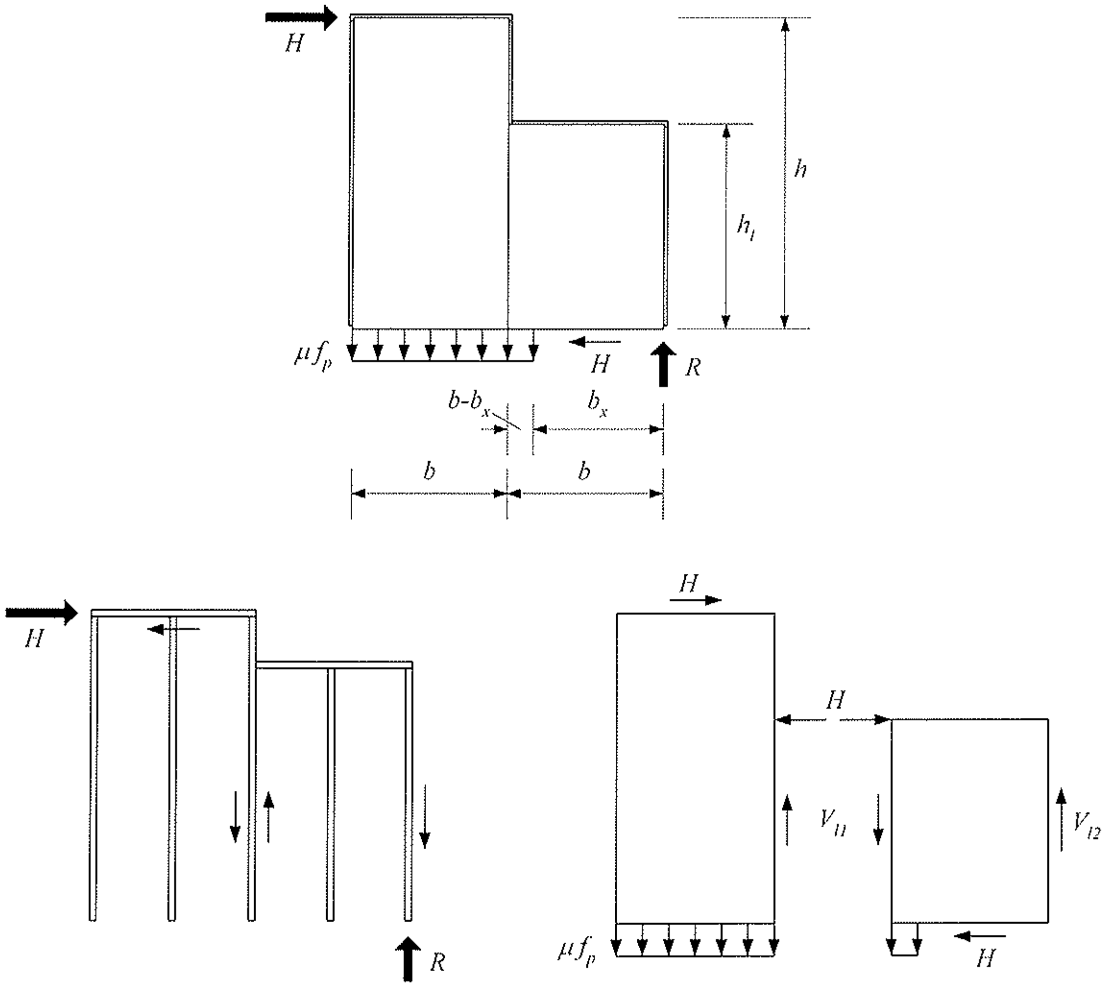

Figure 3: Forces acting on a shear wall in the case of a low sheet on the leeward side ($2/3\ h \leq h_l \leq h_c$).

A moment equation with respect to the left sheet around the lower right corner gives

$$H = \mu f_p \frac{b^2}{2(h - h_l)} \tag{13}$$

The load-carrying capacity H in equation (13) is the same as in equation (9) since the force distribution on the left sheet has not been changed. Vertical force equilibrium for the left sheet gives

$$V_{l1} = \mu f_p b \tag{14}$$

Moment equilibrium of the entire shear wall around the lower right corner can be expressed as

$$Hh = \mu f_p (2b - b_x) \frac{2b + b_x}{2} \tag{15}$$

Insertion of equation (13) into equation (15) gives

$$b_x = b\sqrt{\frac{3h-4h_l}{h-h_l}} \tag{16}$$

Vertical force equilibrium for the entire shear wall gives

$$R = \mu f_p(2b-b_x) = \mu f_p b\left\{2-\sqrt{\frac{3h-4h_l}{h-h_l}}\right\} \tag{17}$$

In Figure 4 the horizontal racking capacity H of the shear wall is shown as function of the depth h_l for the case when $h/b = 2$ and $\mu = 1$. The relationship is given by equation (9) and (13) when $h \le h_c$ and by equation (2) when $h \ge h_c$. An interesting observation is that when the depth h_l approaches zero the capacity H approaches 0,25. This value is close to the value 0,24 obtained for a shear wall consisting of a single sheet of full format, see Källsner et al. (2001). It can of course be questioned if it is reasonable to adopt the proposed model for very small values of the depth h_l. On the other hand we must be aware of that it is a plastic lower bound method and that the limit value (0,25 for $h_l/h = 0$) does not deviate much from the one found for a wall built up of only one sheet of full format (0,24).

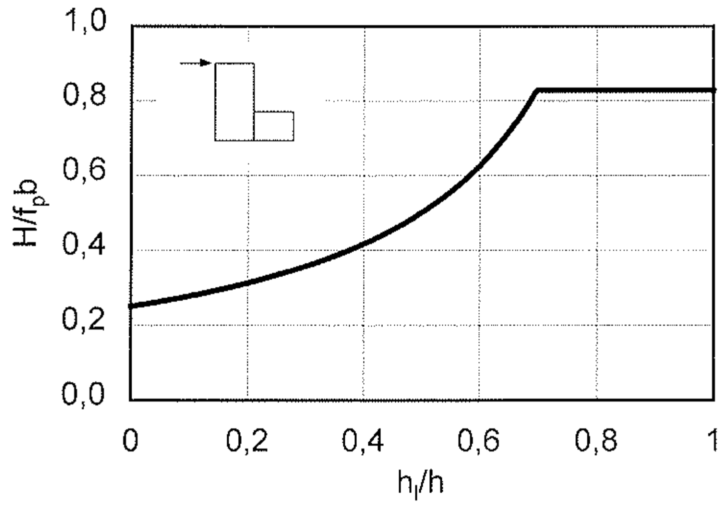

Figure 4: Relationship between load-carrying capacity *H* and depth h_l in the case of a low sheet on the leeward side ($h/b = 2$ and $\mu = 1$).

3.2 Sheets of different depths. Low sheet on the windward side.

In section 3.1 a shear wall consisting of two sheets of different depths was studied for the load case when the low sheet was placed on the leeward side. In this section the same wall configuration will be studied but with the low sheet on the windward side. The same kind of notations as was used in previous section will be used here. First the wall configuration according to Figure 5 will be studied, where the plastic fastener capacity of the sheathing-to-timber joints along the entire bottom rail has been attained. By studying the force equilibrium of the low sheet, the shear force V_l is obtained as

$$V_l = \frac{1}{2}\mu f_p b \tag{18}$$

To ensure that the shear force V_l always is smaller than or equal to the plastic shear capacity $f_p h_l$ along the vertical sides of the low sheet, the condition $h_l \ge 0{,}5\ \mu b$ must always be fulfilled.

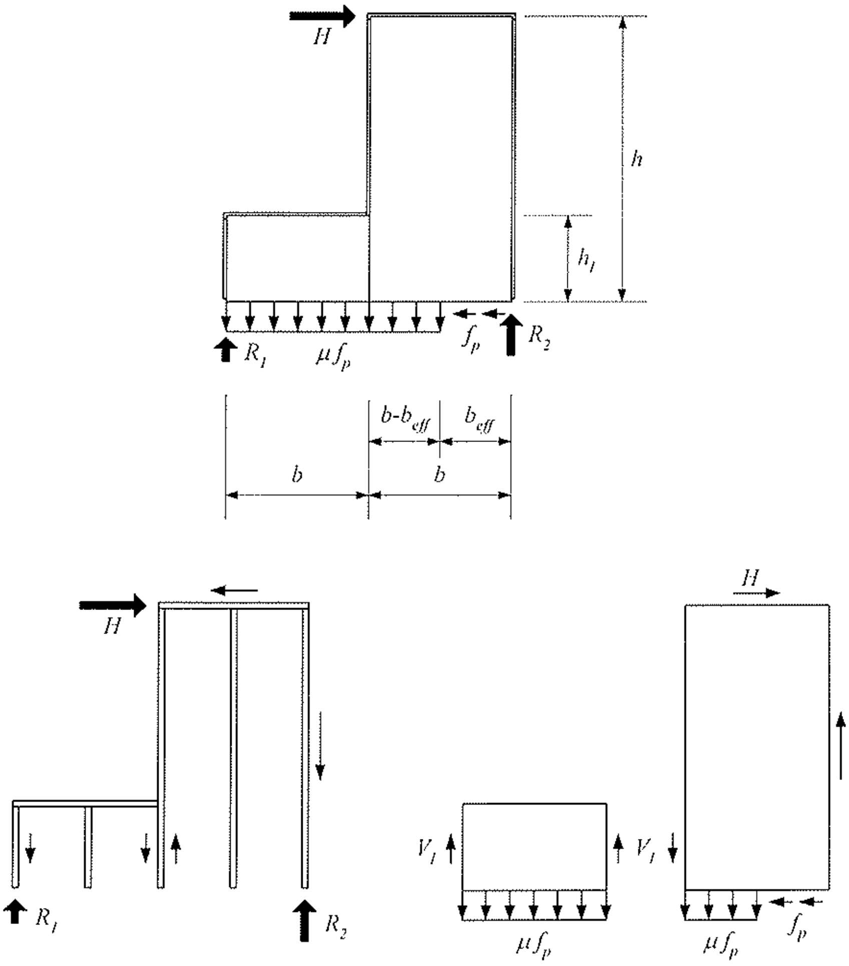

Figure 5: Forces acting on a shear wall in the case of a low sheet on the windward side ($h_l \geq 0{,}5\ \mu b$).

The effective width b_{eff} is obtained by studying the moment equilibrium of the full format sheet (cf. Källsner et al 2001). A moment equation around the lower right corner of the sheet gives

$$Hh - V_l b = \mu f_p (b - b_{eff}) \frac{b + b_{eff}}{2} \tag{19}$$

Force equilibrium in horizontal direction gives

$$H = f_p b_{eff} \tag{20}$$

The vertical load V_l can be expressed by the factor β_l defined as

$$\beta_l = \frac{V_l}{f_p h} \tag{21}$$

By introducing the notation

$$\alpha_s = \frac{b}{h} \tag{22}$$

and using equations (19)-(21) the effective sheet width is obtained as

$$b_{eff} = b\left(\sqrt{1+\left(\frac{1}{\alpha_s\mu}\right)^2+\frac{2\beta_l}{\alpha_s\mu}}-\frac{1}{\alpha_s\mu}\right) \tag{23}$$

Force equilibrium in vertical direction gives

$$R_2 = \mu f_p\left(\frac{3b}{2}-b_{eff}\right) \tag{24}$$

If the depth of the low sheet is fairly small the condition $h_l \geq 0{,}5\ \mu b$ will not be fulfilled and a force distribution according to Figure 6 is reasonable to assume. The distributed force f acting along the lower side of the low sheet is in this case always less than or equal to the plastic capacity μf_p. Assuming that the plastic shear flow f_p is attained along the vertical sides of the low sheet, the shear force V_l is obtained as

$$V_l = f_p h_l \tag{25}$$

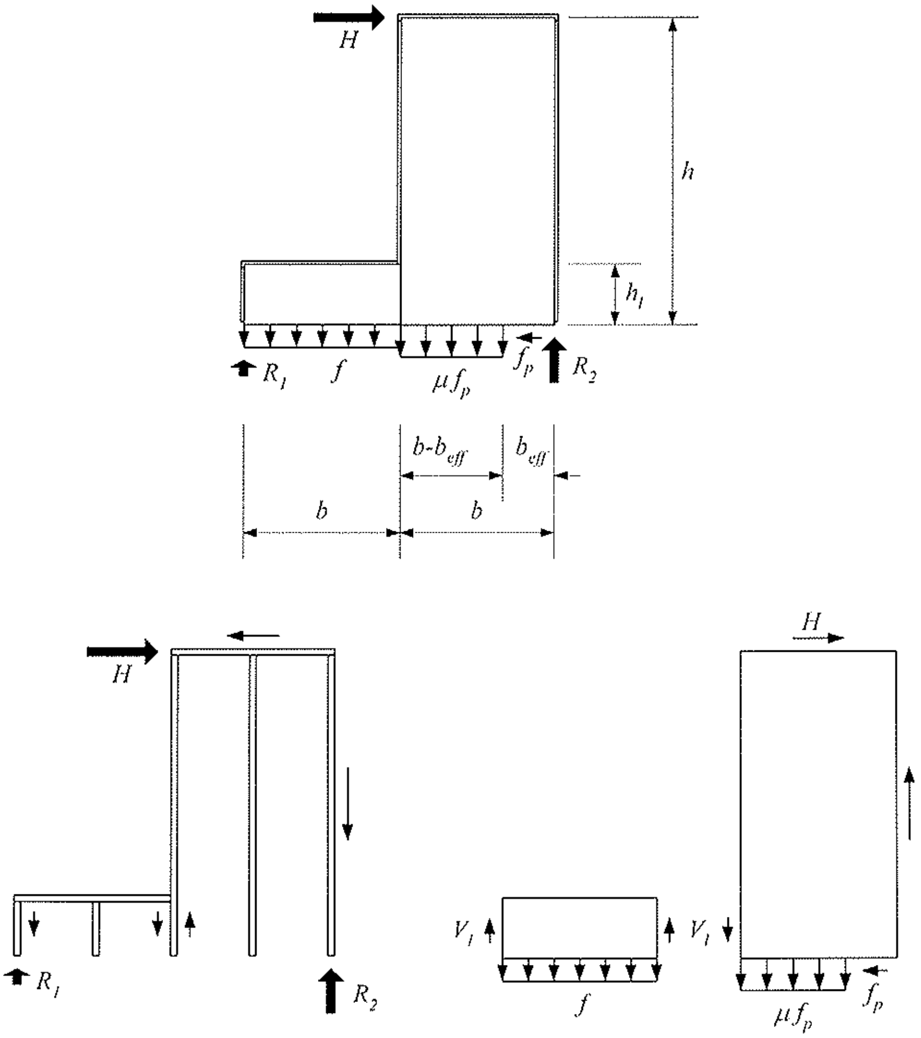

Figure 6: Forces acting on a shear wall in the case of a low sheet on the windward side ($h_l \leq 0{,}5\ \mu b$).

Considering this new relationship, the effective width b_{eff} can be calculated from equation (23). Vertical force equilibrium gives

$$R_2 = f_p(h_l + \mu(b - b_{eff})) \tag{26}$$

According to one of the basic assumptions in section 2 it is assumed that the sheathing-to-timber joints along the vertical studs do not transfer any forces perpendicular to the timber members. The test results presented in section 4 indicate that this assumption may lead to too low racking capacities and that there are cases when it is reasonable to consider this type of forces. First a shear wall, with the forces distributed according to Figure 7, will be studied.

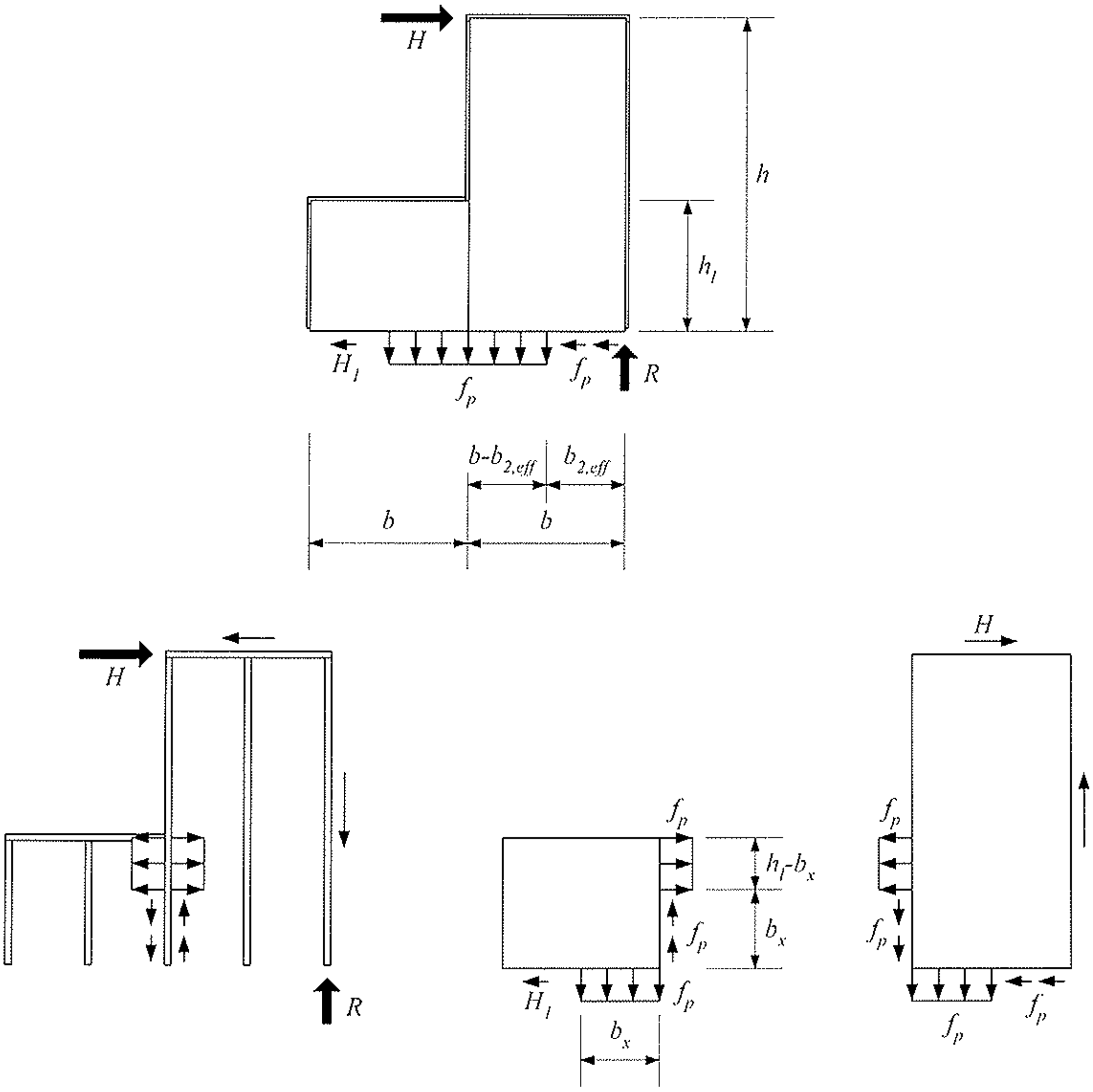

Figure 7: Forces acting on a shear wall in the case of a low sheet on the windward side. Tensile forces perpendicular to the vertical timber stud ($h_l \leq b$ and $\mu = 1$).

It is assumed that the plastic shear flow f_p has been attained along the right side of the low sheet. In order to obtain not too complicated equations, it is assumed that the factor μ is equal to unity. To fulfil the horizontal and vertical force equilibrium of the low sheet these assumptions lead to the condition that the depth h_l must be less or equal to the width b. Considering the moment equilibrium of the small sheet around its lower right corner gives

$$f_p b_x \frac{b_x}{2} = f_p (h_l - b_x) \frac{h_l + b_x}{2} \tag{27}$$

From equation (27) the distance b_x is calculated as

$$b_x = \frac{h_l}{\sqrt{2}} \tag{28}$$

Horizontal force equilibrium of the small sheet gives

$$H_1 = f_p(h_l - b_x) \tag{29}$$

Moment equilibrium of the entire shear wall around its lower right corner gives

$$Hh = f_p(b - b_{2,eff})\frac{b + b_{2,eff}}{2} + f_p b_x (b + \frac{b_x}{2}) \tag{30}$$

Horizontal force equilibrium gives

$$H = H_1 + f_p b_{2,eff} \tag{31}$$

By introducing the notations

$$V = f_p b_x \frac{b + \frac{b_x}{2}}{b} \tag{32}$$

and

$$\beta = \frac{V}{f_p h} \tag{33}$$

and inserting equation (31) into equation (30), the effective width $b_{2,eff}$ is obtained as

$$b_{2,eff} = b\left(\sqrt{1 + \left(\frac{1}{\alpha_s}\right)^2 + \frac{2\beta}{\alpha_s} - \frac{2H_1}{\alpha_s f_p b}} - \frac{1}{\alpha_s}\right) \tag{34}$$

The racking capacity of the shear wall is obtained by inserting equation (34) into equation (31).

If the depth h_l is larger than the width b, it is reasonable to assume that the forces acting on the low sheet are distributed according to Figure 8.

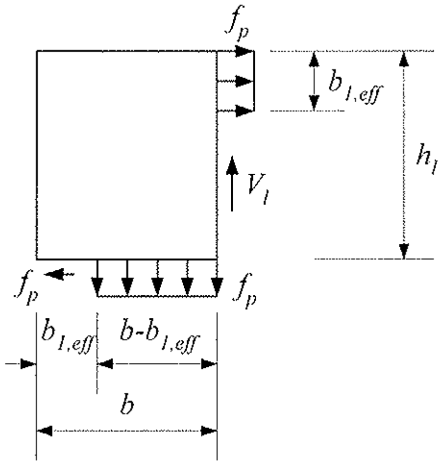

Figure 8: Forces acting on a shear wall in the case of a low sheet on the windward side. Tensile forces perpendicular to the vertical timber stud ($h_l \geq b$ and $\mu = 1$).

For this wall configuration the following equations can be derived

$$b_{1,eff} = \frac{1}{2}(b+h_l) - \frac{1}{2}\sqrt{(b+h_l)^2 - 2b^2} \tag{35}$$

$$V_l = f_p(b - b_{1,eff}) \tag{36}$$

$$V = \frac{\frac{1}{2}(3b - b_{1,eff})}{b} V_l \tag{37}$$

$$\beta = \frac{V}{f_p h} \tag{38}$$

$$b_{2,eff} = b\left(\sqrt{1 + \left(\frac{1}{\alpha_s}\right)^2 + \frac{2\beta}{\alpha_s} - \frac{2}{\alpha_s}\frac{b_{1,eff}}{b}} - \frac{1}{\alpha_s}\right) \tag{39}$$

$$H = f_p(b_{1,eff} + b_{2,eff}) \tag{40}$$

In Figure 9 the relationship between the racking capacity H and the depth h_l is shown for the different assumed force distributions. The bold line represents the force distributions according to the basic theory shown in Figure 5 and 6. The thin line represents the force distributions according to the more advanced theory in Figure 7 and 8. It is clearly demonstrated that for h_l larger than $b/2$, the racking capacity H will increase considerably if tensile forces are accepted perpendicular to the vertical studs.

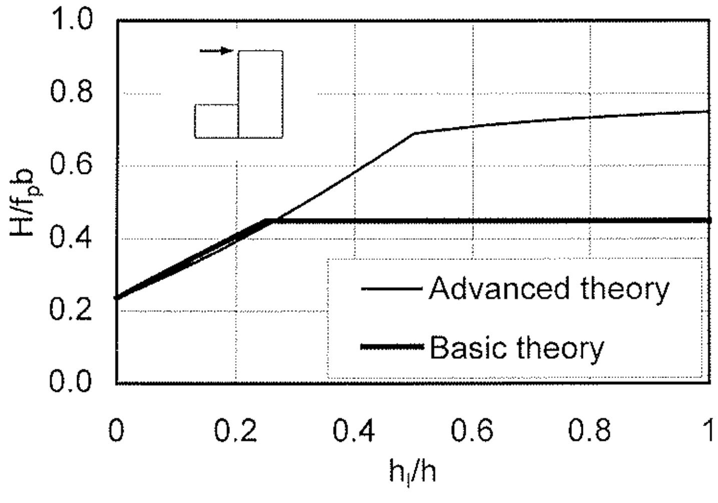

Figure 9: Relationship between load-carrying capacity H and depth h_l in the case of a low sheet on the windward side ($h/b = 2$ and $\mu = 1$).

3.3 Wall with window opening on the leeward side

The shear wall configuration according to Figure 10 can be handled in the same way as the wall in section 3.1 consisting of two sheets of different depths. Due to the basic assumptions in section 2, the sheet above the window opening will not contribute to any additional shear capacity.

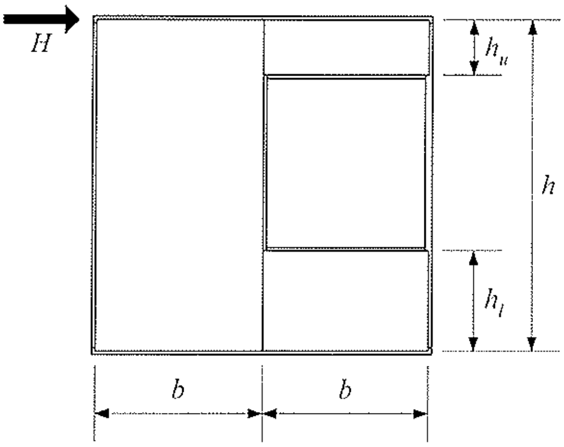

Figure 10: Shear wall with window opening on the leeward side.

3.4 Wall with window opening on the windward side

A shear wall with a window opening on the leeward side will now be studied. The forces acing on the wall are assumed to be distributed according to Figure 11. In this case it is assumed that the plastic capacity of the sheathing-to-timber joints along the bottom rail has been attained. Further, it is assumed that the plastic capacity of the sheathing-to-timber joints in the small sheet above the window opening has been attained along the top rail. Consequently the force H_u is obtained as

$$H_u = f_p b \tag{41}$$

Moment equilibrium for the sheet above the window opening gives

$$V_u = \frac{h_u}{b} H_u = f_p h_u \tag{42}$$

Vertical force equilibrium of the sheet below the window opening gives

$$V_l = \frac{1}{2} \mu f_p b \tag{43}$$

It must here be controlled that the force V_u not is larger than the force V_l. If this is not the case, plastic shear flow between the top rail and the small sheet cannot be assumed.

Horizontal force equilibrium of the shear wall gives

$$H = f_p b_{eff} \tag{44}$$

A moment equation for the body consisting of the small sheet and the full format sheet around the lower right corner gives

$$Hh - V_u 2b - V_l b = \mu f_p (b - b_{eff}) \frac{b + b_{eff}}{2} \tag{45}$$

By introducing the notations

$$V = 2V_u + V_l \tag{46}$$

and

$$\beta = \frac{V}{f_p h} \tag{47}$$

and inserting the equations (42)-(44) in equation (45), the effective width b_{eff} can be expressed as

$$b_{eff} = b\left(\sqrt{1+\left(\frac{1}{\alpha_s \mu}\right)^2 + \frac{2\beta}{\alpha_s \mu}} - \frac{1}{\alpha_s \mu}\right) \tag{48}$$

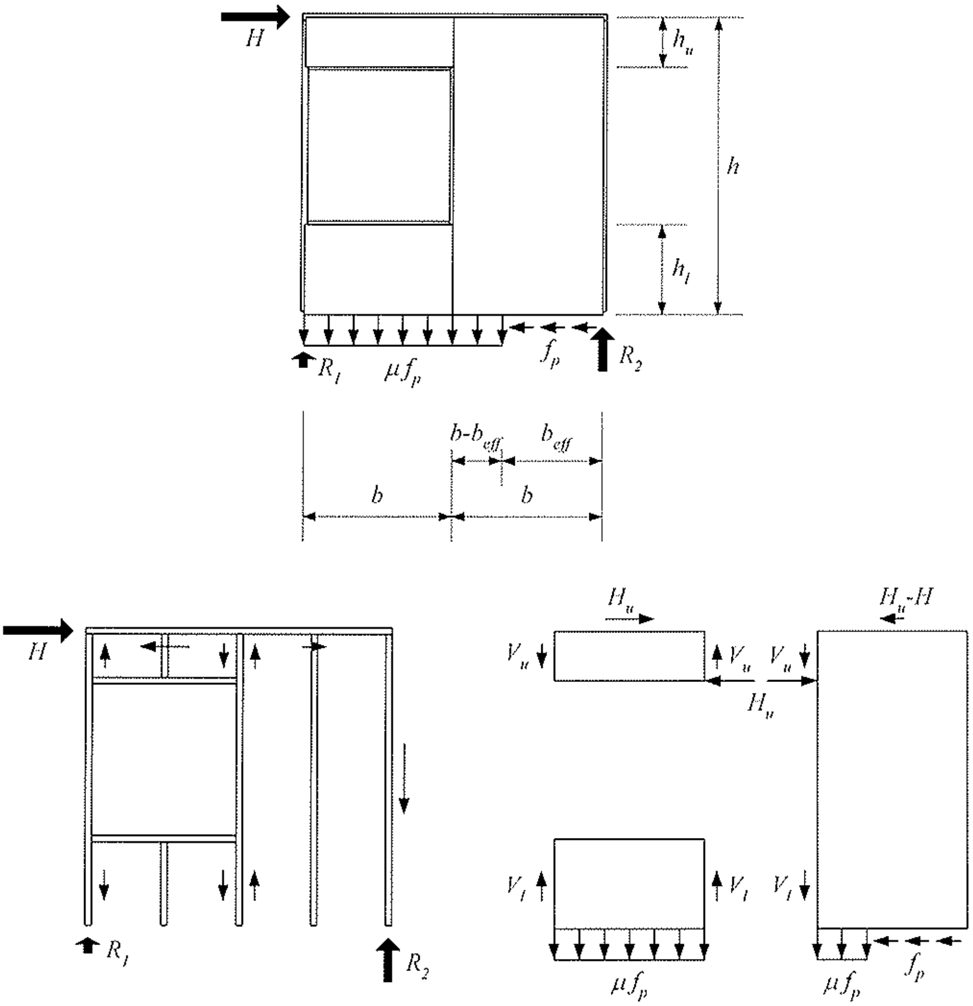

Figure 11: Forces acting on a shear wall in the case of a window opening on the windward side ($h_l \geq 0{,}5\ \mu b$ and $V_l \geq V_u$).

In Figure 12 the racking capacity H of the shear wall is shown as function of the depth h_u for the case when $h_l \geq 0{,}5\ \mu b$, $h/b = 2$ and $\mu = 1$. The left part of the bold curve represents the basic theory according to equation (48). The breakpoint on the curve represents the case when the force V_l is equal to the force V_u. For this value of the depth h_u, the force distribution along the bottom rail is identical to the case when a shear wall is built up of two sheets of full format ($H/f_p b$ = 0,83 according to Källsner et al. 2001). Consequently, for h_u values larger than this value, the window opening has no influence on the racking capacity H of the wall. The thin curve shows the results of a more advanced calculation where transfer of tensile forces between the two sheets via the vertical stud has been accepted. This corresponds to the procedure presented at the end of section 3.2.

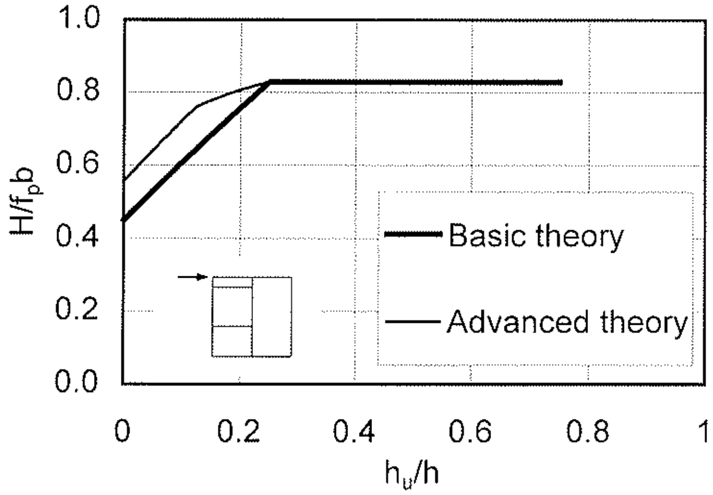

Figure 12: Relationship between load-carrying capacity *H* and depth h_u in the case of a window opening on the windward side ($h_l \geq 0{,}5\ \mu b$, $h/b = 2$, $\mu = 1$).

3.5 Wall with window opening between two sheets of full format

In this section a wall configuration consisting of a window opening between two sheets of full format is studied. This type of structure can be analysed in two stages. First the left sheet including the influence of the window opening is analysed (see section 3.3). Then the right sheet including the influence of the window opening is analysed (see section 3.4), considering the forces introduced during the first stage. The results of such an calculation is shown in Figure 13 where the load carrying capacity *H* is given as a function of the depth h_u. In this case it has been assumed that $h/b = 2$, $\mu = 1$ and $h_l/h = 0{,}375$.

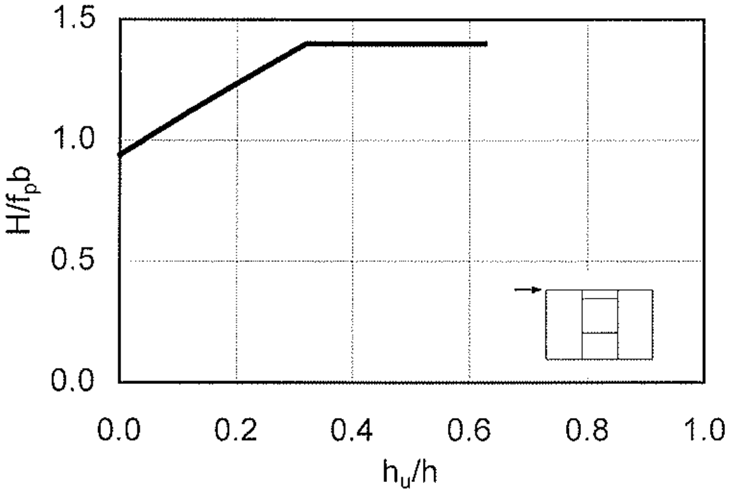

Figure 13: Relationship between load-carrying capacity *H* and depth h_u in the case of a window opening between two sheets of full format ($h/b = 2$, $\mu = 1$, $h_l/h = 0{,}375$).

4 Experimental work

The results of some introductory tests of shear walls without openings were reported by Källsner et al (2001). In those tests the influence of different kinds of anchorage and load configurations were investigated.

In this paper the results of a few tests of shear walls with openings will be reported. As in the previous tests, hard fibreboard of thickness 8 mm was used. The size of the sheets was 1200 x 2400 mm and the dimension of the timber members was 45 x 120 mm. For the sheathing-to-timber connections, annular ringed shank nails of dimension 50 x 2,1 mm were used. The distances between the fasteners were 100 mm along the perimeter of the sheets and 200 mm along the vertical centre lines of the sheets. The nominal edge distance was 11,25 mm along the vertical studs and 22,5 mm along the bottom and top rails. For each framing joint two annular ringed shank nails of dimension 90 x 3,1 mm were used. These nails were applied in the grain direction of the vertical studs. More information about the test specimens and the testing procedure can be found in Källsner et al (2001).

A specification of shear walls tested is shown in Table 1. The depths of the sheets above and below the window openings were 300 and 900 mm respectively. The bottom rail was completely fixed to the substrate.

Table 1: Specification of shear walls tested

Test wall	Load configuration	Anchored bottom rail	Vertical loads [kN]
1	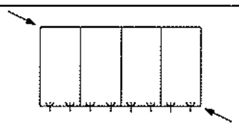	Yes	
2	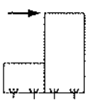	Yes	
3	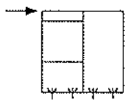	Yes	
4	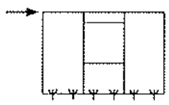	Yes	
5	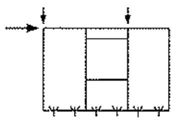	Yes	12,9 (0,50 $f_p h$)

Measured and calculated load-carrying capacities of shear walls tested are shown in Table 2. Test specimen 1 served as a reference test for the other tests. The load was in this case applied in the diagonal direction of the wall diaphragm but the horizontal load component is given in the table. The plastic shear flow is obtained as $f_p = 51{,}7 / 4{,}8 =$ 10,8 kN/m. Calculated capacities are given using both the basic and the more advanced theory. In the basic theory it is assumed that there can only be transferred force components between the vertical studs and the sheets in the length direction of the studs. In the more advanced theory, it is assumed that force components can also be transferred perpendicularly to the length direction of the studs.

The ratios between measured and calculated load-carrying capacity are shown in the last two columns of Table 2. For the basic theory these ratios are in the range between 1,31 and 1,39. For the advanced theory these ratios are lower. A comparison with the results found for shear walls without openings (Källsner et al 2001) indicates that the load-carrying capacity of shear walls with openings are somewhat underestimated by the basic theory. The advanced theory seems to predict the strength of shear walls with openings better than the basic theory.

Table 2: Measured and calculated load-carrying capacities.

Test wall	Load-carrying capacity H			$\frac{H_{measured}}{H_{calculated}}$	
	Measured [kN]	Basic theory [kN]	Advanced theory [kN]	Basic theory	Advanced theory
1	51,7	$(4{,}00\,f_p b)$		1,00 (ref.)	
2	7,58	5,80 $(0{,}449\,f_p b)$	7,20 $(0{,}557\,f_p b)$	1,31	1,05
3	11,53	8,35 $(0{,}646\,f_p b)$	9,84 $(0{,}761\,f_p b)$	1,38	1,17
4	20,20	14,58 $(1{,}128\,f_p b)$		1,39	
5	33,94				

5 Conclusion

A simplified plastic model for design of incompletely anchored wood-framed shear walls has been presented. The model can be used if the sheet material is fixed by mechanical fasteners and if these sheathing-to-timber joints show plastic behaviour. The model can only be applied on static loads in the ultimate limit state.

A few introductory tests of shear walls with openings have been conducted where the bottom rail was completely fixed to the substrate. The test results indicate that the proposed basic theory should be somewhat modified in order to obtain good agreement between measured and calculated load-carrying capacity.

6 Future work

The design method has so far only been checked against some introductory experiments. The intention is to repeat these experiments with specimens that have been manufactured under more controlled conditions and with other sheet materials.

The influence of vertical loads around window openings should be further investigated.

There is a need to develop diagrams and tables that can facilitate a structural design.

7 References

prEN 1995-1-1, Eurocode 5 – Design of timber structures – Part 1-1: General rules and rules for buildings, Final draft September 2001 (CEN/TC 250/SC5 N158).

EN 594:1995, Timber structures – Test methods – Racking strength and stiffness of timber frame wall panels.

Andreasson, S., 2000, Three-dimensional interaction in stabilisation of multi-storey timber frame building systems, Lund University, Report TVBK-1017, Lund.

Källsner, B. and Lam F., 1995, Diaphragms and shear walls, Holzbauwerke nach Eurocode 5 - STEP 3, Arbeitsgemeinschaft Holz e. V., Düsseldorf, pp 15/1-15/19.

Källsner, B., Girhammar, U. A. and Wu, L., 2001, A simplified plastic model for design of partially anchored wood-framed shear walls, CIB-W18 meeting, Venice, Italy.

CIB-W18/35-15-3

INTERNATIONAL COUNCIL FOR RESEARCH AND INNOVATION
IN BUILDING AND CONSTRUCTION

WORKING COMMISSION W18 - TIMBER STRUCTURES

EVALUATION AND ESTIMATION OF THE PERFORMANCE OF THE SHEAR WALLS IN HUMID CLIMATE

S Nakajima

Building Research Institute

JAPAN

Presented by: S Nakajima

S Svensson asked about the moisture content of the components in the tests and S Thelandersson commented on the need for caution when considering appropriate service class allocation and when calculating slip values. S Nakajima clarified the issues raised. B Yeh then commented on the 5-15 % higher strength values described in section 5.2 of the paper and asked for further clarification of the modelling used. S Nakajima clarified that the analysis adopted a process which followed the load-deflection curve of each nail which were then summed to provide an over result.

Evaluation and estimation of the performance of the shear walls in humid climate

Shiro NAKAJIMA
Building Research Institute, JAPAN

1 Abstract

The effect of the moisture content of the lumbers and the sheathing materials on the performance of the plywood or OSB sheathed shear walls was reported in the last paper (Nakajima 2001). And the effect of the moisture content on the panel shear properties of the sheathing materials and the performance of the nail joints was also reported. Additional test data for the nail joints were collected to evaluate the effect of the humid climate on the lateral resistance of the joints. Lateral nail tests were conducted for all possible combination of the surface grain direction of the wood pieces and the sheathing materials and the loading direction.

The strength reduction of the shear walls due to the high moisture content of the composing materials was predicted by analyzing the characteristics of the nail joints and the sheathing panels under the humid condition. A numerical calculation was conducted to predict the strength reduction of the shear walls. The results of the analysis were compared to the test results.

In most cases the lateral nail resistance of the nail joints was reduced in the humid climate and the reduction level depended on the type of the sheathing materials and also the direction of the load and the assembly of the studs and sheathing panels. And the yield and ultimate strength of the nail joints were affected by the failure mode of the nail joints.

At least for the plywood sheathed shear walls the test results of the lacking test and the lateral nail resistance test indicated that the yield strength reduction of the shear walls due to the humid climate can be roughly predicted by looking though the strength reduction of the nail joints conditioned in the same humid climate.

The yield strength reduction of the shear walls caused by the humid climate was well predicted by the simplified model. This simplified model can be a good predictor to evaluate the effect of the moisture contents on the yield strength of the shear walls.

2 Introduction

The moisture contents of wooden materials and components affect on the strength and stiffness properties of the joints and the shear walls of wooden structures. In most cases the strength and stiffness properties of the joints and the shear walls are evaluated from the test results of the test pieces that are conditioned in the standard condition, temperature 20°C and relative humidity 65%. Wooden structures are actually used in various conditions and the performance of the joints and the shear walls of these structures should be properly evaluated according to the conditions in which they are used. As it is quite difficult to conduct full size shear wall tests in various conditions it is quite necessary to develop an appropriate method to estimate the performance of the shear walls from the performance data of the materials and the joints.

In Japan the service classes are stipulated in the Enforcement Order No.1446 that was revised in June 2001. In this Enforcement Order three service classes were stipulated. The three service classes represented the climates "constantly wet", "intermittently wet" and "dry".

The climate "constantly wet" corresponds to the environments in which structural members are directly exposed to the outside or could be perpetually exposed to moisture. The representative temperature and relative humidity for this service class are 20°C and 95%. The climate "intermittently wet" corresponds to the environments in which structural members are indirectly exposed to the outside or could be intermittently exposed to moisture as sheathing materials of exterior wall, roof or floor. The representative temperature and relative humidity for this service class are 20°C and 85%. The climate "dry" corresponds to the environments other than those above-mentioned. The representative temperature and relative humidity for this service class are 20°C and 65%.

The allowable shear strengths of the shear walls constructed by the 2X4-construction system were decided by analyzing the test data of the series of shear wall tests conducted in 1972 (Building Research Institute 1975). In the process of calculating the allowable shear strengths of the shear walls, the strength modification factors were multiplied to the shear strength to give safety factors for the durability issues of the sheathing materials against water. Table 1 shows the values of these strength modification factors. Most of these values were derived from the test results of the lateral nail resistance test of the nailed joints. The strength reductions of the nailed joints after experiencing three cycles of wet and dry procedures were mainly considered when deciding the values for the modification factor. The modification factors were not directly derived from the test data of the shear walls.

Table 1 The shear strength modification factors for sheathed shear walls.

Sheathing Type	Modification factor
Plywood 9mm in thickness	1.00
Plywood 7.5mm in thickness	1.00
Insulation board 12mm in thickness	0.75
Particleboard 12mm in thickness	0.85
Hard board 5mm in thickness	0.65
Hard board 7mm in thickness	0.90
Hard cement particle board 12mm in thickness	0.75
Gypsum board 12mm in thickness	0.75

As there are limitations in the capacity of the testing facilities in most cases it is difficult to condition full size shear walls in a certain climate. And of course it is quite difficult to conduct a full size shear wall test in a chamber controlled to a certain temperature and humidity. For these reasons the durability of the shear walls against humidity should be evaluated from the durability of the composing materials and joints. The object of this research is to evaluate the performance of the nail joints and to predict the effect of the moisture contents on the performance of the shear walls by modeling the shear walls and analyzing the characteristics of the nail joints and the sheathing panels.

3 Previous test results

Shear walls sheathed with plywood or OSB were constructed by the 2X4-construction system and tested in two climates, temperature 20°C & relative humidity 65% and temperature 20°C & relative humidity 90% to clarify the effect of the moisture contents on the racking strength and stiffness of the shear walls. The lateral nail tests were also conducted in these two climates. The following results were derived:

(1) In the humid climate the yield strength, the ultimate strength and the initial stiffness of the plywood sheathed shear walls were reduced to 85%, 87% and 79% respectively.

(2) In the humid climate the yield and the ultimate strength of the OSB sheathed shear walls were reduced to 90% and 91% respectively. And the initial stiffness of the OSB sheathed shear walls increase 5% after conditioned in the climate of 20ºC and 90% R.H.

(3) The reduction of the panel shear modulus of rigidity due to the wet condition was 24% for plywood and 43% for OSB and the reduction of the panel shear strength was 24% for plywood and 23% for OSB. Both sheathing materials particularly OSB becomes more ductile when it is in a wet condition.

(4) The lateral nail resistance of the nail joints measured in the humid climate was almost 10% higher than that measured in the normal climate.

As the lateral nail resistance of the nail joints was not reduced in the humid climate additional tests were conducted to re-evaluate the performance of the nail joints under the humid climate.

4 Reverse-cyclic test of nail joints

4.1 Test specimens

Eight different types of nail joints were tested to re-evaluate the performance of the nail joints. Plywood and OSB panels were connected to the studs (204 lumbers) by the common nails 50mm in length (CN50). Considering the surface grain direction of the lumbers and the sheathing materials and also the loading direction four different types of test specimens were prepared. Figure 1 and figure 2 show the size and shape of the test specimens. The details of the specification of the test specimens are as follows:

Joint A:	Joint A represents the nail joints located at the vertical frames. The surface grain directions of the framing members and the sheathing materials are parallel to each other and the loading direction is parallel to both the surface grain direction of the framing members and the sheathing materials.
Joint B:	Joint B represents the nail joints located at the top and bottom plates. The surface grain directions of the framing members and the sheathing materials are perpendicular to each other and the loading direction is parallel to the surface grain direction of the framing members.

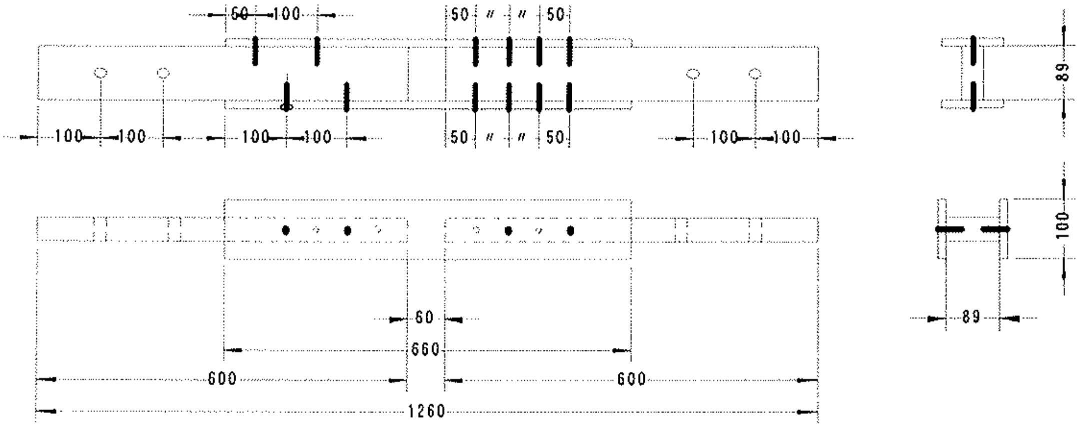

Figure 1 Test specimens, joint A and joint B.

Joint C: Joint C represents the nail joints located at the top and bottom plates. The surface grain directions of the framing members and the sheathing materials are perpendicular to each other and the loading direction is parallel to the surface grain direction of the sheathing materials.

Joint D: Joint D represents the nail joints located at the vertical frames. The surface grain directions of the framing members and the sheathing materials are parallel to each other and the loading direction is perpendicular to both the surface grain direction of the framing members and the sheathing materials.

Twenty test specimens were prepared for all types of nail joints. The test specimens were conditioned in a chamber after being assembled. Half of the test specimens were conditioned to constant mass in the climate of temperature 20ºC and relative humidity 65% and half of them were conditioned in the climate of temperature 20ºC and relative humidity 90%.

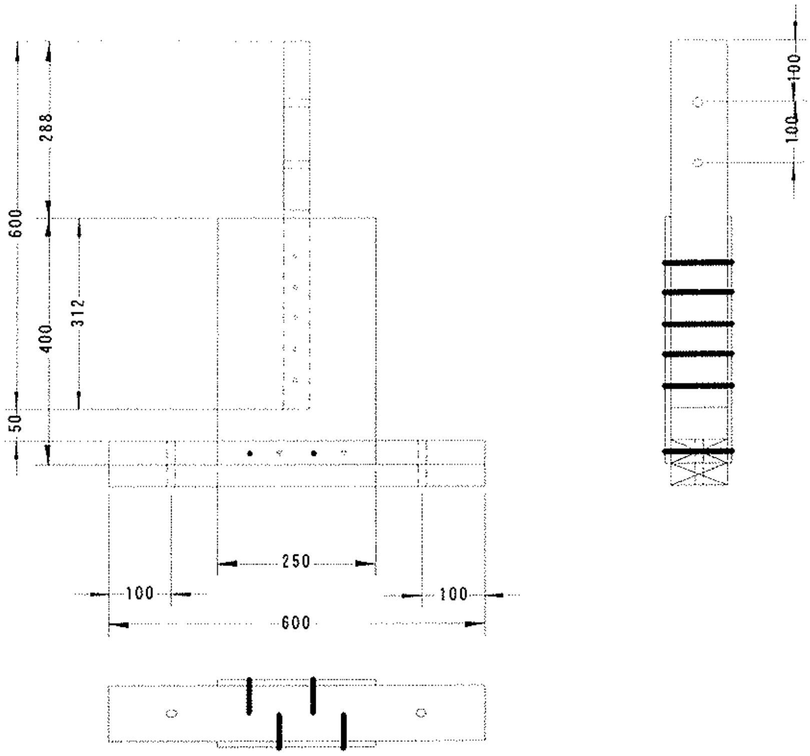

Figure 2 Test specimens, joint C and joint D.

4.2 Testing methods

Both ends of the studs (204 lumbers) were connected to the testing equipment and the reverse-cyclic load was applied to the test specimens. The loading schedule followed the ISO/DIS 16670 protocol. The slip between the sheathing materials and the studs were measured. Photo 1 shows the testing equipment and the testing setups.

5 Test results

5.1 Plywood nailed joints

The yield strength (P_y), the yield deformation (D_y), the ultimate strength (P_u), the ultimate deformation (D_u), the initial stiffness (K) and the typical failure mode of the "plywood - lumber" nailed joints are summarized in table 2. And the bi-linier lines of the envelope curve derived from the first reversed cycles are shown in figure 3.

The yield strength reduction caused by the humid conditioning of the nail joints are summarized as follows:

(1) When the loading direction was parallel to both the surface grain directions of the lumber pieces and the sheathing materials the yield strength was reduced to 84% by the humid condition.

(2) When the surface grain directions of the lumber pieces and the sheathing materials were perpendicular to each other and the loading direction was parallel to the surface grain directions of the lumber pieces the yield strength was reduced to 85 % by the humid condition.

(3) When the loading direction was perpendicular to both the surface grain directions of the lumber pieces and the sheathing materials the yield strength was reduced to 84% by the humid condition.

(4) When the surface grain directions of the lumber pieces and the sheathing materials were perpendicular to each other and the loading direction was parallel to the surface grain directions of the sheathing materials there was no reduction in the yield strength.

The failure mode of the joints seems to affect on the yield and ultimate strength of the nail joints. The dominant failure mode of the nail joint C was nail fatigue in the humid

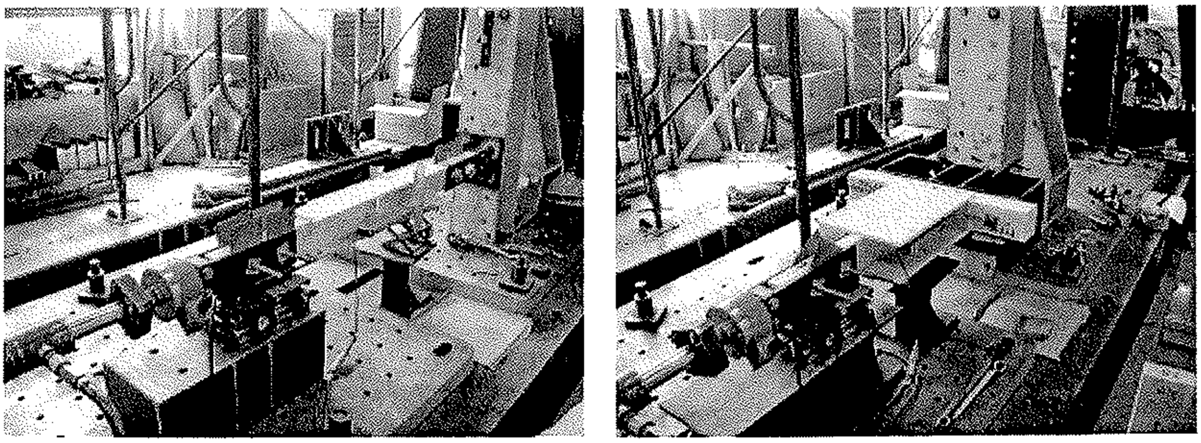

(a) Testing setup for joint A and joint B. (b) Testing setup for joint C and joint D.

Photo 1 Testing equipment and the testing setups.

climate. And this failure mode was different from the dominant failure modes of the other nail joints. The dominant failure mode of the other three types of nail joints was punching out.

The reduction of the initial stiffness of the nail joints due to the humid condition ranged from 0.56 to 1.04. The reduction of the initial stiffness was not affected by the failure mode of the nail joints.

The reduction of the yield strength and the ultimate strength due to the humid condition of the plywood sheathed shear walls were 15% and 13% respectively (Nakajima 2001). The test results of the lacking test of shear walls and the lateral nail resistance test of the nail joints indicates that the yield strength reduction of the shear walls can be roughly predicted by looking though the strength reduction of the nail joints conditioned in the same humid climate.

5.2 OSB nailed joints

The yield shear strength (P_y), the yield shear deformation (D_y), the ultimate shear strength (P_u), the ultimate shear deformation (D_u), the initial stiffness (K) and the dominant failure mode of the OSB to lumber nailed joints are summarized in table 3. And the bi-linier lines of the envelope curve derived from the first reversed cycles are shown in figure 4.

When the load was applied perpendicular to the surface grain of the 204 lumber pieces and parallel to the surface grain of the OSB panels the yield shear strength was reduced to 67% by the humid condition. And the reduction of the yield shear strength due to the humid condition was not observed when the load was applied parallel to the surface grain of the 204 lumber pieces or when the load was applied perpendicular to both the surface grain of the 204 lumber pieces and the surface grain of the OSB panels. In this case the yield shear strength in the humid condition was 5% to 15% higher than those measured in the normal condition.

This test results differs from the test results obtained from the lateral nail test of the plywood to lumber nail joints. This difference was probably caused by the characteristics of the two sheathing materials, plywood and OSB, under the humid climate. As mentioned in the previous paper (Nakajima 2001) similar test results were reported by Arima et.al. in 1972 (Arima et.al. 1975). It was reported that the lateral nail resistance of the particleboard increased almost 10% after immerged in the water at normal temperature for 24 hours.

The effect of the humid climate on the lateral nail resistance of the nail joints depended on types of the sheathing materials and also the direction of the load and the assembly of the studs and sheathing panels.

Table 2 Summary of test results of the reverse-cyclic test of plywood nail joints.

Type of the test specimen	Humidity of the conditioning room1)	Py (kN)	Dy (mm)	K (kN/mm)	Pu (kN)	Du (mm)	Dominant failure mode2)
Joint A	65% R.H.	0.51	0.68	0.82	0.79	14.09	P6, W12, N22
	90% R.H.	0.43	0.61	0.85	0.69	10.97	P40, W0, N0
	Reduction ratio	*0.84*	*0.90*	*1.04*	*0.88*	*0.78*	-
Joint B	65% R.H.	0.54	0.64	0.94	0.86	12.68	P24, W10, N2
	90% R.H.	0.46	0.96	0.53	0.75	12.68	P40, W0, N0
	Reduction ratio	*0.85*	*1.50*	*0.56*	*0.88*	*1.00*	-
Joint C	65% R.H.	0.51	0.73	0.73	0.78	12.24	P13, W27, N0
	90% R.H.	0.51	1.07	0.52	0.78	14.35	P7, W12, N21
	Reduction ratio	*1.01*	*1.45*	*0.72*	*1.00*	*1.17*	-
Joint D	65% R.H.	0.53	0.80	0.72	0.80	12.27	P0, W23, N17
	90% R.H.	0.45	0.95	0.56	0.70	12.33	P39, W0, N1
	Reduction ratio	*0.84*	*1.18*	*0.78*	*0.87*	*0.93*	-

Note 1: The temperature of the conditioning room is 20ºC.

Note 2: Failure mode "P", "W" and "N" represent "punching out", "nail withdrawal" and "nail failure" respectively and the figures beside the alphabet represent the amount of the nails.

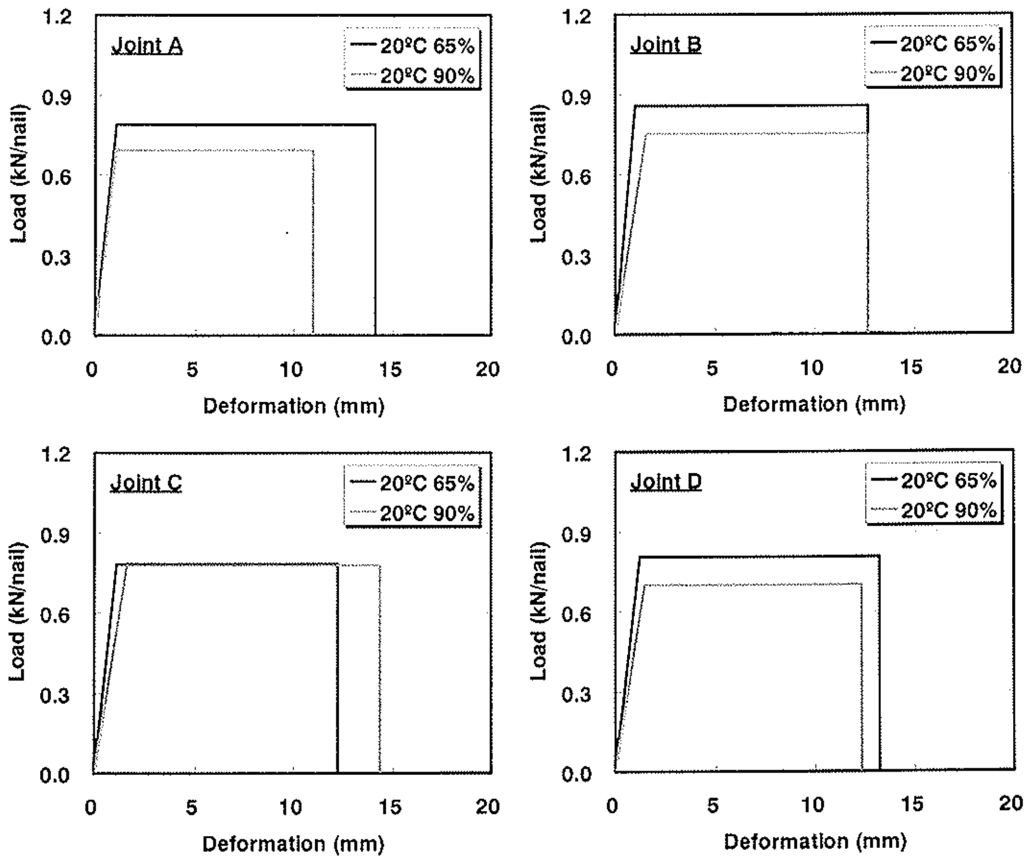

Figure 3 Bi-linier models for the plywood nail joints.

Table 3 Summary of test results of the reverse-cyclic test of OSB nail joints.

Type of the test specimen	Humidity of the conditioning room[1]	*Py* (kN)	*Dy* (mm)	*K* (kN/mm)	*Pu* (kN)	*Du* (mm)	Dominant failure mode[2]
Joint A	65% R.H.	0.57	0.47	1.29	0.86	13.74	P12, W27, N1
	90% R.H.	0.59	0.57	1.15	0.90	13.63	P39, W1, N0
	Reduction ratio	*1.05*	*1.23*	*0.89*	*1.04*	*0.99*	-
Joint B	65% R.H.	0.54	0.54	1.07	0.83	14.40	P4, W31, N5
	90% R.H.	0.62	0.59	1.17	0.95	13.88	P37, W3, N0
	Reduction ratio	*1.15*	*1.10*	*1.09*	*1.15*	*0.96*	-
Joint C	65% R.H.	0.59	0.73	0.99	0.88	12.15	P1, W39, N0
	90% R.H.	0.57	0.69	1.04	0.86	13.30	P10, W11, N19
	Reduction ratio	*0.67*	*0.96*	*1.05*	*0.98*	*1.09*	-
Joint D	65% R.H.	0.57	0.67	0.90	0.84	12.15	P2, W33, N5
	90% R.H.	0.60	0.62	1.07	0.91	12.61	P23, W7, N10
	Reduction ratio	*1.05*	*0.91*	*1.18*	*1.08*	*1.04*	-

Note 1: The temperature of the conditioning room is 20ºC.

Note 2: Failure mode "P", "W" and "N" represent "punching out", "nail withdrawal" and "nail failure" respectively and the figures beside the alphabet represent the amount of the nails.

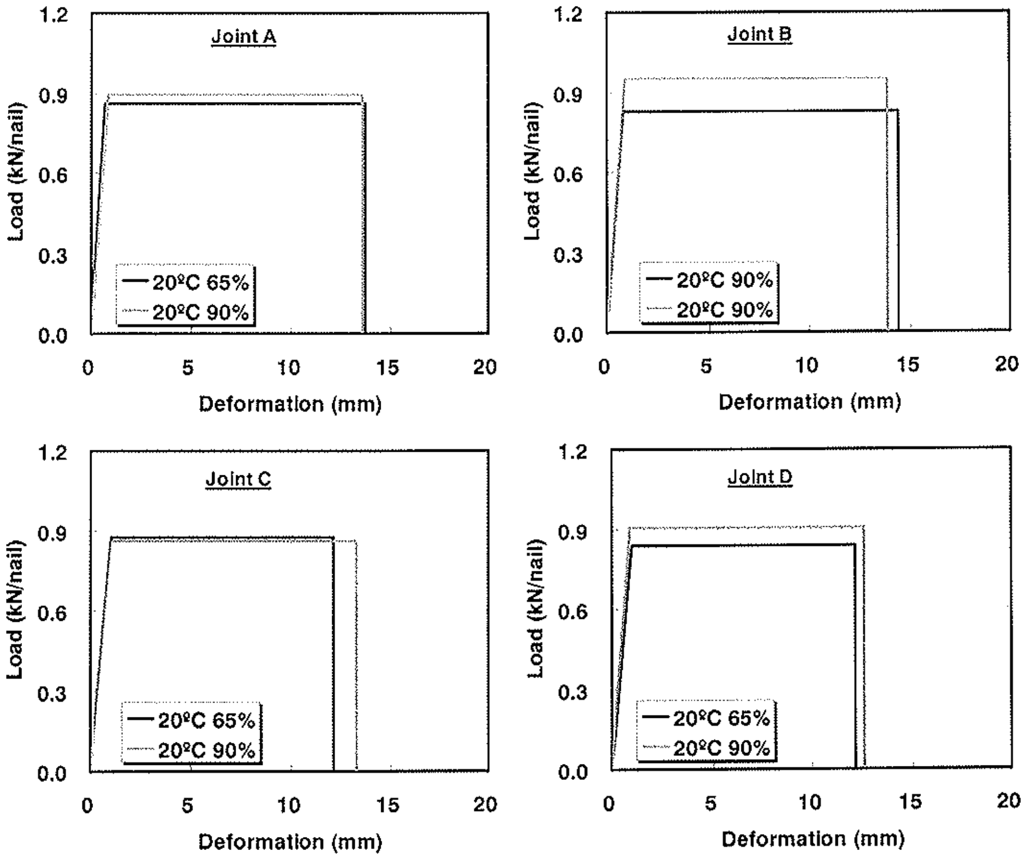

Figure 4 Bi-linier models for the OSB nail joints.

6 Prediction of the yield strength of the shear walls

6.1 Simple numerical estimation model

There are some models and calculation methods (for example Tuomi 1978) that can predict the strength properties of the shear walls by the characteristics values of the nail joints. To predict the reduction of the yield shear strength of the shear walls under the humid climate the simple structural model proposed by Hirai (Hirai et.al. 1999) was referred. The shear wall shown in figure 5 was modeled as shown in figure 6.

The model is a simplified model and the true shear deformation of the shear walls are assumed to be the summation of the shear deformation caused by the slip of the nail joints and the shear deformation of the sheathing panels. When a horizontal load *P* is applied at the top of the shear wall the true shear deformation of the shear wall *ã* can be calculated by summing the shear deformation of the sheathing panels $\tilde{a}_s$ and the shear deformation caused by the slip of the nailed joints $\tilde{a}_n$.

$$\gamma = \gamma_s + \gamma_n \qquad \text{---(1)}$$

where ,

$\tilde{a}_s$ represents the shear deformation of the sheathing panels, and

$\tilde{a}_n$ represents the shear deformation caused by the slip of the nailed joints.

When the load and deformation are in linear the shear deformation of the shear wall *ã* and the load *P* can be easily calculated by a simple numerical calculation. Equation 2 shows the relationship between the load applied at the top of the shear wall and the shear deformation of the shear wall caused by the slip of the nail joints.

$$P = \frac{h_e}{2}\left(\sum_{i=1}^{n} k_{si}\cdot R_i^2 + \sum_{j=1}^{m} k_{si}\cdot R_j^2\right)\cdot \gamma_n \qquad \text{--- (2)}$$

where,

k_{si} is the slip modulus of the nail joints at the horizontal framing members,

k_{sj} is the slip modulus of the nail joints at the vertical framing members,

and,

$$R_i = \frac{1}{1+\lambda^2}\left\{1+\lambda^2\left(1-\frac{2(i-1)}{n-1}\right)^2\right\}^{\frac{1}{2}} \qquad \text{---(3)}$$

$$R_j = \frac{1}{1+\lambda^2}\left\{\lambda^2+\left(1-\frac{2(j-1)}{m-1}\right)^2\right\}^{\frac{1}{2}} \qquad \text{---(4)}$$

$$\lambda = \frac{h_e}{l_e} \qquad \text{---(5)}$$

The slip of the nails nailed to the horizontal framing members s_i and the slip of the nails nailed to the vertical framing members s_j are given as shown in equation 6. The slip modulus of the nail joints located at the horizontal framing members k_{si} and the slip modulus of the nail joints located at the vertical framing members k_{sj} can be derived from the test results of lateral nail tests of the nail joints. Thus equation 2 gives the load *P* that can deform the shear wall to a certain shear deformation $\tilde{a}_n$, the shear deformation caused by the slip of the nail joints.

$$s_i = \frac{h_e\gamma_n}{2}\cdot R_i, \quad s_j = \frac{h_e\gamma_n}{2}\cdot R_j \qquad \text{---(6)}$$

Equation 7 gives the shear deformation of the sheathing panels $\tilde{a}_s$ caused by the load *P* applied at the top of the shear wall.

$$\gamma_s = \frac{P}{G l_e t} \qquad \text{---(7)}$$

where,

G is the panel shear modulus of rigidity, and
t is the thickness of the panel.

Equation 1, 2 and 7 gives the total shear deformation of the shear wall and the load P carried by the shear wall.

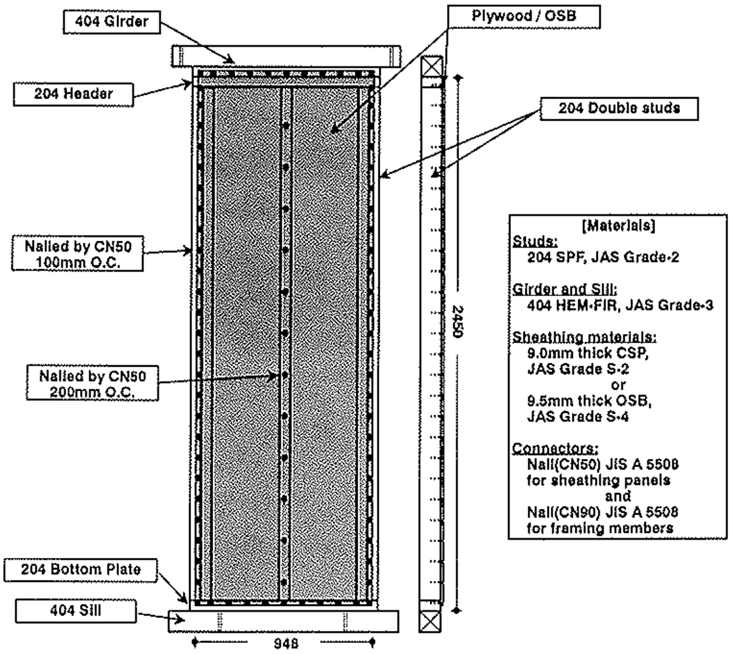
404 Girder
204 Header
Nailed by CN50 100mm O.C.
Nailed by CN50 200mm O.C.
204 Bottom Plate
404 Sill
948
Plywood / OSB
204 Double studs
2450
[Materials]
Studs:
204 SPF, JAS Grade-2
Girder and Sill:
404 HEM-FIR, JAS Grade-3
Sheathing materials:
9.0mm thick CSP, JAS Grade S-2
or
9.5mm thick OSB, JAS Grade S-4
Connectors:
Nail(CN50) JIS A 5508 for sheathing panels
and
Nail(CN90) JIS A 5508 for framing members

Figure 5 Size and assembly of the shear walls.

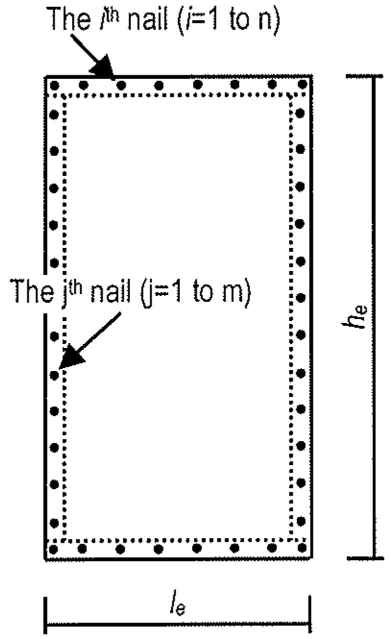
The i^{th} nail (i=1 to n)
The j^{th} nail (j=1 to m)
h_e
l_e

Figure 6 Modeling of the nailed shear walls.

6.2 Results and discussion

The length of the shear wall l_e was 948mm and the height h_e was 2450mm. And the number of the nail joints located at the vertical framing member m was 25 and the number of the nail joints located at the horizontal framing member n was 11. The slip modulus of the nail joints located at the horizontal framing members k_{si}, the slip modulus of the nail joints located at the vertical framing members k_{sj} at a certain displacement level can be derived from the load-slip curve of the nail joints. And to simplify the calculation the actual load-slip curves were express by certain functions.

The panel-shear modulus of rigidity of the sheathing panels is summarized in table 4. Using these values the shear deformation of the shear wall under a certain load was calculated. The results of the calculation are summarized in table 5.

Table 4 The panel shear modulus of rigidity of the sheathing panels.

Climate:	(1) 20°C , 65%		(2) 20°C , 90%	
Sheathing material:	Plywood	OSB	Plywood	OSB
Panel shear modulus of rigidity (Mpa)	460	1650	350	940

Table 5 The predicted and actual yield strength of the shear walls.

Wall type	Humidity of the conditioning room	Yield strength of the shear wall Py (kN)		
		Calculated (Pyc)	Measured (Pym)	Pyc/Pym
Plywood sheathed shear wall	65% R.H.	6.03	5.70	1.06
	90% R.H.	5.09	4.85	1.05
	Reduction ratio	*0.84*	*0.85*	-
OSB sheathed shear wall	65% R.H.	5.51	5.95	0.93
	90% R.H.	4.93	5.36	0.92
	Reduction ratio	*0.89*	*0.90*	-

The reduction of the yield strength of the shear walls caused by the humid climate was well predicted for both plywood sheathed shear walls and OSB sheathed shear walls. The simplified model can be a good predictor to evaluate the effect of the moisture contents on the yield strength of the shear walls. Even though detail analytical models should be proposed to predict the performance of the shear walls precisely and to predict the non-linear characteristics of the shear walls.

7 Conclusion

In most case the lateral nail resistance of the nail joints was reduced in the humid climate and the reduction level depended on the type of the sheathing materials and also the direction of the load and the assembly of the studs and sheathing panels. And the failure mode of the joints to also affected on the yield and ultimate strength of the nail joints.

And at least for the plywood sheathed shear walls the test results of the lacking test and the lateral nail resistance test indicated that the yield strength reduction of the shear walls due to the humid climate can be roughly predicted by looking though the strength reduction of the nail joints conditioned in the same humid climate.

The yield strength reduction of the shear walls caused by the humid climate was well predicted by the simplified model. This simplified model can be a good predictor to evaluate the effect of the moisture contents on the yield strength of the shear walls.

Reference

Building Research Institute MOC 1975. 'Annual Report of the General Technology Development Project – Development of the Construction Methods for the Small Scale Wooden houses'. Building Research Institute MOC.

Roger l. Tuomi and Willain J. McCutcheon, 1978. Racking strength of light-frame nailed walls. Journal of structural division, ASCE, 104 (ST7), 1131-1140.

Takurou Hirai, Pei-Wen Zhang, Yasutaka Irie and Yoshiaki Wakashima, 1999. Lateral resistance of nailed timber joints with structural wooden panels. Journal of Japan Wood Science Society, 45(2), 120-129.

Nakajima S, 2001. The effect of the moisture content on the performance of the shear walls. Proceedings of CIB-W18/34-15-2.

CIB-W18/35-15-4

**INTERNATIONAL COUNCIL FOR RESEARCH AND INNOVATION
IN BUILDING AND CONSTRUCTION**

WORKING COMMISSION W18 - TIMBER STRUCTURES

INFLUENCE OF VERTICAL LOAD ON LATERAL RESISTANCE OF TIMBER-FRAMED WALLS

B Dujič
R Žarnić

University of Ljubljana
Faculty of Civil and Geodetic Engineering, Ljubljana

SLOVENIA

Presented by: B Dujič

G Gonzalez asked about the embedding strength on both sides of the test system used and S Svensson asked for further details of the vertical loading used in the tests. B Dujič confirmed that failure mode d was observed and the vertical load used represented both dead and live loads which can be expected from a 5 storey building. Comments were then made about the need or otherwise for intermediate studs in a 5 storey building. M Yasumura asked for further details about the model used and its applicability to panels with opening. After further description of the test setup and the model used, B Dujič indicated that the test specimen can be classified as a rigid diaphragm. This was followed by further discussions led by S Thelandersson and H J Blaß about the test rig and the loading system used.

Influence of Vertical Load on Lateral Resistance of Timber-Framed Walls

B. Dujič and R. Žarnić
University of Ljubljana, Faculty of Civil and Geodetic Engineering, Ljubljana, Slovenia

Abstract

Laboratory tests are the most reliable source of information about the actual response of the load-carrying walls loaded with combined vertical and horizontal load. The laboratory device, which enables testing of cantilever walls, was developed at the University of Ljubljana. Fourteen cyclic shear tests were carried out on full-scale double panel units with different timber framing (corner connectors, extra vertical stud along the vertical edge of each unit) and OSB sheathing plate. They were preloaded with different vertical loads. The research was focused on hysteretic behavior of sheathing to framing connections, lateral resistance of timber-framed panels, and mathematical modelling of their response to combined vertical and varied horizontal load.

The behavior of timber-framed walls was governed by the non-linear response of connectors and anchors. The influence of vertical load on cyclic horizontally loaded panels was studied in details. It was found out that the magnitude of vertical load has strong effect on lateral resistance of the wall. At small magnitudes of horizontal load the anchorage system increases the racking resistance of the wall. Fully anchored timber-framed shear walls with tie-downs at the leading stud have higher lateral resistance and load carrying capacity than partially anchored walls. At higher magnitudes of vertical load, the anchorage system does not have much influence on lateral resistance of a shear wall.

1 Introduction

There is general lack of information about the behavior of timber frame structures in comparison to the behavior of structures constructed of other types of materials. The main characteristic of this kind of timber structures is a large number of connections with non-linear inelastic behavior when subjected even to low intensity loads where dissipation of energy is significant. The dynamic response of these structures can be calculated only if sufficient amount of experimentally obtained data is available. Therefore, the experimental research is needed to obtain knowledge about the behavior of joints, elements and panels exposed to cyclic loading. Research is also needed to study the development of reliable and efficient mathematical models of timber frame structures.

The timber frame constructions are often considered to have higher earthquake resistance than structures constructed of other materials. The reason for this reputation is their relatively low mass. These systems are often designed without paying enough attention to seismic action impact. However, insufficient knowledge on interaction between wood frames and sheathing and the role of fasteners often result in poor design of such kind of structures. The panel geometry data and the mechanical properties of the used materials are not sufficient for the evaluation of the lateral resistance of timber-framed walls. Reliable information on the actual response of the basic load-carrying element exposed to combined vertical and horizontal loading can be obtained only from laboratory tests. Special attention should be paid to the non-linear behaviour of the mechanical connections between the wood elements, because they govern the response of the entire timber structure. The results of investigations and testing of different structural complexes and connections in various testing laboratories are also difficult to compare because of the diversity of the system of composite elements and the performance of tests with variable boundary conditions.

The aim of extensive experimental research of timber frame wall panels that has been carried out at the University of Ljubljana is to obtain information on seismic resistance of different timber structural elements used by Slovenian manufactures of so called prefabricated timber houses. Based on these results, the mathematical model for seismic time-history analyses was developed, validated and verified.

Evaluation of the influence of vertical dead load on structurall walls behaviour is an important part of the design of structures exposed to earthquake excitation and wind load. The evaluation results enable the appropriate design of a buillding anchorage system. The prevention of uplifting of wall segments using anchorage system is correlated with the magnitude of vertical load. Both anchorage and magnitude of vertical dead load influence significantly the horizontal load-carrying capacity of the timber-framed shear walls.

2 Experimental research of timber-framed walls

Series of double timber panels were tested. The specimens were loaded with constant vertical and cyclic horizontal load as well as with constant vertical and monotonic horizontal load according to EN 594. The influence of anchors and different frame connectors as well as the influence of different magnitudes of vertical load were studied. The universal set-up (Fig. 1) was developed in the scope of research of the mechanical properties of panels and walls as structural elements in timber frame buildings with flexible horizontal diaphragms.

2.1 The set-up for testing of cantilever panels

The construction of set-up enables shear testing of panels exposed to constant verical load withouth influencing movement and rotation of free edge of specimen. The horizontal load is applied by gradual imposition of displacements along the free edge of specimen. Taking into account the limits of the available funds, the simple device based on principle of balance and lever was constructed. The set-up facilitates the testing of specimens in the form of cantilever panels turned upside-down and supported along the upper edge by the steel frame structure. The bottom (free) edge of the tested panel is supported by hinged and horizontally movable mechanism, which allows its free horizontal movement and rotation during the test.

The test set-up for combined constant vertical and displacement-controlled horizontal loading is composed of five major parts, marked in Figure 1 by numbers 1 to 5. The pair of lever beams (1) follows the vertical deformation of a specimen, while constant vertical load provided by counterbalance acts on the specimen. The horizontal load is applied along the lower horizontal edge of the specimen by a single displacement-controlled actuator (5) that moves the roller beam (3). The beam rolls along the supporting beam (2) that is hinged between the pair of leaver beams. The specimen is tested as cantilever panel turned upside-down and supported along the upper edge by the steel frame (4).

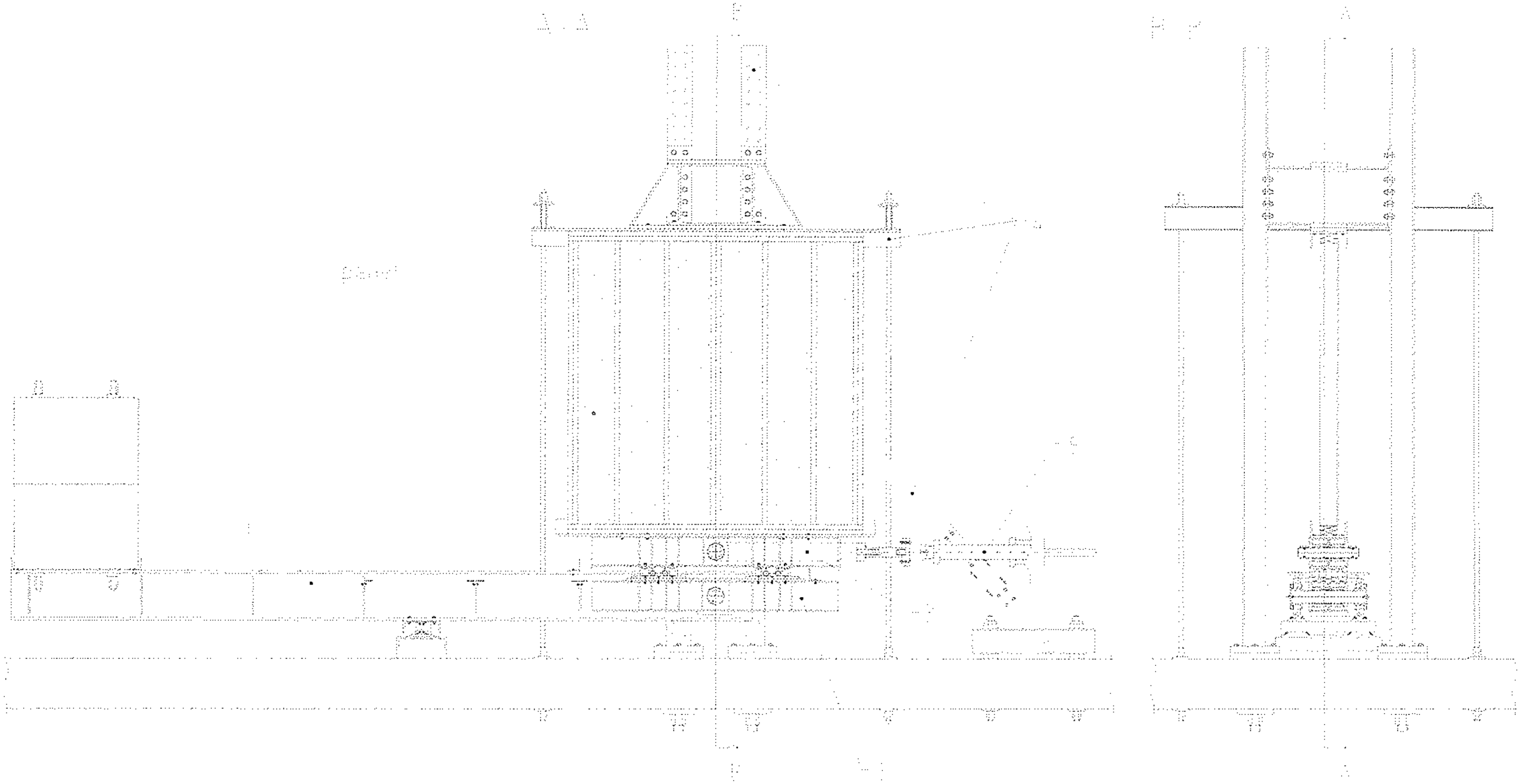

Figure 1: The set-up for shear testing of cantilever panels turned upside-down and along the bottom edge supported by hinged and horizontally movable mechanism.

During the testing, the lower edge of the panel is supported by hinged (2) and horizontally movable mechanism (3), which allows its free horizontal movement and rotation. The set-up is calibrated for vertical and horizontal load.

2.2 Description of panels and testing procedures

The timber-framed panels were tested to obtain data on the lateral behaviour of the Canadian platform construction system for residential buildings that has recently come to Slovenian market. The basic structural wall elements were constructed of the Canadian OSB single face sheathing and Spruce-Pine-Fir (S-P-F) framing wood elements. The OSB sheaths were 1.22m long, 2.44m high and 12.7mm thick with material density of 620kg/m^3. The basic frame was constructed of four evenly spaced vertical studs and two horizontal studs (top and bottom rail) with rectangular cross-section measuring 38 by 138 mm and material density of 450kg/m^3 (wood strength class C27 according to EN 338). In each joint the studs were fastened together by three 90mm long helically threaded nails with a diameter of 3.3mm and tensile strength above 600MPa. The total length and height of the frame was equal to the corresponding dimensions of OSB sheathing. The OSB plate was fastened to frame by 75mm long annularly threaded nails with a diameter of 2.8mm. They were distributed evenly along peripheral and inner studs with nailing density of 100mm.

Two different types of basic panels were developed from the above-described one (Table 1). The first type of panel (marked with **2ec**) had additionally strengthened peripheral frame joints where BMF steel angle (2,5/60/90mm) with a rib was fixed by twelve 40mm long annularly threaded BMF nails of 4.0mm diameter. The second type of panel (**2ev**) was strengthened by an additional vertical stud positioned along the inner side of the external vertical edge of frame. The internal vertical edge of frame is considered the one that is connected together with another panel unit to form a double unit specimen. The additional vertical stud was fastened to primary vertical stud in the same way as the inner studs when they were connected together to form specimens described in the next paragraph. The OSB plate was fastened to the additional stud in the same way as the other studs.

The tested specimens were composed of the two above described wall panels. They were connected along the inner peripheral vertical frame studs by helically threaded nails (3.3/90 mm) with each side density of 300 mm. The nails were threaded inclined to vertical axis of stud in approximate angle of 75°. The additional connection of basic panels was obtained by horizontal boundary studs (head binder and timber packer) fastened to panels along the upper and lower horizontal edges of the frames. The boundary studs were of the same cross-section dimensions and material as the frame studs. Each horizontal edging stud of frame (top and bottom rail) was fastened to additional boundary stud with eight nails threaded inclined to vertical in approximate angle of 15°. The head binder and the timber packer were fastened to test the set-up with sixteen metric type M8 bolts. The specimens were anchored only through bottom rail to the set-up with two metric type M14 bolts positioned 150 mm from the corners of the specimen. The square steel plate washers, 5 mm thick and 50 mm in square, were used under the bottom plate bolts.

The panels were tested by monotonic load in accordance to EN 594 and by cyclic load with increasing reversed cycles (Fig. 3). At every step, the cyclic amplitude was repeated three times. The herein presented test results are those of the walls strengthened in two different ways and loaded with quasi-static cyclic horizontal load and three different magnitudes of vertical load (Table 1). The magnitudes of vertical load were calculated from the example of the five-story building with a 100 m^2 of floor area.

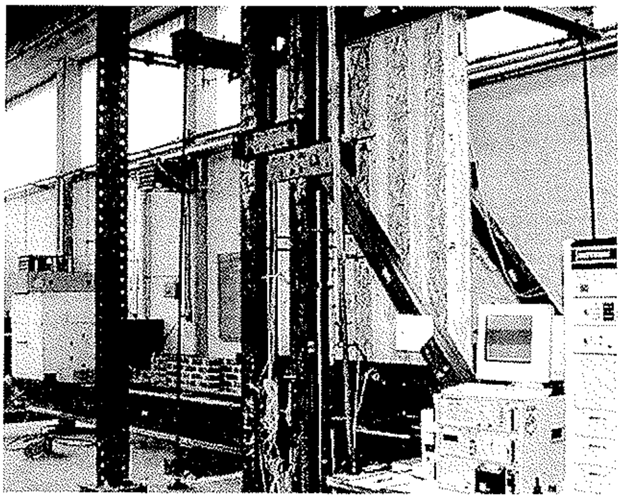

Figure 2: Experimental shear test of timber-framed wall.

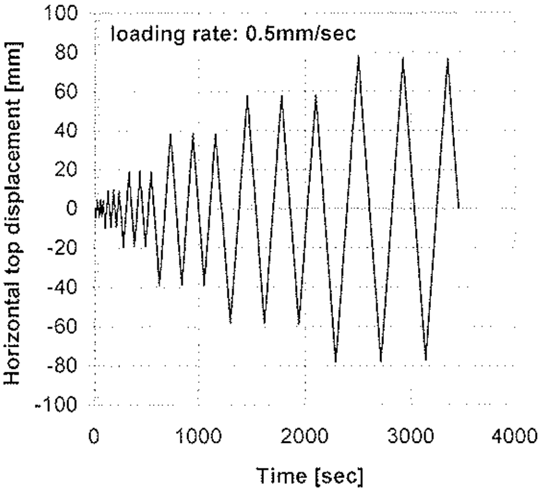

Figure 3: The quasi-static cyclic loading protocol.

To obtain the basic properties of wall panels exposed to the seismic action the quasi-static cyclic loading protocol is more appropriate than the monotonous loading protocol defined in EN 594 The shapes of histeresis loops and peak load degradation after reversed cycles within the same amplitude and energy dissipation are the main data obtained from cyclic tests that enables the evaluation of seismic resistance of timber structures.

2.3 Evaluation of cyclic test results

The behaviour mechanisms of walls are different because of different configuration and detailing of panels as well as because of different magnitudes of vertical loading. In the majority of cases, the failure of wall panels developed due to the failure of anchored corners. The failure propagates through the contact between framing and sheathing as well as the contact between frame studs locally in the corner of the panel. Because of the high in-plane stiffness of sheathing plate, the exterior vertical frame stud is usually deformed out-of-plane, which can lead to instability and thus collapse of entire wooden frame. Hysteresis responses of two types of specimens tested by cyclic loading and loaded with three different vertical loads of 10 kN, 51 kN and 84 kN are presented in Table 1. These loads represent vertical loads on walls positioned in the fifth, third and first story, respectively.

The sequentially phased displacement procedure [7] introduced the concept of the First Major Event (FME). FME is defined as the first significant limit state that occurs during the cyclic test with repeated load reversals to predefined displacements. This limit can be observed as an event that signifies the demarcation between two behaviour states. For instance, FME occurs when the shear load capacity drops noticeably from the initial one due to the recycling of the load to the same wall displacement increment. The transition of the specimen behaviour from elastic to inelastic response is FME called the Yield Limit State. There is a number of different concepts for YLS evaluations or determinations. Often YLS is defined as the point of intersection of secants or/and tangents on the skeleton curve of hysteretic response of timber-framed walls. In our case, because of big step between displacement amplitudes, YLS was defined as the point of intersection between two lines. The lines are the secant of the skeleton curve defined by points at $0.1F_{max}$ (10% of maximal horizontal load capacity) and $0.4F_{max}$ and tangent on the upper part of the envelope, which is parallel to the secant through the skeleton curve at $0.4F_{max}$ and $0.9F_{max}$ (Fig. 4).

Table 1: The hysteresis response of the tested timber-framed walls.

Description of wall type **Magnitude of vertical load**	**P-2ec** (with corner conectors) 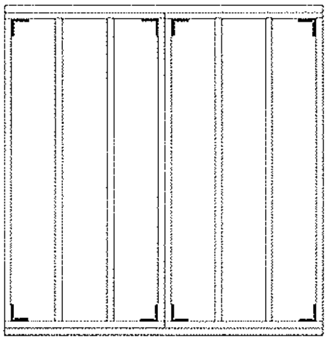	**P-2ev** (with extra vertical studs) 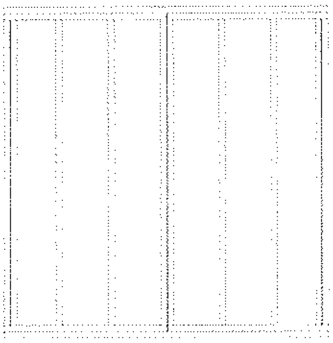
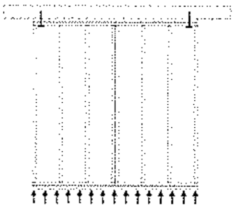 **10kN**	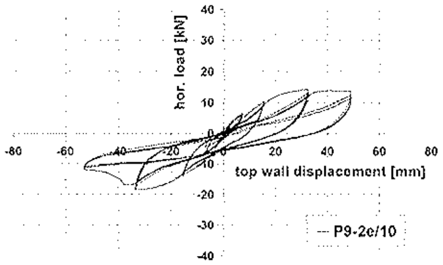 	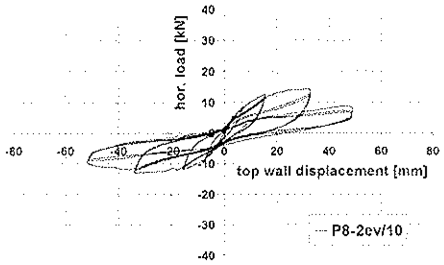
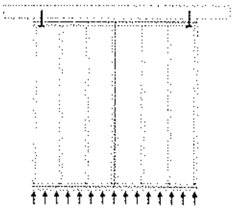 **51kN**	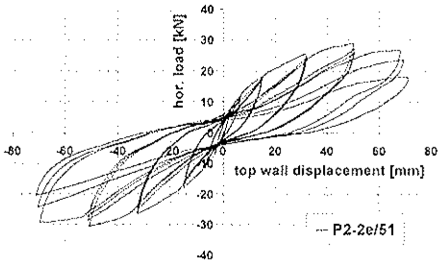 	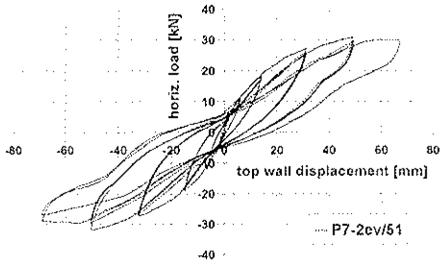
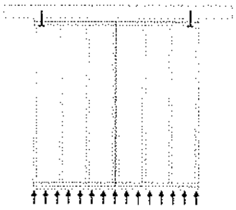 **84kN**	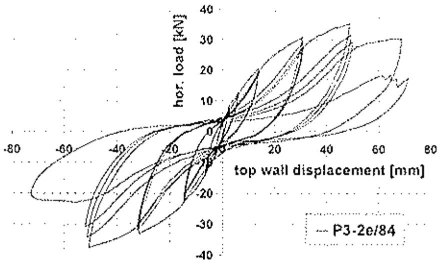 	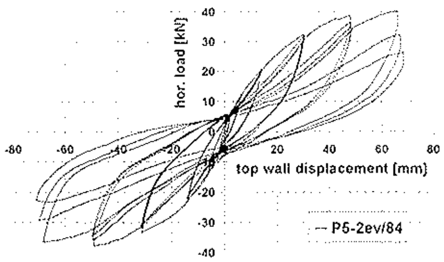

The skeleton curves of hysteresis response of specimens presented in Table 1 are compared in the diagram presented in Figure 4. It is obvious that the magnitude of vertical load had a major influence on the all over shear response of the tested panels. On the contrary, the type of strengthening does not influence very much on the shear strength of the panels. Some differences can be observed at YLS and at maximal horizontal load capacity in cases of low and high magnitudes of vertical loads. At medium magnitude of vertical load (51 kN), there is only slight difference between the types of strengthening. The panels with corner strengthening of frame have higher ductility than those with additional vertical studs. The corner connectors provide additional anchorage of frame studs, which results in higher lateral resistance of the wall at lower magnitudes of vertical load. In the case of higher vertical load the panels with additional studs experience transition into inelastic response at higher magnitude of shear force. The horizontal load capacity of specified basic configuration of the timber frame wall was also calculated according to Eurocode 5 (Section 3) and compared with actual response of the tested specimens (Fig. 4).

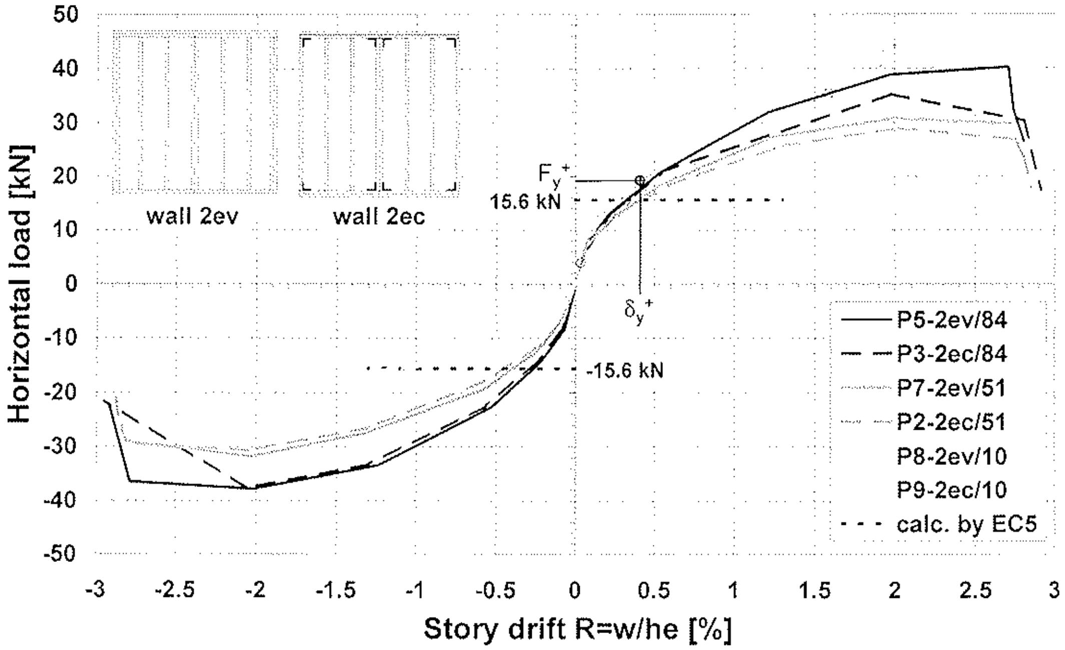

Figure 4: Skeleton curves of two types and at different magnitudes of vertical load in comparison to the calculated one according to EC 5.

The values of YLS (K_y, F_y and δ_y) and the maximal horizontal load capacity (F_{max}) at the corresponding displacement (δ_{Fmax}) presented in Table 2 are the average values of two tests. Because the results of two tests were within the scatter of 5%, the third test was not performed.

Table 2: Mechanical properties of timber-framed walls with configuration 2ev and 2ec preloaded with vertical load of 10 kN, 51 kN in 84 kN.

Type of timber frame wall	Uniform vertical load per meter	K_y [kN/mm]	δ_y [mm]	F_y [kN]	F_{max} [kN]	δ_{Fmax} [mm]
2ev/10	4.0 kN/m	2,23	3,1	6,9	13,6	32,9
2ec/10	4.0 kN/m	0,97	9,4	9,1	16,3	32,8
2ev/51	20.9 kN/m	1,71	9,2	15,7	29,7	51,0
2ec/51	20.9 kN/m	1,51	10,2	15,4	29,0	49,8
2ev/84	34.4 kN/m	1,99	9,6	19,1	38,2	48,3
2ec/84	34.4 kN/m	1,94	9,0	17,5	35,6	49,1

The lateral resistance of the timber frame wall is significantly affected by the magnitude of vertical load (Fig. 5). In the case of low vertical load, the anchorage system increases the racking resistance of the wall. Fully anchored timber-framed shear walls with tie-downs at the leading stud have higher lateral resistance and load carrying capacity than partially anchored walls. At the magnitudes of vertical load above 50 kN or 20 kN per meter length of the wall the anchorage system does not have very important influence on lateral resistance of the shear wall. In this case, the failure mode is not governed by up-lifting of leading stud with cutting and pulling through the nails at the corner of the OSB plate.

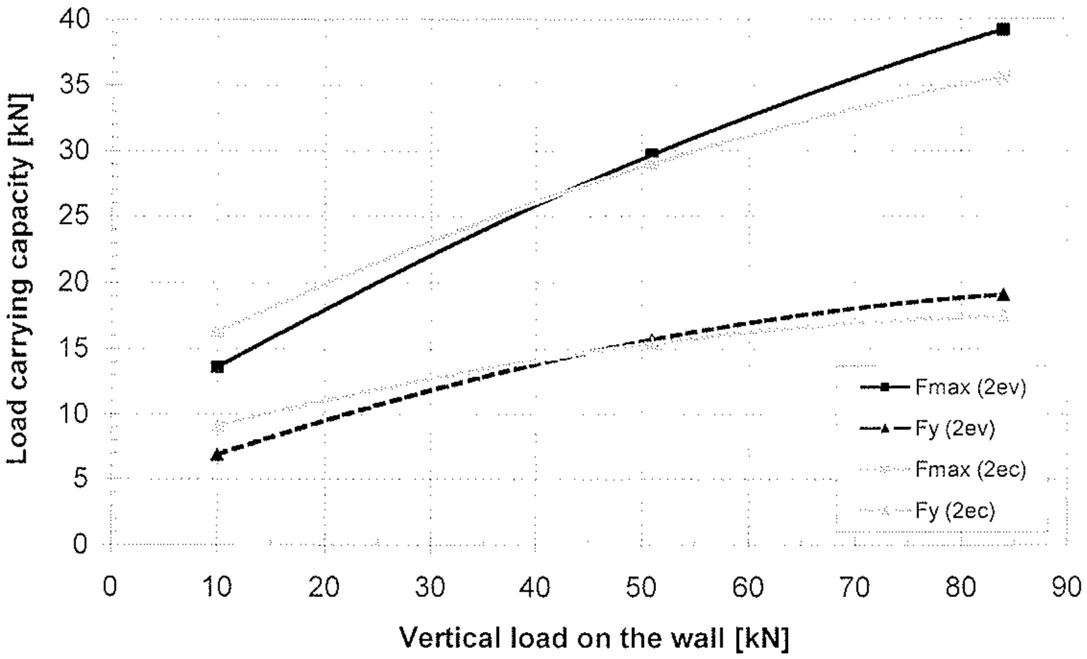

Figure 5: Influence of common vertical load on lateral strenght of timber-framed wall with the length of 244 cm assembled from to panel units.

3 Racking strength of the wall calculated according to EC5

Section 5.4.3 of Eurocode 5 states that racking strength shall be determined by an analytical method according to EC5 or by test method according to EN 594. The test method is more suitable for the evaluation of lateral resistance of specific panel configurations than analytical method, because it does not take into account the versatility of the construction details. The test provides data on the entire response of the structural element, while the calculation supplys only the shear strength of a panel. The results of the calculation according to EC5 are very sensitive to the values of basic input parameters that should be experimentally evaluated for every type and configuration of fasteners. The calculation can be based on the empirical equations given in EC5 or on the data obtained by experiments according to EN 409 and EN 383. The calculation method for the evaluation of racking strength is approximate and does not take into account the vertical load and properties of details (anchoring of different types, fastening). The calculated strength of panel is governed only by bearing capacity of edge nails that are distributed along the bottom rail of the timber frame. The calculated resistance of 15.6 kN without taking into account the safety factors was in the range of the resistance obtained by the testing of panels, where vertical loading was 10 kN (Fig. 5). The resistance of panels loaded with higher vertical loading was much higher because of "pre-stressing effect" caused by induced vertical axial load.

4 Mathematical modelling

4.1 Non-linear spring element for mechanical connections

The new non-linear spring element in DRAIN-2DX was developed at the University of Ljubljana and is named "ULS" element (Universal Longitudinal Spring). Experimentally supported development started in 1980's by Žarnić. The element is based on significantly modified hysteresis rules that were originally proposed by the authors of IDARC program (Park et at., 1987) and own skeleton curve. ULS element is included in the DRAIN-2DX program (Prakash and Powel, 1993) as a longitudinal inelastic spring element. This element is suitable for mathematical modelling of inelastic behaviour of structural connectors and for structural struts as well as for the simulation of displacement responses of different entire timber frame wall compositions.

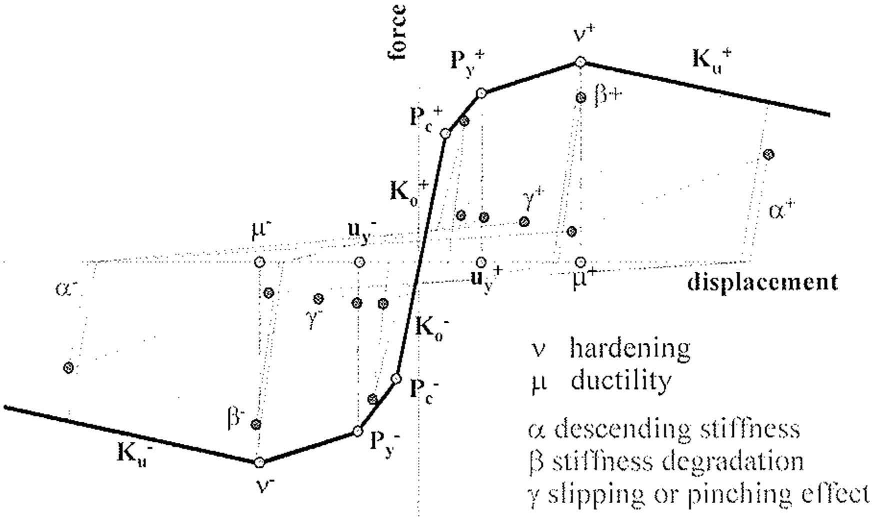

Figure 6: ULS model with trilinear part and descending curves controlled separately in the compression and tension zone by 10 parameters.

The trilinear skeleton curve governs the non-linear spring responses, while the shapes of hysteresis loops are influenced by three additional parameters. The trilinear envelope (Fig. 6) is defined as non-symmetric by three points – crack, yield and rupture point – separately in tension and in compression. The additional characteristic of the envelope is its strength deterioration after the deformation defined by rupture point. The independent parameters, relevant for our case, define: degrading reversal stiffness of spring, deteriorating of stiffness due to damage propagation, and pinching effect due to the slip of connectors.

Non-linear inelastic behaviour of the mechanical connections between the wood elements dictates the response of the entire timber structure. The basic parameters, which are needed for modelling the behaviour of the structure subjected to earthquake loading, can be defined only by experimental research of the typical connections. For fitting the parameters of hysteretic rules and skeleton curve of ULS element, the experimental data of sheathing to framing connection obtained by cyclic tests with loading in both grain directions of woodframe are needed. Both parallel and perpendicular framing member grain orientations were modelled separately. Therefore, the nail behaviour is represented by two non-liner longitudinal springs (Fig. 7), which act independently in two directions.

4.2 Mathematical model of timber-framed walls and whole structure

The mathematical model of timber-framed panels represents the assemblage made of OSB sheathing connected to wooden frame by the same number and distribution of nails as in the prototype structural element (Fig. 7). The contribution of intermediate studs was assumed to be of less significance to lateral resistance than the influence of boundary studs. Therefore, the mathematical model includes only boundary nailing. In mathematical model, each nail is represented by two longitudinal non-linear spring elements.

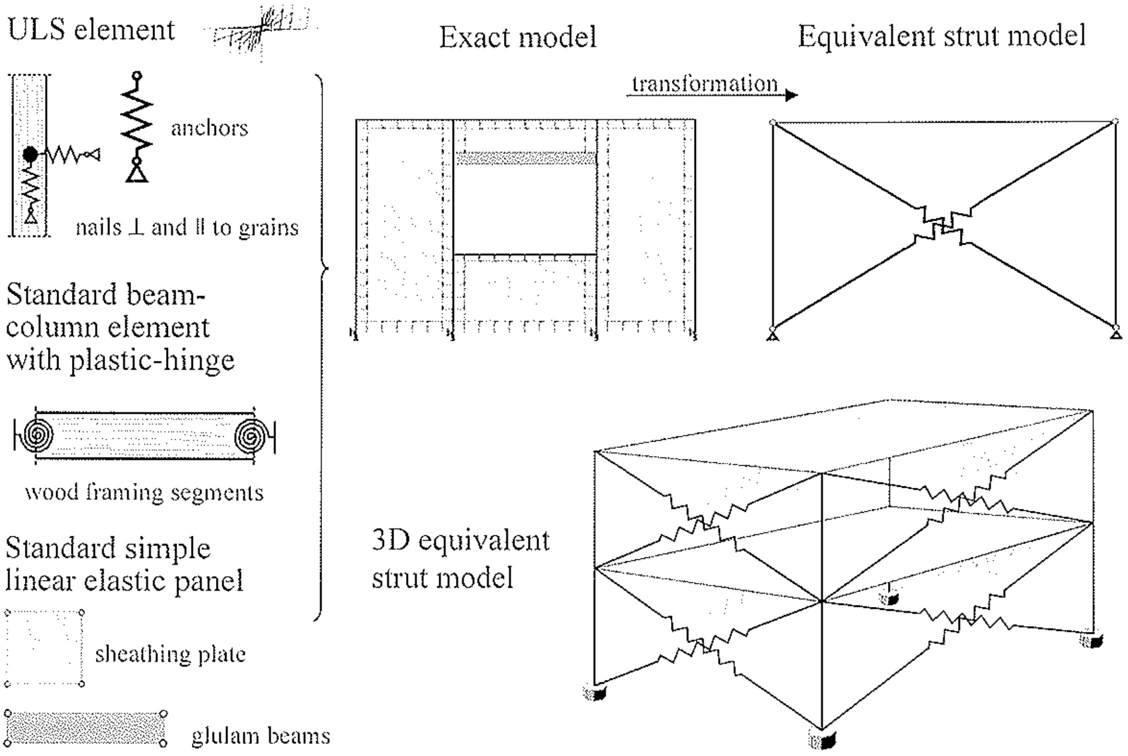
ULS element
anchors
nails ⊥ and ∥ to grains
Standard beam-column element with plastic-hinge
wood framing segments
Standard simple linear elastic panel
sheathing plate
glulam beams
Exact model
transformation
Equivalent strut model
3D equivalent strut model

Figure 7: Two-stage mathematical model of timber frame structures.

The first spring element simulates the behaviour of a nail parallel to the grain of wood connection, while the second one represents its behaviour perpendicular to the grain of wood connection. The studs at the edges of sheathing segments were fully anchored by tie-downs. The initial stiffness of the tie-down should be estimated, measured, or governed by deformability of the used number of nails loaded in parallel to the grain of wood member.

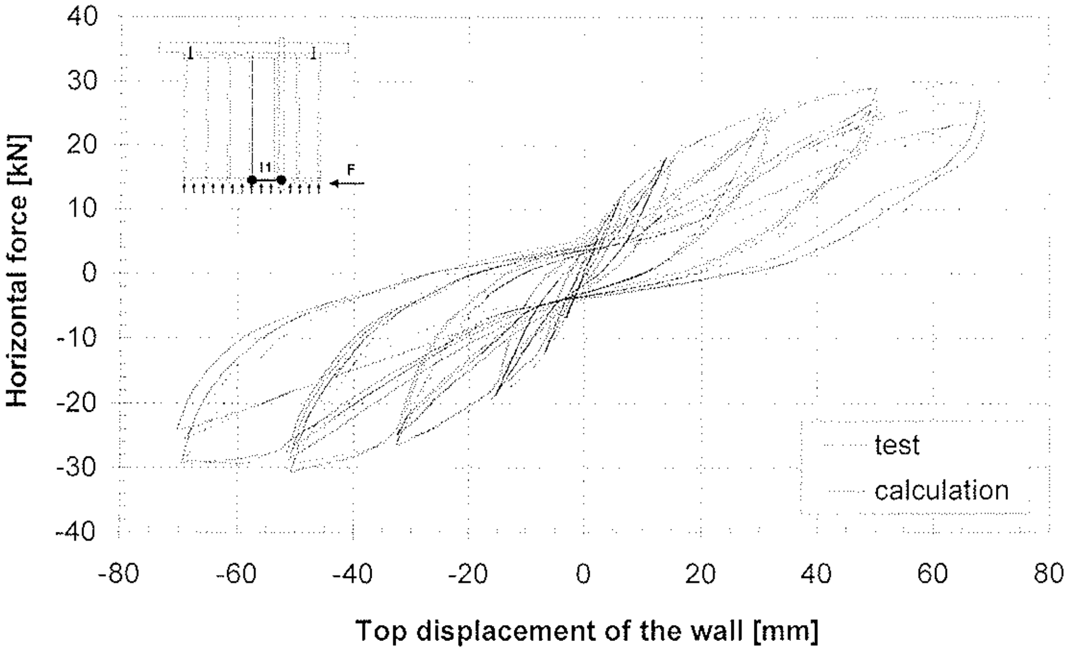

Figure 8: Comparison between experimentally obtained and calculated hysteresis response of the wall with 2ec configuration at 51 kN of vertical load for the same cyclic excitation.

The scheme of the mathematical model of timber-framed structures is presented in Figure 7. The main advantage of the macro modelling approach in comparison to FEM modelling is in better matching of the real non-linear behaviour of fasteners and in shorter time needed for the simulation of the response of real structural systems. The herein proposed approach is a two-stage approach based on the behaviour of the mechanical connections. At the first level of structural analysis, each wall of system is analysed knowing the behaviour of the frame to sheeting mechanical connection. The second level of the analysis is based on the calculated response of the single walls obtained from the first stage of analysys. The walls are represented with equivalent strut models that compose the model of entire structural system of the timber building.

In Figure 8 the calculated hysteresis response is compared with the response obtained from testing panel with 2ec configuration preloaded with vertical load of 51 kN. Good matching even in the shape of hysteresis loops confirms the quality of the mathematical model.

The quality of the mathematical model can be judged also on the energy dissipation calculated from the histeresis loops (Fig. 9). Model is not able to simulate the dissipation of hysteric energy until the yielding point is reached. After reaching YLS, the mathematical model starts to dissipate energy with the same intensity as the tested wall. This is reflected in constant difference within the dissipated energy form the beginning until the failure. It is well known that all kinds of dowel type connections between the mechanical fastener and the wood medium have a characteristic non-linear behaviour from the start of loading at very small deformation because of the embedding of the connector into the wood medium. Taking into account this phenomenon is almost impossible within a mathematical model.

The influence of vertical load to shear response of panels is demonstrated by using a calculation (Fig. 10) in the similar way as by testing of panels. The calculated and measured responses differ to certain extend in the cases of lower vertical load because of the influence of different anchorage system used in the mathematical model. The mathematical model assumes full anchorage, while the tested walls were partially anchored. From the difference evaluated from graphs (Fig. 5 and 10) it can be concluded that the tie-downs at external studs of panels could at the vertical load of 10 kN increase the horizontal load carrying capacity by more than 50 %.

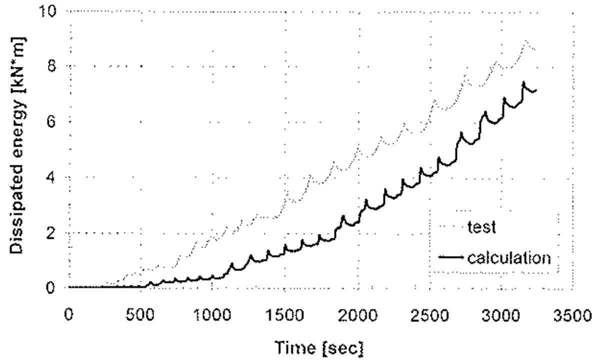

Figure 9: Comparison between experimentally obtained and calculated energy dissipation of the tested wall.

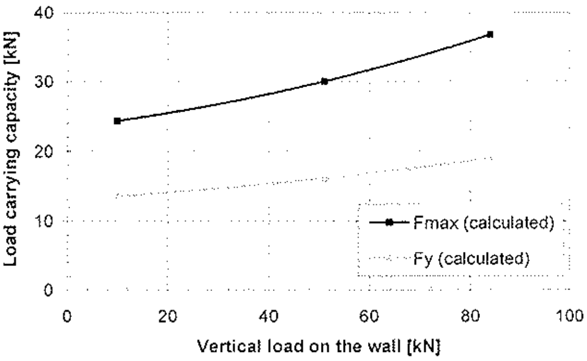

Figure 10: Influence of vertical load on calculated load carrying capacity of fully anchored timber frame wall.

The developed mathematical model was also verified by blind prediction of dynamic response of a wood framed residental building at International Benchmark Workshop in June 2001 in San Diego. The two-story house was tested on uniaxial seismic simulation system at the University of California, San Diego, in the scope of CUREE-Caltech Woodframe Project. The calculated dynamic response shows good agrement with the measured one [4, 1 and 2], which proves the model's efficiency.

5 Conclusions

The main conclusions derived from herein presented experimental research are that the shear tests on cantilever timber-framed walls are very sensitive to boundary conditions and the magnitude of vertical load. Very important is also the way of applying loading on the test specimens. The tests results show that moderate additional investment in slight variation of panel composition (anchors, tie-downs) can significantly upgrade the shear resistance of the wall at the same magnitude of vertical load. Due to weak connections of framing elements and unsuitable anchoring, the magnitude of vertical load has a beneficial influence on racking strength of the wall. The bearing wall preloaded with lower vertical load should be fully anchored with the tie-downs on the exterior studs of the frame.

The proposed non-linear spring element is capable to simulate the behaviour of all kinds of connectors and anchors with typical characteristics of hysteresis loops. The simulation of inelastic behaviour of nailed connection is of crucial importance for successful prediction of the behaviour of timber frame walls and timber structures on seismic excitation. The presented mathematical model is also suitable for modelling the response of largely fenestrated panels. The whole layout of openings can be taken into account with real distribution and dimension of OSB sheathing including the sheathing beneath the windows as well as sheathing and glued laminated timber beams above the openings. The comparison of calculated and experimentally obtained response of the tested timber frame wall shows excellent agreement even in the shape of hysteresis loops. For accurate analysis it is important to calibrate the mathematical model parameters for mechanical connectors with experimentally obtained results.

6 References

[1] Dujič, B., 2001. "Experimental Supported Modelling of Response of the Timber Frame Wall Panels to Horizontal Cyclic Load", Ph.D. thesis (in Slovenian), Faculty of Civil and Geodetic Engineering, University of Ljubljana, Slovenia.

[2] Dujič, B., Žarnić, R., 2001. "Blind Prediction of Seismic Response of a Wood Framed Residential Building Performed at University of Ljubljana, Slovenia"; CUREe-Caltech Wood Frame Project - International Benchmark; Report N^{o} UL FGG KPMK 01/01, 43 p., University of Ljubljana, Slovenia.

[3] EN 594:1995, Timber structures - Test methods - Racking strength and stiffness of timber frame wall panels, CEN, European Committee for Standardization, Brussels.

[4] Folz, B., Filiatrault, A., Uang, C.-M., Seible, F., 2001. "Blind Predictions of the Seismic Response of a Two-Story Woodframe House: An International Benchmark", Report N^{o} SSRP – 2001/15, Report to the CUREE as part of the CUREE-Caltech Woodframe Project, Division of Structural Engineering, University of California, San Diego, La Jolla, California, September 2001.

[5] Gostič, S., Dujič, B., Žarnić, R., 2001. "Inelastic Computational Model (ULS) of Nail Connections", Proceedings of the International RILEM Symposium, Aicher and Reinhardt (editors), Stuttgart, Germany, 12-14 September 2001.

[6] Källsner, B., 2001. "A Simplified Plastic model for Design of Partially Anchored Wood-Framed Shear Walls", Proceedings CIB-W18, paper 34-15-1, Venice, Italy.

[7] Shepherd R., "Standardized Experimental Testing Procedures for Low-Rise Structures", Earthquake Spectra, EERI, Vol. 12, No.1, 1996, pp. 111-127.

[8] Žarnić, R., Gostič, S., 1997. "Masonry Infilled Frames as an Effective Structural Sub-Assemblage", Proc. of the Int. Workshop on Seismic Design Methodologies for the Next Generation of Codes, Fajfar and Krawinkler (ed.), Bled, Slovenia.

CIB-W18/35-15-5

INTERNATIONAL COUNCIL FOR RESEARCH AND INNOVATION
IN BUILDING AND CONSTRUCTION

WORKING COMMISSION W18 - TIMBER STRUCTURES

CYCLIC AND SEISMIC PERFORMANCES OF A TIMBER-CONCRETE SYSTEM

- LOCAL AND FULL SCALE EXPERIMENTAL RESULTS -

E Fournely
P Racher

Lermes – MSGC/CUST - Blaise Pascal University of Clermont-Ferrand

FRANCE

Presented by: E Fournely

In answer to a question by G Gonzalez, E Fournely indicated that the slip modulus was measured. H J Blaß asked if bonding between the timber and concrete was prevented during the test. E Fournely replied that plastic sheeting were only provided on the sides of the test specimens and so bonding between the concrete and timber was not prevented.

Cyclic and seismic performances

# of a timber-concrete system

- local and full scale experimental results -

Eric Fournely, Patrick Racher
Lermes – MSGC/CUST - Blaise Pascal University of Clermont-Ferrand
CUST BP 206 – F 63174 Aubiere Cedex

1 Introduction

Timber-concrete composite floors are light solutions to comply with design criteria: stiffness, load capacity, fire barrier and resistance, phonic isolation, comfort toward vibrations... Most of these characteristics are particularly important in seismic zone. A lot of mechanical functions have to be assumed by a floor in a structure undergoing severe vertical and horizontal loading. Obviously, bending strength is the first function of a floor. Nevertheless, diaphragm function and connection with vertical structure is also extremely important. The total or semi-rigid connection of to layers provides a large strength for floor elements in bending. This connection also undergoes shear forces in order to transfer horizontal loading (wind, buckling effects, seismic actions…) from beams to diaphragm and from diaphragm or beams to vertical structures. Figure 1 gives an illustration of different configurations for a composite floor.

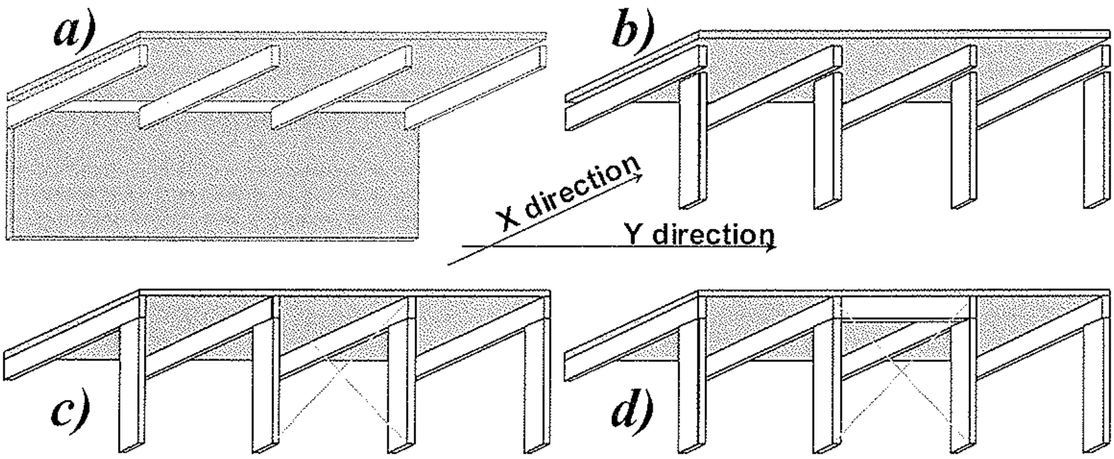

Figure 1 : illustration of a composite floor integration in different vertical structures

The *a)* configuration corresponds to a reinforced diaphragm layer directly connected with concrete wall. In this case, horizontal loads can be transfer by usual RC system and connected beams are essentially used for bending function. For *b)* structure and loading in x direction, horizontal forces are equally distributed on the different portal frames. For Y axis loading direction, *c)* configuration induces layer interface forces perpendicular to the beam. The integration of a longitudinal beam as in *d)* illustration allows to reduce these perpendicular forces. A complete side-line of connected beams as anchoring flat may be more efficient. Nevertheless, with torsion displacement modes the perpendicular to beam forces can not be totally suppressed.

The types of behaviour are often different among Service Limit States and Ultimate Limit States. The concreting technology is quite important on the global characteristics of a timber-concrete element. The possible semi rigidity for one connection can be differently integrated in global behaviour. The number of points of connection or its continuity can induce various types of global mechanical response. For a composite floor, it is important to have a global approach, without a unique limitation to a regular bending problem.

This paper deals with stiffness, strength and ductility experimentally observed on increasing sizes of shear specimens as well as on full scale floor in bending.

2 Sylvabat system and experimental programme

The technology analysed here is based on a mechanical connection realized by steel tube, circular hollow section, between reinforced concrete layer and glulam beams. One part of the tube is inserted in timber component by drilling, the other part is sealed during concreting in the slab. This technical solution, Sylvabat system, can be used as well as for new construction or for refurbishment. Figure 2 presents two examples of recent realizations with this technique.

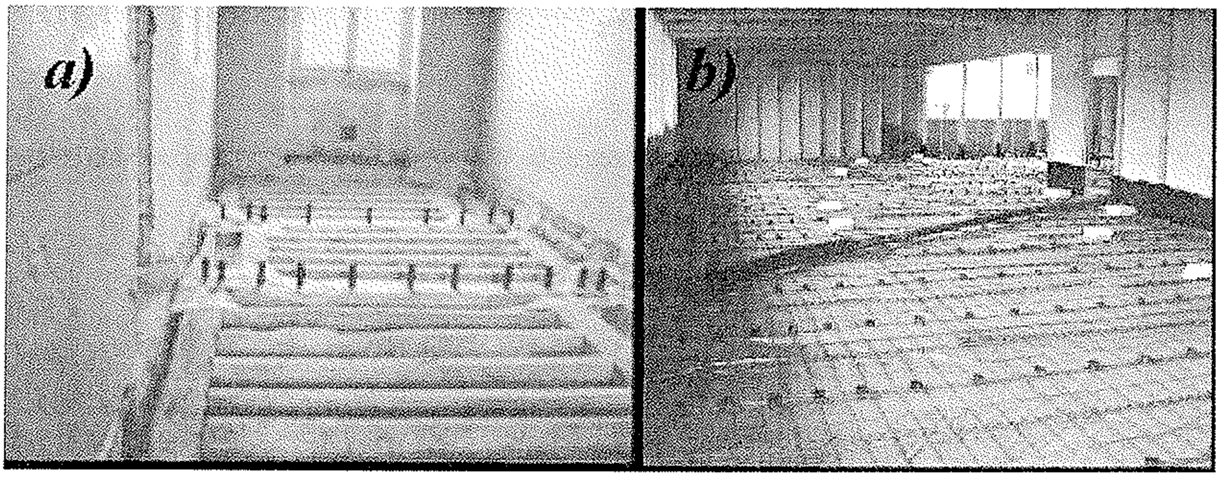

Figure 2 : examples of Syylvabat system realisations:
a) refurbishment of Esquirol hospital in Paris region (530m^2),
b) construction of a secondary school in the Alps (1760 m ^{2})

Standard CEN,EN 12512 [2] is used to perform the static tests, amplitudes of cyclic loading signal are determined from it. Indeed, this standard is relative to experimentations on timber elements. In our case, the mixed building technology with the presence of a thin concrete slab, brought us to increase the number of cycles, in each sequence of a constant amplitude of the controlled signal, from 3 to 20 better to exhibit possible concrete damage in the connecting zone. Increment of amplitude of loads are determined in comparison to ultimate displacement as proposed in ISO standard [4]. Loading histories are recapitulated in figure 3.

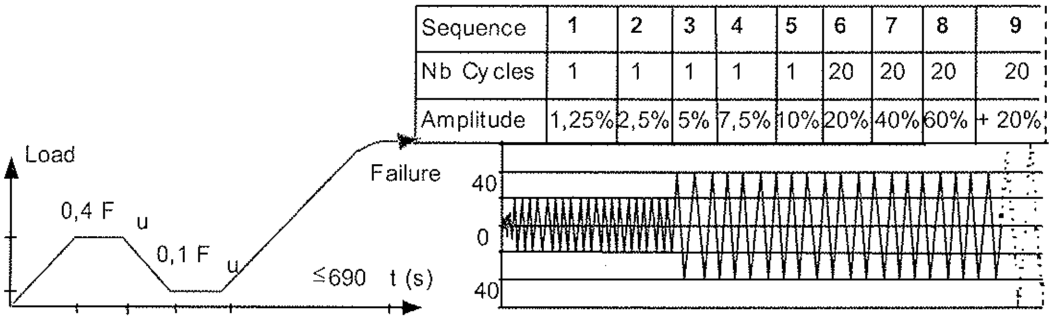

Sequence	1	2	3	4	5	6	7	8	9
Nb Cycles	1	1	1	1	1	20	20	20	20
Amplitude	1,25%	2,5%	5%	7,5%	10%	20%	40%	60%	+ 20%

Figure 3. static and growing cyclic loading

Three scales of shear specimens are tested with 1, 2 and 4 or 8 connectors. These different scales of specimens allow us to obtain information about interaction effects and distribution of load between connectors. For each configuration, every test is repeated three times to estimate the variability of the behaviour. The constitution of the simplest specimens is summarized in table 1.

	Code name	1-a	1-b	1-d
	Timber type	GL26h	GL26h	C24
specimen	L (mm)	600	600	600
	b (mm)	110	110	90
	h (mm)	270	270	220
Connector	ha (mm)	40	70	40
	D (mm)	50	70	50

Table 1: shear specimen configuration and dimension

Connectors with a diameter of 70mm are used for 2 and 4 connector specimens. Finally tests carried out on 27 m² floors give global in formation in order to calibrate the integration of basic single connector behaviour, interaction effect on global response of the whole structure.

The characteristics of the materials are the following ones :
Concrete slab: concrete B25 (fc28=25MPa) , with a reinforcing steel mesh,
Timber beam: GL26H, $\bar{d} = 465\ \mathrm{kg} / \mathrm{m}^3$ and solid wood, C24, $\bar{d} = 438\ \mathrm{kg} / \mathrm{m}^3$
Connections: steel Tube S235, thickness=2 mm.

3 Basic scale: one connector

3.1 Experimental set up

Tests are carried out on specific test vertical portal frame. Controlled displacement signal is applied on the extremities of the timber beam (fig. 4), it is applied with an hydraulic jack "Instron" and controlled by an electronic system "S56". The forces induced by this displacement are recorded by a force sensor "Z12 HBM". The slab is supported on each side by a trimmer beam. This beam is pin connected on two force sensors "H2 HBM". H2 and Z12 sensors allow us to compare the loads applied on the beam and the slab, and so, to have an estimation of the friction on lateral, back and front simply support (less than five percent of the applied load in our tests, with a validation for each test) [5]. The slip between timber and concrete elements is measured by two symmetrical LVDT sensors fixed on both sides of the timber beam. Difference between the two sensors allows to make sure of the weak importance of a rotation around the tube axis. Specimens are placed with a gap of some mm perpendicularly to the plan of connection but without gap in the direction of the load.

Therefore the preloading phase is integrated into the phase of implementation ; it is limited to 30 % of the estimated static strength.

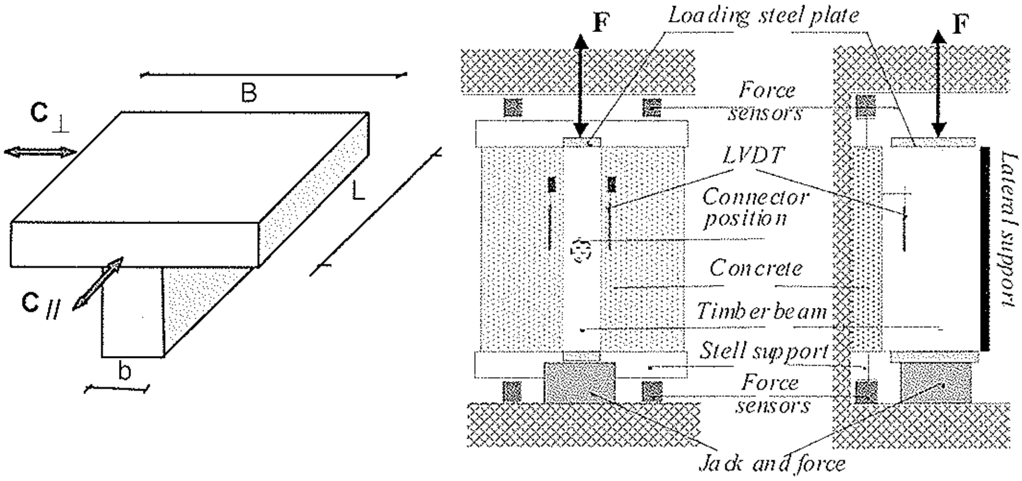
B
$C_\perp$
L
$C_{//}$
b
F
Loading steel plate
F
Force sensors
LVDT
Connector position
Concrete
Timber beam
Stell support
Force sensors
Jack and force
Lateral support

Figure 4. Shear specimen and experimental set up

3.2 Static loads results

Static loads results are illustrated on figure 5. Rigidity, strength and static ductility are presented in the table 2 [6]. These figure and table show the good homogeneity of the results obtained for each configuration; the biggest homogeneity is observed for specimens with the glulam beams. The little more important dispersion of results with solid timber beam component can be attributed to the biggest dispersion of the characteristics of the solid wood itself. Specimens undergoing longitudinal loading, in the various configurations of connection, present a good static ductility.

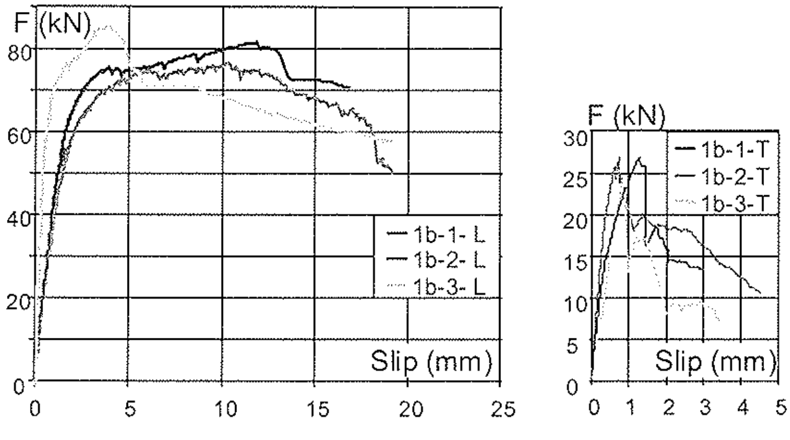

Figure 5: Static behaviour for basic tests longitudinally and transversally loaded

		K (kN/mm)	Fmax (kN)	Ductility
Longitudinal shear	**1-a-L**	39,5	61	11
	1-b-L	38,5	75	8
	1-d-L	28,2	60	4 to 10
Transverse shear	**1-a-T**	28	21,7	1
	1-b-T	40	27,0	1
	1-d-T	23,5	16,2	1

Table 2: basic specimen shear tests, strength, stiffness and ductility

The connectors with a diameter of 70mm and an anchorage of 70mm bring a wider linear elastic domain, but not a biggest static ductility. Strength in transverse shear of this type of connection is about 30% of the longitudinal one, failure is brittle and experimental results obtained after this first failure correspond to the behaviour of a half-beam in three point transverse bending (tow points for the applied load and the connector as support).

3.3 Cyclic results

Cyclic results are presented on figure 6. On this figure, curves in wide lines correspond to static envelop curves; cyclic curves well join the static domain. The strength diminution during a sequence of 20 cycles remains very weak until 40 % of the static strength, After this threshold, until yield strength, the diminution does not exceed 20 %, even with 20 cycles per sequence. Observations made for static results can be duplicated for cyclic results. Differences between static and cyclic results appear on the shape and the location of the collapse. Indeed, the observation after testing of the static specimens indicates an embedding of the wood, a plastic hinge with shear in the connector and cracks in concrete in joint zone. In contrast, after cyclic loading, the specimens show preferentially a large damage of concrete in embedment, without significant embedding in wood or deformation of the connector.

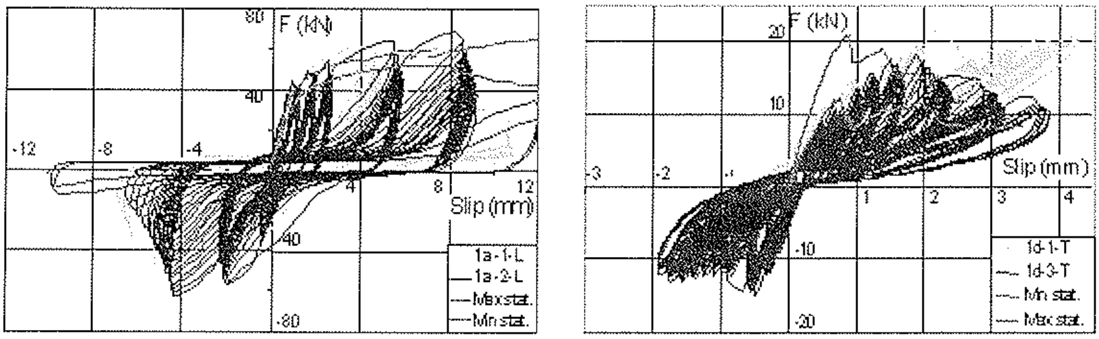

Figure 6: cyclic behaviour for basic tests longitudinally and laterally loaded

3.4 Seismic results

In order to complete these static and cyclic results, static and seismic type loads are applied on single connected specimens close to 1-b type with concrete throughout the tube, including in the thickness of the beam. Loading and behaviour are presented on figure 7. The three signals of loading are deduced from Kobe earthquake. Between the first and the second loading, the duration of the load is modified. Between the second and the third loading, the amplitude of the required displacement is modified. The widest curves on right graphics correspond to the static relationship between displacement and load. The fine lines indicate the seismic behaviour. Together, the different seismic behaviours are in a good accuracy. The seismic loads are Slightly greater than those of static skeleton curve (wide lines). First and second loadings are particularly severe and for the end of loading a large gap in the connection can be observed. After the third loading, only little damage of the specimen can be detected. A good ductility is also observed during these specific loadings.

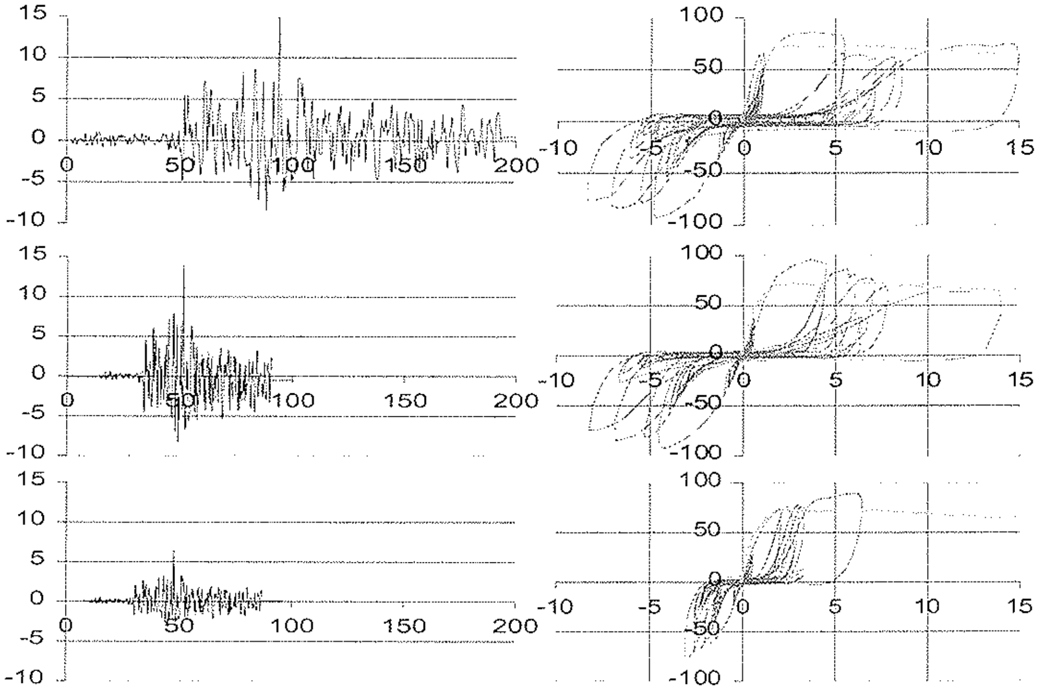

Figure 7: Seismic behaviour of a single connected shear specimen
Left: time(s)-displacement(mm) loading - Right: slip(mm)-load (kN) curve

4 Multi connected shear specimens

The dimensions of these specimens are the same as basic ones, except the length. Tests reported here correspond to specimens with:
- two connectors (1-c) placed at minimal distance indicated in the technical approval [7] of the process (dc/c=200 mm), L=900mm, D=70mm, ha=70mm,
- four connectors (2-a) dc/c=250mm, L=1200mm, D=70mm, ha=40mm,
- eight connectors placed in staggered rows (2-b), dc/c=170/80mm, L=1200mm, D=50mm,ha=40mm

Stiffness, strength and ductility are given in table 3. Stiffness, resistance per connector and ductility seem to be quite dependant to the number of connectors and to the distance between these connectors.

SERIES	Multi-connected specimens			Equivalent single connected specimens		
	K_n (kN/mm)	Fumax $_n$ (kN)	SD	K_1 (kN/mm)	$Fumax_1$ (kN)	SD
1 – c	94 = 2,4.K_1	116 = 1,5.F_1	6,1	38,5	75	8
2 – a	170 = 4,4.K_1	259 = 3,5.F_1	6,3	38,5	75	8
2 – b	218 = 5,5.K_1	283 = 4,6.F_1	5	39,5	61	11

Table 3 – stiffness, strength and static ductility of multi connected specimens

5 Floors in bending

Tests on two types of connected floors have been carried out. The two diameters of connectors have been used. Here is only presented the test and the results relative to the third floor with 70 mm diameter connectors and an alternated loading. Constitution of the floor, dimension and position of the beams are given on figure 8. On this figure, experimental set up for a three point bending is also describe. Realization of the floor before and after concreting is illustrated on figure 9. Steel frame specially designed to apply ascendant and descending loading, equipment used to record displacements and forces are also shown on this figure. Design of the floor with four beams and usual concrete slab is able to take into account and to exhibit influence of the effective compressed concrete zone due shear lag. Configuration of the loading induces linear bending moment and constant vertical load effect and so, a biggest zone for transfer of connecting forces.

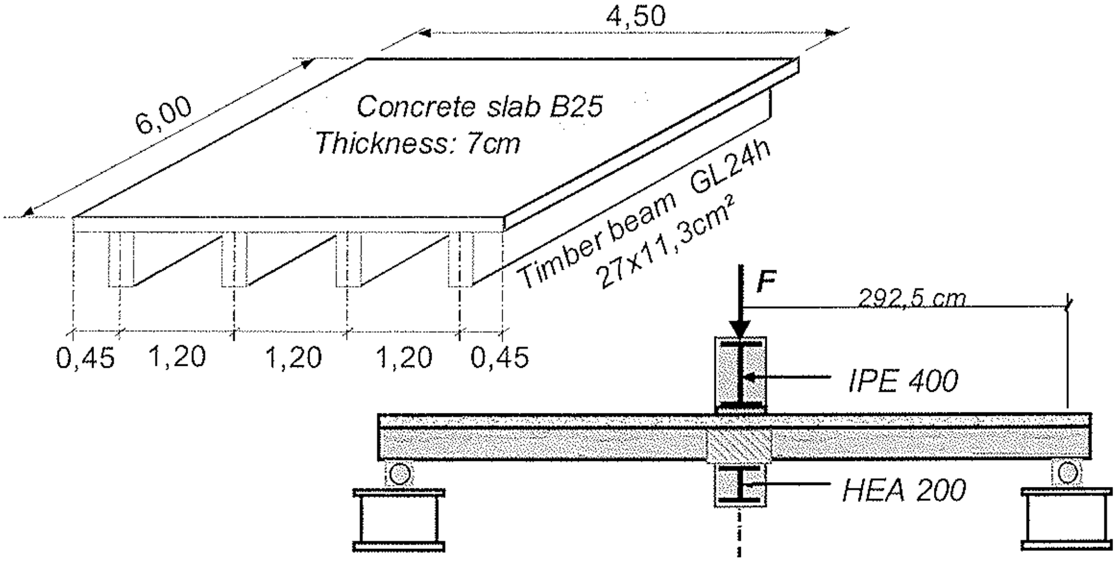
4,50
6,00
Concrete slab B25
Thickness: 7cm
Timber beam GL24h
27x11,3cm²
0,45
1,20
1,20
1,20
0,45
F
292,5 cm
IPE 400
HEA 200

Figure 8: description of the floor and experimental set up

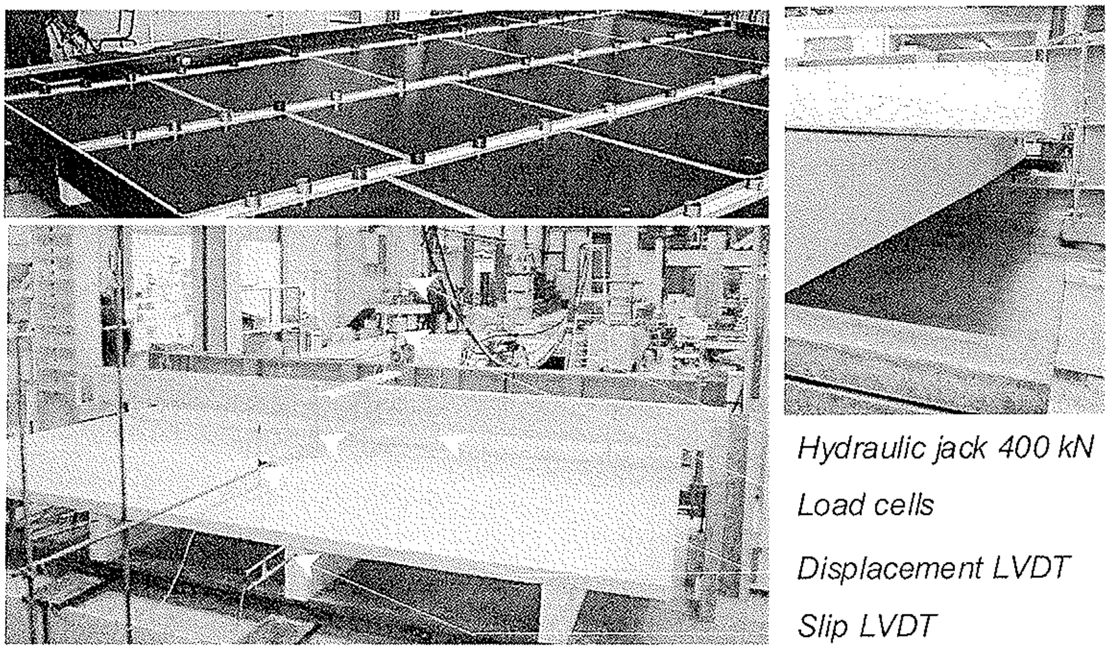
Hydraulic jack 400 kN
Load cells
Displacement LVDT
Slip LVDT

Figure 9: framework, connection, loading apparatus and measurement equipment

A same evolution of number of cycles and amplitude of displacement of each sequence is defined for cyclic loading. Nevertheless, asymmetric signal is assumed between downward and upward controlled displacement loading. All these actions are applied on concrete layer, directly on the upper face, or on the lower face between the timber beams. Vertical displacements are recorded in different points on a half part of the floor. mid span deflection is illustrated on figure 10. Interesting stiffness, strength, and lower cyclic damage can be observed. However, global ductility is very low; collapse is not induced by connecting failure. Collapse appears in bending in one or two timber beams. Maximum of bending moment is close to 340 m.kN. After this failure, the floor still undergoes a moment about 180 m.kN, equivalent to a deflection of l/300 before the first failure.

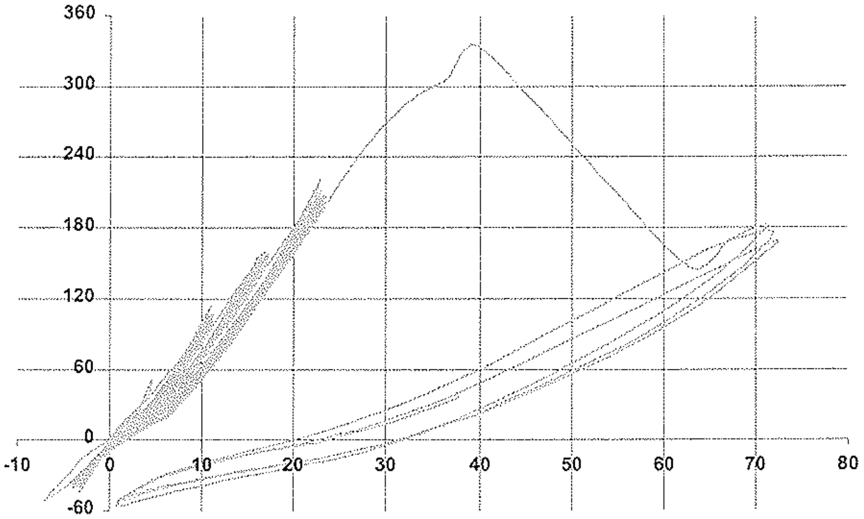

Figure 10: floor Nb. 3, Bending moment (m.kN) versus central displacement (mm)

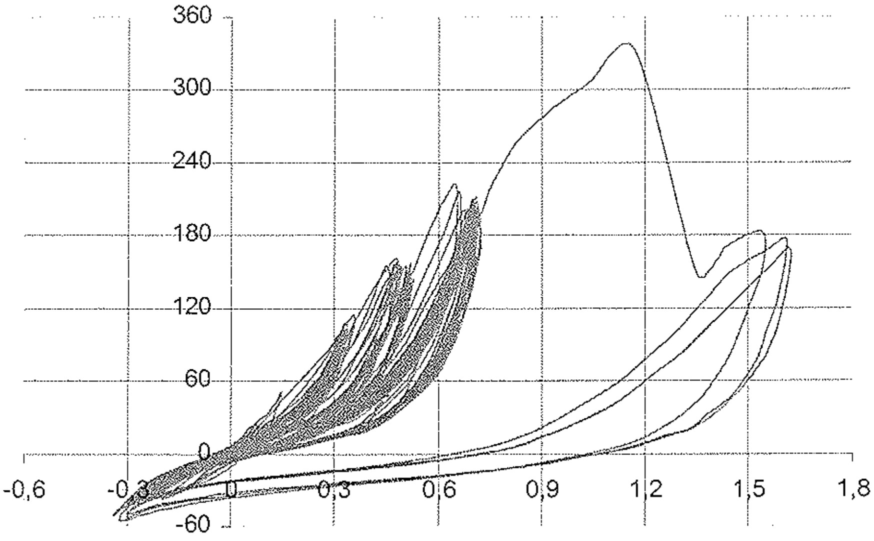

Figure 11: floor Nb. 3, Bending moment (m.kN) versus slip between layers (mm)

Displacements between timber beams and concrete layer are measured on the ends of the floor; they are presented on figure 11. For a deflexion corresponding to l/300, the slip between the two component is 0,7 mm. The failure appears for a value of slip of 1,1 mm. This value increase only to 1,6 mm during the next loops.

6 Analysis and conclusion

Results of test carried out on the floors and shear specimens are compared with modelling proposed by Eurocode 5- part 1.1 (Annex B – Informative- Mechanically jointed beams) [1], [3]. Values parameter used for the modelling are the following:
Concrete MOE (E_c): 30 Gpa,
Timber MOE ($E_{0,moy}$/): 12 et 11,7 Gpa,
Stiffness connection: 38,5 kN/mm for D=70mm, 39,5 kN/mm for D=50mm.

Effective part of concrete slab taken into account with a timber beam is defined as:

$$b_{eff} = min\ (b_w + L/5\ ;\ b)\ x\ (E_{0,moy}/E_c)$$

Results of annex B modelling applied to our floors in these conditions for bending moment of 200 m.kN are presented in table 4. Experimental values of deflection and slip are also given for the same moment in this table.

	u_{exp} (mm)	g_{exp} (mm)	b_{eff} (mm)	u_{th} (mm)	g_{th} (mm)	**Forces in conncetors (kN)**
P1 , P3	22	0,6	480	20	0,644	**25,8**
P2	25	0,56	468	19	0,547	**21,1**

Table 4 – Experimental modelling results for floors in bending

Study of the local behaviour of Sylvabat system connection exhibits different failure modes according to the loading signal (static or cyclic). The full scale floor shows another dominating mode of failure. In this case, the failure is due to timber beams in bending. Brittle behaviour in tension of timber and limited capacity of deflection give some explication of this observation.

Strength variation of concrete layer does not appear to be an important element in the strength of the composite floor. In fact, the three floors reach equivalent levels of resistance (≈340 m.kN) [8]. Evolutions of distance between the connectors along the span proposed in annex B correspond to larger distances than in the actual technical approval and seems to be enough to obtain the observed strength (*600 mm* for a diameter of 70mm in middle span zone and 300 mm close to support). With regard to the two components without connection, Sylvabat system presents a gain of efficiency from 2,5 to 3,5. This ratio is about 0,75 to 0,85 by considering stiff interfaces. The previous variations depend on the definition of the shear lag effect. Complementary studies have to precise this point.
Beyond the validation of the cyclic behaviour of Sylvabat floor (designed for static action), its realization in seismic zone requires definition of specific details in connection with vertical structures in order to transfer horizontal forces.

7 References

1 Ceccotti A. "Timber to concrete structures", STEP/Eurofortech, Timber engineering Vol.2, lecture E13, Centrum Hout, Almere, The Nederlands 1995

2 CEN, EN12512. "Timber structures – Test methods – Cyclic testing of joints made with mechanical fasteners", 1977

3 CEN/TC250/SC5 prENV1995-1-1. "Eurocode 5, Design of timber structures Part 1.1, Informative Annex B : Mechanically Jointed Beams", final draft, stage 34

4 ISO, TC 165 WG7. "Timber Structures – Joints made with Mechanical fasteners – Quasi Static Reversed-cyclic Test Method", draft

5 Fournely E., Racher P.. "Comportement dynamique du plancher mixte et de la connexion bois-béton du système Paris-Ouest", contract report, June 2002

6 Fournely E., Lecrompt C., Racher P., Sauvat N.. "Behaviour of a timber-concrete connection, application to shear specimens and floors undergoing repeated loads", COST C12-WG1 Mixed building technology – Proceedings of Bled meeting, Slovenia – sept. 2001 – 7 pages

7 Paris Ouest : Technical approval «Sylvabat »,1989

8 Racher P. "Eléments mixtes dans les structures bois : assemblages bois-métal et plancher bois-béton", Int. Holzbau Forum 2001, 11 p, Garmisch Allemagne, déc. 2001

CIB-W18/35-15-6

INTERNATIONAL COUNCIL FOR RESEARCH AND INNOVATION IN BUILDING AND CONSTRUCTION

WORKING COMMISSION W18 - TIMBER STRUCTURES

DESIGN OF TIMBER-CONCRETE COMPOSITE STRUCTURES ACCORDING TO EC5 – 2002 VERSION

A Ceccotti
NRC - TTI, Florence

M Fragiacomo
University of Trieste, DCE

ITALY

R M Gutkowski
Colorado State University

USA

Presented by: R M Gutkowski

H J Blaß asked if the proposed calculation methods presented were compared against test data. G Gutkowski replied that the presentation refers only to numerically generated data as the testing intended by the authors have yet to be conducted. H J Blaß then commented that the deformations obtained from recent tests conducted at Karlsruhe University were twice the values predicted by EC5 and as such perhaps an approach which is simpler but more accurate than those proposed in the latest version of EC5 or the authors is needed.

Design of timber-concrete composite structures according to EC5 – 2002 version -

A. Ceccotti

NRC – TTI, Florence, Italy

M. Fragiacomo

University of Trieste, DCE, Italy

R. Gutkowski

Colorado State University, USA

1. Introduction

This paper is about the design of timber-concrete structures with semi-rigid connections -beams in particular-, according to the provisions given by Eurocode 5 (EC5). In fact the new pre-version of this Standard (prEN 1995-1-1, final draft, April 2002 [1]) has introduced some changes in the way of evaluating the long-term effects of sustained loads, which allows for some modification of the currently employed design procedure for this kind of composite beams (presently ENV 1995-Part 1-1 [2] and ENV 1995-Part 2 [3]).

Therefore the scope of this paper is the long-term performance of timber-concrete composites, aiming to propose a simplified procedure for its evaluation.

2. Basics of design

The deformability of the semi-rigid connection system play a very important role on the structural response of mechanically jointed structures. EC5 takes it into account by using the formulas for timber-to-timber composite beams with semi-rigid joints firstly proposed by K. Möhler [4] (see Appendix).

Strictly speaking, these formulas are rigorous only for linear-elastic materials. Concrete and timber are therefore regarded as linear-elastic, and their average Young's moduli $E_{cm}\ (t)$ and $E_{0,mean}$ are evaluated according to provisions given by Eurocode 2-Part 1-1 [5] and EC5-1-1 related product-standards respectively[1].

The connection system is usually characterized by a load-slip non-linear constitutive law, but in order to apply the elastic formulas it is also considered as linear-elastic. The slip moduli K_{ser} and K_u are therefore secant slip moduli that are employed respectively for serviceability and ultimate limit state verifications. They should be evaluated by experimental tests (i.e. ISO-EN 26891), however EC5-1-1 provides some approximate formulas for timber-to-timber connection systems that are extended to timber-concrete connection systems by simply doubling these values. In addition, it states that a value $K_u = 2/3\,K_{ser}$ is admissible for design calculations.

---

[1] Since concrete is an aging material, its Young's modulus increases in time and is a function of the instant t ($E_{cm}\ (t)$) at which the load is applied, according to the formulas given by [6]. Nevertheless, for the sake of simplicity, this dependency of the concrete Young's modulus on the time, is not considered by Eurocode 2.

Both ultimate and serviceability limit states have to be checked at short-term and long-term.

3. Evaluation

Let E^F be a generic effect (stress, displacement) produced by the load combination F, and F_u, F_s be the load combinations for ultimate and serviceability limit state. The value of E^F can be calculated using the formulas provided by EC5. *Ceteris paribus,* this value depends on the load applied on the beam, and on the Young's and slip moduli of the component materials:

$$\mathrm{E}^{F_s} = \mathrm{E}^{F_s}\left(E_{cm}, E_{0,mean}, K_{ser}\right) \qquad \mathrm{E}^{F_u} = \mathrm{E}^{F_u}\left(E_{cm}(t_0), E_{0,mean}, K_u\right) \qquad (1)\quad(2)$$

The quantities E^{F_s} and E^{F_u} would be different even if the same load combination was applied, being $K_{ser} \neq K_u$.

The problem is complicated by the rheological phenomena that occur in all the component materials. Concrete, timber and connection system are characterized by important creep phenomena, and the moisture content affects the behaviour of both timber and connection. For the concrete, EC2-1-1 provides some formulas and tables for evaluating the creep coefficient $\phi(t,t_0)$, t and t_0 being the final and loading instant respectively. EC5-1-1 tables the values of the creep coefficients k_{def} for both timber and connection. The creep phenomenon produces two types of effect on the composite beam:

- increment in time of strains and displacements;
- different distribution in time of stresses and internal forces in the component materials, because of the different creep properties.

Consequently the creep affects both the ultimate and serviceability limit states, and should not be neglected. Thus, the composite beam has to be checked with regard to:

- the initial state (short-term verifications), i.e. immediately after the construction (instant t_0): the loads are applied instantaneously, and there is no creep effect;
- the final state (long-term verifications), i.e. at the end of the technical life (instant t): the rheological phenomena affect the behaviour of the beam.

The short-term verifications can be performed according to the aforementioned procedure, based on Young's modulus values, while for the long-term verifications, the *effective modulus* method can be employed [1,2,3,5], i.e.

$$E_{c,fin} = \frac{E_{cm}(t_0)}{1+\phi(t,t_0)} \qquad E_{t,fin} = \frac{E_{0,mean}}{1+k_{def,t}} \qquad K_{fin} = \frac{K}{1+k_{def,f}} \qquad (3)\quad(4)\quad(5)$$

In the case of timber-concrete composite structures, being the concrete more viscous than timber in most cases, concrete stresses tend to decrease in time while stresses on timber tend to increase. Therefore the long-term situation is the most demanding for timber. For this reason short term performance is not considered in this paper.

The long-term calculation procedure is described in the following Sections with regard to the old (ENV, 1993) and the new version (prEN 2002) of Eurocode 5.

4. Design procedure according to ENV version

In the ENVversion of EC5, in force at present time, the creep coefficient k_{def} is tabled as a function of the *service class*, which accounts for the moisture content of timber, and of the *load duration class*. Since loads with different duration classes may exist in the same combination, different values of k_{def} should be used. For serviceability and ultimate limit states, the design load combinations are respectively:

$$F_{d,s} = \sum_{j\geq 1} G_{k,j} + Q_{k,1} + \sum_{i>1} \psi_{1,i} Q_{k,i} \qquad F_{d,u} = \sum_{j\geq 1} \gamma_{G,j} G_{k,j} + \gamma_{Q,1} Q_{k,1} + \sum_{i>1} \gamma_{Q,i} \psi_{0,i} Q_{k,i} \qquad (6) \quad (7)$$

where G denotes the permanent and Q the variable actions, characterized by different values of creep coefficients, and γ, ψ are coefficients tabled in Eurocode 0 [8].

Long-term verifications

Serviceability limit state

The long-term maximum vertical displacement u_{fin} can be calculated by superposing the effects of the different loads:

$$u_{fin} = u_{fin}^{F_{d,s}} = \sum_{j\geq 1} u_{fin}^{G_{k,j}} + u_{fin}^{Q_{k,1}} + \sum_{i>1} \psi_{1,i} u_{fin}^{Q_{k,i}} \qquad (8)$$

Each contribute u_{fin}^{F} is evaluated using the effective moduli of the materials [7]:

$$u_{fin}^{F} = u^{F}\left(E_{c,fin}, E_{t,fin}, K_{ser,fin}\right) \qquad (9)$$

that are given by Eqs. (3) to (5), adopting the creep coefficients calculated according to the load duration class.

Ultimate limit state

The ultimate limit state at the final stage can be checked using the formulas given by EC5 to evaluate σ_{fin} stresses, replacing the Young's moduli of the materials with the effective moduli E_{fin}:

$$\sigma_{fin} = \sigma_{fin}^{F_{d,u}} = \sigma^{F_{d,u}}\left(E_{c,fin}, E_{t,fin}, K_{u,fin}\right) \qquad (10)$$

where the load combination $F_{d,u}$ is given by Eq. (7). Because of the different values of k_{def} for the loads G and Q, the effective moduli are calculated as average values of the k_{def} coefficients *weighted* according to the loads [7]:

$$E_{fin} = \frac{E}{\sum_{j>1} G_{k,j} + \sum_{i>1} Q_{k,i}} \cdot \left(\sum_{j>1} \frac{G_{k,j}}{1 + k_{def,G_{k,j}}} + \sum_{i>1} \frac{Q_{k,i}}{1 + k_{def,Q_{k,i}}} \right) \qquad (11)$$

where E is the Young's modulus of concrete, timber or the slip modulus of connection. The Eq. (11) applies for both timber and connection (the creep coefficients are assumed equal for both materials), and also for concrete, as long as the creep coefficients k_{def} are substituted with $\phi(t,t_0)$, according to the corresponding load duration class. While correct this procedure lacks of physical sense, somehow.

5. Design procedure according to prEN version

In prEN version of Eurocode 5 (2002) while the load combination for ultimate limit state design has been retained unaltered, the load combination for the serviceability limit state has been changed as anticipated in [9]. In fact, according to Eurocode, *Basis of structural design* [8], three combinations - characteristic, frequent and quasi-permanent - are now considered:[2]

$$F_{d,r}=\sum_{j\geq 1}G_{k,j}+Q_{k,1}+\sum_{i>1}\psi_{0,i}Q_{k,i} \quad F_{d,f}=\sum_{j\geq 1}G_{k,j}+\Psi_{11}Q_{k,1}+\sum_{i>1}\Psi_{2,i}Q_{k,i} \quad F_{d,p}=\sum_{j\geq 1}G_{k,j}+\sum_{i\geq 1}\psi_{2,i}Q_{k,i} \quad (12)\ (13)\ (14)$$

In particular the characteristic $F_{d,r}$ and the quasi-permanent $F_{d,p}$ load combinations are employed respectively for evaluating the effects of instantaneous and sustained loads.2

Only *one value* per material is now provided for k_{def}, i.e. the *permanent* value. In case of other duration loads the relevant k_{def} is simply calculated as $\psi_2\ k_{def,perm}$, basically re-introducing the load-duration based k_{def} values of ENV version. Therefore, basically nothing has changed. In fact in order to calculate the final deformation each load contribute is calculated using the *effective* modulus. In order to calculate the stress state at long-term, the effective moduli are again used and calculated on the basis of the *weighted* k_{def} coefficients according to the loads.

The creep coefficient of connection $k_{def,f}$ is now assumed to be twice the timber one, in order to take into account the actual higher creep deformation of joints.

Other difference between ENV and prEN is the way of evaluating the mean value of connection stiffness K_{ser} (ENV formulas refer to characteristic timber density ρ_k while prEN refer to mean value of density ρ_m : actual difference is very small indeed).

In conclusion the actual differences between ENV and prEN calculation procedure are very limited.

6. Simplified procedure

An alternative procedure, which allows to avoid the *weighting* k_{def} factors, is hereby described and proposed.

Long-term verifications

Serviceability limit state

The creep effects are due only to the quasi-permanent part of the load $F_{d,p}$ considered as acting on the structure for the whole technical life. The long-term maximum vertical displacement can be calculated by superposing to the long-term displacement due to the quasi-permanent part of the load, and the instantaneous displacement due to the difference between the rare and the quasi-permanent combinations applied at the end of the technical life t:

$$u_{fin}=u_{fin}^{F_{d,p}}+u_{inst}^{F_{d,r}-F_{d,p}}=u^{F_{d,p}}\left(E_{c,fin},E_{t,fin},K_{ser,fin}\right)+u^{F_{d,r}-F_{d,p}}\left(E_{cm}(t),E_{0,mean},K_{ser}\right) \quad (15)$$

with $E_{c,fin}$, $E_{t,fin}$ and $K_{ser,fin}$ given by Eqs. (3) to (5). The load combination $F_{d,p}$ is given by Eq. (14), and $F_{d,r}-F_{d,p}$ by:

---

[2] "The combinations of actions to be taken into account in the relevant design situations should be appropriate for the serviceability requirements and performance criteria being verified".

$$F_{d,r} - F_{d,p} = (1-\psi_{2,1})\cdot Q_{k,1} + \sum_{i>1}(\psi_{0,i}-\psi_{2,i})\cdot Q_{k,i} \tag{16}$$

Ultimate limit state

Only the quasi-permanent part $F_{d,p}$ of the ultimate limit state combination $F_{d,u}$ has to be considered as acting during the whole technical life of the structure. The effects due to the load $F_{d,p}$ can be evaluated using the effective moduli E_{fin}. The difference between the ultimate and the quasi-permanent load combination is instead applied instantaneously: thus for this part of load the Young's moduli at the instant t have to be employed. In symbols, the following equation can be written:

$$S_{fin} = S_{fin}^{F_{d,p}} + S_{inst}^{F_{d,u}-F_{d,p}} = S^{F_{d,p}}(E_{c,fin}, E_{t,fin}, K_{ser,fin}) + S^{F_{d,u}-F_{d,p}}(E_{cm}(t), E_{0,mean}, K_u) \tag{17}$$

with $F_{d,p}$ given by Eq. (14) and $F_{d,u}-F_{d,p}$ by:

$$F_{d,u}-F_{d,p} = \sum_{j\geq 1}(\gamma_{G,j}-1)\cdot G_{k,j} + (\gamma_{Q,1}-\psi_{2,1})\cdot Q_{k,1} + \sum_{i>1}(\gamma_{Q,i}\psi_{0,i}-\psi_{2,i})\cdot Q_{k,i} \tag{18}$$

7. Numerical examples

Two different timber-concrete composite beams, the cross sections of which are represented in Figure 1, have been used as an example. The beam denoted as "GL", 8 meters span, is typical of new structures and is made by two high glued-laminated timber beams and a concrete slab cast above a corrugated steel sheet. The beam denoted as "S", 4 meters span, is typical of restoration of ancient timber floors, and it is made by a solid timber beam.

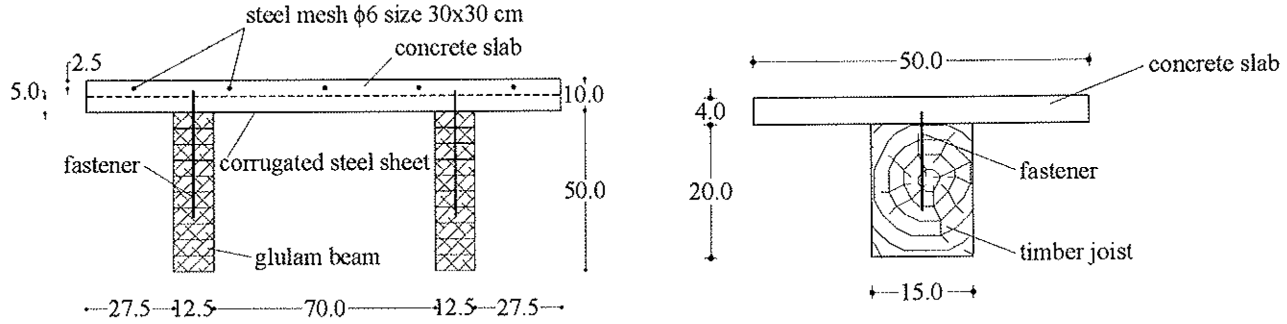

Figure 1: Cross section of the "GL", long span, and "S", short span, composite beams - Measures in cm

Geometrical and mechanical properties

The geometrical properties of the two composite beams are summarised in Table 1. Both the beams are one-span simply supported and uniformly loaded. The spacing of the fasteners varies between a minimum and a maximum value, s_{min} and s_{max} respectively. According to EC5, an effective value of fastener spacing s_{ef} can be used into the elastic formulas:

$$s_{ef} = 0.75 s_{min} + 0.25 s_{max} \tag{19}$$

Table 1: Geometrical properties and loads on the two beams

Symbol	Meaning	Measure	GL Beam	S Beam
b_c	Slab width	cm	150	50
h_c	Slab height	cm	10	4
b_t	Timber beam width	cm	2x12.5	15
h_t	Timber beam height	cm	50	20
l	Length of the beam	cm	800	400
$s_{\min}$	Minimum connector spacing	cm	15	8
$s_{\max}$	Maximum connector spacing	cm	45	24
s_{ef}	Effective connector spacing	cm	11,25	12
d	Diameter of the connector	mm	18	10
G_k	Permanent load	kN/m	3.3	0.70
Q_k	Variable (medium or long term) load	kN/m	16	4.15
Ψ_2	Factor for quasi-permanent value of a variable long term action		0.6	0.6
Ψ_2	Factor for quasi-permanent value of a variable medium term action		0.3	0.3

The same kind of concrete and steel has been used for the two beams: concrete strength class C25/30 according to Eurocode 2 , steel bars for reinforced concrete are used for the fasteners. The timber classes are: glued-laminated timber, strength class GL24h according to prEN 1194 [10], for the "GL" beam; solid timber, strength class C22 according to EN 338 [11], for the "S" beam. The service classes are the 3rd and the 1st for both beams "GL" and "S".

The mechanical properties can be evaluated according to the formulas given by Eurocodes and summarized in [7].

Table 2: Mechanical properties of the **timber** *used for the two beams*

Symbol	Meaning	Measure	GL Beam	S Beam
$E_{0,mean}$	Medium Young's modulus	N/mm^2	11600	10000
ρ_k	Characteristic density	kg/m^3	380	340
ρ_m	Medium density	kg/m^3	450	410

		Service class 3	Service class 1
$k_{def,G_k,t}$	Creep coefficient for permanent load (ENV and prEN)	2	0.6
$k_{def,Q_k,t}$	Creep coefficient for long term load (ENV)	1.5	0.5
$k_{def,Q_k,t}$	Creep coefficient for medium term load (ENV)	0.75	0.25
$k_{def,Q_k,t}$	Creep coefficient for long term load (prEN)	$\Psi_2 k_{def,G_k,t} = 1.2$	$\Psi_2 k_{def,G_k,t} = 0.36$
$k_{def,Q_k,t}$	Creep coefficient for	$\Psi_2 k_{def,G_k,t} = 0.6$	$\Psi_2 k_{def,G_k,t} = 0.18$

	medium load (prEN)		

Table 3: Mechanical properties of the **concrete** *used for the two beams*

Symbol	Meaning	Measure	GL Beam	S Beam
$E_{cm}(t_0)$	Medium Young's modulus at instant t_0	N/mm^2	30000	30000
$E_{cm}(t)$	Medium Young's modulus at instant t	N/mm^2	30000	30000

		Service class 3	Service class 1
$\phi(t,t_0)$	Assumed Creep coefficient for permanent load	2.20	2.25
$\phi(t,t_0)$	Assumed Creep coefficient for long term load	1.85	1.90
$\phi(t,t_0)$	Assumed Creep coefficient for medium term load	1.30	1.35

Table 4: Mechanical properties of the **fasteners** *used for the two beams*

Symbol	Meaning	Measure	GL Beam	S Beam
$K_{ser} = 2 \cdot \frac{\rho_k^{1,5} d}{20}$	Slip modulus (ENV)[3]	N/mm	13330	6270
$K_u = \frac{2}{3} K_{ser}$	Slip modulus (ENV)	N/mm	8890	4180
$K_{ser} = 2 \cdot \frac{\rho_m^{1,5} d}{25}$	Slip modulus (prEN)	N/mm	13740	6640
$K_u = \frac{2}{3} K_{ser}$	Slip modulus (prEN)	N/mm	9160	4430

		Service class 3	Service class 1
$k_{def,G_k,f}$	Creep coefficient for permanent load (ENV)	2	0.6
$k_{def,G_k,f}$	Creep coefficient for permanent load (prEN)[4]	4	1.2
$k_{def,Q_k,f}$	Creep coefficient for long term load (ENV)	1.5	0.5
$k_{def,Q_k,f}$	Creep coefficient for medium term load (ENV)	0.75	0.25
$k_{def,Q_k,f}$	Creep coefficient for long term load (prEN)	$2\Psi_2 k_{def,G_k,t} = 2.4$	$2\Psi_2 k_{def,G_k,t} = 0.72$
$k_{def,Q_k,f}$	Creep coefficient for medium load (prEN)	$2\Psi_2 k_{def,G_k,t} = 1.2$	$2\Psi_2 k_{def,G_k,t} = 0.36$

---

[3] The slip modulus of connection for the serviceability limit state K_{ser} is evaluated doubling the corresponding value obtained for timber-timber connections, which is calculated as a function of the characteristic or medium density of timber in the ENV and prEN versions of EC5, respectively.

[4] The creep coefficients are assumed equal or twice the corresponding values adopted for timber, in the ENV,and prEN, respectively.

8. Computation

Env and prEN

The results are reported in Table 5. They have been obtained from Eqs. (42) to (57) as reported in Appendix, where:

1) for the serviceability limit state, the long-term solutions $u_{fin}^{G_k}$ and $u_{fin}^{Q_k}$ due to the loads G_k and Q_k have been superposed. These solutions have been calculated by adopting the effective moduli:

$$E_c = E_{c,fin} \qquad E_t = E_{t,fin} \qquad K = K_{ser,fin} \qquad (20)\quad (21)\quad (22)$$

evaluated according to Eqs. (3) to (5), assuming the creep coefficients corresponding to the duration class of the loads G_k and Q_k;

2) for the ultimate limit state, the long-term solution has been evaluated by adopting the effective *weighted* moduli given by Eq. (11) under the load combination $F_{d,u}$:

$$E_c = E_{c,fin} \qquad E_t = E_{t,fin} \qquad K = K_{u,fin} \qquad F_{d,u} = \gamma_G G_k + \gamma_Q Q_k \qquad (23)\quad (24)\quad (25)\quad (26)$$

Proposed procedure

The results are reported in Table 5 as well. They have been obtained from from the same Eqs. (42) to (57).

For the serviceability limit state, two elastic solutions have been superposed:

1) the long-term solution $u_{fin}^{F_{d,p}}$ due to the load combination $F_{d,p}$, obtained using the effective moduli:

$$E_c = E_{c,fin} \qquad E_t = E_{t,fin} \qquad K = K_{ser,fin} \qquad (27)\quad (28)\quad (29)$$

evaluated according to Eqs. (3) to (5);

2) the short-term solution $u_{inst}^{F_{d,r}-F_{d,p}}$ due to the load combination $F_{d,r} - F_{d,p}$, obtained using the elastic moduli:

$$E_c = E_{cm}(t) \qquad E_t = E_{0,mean} \qquad K = K_{ser} \qquad (30)\quad (31)\quad (32)$$

The load combinations are given by Eqs. (14) and (16):

$$F_{d,p} = G_k + \psi_2 Q_k \qquad F_{d,r} - F_{d,p} = (1-\psi_2)Q_k \qquad (33)\quad (34)$$

For the ultimate limit state, two elastic solutions have been superposed:

1) the long-term solution $S_{fin}^{F_{d,p}}$ due to the load combination $F_{d,p}$, obtained using the effective moduli:

$$E_c = E_{c,fin} \qquad E_t = E_{t,fin} \qquad K = K_{ser,fin} \qquad (35)\quad (36)\quad (37)$$

evaluated according to Eqs. (3) to (5);

2) the short-term solution $S_{inst}^{F_{d,u}-F_{d,p}}$ due to the load combination $F_{d,u} - F_{d,p}$, obtained using the elastic moduli:

$$E_c = E_{cm}(t) \qquad E_t = E_{0,mean} \qquad K = K_u \qquad (38)\quad (39)\quad (40)$$

The load combination $F_{d,u} - F_{d,p}$ is given by Eq. (18):

$$F_{d,u} - F_{d,p} = (\gamma_G - 1)G_k + (\gamma_Q - \psi_2)Q_k \tag{41}$$

9. Comparisons

From a designer point of view the differences among the three calculation procedures, as exposed in Table 5, are negligible. Therefore the here discussed "different" calculation procedures are in fact equivalent each other.

However, the method proposed by the Authors seems to be more appealing: in fact at the ultimate limit state verifications there is no need to use the effective *weighted* moduli E_{fin} given by Eq. (11), i.e a procedure that lacks of a clear physical sense. In addition only one k_{def} value ($k_{def,perm}$) needs to be used.

10. Conclusions

The Eurocode 5 available calculation procedures for long-term performance of timber-concrete composite beams lead to similar results (ENV 1993 and prEN 2002 versions).

The Authors propose an alternative procedure based on the superposition of two simple solutions:

- the long-term solution under the quasi-permanent load combination;
- the short-term solution under the difference between the rare or the ultimate limit state combination and the quasi-permanent one, for the serviceability and ultimate limit states respectively.

These solutions are obtained using the elastic formulas for composite beams with semi-rigid connections, ad employing the effective and the Young's moduli of the materials at long and short-term combination respectively.

9. References

[1] CEN - Eurocode 5 – Design of timber structures – Part 1.1: General rules and rules for buildings. prEN 1995-1-1. Fal draft, April 2002, Bruxelles, Belgium

[2] CEN - Eurocode 5 – Design of timber structures – Part 1.1: General rules and rules for buildings. ENV 1995-1-1. 1993, Bruxelles, Belgium.

[3] CEN - Eurocode 5 – Design of timber structures – Part 2: Bridges. ENV 1995-2. 1996. Bruxelles, Belgium.

[4] Möhler, K. 1956. Über das Tragverhalten von Biegerträgern und Druckstäben mit zusammengesetzten Querschnitten und nachgiebigen Verbindungsmitteln. Habilitation, Technische Universität Karlsruhe, Germany.

[5] CEN. Eurocode 2 – Design of concrete structures – Part 1.1: General rules and rules for buildings. ENV 1992-1-1. 1991. Bruxelles, Belgium.

[6] Comité Euro-International du Béton. CEB Bull. N°213/214: CEB-FIP Model Code 90. 1993. Lausanne, Switzerland.

[7] Ceccotti, A. STEP lecture E13: Timber-concrete composite structures. Timber Engineering – STEP 2. 1995. First edition, Centrum Hout, The Netherlands. E13/1-E13/12.

[8] CEN. Eurocode 0 – Basis of structural design – prEN 1990-1. Final draft, July 2001, Bruxelles, Belgium.

[9]Racher, P. and Rouger, F. 1994. Serviceability limit states: a proposal for updating Eurocode 5 with respect to Eurocode 1[5]. CIB W18 Meeting 27th, paper 27-20-3, Sidney, Australia.

[10] CEN/TC124 "Structural timber", Work Group 2, prEN 1194 "Timber structures – Glued laminated timber – Strength classes and determination of characteristic values", Februray 1998.

[11] CEN/TC124 "Structural timber", Work Group 2, EN 338 "Structural timber – Strength classes", March 1997.

---

[5] The ENV Eurocode 1 "Basis of design and actions on structures, part 1: Basis of design" has been split in two parts. Basis of design became Eurocode 0 (zero).

Serviceability Limit State

		ENV	**PrEN**	**proposed**
Long span GL beam	Service class	*Mid-span deflection at final time (in mm)*	*Mid-span deflection at final time (in mm)*	*Mid-span deflection at final time (in mm)*
Qk medium term $\Psi_2 = 0.3$	1	***19.36***	***21.16***	***19.01***
	3	***27,86***	***29.70***	***28.63***
Qk long term $\Psi_2 = 0.6$	1	***22.47***	***24.10***	***22.11***
	3	***36.18***	***38.16***	***37.43***
Short span S beam	Service class	*Mid-span deflection at final time (in mm)*	*Mid-span deflection at final time (in mm)*	*Mid-span deflection at final time (in mm)*
Qk medium term $\Psi_2 = 0.3$	1	***11.48***	***11.56***	***11.25***
	3	***16.51***	***17.16***	***16.79***
Qk long term $\Psi_2 = 0.6$	1	***13.37***	***13.32***	***13.07***
	3	***21.73***	***22.47***	***22.13***

Ultimate Limit State

		ENV	**PrEN**	**proposed**
Long span GL beam	Service class	*Maximum timber tension stress at finaltime (in MPa)*	*Maximum timber tension stress at finaltime (in MPa)*	*Maximum timber tension stress at final time (in MPa)*
Qk medium term $\Psi_2 = 0.3$	1	***13,61***	***14.05***	***13.61***
	3	***13,27***	***12.72***	***13.53***
Qk long term $\Psi_2 = 0.6$	1	***13,64***	***14.31***	***13.98***
	3	***13.15***	***14.32***	***13.86***
Short span S beam	Service class	*Maximum timber tension stress at final time(in MPa)*	*Maximum timber tension stress at final time(in MPa)*	*Maximum timber tension stress at final time (in MPa)*
Qk medium term $\Psi_2 = 0.3$	1	***10.21***	***10.50***	***10.22***
	3	***9.99***	***9.91***	***10.20***
Qk long term $\Psi_2 = 0.6$	1	***10.22***	***10.67***	***10.45***
	3	***9.92***	***10.72***	***10.42***

Table 5 numerical results summary according to different methods of calculation

Appendix : The design *elastic* formulas

The design elastic formulas for mechanically jointed composite beams are reported here below:

$$(EI)_{ef} = E_c I_c + E_t I_t + \gamma_c E_c A_c a_c^2 + \gamma_t E_t A_t a_t^2 \qquad \gamma_c = \frac{1}{1+\frac{\pi^2 E_c A_c s_{ef}}{K l^2}} \qquad \gamma_t = 1 \; (42) \qquad (43)$$

(344)

$$A_c = b_c h_c \qquad I_c = \frac{b_c h_c^3}{12} \qquad A_t = b_t h_t \qquad I_t = \frac{b_t h_t^3}{12} \qquad (45) \quad (46) \qquad (47)$$

(48)

$$a_c = \frac{\gamma_t E_t A_t H}{\gamma_c E_c A_c + \gamma_t E_t A_t} \qquad a_t = \frac{\gamma_c E_c A_c H}{\gamma_c E_c A_c + \gamma_t E_t A_t} \qquad H = h_c/2 + a + h_t/2 \qquad (49) \quad (50) \quad (51)$$

$$u = \frac{5 F_d l^4}{384 (EI)_{ef}} \qquad \sigma_c(x) = -\frac{\gamma_c E_c a_c M(x)}{(EI)_{ef}} \qquad \sigma_t(x) = \frac{\gamma_t E_t a_t M(x)}{(EI)_{ef}} \qquad (52) \quad (53) \quad (54)$$

$$\sigma_{m,i}(x) = \frac{1}{2} \cdot \frac{E_i a_i M(x)}{(EI)_{ef}} \text{ with } \quad i = c,t \; \tau_{t,\max}(x) = 1.5 \cdot \frac{V(x)}{A_t} \qquad F(x) = \frac{\gamma_c E_c A_c a_c s(x)}{(EI)_{ef}} \cdot V(x) \quad (55) \qquad (56)$$

(57)

where:
the superscripts c and t refer to concrete and timber, respectively;
E and K are the Young's and slip modulus;
A and I are the area and the inertia moment of the cross section;
$(EI)_{ef}$ is the effective flexural stiffness of the composite beam, evaluated neglecting the reinforcement into the slab;
a is a possible gap between concrete salb and timber element;
u is the mid-span vertical displacement;
F_d is the design load combination, uniformly distributed along the beam;
σ_c and σ_t are the normal stresses due to the normal force into the concrete and timber, respectively;
$\sigma_{m,c}$ and $\sigma_{m,t}$ are the maximum normal stresses due to the bending moment into the concrete and timber, respectively;
$\tau_{t,\max}$ is the maximum shear stress into the timber, evaluated neglecting the presence of the concrete slab;
F is the shear force in the connection system;
s is the spacing between the connectors;
V and M are the shear force and bending moment;
x is the abscissa along the beam axis.

CIB-W18/35-15-7

INTERNATIONAL COUNCIL FOR RESEARCH AND INNOVATION IN BUILDING AND CONSTRUCTION

WORKING COMMISSION W18 - TIMBER STRUCTURES

DESIGN OF TIMBER STRUCTURES IN SEISMIC ZONES ACCORDING TO EUROCODE 8 – 2002 VERSION

A Ceccotti
NRC – TTI, Florence

ITALY

T Toratti
VTT, Espoo

FINLAND

B Dujič

University of Ljubljana
Faculty of Civil and Geodetic Engineering, Ljubljana

SLOVENIA

Presented by: B Dujič

There were no comments or questions for the authors.

Design of Timber Structures in Seismic Zones According to Eurocode 8 – 2002 Version

A. Ceccotti
NRC – TTI, Florence, Italy
T.Toratti
VTT, Espoo, Finland
B. Dujič
University of Ljubljana, Slovenia

1. Introduction

Eurocode 8 is the European code for "Design of structures for earthquake resistance". Part 1 includes "General rules, seismic actions and rules for buildings". Chapter 5 of Part 1 is devoted to specific rules for concrete buildings, chapter 6 is for steel buildings, chapter 7 for steel-concrete composite buildings, chapter 8 for timber buildings, and finally chapter 9 is for masonry buildings. The final draft (prEN 1998-1) [1] is dated May 2002 and it is now ready to undergo the procedure to be accepted as an EN standard. This version of the code supersedes the previous 1994 version (ENV 1998-1) [2,3]. The intention of this paper is to highlight the major differences between the two versions and their consequences on timber buildings design. Finally a four storey building design example is provided to non-European Colleagues for possible inter-codes comparisons.

2. General

Eurocode 8 approach to the design of structures in seismic regions does not differ from other Limit States Design format codes. The so-called "service" earthquake, "moderate" but not "likely", without important deformations and without any damage to the structural elements, has a Peak Ground Acceleration (PGA) with an average return period of 50 years. The "ultimate" earthquake, "severe" but "accidental", even with severe damages to structural elements but without the total ruin of the building, has a return period of 475 years.
Because timber elements exhibit a generally elastic behaviour under alternate loading, with brittle failure primarily due to natural defects like knots, plasticity and capacity to dissipate energy are taken into account in the connections between the various structural elements provided that they are "semi-rigid" (as most mechanical ones are [4]).

Therefore in Eurocode 8 structures are classified into categories taking into account their plastic behaviour and their ability to dissipate energy. The bigger these features are, the higher is the possibility to resist a stronger earthquake. In principle the earthquake design base shear E_d is definitively written in the following way:

$$\frac{M \cdot R(T_o, v) \cdot A_u}{q} = E_d \tag{1}$$

where M is the mass of the structure; $R(T_o, v)$ is the amplification factor of the PGA according to the site seismology nature, depending on the fundamental period of vibration T_o of the structure; v is the viscous damping in the elastic field. A_u is the design PGA depending on the seismicity of the site. As a rule A_u values are reported in the National codes of single European Countries and they definitely represent the level of seismicity of the site (e.g. in Italy there are three zones with A_u = 0.35g, A_u = 0.25g and A_u = 0.15g from highest to lowest seismic intensity, respectively).

Finally q is the design Action Reduction Factor (ARF), i.e. *"simply the factor to be used in calculating design inertia forces so that a structure designed linearly elastic using the static code strength values can survive the design quake intensity, even if heavily damaged, but without its ruin"* [5][1].

3. PrEN 1998-1 final draft

3.1 Design base shear

In the PrEN 1998-1 final draft the design base shear, now called F_b, is evaluated as:

$$F_b = S_{d\,(T_o)}\, W \tag{3}$$

Where:
$S_{d\,(T_o)}$ is the ordinate of the design spectrum
W is the total weight of the building

S_d value is evaluated from the a set of equations (see Appendix), depending on the fundamental period of the building T_0. For timber houses usual range of T_0 values, the equation to be used is normally this one:

$$S_d = \alpha\, S \frac{2.5}{q} \tag{4}$$

Where:
α is the design peak ground acceleration value/acceleration of gravity g,
S is the soil parameter factor (>1) depending on T_0,
q is the behaviour factor (ARF)

Substantially equation (4) is the very same as the equation (1) being the *2.5 S* factor corresponding to the amplification factor $R(T_o, \nu)$.

3.2 Amplification factor

In the prEN version a larger number of soil conditions are considered (A to E) instead of (A to C)

---

[1] According to this definition, one way for determining the suitability of a chosen ARF value is to design the structure using the ARF according to the code. Then using a suitable non-linear analysis programme capable of following the displacement history of the building under a quake in the time domain, the PGA_u that the building will survive without exceeding a failure limit can be determined (for example based on a maximum inter-storey drift, or a rupture in joints or in timber elements). Finally, this PGA_u can be compared against PGA_{code} prescribed by the code: if

$$PGA_u > PGA_{code} \tag{2}$$

the previously chosen design ARF value is good enough [6].
Please note that in this case a definition of yielding limit is not needed, but only the definition of ultimate limit is necessary. This allows us to get rid of the definition of yielding limit, but, on the other hand the value of ARF becomes strictly code dependent this time. Actually consider the following:
if the design code values are artificially low, the structure will be over-designed and consequently it will resist a greater PGA resulting in a greater margin between PGA_u and PGA_{code};
if the calculated fundamental period of the structure, T_o is too conservative, once again this will result in over-design and greater values of PGA_u will be found.
There is nothing wrong with that but this leads to the conclusion that with the same structural type, ARF can be different in different countries.

as in ENV. In addition, two different types of quakes: Type 1 (Magnitudo $M_s>5.5$), and Type 2 ($M_s<5.5$) are considered for each soil condition [7].
In Figures 1 and 2 amplification factors according to different quake nature and soil conditions are shown in comparison with class B soil, ENV spectrum.

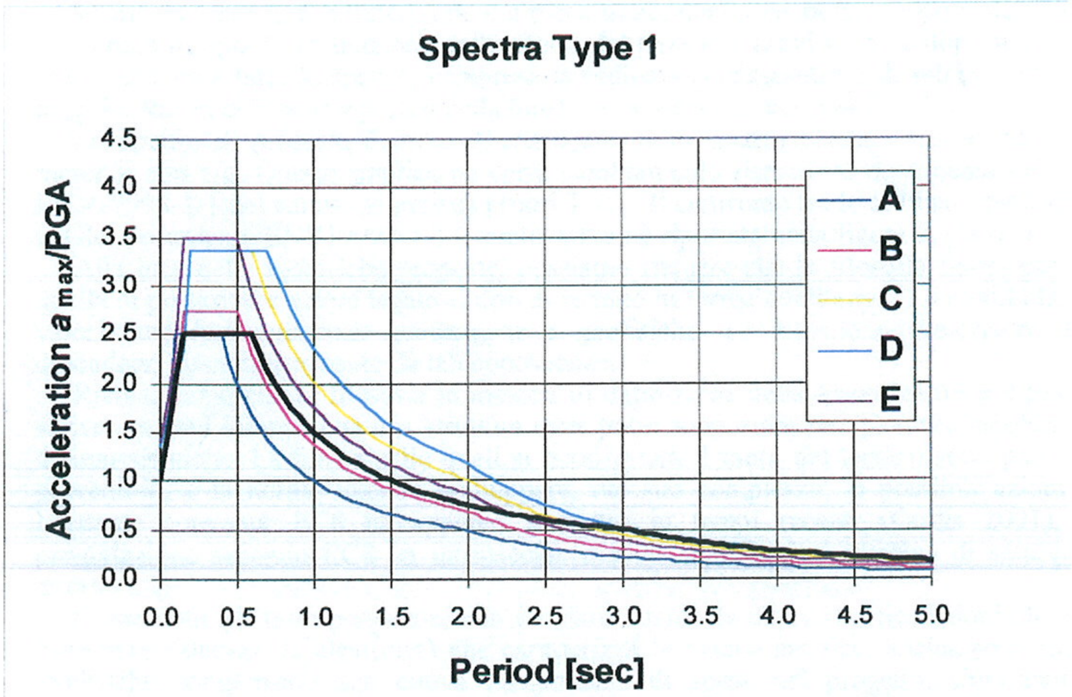

Figure 1: Amplification factors $R(T_0,5\%)$ according to near fault quake nature ($M_s>5.5$) and soil conditions are shown in comparison with class B soil, ENV spectrum (black line).

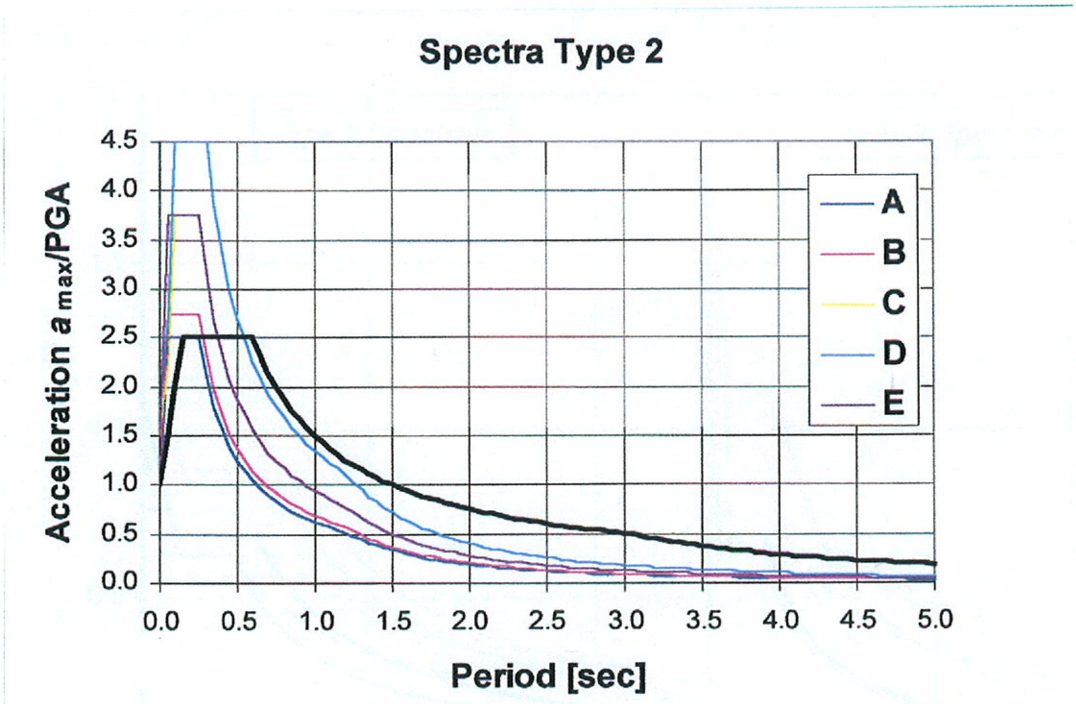

Figure 2: Amplification factors $R(T_0,5\%)$ according to quake nature ($M_s< 5.5$) and soil conditions are shown in comparison with class B soil, ENV spectrum (black line).

It can be said that an amplification factor maximum value of 2.5 was anticipated in ENV version, while in prEN version the amplification factor can reach up to 4.5 (1.8 times higher, in the worst case).

3.3 Behaviour factor

In order to take into account the so-called over-strength, q factors have been changed according to Table 1a. For reference, ENV values are reported in table 1b.

Type DCL Structures having low capacity to dissipate energy	q = 1.5	Cantilevers; beams; arches with two or three pinned joints; trusses joined with connectors.
Type DCM, Structures having medium capacity to dissipate energy	q = 2,0	Glued wall panels with glued diaphragms, connected with nails and bolts; trusses with doweled and bolted joints; mixed structures consisting of timber framing (resisting the horizontal forces) and non-load-bearing infill.
"	q = 2.5	Hyperstatic portal frames with doweled and bolted joints
Type DCH, Structures having high capacity to dissipate energy	q = 3.0	Nailed wall panels with glued diaphragms, connected with nails and bolts, trusses with nailed joints
"	q = 4.0	Hyperstatic portal frames with doweled and bolted joints
"	q = 5.0	Nailed wall panels with nailed diaphragms, connected with nails and bolts.

Table 1a: q factors according to prEN version

Type A Non-dissipative structures	q = 1	Without or with only a few joints with mechanical fasteners beyond the dissipative zones (e.g. arches with hinged joints, cantilever structures with rigid connections at the base, buildings with wall-diaphragms resisting the horizontal forces without mechanical fasteners for both interconnection and between sheathing and timber framing
Type B Low-dissipative structures	q=1.5	With few but effective dissipative zones, structures with semi-rigidly fixed-based columns.
Type C Medium-dissipative structures	q = 2	Frames or beam-column structures with semi-rigid joints between all members. Connections with foundations may be semi-rigid as well as hinged; braced frame structures with mechanical fasteners in the joints of the frame and/or the connections of the bracing system; buildings with vertical diaphragms resisting the horizontal forces, where sheathing is glued to the framing. Diaphragms are interconnected by mechanical; mixed structures consisting of timber framing (resisting the horizontal forces) and non-load-bearing infillment.
Type D Well-dissipative structures	q = 3	Buildings with vertical diaphragms resisting the horizontal forces, where sheathing is fixed to the framing by mechanical fasteners a well as the interconnection of the wall-elements (horizontal diaphragms may be glued or nailed).

Table 1b: q factors according to ENV version

Comparing Table 1a and Table 1b it is possible to say that an average increase of 1.5 times has been set up for q factors.

3.4 γ_M factors

In the ENV version the mechanical connections loss of strength due to differences from static to cyclic behaviour, was taken into account by using the partial safety factor for fundamental load combination, i.e. γ_m=1.3, instead of the classical γ_m=1 for accidental load combination. On the contrary, for non-dissipative structures γ_m = 1 was retained.

In the EN version this point has been reversed: in case of non-dissipative structures the fear of brittle failure has been privileged and the safety coefficient increased, i.e. γ_m=1.3, while in the case of dissipative structures, the cyclic impairment of strength [4] has been considered limited and the safety coefficient for accidental load combination is used, i.e. γ_m=1.

Structural type ENV	γ_M ENV	**Structural type** prEN	γ_M prEN
A	1.0	DCL	1.3
C	1.3	DCM	1.0
D	1.3	DCH	1.0

Table 2: γ_M factors, ENV version versus prEN version.

4. Comparisons between ENV version and prEN version

The $R(T_0,\nu)\frac{\gamma_M}{q}$ factor well detects the differences in the design base shear evaluation: in table 3 results for the **worst** possible soil and quake type combination are shown.

A	$2.5\frac{1.0}{1}=$	**2.50**	DCL	$4.5\frac{1.3}{1.5}=$	**3.90**	+*56*%
B	$2.5\frac{1.3}{2}=$	**1.63**	DCM	$4.5\frac{1.0}{2.5}=$	**1.80**	+*10*%
C	$2.5\frac{1.3}{3}=$	**1.08**	DCH	$4.5\frac{1.0}{5}=$	**0.90**	-*17*%
ENV	ENV	ENV	prEN	prEN	prEN	difference %

Table 3: the $R(T_0,\nu)\frac{\gamma_M}{q}$ factor according to structural types (ENV versus EN).

In conclusion: for "dissipative" design a moderate variation of the design base shear, plus or minus, can be anticipated. On the contrary a large increase must be expected for "non-dissipative" design.[2]

5. Example: a four-storey timber house, calculation of the seismic load according to prEN version.

Input values:
Ground acceleration 0.35 g,
Subsoil class B

---

[2] Nevertheless this should not alarm when in case of large roof structures where the snow will remain the dimensioning load condition [8].

Floor dead load 1 KN/m^2 *(the weight of the walls is assumed to be included in this figure)*
Roof dead load 0.75 KN/m^2
Live load q_h = 2.0 KN/m^2
Importance factor γ_{III} = 1.0 (residence)

Building braced with shear walls of plywood sheathing and mechanical fasteners, $q = 5.0$.
Building area: 288 m^2

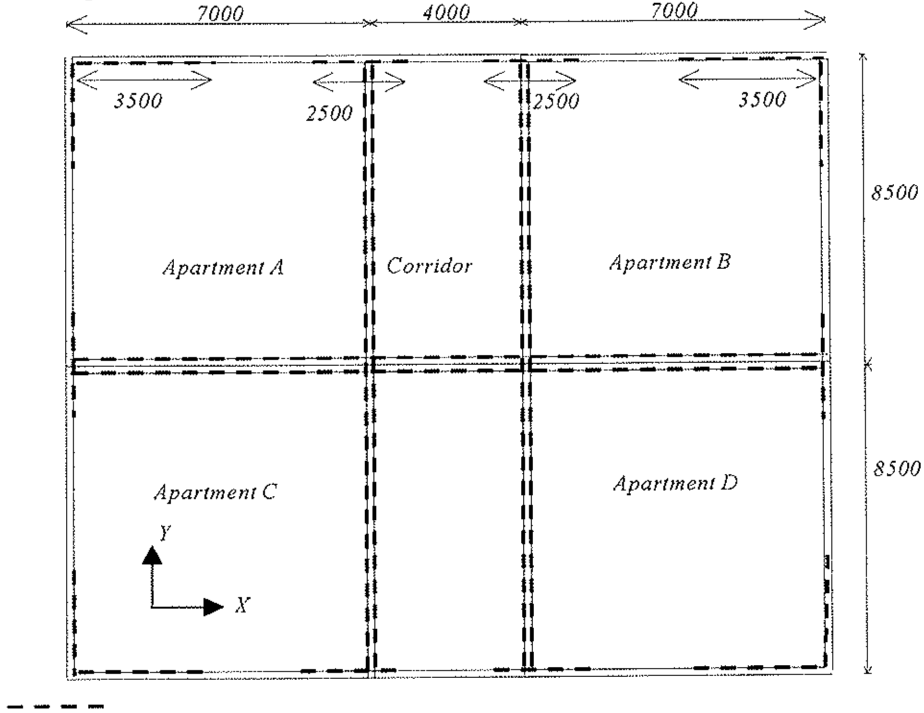

Figure 3: A schematic diagram of the shear walls in the first storey of the building (measures in mm).

The seismic load is determined considering the vertical loads present in the different storeys of the building. This load is calculated using eq. A5, see Appendix:

$$\sum G_{kj} + \sum \psi_{EI} Q_{ki} \tag{A5}$$

G_{kj} is the characteristic dead load and $\psi_{EI}Q_{ki}$ is the probable live load during a seismic event.

Combination coefficient: $\psi_{EI} = \varphi \psi_{2i}$

ψ_{2i} is 0.3 (the quasi-permanent value of the live load (EC1 and EC5) ,
φ is 0.5 except for the top storey for which it is 1.0 (EC8)

Storey	G_{kj}	Q_{ki}	ψ_{2i}	φ	ψ_{EI}	$G_{kj} + \psi_{EI}Q_{ki}$
Roof	0.75					0.75
Storey 4	1.0	2.0	0.3	1	0.30	1.60
Storeys 2 and 3	1.0	2.0	0.3	0.5	0.15	1.30
Storey 1	Loads transferred directly to the foundations					

Table 4. Combining the loads in the different storeys.

Following the table above, the total vertical load is:

$$\sum G_{kj} + \sum \psi_{EI} Q_{ki} = 0.75 + 1.60 + 1.30 + 1.30 = 4.95 \text{ KN/m}^2$$

Building height H: 12 m

Building fundamental period T_0

$H := 12$ $S := 1.2$ $T_b := 0.15 \cdot s$ $T_c := 0.5 \cdot s$ $T_d := 2 \cdot s$

$\alpha := 0.35$ $q := 5.0$

$T_0 := 0.05 \cdot H^{\frac{3}{4}} \cdot s$

$T_0 = 0.322 s$

$$S_d(T) := \begin{cases} \alpha \cdot S \cdot \left[1 + \frac{T}{T_b} \cdot \left(\frac{2.5}{q} - 1\right)\right] & \text{if } T < T_b \\ \alpha \cdot S \cdot \frac{2.5}{q} & \text{if } T_b < T < T_c \\ \alpha \cdot S \cdot \frac{2.5}{q} \cdot \left(\frac{T_c}{T}\right) & \text{if } T_c < T < T_d \\ \alpha \cdot S \cdot \frac{2.5}{q} \cdot \frac{T_c \cdot T_d}{T^2} & \text{if } T_d < T \end{cases}$$

$S_d(T_0) = 0.21$

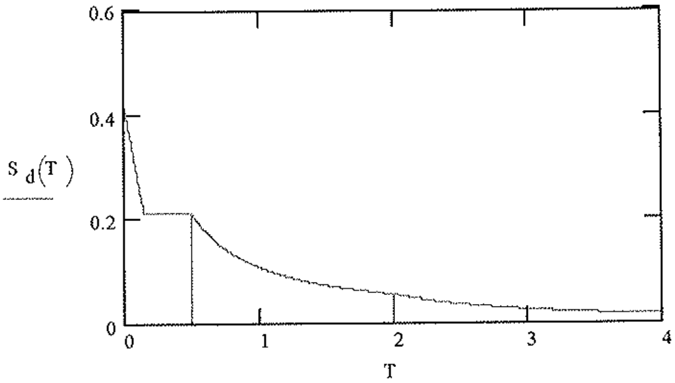

Vertical load , W = Σ (G+$\psi_{Ei}Q_{ki}$) x building area

$W := (0.75 + 1.6 + 1.3 + 1.3) \cdot 288$

$W = 1.426 \cdot 10^3$ KN

Base shear load

$Fb := W \cdot S_d(T_0)$ Importance factor = 1.0

$Fb = 299.4$ KN

Comparison to the wind load below

Q_{wind} = 20 x 12 x 0.7 KN/m ^{2} = 168 KN

The base shear force is distributed in elevation according to eq. A3 :

$$F_i = F_b \frac{z_i W_i}{\sum_j z_i W_i} \qquad \text{(A3)}$$

F_b is the base shear force

The shear force acting on the shear walls of each storey

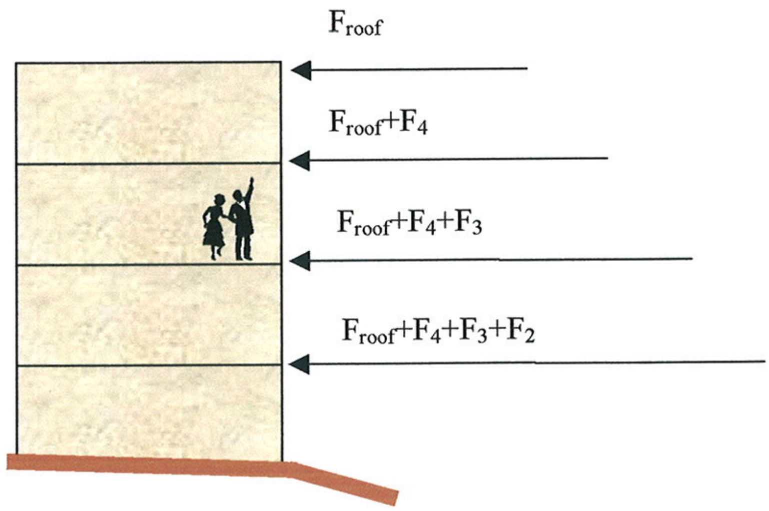

The force distribution according to eq. A3

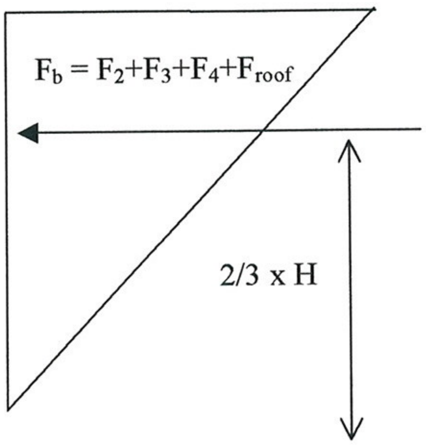

$F_b = F_{roof}+F_4+F_3+F_2$

Storey, *i*	Height of storey from ground z_i [m]	The load on each floor *(Table 4)* W_i [KN]	F_i , shear force in the storey level $F_i = F_b \frac{z_i W_i}{\sum_j z_i W_i}$ [KN]	Cumulative shear force acting on the shear walls at the different storey levels $F_v = \sum_i^4 F_i$ [KN]
Roof	12	$0.75 \times 288 = 216$	77	77
4	9	$1.6 \times 288 = 461$	123	200
3	6	$1.3 \times 288 = 375$	67	267
2	3	$1.3 \times 288 = 375$	33	300

Table 5. The design shear forces in the different storeys

$\Sigma z_i W_i = 10116$ KNm ;
$F_b \cong 300$ KN

The shear walls will be composed of 9-mm-thick plywood panels connected with threaded nails 28×60 k70. In this case the shear wall capacity per length (from Table 6) is $F_{v,d} = 9.59$ KN/m.

This means that the lengths of shear walls needed in the different storeys are:
first storey at least 300/8.99 = 34 m
second storey at least 267/8.99 = 30 m
third storey at least 200/8.99 = 23 m
fourth storey at least 77/8.99 = 9 m

The sheathing panel is nailed along all edges to the timber frame at spacing 70 mm and to the middle of the panel at spacing 300 mm.

The total length of shear walls in X-direction

- internal walls	18 m × 2 – 3 × 1.2 m (doors) =	32.4 m
- external walls	(3.5 m + 2.5 m + 2.5 m + 3.5 m) × 2 =	24 m
	total 56.4 m	

The total length of shear walls in Y-direction

- internal walls	17 m × 4 – 4 × 1.2 (doors) =	63.2 m
- external walls	(3.5 m + 2.5 m + 2.5 m + 3.5 m) x 2 =	24 m
	total 87.2 m	

As seen from above, there are more than enough possibilities to place shear walls in the house and more openings in the shear walls may be designed.

It is advantageous to use the walls between apartments and corridors as shear walls with panelling on both sides of the wall. In this example, the shear walls are situated symmetrically to avoid a torsion effect (for simplicity). In practice, gypsum boards could also be used as an additional reinforcement for the shear walls. EC5 allows the use of two different panels in shear walls, but only 50% of the capacity of the weaker gypsum panel could be included.

The complete design can be found in [9] along with some detailing.

Panel	**Nail (helically threaded)**		**Screw**	
Spruce plywood 9 [mm]	**25x45**	**28x60**	**d = 3.5**	**d = 4.5**
Fastener spacing [mm]				
150	3,59	4,20	5,82	7,72
100	5,38	6,29	8,73	11,57
70	7,69	8,99	12,47	16,54
50	10,77	12,59	17,45	23,15
Spruce plywood 12 [mm]	**25x45**	**28x60**	**d = 3.5**	**d = 4.5**
Fastener spacing [mm]				
150	4,03	4,62	6,19	8,01
100	6,04	6,94	9,29	12,02
70	8,64	9,91	13,27	17,17
50	12,09	13,87	18,57	24,04

Table 6: Shear design capacity with different panels and fasteners [KN/m] in seismic design, note the following: 1) $k_{mod} = 1.1$, $\gamma_M = 1.0$ *, 2) values are for only one panel on one side, 3) the fastener spacing is constant all around the panel, in the inner part the spacing may be up to double (and < 300 mm).*

4. Conclusions

Eurocode 8 is a seismic design code that considers the same design philosophy for all building materials. In particular the designer of timber structures is allowed to perform a global elastic analysis . Eurocode 8 presents few relatively simple and conservative design rules, wich are easy to apply, for the most important structural forms, classified according to their ductility and energy dissipation level. Last version of the code (prEN, 2002) leaves basically untouched the design of dissipative structures while increases the demand for non-dissipative designed structures.

5. References

[1] Eurocode 8. 2002. Design of structures for earthquake resistance. PrEN 1998-1 May 2002 final draft. CEN, Brussels, Belgium

[2] Eurocode 8. 1994. Design Provisions for Earthquake resistance of structures. ENV 1998-1-1, seismic actions and general requirements of structures; 1998-1-2, general rules for buildings; 1998-1-3, specific rules for various materials and elements. CEN, Brussels, Belgium.

[3]K. Becker, A. Ceccotti, H.Charlier, E. Katzaragakis, H.J. Larsen and H. Zeitter: Eurocode 8 – part. 1.3 – Chapter 5, Specific Rules for Timber Buildings in Seismic Regions. Paper 26-15-2, CIB W18 Meeting, Athens, USA, August 1993.

[4] EN 12512. 2001. Timber Structures - Test methods - Cyclic testing of joints made with mechanical fasteners. CEN, Brussels, Belgium.

[5] A.Ceccotti: "Analysis and design of woodframe construction according to Eurocode 8", Proceedings of Invitational Workshop on Seismic Testing, Analysis and Design of Woodframe construction, 1999, University of San Diego, California, USA.

[6] A: Ceccotti and E. Karacabeyli: Dynamic Analysis of Nailed Wood-Frame Shear Walls. Proceedings of 12 WCEE, Auckland, New Zealand, January 2000.

[7] Z.A. Lubkowski and X. Duan: EN 1998 Eurocode 8 : Design of Structures for Earthquake Resistance. Civil Engineering , vol. 144, Issue 2, November 2001, London, UK

[8] A.Ceccotti, M.Lauriola and A.Vignoli: "About the seismic resistance of the Hamar hall", Proceedings of '96 International Wood Engineering Conference, Ottobre 1996, New Orleans, USA.

[9] T. Toratti: Seismic Design of Timber Structures according to Eurocode 8 : Design of structures for earthquake resistance, Final Draft No 5, May 2002

Appendix: A summary of the evaluation of the seismic load according to Eurocode 8

The seismic design of a building starts with an evaluation of the regularity of the building in both layout and elevation. Generally regularity increases the seismic resistance of the building. Usually timber residential buildings are regular in plan and in height.

The initial values are given, the subsoil class according to the ground conditions and the peak ground acceleration value, a_g, according to the site seismicity.

It should be noted that for a different country, the authorities may enforce values or parameters different from the ones given in EC8, which are so-called boxed values. The values given in this Appendix are the ones recommended by EC8. Such information is given in the national application documents.

Base shear force

The base shear force acts in both principal directions of the building.

$$F_b = S_d(T_0)\, W\, \lambda \qquad \text{(A1)}$$

Where T_0 is the fundamental period of the building

S_d is the ordinate of the design spectrum

W is the total weight of the building

λ is a correction factor, having a value of 0,85 if $T_0 < T_C$ or 1,0 otherwise.

Fundamental period

To estimate the fundamental period, T_0, of the building, EC8 has a simple procedure:

$$T_0 = 0.05\, H^{0.75} \qquad \text{(A2)}$$

Where the building height is in metres and the time in seconds.

Distribution of the base shear force in elevation

If the floor loads are equal in the different storeys, the base shear force is distributed in a triangular manner so that higher forces are higher up. This is given by the equation:

$$F_i = F_b \frac{z_i W_i}{\sum_j z_i W_i} \qquad (A3)$$

Where F_i is the lateral load in storey i

F_b is the base shear force

z_i is the distance of the floor from the ground

W_i is the vertical load on the floor

Design spectrum

$$S_d = \alpha\ S\left[1+\frac{T_0}{T_b}\left(\frac{2.5}{q}-1\right)\right] \qquad if T < T_b \qquad (A4.a)$$

$$S_d = \alpha\ S\frac{2.5}{q} \qquad if T_b < T_0 < T_c \qquad (A4.b)$$

$$S_d = \alpha\ S\frac{2.5}{q}\left(\frac{T_c}{T_0}\right) \qquad if T_c < T_0 < T_d \qquad (A4.c)$$

$$S_d = \alpha\ S\frac{2.5}{q}\left(\frac{T_c T_d}{T_0^{\,2}}\right) \qquad if T_d < T_0 \qquad (A4.d)$$

According to the subsoil class, the parameter values are as in the following table.

Subsoil class	S	T_b [s]	T_c [s]	T_d [s]	S	T_b [s]	T_c [s]	T_d [s]
	Type 1 recommended for large earthquakes				Type 2			
A	1.0	0.15	0.40	2.00	1.0	0.05	0.25	1.2
B	1.2	0.15	0.50	2.00	1.35	0.05	0.25	1.2
C	1.15	0.20	0.60	2.00	1.5	0.10	0.25	1.2
D	1.35	0.20	0.80	2.00	1.8	0.10	0.30	1.2
E	1.4	0.15	0.50	2.00	1.6	0.05	0.25	1.2

Table A.1 Parameters for the spectrum equations for the different subsoil classes (EC8). The national authorities will decide which type response spectrum will be used.

EC8 gives the behaviour factor q values for different structural types as shown in table 1a.
If the building is non-regular in elevation the above q-values should be reduced by 20 %, but need not be lower than 1.5.
To ensure the above classification of structures, the dissipative zones should be able to deform plastically for at least three fully reversed cycles at a static ductility ratio 4 for type DCM structures and 6 for type DCH structures, without more than 20 % reduction of their resistance.
These provisions will be met by all structures if :
a) In doweled, bolted and nailed timber-to-timber and steel-to-timber joints, the minimum thickness of the connected member is 10 d and the fastener diameter d does not exceed 12 mm.
b) In shear walls and diaphragms, the sheathing material is wood-based with a minimum thickness of 4 d, where the nail diameter does not exceed 3.1 mm.

The mass in seismic design

$$W = \sum G_{kj} + \sum \psi_{EI} Q_{ki} \qquad (A5)$$

G_{kj} is the characteristic dead load and

$\psi_{EI}Q_{ki}$ is the probable live load during an earthquake.

$$\psi_{EI} = \varphi \psi_{2i} \qquad (A6)$$

ψ_{2i} is the long-term value 0.3 for live loads,
or 0.2 for snow loads (EC1 and EC5),

φ is 0.5 for all storeys except the top storey for which it is 1.0
(no correlation between storey loads). (EC8)
φ is 1.0 for storage loads (EC8)

Combining loads in seismic design

The design loads needed in seismic design consist of dead loads and seismic loads. Wind loads do not need to be considered.

$$E_d = \sum G_{kj} + \gamma F_b + \sum \psi_{2i} Q_{ki} \qquad \text{(A7)}$$

Where, γ is the importance factor (γ_I = 1.4 hospitals, fire stations, power stations; γ_{II} = 1.2 schools, cultural buildings; γ_{III} = 1.0 residential and commercial buildings; γ_{IV} = 0.8 agricultural buildings),
G_{kj} and Q_{ki} are the characteristic values of the dead and live load,
ψ_{2i} is the combination coefficient of the quasi-permanent value of the live load.

Seismic design

Ultimate limit state

$$E_d = f\left\{\sum G_{kj}, \gamma F_b, \sum \psi_{2i} Q_{ki}\right\} \le R_d = R\{\frac{f_k}{\gamma_M}\} \qquad \text{(A8)}$$

The load duration class is 'instantaneous' and such k_{mod} values are used. The material safety factor is γ_M = 1.0, when the structure is energy dissipative (type DCM or DCH) and γ_M = 1.3, when the structure is non-dissipative (type DCL). The importance factor, γ, in the above equation is as given for eq. A7.

Ductility

The structures and the building as a whole should be adequately ductile. The ductility should be as considered in the design, where it is taken into account as a load reducing factor, the behaviour factor q was explained previously.

Equilibrium

The building should be stable during a seismic event. The seismic load combinations should be considered when designing for the anchorage of the building in the following two cases:

- anchorage for overturning: upward tension at ends of shear walls,
- anchorage for sliding, base shear at the bottom of shear walls

Serviceability limit state

In order to avoid excessive damage, EC8 gives rules for the inter-storey drift during a seismic event. The design earthquake may be one, which is more likely (lower return period), and the peak ground acceleration is lower than for the ultimate limit state. The inter-storey drift is limited to the following values:

$d_r/\nu \le 0.005\,h$, buildings having non-structural elements of brittle or materials attached to the structure
$\le 0.0075\,h$, buildings having non-structural elements fixed in a way as not to interfere with structural deformations

Where d_r is the inter-storey drift
h is the storey height
ν reduction factor to take into account the lower return period of the seismic event associated with the serviceability limit state (recommended values are 0.4 for importance classes I and II and 0.5 for importance classes III and IV).

CIB-W18/35-15-08

**INTERNATIONAL COUNCIL FOR RESEARCH AND INNOVATION
IN BUILDING AND CONSTRUCTION**

WORKING COMMISSION W18 - TIMBER STRUCTURES

DESIGN METHODS TO PREVENT PREMATURE FAILURE OF JOINTS AT SHEAR WALL CORNERS

N Kawai
National Institute for Land and Infrastructure Management

H Okiura
Mitsui Home Co., Ltd. Technology Research and Development Institute

JAPAN

Presented by: N Kawai

N Kawai confirmed H J Blaß's observation that although the calculated results are in general larger than test data, this was not so for certain ultimate conditions. B S Choo asked if the assumption that the beams are rigid in the vertical plane is valid and if that could be a reason for large differences observed between calculated and test results. N Kawai agreed that this is possible, especially for the simplified analytical methods but does not explain the differences for the most precise analytical approach. G Gonzalez asked how the yield values were estimated. N Kawai replied that a modified European approach described earlier by B Dujič was used. M Yasumura asked for if the beams used in the tests were of normal proportions or if they could be considered to be rigid. N Kawai confirmed that normal sized glulam beams were used. This was followed by a general discussion relating to the holding down straps and the corner panel size and construction.

Design Methods to Prevent Premature Failure of Joints at Shear Wall Corners

Naohito KAWAI
National Institute for Land and Infrastructure Management, Japan

Hiroshi OKIURA
Mitsui Home Co., Ltd. Technology Research and Development Institute, Japan

1 Introduction

In a simple method to confirm the structural performance of timber buildings with shear walls against earthquake and wind forces, shear strength of each story in one direction is assumed to be equal to the summation of those of shear walls in the same direction. And each shear wall is regarded to have the same shear strength as is obtained by experiments with preventing uplift of the shear walls. However, this assumption is available at least when the premature failure of the joints at the corners of each shear wall is prevented.

Some calculation method to predict the tensile force and some design methods to prevent premature failure at these joints have been proposed, and one method was provided in a Notification under the Building Standard Law of Japan in 2000.

First in this paper, these calculation methods are introduced. Next, the results of lateral loading test on two-storey structures with wood framed shear walls, are summarized. Finally, the calculation results by these methods are compared with the test results and numerical analysis results, and the applicability of these design methods is discussed.

2 Design methods

There are some theories and design methods proposed in design manuals for post and beam construction with shear walls or braces, and for wood frame construction in Japan.

2.1 Empirical design method

An empirical design method for joints at the bottom of post at shear wall end, have been used in structural design of wooden houses with Japanese conventional (post and beam) construction. Equation 1 shows the calculation method to obtain the required tensile strength considering transmitted tensile force from the shear walls on the upper floors. This calculation method was described in a structural design manual for allowable stress design of post and beam construction (HOWTEC 1988).

$$F_{a,i,j} = \sum_{i=k}^{n} \frac{L_{r,i}}{L_{e,i}} \frac{Q_{a,i,j}}{l_{i,j}} \beta_{i,j} h_i - G_{i,j} \qquad (1)$$

where, $F_{a,i,j}$ is the tensile force at the bottom joint of shear wall number j on floor number i against the external force for allowable stress design, $L_{r,i}$ is required total effective wall length on floor number i, $L_{e,i}$ is existing effective wall length on floor number i, h_i is the height of the shear wall, $l_{i,j}$ is the length of the shear wall, $\beta_{i,j}$ is a factor considering the effect of restraint by surrounding members, $Q_{a,i,j}$ is the allowable shear strength of the shear wall and $G_{i,j}$ is the vertical load due to fixed load and superimposed load transmitted to the joint.

Effective wall length means the value obtained by multiplying actual wall length and multiplier, which is determined according to the allowable shear strength of the shear wall. Therefore, the ratio $L_{r,i}/L_{e,i}$ means the ratio of external force to existing strength and is used to obtain the shear force generated in each shear wall in linear behaviour with the assumption that the shear stiffness is proportional to the shear strength of the shear wall. The value of $\beta_{i,j}$ is 0.8 for shear wall that reaches the end of building, and 0.5 for others, which was determined empirically by some experimental results.

2.2 Modification considering ultimate state

Equation (1) is applicable only in allowable stress design or for the structures with linear behaviour. In the ultimate state, shear force of each shear wall reaches the ultimate shear strength even if the total length of existing shear walls are far larger than required length. Therefore, it is necessary to modify the equation for the structural design considering ultimate state. Equation (2) gives the required tensile strength in ultimate state not only for posts at shear wall end but for posts between shear walls.

$$F_{u,i,j} = \sum_{i=k}^{n} \left| \frac{Q_{u,i,j}}{l_{i,j}} - \frac{Q_{u,i,j-1}}{l_{i,j-1}} \right| \beta_{i,j} h_i - G_{i,j} \qquad (2)$$

where, $F_{u,i,j}$ is the tensile force at the bottom joint of shear wall number j on floor number i against the external force in the ultimate state, $Q_{u,i,j}$ is the ultimate shear strength of the shear wall and others are same as equation (1).

If the ratio between the ultimate strength and the allowable strength of shear wall is almost equal to that of joint, then equation (2) can be modified to the expression of allowable strength. This equation is used in revised structural design manual for post and beam construction (HOWTEC 2001), and was also used as the bases of a provision of Notification No. 1460 in 2000 under the Building Standard Law of Japan.

2.3 Rigid frame model

In a structural calculation manual for wood frame construction (Japan 2×4 builders association 2002), rigid frame model has been used to calculate the tensile force of joints at the bottom of shear wall end. In the rigid frame model used in this hand calculation method, the height of the inflection point of each post may be assumed to be a half of the post height and the distributed moment at the post-beam joints to the beams in both direction are assumed to be equal. Tensile force at the joint is calculated by summation of axial force (which is usually positive value) due to horizontal force of the post of the rigid frame model, axial force (which is usually negative value) due to fixed load and superimposed load, and axial force that can be obtained by dividing the moment at post bottom by the original wall length.

This calculation method was originally developed for allowable stress design, but is applicable for the ultimate state with using ultimate shear strength instead of allowable shear strength of shear walls.

2.4 Precise model with rigid beam assumption

In the revised structural manual for houses with post and beam construction (HOWTEC 2001), equations (3) and (4) are proposed as a precise method to calculate tensile or compression force of the joints at the top and the bottom of the posts used in shear walls (see Figure 1), based on the study by Inayama et al. (2001).

$$F_{a,1,i} = \frac{Q_{a,i-1}h}{2l_{i-1}} - \frac{Q_{a,i}h}{2l_i} - \frac{G\{l_{GL}L_L - L_{LR} - l_{Ri}(L_R - nl_{GR})\} + \left(\frac{h}{2} + h_u\right)(L_R - nl_{Ri})\sum Q_a}{L_L L_R - nL_{LR}} \tag{3}$$

$$F_{a,2,i} = F_{a,1,i} - \frac{Q_{a,i-1}h}{l_{i-1}} + \frac{Q_{a,i}h}{l_i} \tag{4}$$

where, $F_{a,1,i}$ is the tensile force at the bottom joint and $F_{a,2,i}$ is the tensile force at the top joint of the post number i against the external force for allowable stress design, n is the number of posts, $Q_{a,j}$ is the allowable shear strength of the shear wall, h is the height of the shear wall, $\sum Q_a$ is summation of horizontal force applied to upper storey, l_j is the length of the shear wall, G is the vertical load due to fixed load and superimposed load transmitted to the upper beam, l_{GL} and l_{GR} are the distance between the vertical load G and left end post and right end post, l_{Li} is the distance between post number i and left end post, l_{Ri} is the distance between post number i and right end post, L_L, L_R and L_{LR} are the summation of the length l_{Li}, l_{Ri} and the product $l_{Li}l_{Ri}$, respectively, as;

$$L_L = \sum_{i=1}^{n} l_{Li}\ ,\ L_R = \sum_{i=1}^{n} l_{Ri}\ ,\ L_{LR} = \sum_{i=1}^{n} (l_{Li}l_{Ri})$$

and h_u is the height of centre of external forces applied to the upper floors, which can be calculated by equation (5).

$$h_u = \frac{\sum_{i=k+1}^{m} Q_i h_i}{Q_k} \tag{5}$$

where, Q_k is the shear force generated in the said storey number k, Q_i is the shear force generated in the storey number i, h_i is the height of the storey number i.

Equations (3) and (4) are derived for the model as shown in figure 1, using assumptions as follows;

- Upper beam behaves as a rigid body,

- All the joints at the top and bottom of posts are in elastic behaviour, and have the same stiffness.

Although these equations give the tensile forces against external force of allowable stress design, it can be applicable to obtain tensile forces in ultimate state if the ultimate strength of shear walls are used instead of allowable strength.

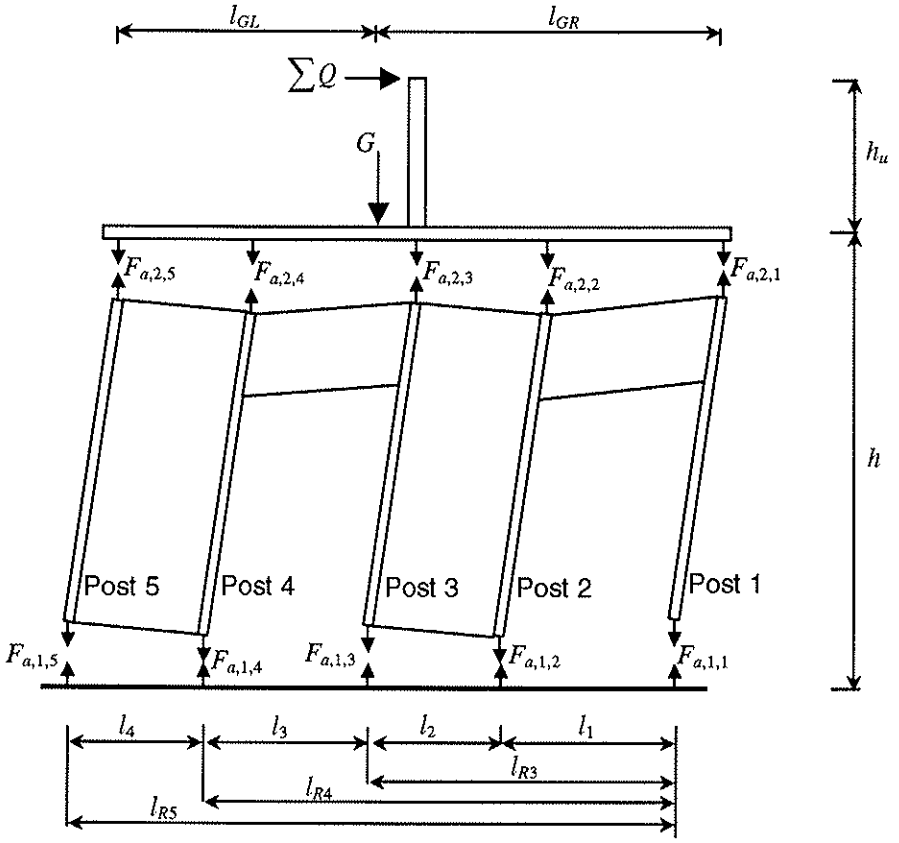

Figure 1 Precise model with rigid beam assumption (in case n = 4).

3 Experimental Results

3.1 Test method

3.1.1 Specimen

To study the applicability of the calculation and design methods mentioned above, cyclic loading test was conducted on a two-storied frame with shear walls and openings by wood frame construction. Figure 2 shows the configuration of the specimen.

Framing materials are 204 S-P-F (JAS 2nd Grade of A Class Framing Lumber). Structural glulam is used for sill and loading beams in both storey. Shear walls are sheathed with plywood (JAS Structural Plywood Class 2, CPS, t = 9.5mm), which are nailed by CN50 (JIS A5508) with spacing 100mm along the edges and 200mm for other areas.

Hold-down bolts were used at the bottom of the studs at both ends in first storey (HD-S and HD-N in figure 2) and four types of strap were used for the other connections at the top and the bottom of studs (large straps at S-1, S-6, S-7, S-12 and S-13 to S-16, and small straps at S-2 to S-5 and S-8 to S-11 in figure 2).

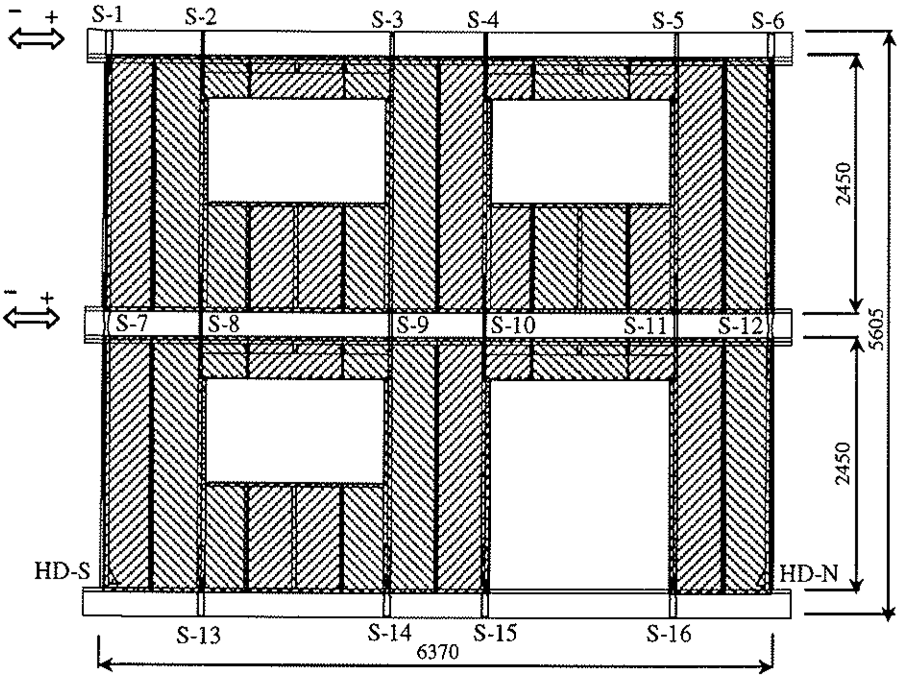

Figure 2. Configuration of the test specimen.

3.1.2 Testing methods

Lateral loads were applied to the loading beams of both storey using oil jacks, with keeping the ratio of the second storey displacement to the first storey displacement as 1.4, which was determined considering distribution of seismic force for ordinary two-storey houses. Figure 3 shows the loading protocol, in which the value of yield displacement D_y was determined by preceding one-story shear wall test. Displacement of each point was measured by LVDT, and the strain of each strap and hold-down bolt was measured using strain gauge.

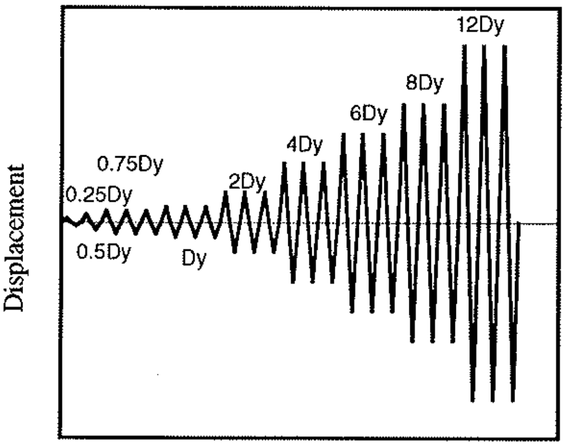

Figure 3 Loading protocol.

3.2 Test results

Table 1 shows the observed properties of first storey and Figure 4 shows the load-displacement curve of both storey. Figure 5 shows the tensile force of each strap and hold-down bolts. As the straps yielded during the test, the tensile force of strap was calculated using relationship of tensile force and residual strain obtained by loading test of the joint.

Table 1. Summary of test results – properties of first storey

Loading direction	P_y (kN)	D_y (mm)	K (kN/mm)	P_{max} (kN)	P_u (kN)	μ
+	22.40	13.09	171.2	42.00	37.85	5.06
–	24.91	13.22	188.5	44.84	39.65	5.13
Average	23.66	13.16	179.9	43.42	38.75	5.10

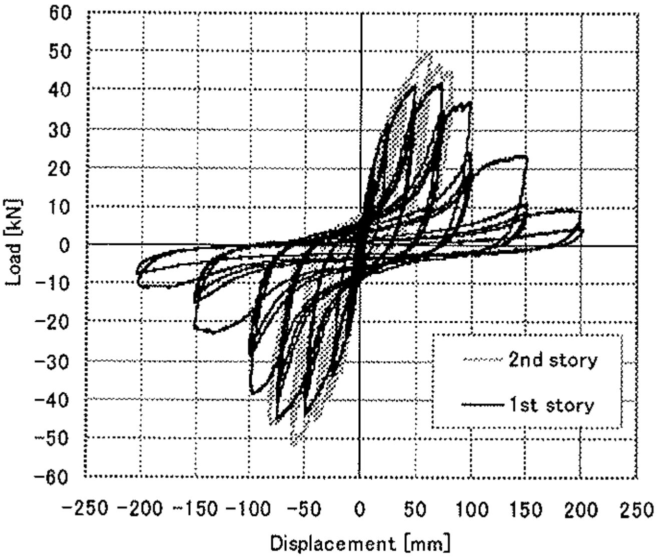

Figure 4. Load-displacement curve.

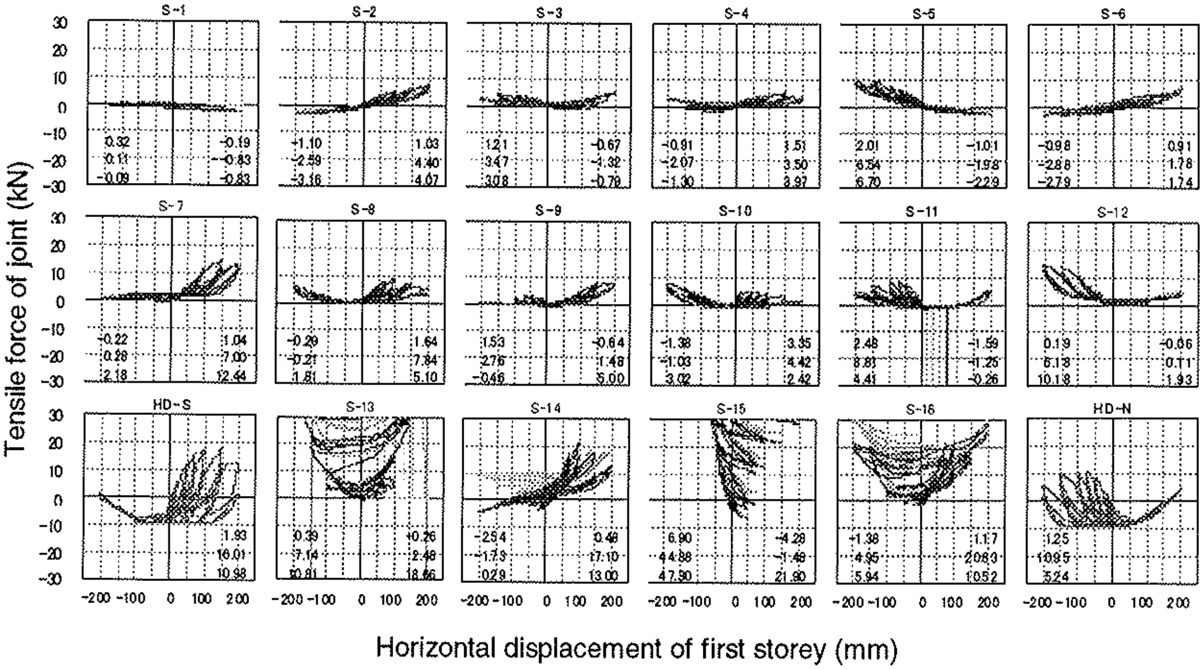

Figure 5. Tensile force of joint versus horizontal displacement of first storey
Three values in left side in each graph are respectively the values of tensile force of joints at Py, Pmax and Du, from up to down, when loaded in minus side, in right side are respectively at Py, Pmax and Du, when loaded in plus side,.

4 Numerical Analysis

4.1 Method

Figure 6 shows the analytical model, which is substituted bracing model for shear walls.

Figures 7 (1) to (4) show the stress-strain or load-displacement relationship used for the elements, equivalent brace, large strap, small strap and hold-down bolt. These relationships are determined to trace the preceding test results on a shear wall and joints with same configurations.

As the executive condition of the analysis, displacement at the top of second storey is kept to be 1.4 times of that of first storey, so that it traces the experimental condition.

ANSYS/ED® 5.7 was used as the software of this analysis.

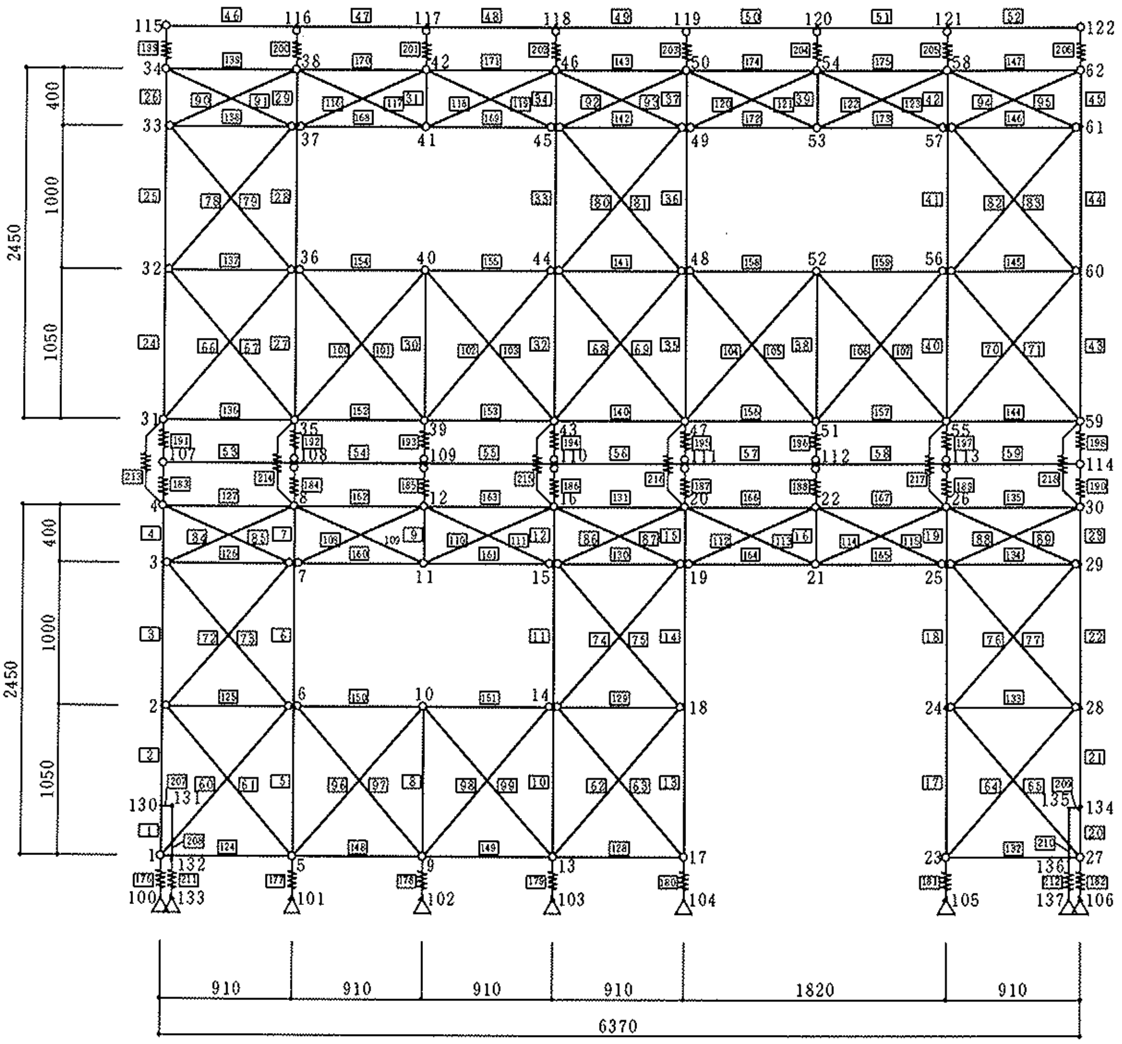
115
116
117
118
119
120
121
122
34
38
42
46
50
54
58
62
33
37
41
45
49
53
57
61
32
36
40
44
48
52
56
60
31
35
39
43
47
51
55
59
107
108
109
110
111
112
113
114
4
8
12
16
20
22
26
30
3
7
11
15
19
21
25
29
2
6
10
14
18
24
28
130
131
134
135
1
132
5
9
13
17
23
27
136
100
133
101
102
103
104
105
137
106
2450
400
1000
1050
2450
400
1000
1050
910
910
910
910
1820
910
6370

Figure 6. Analytical model using equivalent braces

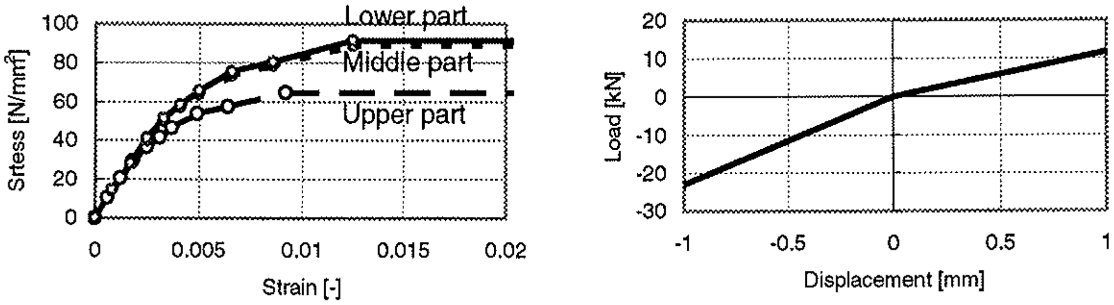
(1) Equivalent brace (Section area 100 mm^2)

(2) Joint with large strap

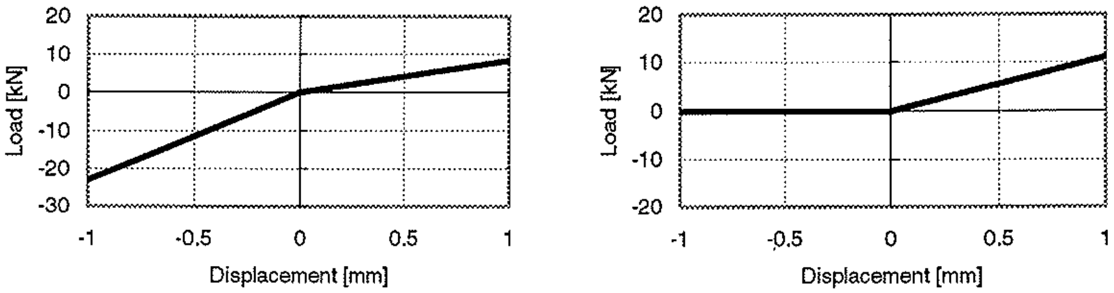
(3) Joint with small strap

(4) Hold down bolt

Figure 7. Stress-strain and load-displacement relationship of the model elements

4.2 Analytical results

Figure 8 shows the Load-displacement curves of first and second storeys obtained by the analysis, compared with the test results. Figure 9 shows the tensile force of joints by analysis at the displacement of yield strength and maximum strength of the test results, also compared with the test results.

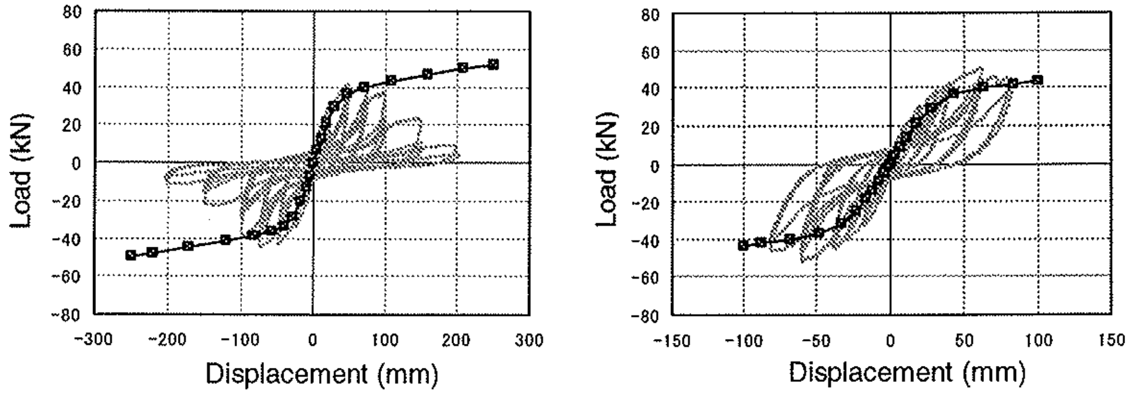
(1) Load-displacement curve of first storey

(2) Load-displacement curve of second storey

Figure 8. Load-displacement curves by the analysis, compared with the test results

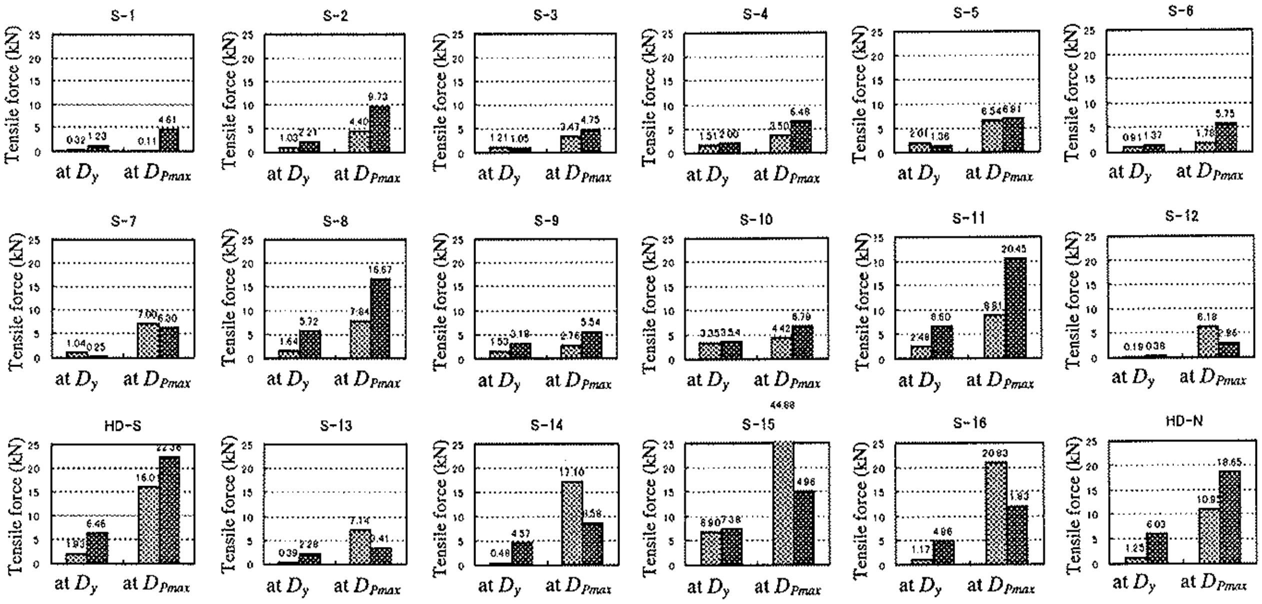

Figure 9. Tensile force of joints by the analysis, compared with the test results

5 Comparison of test result and design methods

5.1 Calculation of tensile force of joints

To discuss the adequacy of the design method mentioned above, tensile forces of joints at bottom corner of shear wall test specimens were calculated according those method, i.e.;

- Method 1: using empirical factor of 0.8 and 0.5 (see 2.1 and 2.2),
- Method 2: using rigid frame model (see 2.3), and
- Method 3: precise model with rigid beam assumption (see 2.4),

for the two states, yield point of first storey and ultimate state, respectively;

To apply these method to the test specimen, yield strength of a shear wall with the length of 0.91m, and the effect of suspended wall and waist-high wall were calculated according to the structural calculation manual for wood frame construction. And the shear force generated in shear walls in second storey were assumed to be 40% of their yield strength when the first storey reaches yield strength, because the relative shear deformation of second storey was controlled to be 40% of that of first storey during the loading test.

Ultimate shear strength was assumed to be 1.64 times of the yield shear strength for each part, which is the ratio of the ultimate strength to the yield strength observed in the loading test. No vertical load was considered in the calculation.

Figure 10 shows the calculated or assumed shear strength of each part of the specimen.

5.2 Calculation results and discussions

Tables 2 and 3 show the calculation results with the results of test and numerical analysis.

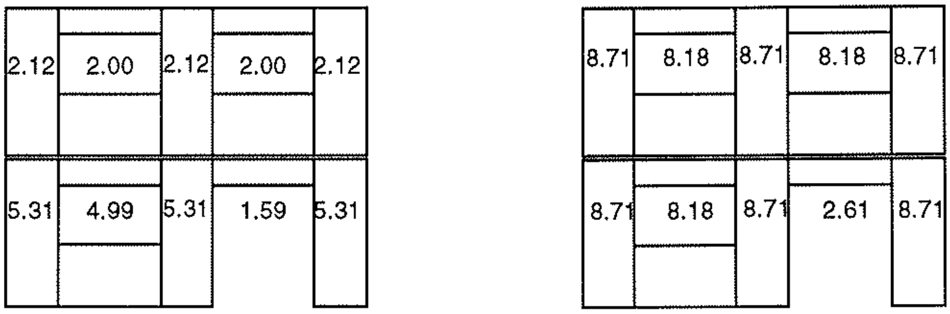
(1) Yield point of first storey

(2) Ultimate state

Figure 10. Calculated or assumed shear strength (kN) of each part of the specimen

Table 2. Comparison of tensile force of joints (kN) at yield strength of first storey – test results, numerical analysis results, and calculated according to three design methods

Test or Method	Joint S-7	S-8	S-9	S-10	S-11	S-12
Test	1.04	-0.29	-0.64	-1.38	-1.59	0.19
Analysis	0.25	0.00	1.04	0.48	0.00	0.38
Method 1	5.00	1.65	1.65	1.65	1.65	5.00
Method 2	4.70	4.70	3.13	3.13	4.70	4.70
Method 3	3.13	1.65	1.65	1.65	1.65	3.13
Test or Method	Joint HD-N	S-13	S-14	S-15	S-16	HD-S
Test	1.93	0.39	0.48	6.90	1.17	1.25
Analysis	6.46	2.28	4.57	7.38	4.96	6.03
Method 1	17.53	5.80	5.80	8.31	8.31	17.53
Method 2	14.89	14.89	7.84	7.84	14.89	14.89
Method 3	13.79	-0.10	5.00	7.51	2.41	13.79

Table 3. Comparison of tensile force of joints (kN) at ultimate strength – test results, numerical analysis results, and calculated according to three design methods

Test or Method	Joint S-7	S-8	S-9	S-10	S-11	S-12
Test	7.00	-0.21	1.48	-1.03	-1.25	6.18
Analysis	6.30	0.00	5.83	4.69	0.00	2.96
Method 1	20.56	6.81	6.81	6.81	6.81	20.56
Method 2	19.27	19.27	12.85	12.85	19.27	19.27
Method 3	12.85	6.82	6.82	6.82	6.82	12.85
Test or Method	Joint HD-N	S-13	S-14	S-15	S-16	HD-S
Test	16.01	7.14	17.10	44.88	20.83	10.95
Analysis	22.38	3.41	8.58	14.96	11.83	18.65
Method 1	41.11	13.62	13.62	17.73	17.73	41.11
Method 2	32.11	32.11	12.85	12.85	32.11	32.11
Method 3	29.63	18.80	9.21	13.32	22.91	29.63

As a whole, there are tendencies that the numerical analysis gives larger values than the test results, and all design methods give still larger values than the numerical analysis especially for the tensile force at hold down bolts. In the three design methods, Method 3 (precise model with rigid beam assumption) tends to give nearer values to the analytical values.

One possible reason for the difference between the test results and calculation results including numerical analysis, is that the resistance of nails from plywood to framing members is not considered in the calculations.

As the reason of the difference between design methods and analysis in tensile forces of hold down bolts, it can be pointed out that the distance of the stress centre of hold down bolts from the centre of stud is considered only in the numerical analysis. This eccentric setting of hold down bolts possibly decrease the tensile force generated in hold down bolts.

Method 1 gives far larger values at the end of the frame (S-7, S-12, HD-N and HD-S) than the test results and analytical results. The empirically determined factor 0.8 seems to be too large for wood frame construction.

Method 2 gives larger values for inner joints such as S-8, S-11, S-13 and S-16. In Method 2, neither the effect of suspended wall nor waist-high wall is considered, which seems effective to reduce the tensile force at the joints. It seems to be the reason why Method 2 gives larger values at inner joints.

6 Conclusions

There are some design methods to calculate tensile forces of joints at the shear wall corner were introduced. To discuss the adequacy of these design method for wood frame construction, lateral loading test was conducted on a two-storey structure with plywood sheathed shear walls with openings, and the tensile forces at the joints obtained by these design methods, numerical analysis and test results were compared.

As the results, there are tendencies that numerical analysis gives larger values than the test results, and all design methods give still larger values than the numerical analysis especially for the tensile force at hold down bolts at the end of the frame. In the three design methods, precise model with rigid beam assumption seems to give nearer values to the analytical values.

There are some possible reasons for the difference, such as lack of consideration for the effect of nails from plywood to framing members, distance between hold down bolt and centre of stud, effect of suspended walls and waist-high walls.

References

HOWTEC. 1988. Guideline for the structural design and fire- proof design for three storey wooden houses (in Japanese).

HOWTEC. 2001. Allowable stress design for wooden houses by post and beam construction (in Japanese).

Inayama, M. and Murakami, M. 2001. Development of structural design method on conventional post and beam structures, Part 53 (in Japanese). Summaries of technical papers of annual meeting, Architectural Institute of Japan. Vol. C-1, pp369-370.

Japan 2×4 builders association. 2002. Structural design manual for buildings by wood frame construction (in Japanese)

CIB-W18/35-16-1

INTERNATIONAL COUNCIL FOR RESEARCH AND INNOVATION
IN BUILDING AND CONSTRUCTION

WORKING COMMISSION W18 - TIMBER STRUCTURES

BASIC AND NOTIONAL CHARRING RATES

J König

Trätek – Swedish Institute for Wood Technology Research

SWEDEN

Presented by: J König

H J Blaß asked why the close comparison of cross-sectional moduli calculated from test data against EC5 values was not reflected in the comparison for beams. J König replied that in the data he presented, he merely wanted to compare the single beam values. J König then commented that EC5 values tend to be conservative for members with narrow cross-sections and is an issue which should be investigated. This was followed by a brief discussion initiated by R Gutkowski around the issues of the needs of the practising designer for simple but generally conservative calculations versus detailed calculations which seek to be accurate and as such may or may not be conservative from a design view point.

Basic and notional charring rates

Jürgen König
Trätek — Swedish Institute for Wood Technology Research

Summary

In the Fire Part of Eurocode 5 basic and notional charring rates. In order to simplify the determination of the load bearing capacity of cross sections, a notional charring rate is given to be used on all sides of the cross section. It is shown that the same notional charring rate can be used also for very small or narrow cross sections with a great influence of two-dimensional heat transfer, for example very narrow timber joists exposed on three sides.

The basic charring rate is strictly valid only in the case of one-dimensional heat flux and its use requires separate consideration of corner roundings of the char line. A criterion is derived to define when the notional charring rate should be applied.

From the results of recent fire tests notional charring rates are derived to be applied to heavy laminated timber plates, such as nail laminated timber decks and walls where gaps may open between laminations due to drying in service.

1 Introduction

The Fire Part of Eurocode 5 (prEN 1995-1-2) makes a distinction between

- the *basic charring rate* β_0, which is valid for one-dimensional heat transfer as in the case of a semi-infinite slab, or in parts of cross-sections where heat transfer is predominantly one-dimensional, and
- the *notional charring rate* β_n which implicitly includes effects of two-dimensional heat transfer in the vicinity of corners and large fissures, that is the corner roundings need not be taken into account separately.

For softwood, the basic charring rate is given as 0,65 mm/min; the notional charring rates for glued laminated and solid timber are 0,7 and 0,8 mm/min respectively. For solid timber, the relationship given by between the notional and basic value of charring rate is given by

$$\frac{\beta_n}{\beta_0} = \frac{0,8}{0,65} = 1,23 \qquad (1)$$

König et al. (2001) have shown that this ratio is a reasonable approximation when the real residual cross-section is replaced by a rectangular cross-section such that the section modulus is the same. See Figure 1. For small cross sections, e.g. a cross section of size

45 mm × 120 mm, the figure shows that this approximation is safe during the first 9 to 10 minutes of fire exposure. For larger times the ratio of 1,23 would be non-conservative, however this stage is normally not reached since the timber member would fail due to exhaustion of mechanical resistance.

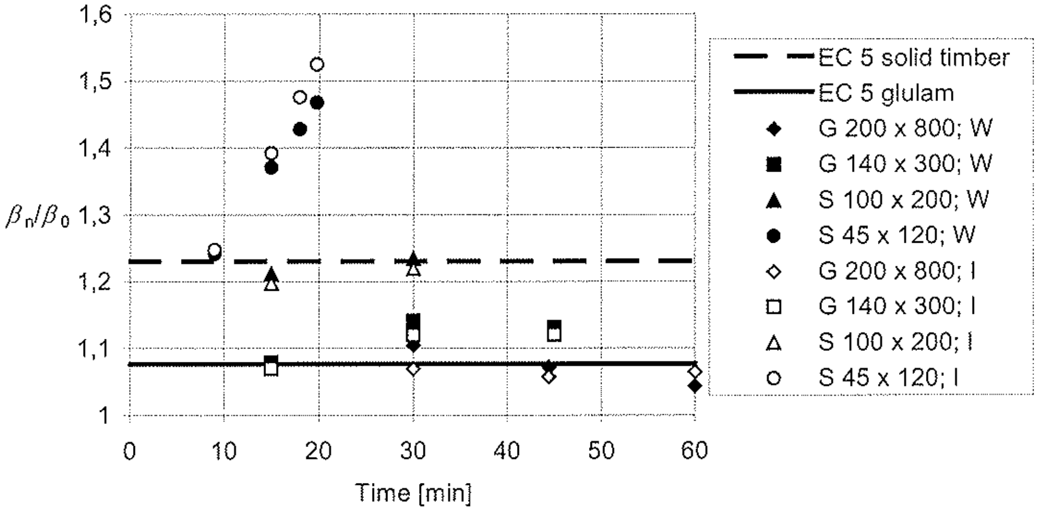

Figure 1 — Charring rate ratios vs. time: Comparison of calculated values with Eurocode 5 for solid (S) and glued-laminated (G) timber cross sections exposed on four sides (from König et al, 2001)

The values of figure 1 include that the charring depth on the narrow side is greater than the charring depth on the wide side. For example, for the cross-section 45 mm × 120 mm, at 15 minutes the calculated charring depth is 10,4 mm while it is 14,7 mm on the narrow side, that is it is 41 % larger on the narrow side. The reason is that heat flux is pronounced two-dimensional.

During the discussion of prEN 1995-1-2, it was argued against a fixed value of β_n/β_0 for small narrow cross-sections, since tests have shown that the charring rate of the narrow edge would, after some time, increase considerably compared to the charring rate on the wide side of the cross-section.

The concept of notional charring rates is also applied in annex C of prEN 1995-1-2 dealing with insulated timber frame assemblies, see also König (2000). Here, the use of the real shape of the residual cross-section would imply considerable difficulties for the designer.

2 Test results by van de Haar

Van de Haar (1983) made two fire tests on loaded floor assemblies consisting of two timber joists of dimension 59 mm × 196 mm spaced at 650 mm and a decking consisting of 19 mm plywood and 10 mm calcium silicate board on top of it. The joists were initially unprotected and exposed to the fire on three sides. Since the loading was different, the failure times were different: 25 minutes for floor 1 and 32 minutes for floor 2.

In Figure 2 and 3 the some of the residual cross sections recorded after the fire tests are shown. The graphs were reproduced from the original report by recording the co-ordinates of the border of the residual cross-section using a digitising device. In order to illustrate the degree of charring also the shapes of the original cross-sections are shown, however their horizontal position in relation to the residual cross-sections is not exact.

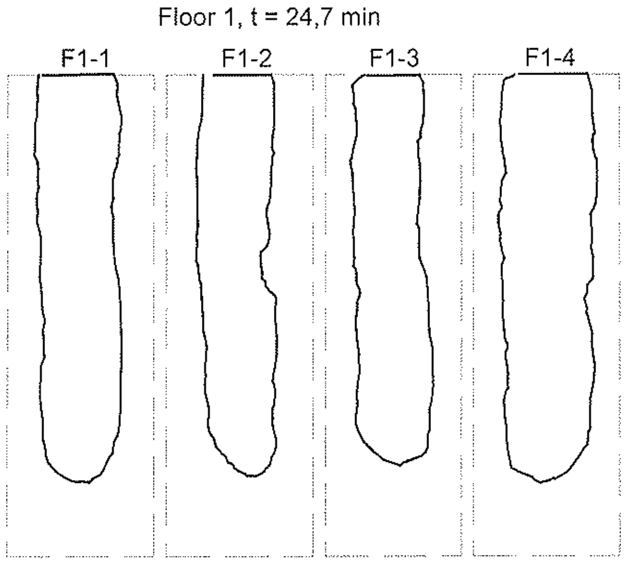

Figure 2 — Recorded residual cross sections at four locations of floor 1 (their horizontal position in relation to the original cross-section is approximate)

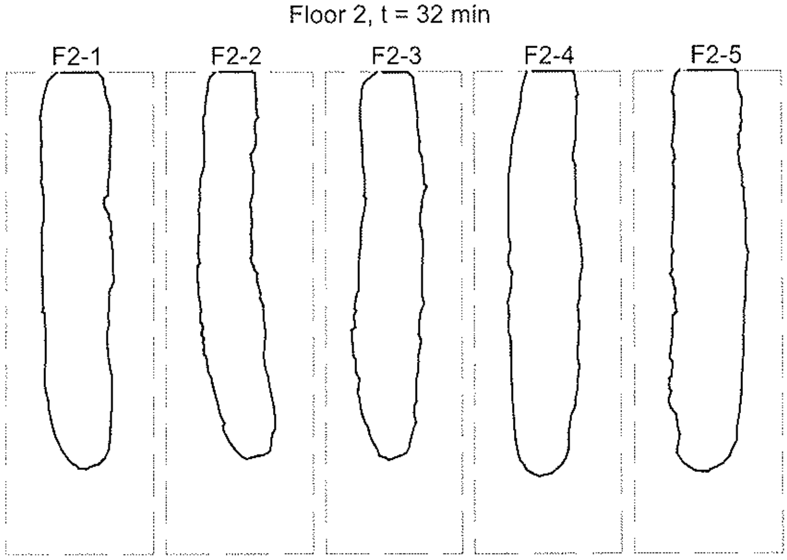

Figure 3 — Recorded residual cross sections at five locations of floor 2 (their horizontal position in relation to the original cross-section is approximate)

The residual cross-sections show considerably larger charring depths on the narrow sides than on the wide sides. For a charring depth on the wide side equal to *b*/4, the difference is between 45 and 85 %, that is about the same order of magnitude as calculated for a cross-section of 45 mm × 120 mm with a charring depth of 23 % of the width.

The section moduli W_{test} of the recorded residual cross-sections we calculated using the recorded co-ordinates of the border and a computer program for the determination of cross-sectional of arbitrary cross-sections, see Table 1. These section moduli were compared with section moduli W_{EC5}, obtained by assuming a notional charring depth equal to 1,23 times the experimental charring depth on the wide sides of the joists. (see equation (1). The average value of the ratio W_{test}/ W_{EC5} is with 1,037 slightly conservative. These values are illustrated in Figure 4 and 5. It can be seen that the relationship (1), derived from prEN 1995-1-2, takes fairly into account increased charring of the narrow sides of small timber cross-sections.

Table 1 – Relative section moduli – comparison of test results and values calculated according to prEN 1995-1-2

Cross-section	W_{test}	W_{EC5}	W_{test}/W_{EC5}
F1-1	0,406	0,414	1,020
F1-2	0,317	0,346	1,091
F1-3	0,407	0,35	0,860
F1-4	0,481	0,452	0,940
F2-1	0,360	0,310	0,861
F2-2	0,199	0,259	1,302
F2-3	0,246	0,265	1,077
F2-4	0,281	0,312	1,110
F2-5	0,315	0,338	1,073
Average			1,037

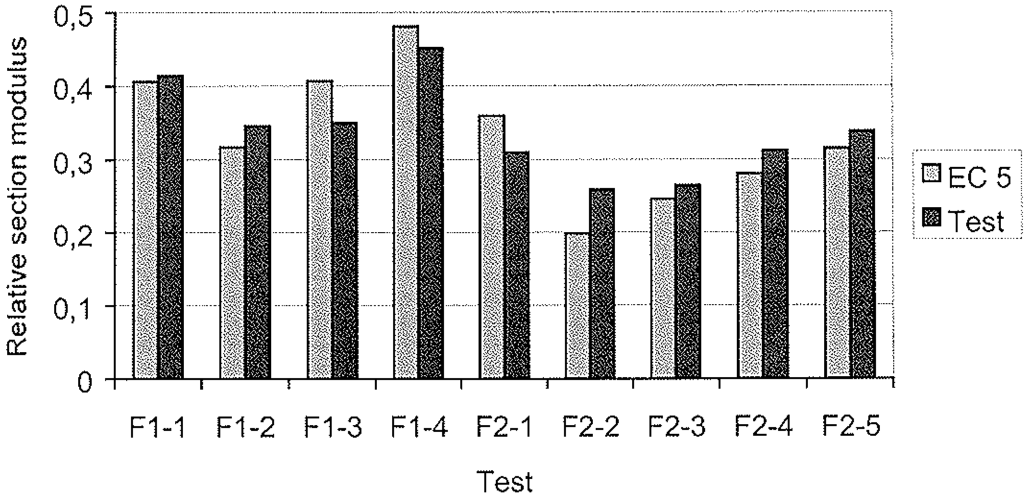

Figure 4 – Comparison of relative section moduli

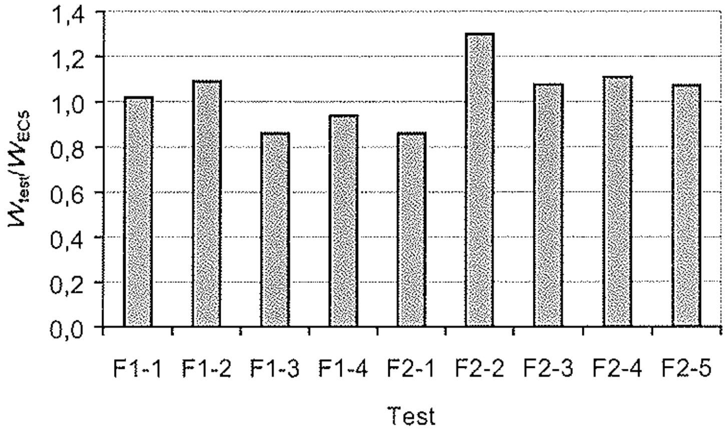

Figure 5 – Comparison of relative section moduli

3 When should the basic charring rate be used?

We can expect that some designers wish to use the concept of basic charring depth values plus separate addition of corner roundings in order to obtain more favourable results. Basic charring rates are valid only for one-dimensional heat transfer. As we have seen above, rectangular cross-sections may exhibit an extensive degree of two-dimensional heat transfer in the vicinity of the narrow sides. Therefore an application limit should be given in order to prevent non-conservative results.

Performing a heat transfer analysis using the thermal properties (conductivity and specific heat) as given in prEN 1995-1-2, for a cross-section of 100 mm × 200 mm, at 30 minutes the calculated charring depth is 20,3 mm on the wide side and 21,8 mm on the narrow side, that is it is 7,3 % greater on the narrow side. The conditions on the narrow side are influenced by two-dimensional heat flux to some degree, since the width of residual cross-section of about 60 mm is less than twice the temperature profile we get in the case of one-dimensional heat transfer when the timber is exposed on one side only. A stable temperature profile is developed after 20 minutes, see figure 6 showing temperature profiles of three specimens after 5, 10 and 20 minutes according to tests made by König et al. (1999). After 20 minutes, the depth d_Θ of the zone below the char layer which is affected by increased temperature is about 40 mm and does not increase significantly.

The use of the basic charring rate is permitted only when charring is one-dimensional. For application to rectangular cross-sections of beams and columns, from the depth of heat affected zone can be derived minimum width $b_{\min}$ of the cross-section to satisfy this requirement. For $b = b_{\min}$ heat transfer changes in the middle of the narrow side from being one-dimensional to two-dimensional.

For a temperature profile of depth d_Θ below the char layer, the required minimum width of the cross-section (see Figure 6) is

$$b_{\min} = 2\left(d_{\text{char},0} + d_\Theta\right) \qquad (2)$$

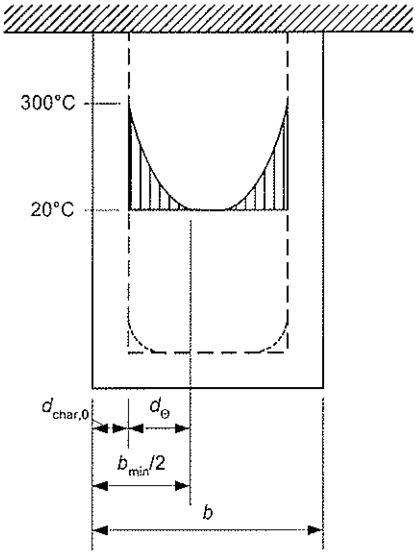

Figure 6 — Definition of minimum width for use of basic charring rate

For simplicity, a linear increase of the depth d_Θ of the temperature affected zone is assumed during the first twenty minutes (from 0 to 40 mm), although the increase is somewhat greater in the beginning (see Figure 7).

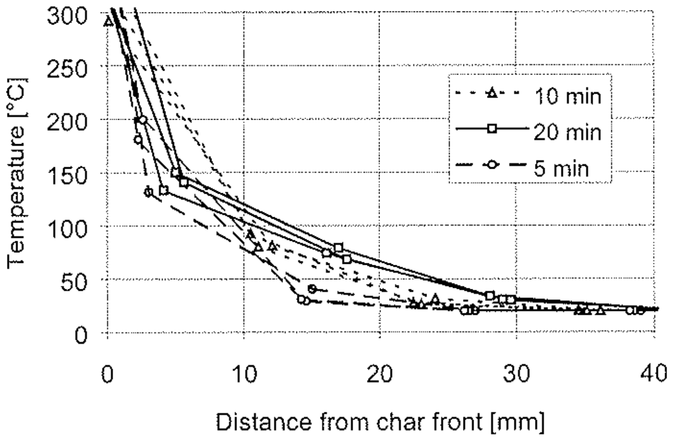

Figure 7 — Temperature profiles for one-dimensional heat transfer at 5, 10 and 20 minutes fire exposure

For practical use, with β_0 = 0,65 mm/min, after 20 minutes fire exposure the charring depth is 20 × 0,65 = 13 mm, criterion (2) can be expressed as:

$$b_{\mathrm{min}} = 2\, d_{\mathrm{char},0} + 80 \quad [\mathrm{mm}] \qquad \text{for } d_{\mathrm{char},0} \geq 13 \text{ mm} \tag{3}$$

and for the first twenty minutes of fire exposure as:

$$b_{\mathrm{min}} = 8{,}15\, d_{\mathrm{char},0} \qquad \text{for } d_{\mathrm{char},0} < 13 \text{ mm} \tag{4}$$

Graphs of expressions (3) and (4) are shown in Figure 8.

For example, for a 45 mm wide timber frame joist the concept of basic charring rate should not be used when the charring depth on the wide side exceeds 45/8,15 = 5,5 mm, that is for times greater than 5,5/0,65 = 8,5 minutes.

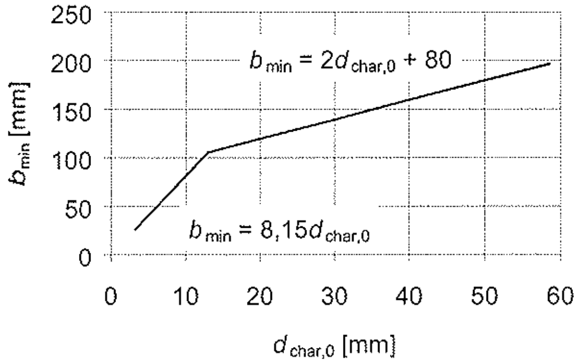

Figure 8 — Minimum width of cross section for use of basic charring rate as a function of basic charring depth $d_{char,0}$

4 Stress and nail-laminated timber plates

The fire resistance of heavy laminated timber plates used as floor and wall components is in general high. Such laminated timber plates may be glued-laminated, stress-laminated or nail-laminated. Also after a long time of fire exposure, considerable parts of the cross-section are uncharred and provide sufficient load-bearing capacity in a fire situation. Checking the load-bearing capacity of such construction, it would be natural for the designer to use the basic charring rate, since the heat transfer conditions would be one-dimensional. For glued-laminated heavy timber plates, that is glued-laminated beams in a flatwise position, this would be correct. In order to minimise the risk of shrinkage due to drying and the subsequent occurrence of fissures or gaps between the laminations, when assembling the laminations the moisture content of the timber should be as close to the final moisture content as possible. In Germany, it is recommended to use timber with a moisture content of 15 % ± 3 % (Werner, 1997). In Sweden it is recommended to use dry timber with a moisture content of not more than 12 %. The final moisture content is normally about 8 to 9 %, in areas of cold climate it may be even lower. The order of magnitude of drying shrinkage is about 0,2 percent per percent moisture content. A laminated timber plate will then shrink by 1,4 % when the moisture content is reduced from 15 to 8 %. In nail-laminated plates with 45 mm thick laminations, the mean gap width between the laminations would be 0,6 mm. In reality, it can be expected that there is a considerable variation of gap widths in a nail-laminated plate.

At Trätek, a series of seven fire tests was performed in order to study the effect of imperfect contact of laminations on charring. The specimens were made of seven timber members of size 43 mm × 97 mm glued against a sheet of 12 mm thick plywood in order to get a tight construction, see Figure 9. The fire exposed length of the specimen was one metre. The gap width between the wide sides of the laminations was 0, 1 or 2 millimetres; two of the specimens were glued against the backing plywood at a moisture content of 13 percent and were tested when the moisture content had decreased to 9 percent. Due to the shrinking of the laminations gaps opened between them with a width between 0 and 5 mm.

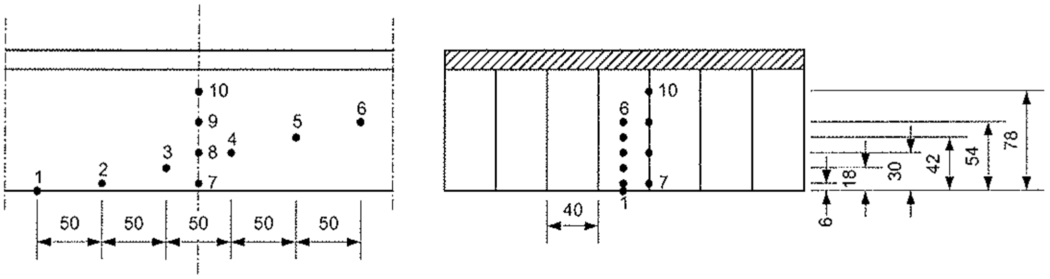

Figure 9 — Specimen configuration representing a heavy laminated timber plate

The progression of the char-line in the middle member is shown as the position of the 300-degree isotherm from temperature measurements of thermocouples 1 to 6, see Figure 10. Since the thermocouples were located in the middle plane of the middle member, no significant influence can be seen due the different gap widths, that is at this position the thermal conditions can be regarded as one-dimensional.

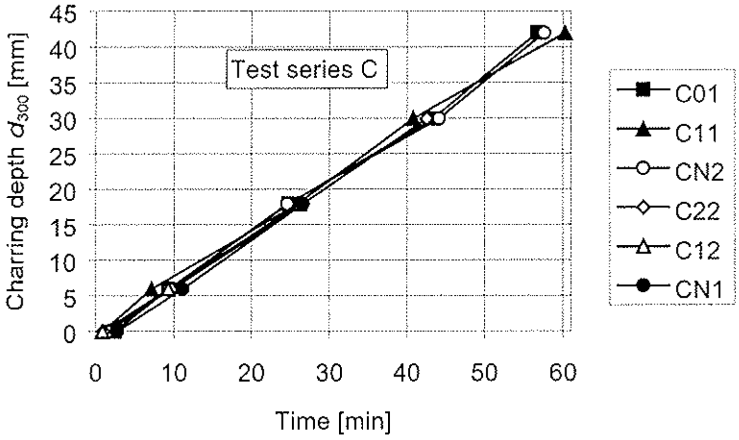

Figure 10 — Charring depth vs. time in middle member (thermocouples 1 to 6)

In stress-laminated plates, due to the pre-stressing of the laminations, e.g. planks of thickness from about 25 to more than 100 mm, the sides of the laminations are in contact, that is there is no gap between two neighbouring members. Figure 11 shows residual cross-sections of the five inner laminations at five different positions at equal distances in longitudinal direction. Although there is a considerable variation of charring at different locations, no significant corner roundings can be seen at the interfaces between two laminations. It is reasonable to assume purely one-dimensional conditions in the design.

In Figure 12 and Figure 13 corresponding residual cross-sections are shown for two specimens with gap widths of 1 and 2 mm respectively. We can see that charring near corners of laminations is influenced by the gap width. There is a considerable variability between the shape of residual cross-sections at different locations.

For each of the cross-sections of specimens with gap widths of 1 and 2 mm, an equivalent rectangular cross-section was determined such that the section modulus remained unchanged. This would require notional charring depth somewhat greater than the measured minimum charring depth. The average values and 95 % confidence intervals of the ratio of the notional charring depth and the minimum charring depth are shown in Figure 14.

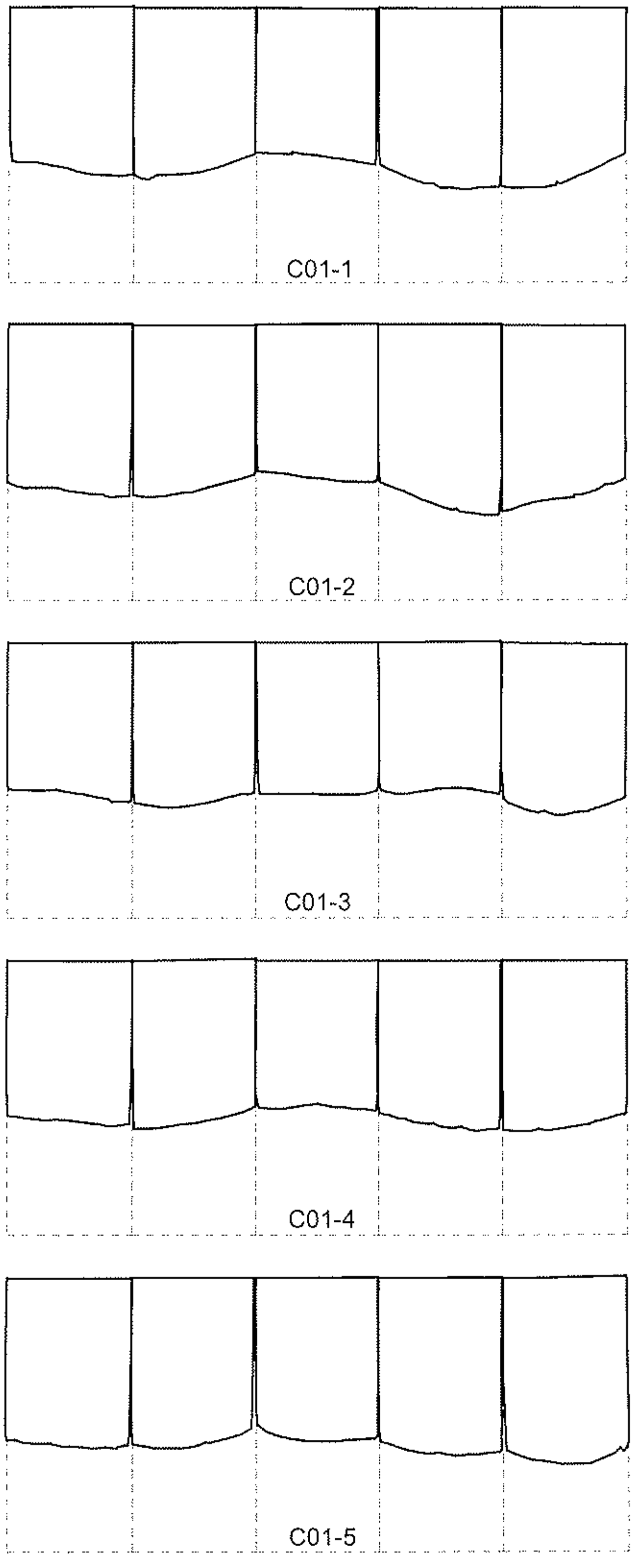
C01-1
C01-2
C01-3
C01-4
C01-5

Figure 11 — Residual cross-sections of specimen C01 without gaps after 61 minutes fire exposure

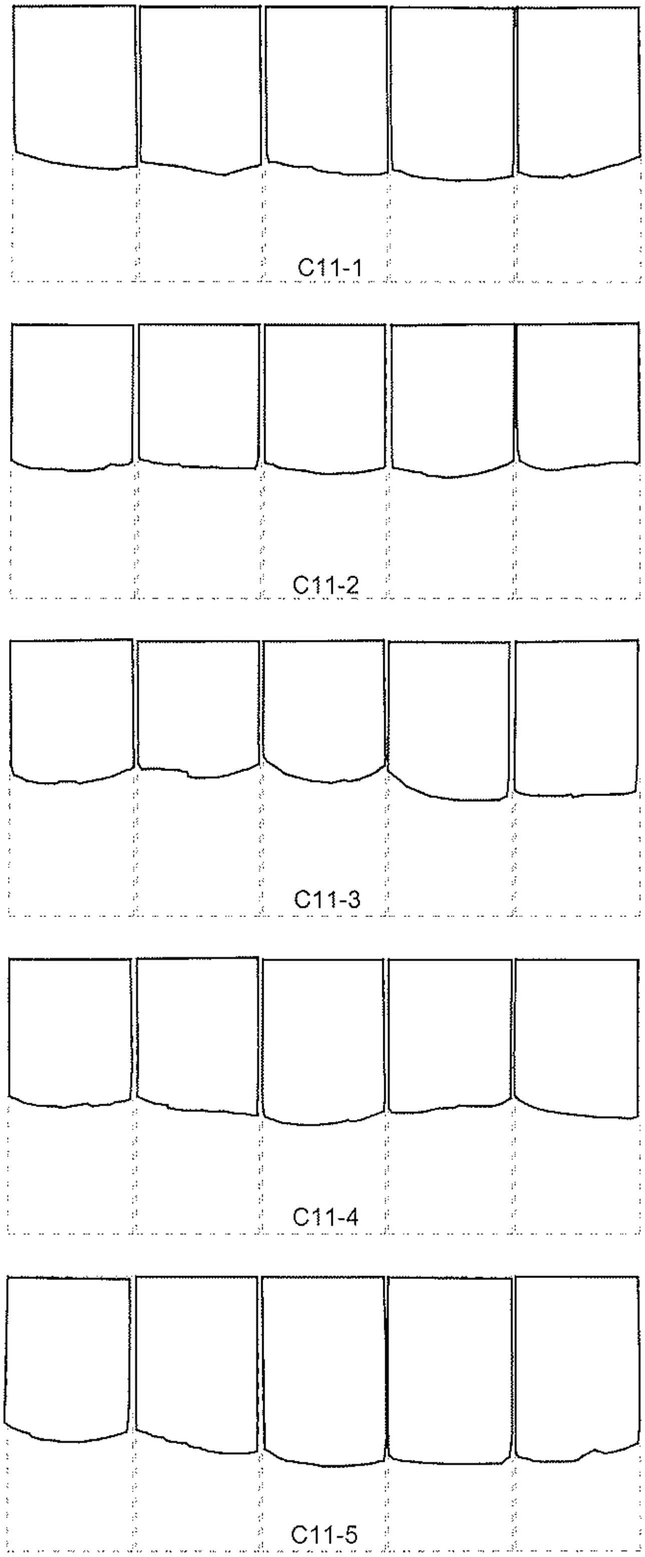
C11-1
C11-2
C11-3
C11-4
C11-5

Figure 12 — Residual cross-sections of specimen C11 with a gap width of 1 mm after 63 minutes fire exposure

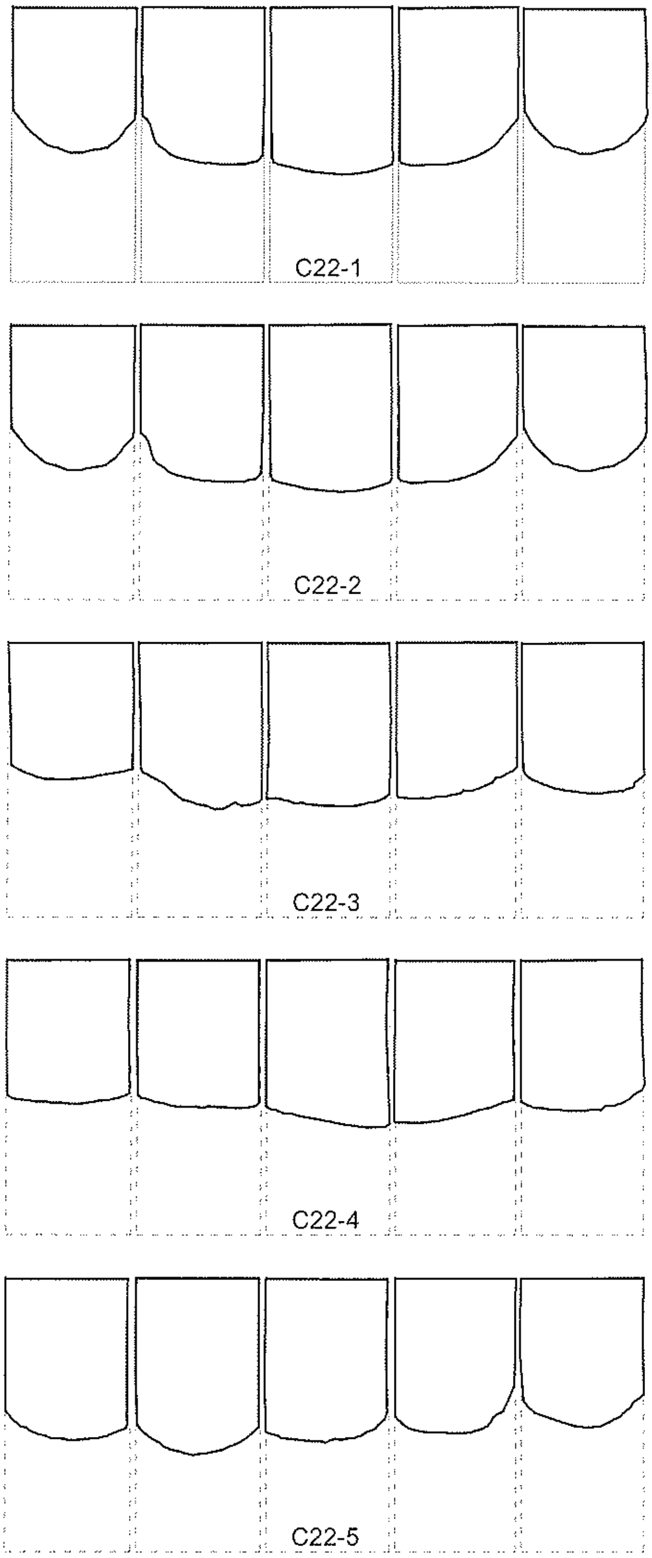
C22-1
C22-2
C22-3
C22-4
C22-5

Figure 13 — Residual cross-sections of specimen C22 with a gap width of 2 mm after 60 minutes fire exposure

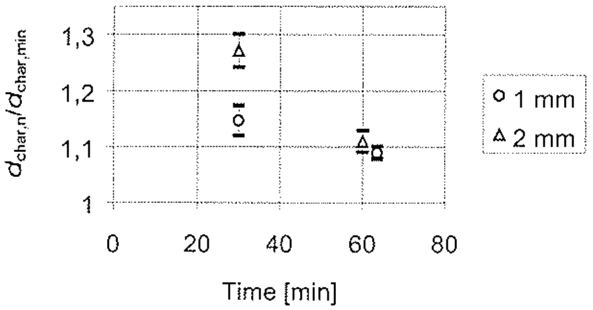

Figure 14 — Effect of corner roundings due to gap widths of one and two millimetres between laminations

The ratio is decreasing with time (or with the charring depth). Only for a gap width of 2 mm and fire exposure times up to about 30 minutes, the value is greater than 1,23 (see equation (1)). For normal gap widths of less than 1 mm, a notional charring rate which is 15 % greater than the basic charring rate should be used.

5 Conclusions

It has been shown that the concept of notional charring rates is a tool that can be widely used to simplify the calculation of cross-sectional parameters by determining an equivalent rectangular residual cross-section. This is an option in order to simplify the calculation or when the real shape of the residual cross-section cannot be determined unless advanced heat transfer calculations are performed.

6 References

König, J. and Walleij, L., 1999, One-dimensional charring of timber exposed to standard and parametric fires in initially unprotected and post-protection situations. Swedish Institute for Wood Technology Research. Report I 9908029

König, J., 2000, A design model for load-carrying timber frame members in walls and floors exposed to fire. Proceedings of CIB W18, Meeting 33, Paper 33-16-1

König, J. and Källsner, B., 2001, Cross section properties of fire exposed rectangular timber members. Proceedings of CIB W18, Meeting 34, Paper 34-16-2

prEN 1995-1-2, Eurocode 5: Design of timber structures – Part 1-2: General – Structural fire design. Final draft 2002.

Van de Haar, P. W., 1983, Onderzoek naar de invloed van de grootte van de veranderlijke belastning op de brandwerendheid op bezwijken van HSB-vloeren. TNO, Rijswijk, Netherlands

Werner, H., 1997, Brettstapelbauweise. Informationsdienst Holz, Arbeitsgemeinschaft Holz e.V., Düsseldorf

CIB-W18/35-17-1

INTERNATIONAL COUNCIL FOR RESEARCH AND INNOVATION
IN BUILDING AND CONSTRUCTION

WORKING COMMISSION W18 - TIMBER STRUCTURES

PROBABILISTIC MODELING OF DURATION OF LOAD EFFECTS IN TIMBER STRUCTURES

J Köhler
Swiss Federal Institute of Technology ETH

SWITZERLAND

S Svensson
Dept. Building Technology and Structural Engineering, Aalborg University

DENMARK

Presented by: S Svensson

S Thelandersson asked for clarification regarding the stated intention of the author to model uncertainties versus what was presented which is merely a comparison of the uncertainties between the test data and the model results. This was followed by a detailed discussion about the fundamental assumptions in the 3 models considered and their validity for the cases under consideration. S Svensson cautioned that the test data he presented were derived from specimens with a high moisture content which is not representative of normal building structures and commented on the possible effects on values of k_{mod}.

Creep testing wood adhesives for structural use

Björn Källander and Charlotte Bengtsson
SP Swedish National Testing and Research Institute, Wood Materials and Structures,
Sweden

1 Introduction and background

Lack of approval procedures for adhesives is hampering the development of wood products. There is an urgent need for fast and reliable approval procedures for new wood adhesive types, new gluing processes and new glued wood based products. SP is conducting research on test procedures to determine creep properties of wood adhesives for structural purposes. The research has been aimed at developing fast and reliable methods for approval of structural adhesives. The work is carried out within the framework of CEN / TC193 / SC1 / WG4 with financial support from the Swedish Wood Association.

Existing test methods for adhesives for structural use have been developed for aminoplastic and phenolic adhesives such as Phenol Resorcinol Formaldehyde (PRF) and Urea Formaldehyde (UF). These adhesives show very little or no creep and hence no test procedures for creep deformation or creep rupture testing of structural wood adhesives have been established. New adhesives such as PolyUrethane (PU) and Emulsified Polymer Isocyanates (EPI) show certain creep tendencies. In order to approve such adhesives, the amount of creep must be determined and related to demands of the finished products.

As for all accelerated test methods, it is crucial that the developed test methods reflect the expected failure modes in the climates that the glued structure will meet in practice. An important aspect regarding creep is the glass transition temperature of the adhesive. An accelerated test at high temperature and moisture could result in failures that never would occur at lower temperatures. There is also the question of whether a test for wood, adhesive or glulines is developed. The combined effects of temperature and moisture on the adhesive as well as the wood properties will limit the possibilities to accelerate creep tests if failure modes are to maintain unaltered.

A serious difficulty regarding accelerated creep test methods for adhesives is the question on how to set the requirements for the tests. Without long term experience of the actual adhesive types in real practice, we need to establish initial requirements based on theoretical assumptions. SP suggests that such initial requirements should be based on the load levels, climates and time spans set in Eurocode 5.

Although the developed test methods should be as fast and cheap as possible in order to simplify the introduction of new products, it is crucial that the developed test methods produce safe and reliable results. One important aspect is then that the limited experience of the test methods and the lack of established requirements make it important that the test methods produce results that can be re-evaluated when new experience is gathered.

2 Experimental work and theoretical studies

The study has been focused on two test methods based on the American standards ASTM D 3535 and ASTM D 4680 [1,2]. The primary aims of the study have been to determine if the two methods are capable of separating adhesives with different creep properties and to determine the suitability of the methods for evaluation of adhesives for structural purposes.

Results from tests with the two methods have been compared to results from a reference test method developed at SP.

In addition to the experimental work, FE analysis of the stress patterns in the test samples used have been made by Lund University [11,12] and calculations of test climates and of requirement levels based on Eurocode 5 have been made at SP [4,5].

2.1 Adhesives in test

The research projects at SP have primarily been using six different adhesives ranging from thermoplastic PVA to PRF with virtually no measurable creep in the glulines, see Table 1.

Table 1. Adhesives used in tests at SP.

Adhesive	Adhesive class	Comment
PVA D4	EN 204 class D4 exterior surface coated	Two component, thermoplastic, not for structural applications.
PU 1	EN 301 Type II ASTM D 2559-99 Exterior use	30 min curing one component PU adhesive
PU 2	EN 301 Type II ASTM D 2559-99 Exterior use	3 h curing one component PU adhesive
EPI	EN 204 class D4, exterior surface coated JAS 111	Adhesive type used for structural applications in Japan, but as of today not approved for structural applications in Europe.
MUF	EN 301 Type II	
PRF	EN 301 Type I	

2.2 Test methods studied

Two of the methods studied are based on the American standards ASTM D 3535 - 92 and ASTM D 4680 - 92, using samples subjected to compression shear at constant spring loading [1,2]. The "European 3535" is developed by Norwegian Institute of Wood Technology (NTI) and the "European 4680" by SP [6,7,8]. The third method developed by SP uses test samples similar to European standard EN 302-1 subjected to constant tensile shear load by cantilevers.

All the three test methods studied have primarily been aimed at determining the time to failure at constant load rather than creep deformation, even though deformation has been measured for all three methods. The research project has only covered short and medium term tests of small samples. Correlated long term creep tests of full size specimens are recommended.

2.2.1 Description of the European 3535 test method

The European 3535 uses an identical test rig as ASTM D 3535 but smaller test samples, see Figure 1. The test sample of European 3535 differs from the sample of ASTM D 3535 as the size has been reduced from thirty to twelve 12.5 x 50 mm glulines. The European 3535 sample is symmetrical, with plane surfaces in both ends.

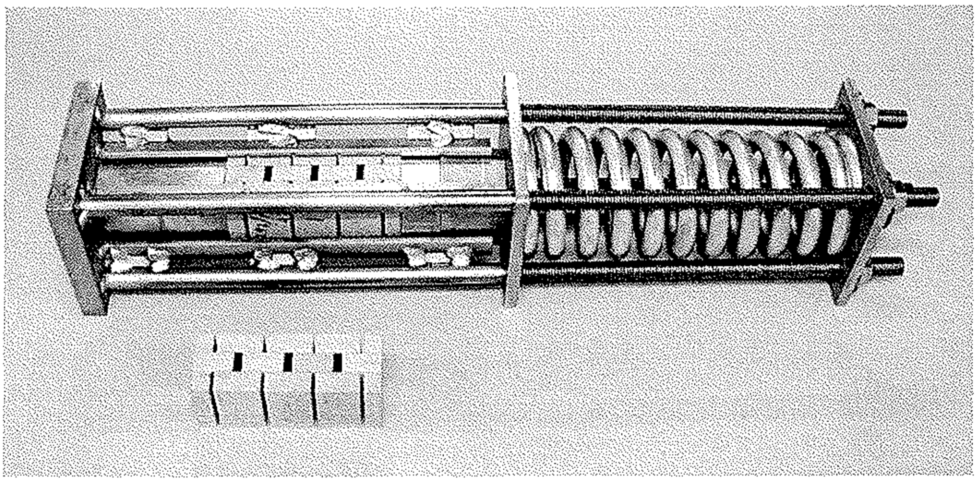

Figure 1. Test rig and sample for European 3535 test. Sample size 50 x 50 x 135 mm.

Six replicates are tested with each adhesive. Each sample is inserted into the rig, a compression load corresponding to 3 N/mm^2 shear stress is applied by a universal testing machine and the nuts on the rig are tightened to maintain spring compression.

The shear stress level used in European 3535 has been chosen by NTI after several pilot tests at various shear stress levels [7,8]. The 3 N/mm^2 shear stress level was chosen in order to result in failures within the six weeks test period to separate different adhesives, without unacceptable deformations or failures in the wood. The 3 N/mm^2 shear stress level is also in part supported by theoretical calculations [9].

After the load is applied, the rig is placed in a climatic chamber and stored for six weeks in a series of climates:

Table 2. Climate series used in European 3535. The proposed sequence of test climates has been altered after the tests at SP.

Climate	Climates series used in tests at SP	New proposed climate series
1	14 days at 80 °C / 10-15 % RH	14 days at 80 °C / 10-15 % RH
2	14 days at 50 °C / 75 % RH	14 days at 20 °C / 85 % RH
3	14 days at 20 °C / 85 % RH	14 days at 50 °C / 75 % RH

The rigs are removed after the six weeks period. In order to pass the test, no gluline in any of the six samples are allowed to fail.

2.2.2 Description of the European 4680 test method

The European version of ASTM D 4680 has been developed by SP. The method follows established principles used for determination of duration of load factors for solid wood and wood based panels [3].

The European 4680 method is primarily a creep rupture test method although deformation can be measured. It fairly closely resembles the American original. The most important modifications are:

1) the two test climates used,
2) prediction of shear stress level corresponding to 10000 h failure time is based on median time to failure at each stress level rather than on individual tested samples.

The test sample and test rig in European 4680 are identical to the American ASTM D 4680, with the exception that the test surface of the sample is 25x25 mm instead of 1x1", see Figure 2.

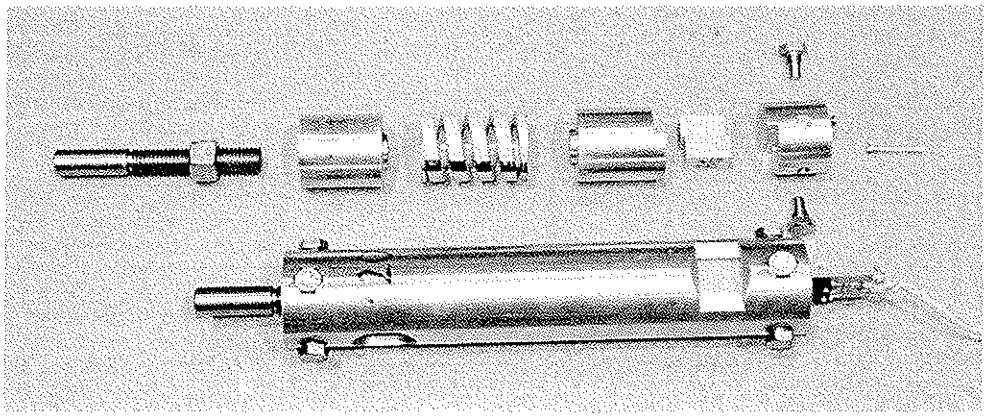

Figure 2. Test rig and sample for European 4680 test. Shear test surface 25 mm x 25 mm.

Two test climates are used: 50 °C / 75 % RH and 80 °C / dry (10-15 % RH, not controlled). The choice of climates is based on the climates and requirements defined in Eurocode 5 and the definition of adhesives of Type I and Type II in EN 301 [5,6].

50 °C / 75 % RH is an extreme climate for timber structures. The temperature may occur in the vicinity of the wood members in a roof structure due to absorption of heat from sun radiation. The duration is likely to be less than 12 hours for each occasion. The combination 50 °C / 75 % RH can normally not occur. Additional moisture is required; conditions which might occur in for instance process industries.

80°C / dry is a climate or temperature which is not likely to occur except for in very special application and situation and with short duration. A climate of this nature is not likely to affect the adhesive bond line only, but also the wood itself with increased creep and reduced strength. It is for instance a temperature that will occur during fire close to the charring zone.

At 80 °C the test samples are loaded at 3 N/mm^2. The stress levels at 50 °C / 75 % RH are chosen to be as high as possible without leading to high proportions of wood failure, as will be described in Section 3.5.

Ten test samples are loaded at each climate and shear stress level, which gives a total of 50 samples for each adhesive tested. In addition to this, short term shear strength is determined according to the ASTM D 905 method. Time to failure is recorded for each sample and median time to failure is calculated at each shear stress level.

The load corresponding to 10000 h median time to failure at 50 °C / 75 % RH is calculated based on the median time to failure at each shear stress level, see Figure 3.

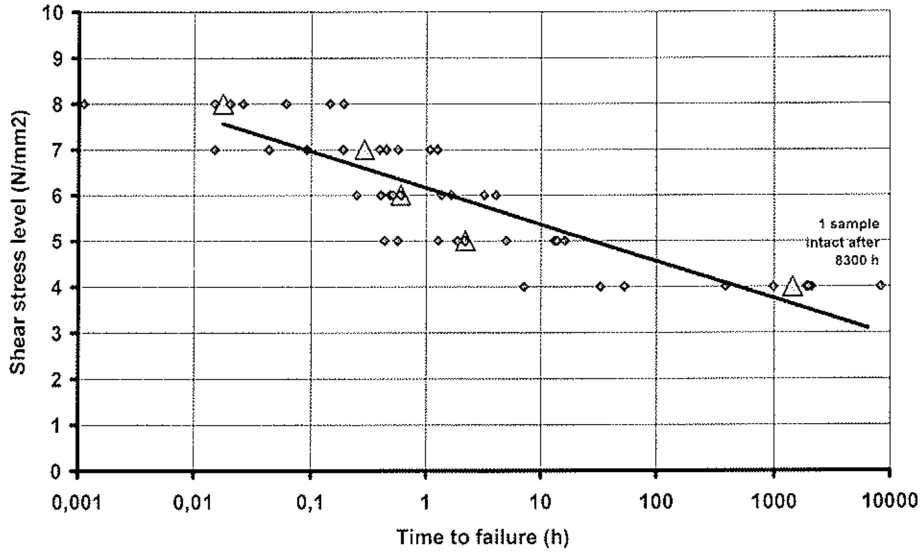

Figure 3. Prediction of shear stress at 50 °C / 75 % RH corresponding to 10000 h time to failure is based on median time to failure at each load level. Triangles mark median time to failure at each shear stress level.

The two suggested requirements used in European 4680; 10000 h predicted time to failure in 50 °C / 75 % RH and 1 000 h median time to failure in 80 °C / dry at 3 N/mm^2 shear stress have been set after calculations based on Eurocode 5 [4].

2.2.3 Description of the SP cantilever method

The SP cantilever method was developed at SP to be used as a reference test method to the European 3535 and European 4680 methods. By using a cantilever system and applying tension shear stress, a constant and fairly well defined stress is applied to the samples, see Figure 4.

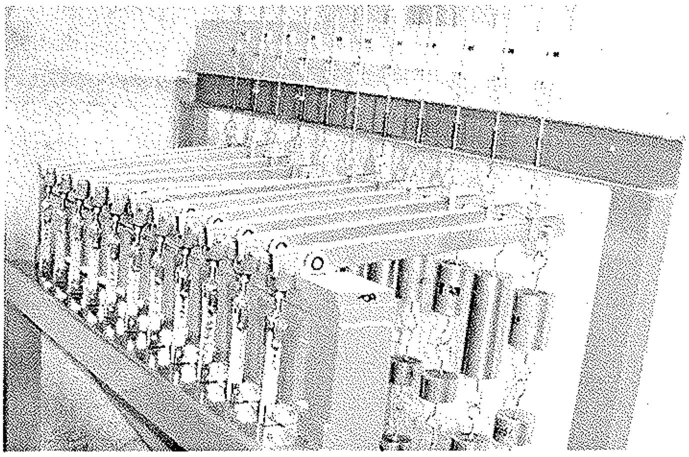

Figure 4. SP cantilever rig. EN 302 samples subjected to constant tensile load. When a sample fails, the cantilever is caught by a damping device designed to carry the weights and to reduce the impact shock to other samples.

The SP cantilever method uses the test sample described in European standard EN 302-1. Two 10.5 mm holes are drilled in the sample and a mark is inscribed across the gluline by a needle for measuring deformation.

Time to failure is recorded by timers attached to the damping device of each cantilever. Deformation is measured by means of a digital camera with high resolution for selected samples. Tests have presently only been made in the climate 20 °C / 65 % RH.

2.3 FE calculations

Numerical finite element studies have been carried out on the three methods studied. The studies have been focused on the sensitivity of the test methods to geometrical imperfections of the test samples and the not centred load caused by the coil spring [11,12].

The FE calculations have been made with non linear material description of the behaviour of the bond line and adhesive properties ranging from brittle to ductile adhesives. The ongoing FE studies are made by Lund University on behalf of SP.

3 Experimental results and discussion

3.1 European 3535

The production of test samples for European 3535 requires extremely high precision in order to guarantee that the tested glulines have equal size. Also very small variations in positioning of the milling tools during the cutting of the samples will lead to differently sized gluline surfaces and resulting stress variations. Such differences are serious since the method is measuring the time to failure of the weakest tested gluline surface.

The 3535 tests performed at SP have lead to very short times to failure for PVA and PU adhesives tested. All tested samples but one failed during the first climate, 80 °C. No failures have been recorded in PRF, MUF or EPI adhesives.
The very short times to failure make it difficult to differentiate between adhesives with "little creep" and "a little more creep". However, it is obvious that the method separates adhesives with creep tendency and adhesives with no creep tendency. The very fast failures could also indicate that the suggested load in the test, 3 N/mm^2, leads to a very severe test.

3.1.1 Comments to the European 3535 method

The European version of ASTM D 3535 differs from the American original as it uses a smaller test sample, a higher shear stress load level and a longer test period comprising of three different climates in series. The European test method is performed on beech samples rather than the species actually used industrially.

The modifications of the original ASTM D 3535 have in reality turned the test method from a "creep deformation" to a "creep rupture" test method. The two separate test climates used in ASTM D 3535 have in European 3535 been turned into a sequence of three climates. The modifications of the test procedure makes it difficult to apply experience gathered from the ASTM D 3535 method to the results of European 3535.

The primary advantage of the European 3535 method is that it is fairly rapid as the results are obtained within 8 weeks after production of the test samples. The primary drawbacks are that the method only gives a pass/fail answer and that we today lack experience from comparative tests of the European 3535 method and long term tests of full size members. Lacking such experience, it is difficult to set requirements for the test. Since the European

3535 method is a pass/fail test and does not differentiate between the effects of shear stress load and climate load, it could be difficult to re-evaluate existing test results if the test procedure or requirements were to be modified when new experience is gathered.

3.2 European 4680

The results show that the European 4680 method is capable of separating adhesives also with relatively similar creep tendencies.

The results of the duration of load tests at 3 N/mm^2 and 80 °C have been completed with all tested adhesives. Of the six adhesive types tested, only PVA, PU1 and PU2 show failures. No failures had been recorded for PRF, MUF or EPI adhesives when the test was terminated after 10100 h. Median time to failure for the PVA D4 samples was 46 minutes, as compared to the suggested requirement 1000 h. Median time to failure for PU1 and PU2 was 2269 h and 1891 h respectively.

The results of tests in climate 50 °C / 75 % RH have so far been completed for PVA D4, PU1 and PU2 adhesives. The results show a large variation in time to failure between samples at the same load level, see Figure 5.

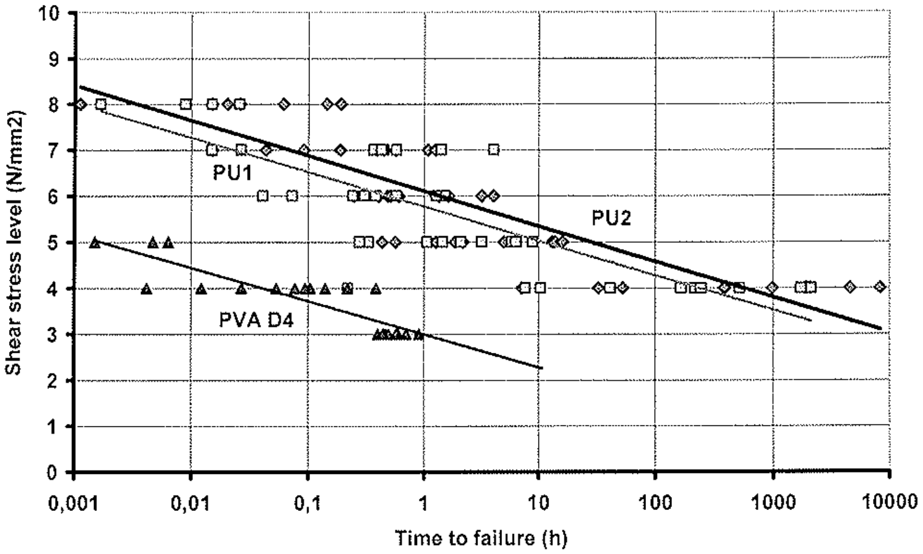

Figure 5. Predicted load corresponding to 10000 h median time to failure is calculated from the median time to failure in the test. The figure shows results from tests with two 1k PU adhesives and one PVA D4 adhesive.

3.2.1 Repeatability

Results from repeated tests with samples of the same adhesive glued at separate occasions show different shear strength level but similar "slope" of the time to failure / shear stress - regression lines, see Figures 6 and 7.

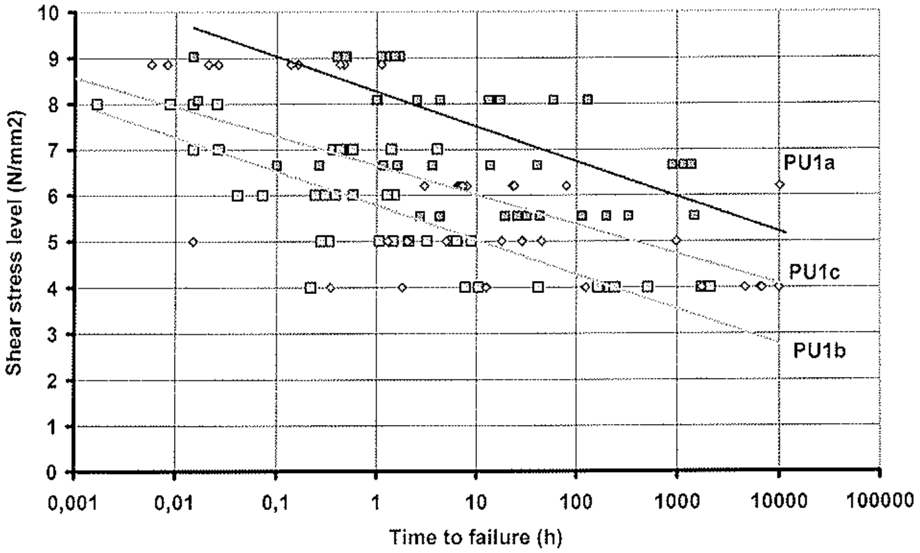

Figure 6. Results of repeated tests with the same type of adhesive indicate that the results are greatly influenced by variations in initial gluline shear strength. The slope of the shear stress / time to failure regression line is relatively constant which could indicate that the test truly reflects the creep properties of the adhesive.

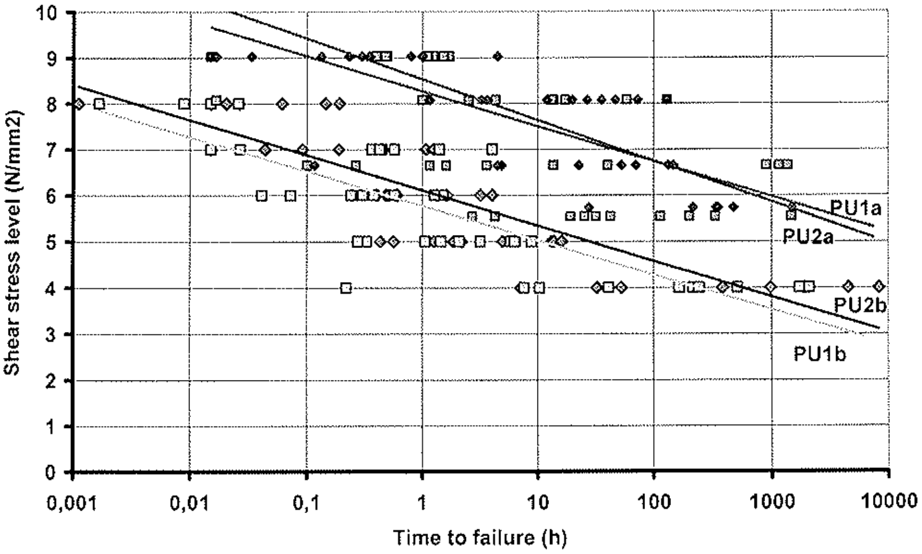

Figure 7. Results of repeated tests with two adhesives with samples glued at two different occasions. The initial gluline strength varies between gluing occasions but not between the two adhesive types.

The test results show that the initial shear strength of the glulines vary between different production batches of test samples. If this is caused by variations in properties between different adhesive batches, different wood properties or variations in the gluing process is not determined.

The similar "slope" of the regression curve of time to failure / load indicate that the time dependent reduction of failure load is independent of the initial shear strength. The results indicate that the test method measures actual creep properties of the test adhesives.

3.2.2 Variation between samples

The test results have shown a large variation in time to failure for different samples tested at the same shear stress level. The median time to failure at each shear stress level can thus differ considerably from the average time to failure. In the tests performed, this has had the effect that the predicted shear stress corresponding to 10000 h failure time is reduced significantly if the prediction is based on median time to failure (as in European 4680) rather than all measured values (as in ASTM D 4680), see Figure 8.

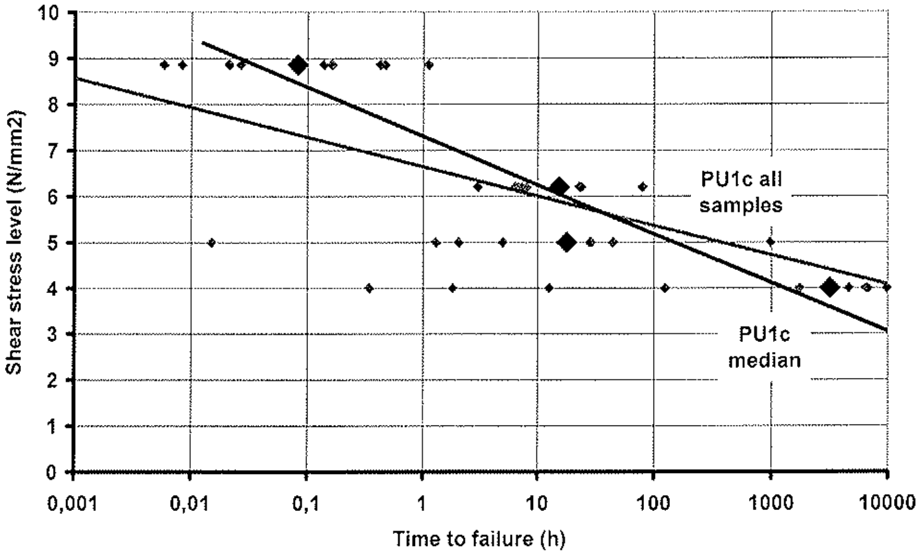

Figure 8. Predicted shear stress corresponding to 10000 h failure time will be lower if the prediction is based on median times to failure rather than on all samples.

3.2.3 Very good adhesives cause problems

The European 4680 test procedure is based on prediction of the shear stress level corresponding to 10000 h time to failure based on time to failure at higher shear stress levels. If the adhesive does not show creep related failures even at these higher shear stress levels, no data for the prediction are available. Hence a very good adhesive will not suit the test procedure. The problem can be solved by establishing a limit for the minimum median time to failure at each shear stress level.

3.3 SP cantilever method

Tests results are presently available from tests with PVA D4, PU1, PU2. The results show great similarities with the tests made according to European 4680, see Figure 9.

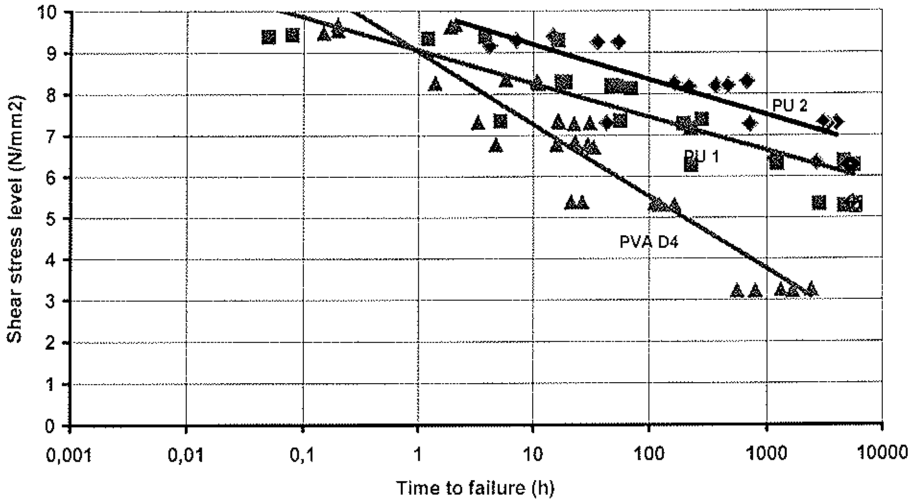

Figure 9. Results from tests of PU1, PU2 and PVA adhesive in SP cantilever rig. Failed samples marked with filled symbols. Intact samples marked with frames.

The SP cantilever test separates adhesives in same way as 4680 in spite of the different stress pattern, which indicates that both methods reflect the same adhesive properties.

3.4 FE calculations

The FE simulations of all three methods have shown that the mechanical behaviour in terms of estimated bond line strength, i.e. load bearing capacity of the test sample is highly dependent not only on the properties of the adhesive, but also on the specimen and loading geometry.

The FE simulations show that the load bearing capacity of the European 3535 test sample is seriously affected by the non centred force caused by the large diameter of the coil spring. Significant deformations of the test sample with resulting stress concentrations and tensile stresses will occur if the force is applied perpendicularly to the glulines, se Figure 10.

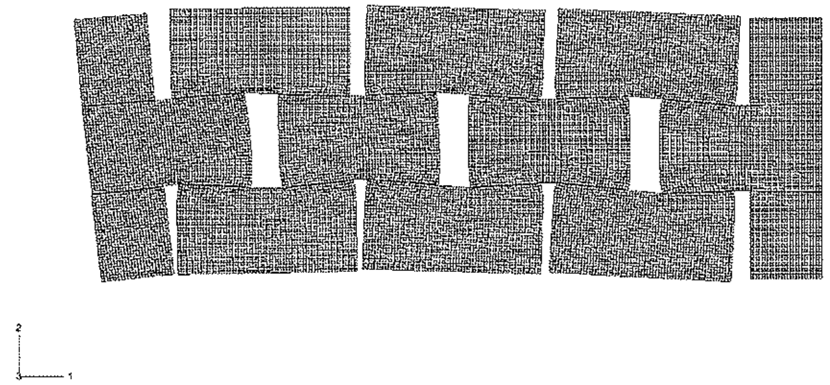

Figure 10. The deformation of eccentric loaded European 3535 specimen, load of 1250 N at 5 mm off-centre. The deformations are magnified by a factor 10. From [11].

If, on the other hand, the force is applied parallel to the glulines, a torsion factor to the gluline stresses is introduced. The simulations indicate that the load bearing capacity can vary as much as 25 % depending on where along the spring periphery the force is applied.

Also the simulations of the European 4680 method have shown that the test results are influenced by how the force is applied to the specimen. If the surfaces where the force is applied are non parallel or if the force is applied at a distance from the gluline, the load bearing capacity of the sample is reduced. On the other hand, friction between the loading device and the sample as well as within the gluline can increase the failure load.

The simulations of the EN 302 - 1 test sample in the cantilever system show the test sample deforming as the load is applied, resulting in tensile stresses perpendicularly to the gluline in addition to the shear stresses.

3.5 Maximum shear stress in a creep test for beech wood samples

The test results from the SP cantilever method show that the wood failure proportion increase with increased shear stress, see Figure 11.

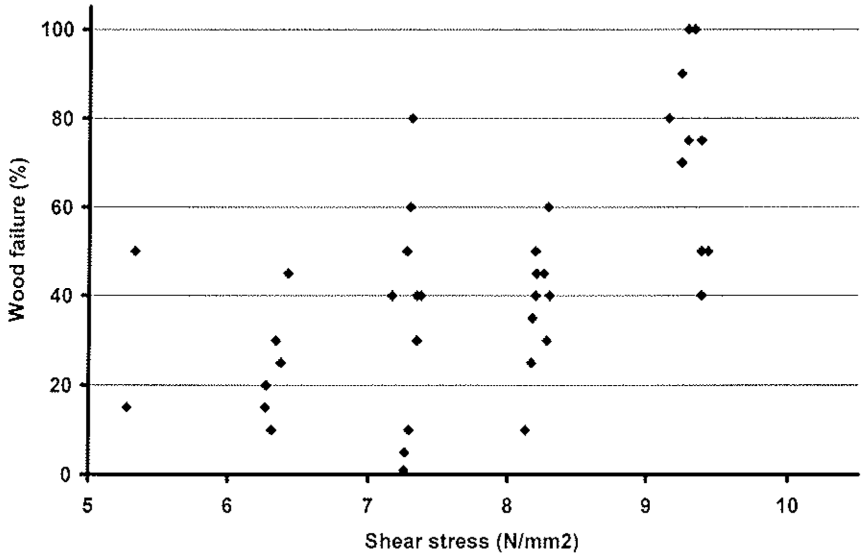

Figure 11. Wood failure increase as load is increased in SP cantilever tests of PU1 and PU2. A high wood failure proportion indicates that the wood rather than the adhesive has failed.

The results seem to indicate that the maximum suitable shear stress level on smaller samples tested at 20 °C is 8 - 9 N/mm^2. If a higher shear stress is applied, the test will actually test the wood rather than the adhesive.

A sample that fails with a high percentage of wood failure indicates that the adhesive would have been able to carry the load for a longer period than the wood. In a short term test, this is usually considered acceptable, the adhesive is "stronger" than the wood. However this is not the case if the result is to be used in predicting the creep behaviour of the adhesive. The wood failure results in a "too quick" failure at high shear stress levels, which in turn reduces the slope of the regression line based on the median times to failure. Hence, the predicted load corresponding to 10000 h median failure time will be too high.

3.6 Effect of post curing

One important aspect of the suggested test procedures in European 3535 and European 4680 is if the samples are heated prior to the application of the load or not. Heating prior to loading can have the effect that post curing adhesives would show a better test result than if the load is applied to a cold sample. Improved performance by 1k PU adhesives has been shown by tests at FMPA with the European 3535 method where samples that had been treated in 80 °C passed the test and samples stored at 20 °C / 65 % RH failed [10]. The mechanisms leading to this effect in 1K PU glulines have not yet been identified.

In the suggested test procedure for the European 3535 method, the load is applied prior to heating. The procedure prevents post curing before the load is applied. In the suggested test procedure of the European 4680 method, the samples are heated to the test temperature prior to the load being applied, and thus post curing can take place. This is done in order to guarantee that the load is not changed as the aluminium tube and steel spring are heated.

It has to be determined what procedure is best suited for a creep test at elevated temperature. Application of the load prior to heating could lead to a test "on the safe side", if the load after heating is the same as before heating. It could also be argued that a large structure most likely will be subject to heat during summer and heavy constant load during winter, resulting in post curing prior to loading.

3.7 Possibility to improve the methods

Both the methods "European 3535" and "European 4680" use coil springs to maintain the load during the test. This has the obvious effect that the load will be reduced slightly when the samples deform. A more serious effect is caused by the coil spring introducing the force along its periphery. The peripheral load has the double effect that the test samples will not be loaded symmetrically and that the stress pattern of each sample will depend on where along the periphery the force is introduced.

The negative effect of the coil spring loading can possibly be reduced by introducing a centred ball bearing between the spring and the sample. Such a modification could lead to altered test procedures and requirements for the tests.

4 Conclusions and recommendations

The results have shown that both methods European 3535 and European 4680 can differentiate between adhesives with different creep properties. Possibly both methods can in the future be used in approval of PU adhesives for structural purposes.

The tests with European 4680 show large variations in results of the same 1 component PU adhesive type, both between individual test samples as well as between different batches. Similar variations are likely to influence also results of the European 3535 test method. The effects of such variations on the testing and approval procedure need to be evaluated.

4.1 Conclusions regarding the European 3535 method

The European 3535 method gives a fail / pass test result within an eight weeks period after production of test samples. The test result depends on time to failure for the weakest of 72 gluline surfaces. The complicated sample design and non centred load application makes the method sensitive to variations in sample production and orientation of the coil springs.

Since climatic load, mechanical load and test requirements are closely linked in the test procedure, it is difficult to re-evaluate earlier tests results as new knowledge is made available.

As of today no tests have been made to determine proper requirement levels for the European 3535 method. Neither has it been possible to calculate suitable requirement levels based on Eurocode 5 due to the complexity of the test sample, the not centred load application and the mixed climates in the test. This has had the effect that the suggested requirements for European 3535 lack both experimental and theoretical foundation and would, if implemented, lead to the disqualification of already established adhesive systems.

Additional comparative tests between the European 3535 method and alternative long term duration of load tests are needed in order to establish proper requirements.

4.2 Conclusions regarding the European 4680 method

The European 4680 method follows established principles for determination of duration of load and creep factors. The European 4680 method predicts the shear stress level corresponding to 10000 h time to failure for samples tested at constant climate 50 °C / 75 % RH. In addition to this, the method determines that the samples show acceptable time to failure at 80 °C and 3 N/mm^2 shear stress level.

The method separates the effects of climate, shear stress level and time. The European 4680 method produces numerical data that can be used to pass or fail an adhesive as well as determine and compare properties of different adhesives. The data provided by the European 4680 method can be re-evaluated when new knowledge is made available. The suggested test procedure and the requirements for the European 4680 method are supported by Eurocode 5.

The test results indicate that the European 4680 method can measure creep properties of adhesives. The method has shown a large variation in times to failure between samples tested at the same shear stress level. This can be influenced by variations in gluline properties, but can also be influenced by the sensitivity of the method to irregularities in specimen geometry and application of the load from the coil spring. The test procedure could be improved if the load would be introduced to the centre of the gluline.

The method can as it is designed today be implemented as a European test method. Further tests incorporating comparative tests with the European 4680 method and long term duration of load tests of full size structural members could later be used to adjust requirements levels.

5 Acknowledgements

We wish to express our gratitude to the Swedish Wood Association for supporting this research project.

6 References

[1] American standard ASTM D 3535 - 92. Standard test method for resistance to deformation under static loading for structural wood laminating adhesives used under exterior (wet use) exposure conditions.
[2] American standard ASTM D 4680 - 92. Standard test method for creep and time to failure of adhesives in static shear by compression loading (wood-to-wood).
[3] European standard draft ENV 1156 Wood based panels- Determination of duration of load and creep factors. CEN/TC112/WG4, 1996.
[4] Johansson, Carl-Johan: Stress level for creep rupture test of adhesive bonds according to ASTM 4680. 3rd draft. SP, Borås, 2002.
[5] Källander, Björn: test climates for creep testing. SP, Borås, 2000
[6] Källander, B., Kemmsies, M., Johansson, C.-J.: ASTM D4680 - 92 Standard test method for creep and time-to-failure of adhesives in static shear by compression loading - Experience using the method on 3 adhesives. SP, Borås, 2000.
[7] Lind, Per: ASTM D 3535- 90 - NTI version. Proposal for test cycle and test method when using the standard's test jig and test piece. NTI, Oslo, 2000.
[8] Lind, Per: NTI modified ASTM-D3535. NTI, Oslo, 2000.
[9] Riberholt, Hilmer: Stress level for long term testing of gluelines in glulam. 1999.
[10] Rothkopf, Claus: Results of comparative tests with ASTM 3535 mod. between NTI und FMPA. FMPA, Stuttgart, 2002.
[11] Serrano, Erik: A preliminary study on the linear elastic stress distribution of the ASTM-D3535-like specimen. Lund University, 2001.
[12] Serrano, Erik: On the mechanical behaviour of test specimens for wood-adhesive bonds. Lund University, 2002.

CIB-W18/35-18-1

**INTERNATIONAL COUNCIL FOR RESEARCH AND INNOVATION
IN BUILDING AND CONSTRUCTION**

WORKING COMMISSION W18 - TIMBER STRUCTURES

CREEP TESTING WOOD ADHESIVES FOR STRUCTURAL USE

B Källander
C Bengtsson

SP Swedish National Testing and Research Institute, Wood Materials and Structures

SWEDEN

Presented by: C Bengtsson

S Aicher challenged the authors' recommendation that the 4680 rather than the 3535 test procedures be adopted as the European standard practice for glue testing. The challenge is based on the assertion that the test time to failure obtained ranged from values around 200 to over 10000 hours. Additionally, S Aicher was of the view that the study is not sufficiently detailed or complete to justify the recommendations made. C Bengtsson replied that the authors are not dismissing the 3535 approach completely but the method is only able to differentiate between glues with very different strengths and does not provide data beyond a pass-fail conclusion. C Bengtsson acknowledged that further testing, especially with large or full scale specimens, may well provide data which are able to differentiate and/or confirm the advantages of the two approaches, however until such data is available, C Bengtsson is of the view that the 4680 approach is more sophisticated and should be adopted as the standard European glue testing method.

Creep testing wood adhesives for structural use

Björn Källander and Charlotte Bengtsson
SP Swedish National Testing and Research Institute, Wood Materials and Structures, Sweden

1 Introduction and background

Lack of approval procedures for adhesives is hampering the development of wood products. There is an urgent need for fast and reliable approval procedures for new wood adhesive types, new gluing processes and new glued wood based products. SP is conducting research on test procedures to determine creep properties of wood adhesives for structural purposes. The research has been aimed at developing fast and reliable methods for approval of structural adhesives. The work is carried out within the framework of CEN / TC193 / SC1 / WG4 with financial support from the Swedish Wood Association.

Existing test methods for adhesives for structural use have been developed for aminoplastic and phenolic adhesives such as Phenol Resorcinol Formaldehyde (PRF) and Urea Formaldehyde (UF). These adhesives show very little or no creep and hence no test procedures for creep deformation or creep rupture testing of structural wood adhesives have been established. New adhesives such as PolyUrethane (PU) and Emulsified Polymer Isocyanates (EPI) show certain creep tendencies. In order to approve such adhesives, the amount of creep must be determined and related to demands of the finished products.

As for all accelerated test methods, it is crucial that the developed test methods reflect the expected failure modes in the climates that the glued structure will meet in practice. An important aspect regarding creep is the glass transition temperature of the adhesive. An accelerated test at high temperature and moisture could result in failures that never would occur at lower temperatures. There is also the question of whether a test for wood, adhesive or glulines is developed. The combined effects of temperature and moisture on the adhesive as well as the wood properties will limit the possibilities to accelerate creep tests if failure modes are to maintain unaltered.

A serious difficulty regarding accelerated creep test methods for adhesives is the question on how to set the requirements for the tests. Without long term experience of the actual adhesive types in real practice, we need to establish initial requirements based on theoretical assumptions. SP suggests that such initial requirements should be based on the load levels, climates and time spans set in Eurocode 5.

Although the developed test methods should be as fast and cheap as possible in order to simplify the introduction of new products, it is crucial that the developed test methods produce safe and reliable results. One important aspect is then that the limited experience of the test methods and the lack of established requirements make it important that the test methods produce results that can be re-evaluated when new experience is gathered.

2 Experimental work and theoretical studies

The study has been focused on two test methods based on the American standards ASTM D 3535 and ASTM D 4680 [1,2]. The primary aims of the study have been to determine if the two methods are capable of separating adhesives with different creep properties and to determine the suitability of the methods for evaluation of adhesives for structural purposes.

Results from tests with the two methods have been compared to results from a reference test method developed at SP.

In addition to the experimental work, FE analysis of the stress patterns in the test samples used have been made by Lund University [11,12] and calculations of test climates and of requirement levels based on Eurocode 5 have been made at SP [4,5].

2.1 Adhesives in test

The research projects at SP have primarily been using six different adhesives ranging from thermoplastic PVA to PRF with virtually no measurable creep in the glulines, see Table 1.

Table 1. Adhesives used in tests at SP.

Adhesive	Adhesive class	Comment
PVA D4	EN 204 class D4 exterior surface coated	Two component, thermoplastic, not for structural applications.
PU 1	EN 301 Type II ASTM D 2559-99 Exterior use	30 min curing one component PU adhesive
PU 2	EN 301 Type II ASTM D 2559-99 Exterior use	3 h curing one component PU adhesive
EPI	EN 204 class D4, exterior surface coated JAS 111	Adhesive type used for structural applications in Japan, but as of today not approved for structural applications in Europe.
MUF	EN 301 Type II	
PRF	EN 301 Type I	

2.2 Test methods studied

Two of the methods studied are based on the American standards ASTM D 3535 - 92 and ASTM D 4680 - 92, using samples subjected to compression shear at constant spring loading [1,2]. The "European 3535" is developed by Norwegian Institute of Wood Technology (NTI) and the "European 4680" by SP [6,7,8]. The third method developed by SP uses test samples similar to European standard EN 302-1 subjected to constant tensile shear load by cantilevers.

All the three test methods studied have primarily been aimed at determining the time to failure at constant load rather than creep deformation, even though deformation has been measured for all three methods. The research project has only covered short and medium term tests of small samples. Correlated long term creep tests of full size specimens are recommended.

2.2.1 Description of the European 3535 test method

The European 3535 uses an identical test rig as ASTM D 3535 but smaller test samples, see Figure 1. The test sample of European 3535 differs from the sample of ASTM D 3535 as the size has been reduced from thirty to twelve 12.5 x 50 mm glulines. The European 3535 sample is symmetrical, with plane surfaces in both ends.

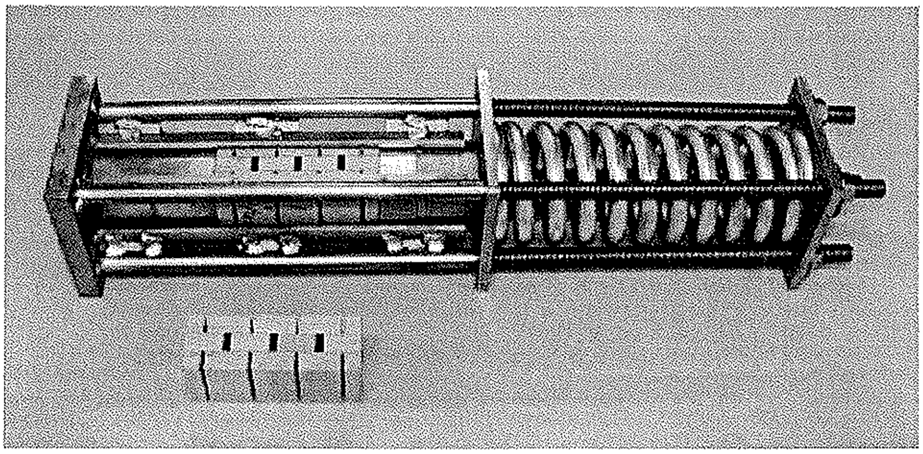

Figure 1. Test rig and sample for European 3535 test. Sample size 50 x 50 x 135 mm.

Six replicates are tested with each adhesive. Each sample is inserted into the rig, a compression load corresponding to 3 N/mm^2 shear stress is applied by a universal testing machine and the nuts on the rig are tightened to maintain spring compression.

The shear stress level used in European 3535 has been chosen by NTI after several pilot tests at various shear stress levels [7,8]. The 3 N/mm^2 shear stress level was chosen in order to result in failures within the six weeks test period to separate different adhesives, without unacceptable deformations or failures in the wood. The 3 N/mm^2 shear stress level is also in part supported by theoretical calculations [9].

After the load is applied, the rig is placed in a climatic chamber and stored for six weeks in a series of climates:

Table 2. Climate series used in European 3535. The proposed sequence of test climates has been altered after the tests at SP.

Climate	Climates series used in tests at SP	New proposed climate series
1	14 days at 80 °C / 10-15 % RH	14 days at 80 °C / 10-15 % RH
2	14 days at 50 °C / 75 % RH	14 days at 20 °C / 85 % RH
3	14 days at 20 °C / 85 % RH	14 days at 50 °C / 75 % RH

The rigs are removed after the six weeks period. In order to pass the test, no gluline in any of the six samples are allowed to fail.

2.2.2 Description of the European 4680 test method

The European version of ASTM D 4680 has been developed by SP. The method follows established principles used for determination of duration of load factors for solid wood and wood based panels [3].

The European 4680 method is primarily a creep rupture test method although deformation can be measured. It fairly closely resembles the American original. The most important modifications are:

1) the two test climates used,
2) prediction of shear stress level corresponding to 10000 h failure time is based on median time to failure at each stress level rather than on individual tested samples.

The test sample and test rig in European 4680 are identical to the American ASTM D 4680, with the exception that the test surface of the sample is 25x25 mm instead of 1x1", see Figure 2.

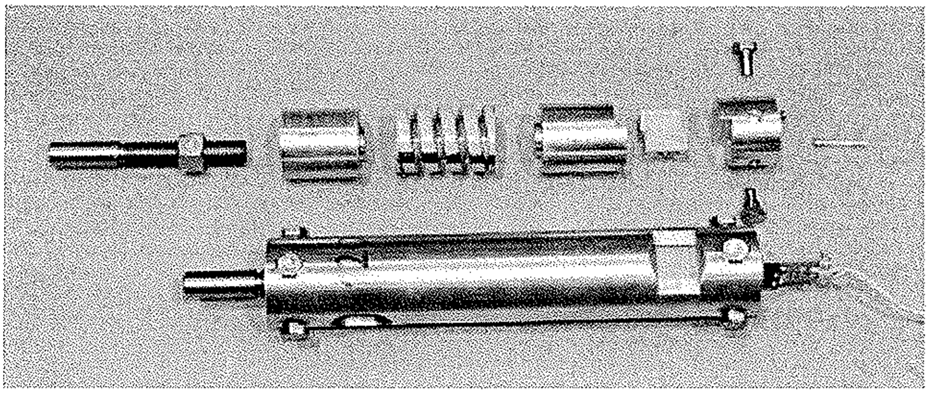

Figure 2. Test rig and sample for European 4680 test. Shear test surface 25 mm x 25 mm.

Two test climates are used: 50 °C / 75 % RH and 80 °C / dry (10-15 % RH, not controlled). The choice of climates is based on the climates and requirements defined in Eurocode 5 and the definition of adhesives of Type I and Type II in EN 301 [5,6].

50 °C / 75 % RH is an extreme climate for timber structures. The temperature may occur in the vicinity of the wood members in a roof structure due to absorption of heat from sun radiation. The duration is likely to be less than 12 hours for each occasion. The combination 50 °C / 75 % RH can normally not occur. Additional moisture is required; conditions which might occur in for instance process industries.

80°C / dry is a climate or temperature which is not likely to occur except for in very special application and situation and with short duration. A climate of this nature is not likely to affect the adhesive bond line only, but also the wood itself with increased creep and reduced strength. It is for instance a temperature that will occur during fire close to the charring zone.

At 80 °C the test samples are loaded at 3 N/mm^2. The stress levels at 50 °C / 75 % RH are chosen to be as high as possible without leading to high proportions of wood failure, as will be described in Section 3.5.

Ten test samples are loaded at each climate and shear stress level, which gives a total of 50 samples for each adhesive tested. In addition to this, short term shear strength is determined according to the ASTM D 905 method. Time to failure is recorded for each sample and median time to failure is calculated at each shear stress level.

The load corresponding to 10000 h median time to failure at 50 °C / 75 % RH is calculated based on the median time to failure at each shear stress level, see Figure 3.

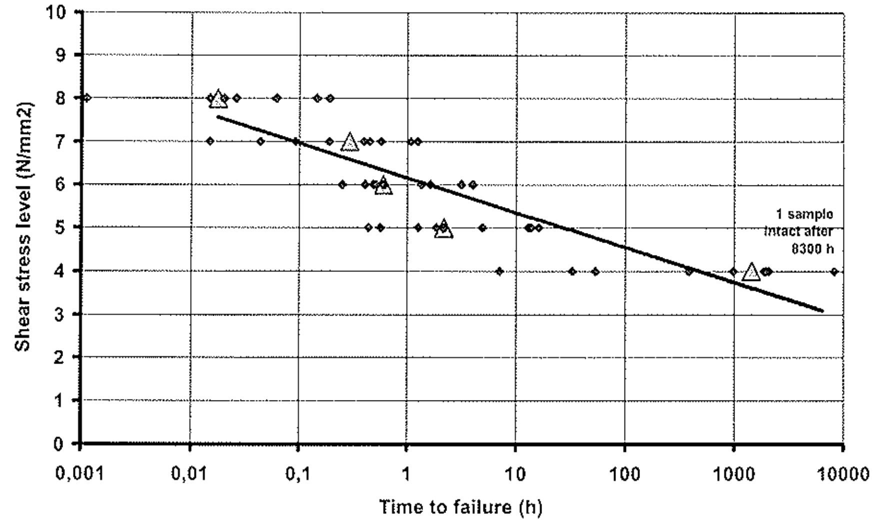

Figure 3. Prediction of shear stress at 50 °C / 75 % RH corresponding to 10000 h time to failure is based on median time to failure at each load level. Triangles mark median time to failure at each shear stress level.

The two suggested requirements used in European 4680; 10000 h predicted time to failure in 50 °C / 75 % RH and 1 000 h median time to failure in 80 °C / dry at 3 N/mm^2 shear stress have been set after calculations based on Eurocode 5 [4].

2.2.3 Description of the SP cantilever method

The SP cantilever method was developed at SP to be used as a reference test method to the European 3535 and European 4680 methods. By using a cantilever system and applying tension shear stress, a constant and fairly well defined stress is applied to the samples, see Figure 4.

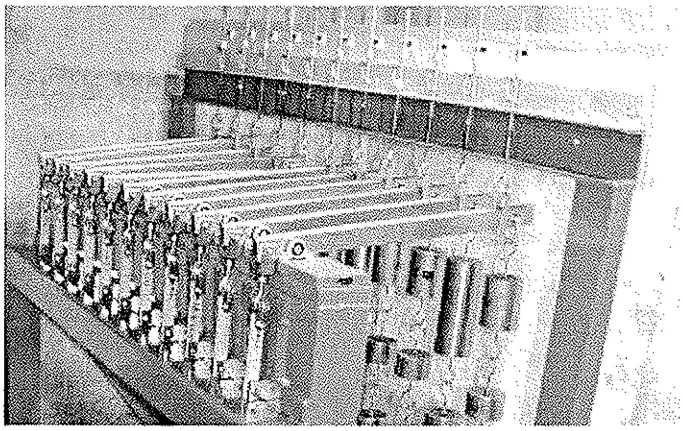

Figure 4. SP cantilever rig. EN 302 samples subjected to constant tensile load. When a sample fails, the cantilever is caught by a damping device designed to carry the weights and to reduce the impact shock to other samples.

The SP cantilever method uses the test sample described in European standard EN 302-1. Two 10.5 mm holes are drilled in the sample and a mark is inscribed across the gluline by a needle for measuring deformation.

Time to failure is recorded by timers attached to the damping device of each cantilever. Deformation is measured by means of a digital camera with high resolution for selected samples. Tests have presently only been made in the climate 20 °C / 65 % RH.

2.3 FE calculations

Numerical finite element studies have been carried out on the three methods studied. The studies have been focused on the sensitivity of the test methods to geometrical imperfections of the test samples and the not centred load caused by the coil spring [11,12].

The FE calculations have been made with non linear material description of the behaviour of the bond line and adhesive properties ranging from brittle to ductile adhesives. The ongoing FE studies are made by Lund University on behalf of SP.

3 Experimental results and discussion

3.1 European 3535

The production of test samples for European 3535 requires extremely high precision in order to guarantee that the tested glulines have equal size. Also very small variations in positioning of the milling tools during the cutting of the samples will lead to differently sized gluline surfaces and resulting stress variations. Such differences are serious since the method is measuring the time to failure of the weakest tested gluline surface.

The 3535 tests performed at SP have lead to very short times to failure for PVA and PU adhesives tested. All tested samples but one failed during the first climate, 80 °C. No failures have been recorded in PRF, MUF or EPI adhesives.
The very short times to failure make it difficult to differentiate between adhesives with "little creep" and "a little more creep". However, it is obvious that the method separates adhesives with creep tendency and adhesives with no creep tendency. The very fast failures could also indicate that the suggested load in the test, 3 N/mm^2, leads to a very severe test.

3.1.1 Comments to the European 3535 method

The European version of ASTM D 3535 differs from the American original as it uses a smaller test sample, a higher shear stress load level and a longer test period comprising of three different climates in series. The European test method is performed on beech samples rather than the species actually used industrially.

The modifications of the original ASTM D 3535 have in reality turned the test method from a "creep deformation" to a "creep rupture" test method. The two separate test climates used in ASTM D 3535 have in European 3535 been turned into a sequence of three climates. The modifications of the test procedure makes it difficult to apply experience gathered from the ASTM D 3535 method to the results of European 3535.

The primary advantage of the European 3535 method is that it is fairly rapid as the results are obtained within 8 weeks after production of the test samples. The primary drawbacks are that the method only gives a pass/fail answer and that we today lack experience from comparative tests of the European 3535 method and long term tests of full size members. Lacking such experience, it is difficult to set requirements for the test. Since the European

3535 method is a pass/fail test and does not differentiate between the effects of shear stress load and climate load, it could be difficult to re-evaluate existing test results if the test procedure or requirements were to be modified when new experience is gathered.

3.2 European 4680

The results show that the European 4680 method is capable of separating adhesives also with relatively similar creep tendencies.

The results of the duration of load tests at 3 N/mm^2 and 80 °C have been completed with all tested adhesives. Of the six adhesive types tested, only PVA, PU1 and PU2 show failures. No failures had been recorded for PRF, MUF or EPI adhesives when the test was terminated after 10100 h. Median time to failure for the PVA D4 samples was 46 minutes, as compared to the suggested requirement 1000 h. Median time to failure for PU1 and PU2 was 2269 h and 1891 h respectively.

The results of tests in climate 50 °C / 75 % RH have so far been completed for PVA D4, PU1 and PU2 adhesives. The results show a large variation in time to failure between samples at the same load level, see Figure 5.

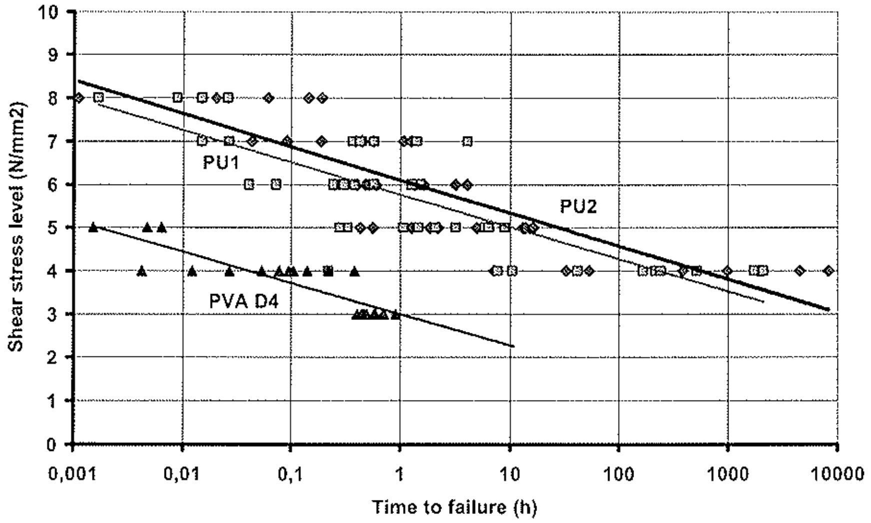

Figure 5. Predicted load corresponding to 10000 h median time to failure is calculated from the median time to failure in the test. The figure shows results from tests with two 1k PU adhesives and one PVA D4 adhesive.

3.2.1 Repeatability

Results from repeated tests with samples of the same adhesive glued at separate occasions show different shear strength level but similar "slope" of the time to failure / shear stress - regression lines, see Figures 6 and 7.

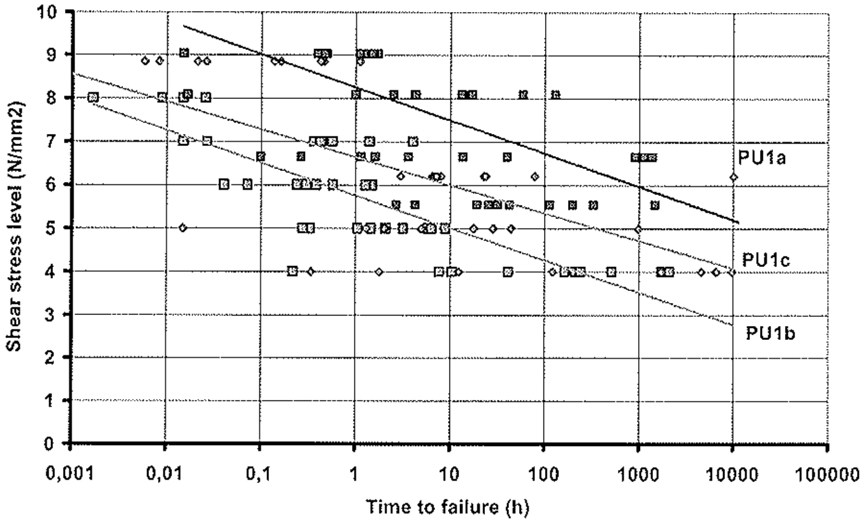

Figure 6. Results of repeated tests with the same type of adhesive indicate that the results are greatly influenced by variations in initial gluline shear strength. The slope of the shear stress / time to failure regression line is relatively constant which could indicate that the test truly reflects the creep properties of the adhesive.

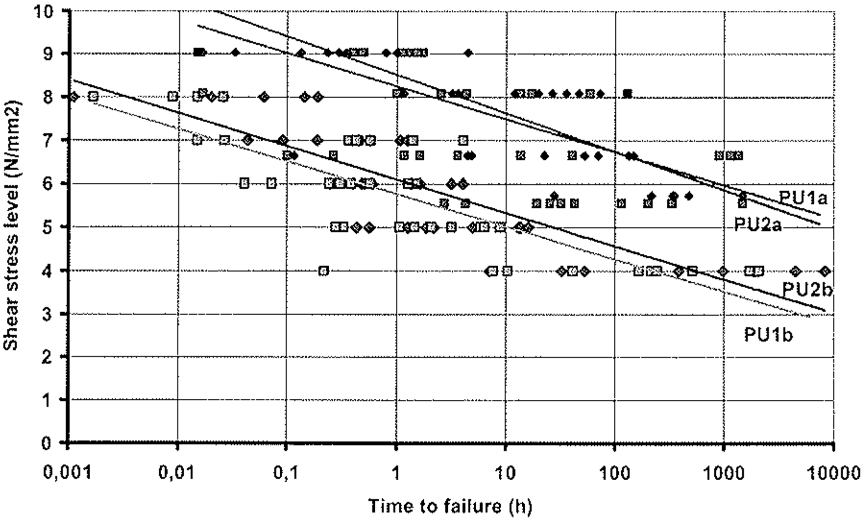

Figure 7. Results of repeated tests with two adhesives with samples glued at two different occasions. The initial gluline strength varies between gluing occasions but not between the two adhesive types.

The test results show that the initial shear strength of the glulines vary between different production batches of test samples. If this is caused by variations in properties between different adhesive batches, different wood properties or variations in the gluing process is not determined.

The similar "slope" of the regression curve of time to failure / load indicate that the time dependent reduction of failure load is independent of the initial shear strength. The results indicate that the test method measures actual creep properties of the test adhesives.

3.2.2 Variation between samples

The test results have shown a large variation in time to failure for different samples tested at the same shear stress level. The median time to failure at each shear stress level can thus differ considerably from the average time to failure. In the tests performed, this has had the effect that the predicted shear stress corresponding to 10000 h failure time is reduced significantly if the prediction is based on median time to failure (as in European 4680) rather than all measured values (as in ASTM D 4680), see Figure 8.

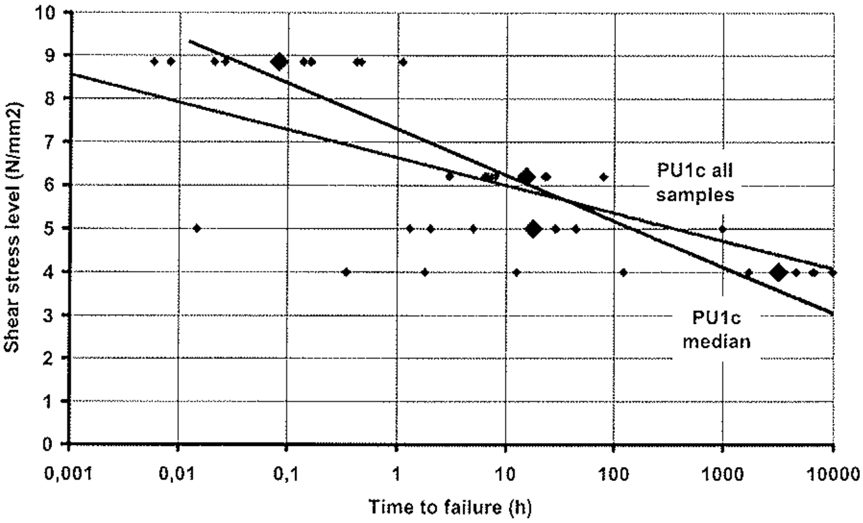

Figure 8. Predicted shear stress corresponding to 10000 h failure time will be lower if the prediction is based on median times to failure rather than on all samples.

3.2.3 Very good adhesives cause problems

The European 4680 test procedure is based on prediction of the shear stress level corresponding to 10000 h time to failure based on time to failure at higher shear stress levels. If the adhesive does not show creep related failures even at these higher shear stress levels, no data for the prediction are available. Hence a very good adhesive will not suit the test procedure. The problem can be solved by establishing a limit for the minimum median time to failure at each shear stress level.

3.3 SP cantilever method

Tests results are presently available from tests with PVA D4, PU1, PU2. The results show great similarities with the tests made according to European 4680, see Figure 9.

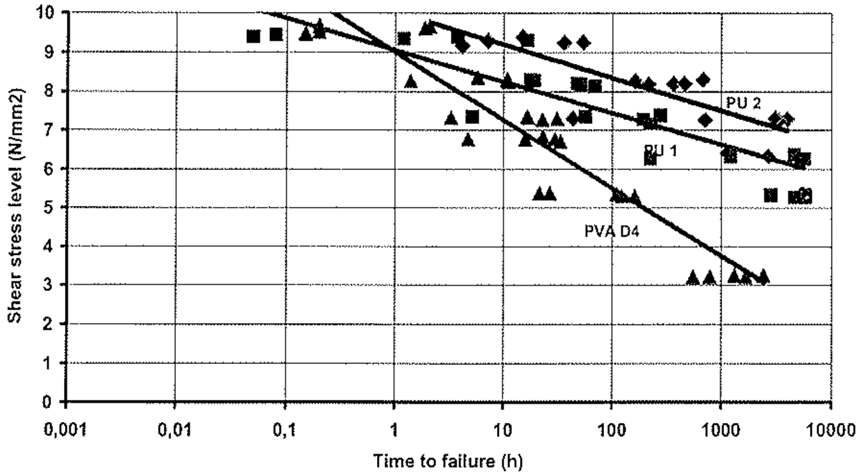

Figure 9. Results from tests of PU1, PU2 and PVA adhesive in SP cantilever rig. Failed samples marked with filled symbols. Intact samples marked with frames.

The SP cantilever test separates adhesives in same way as 4680 in spite of the different stress pattern, which indicates that both methods reflect the same adhesive properties.

3.4 FE calculations

The FE simulations of all three methods have shown that the mechanical behaviour in terms of estimated bond line strength, i.e. load bearing capacity of the test sample is highly dependent not only on the properties of the adhesive, but also on the specimen and loading geometry.

The FE simulations show that the load bearing capacity of the European 3535 test sample is seriously affected by the non centred force caused by the large diameter of the coil spring. Significant deformations of the test sample with resulting stress concentrations and tensile stresses will occur if the force is applied perpendicularly to the glulines, se Figure 10.

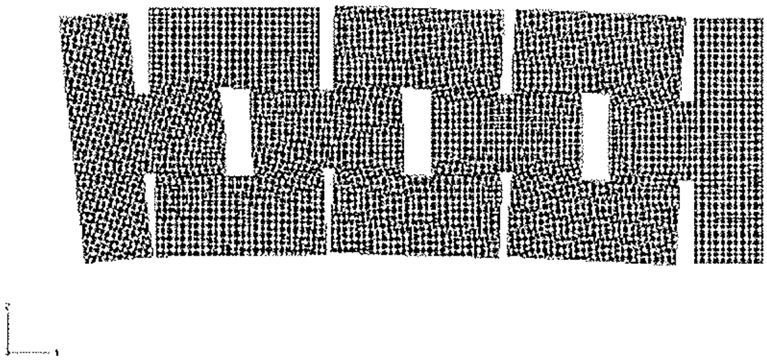

Figure 10. The deformation of eccentric loaded European 3535 specimen, load of 1250 N at 5 mm off-centre. The deformations are magnified by a factor 10. From [11].

If, on the other hand, the force is applied parallel to the glulines, a torsion factor to the gluline stresses is introduced. The simulations indicate that the load bearing capacity can vary as much as 25 % depending on where along the spring periphery the force is applied.

Also the simulations of the European 4680 method have shown that the test results are influenced by how the force is applied to the specimen. If the surfaces where the force is applied are non parallel or if the force is applied at a distance from the gluline, the load bearing capacity of the sample is reduced. On the other hand, friction between the loading device and the sample as well as within the gluline can increase the failure load.

The simulations of the EN 302 - 1 test sample in the cantilever system show the test sample deforming as the load is applied, resulting in tensile stresses perpendicularly to the gluline in addition to the shear stresses.

3.5 Maximum shear stress in a creep test for beech wood samples

The test results from the SP cantilever method show that the wood failure proportion increase with increased shear stress, see Figure 11.

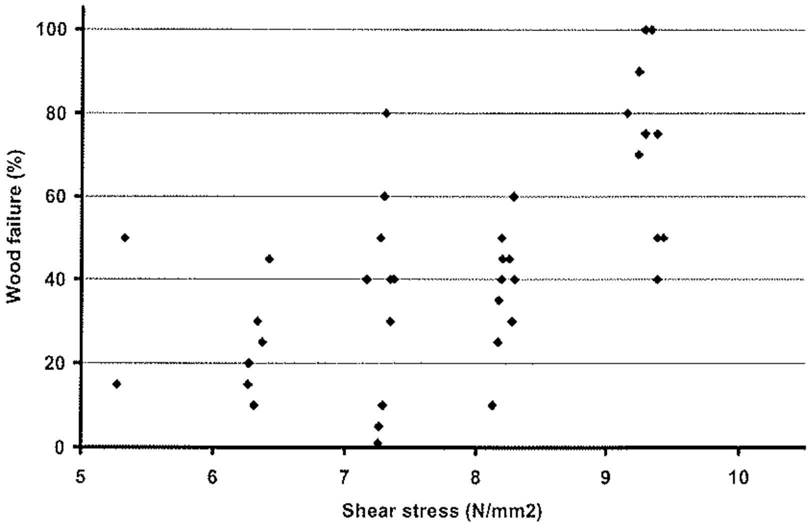

Figure 11. Wood failure increase as load is increased in SP cantilever tests of PU1 and PU2. A high wood failure proportion indicates that the wood rather than the adhesive has failed.

The results seem to indicate that the maximum suitable shear stress level on smaller samples tested at 20 °C is 8 - 9 N/mm^2. If a higher shear stress is applied, the test will actually test the wood rather than the adhesive.

A sample that fails with a high percentage of wood failure indicates that the adhesive would have been able to carry the load for a longer period than the wood. In a short term test, this is usually considered acceptable, the adhesive is "stronger" than the wood. However this is not the case if the result is to be used in predicting the creep behaviour of the adhesive. The wood failure results in a "too quick" failure at high shear stress levels, which in turn reduces the slope of the regression line based on the median times to failure. Hence, the predicted load corresponding to 10000 h median failure time will be too high.

3.6 Effect of post curing

One important aspect of the suggested test procedures in European 3535 and European 4680 is if the samples are heated prior to the application of the load or not. Heating prior to loading can have the effect that post curing adhesives would show a better test result than if the load is applied to a cold sample. Improved performance by 1k PU adhesives has been shown by tests at FMPA with the European 3535 method where samples that had been treated in 80 °C passed the test and samples stored at 20 °C / 65 % RH failed [10]. The mechanisms leading to this effect in 1K PU glulines have not yet been identified.

In the suggested test procedure for the European 3535 method, the load is applied prior to heating. The procedure prevents post curing before the load is applied. In the suggested test procedure of the European 4680 method, the samples are heated to the test temperature prior to the load being applied, and thus post curing can take place. This is done in order to guarantee that the load is not changed as the aluminium tube and steel spring are heated.

It has to be determined what procedure is best suited for a creep test at elevated temperature. Application of the load prior to heating could lead to a test "on the safe side", if the load after heating is the same as before heating. It could also be argued that a large structure most likely will be subject to heat during summer and heavy constant load during winter, resulting in post curing prior to loading.

3.7 Possibility to improve the methods

Both the methods "European 3535" and "European 4680" use coil springs to maintain the load during the test. This has the obvious effect that the load will be reduced slightly when the samples deform. A more serious effect is caused by the coil spring introducing the force along its periphery. The peripheral load has the double effect that the test samples will not be loaded symmetrically and that the stress pattern of each sample will depend on where along the periphery the force is introduced.

The negative effect of the coil spring loading can possibly be reduced by introducing a centred ball bearing between the spring and the sample. Such a modification could lead to altered test procedures and requirements for the tests.

4 Conclusions and recommendations

The results have shown that both methods European 3535 and European 4680 can differentiate between adhesives with different creep properties. Possibly both methods can in the future be used in approval of PU adhesives for structural purposes.

The tests with European 4680 show large variations in results of the same 1 component PU adhesive type, both between individual test samples as well as between different batches. Similar variations are likely to influence also results of the European 3535 test method. The effects of such variations on the testing and approval procedure need to be evaluated.

4.1 Conclusions regarding the European 3535 method

The European 3535 method gives a fail / pass test result within an eight weeks period after production of test samples. The test result depends on time to failure for the weakest of 72 gluline surfaces. The complicated sample design and non centred load application makes the method sensitive to variations in sample production and orientation of the coil springs.

Since climatic load, mechanical load and test requirements are closely linked in the test procedure, it is difficult to re-evaluate earlier tests results as new knowledge is made available.

As of today no tests have been made to determine proper requirement levels for the European 3535 method. Neither has it been possible to calculate suitable requirement levels based on Eurocode 5 due to the complexity of the test sample, the not centred load application and the mixed climates in the test. This has had the effect that the suggested requirements for European 3535 lack both experimental and theoretical foundation and would, if implemented, lead to the disqualification of already established adhesive systems.

Additional comparative tests between the European 3535 method and alternative long term duration of load tests are needed in order to establish proper requirements.

4.2 Conclusions regarding the European 4680 method

The European 4680 method follows established principles for determination of duration of load and creep factors. The European 4680 method predicts the shear stress level corresponding to 10000 h time to failure for samples tested at constant climate 50 °C / 75 % RH. In addition to this, the method determines that the samples show acceptable time to failure at 80 °C and 3 N/mm^2 shear stress level.

The method separates the effects of climate, shear stress level and time. The European 4680 method produces numerical data that can be used to pass or fail an adhesive as well as determine and compare properties of different adhesives. The data provided by the European 4680 method can be re-evaluated when new knowledge is made available. The suggested test procedure and the requirements for the European 4680 method are supported by Eurocode 5.

The test results indicate that the European 4680 method can measure creep properties of adhesives. The method has shown a large variation in times to failure between samples tested at the same shear stress level. This can be influenced by variations in gluline properties, but can also be influenced by the sensitivity of the method to irregularities in specimen geometry and application of the load from the coil spring. The test procedure could be improved if the load would be introduced to the centre of the gluline.

The method can as it is designed today be implemented as a European test method. Further tests incorporating comparative tests with the European 4680 method and long term duration of load tests of full size structural members could later be used to adjust requirements levels.

5 Acknowledgements

We wish to express our gratitude to the Swedish Wood Association for supporting this research project.

6 References

[1] American standard ASTM D 3535 - 92. Standard test method for resistance to deformation under static loading for structural wood laminating adhesives used under exterior (wet use) exposure conditions.
[2] American standard ASTM D 4680 - 92. Standard test method for creep and time to failure of adhesives in static shear by compression loading (wood-to-wood).
[3] European standard draft ENV 1156 Wood based panels- Determination of duration of load and creep factors. CEN/TC112/WG4, 1996.
[4] Johansson, Carl-Johan: Stress level for creep rupture test of adhesive bonds according to ASTM 4680. 3rd draft. SP, Borås, 2002.
[5] Källander, Björn: test climates for creep testing. SP, Borås, 2000
[6] Källander, B., Kemmsies, M., Johansson, C.-J.: ASTM D4690 - 92 Standard test method for creep and time-to-failure of adhesives in static shear by compression loading - Experience using the method on 3 adhesives. SP, Borås, 2000.
[7] Lind, Per: ASTM D 3535- 90 - NTI version. Proposal for test cycle and test method when using the standard's test jig and test piece. NTI, Oslo, 2000.
[8] Lind, Per: NTI modified ASTM-D3535. NTI, Oslo, 2000.
[9] Riberholt, Hilmer: Stress level for long term testing of gluelines in glulam. 1999.
[10] Rothkopf, Claus: Results of comparative tests with ASTM 3535 mod. between NTI und FMPA. FMPA, Stuttgart, 2002.
[11] Serrano, Erik: A preliminary study on the linear elastic stress distribution of the ASTM-D3535-like specimen. Lund University, 2001.
[12] Serrano, Erik: On the mechanical behaviour of test specimens for wood-adhesive bonds. Lund University, 2002.

CIB-W18/35-21-1

INTERNATIONAL COUNCIL FOR RESEARCH AND INNOVATION IN BUILDING AND CONSTRUCTION

WORKING COMMISSION W18 - TIMBER STRUCTURES

FULL-SCALE EDGEWISE SHEAR TESTS FOR LAMINATED VENEER LUMBER

B Yeh
T G Williamson

APA - The Engineered Wood Association

U.S.A.

Presented by: B Yeh

H J Blaß asked if the author has also tested glulam beams in the same manner as that presented for LVL and if so, how the values compared. B Yeh replied that similar tests were conducted on glulam beams a year ago and that in general the shear strength values for LVL are higher than those for glulam beam. B Yeh felt that the reason for this is the higher volume of glue in the LVL and that the ply in the LVL has been densified.

Full-Scale Edgewise Shear Tests for Laminated Veneer Lumber

Borjen Yeh, Ph.D., P.E.
Thomas G. Williamson, P.E.
APA - The Engineered Wood Association, U.S.A.

Abstract

The shear strength of laminated veneer lumber (LVL) has traditionally been determined based on the results of small block shear tests conducted in accordance with ASTM D 143 [1]. In recent years, there has been a significant interest in determining the shear strength of engineered wood products using full-scale bending test methods [2,3,4,5,6] in lieu of small block shear tests. However, due primarily to different shear-to-bending strength ratios among a variety of engineered wood products, the use of a prismatic cross section and test setup similar to those adopted for full-scale shear tests of glulam [6] does not normally produce an acceptable shear failure rate in the edgewise or joist orientation (loads are applied parallel to gluelines), as required for LVL. Therefore, special considerations should be given to the test setup and specimen configuration for LVL edgewise shear tests.

This paper describes the development of shear test methods for both LVL edgewise full-scale and small-scale tests. The full-scale test method can be used for product qualification of the LVL shear strength and the small-scale test method can be used as an in-plant quality assurance tool to monitor the LVL shear strength on an on-going basis. A noticeable size effect is discussed. The moisture effect on the full-scale LVL edgewise shear specimens is also presented.

1. Introduction

Laminated veneer lumber (LVL) has been used in North American for more than 30 years as both flanges for I-joists and as beams and headers. With improved technology in veneer grading, adhesives, and machining, LVL is known for its excellent load-carrying capacities and consistent quality. Since the grade and quality of each individual layer of veneers can be closely controlled in the LVL manufacturing processes, the variability in product properties is typically much lower than that of sawn lumber. Due to its manufacturing processes, LVL can be customized to a wide variety of widths, thickness, and lengths. Most importantly, the end (scarf or lap) joints between adjacent veneer layers can be staggered to minimize the strength reducing effect of those joints on the bending and tensile strengths of LVL.

In North America, the design stress for LVL is traditionally determined based on the procedures set forth in ASTM D 5456 [7] using ASTM D 143 [1] small block shear specimens with a shear area of only 2581 mm^2 (4 $in.^2$). In recent years, there have been significant interests in determining the shear strength of engineered wood products using full-scale bending test methods [2,3,4,5,6]. A review of various full-scale shear test methods for engineered wood products has been provided by Lam and Craig [4]. However, due primarily to different shear-to-bending strength ratios among a variety of engineered wood products, the use of a prismatic cross section and test setup similar to those adopted for the full-scale shear tests of glulam [6] does not normally produce an acceptable shear failure rate in the edgewise or joist orientation (see Figure 1), as required for LVL. Therefore, special considerations should be given to the test setup and specimen configuration for full-scale LVL edgewise shear tests.

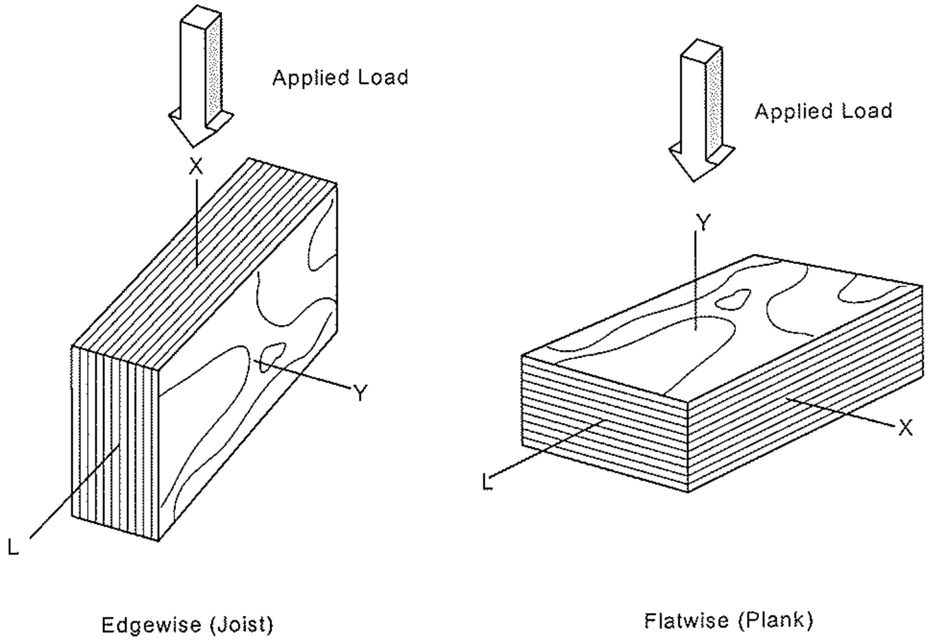

Figure 1. Orientations for LVL

2. Objective

This paper describes the special considerations given to the development of LVL edgewise shear test methods for both full-scale qualification and small-scale quality assurance tests. The size and moisture effects on the full-scale LVL edgewise shear specimens are also presented.

3. Development of Test Methods

It has been reported that it is very difficult to fail LVL in edgewise shear using a prismatic cross section due to the high shear-to-bending strength ratio of the LVL, as compared to other engineered wood products such as glulam [3,4]. One solution to increase the edgewise shear failure rate in full-scale shear tests is to decrease the shear-to-bending strength ratio by either reinforcing the edgewise bending capacity of the LVL or using an I-section. The reinforcement approach, such as by using fiber-reinforced plastics, is considered unfeasible due to the requirement of determining the transformed section and the need for sophisticated specimen preparation processes.

Lam and Craig [4] tested edgewise shear of Douglas-fir LVL, southern pine Parallel Strand Lumber (PSL), and Douglas-fir PSL using I-shaped specimens, as shown in Figure 2. The I-sections were 44 x 184 mm (1-3/4 x 7-1/4 in.) and 44 x 305 mm (1-3/4 x 12 in.), and were prepared by using a router. The specimens were tested using the center-point load as well as five-point load methods. The on-center span was 6 times the specimen depth (6d) for the center-point load method and 5d for the five-point load method. However, as the shear stress induced by the five-point load method at the intermediate reaction can be interfered by the cross-grain stresses, the wood industry in the United States has not considered the five-point load method an appropriate test method for evaluating the edgewise shear strength of glulam and LVL. Therefore, for the purpose of this study, only the LVL test results using the center-point load method are reviewed below.

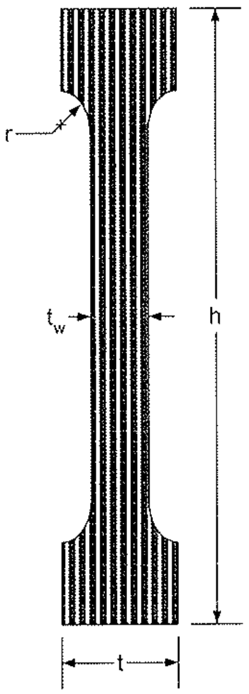

Figure 2. The I-shaped specimen used by Lam and Craig [4] (t = LVL thickness)

The shear failure rate reported by Lam and Craig [4] using the center-point load method was excellent (89 out of 96 specimens or 93%). When compared to the ASTM D 143 block shear test results, the center-point load method yielded a shear strength of 83% on average for the 44 x 184 mm (1-3/4 x 7-1/4 in.) and 73% on average for the 44 x 305 mm (1-3/4 x 12 in.) specimens, indicating a likely size effect.

While the center-point load method has been demonstrated as appropriate for edgewise shear tests, some concerns may be raised on the specimen preparation technique. Among them, the most significant one is that the high-quality face veneers that are normally densified are required to be removed for making the I-section. Therefore, the shear strength obtained from this type of specimens is likely to be conservative. In addition, the router used to prepare the specimens requires multiple passes for deeper specimens, which could be quite time-consuming.

In 1996, APA -The Engineered Wood Association initiated a full-scale LVL edgewise shear test program based on prior experience on full-scale glulam shear tests [6]. In developing the specimen configuration, it was decided through a preliminary study that an I-section, as shown in Figure 3, should be used to ensure a high percentage of shear failure. The flanges of the I-section were cut from materials adjacent to the web and face-glued to the web so that the gluelines for both flanges and web were parallel to each other, resulting in a net flange width of 3 times the web thickness.

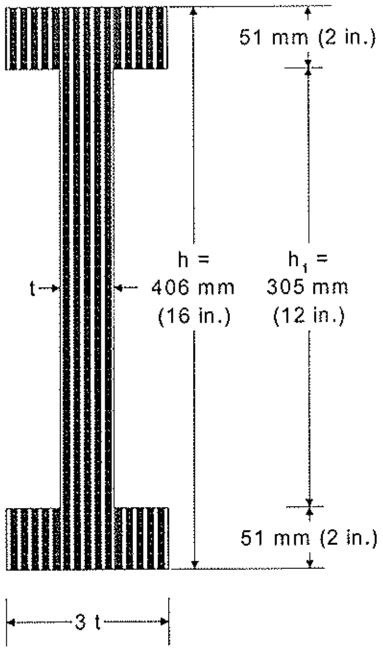

Figure 3. Specimen dimension used in APA full-scale edgewise shear tests (t = LVL thickness)

By selecting the matched flanges and web materials, and orientating the web and flange materials, the moduli of elasticity for the entire I-section could be assumed as the same in the edgewise orientation. As a result, a calculation of the transformed section is not required. Furthermore, this specimen configuration does not require the removal of face veneers and therefore, the shear strength obtained from this specimen configuration reflects the best estimate of the LVL edgewise shear strength.

The specimen size is an important consideration for evaluating the edgewise shear strength of LVL due to the consideration of size effect. Since most LVL products used in light-frame construction in North America are generally limited to 406 mm (16 in.) in depth, this was selected as the specimen depth. The length of the specimen was determined based on prior experience from glulam tests [6]. Specifically, it was considered desirable to use a 4-point load method so that the applied load could be spread over 2 load heads, which were set 152 mm (6 in.) apart, to reduce the likely crushing under the load. In this loading configuration, each load head applied the same load carried by each reaction (bearing plate). In addition, the clear distance between the bearing plate and the nearest load head was maintained at least 2 times the specimen depth to avoid the interference of cross-grain stresses to the shear strength. Figure 4 shows the resulting test setup. It is expected that bending or deflection criteria will govern the design when the span-to depth ratio of the LVL increases. Therefore, the shear strength derived from this specimen configuration represents the near maximum size of the LVL governed by the shear strength in design. This is the same concept used to develop the glulam shear test setup given in Annex A5 of ASTM D 3737 [8].

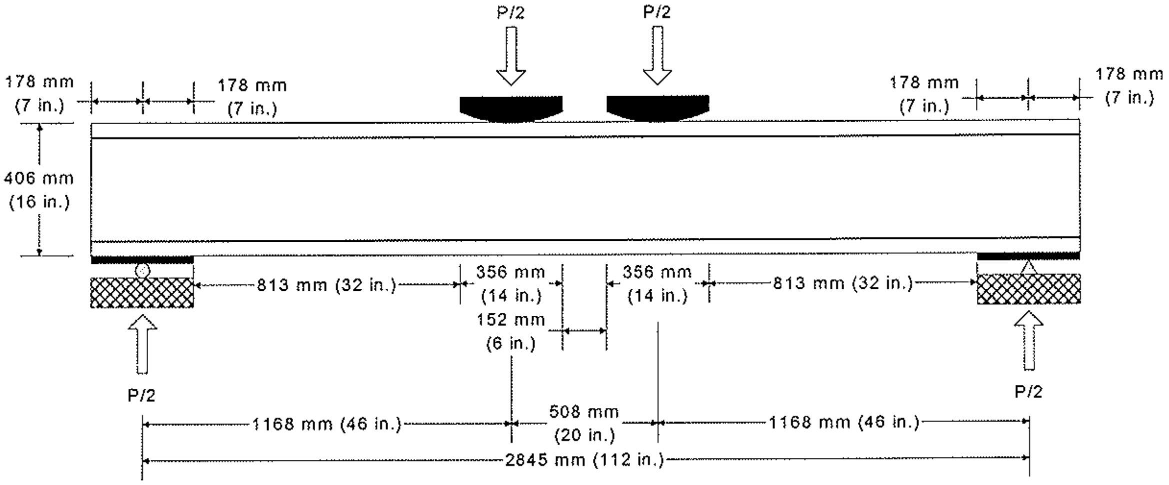

Figure 4. Test setup for LVL edgewise shear tests

The likelihood of shear failure could be estimated using the loading configuration given in Figure 4 if the bending and shear strengths of the LVL can be estimated. For example, if the characteristic bending strength of LVL is 43.4 MPa (6,300 psi) with a COV of 0.15 based on the depth of 305 mm (12 in.) and a volume effect factor of $(h/305)^{(1/8)}$, where h is the LVL depth (mm), the 5th percentile ultimate load required for bending failure using the test setup given in Figure 4 can be estimated as 200 kN (45,000 lbf). If the same LVL has a characteristic shear strength of 1/10 of the characteristic bending strength, but with a COV of 0.10, the 99th percentile ultimate load required for shear failure can be estimated as 177 kN (39,900 lbf). Since the 99th percentile of shear capacity is lower than the 5th percentile of bending capacity, the shear failure rate based on the test setup given in Figure 4 is expected to be 94% or higher. The probability of shear failure will increase with a decreasing shear-to-bending strength ratio. For example, when the shear-to-bending strength ratio is reduced to 1/12 for the example given above, the 99.9th percentile of shear capacity is approximately the same as the 0.4th percentile of the bending capacity, which ensures a near perfect shear failure rate.

To assemble the I-section, a white glue readily available from retail stores was applied to both web and flange faces (double applications). Soon after the application of the white glue, 24 - 8d ring-shank screws (64-mm or 2-1/2-inch long) were applied at 76 mm (3 in.) on center for the outer 457 mm (18 in.) from both ends and both faces. The first screw were located 76 mm (3 in.) from each end. The screws were staggered vertically on both faces to avoid splitting. Additional 28 - 8d ring-shank screws were applied at 152 mm (6 in.) on center for the remaining length on both faces. It should be noted that the main purpose of using those screws was to provide pressures for the white glue to cure. If the glue can be cured by other mechanical or chemical means, the use of those screws is not necessary. Through a preliminary study, it was determined that smooth-shank nails do not provide adequate pressures for the white glue to cure due likely to the effect of stress relaxation.

4. Materials and Methods

Forty-two pieces of 44 mm x 406 mm x 8,230 mm (1-3/4 in. x 16 in. x 27 ft) LVL were sampled by an APA auditor at a commercial LVL plant and shipped to the APA Research Center in Tacoma, Washington for testing. These materials were manufactured with 8 plies of 3.2-mm (1/8-inch) thick Douglas fir Grade 1 veneers and 7 plies of 3.2-mm (1/8-inch) thick Western Hemlock Grade 2 veneers. APA staff witnessed the veneer peeling, sorting, and drying processes, and the LVL manufacturing.

Upon the receipt of those materials, each LVL was cut in half in the lengthwise direction. All materials were then conditioned at the APA Research Center at 65 ± 5% relative humidity and 68 ± 11°F until reaching an equilibrium moisture content. Fifty-four I-shaped specimens were then manufactured at the APA Research Center using matched materials as web and flange sections, as shown in Figure 3. As previously noted, the flange sections were attached to the web sections using a commercially available white glue and 8d ring-shank screws. All I-shaped specimens were kept in the conditioning chamber until the full-scale shear tests were conducted.

The remainder of the LVL materials was manufactured into an additional 15 I-shaped specimens for testing without moisture conditioning. Results from these tests were compared with those obtained from conditioned specimens to evaluate the effect of moisture conditioning, if any, on full-scale shear tests. In the meantime, some LVL materials randomly selected from the same production lot were tested using the small block shear test setup in accordance with ASTM D 143.

The 4-point load method shown in Figure 4 was used to test all 69 I-shaped specimens. The test apparatus, including rocker-type reaction supports, reaction bearing plates and rollers, load bearing blocks, and load bearing rollers were set up following ASTM D 198 [9]. The curved load bearing blocks had a chord length of 356 mm (14 in.) and a radius of curvature of 711 mm (28 in.). The clear distance between the edge of the reaction bearing plate to the edge of the nearest load bearing block was 2 times the specimen depth or 813 mm (32 in.) for all specimens. A load button was installed between a 890-kN (200,000-lbf) capacity load cell and load bearing block/rollers to function as a load-alignment device. Lateral supports were provided at 610-mm (2-ft) intervals along the test span to prevent lateral buckling. All specimens were cut to the exact length of 3,200 mm (126 in.) and no end overhangs were allowed.

Before testing, the web thickness for each specimen was measured at both reaction points. The mean of the readings was used to calculate the sectional properties of the specimen. Load was applied by a hydraulic cylinder at a constant rate so as to reach the ultimate load in about 10 minutes. The load readings were continuously recorded by a computerized data acquisition system up to the ultimate load. As verification of LVL stiffness was not part of this study, no deflection readings were recorded.

After testing, a 152 x 152 mm (6 in. x 6 in.) section was cut from the web of each tested specimen at about 305 mm (12 in.) away from each specimen end for determining the moisture content and specific gravity of each specimen in accordance with the oven-drying method of ASTM D 4442 [10] and D 2395 [11], respectively.

Based on the theory of elasticity, the maximum applied shear stress (f_v) can be calculated using the following equations:

$$f_v = \frac{VQ}{It} = \frac{3V[b(h^2 - h_1^2) + th_1^2]}{2t(bh^3 - bh_1^3 + th_1^3)} \qquad [1]$$

where f_v = calculated shear strength (MPa)
V = applied ultimate shear force (N) = 1/2 of the ultimate load
Q = first moment (mm^3)
I = moment of inertia (mm^4)
t = measured web thickness (mm)
b = measured flange width (mm)
h = measured height of the I-section (mm)
h_1 = net height of the web between flanges (mm)

As previously mentioned, the materials used for the flanges were intentionally matched with those used for the web. Therefore, the first moment (Q) for each specimen can be determined without calculating the transformed section.

5. Results and Discussions

All 54 specimens that were conditioned and 15 specimens that were not conditioned (as-received) failed in shear. The typical failure mode was shear through the web at one of the supports near the neutral axis of the I-section, as shown in Figure 5. Table 1 summarizes the test results.

Data distributions for both conditioned and as-received specimens are shown in Figure 6 with an empirical normal distribution overlaid. As seen from Figure 6, the normal distribution fits the test data well. Based on the Kolmogorov-Smirnov statistical test, the assumed normality for the distribution function cannot be rejected at the 20% statistical significance level (the higher the significance level, the easier to reject the null hypothesis assuming the test data have the same distribution as the underlying empirical function).

Table 1. Summary statistics for all shear specimens

	Moisture-Conditioned			Without Moisture Conditioned		
	MC, %	SG(a)	f_v(b), MPa	MC, %	SG(a)	f_v(b), MPa
N	50(c)	50(c)	54	15	15	15
Mean	9.0	0.51	5.10	6.8	0.52	5.04
COV	0.030	0.028	0.060	0.057	0.035	0.045
Range	8.3 - 9.8	0.48 - 0.55	4.29 - 5.87	6.3 - 7.6	0.47 - 0.55	4.61 - 5.51

(a) Based on the oven-dry weight and as-received volume of the web.
(b) Shear stress calculated based on Equation 1.
(c) Data for 4 specimens were unavailable.

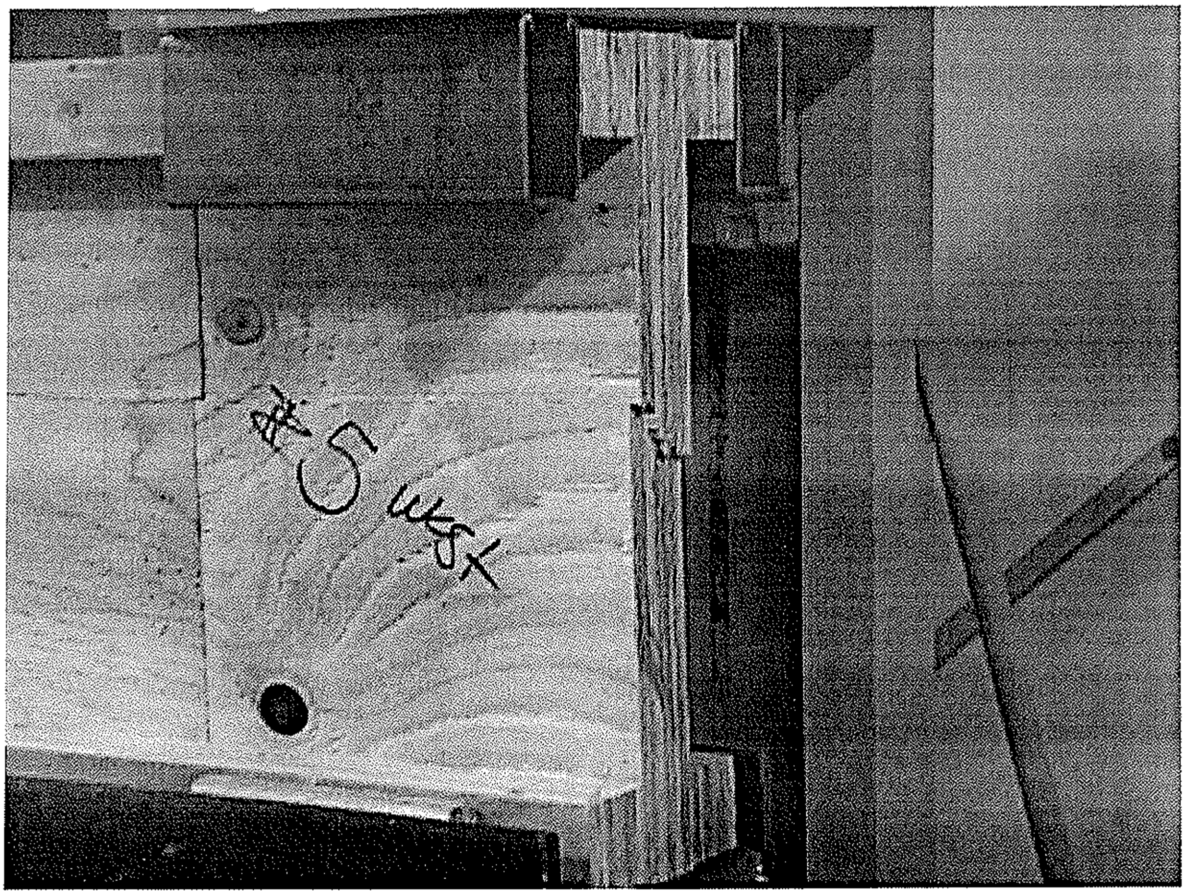

Figure 5. Typical shear failure from full-scale LVL shear tests

Characteristic values (the 5th percentile with 75% confidence) for the conditioned and as-received specimens are given in Table 2, which shows that the characteristic values are practically identical between the specimens with and without the moisture conditioning. The standard error on the characteristic value is approximately 1.5% for the conditioned specimens and 2.0% for the as-received specimens, which are within the typically acceptable range of 5% for the mechanical properties of engineered wood products.

Table 2 and Figure 6 also show the small block shear test results in the edgewise orientation. As shown, the ratio of the mean shear strength between the small block shear and moisture-conditioned full-scale shear is 1.52. However, due to the higher COV in the block shear test results, the ratio of the characteristic shear strength between the small block shear and full-scale shear tests is only 1.42. It should be noted that the mean block

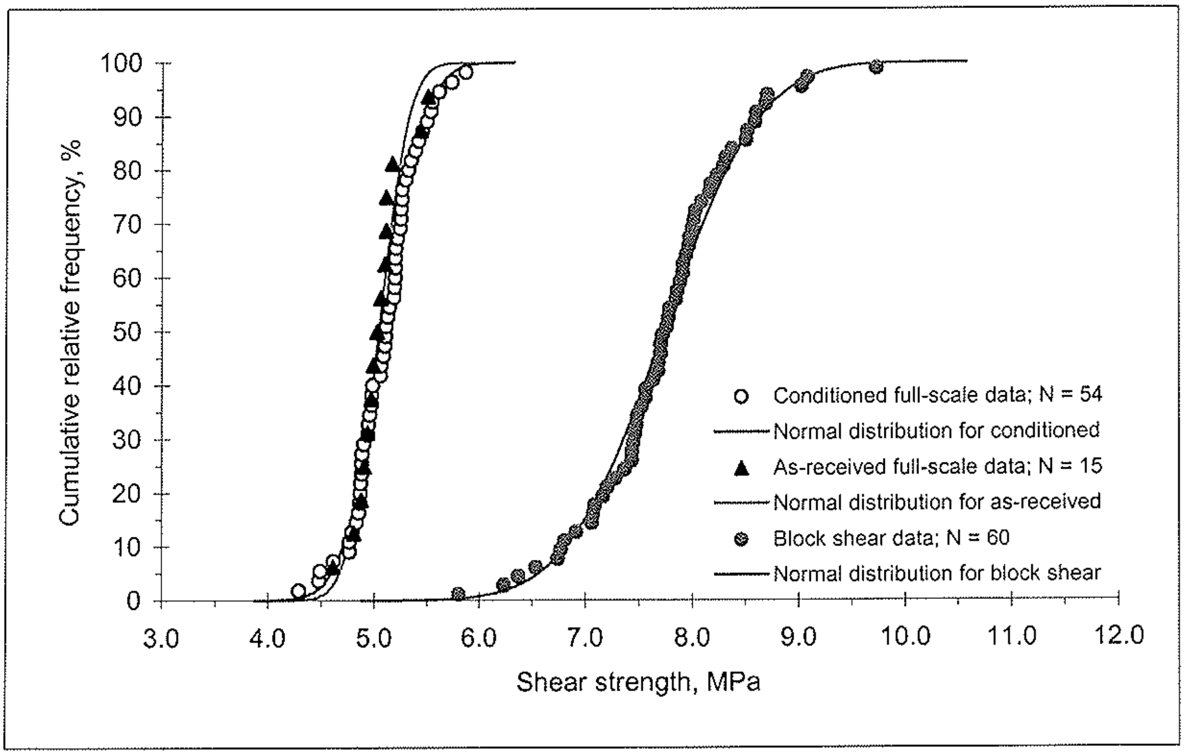

Figure 6. Data distribution for full-scale (conditioned & as-received) and block shear tests

shear value of 7.73 MPa is comparable to the value of 7.52 MPa, as published by Lam and Craig [4]. However, the mean full-scale shear value obtained from this study (5.10 MPa) is much lower than the value of 6.83 MPa (44 x 184 mm specimens) or 6.39 MPa (44 x 302 mm specimens) reported by Lam and Craig [4].

Table 2. Characteristic shear strengths

	Small block shear	Full-scale shear	
	Moisture conditioned		As-received
N	60	54	15
Mean, MPa	7.73	5.10	5.04
COV	0.092	0.060	0.045
K[a]	1.795	1.804	1.991
LTL[b], MPa	6.45	4.54	4.59
SE[c], %	2.3	1.5	2.2

[a] Obtained from Table 3 of ASTM D 2915 [12] at the 5th percentile with 75% confidence

[b] Lower tolerance limit = Mean x (1 - K x COV) based on an assumed normal distribution

[c] Standard error on the lower tolerance limit estimate determined in accordance with ASTM D 2915 [11]

A significance difference between these 2 reports is the specimen size (44 mm x 302 mm x 1812 mm used by Lam and Craig [4], and 44 mm x 406 mm x 2845 mm used in this study). It is recognized that the specimens used between these 2 studies were not manufactured by the same producer, and the layup and species were not the same. Nonetheless, the specimen configuration and test setup used between these 2 studies were similar. Therefore, if the small block shear strength is an indication of the similarity in the LVL materials tested between these 2 studies, the difference in the test results seems to suggest a notable size effect. As a result, for the development of a design shear value, it is imperative that the size effect on the LVL shear strength be addressed by selecting an appropriate specimen size for full-scale shear tests. As previously mentioned, since most LVL products used in light-frame construction in North America are generally limited to 406 mm (16 in.) in depth, the specimen size selected for this study seems to be reasonable and practical. Alternatively, a minimum of 4 sizes should be tested so that the appropriate size effect can be quantified in a similar manner as the volume effect required in ASTM D 5456 [7].

6. Additional Data

In a separate study undertaken soon after the completion of this study, another set of 29 pieces of 44 mm (1-3/4 in.) specimens made with 6 plies of 3.2-mm (1/8-inch) thick Western Hemlock Grade 1 and 7 plies of 4.2 mm (1/6-inch) thick Western Hemlock Grade 2 veneers was tested in the same manner as those reported above. All 29 specimens failed in shear. The mean value obtained from the full-scale shear tests was 4.55 MPa (660 psi) with a COV of 0.07. The matched small block shear tests gave a mean of 6.83 MPa (990 psi) with a COV of 0.16. Figure 7 shows the data distribution.

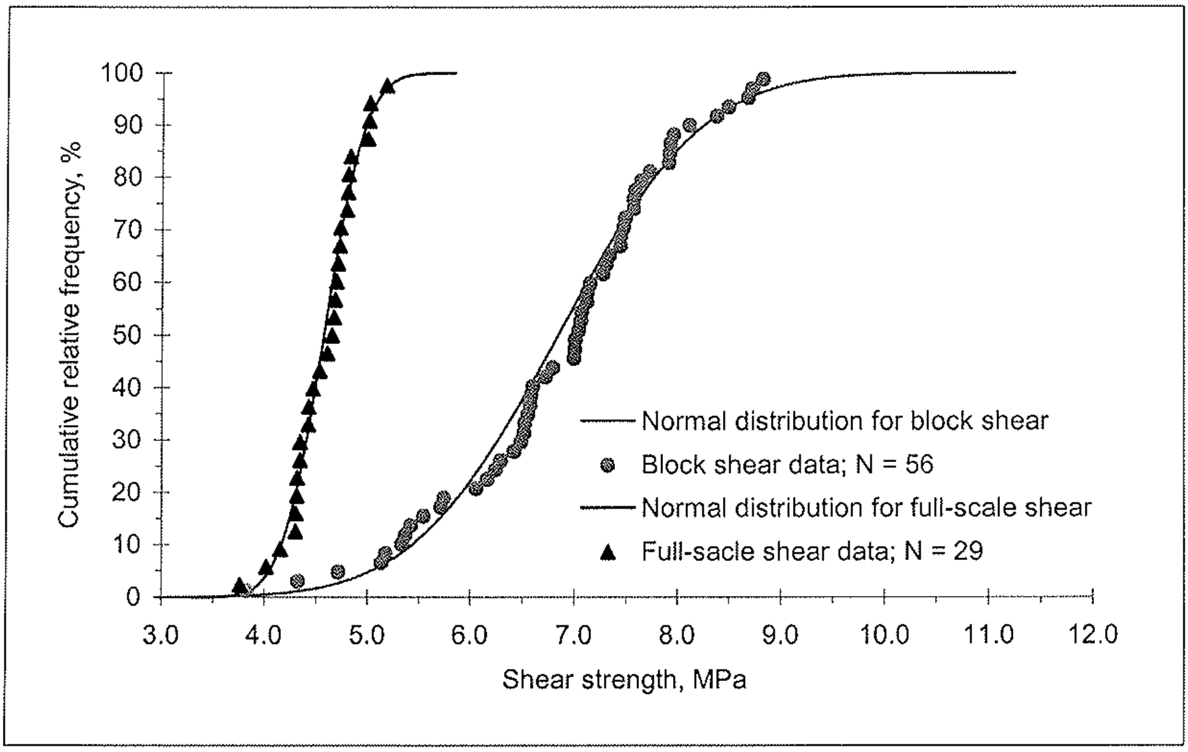

Figure 7. Data distribution for full-scale and block shear tests of Western Hemlock LVL

As shown in Figure 7, the difference in the COV between the block shear and full-scale shear test results is substantial, suggesting that the full-scale shear test method is a more reliable test method for evaluating the LVL edgewise shear strength. Incidentally, the ratio of the mean shear strength between the small block shear and full-scale shear tests is also 1.5. However, due to the higher COV for the small block shear test results, the ratio of the characteristic shear strength between the small block shear and full-scale shear tests is only 1.22.

7. Small-Scale QA Shear Test Method

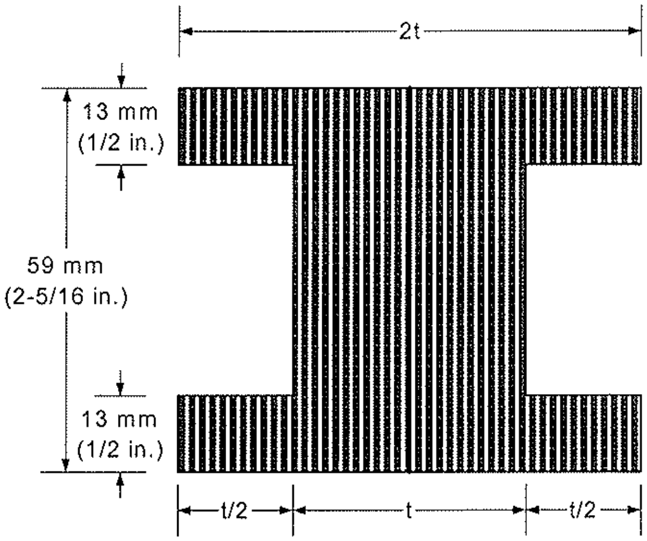

Figure 8. Specimen dimension for small-scale QA shear tests (t = LVL thickness)

It is impractical to use full-scale shear specimens for in-plant quality assurance (QA) tests. For monitoring the LVL edgewise shear strength on an on-going basis, a small-scale QA shear test method is needed, as shown in Figure 8.

The small-scale QA specimen is manufactured by gluing 2 matched LVL's back-to-back using a white glue. The web of the I-section is then created by using a router. As the specimen is small, the web can be readily produced in one single router run. Most importantly, since the web is composed of 1/2 of LVL thickness from each half specimen, the net web thickness is exactly the same as the LVL thickness, thereby preserving the high-grade and densified face veneers in the shear-resistive cross-sectional area.

Due to the small specimen depth (59 mm or 2-5/16 in.), a center-point load method with a span-to-depth ratio of approximately 6 was employed, as shown in Figure 9, for the edgewise QA shear tests. The adoption of the center-point load method, instead of four-point load method, was intended to simplify the test setup for a typical lab at a manufacturing plant. The length of the bearing plates was 51 mm (2 in.) and the loading plate had a length of 76 mm (3 in.). The testing procedures followed ASTM D 4761 [13] with a targeted time to failure of approximately 1 minute. The shear strength was calculated using Equation 1.

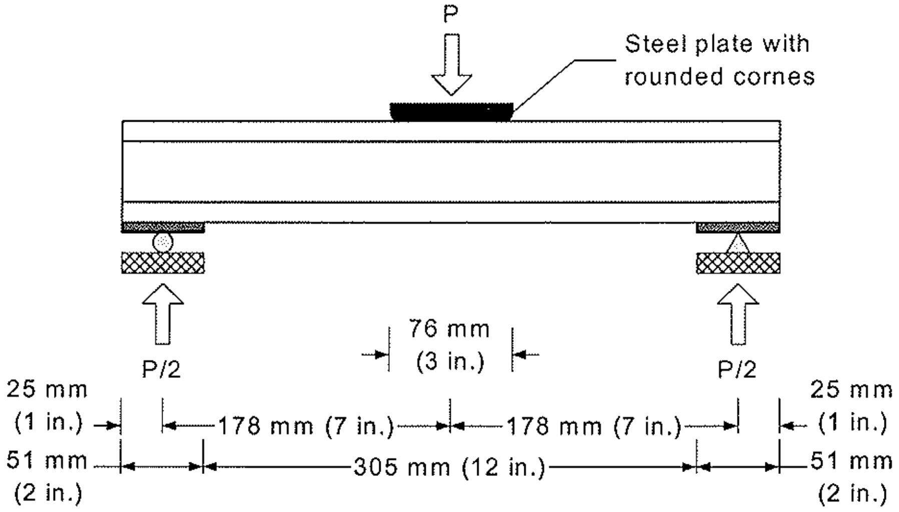

Figure 9. Test setup for edgewise QA shear tests.

The likelihood of shear failure could be estimated using the loading configuration given in Figure 9 if the bending and shear strengths of the LVL can be estimated. For example, if the characteristic bending strength of LVL is 43.4 MPa (6,300 psi) with a COV of 0.15 based on the depth of 305 mm (12 in.) and a volume effect factor of $(h/305)^{(1/8)}$, where h is the LVL depth (mm), the 5th percentile ultimate load required for bending failure using the test setup given in Figure 9 can be estimated as 25.6 kN (5,750 lbf). If the same LVL has a characteristic shear strength of 1/9 of the characteristic bending strength, but with a COV of 0.12, the 99th percentile ultimate load required for shear failure can be estimated as 24.9 kN (5,590 lbf). Since the 99th percentile of shear capacity is lower than the 5th percentile of bending capacity, the shear failure rate based on the test setup given in Figure 9 is expected to be 94% or higher. When compared to the example given for the full-scale shear tests, this example uses a higher shear-to-bending strength ratio (1/9 vs. 1/10) and a higher COV (0.12 vs. 0.10) for the shear strength.

In order to demonstrate the feasibility of using the small-scale edgewise QA shear test method, a total of 35 pieces of 38-mm (1-3/4-in.) thick Douglas fir and southern pine LVL were sampled by an APA auditor at a commercial LVL plant and shipped to the APA Research Center for testing. Eighteen of these specimens were Douglas-fir LVL's made with 2 plies of 3.2-mm (1/8-in.) thick G1, 8 plies of 3.2-mm (1/8-in.) thick G2, and 3 plies of 2.5-mm (1/10-in.) thick G1 veneers. The remaining 17 specimens were southern-pine LVL made with 14 plies of 3.2-mm (1/8-in.) thick G1 veneers. APA staff witnessed the veneer peeling, sorting, and drying processes, and the LVL manufacturing.

Table 3 shows the summary of the test results. All 18 Douglas-fir specimens and 14 out of 17 southern pine specimens failed in shear through the web. Figure 10 shows the typical failure mode, which is similar to the full-scale shear tests. Overall, the shear failure rate was 32/35 or 91%, indicating that the test method can be used for edgewise QA shear tests. The relatively low shear failure rate for the southern pine LVL reflects the higher shear-to-bending strength ratio. A change in the specimen configuration, such as an increase in the flange depth from 13 mm (1/2 in.) to 16 mm (5/8 in.) would increase the probability of shear failure for southern pine LVL.

Table 3. Summary of small-scale edgewise QA shear tests

Species	Douglas-fir LVL	Southern Pine LVL
Sample size	18	14[(a)]
Mean MC, %	7.1	9.9
Mean shear strength, MPa	6.13	8.26
COV	0.079	0.097

[(a)] Shear failure only.

The appropriate QA shear value using the small-scale edgewise QA shear test method should be established in accordance with the correlation between the test results obtained from the small-scale edgewise QA shear (Figure 9) and the full-scale edgewise shear qualification tests (Figure 4). As a result of the size effect, the QA value is expected to be higher than the published characteristic shear strength. Unfortunately, due to the proprietary nature of most LVL products and the lack of a broad database available to the public today, the correlation between the small-scale edgewise QA shear and the published characteristic shear strength should be established from qualification tests of individual species or layup combinations unless the most critical species or layup is pre-determined and tested.

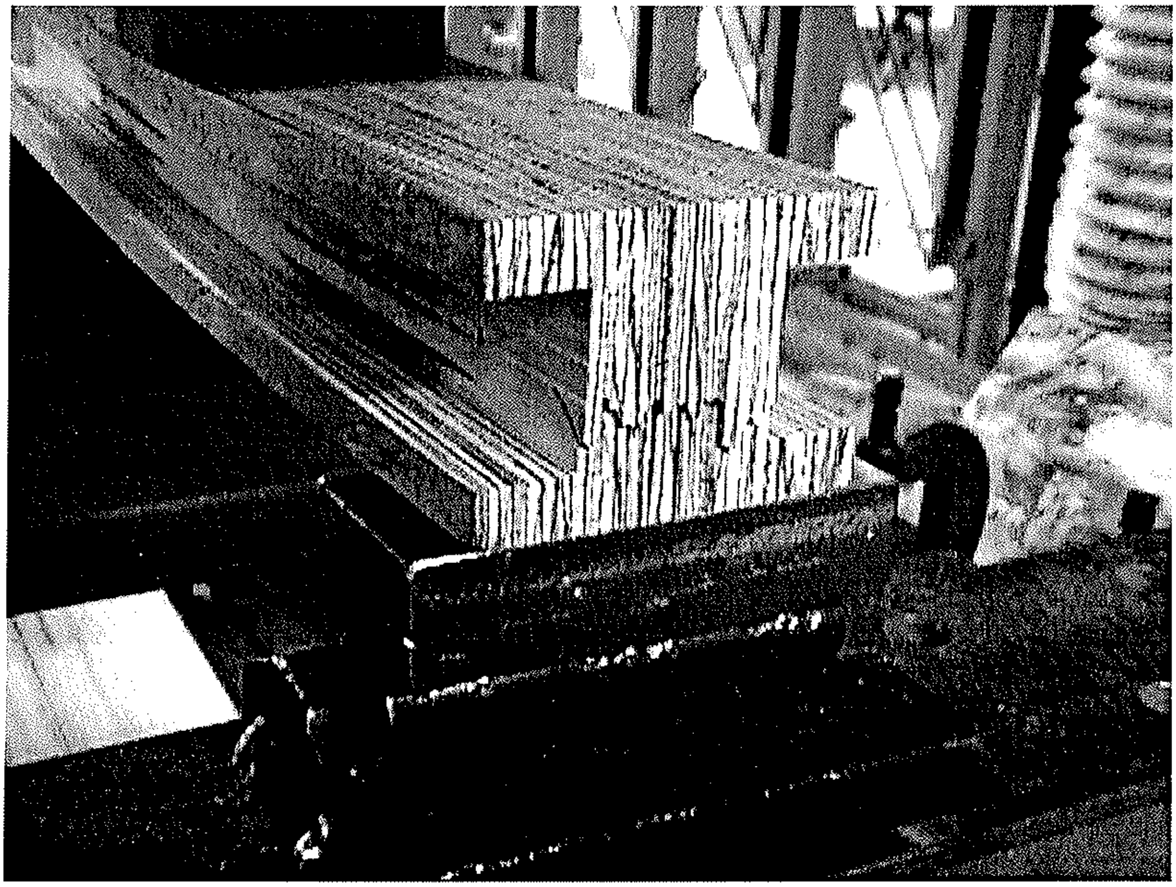

Figure 10. Typical shear failure from small-scale LVL QA shear tests

8. Conclusions

The following conclusions can be substantiated by the test results presented above:

- The full-scale test method used in this study is adequate for qualification of the edgewise shear strength of LVL.

- The difference in the characteristic shear stresses between the specimens tested at the standard environmental conditions (9.0% moisture content in this study) and as-received conditions (6.8% moisture content in this study) are negligible.

- The mean shear strength derived from the ASTM D 143 small block shear tests is approximately 50% higher than the mean shear strength determined from full-scale shear tests, suggesting the necessity of considering a size effect.

- The small-scale QA specimen configuration and test setup used in this study can be used for edgewise QA shear tests.

9. References

1. ASTM. *Standard methods of testing small clear specimens of timber.* ASTM D 143. West Conshohocken, PA, 2001.

2. Rammer D.R. and L.A. Soltis, *Experimental shear strength of glued laminated beams.* Research Report FPL-RP-527. Forest Products Lab., Madison, WI, 1994.

3. Craig, B.A. and F. Lam. *Preliminary investigation of shear strength in structural composite lumber.* Proceeding of International Wood Engineering Conference, 3:407-414, 1996.

4. Lam F. and B.A. Craig, *Shear strength in structural composite lumber.* Journal of Materials in Civil Engineering, 12(3): 196-204, 2000.

5. Schickhofer, G. *Determination of shear strength value for GLT using visual and machine graded spruce laminations.* CIB-W18 paper 34-12-6, August 2001.

6. Yeh, B. and T.G. Williamson. *Evaluation of glulam shear strength using a full-size four-point test method.* CIB-W18 paper 34-12-2, August 2001.

7. ASTM. *Standard specification for evaluation of structural composite lumber products.* ASTM D 5456. West Conshohocken, PA, 2001.

8. ASTM. *Standard test methods of static tests of lumber in structural sizes,* ASTM D 198. West Conshohocken, PA, 2001.

9. ASTM. *Standard practice for establishing stresses for structural glued laminated timber (glulam),* ASTM D 3737. West Conshohocken, PA, 2001.

10. ASTM. *Standard test methods for direct moisture content measurement of wood and wood-base materials.* ASTM D 4442. West Conshohocken, PA, 2001.

11. ASTM. *Standard test methods for specific gravity of wood and wood-base materials.* ASTM D 2395. West Conshohocken, PA, 2001.

12. ASTM. *Standard practice for evaluating allowable properties for grades of structural lumber.* ASTM D 2915. West Conshohocken, PA, 2001.

13. ASTM. Standard test methods for mechanical properties of lumber and wood-base structural material. ASTM D4761. West Conshohocken, PA, 2001.

**INTERNATIONAL COUNCIL FOR RESEARCH AND INNOVATION
IN BUILDING AND CONSTRUCTION**

WORKING COMMISSION W18 - TIMBER STRUCTURES

DESIGN CHARACTERISTICS AND RESULTS ACCORDING TO EUROCODE 5 AND SNIP PROCEDURES

L Ozola
Latvia University of Agriculture

LATVIA

T Keskküla
Estonia Agricultural University

ESTONIA

Presented by: L Ozola

H J Larsen commented that the classification of building types is not part of the Eurocodes because the activity is the responsibility of the national states in other Standards relating to the design and construction of buildings and structures. He also commented that no EU country has yet formally adopted the Eurocodes for practical design purposes. L Ozola then said that she is an enthusiastic about the Eurocodes because of the scientific content and procedures used in its formulation.

DESIGN CHARACTERISTICS AND RESULTS ACCORDING TO EUROCODE 5 and SNiPR PROCEDURES

Lilita OZOLA
Assist. Prof., Latvia University of Agriculture, e-mail: ℓitloak@cs.ℓℓu.ℓv
Tõnu KESKKÜLA
Professor, Estonia Agricultural University, e-mail:Sirje.Keskkyℓa@maiℓ.ee

Abstract. The article presents the comparison of design results of structural timber elements according to different building codes- Soviet SNiP II-25-80 (now- SNiPRR) and ENV 1995-1-1. Design resistance of wood and load bearing capacity of solid timber elements and connections with dowel-type fasteners are chosen to analysis. The differences in results of design are discussed.

Key words: *wood engineering, building codes, design*

1. Motivation for this study

Currently, two building codes- the Eurocode 5 [1] and SNiPR II-25-80 [2] represent two legally acceptable instruments by which an engineer can design a timber structure in Baltic states. Eurocodes were drafted with the purpose to establish common rules for the design of structures within European Community's member states. The use of common codes provides the free movement of construction products without any technical barriers, as well make the situation more favourable for foreign investments. Both codes- the SNiPR and Eurocode 5 are based on the limit states method, however there are some distinctive methodological aspects as well as various partial safety factor values. It is advisable to take into account that most of engineers from Eastern European countries have the erudition in design practice according to Russia SNiPR not Eurocode, and majority of them are not convinced about the advantages of Eurocode because of lack of explanation and information. It is necessary to perform some interpretive actions to do Eurocode more friendly for civil engineers from Eastern Europe.

The article presents a comparison of the economical and some safety aspects of the structural timber elements designed according to Russia SNiPR II-25-80 taking into account actions from SNiPR 2.01.07-85 [4] and ENV 1995-1-1 with actions from ENV 1991 [5,6,7,8].

2. Design and characteristic resistance values of structural timber

Both codes ENV 1995-1-1 and SNiPR II-25-80 follow the same procedure to evaluate a design value of wood resistance. The characteristic value is based on the data from standardised tests of actual structural members under short-term loading. From the data of testing the characteristic value is estimated as 5% lower exclusion level reflecting a normal or lognormal distribution form. So, the same variability assessment methods for strength properties are used. Some differences emerge by comparing to SNiPR design procedure related to the treatment of load duration and moisture content effects to the design values of strength and stiffness properties. SNiPR defines 4 service classes for timber structures: A (in heated buildings), Б (in nonheated buildings), B (outdoor structures), Г (structures in contact with soil and groundwaters). Each class is divided in 3 subgroups dependent on the relative humidity of surrounding air. As a result in some subgroups the moisture conditions are similar, and only four values of service factors are defined in design aims: m_B= 1 for normal conditions (W=12%), m_B= 0.9 for hard conditions in the covered building structures, m_B= 0.85 for outdoor structures, m_B= 0.75 for timber structures in contact with soil under influence of groundwaters.

In SNiPR codes the load duration effects are defined for three characteristic combinations. As a basic combination permanent and short-term (snow) load action is assumed. The tabulated values of design resistance correspond to this basic combination in normal service conditions ($W \leq 12\%$). The reduced time of load is 10^6 up to 10^7 s is determined by the factor $k = 0.66$ [3]. Two additional combinations are described with defined modification factors: permanent and variable load of long duration with the related modification factor $m_d = 0.8$ and combination of permanent and short-term loading with modification factor $m_n = 1.2 \ldots 1.4$.

Let us take the same mean value of resistance f_{mean} (in bending, tension, compression or shear) as a basic value, and estimate the characteristic and design values using both procedures: following Eurocode 5 and SNiPR (see Table 1). To simplify the procedure and to improve the perception the generalization for symbols of like meaning reducing to ENV is made.

It is clear from the diagramms in Fig. 1 that the characteristic values of resistance have the same degree of safety. The design values in standard test conditions for maximal values of sample variability are the same or lower on 5-10% according to ENV in comparison with SNiPR for the minimal coefficient of variability.

Table 1

Characteristic and design values of structural timber using different codes

Eurocode 5 [1]	SNiPR II-25-80 [2] +[3]
Characteristic value:	Characteristic (normative) value:
$f_k = f_{mean} \cdot \exp\left[0.15 - \left(2.645 + 1/\sqrt{n}\right) \cdot v\right]$	$f_k = f_{mean} \cdot (1 - \eta \cdot v)$
Design value of wood resistance in standard test conditions: $f_{d,t} = f_k/\gamma_M$, where γ_M- partial coefficient for material properties:	
$\gamma_M = 1.3$ for samples characterised by limited values of coefficient of variation: $0.1 \leq v \leq 0.3$	$\gamma_M = (1 - \eta_n \cdot v)/(1 - \eta \cdot v)$, where $\eta_n = 1.65$ and $\eta = 2.33$ for 95% and 99% probability levels correspondingly with the restriction for coefficient of variability: $0.15 \leq v \leq 0.25$
Design value of wood resistance in real service conditions:	
$f_d = f_{dt} \cdot k_{mod}$	$f_d = f_{d,t} \cdot 0.66 \cdot m_B \cdot m_d$ or $f_d = f_{d,t} \cdot 0.66 \cdot m_B \cdot m_n$

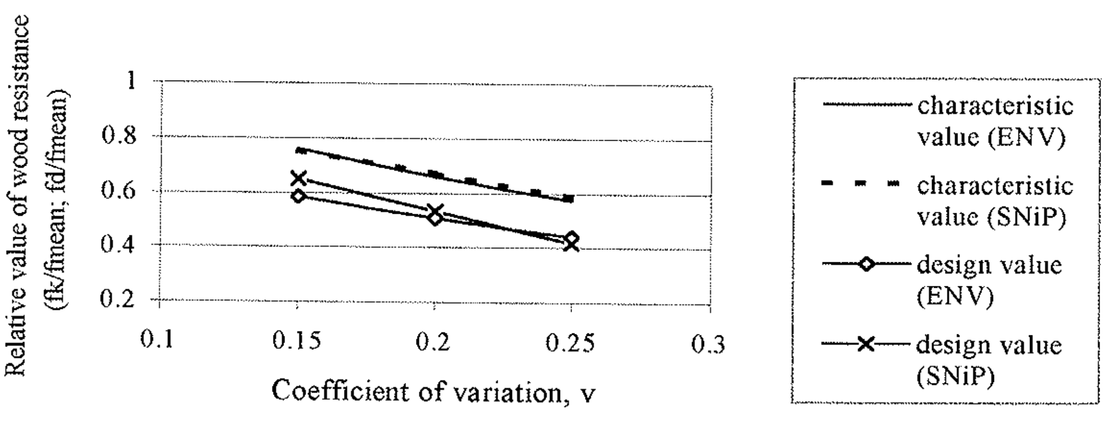

Fig. 1. Relative wood resistance values and variability

Considering the modification factors corresponding to both classification systems of service conditions and load duration we find that Eurocode 5 provide the higher design values of resistance in all cases except short-term loading in heavy conditions (Fig. 2). Eurocode 5 procedure allow to use up to 28% more of the mean value- the ratio of design resistances is f_d(ENV)/f_d(SNiPR)= 1.289 for medium-term loading at the relative air humitity about 85%.

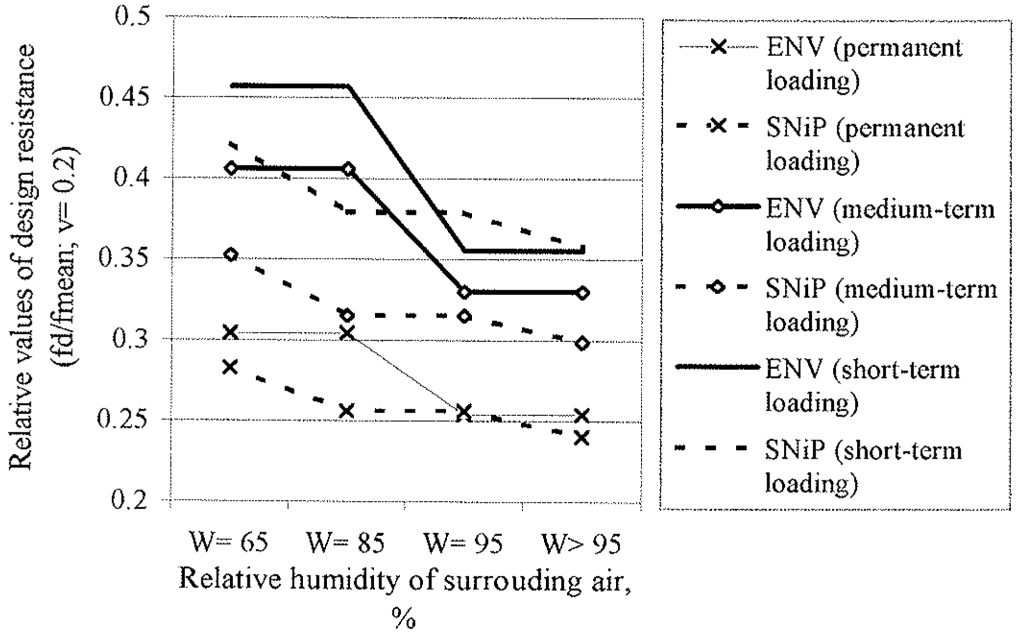

Fig. 2. Design resistance of wood depending from service conditions

It is clear that Eurocode 5 system of modification factors based on five load duration and three moisture content classes is more flexible and leave possibilities for a further develepment as well as using Eurocode 5 procedure we can employ up to 25% a greater part of the mean strength than according to SNiPR codes. Yet it is advisable to note that SNiPR II-25-80 defines the partial factor m_o= 0.8 for tensile elements with cut edgewises estimating the stress concentration that is not found in ENV 1995-1-1.

3. Load bearing capacity of solid timber elements

Assuming the relative design resistance values from Chapter 2 (for the coefficient of variation v= 0.2) we calculate the characteristic value of load bearing capacity under the medium-term snow loading in **axial tension** per 1 unit of the standard element cross section area (b=150 mm):

according to ENV- $N_{k,t}= (f_d/f_{mean})/\gamma_Q$,

according to SNiPR- $N_{k,t}= m_o \cdot (f_d/f_{mean})/\gamma_Q/\gamma_n$,

where γ_Q- partial safety factor for load, m_o- modification factor for tensile resistance of elements with cut edgewises (SNiPR), γ_n- partial factor for building class (SNiPR 2.01-0.7-85 [4]), γ_n= 0.95 for 2-nd class buildings (residential houses, small industrial houses and the like). See results in Table 2.

Design safety reserves of tensile elements are estimated to a considerable extent much more according to SNiPR codes than ENV for light-weight roofs. According SNiPR [4] roof is defined as light-weight if the ratio of characteristic permanent and snow load does not exceed 0.8.

Table 2

Load bearing capacity in tension under medium-term snow loading

Relative humidity of surrounding air	f_d/f_{mean}		Characteristic value of load bearing capacity $N_{k,t}$ in tension (SN-according to SNiPR)								
			ENV γ_Q= =1.5	Heavy roof structure				Light-weight roof structure			
				whole element γ_Q=1.4 m_o=1 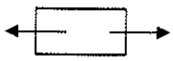		element with cut edgewises γ_Q= 1.4 m_o= 0.8 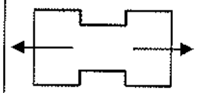		whole element γ_Q= 1.6 m_o= 1 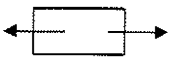		element with cut edgewises γ_Q= 1.6 m_o= 0.8 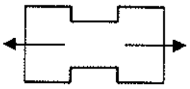	
	ENV	SN		SN	ENV/SN	SN	ENV/SN	SN	ENV/SN	SN	ENV/SN
W=65	0.41	0.35	0.27	0.26	1.02	0.21	1.28	0.23	1.17	0.19	1.46
W=85	0.41	0.32	0.27	0.24	1.14	0.19	1.43	0.21	1.31	0.17	1.63
W=95	0.33	0.32	0.22	0.24	0.93	0.19	1.16	0.21	1.06	0.17	1.33

In similar way we calculate the characteristic values of load bearing capacity of solid wood element in **longitudinal buckling** per 1 unit of cross section area under the medium-term loading (see results in Fig. 3 and Fig. 4):

according to ENV- $N_{k,c}= k_c \cdot (f_d/f_{mean})/\gamma_Q$,

according to SNiPR- $N_{k,c}= \varphi \cdot (f_d/f_{mean})/\gamma_Q/\gamma_n$,

where k_c, φ- buckling factor is estimated from the equations:

ENV [1]: $$k_{c,y} = \frac{1}{k_y + \sqrt{k_y^2 - \lambda_{rel,y}^2}};$$ SNiPR [2]: $$\varphi = 3000/\lambda^2, \text{ if } \lambda > 70;$$ $$\varphi = 1 - 0.8(\lambda/100)^2, \text{ if } \lambda \le 70.$$

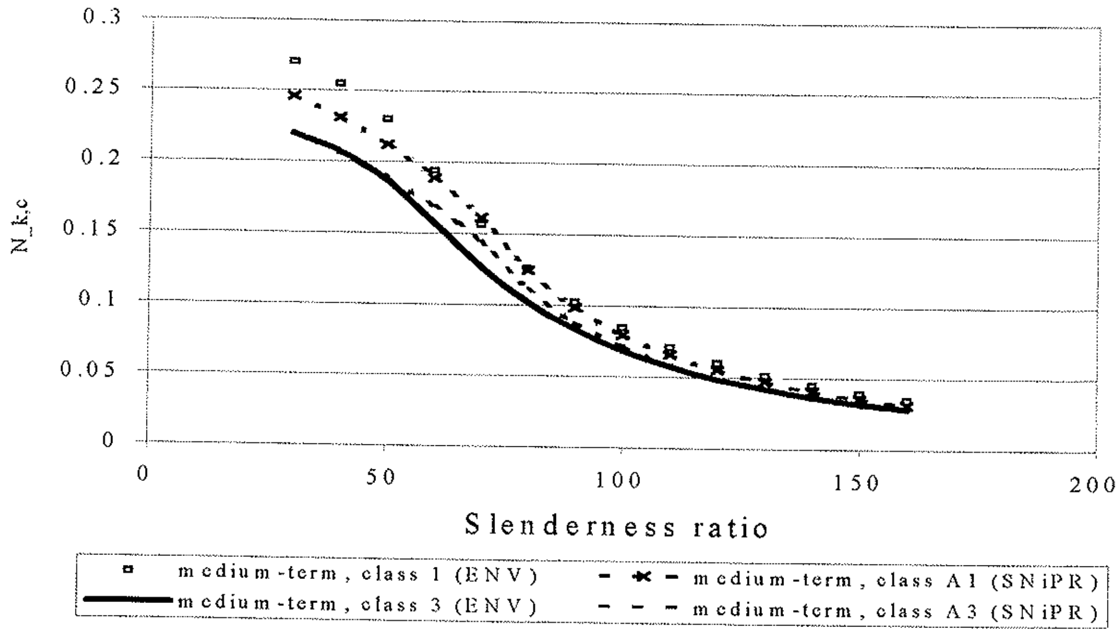

Fig.3. Load bearing capacity of elements in longitudinal buckling in heavy roof structure

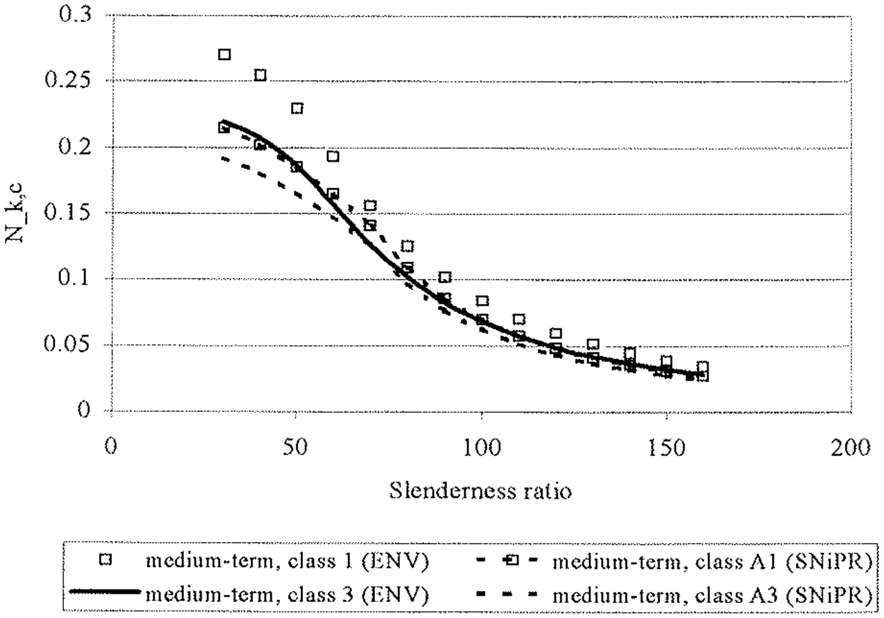

Fig.4. Load bearing capacity of elements in longitudinal buckling in light-weight roof structure

The differences of the load bearing capacity values are not large (up to 10%). However, ENV procedure for determining the buckling factor values is more flexible,- the main influencing factors and properties are included as variables in formulae. In SNiPR code's procedure the influence of timber strength and stiffness properties is involved as constant value.

The comparison of design results of **bending elements** is more complicated because of the amount of influencing factors. Simple supported roof rafters (see Fig.5) for four diferent slope values (α= 15°, 30°, 45°, 60°) are chosen for the analysis. It is a one-storey house with the plan sizes approximately 8 x 12 m.

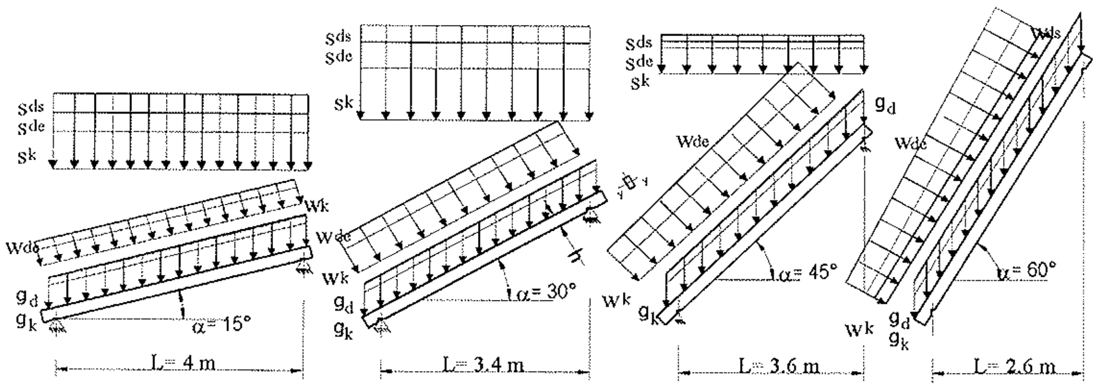

Fig.5. Design diagrams of rafters: $g_{k,}$, $s_{k,}$, w_k- characteristic values of permanent, snow and wind actions, g_{de}- design value of permenent load, $s_{de,}$, w_{de}- design values of snow and wind loads according to Eurocode 1 procedure, $s_{ds,}$, w_{ds}- design values according to SNiPR

Characteristics related to the location of the projected building :

- snow load on the ground: s_k= 1 kN/m²;
- reference wind velocity: $w_{ref} = w_{ref,0}$ = 22 m/s;
- terrain classification: ground category II (farmland);
- the roughness and exposure coefficients: $c_r(z)$= 0.78, $c_e(z)$= 1.64;
- the worse external and internal pressure coefficients: $c_{pe}(z_e)$= +0.2 for α= 15°, $c_{pe}(z_e)$= +0.7 for other slope values, $c_{pi}(z_i)$= -0.5.

The snow load is classified in the medium-term duration, wind action- in the short-term duration class. The factor for the variable load in the combination for persistent and transient situations is ψ_o= 0.6. The spacing of rafters- 0.8 m. Uniformly distributed characteristic value of load on the light-weight roof slope plane- g_k= 0.4 kN/m², on the heavy roof plane- g_k= 0.8 kN/m². The design procedures according to both codes are described in Table 3. The calculation of appropriate cross section sizes is carried out for normal (class 1) and heavy service conditions (class 3) according to Eurocode 5 procedure. The verification according to SNiPR procedure is made for the same cross sections. Design safety reserves are interpreted in diagrams (Fig.6).

Table 3

Design procedures of roof rafters

ENV 1995-1-1	SNiPR II-25-80
Estimation of design values of loads	
permanent load: $g_d = g_k \cdot \gamma_f$ (characteristic value multiple by safety factor)	
$g_d = g_k \cdot \gamma_f$; γ_f = 1.35	$g_d = g_k \cdot \gamma_f \cdot \gamma_n$; γ_f = 1.3; γ_n = 0.95 (takes into account the class of building)
snow load: $s_d = \mu_i \cdot C_e \cdot C_t \cdot s_k \cdot \gamma_f$; γ_f = 1.5	$s_d = s_k \cdot \mu \cdot \gamma_f \cdot \gamma_n$; If $g_k/s_k \ge 0.8$ then γ_f = 1.4 else γ_f = 1.6.
static wind pressure:	
$w_d = q_{ref} \cdot c_e(z_e) \cdot (c_{pe} - c_{pi}) \cdot \gamma_f$; where γ_f = 1.5, $q_{ref} = \rho v_{ref}^2 / 2 = 1.25 \cdot 22^2 / 2 = 303\ \mathrm{N/m^2}$	$w_c = w_o \cdot c_e \cdot k \cdot \gamma_f \cdot \gamma_n$; where γ_f = 1.4, w_o = 300 N/m² (tabulated value [4])
Characteristic values of wood properties:	
C24; $f_{m,k}$=24 N/mm²; $f_{c,0,k}$=21 N/mm² $E_{0,mean}$=11000 N/mm²; $E_{0,05}$=7400 N/mm²	II grade: $f_{m,k}$=24 N/mm²; $f_{c,0,k}$=23 N/mm² $E_{0,mean}$=10000 N/mm²
Design value of wood resistance in real service conditions:	
$f_{m,d} = f_{m,k} \cdot k_{mod} / \gamma_M$; $f_{c,0,d} = f_{c,0,k} \cdot k_{mod} / \gamma_M$;	II grade: $f_{m,d} = f_{c,0,d} = 13 \cdot m_B \cdot m_d$ (N/mm²)
Design conditions for ultimate limit state:	
$\dfrac{N_{c,d}}{k_{c,y} \cdot A \cdot f_{c,0,d}} + \dfrac{M_d}{W_y \cdot f_{m,d}} \le 1$	$N_{c,d}/A + M_d/(\xi \cdot W_y) \le f_{m,d}$, where $\xi = 1 - N_{c,d} \cdot \lambda_y^2 / (3000 \cdot A \cdot f_{c,0,d})$
Strength reserve:	
$c_{str} = \left[1 - \left(\dfrac{N_{c,d}}{k_{c,y} A f_{c,0,d}} + \dfrac{M_d}{W_y f_{m,d}}\right)\right] \cdot 100\%$	$c_{str} = \left[1 - \left(\dfrac{N_{c,d}}{A} + \dfrac{M_d}{\xi \cdot W_y}\right) \Big/ f_{m,d}\right] \cdot 100\%$
Design conditions in serviceability limit states:	
$u_{fin} = u_{inst} \cdot (1 + k_{def}) \le \delta_{max}$ = L/200	$u_{fin} = u_{inst} \le \delta_{max}$ = L/200
Stiffness reserve: $c_{stf} = (1 - u_{fin}/\delta_{max}) \cdot 100\%$	

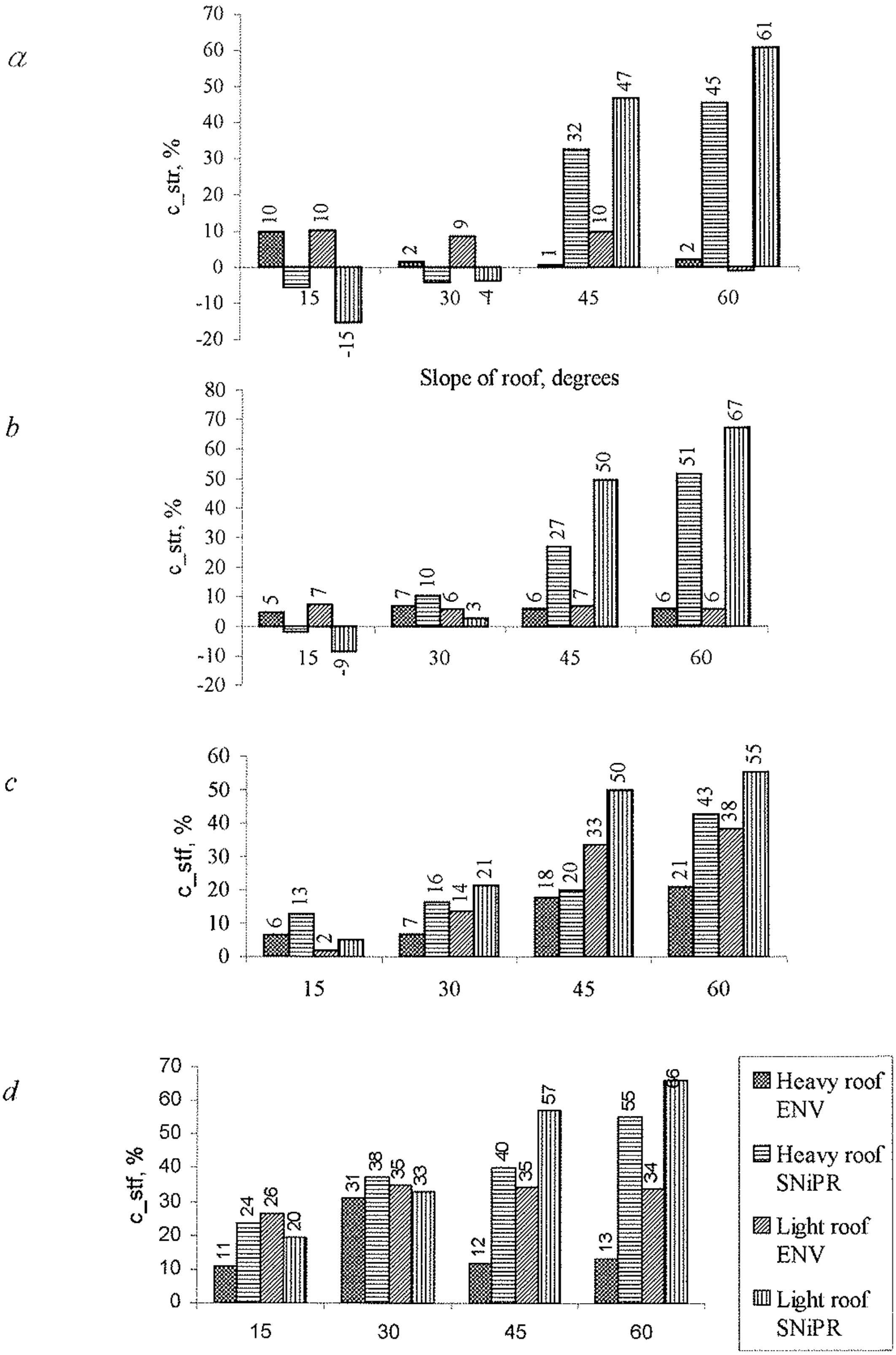

Fig. 7. Design safety reserves of roof rafters dimensioned according to ENV:
a- in strength for 1-st service class conditions, b- the same for 3-rd class,
c- reserves in stiffness for 1-st service class conditions, d- the same for 3-rd class

The results of roof rafter calculations proved that

1) the safety level of light roof elements under permanent self weight and extremal variable of snow loading is provided higher by SNiPR codes for roofs with slope up to 30 degrees;
2) for the roofs of slope 45°-60° the safety of rafters designed according to SNiPR codes is not sufficient because wind loads are determined according to nonsufficient observations;
3) the safety level in stiffness is higher following ENV design criteria because they include the creep factors for the solid timber elements not found in SNiPR.

4. Discussion on joints with dowel type fasteners

The analysed design procedures (see Table 4) of dowel type fasteners in double shear proved that the joints calculated according to SNiPR rules contain an extremely high safety level.

Results of some validatory tests of nailed joints pay attention to the emergence of brittle failure mode in ultimate limit state if the arrangement rules from Eurocode 5 are used in design procedure not observed anywhere with the joints designed according to SNiPR codes. Note that in any case Eurocode 5 procedure provide the sufficient safety level of load bearing capacity value of dowel type joints.

Table 4

Design procedures of load bearing capacity of dowel type fasteners in double shear

ENV 1995-1-1	SNiPR II-25-80
Equations for evaluation of load bearing capacity ($R_{d,i}$, N) per shear plane in double shear:	
$R_{d,1} = f_{h,1,d} \cdot t_1 \cdot d$, where $\rho_k = 350$ kg/m³ $f_{h,1,d} = k_{mod} \cdot 0.082 \cdot \rho_k \cdot d^{-0.3} / \gamma_M$; $\gamma_M = 1.3$	$R_{d,1} = 8 \cdot t_1 \cdot d \cdot m_B \cdot m_n(m_d)$ with suggestion that $R_{d,1} \geq R_{d,3}$ $R'_{d,1} = 8 \cdot t_1 \cdot d \cdot m_B \cdot m_n(m_d)$ with suggestion that $R'_{d,1} \geq R'_{d,3}$
$R_{d,2} = 0.5 \cdot f_{h,1,d} \cdot t_2 \cdot d \cdot \beta$, $\beta = f_{h,2,d} / f_{h,1,d}$;	$R_{d,2} = 5 \cdot t_2 \cdot d \cdot m_B \cdot m_n(m_d)$ with suggestion that $R_{d,2} \geq R_{d,3}$ and $R_{d,2} \geq R'_{d,3}$
$R_{d,3} = 1.1 \cdot \frac{f_{h,1,d} \cdot t_1 \cdot d}{2+\beta} \left[\sqrt{2 \cdot \beta \cdot (1+\beta) + \frac{4 \cdot \beta \cdot (2+\beta) \cdot M_{y,d}}{f_{h,1,d} \cdot d \cdot t_1^2}} - \beta \right]$	bending of smooth common nail: $R_{d,3} = \left(25 \cdot d^2 + 0.1 \cdot t_1^2\right) \cdot \sqrt{m_B \cdot m_d (m_n}$ $R'_{d,3} = \left(25 \cdot d^2 + 0.1 \cdot (t_1 - 1.5 \cdot d)^2\right) \cdot \sqrt{m_i}$ with restriction for bending capacity values in both shear planes: $R_{d,3} \leq 40 \cdot d^2 \cdot \sqrt{m_B \cdot m_d (m_n)}$
$R_{d,4} = 1.1 \cdot \sqrt{\frac{2 \cdot \beta}{1+\beta}} \cdot \sqrt{2 \cdot M_{y,d} \cdot f_{h,1,d} \cdot d}$, where $M_{y,d} = k_{mod} \cdot 0.8 \cdot f_{u,k} \cdot d^3 / 6 / \gamma_M$; $\gamma_M = 1.1$	bending of bolt: $R_{d,3} = \left(18 \cdot d^2 + 0.2 \cdot t_1^2\right) \cdot \sqrt{m_B \cdot m_d (m_n}$ $R_{d,3} \leq 25 \cdot d^2 \cdot \sqrt{m_B \cdot m_d (m_n)}$
Load bearing capacity of dowel in double shear:	
$R_d = 2 \cdot \min(R_{d,1}, R_{d,2}, R_{d,3}, R_{d,4})$	$R_d = R_{d,3} + R'_{d,3}$
Minimum dowel spacings paralel (a_1) and perpendicular to grain (a_2):	
- for nails $a_1 = 10 \cdot d$ and $a_2 = 5 \cdot d$ on condition that $d < 5$ mm and $\rho_k \leq 420$ kg/m³; - for bolts $a_1 = 7 \cdot d$ (if $\alpha = 0°$) and $a_2 = 4 \cdot d$	- for nails $a_1 = 15 \cdot d$ and $a_2 = 4 \cdot d$ on condition that $t_{min} \geq 10 \cdot d$; - for bolts $a_1 = 7 \cdot d$ and $a_2 = 3.5 \cdot d$

According to Eurocode 5 and SNiPR procedures load bearing capacity of dowel in double shear (Fig. 8) is calculated for nail (d= 4 mm) with joint parameters t_1= t_2= 40 mm, and for bolt (d= 12 mm, tensile strength of steel $f_{u,k}$= 400 N/mm², t_1= 60 mm, t_2= 100 mm). Density of wood is assumed as ρ_k= 350 kg/m³ in both cases. Minimum necessary plane area per 1 N of load bearing capacity is determined as criteria for comparison (see Fig. 9). Joints designed according SNiPR codes require 1.4...1.8 times larger area of as the ones based on Eurocode 5 procedure.

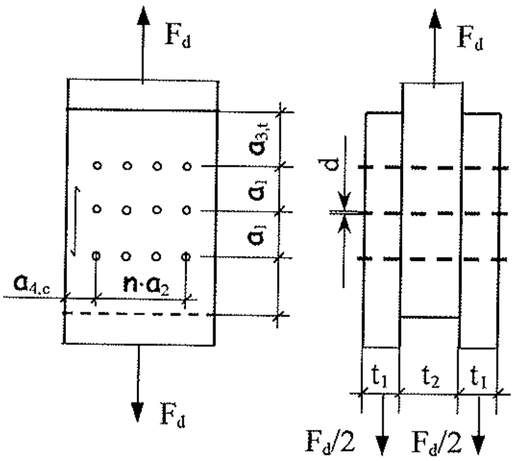

Fig. 8. Laterally loaded joint with dowel-type fasteners in double shear

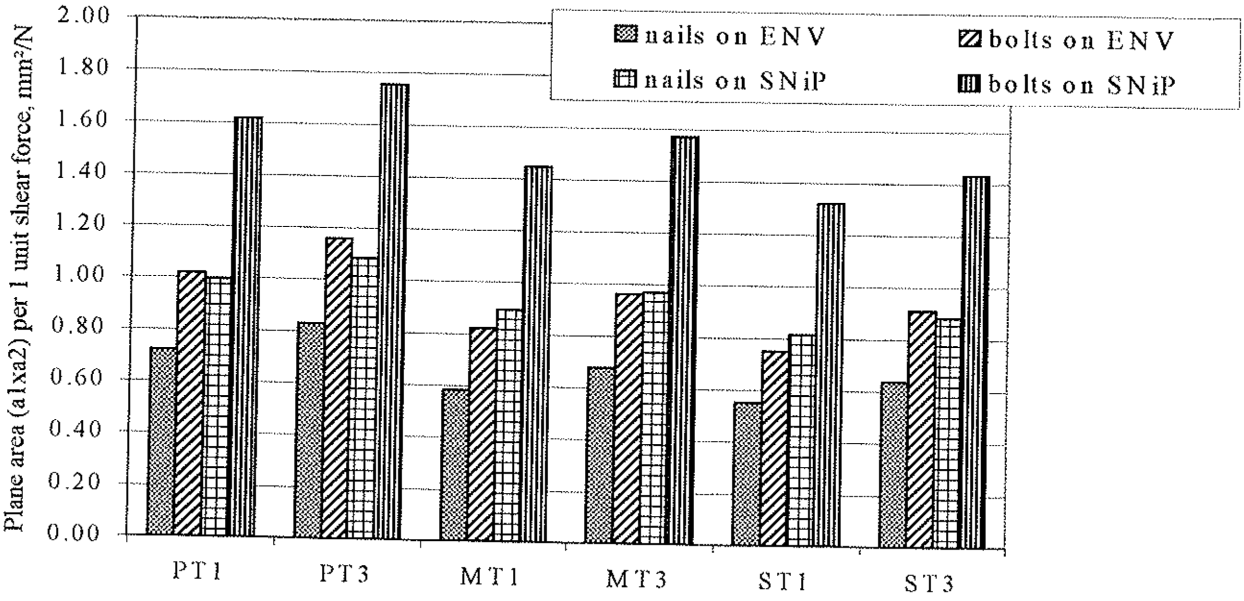

Conditions: PT1- permanent loading, 1-st class, PT3- permanent, 3-rd cl, MT1- middle-term, 1-st cl, MT3- middle-term, 3-rd cl, ST1- shortterm, 1-st cl, ST3- shortterm, 3-rd cl

Fig. 9. Comparison of dowel type joint characteristics in double shear

5. Summary

1. Eurocode 5 procedure to modify the strength properties according to 3 service classes is more appropriate for using in design and future development.
2. SNiPR procedure provides an higher safety level for tensile elements.
3. Eurocode 5 procedure is more flexible in evaluation of the influence of the strength and stiffness properties on the critical axial force in longitudinal buckling, so the characteristics may be used as variables in design procedure.

4. The comparison of design procedures for bending elements (roof rafters, ceiling joists [10]) proved that considerable differences are in the action side. Design value of static wind pressure on buildings is 4-8 times larger then the ones according to SNiPR. The design values of imposed loads on ceilings are 1.5...2 times greater then the ones following SNiPR codes. Result in differences in material consumption for roof rafters and ceiling joists are not considerable.
5. The mechanism should be developed for including the snow and wind load characteristics of Eastern European areas in the appendixes of Eurocode 1. Or on the other hand it is necessary to provide analogue procedures for determining the characteristic values of load from the meteorological data populations. While using a unique procedure we can obtain the target safety level.
6. SNiPR codes do not contain the design criteria for such types of mechanical fasteners as split rings, toothed rings and nail plates which are used for dozen of years in the developed countries.
7. The design procedure according to Eurocode 5 for dowel type fasteners is more flexible as regards the material properties involved and the result is about 1.5...1.8 times less material consumption in comparison with SNiPR codes. Yet it is necessary to note that a lower reliability level may be expected if the safety or reliability is defined as the complement to it's probability of brittle failure. The possibility of human errors is expected if the arrangement conditions for nailed joints are so complicated.
8. It is necessary to adopt the limit values for the slenderness ratio of structural elements and to include them in Eurocode 5.
9. Generally Eurocode should contain all basic design criteria, and therefore Eurocode 5 may be adopted as a complete document by any country.
10. The partial factors corresponding to the class of building should be involved in Eurocode. In such a case the growth of material economy should be expected, as well the related reliability level should be determined.

References

1. ENV 1995-1-1. Eurocode 5: Entwurf, Berechnung und Bemessung von Holzbauwerken. Teil 1-1. Allgemeine Bemessungsregeln, Bemessungsregeln für den Hochbau. (Juni, 1994)
2. СНиП II-25-80. Деревянные конструкции/ Госстрой СССР.- М.: Стройиздат, 1983
3. Пособие по проектированию деревянные конструкций (к СНиП II-25-80)/ ЦНИИСК им. Кучеренко.- М.: Стройиздат, 1986
4. СНиП 2.01.07-85. Нагрузки и воздействия/ Госстрой СССР.- М.: ЦИТП Госстроя СССР, 1986
5. Eurocode 1: Basis of design and actions on structures- Part 1: Basis of design/ CEN.- Brussels, 1996
6. Eurocode 1 - Basis of design and actions on structures- Part 2-1: Actions on structures - Densities, self -weight and imposed loads/ CEN.- Brussels, 2000
7. Eurocode 1 - Basis of design and actions on structures- Part 2-3: Actions on structures - Snow loads/ CEN.- Brussels, 2000
8. Eurocode 1 - Basis of design and actions on structures- Part 2-4: Actions on structures - Wind loads/ CEN.- Brussels, 2000
9. Timber Engineering. Step 1. Basis of design, material properties, structural components and joints. Netherlands: Centrum Hout, 1995
10. T.Keskküla, L.Ozola. Design Results of Structural Wood Elements according to European and Russia Building Codes// Proceedings of the Latvia University of Agriculture. B- technical sciences, building, engineering.- 1998. Vol. 16 (293): Jelgava: LLU 1998, pp: 33-39.

CIB-W18/35-102-2

INTERNATIONAL COUNCIL FOR RESEARCH AND INNOVATION
IN BUILDING AND CONSTRUCTION

WORKING COMMISSION W18 - TIMBER STRUCTURES

MODEL CODE FOR RELIABILITY-BASED DESIGN OF TIMBER STRUCTURES

H J Larsen

BYG DTU: Department of Civil Engineering
Technical University of Denmark

DENMARK

Presented by: H J Larsen

S Thelandersson suggested the use of a single variable instead of (1 + y) in equation 1 as the use of a single variable will not permit the result being negative. S Thelandersson also commented that the present proposed approach enforces the use of a time-variation approach and advocated the possible inclusion of a simple approach based on modification factors instead of a fully reliability based approach. H J Larsen is in sympathy with the points made and is of the view that a lower limit may be included in the current proposed approach to exclude unreasonable answers. H J Larsen agreed with H J Blaß about the need to include the creep properties of connections on structural systems but that due to the complexity involved, H J Larsen will only be able to deal with the issue in the “next chapter”.

Model Code for reliability-based design of timber structures

H. J. LARSEN
BYG•DTU: Department of Civil Engineering, Technical University of Denmark

1. Abstract

One of the main activities of the Joint Committee on Structural Safety is to establish a Probabilistic Model Code for reliability-based design of structures. It is the intention to include in the code a section covering reliability assessment of structures based on timber, glulam and other wood-based building products. It is expected that CIB W18 will be instrumental in drafting and discussing proposals for this section of the code. This paper contains brief information about the Committee and a first draft for the code (chapter 3). The background for the code is given in chapter 4. It is assumed that the structure is constructed from structural timber boards composed of sections with constant strength varying randomly around a basic strength characteristic for the board. The basic strength is related to a reference property (5-percentile strength values, determined by standardised short-term tests). It is argued that for the reliability calculations, a log-normal distribution should be assumed and values for the coefficient of variation are given. The effect of load duration should be assessed using a damage model, and it is proposed to use either Gerhards' model because of its simplicity or Nielsen's model because of its suitability for complicated load histories. Other wood-based materials such as glulam, panels and LVL are treated only briefly.

2. Background

The Joint Committee on Structural Safety (JCSS), created in 1971 by CIB, ECSS, CEB, fip, IABSE and RILEM, has been responsible for establishing the philosophy on which all modern design codes – including the Eurocodes are based; not only the safety codes but also the related design codes.

During the last 2-3 decades, one of the Committee's main activities has been to establish a Probabilistic Model Code for reliability-based design of structures. A first version of the JCSS Model Code was published in early 2001. The Model Code currently contains information regarding the general probabilistic modelling of loads and load combinations together with probabilistic models for the resistance of related materials characteristics of concrete and steel materials. One of the elements needed to complete the JCSS Model Code is a similar model for reliability assessment of structures based on timber, glulam and other wood-based building products.

This, in fact, was initiated some 6-8 years ago, at which time the JCSS asked CIB W18 for assistance in accomplishing this important task. A very primitive document was drafted for discussion in CIB W18 (Larsen et al., 1996), but it had to be concluded that the existing knowledge base was insufficient. As a consequence the European Community COST E24 action entitled Reliability of Timber Structures was initiated, an action that is now almost 18 months old and close to it's mid-term. The COST E24 action aims at establishing an operational basis for reliability analysis of timber structures and subsequently reliability-based code calibration for design codes for timber structures. CIB W18 with its broad base in the timber construction and research community should, however, play an important role as a forum for drafting and discussing the proposal for the code at an early stage.

3. Proposal for a model code for structural timber

3.1.1 Basic model

It shall be assumed that the structure consists of n boards for which the strength of board i varies as shown in figure 1.

The board consists of sections with constant strength. The strength of section j in board i is:

$$f_{j,i} = k\, k_{size.} f_i\, (1 + Y) \tag{1}$$

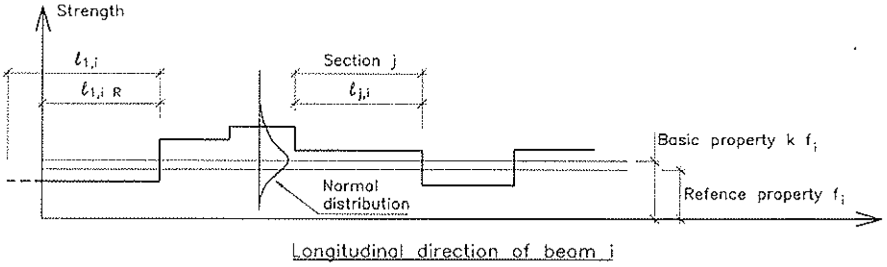
Strength
$\ell_{1,i}$
$\ell_{1,i}$ R
Section j
$\ell_{j,i}$
Basic property k f_i
Normal distribution
Refence property f_i
Longitudinal direction of beam i

Figure 1 – Basic model.

where

- f_i is the reference property of board i, see 3.2
- k is the ratio (≥1) between the basic property and the reference property of board i
- k_{size} is a factor taking into account any geometrical deviations from the reference geometry
- Y is a standardised normal variable with mean = 0 and coefficient of variation COV = 0.4 v. Values of Y outside the interval 0.3 and 1.7 shall be disregarded.
- v is the coefficient of variation for the reference property, see 3.2.

The distance between the mid-points of the sections with constant strength, i.e. the distance between sections with major defects, shall be assumed to be gamma-distributed:

$$\Gamma = \Gamma(k, \lambda) \tag{2}$$

where

$$k = m^2/s^2 \tag{3}$$

Values of $l_{j,i}$ below 150 mm shall be disregarded.

$$\lambda = m/s^2 \tag{4}$$

m is the mean distance and

s is the standard deviation.

The distance from the end of the board to the most distant point of the first section (length $l_{1,i}$) shall be assumed to be

$$a = l_{1,i} R \tag{5}$$

where R is rectangularly distributed.

The length L of the boards shall be assumed to be normally distributed with mean $m(L)$ and coefficient of variation $v(L)$. Values outside the interval 900 mm to 6000 mm shall be disregarded.

3.2 Reference properties

The reference properties (f_i) are

- the characteristic strengths (5-percentiles) in bending (f_m), tension and compression parallel and perpendicular to grain ($f_{t,0}$, $f_{t,90}$, $f_{c,0}$ and $f_{c,90}$) and shear parallel to grain (f_v)
- the characteristic values of modulus of elasticity in bending , E (5-percentile or mean value)
- the characteristic density, ρ (5-percentile)

determined in accordance with EN 1995-1-1 (Eurocode 5) and EN 408.

This means that

- test specimens shall have the reference sizes given in these standards, or test results shall be corrected to these sizes (factor k_{size})
- test specimens shall be conditioned in the reference climate 23^0C and 65% RF, or test results shall be corrected to this climate,
- test specimens shall be loaded to failure in short-term ramp loading with a time to failure of 5 minutes
- beams shall be tested in 4-point bending with distances of $6h$ between loading points where h is the beam depth, and the estimated weakest cross-section (the critical section) shall be placed in the middle part where the moment is constant.

Ideally all properties should be determined by tests. As a minimum, the distribution of bending strength, the modulus of elasticity and the density shall be determined. It may then be assumed that the distribution of the other properties, the shear modulus (G) and the modulus of elasticity perpendicular to grain (E_{90}) may be derived by multiplying the bending strength distribution respectively the density distribution by:

$$\begin{array}{ll} f_{t,0} = 0.60 f_m & f_{t,90} = \min\{0.6\ ;\ 0.0015\rho\} \\ f_{c,0} = 5 f_m^{\ 0.45} & f_{c,90} = 0.007\rho \\ G = E/16 & E_{90} = E/30 \\ f_v = \min\{3.8\ ;\ 0.2 f_m^{\ 0.8}\}. & \end{array} \tag{6}$$

It shall be assumed that the basic property has a log-normal distribution with a coefficient of variation of $0.8v$ where v is the coefficient of variation for the reference property.

The parameters of the distribution shall be determined by fitting to the lowest 15 % of the test data.

3.3 Section lengths and board lengths

m and s shall be determined by measurements for the actual species and growth area. For softwood of Nordic origin, the following values should be assumed

m = 500 mm
s = 250 mm

The board lengths shall be determined by typical trade conditions.

3.4 Basic properties

The basic properties are found by multiplying the reference properties by a factor k.

For Nordic grown softwoods the following values should be used:

- for strength properties: $k = 1.06$ (7)
- for stiffness properties: $k = 1$ (8)

3.5 Safety verifications

It shall be verified that the following conditions with a prescribed probability (expressed e.g. as a reliability index) is fulfilled for any member at any time during the intended life of the structure:

(1) $\sigma_{j,i} \leq k_w f_{j,i}$ (9)

(2) $\alpha_i \leq 1$ (10)

where

$\sigma_{j,i}$	is the maximum stress in section j of board i. In cases where failure is due to a combination of stresses, $\sigma_{j,i}$ is the maximum value of this combination and $f_{j,i}$ is the corresponding failure value
k_w	$k_w = 1.10$ is the ratio between the strength under short-term actions such as wind and the strength determined by a (5-minute) standard test
α	is a parameter expressing the damage in a point due to the loading and moisture history. $\alpha = 0$ corresponds to undamaged material and $\alpha = 1$ to failure.

3.6 Damage function

Disregarding the interaction (the mechano-sorptive effect) between load and moisture history, i.e. assuming that

$$\alpha = \alpha_{\text{load}} \alpha_{\text{moisture}} \tag{11}$$

the following expression may be used for α_{load}:

$$\mathrm{d}\alpha_{\text{load}}/\mathrm{d}t = \exp(A - B\ \sigma/f_l) \tag{12}$$

A and B are constants, σ is the applied stress and f_l is the basic strength.

3.7 Stress-strain curve

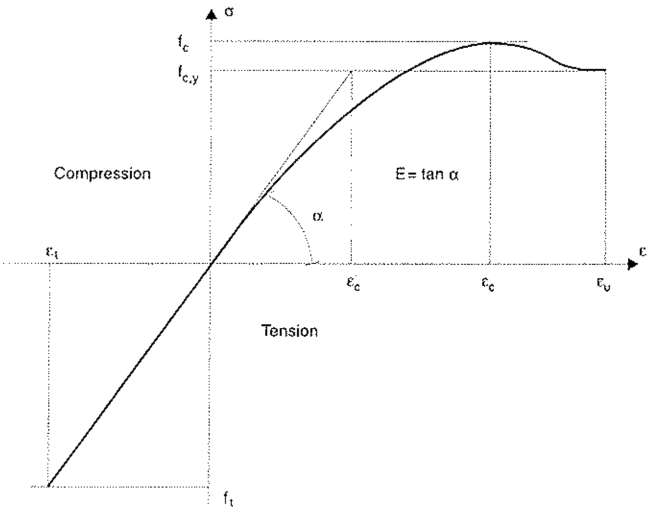

Figure 9 - Stress-strain relation according to (Blass, 1988). A simplified linear elastic plastic-stress-strain curve is represented by thin lines.

According to Blass (1988) the stress-strain curve under axial load shown in figure 9 is appropriate. In tension there is a linear relationship. In compression the relation is described by the initial modulus of elasticity $E = \tan\alpha$, the compression strength f_c, the asymptotic final compression stress $f_{c,y}$, the strain ε_c at maximum stress and the ultimate strain ε_u. The following empirical relation is assumed:

$$\sigma = \frac{E\varepsilon + k_1 (\frac{\varepsilon}{\varepsilon_c})^7}{1 + k_2\varepsilon + k_1 \frac{(\varepsilon/\varepsilon_c)^7}{f_{c,y}}} \tag{13}$$

where

$$k_1 = \frac{f_{c,y}}{6(1 - f_{c,y}/f_c)} \tag{14}$$

$$k_2 = \frac{E}{f_c} - \frac{7}{6\varepsilon_c} \tag{15}$$

Typical values for the parameters are:

$$f_{c,y}/f_c \sim 0.8 \qquad \varepsilon_c = 0.8\text{–}1.2\ \% \qquad \varepsilon_u \sim 3\varepsilon_c \tag{16}$$

4 Background for chapter 3

4.1 Basic model

A probable lengthwise variation of strength is shown in figure 2, together with a model for an idealised variation. In this model it is assumed that timber is composed of localised weak zones connected by segments of clear wood and that failure is primarily initiated in these weak zones. The weak zones correspond to growth defects, especially knots or groups of knots, distributed stochastically along the length.

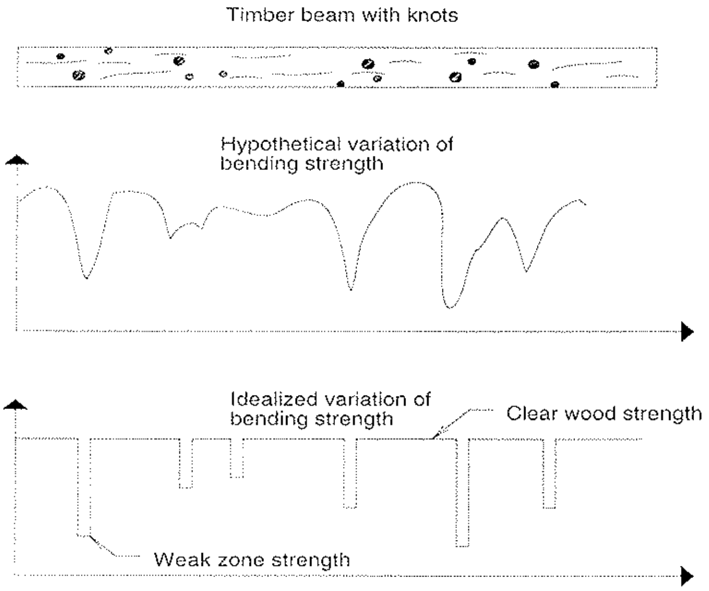
Timber beam with knots
Hypothetical variation of bending strength
Idealized variation of bending strength
Clear wood strength
Weak zone strength

Figure 2 - Modelling of the lengthwise variation of strength. From (Isaksson, 1999).

As a further simplification it is proposed to disregard the influence of the clear wood strength and use a model for which the strength is regarded stepwise constant corresponding to the strength of the weak zone as shown in figure 3. Each section spans half-way from a weak zone to the neighbouring weak zones.

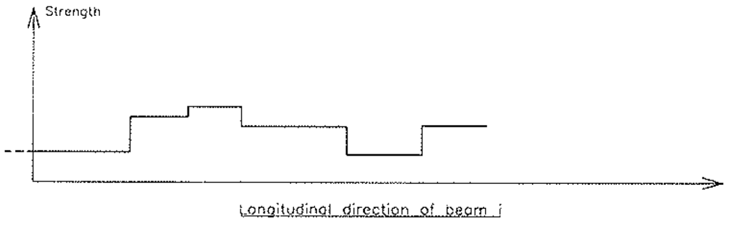

Figure 3 - Simplified model.

4.2 Reference property

To characterise the strength of structural timber in a simple and unambiguous way it is necessary to agree on a reference property based on standardised tests and with standardised specimen size and geometry. Unfortunately it has not been possible to obtain international agreement and at least 3 different systems exist. The crucial difference regards how the estimated critical section (section at which failure is expected to occur) shall be located. In all 3 systems, the bending strength is based on 4-point bending with 3 equal spans and with a total length of 15-18 times the depth, and ramp loaded to failure in 1-3 minutes.

- The European system requires that the critical (weakest) section should be placed inside the inner load points. The selection of this section should be based on a visual inspection assisted if available by non-destructive measurements, e.g. of the stiffness. The European system is linked to careful measurements of defects and deformations etc. and has been developed to obtain maximum information from the tests and safe estimates of the characteristic values.
- In the North American system the tested length should contain the critical section, but the specimen is otherwise placed at random in the testing machine.
- In the Australian system the specimen is placed completely at random, i.e. the tested length does not necessarily belong to the specified grade, provided some of the non-tested parts (the overhang) do.

The distribution function for the reference property of Nordic softwoods has been investigated in a project supported by Nordisk Industrifond (Nordic Industrial Development Fund), see (Ranta-Maunus et al., 2001). A short summary is given in (Ranta-Maunus, 2002).

In the project, data from several large Nordic databases was evaluated. The following distributions were fitted to the data both to the complete dataset and to the lower test values (truncation at 10-15 %): Normal, log-normal, Weibull 2-parameter and Weibull 3-parameter.

Generally the log-normal distribution gave the biggest coefficient of variation, with no clear trend for the other distributions. It was found that distributions fitted to the truncated data gave the best description of the lower tail and the safest estimate of the 5-percentile. Examples of the data and the fitted distributions are given in figure 4.

The following is quoted from the summary in (Ranta-Maunus, 2000):

> The data available suggests that engineered wood products follow the log-normal distribution well. Sawn timber could be better described by normal or Weibull distributions. However, it is suggested that log-normal distribution is used for all timber materials in structural reliability analyses, as it is widely used for other materials and it seems to be the best for timber materials used for-long span structures as well.

When more specific information is unavailable, the COV parameters of lognormal distribution can be taken from table 3.

It would be valuable, especially for glulam, which is used in long-span structures, if a much bigger population were analysed.

Table 3. Suggested values for COV-parameter of lognormal distribution when used in structural reliability analyses.

Material	v [%]
Machine-graded sawn timber	30
Plywood*)	20
Glulam*), I-beam*)	15
LVL	10

*) inadequate population (N < 300).

The variation is due partly to within-member variations and partly to between-member variations. According to Isaksson (1999), the within-member variations are the smaller – about half the between-member variations. It is, therefore, proposed that a coefficient of variation of 80 % of the values found from testing for between-member variations is used and half this value for the within-member variation.

4.3 Section lengths

Riberholt (1979) and Isaksson (1999) assume that the occurrence of defects along the beam can be described by a Poisson process with constant intensity along the beam, which implies that the distance between defects is gamma-distributed. However, this is not strongly supported by statistical tests.

Riberholt (1979) reports distances between 360 mm and 550 mm (cross-sections 50-100 to 30x175 mm) with a typical coefficient of variation of about 0.6. There are indications that the distances are grade and size dependent but the trend is not clear and may be explained by log selection and sawing practices.

Isaksson (1999) reports distances of between 440 mm and 500 mm with a typical coefficient of variation of about 0.6-0.7.

Larsen (1980) investigated boards for glulam (38 mm x150 mm) and found mean distances of 350 mm with a coefficient of variation of 0.35).

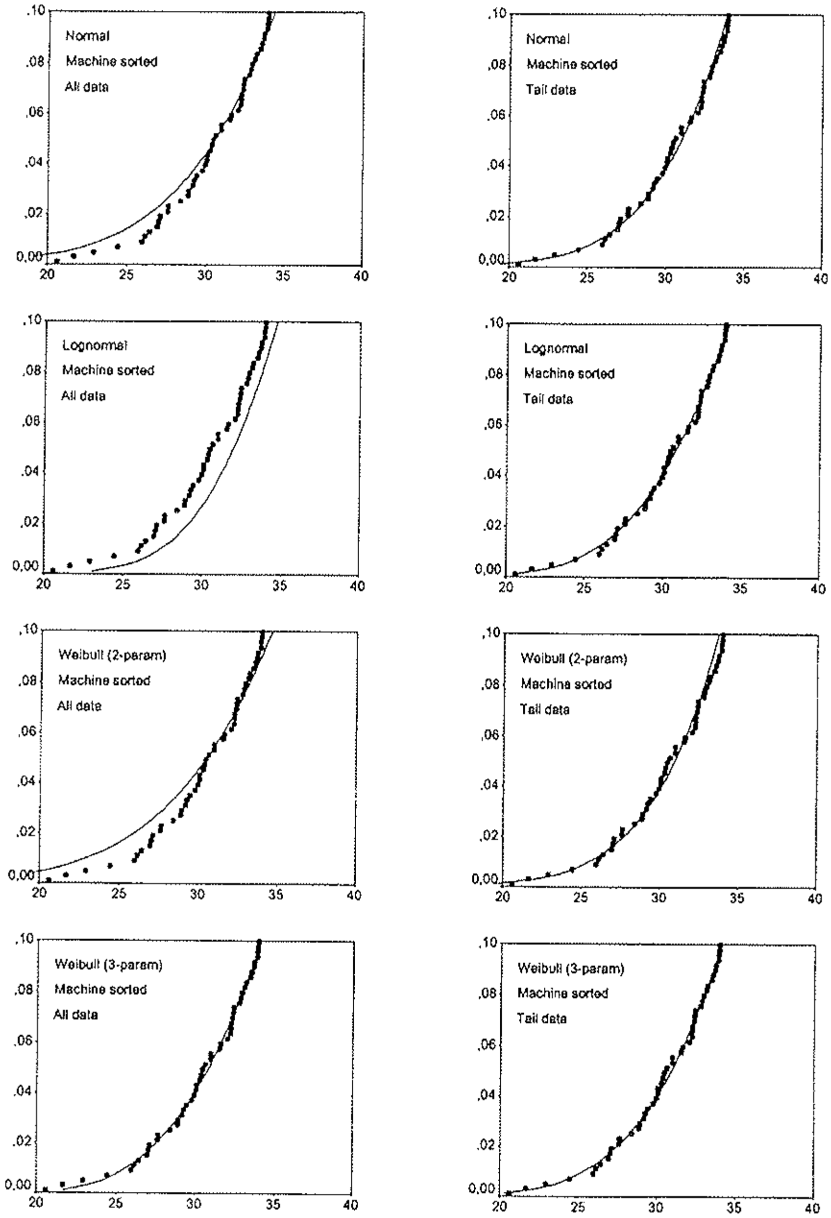

Figure 4 –Example of test data and fitted cumulative distributions of bending strength for spruce with a depth of 150 mm machine graded to European class C30.

Log, log-normal and Weibull distributions are fitted to all data and to the tail data (truncated at 10 %).

4.4 Basic properties

The basis for the model is the basic strength, i.e. the distribution of the properties of the (weak) sections but the test data available relates to the reference properties. It is, therefore, necessary to establish a relation between these two properties

Isaksson (1996) and (1999) has investigated the strength of weak sections in Norway spruce. He aimed to determine the bending strength in several sections. The problem with testing a board in more than one section is that it is difficult to control the location of the failure, and after testing one section, further tests under the same conditions as the first are difficult to accomplish. Another problem concerns testing different sections located within a short distance, which requires that the rest of the board remains unloaded. The intention was to accomplish a constant bending moment over a selected, isolated section, as shown in figure 5.

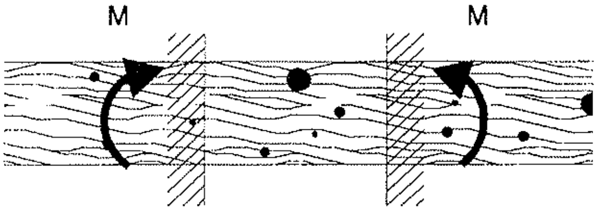

Figure 5 – Intended load situation with a constant bending moment over a selected, isolated section. From (Isaksson, 1996).

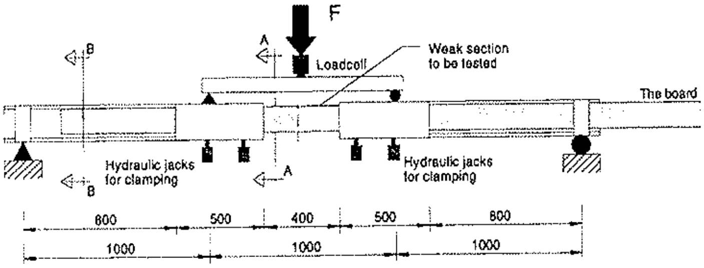
F
A
B
Loadcell
Weak section to be tested
The board
Hydraulic jacks for clamping
Hydraulic jacks for clamping
A
B
800
500
400
500
800
1000
1000
1000

Figure 6 – Test arrangement in principle. From (Isaksson, 1996).

This was achieved with the arrangement shown in figure 6. The board was clamped on both sides of the selected test section, thus leaving the rest of the board unloaded.

To compare the strength of the weak section with the reference property, two as far as possible identical series – A and B – each with 150 specimens of Norway spruce were investigated. Both series were graded visually and by grading machines (Cook-Bolinder and Finnograder). The section corresponding to the lowest Cook-Bolinder stiffness (denoted the CB-section) was determined. This section was assumed to be the critical section.

Series B was tested according to EN 408. Where possible, the CB-section was placed in the middle. If this was not possible, the section with the second-lowest CB reading was tested.

For the specimens in series A the bending strength was determined in several sections using the arrangement shown in figure 6. For series A, the following strength values were reported: The lowest value for a board, the strength of the CB-section, and the strength value that would have been found if testing had been done in accordance with EN 408.

The test results are summarised in table 1.

Table 1 – Bending strength in MPa

	Series B	Series A			
	EN 408	Weakest	CB	EN 408	All
Mean	55.1	47.3	54.2	54.3	57.4
COV	27	23	23	23	23

The ranking reflects that the Cook-Bolinder machine is not able in all cases to identify the weakest section – as assumed in EN 408. If this were the case, the strength of the weakest section and the CB section would be identical. The results according to EN 408 are influenced by adding results from the second-lowest CB readings, and the strong sections influence the mean of the strength for all sections.

The ratio between the mean values is 57.4/54.3 = 1.06.

The characteristic bending strength (5-percentile) according to the different test systems has been estimated from the distribution of the strength of the weak sections using Monte Carlo simulations. The results are shown in table 2.

Table 2 – Characteristic bending strength. (From Isaksson, 1999)

Test system	European (EN 408)	USA	Australien
Strength in MPa	30.8	31.9	32.8
Relative strength	1	1.04	1.06

4.4 Safety verifications – failure criteria

For some materials the failure criterion is quite simple: Failure takes place at first passage of a threshold value. The situation is more complicated for materials –e.g. timber and other wood based materials – where the load (and moisture) history plays an important role:

- The strength of timber under sustained load depends on the load duration or perhaps more precisely: for load levels above a certain threshold (some maintain that the threshold value is zero) failure will take place after a limited period of time: the higher the load levels, the shorter the time to failure.
- The short term-strength is only marginally influenced by a preceding sustained loading:

The phenomena are illustrated in figures 7 and 8, which have been calculated in accordance with Nielsen's theory, see below. The abscissa is a non-dimensional expression of time and the ordinate is the load level. As a rough approximation, it may be assumed that the residual strength is the same as the short-term strength.

For timber structures two verifications are thus needed:

- The time to failure under permanent and sustained variable actions should be greater than the prescribed life time of the structures
- The stress after a sudden increase in the load level (e.g. due to wind or snow) should not exceed the short-term strength.

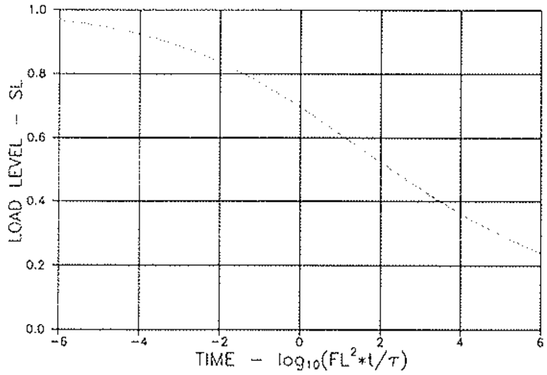

Figure 7 – Time to failure under permanent load dependent on load level relative to strength under short term load. From (Nielsen, 1996).

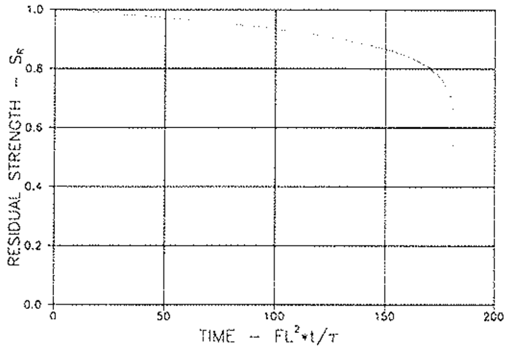

Figure 8 – Residual strength after a permanent load that would lead to failure after a dimensionless time of about 180. From (Nielsen,1996).

The following is from (Thelandersson et al, 1999):

> Various models have been proposed to explain the long-term behaviour of timber. The models use a variable $\alpha(t)$ to describe damage over time, t. This variable increases over time, depending on the intensity and duration of applied stress from $\alpha = 0$ in the undamaged state, until failure occurs, at which time α is taken to be equal to unity.
>
> One of the simplest damage models is the one proposed by Gerhards & Link (1986):
>
> $$\mathrm{d}\alpha/\mathrm{d}t = \exp(A - B\sigma/f) \qquad (17)$$
>
> A and B are constants, σ is the applied stress and f is the short-term strength.
>
> The best-known damage models are probably those proposed by Ricardo O. Foschi. They are not based on theoretical considerations, but a reasonable differential equation is proposed for damage development and the parameters in the model are determined by curve fitting. The first model, proposed in (Barrett & Foschi, 1978),can be expressed
>
> $$\mathrm{d}\alpha/\mathrm{d}t = A(\sigma/f - \sigma_0/f)^B + C\alpha \qquad (18)$$

σ_0 is a threshold stress, below which no damage occurs.

A more complicated model was proposed in (Foschi & Yao, 1984), the model normally referred to as Foschi´s model:

$$\mathrm{d}\sigma/\mathrm{d}\alpha = A(\sigma - \sigma_0)^B + C\sigma^n(\sigma/f - \sigma_0/f)^n\alpha \tag{19}$$

A model based on fracture mechanics is presented in (Nielsen & Kousholt, 1980). A brief presentation can be found in (Madsen, 1992).

The theory is based on the assumption that cracks with a length $2l_0$ already exist in the initial unloaded situation. When loaded, the cracks will open but their growth will be arrested by coherence stresses at the front zone. If the load is increased above a threshold, the cracks will grow in thickness until a critical thickness δ_{cr} is reached. This represents the end of phase 1, see figure 9. The cracks will now start to grow in length until a critical length $2l_{cr}$ is reached and catastrophic failure takes place.

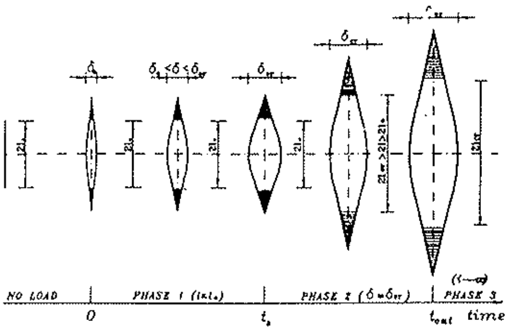

Figure 9 – Crack development. From (Nielsen, 1996).

The theory can be used to calculate the time to failure for a given load level, see figure 7. It is also possible to calculate the residual short-term strength after loading. An example is shown in figure 8 for high-grade timber loaded at 50 percent of the short-term strength. As shown, the reduction in strength is moderate until close to failure.

The models are discussed in (Foschi & Yao, 1986). The following is quoted from the conclusions:

"…the fracture mechanics approach and the damage accumulation model by Foschi were found suitable to represent accurately the experimental trends… The model by Gerhards was found to be lacking in the flexibility needed to follow the experimental trends. The fracture mechanics model is not easy to use, since it requires numerical integration to obtain the time-to-failure in all cases when the applied stress varies with time…"

The models (18) and (19) are discussed in (Ellingwood & Rosowosky, 1991). They conclude:

> "...The damage rate models in (18) and (19) are nearly the same except at stress levels below about 0.65. Equation (19) is more difficult to implement because it cannot be non-dimensionalized..."

> The models are used in (Ellingwood & Rosowosky, 1991) to calculate the effect of live load and snow load. They conclude:

> "...Detailed examination of the simulated damage accumulation processes...revealed that for both light occupancy live and snow loads, damage usually accumulates only during one or two of the largest load pulses to occur during 50 years...This behaviour is a result of the highly nonlinear nature of the damage-rate models..."

In the model code in chapter 3, the use of Gerhards' model is preliminary proposed despite it's shortcomings because of it's simplicity, but studies on the use of the Nielsen model are under way in the COST E24 action and it may eventually replace Gerhards'as the preferred model.

5 Other wood based materials

For wood-based panels and LVL, the effect of the loading history – in principle as for structural timber (section 3.5 and 4.5) – must be taken into account. The reliability analysis is otherwise the same as for other materials.

For glued laminated timber there are two possibilities:

- To establish a model from which the properties may be derived from the properties of the boards with finger joints. This possibility is discussed in (Serrano, 2002).
- To treat glulam as LVL.

The latter approach is recommended. The models for glulam are primitive and generally not able to predict failure behaviour reasonably well.

6 References

Blass, H. J. (1988): Tragberechnung von Druckstäben aus Brettschichtholz. Bauingenieur 63, pp. 245-251.

Barrett, J. D. & Foschi, R. O. (1978): Duration of load and probability of failure in wood, parts I and II. Canadian Journal of Civil Engineering, 5(4) 505-532.

Ellingwood, B. & Rosowsky, D. (1991): Duration of load effects in LRFD for wood construction. Journal of Structural Engineering, 117(2).

EN 408 (2002): European Standard, Timber Structures – Structural and glued laminated timber – Determination of some physical and mechanical properties.

EN 1995-1-1 (2002) Eurocode5: European Standard, Design of Timber Structures, Part 1-1: General rules and rules for buildings.

Foschi, R. O., Folz, B. R. & Yao, F. J. (1989): Reliability based design of wood structures. Structural Research Series Report No. 34. University of British Columbia, Vancouver, Canada.

Gerhards, C. & Link, C. (1986): Effect of loading rate on bending strength of Douglas-fir 2 by 4-s. Forest Products Journal 36(2), 63-66.

Isaksson, T. (1996): Variability of bending strength within timber elements. Report TVBK-1011, Division of Structural Engineering, Lund Institute of Technology, Sweden.

Isaksson, T. (1999): Modelling the variability of bending strength in structural timber. Report TVBK-1015, Division of Structural Engineering, Lund Institute of Technology, Sweden.

Larsen, H. J. (1980): Strength of glued laminated beams, part 2: Properties of glulam laminations. Institute of Building Technology and Structural Engineering, Aalborg University Centre, Aalborg, Denmark.

Larsen, H.J. (2002): Nordic Wood: Safety of timber structures, Summary reports. Report TVSM-3062, Division of structural engineering, Lund Institute of Technology, Sweden.

Larsen, H.J., Isaksson, T. & Thelandersson, S. (1996): Model Code for the Probabilistic Design of Timber Structures. Paper CIB W18 29-02-1.

Madsen, B. (1992): Structural behaviour of timber. Timber Engineering Ltd., Vancouver.

Nielsen, L. F. & Kousholt, K. (1980): Stress-strength-lifetime relationship for wood. Wood Science, 12.

Nielsen, L. F. (1996): Lifetime and residual strength of wood. Report Series R No. 6. Department of Structural Engineering and Materials, Technical University of Denmark.

Ranta-Maunus, A., Fonselius, M., Kurkela & J., Torratti, T. (2001): Reliability of timber structures. VTT Research Notes 2109, Espoo, Finland.

Ranta-Maunus, A. (2002): Summary report on existing strength data, in (Larsen, 2002)

Riberholt, H. & Madsen, P.H. (1979). Strength distribution of timber structures, Measured variation of the cross sectional strength of structural lumber. Structural Research Laboratory, Technical University of Denmark.

Serrano, E. (2002): Mechanical performance and modelling of glulam. In Thelandersson, S. & Larsen, H. J. (ed) 2002: Timber Engineering, Wiley and Sons.

Thelandersson, S., Larsen, H. J., Östlund, L., Isaksson, T. & Svensson, S. (1999): Report TVBK-3039, Division of Structural Engineering, Lund Institute of Technology, Sweden